Development of Optical Instrumentation and Methods to Monitor Brain Oxygen Metabolism: Application to Neonatal Brain Injury

Gemma Margaret Bale

A thesis submitted to University College London
for the Degree of Doctor of Philosophy (Ph.D)

Department of Medical Physics and Biomedical Engineering
University College London

2016

Declaration

I, Gemma Margaret Bale, declare that the work presented in this thesis is my own, and where information has been derived from other sources, those sources are credited.

Abstract

Hypoxic-ischaemic encephalopathy (HIE) is a relatively common and potentially devastating form of perinatal brain injury, associated with neurodevelopmental problems and mortality. HIE is an evolving process and so there is a need for real-time, in-vivo measurements of brain oxygenation and metabolism for clinical assessment in the first days of life, to detect those at risk of further brain injury who may benefit from redirection of care.

This thesis describes the development of a broadband near-infrared spectroscopy (NIRS) system to monitor changes in metabolism and haemodynamics in HIE infants at the cotside. This system uses multiple wavelengths (λ = 136, 770-905nm) to monitor changes in concentration of the oxidation state of cytochrome-c-oxidase (CCO) as well as haemoglobin oxygenation. Changes in the oxidation state of CCO (oxCCO) are indicative of CCO redox state changes within mitochondria and therefore represent oxygen utilisation. The 2-channel system incorporates a broadband source, optical fibres, spectrograph and CCD. This set-up is flexible and robustly monitors changes in haemoglobin and oxCCO.

The system was developed specifically for the neonatal intensive care unit (NICU) and has been demonstrated on 38 brain-injured newborn infants (28 with HIE). NIRS data were continuously collected over the frontal lobe simultaneously with systemic data for multimodal analysis. This allows the study of cerebral changes in response to global pathophysiological events. HIE was assessed by magnetic resonance spectroscopy measurement of lactate to NAA ratio (Lac/NAA), the gold standard for neurodevelopmental outcome.

Initially the analysis focussed on spontaneous hypoxias. The relationship between haemoglobin oxygenation and oxCCO during hypoxic events was significantly associated with Lac/NAA (n=22, r=0.51, p=0.02). Further investigation of the dynamics of the cerebral changes during hypoxias found oxCCO differences with injury severity that was not observed in haemoglobins (n=17). Finally, the relationship between cerebral signals and systemic physiology was investigated with a multivariate statistical technique. A strong relationship between oxCCO and systemic changes indicated severe brain injury (n=11, p=0.04).

Acknowledgements

I would first like to thank my supervisors: Ilias Tachtsidis, who has provided a wonderful subject matter for me to explore, been always available for discussion and has been incredibly supportive; and Judith Meek, who has not only been a wonderful source of wisdom, but also a source of kindness, which is especially important when dealing with such a difficult subject matter.

I am indebted to Subha Mitra as this project would not have been successful without his hard work. He has been patient, kind, knowledgeable and always smiling. My thanks go to all of the clinical team at UCLH: Alan Bainbridge, Sean Mathieson, Cristina Uria, Mary Dinas, Nicola Robertson, and all of the staff who have assisted with the studies. I must also thank the families of the children recruited.

I have been very fortunate to undertake this PhD in the Biomedical Optics Research Laboratory (BORL) at UCL. Thank you in particular to those who have contributed to this work: Robert Cooper, Sabrina Brigadoi, Clare Elwell, Felix Scholkmann, Alexander Caicedo-Dorado, Terence Leung, David Highton, Matthew Caldwell, Pardis Kaynezhad and Isabel de Roever (who is bravely taking on CYRIL and all of 'his' flaws).

I have made some wonderful friends in Medical Physics: Teedah, Emma, Sophie, Nick, Andy, Jamie and Sam - thank you all for making every day in the office a pleasure, I'm lucky to know you all. This PhD was made so enjoyable because I was sat next to Luke Dunne; he deserves special thanks for dealing with my LabVIEW mess and auditing my jokes for three years.

I must also thank my non-BORL friends: Leanne, your unwavering friendship has shaped me as a person and I'm so lucky to have had your support throughout this PhD (and life, in general). Sian, my 'PhD friend', who I'm so glad I could share this experience with and who has inspired me to be the best version of myself. Not forgetting Soraya, who I would not be in Biomedical Optics without!

I am so grateful to my parents who have genuinely made me believe that I can do anything; your support and love has been incredible. Thank you to Andrew, for allowing me to be your friend as well as your sister. Thanks to Maxine and Christopher, it has been wonderful to have family close by throughout this experience. Finally to my new little family: Matt - thank you for your unconditional love and support, I genuinely wouldn't have been able to do this without you - and Archie - thanks for staying up all night with me while I was writing (I know you don't understand), and thanks for being my dog.

Publications Resulting from this Work

Peer-Reviewed Journal Papers

- **Gemma Bale**, Clare Elwell, Ilias Tachtsidis "From Jobsis to the Present Day: A Review of Clinical Near-Infrared Spectroscopy Measurements of Cerebral Cytochrome-C-Oxidase" *Journal of Biomedical Optics* (in press)
- **Gemma Bale**, Subhabrata Mitra, Isabel de Roever, Marcus Chan, Alexander Caicedo-Dorado, Judith Meek, Nicola Robertson, Ilias Tachtsidis "Interrelationship between broadband NIRS measurements of cerebral cytochrome-c-oxidase and systemic changes indicates injury severity in neonatal encephalopathy" *Advances in Experimental Medicine and Biology* (in press)
- Subhabrata Mitra, **Gemma Bale**, Judith Meek, Cristina Uria, Nicola J Robertson and Ilias Tachtsidis "Relationship between cerebral oxygenation and metabolism during rewarming in newborn infants after therapeutic hypothermia following hypoxic-ischaemic brain injury" *Advances in Experimental Medicine and Biology* (in press)
- Subhabrata Mitra, **Gemma Bale**, Sean Mathieson, Cristina Uria, Judith Meek, Ilias Tachtsidis, Nicola Robertson "Changes in cerebral oxidative metabolism during recurrent neonatal seizures" *Developmental Medicine & Child Neurology* (under review)
- Subhabrata Mitra, **Gemma Bale**, Judith Meek, Sean Mathieson, Cristina Uria, Giles Kendall, Nicola Robertson, Ilias Tachtsidis "In vivo measurement of cerebral mitochondrial metabolism using broadband near-infrared spectroscopy following neonatal stroke" *Advances in Experimental Medicine and Biology* 876 pp.493-499, 2016
- **Gemma Bale**, Subhabrata Mitra, Judith Meek, Nicola Robertson, Ilias Tachtsidis "A new broadband near-infrared spectroscopy system for in-vivo measurements of cerebral cytochrome-c-oxidase changes in neonatal brain injury" *Biomedical Optics Express* 5(10) pp. 3450-3466, 2014
- **Gemma Bale**, Aaron Oliver-Taylor, Igor Fierens, Kevin Broad, Jane Hassell, Go Kawano, Jamshid Rostami et al. "Investigation of Cerebral Autoregulation in the Newborn Piglet During Anaesthesia and Surgery" *Advances in Experimental Medicine and Biology* 812 pp.165-171, 2014

Conference Presentations

- **Oral Presentation** "Relationship Between Cerebral Cytochrome-C-Oxidase and Oxygenation is Associated with Brain Injury Severity in Birth Asphyxiated Infants" *OSA Biomed 2016 Miami, USA*
- **Poster Presentation** "Relationship between haemodynamics and metabolism in the injured neonatal brain during spontaneous oxygen desaturations" *Institute of Physics: Optics in Medicine 2015 Nottingham, UK*
- **Oral Presentation** "Relationship between haemodynamics and metabolism in the injured neonatal brain during spontaneous oxygen desaturations" *ISOTT 2015 Wuhan, China*
- **Poster Presentation** "Interrelationship between NIRS measurements of cerebral cytochrome-c-oxidase and systemic changes indicates injury severity in neonatal encephalopathy" *ISOTT 2015 Wuhan, China*
- **Oral Presentation** "Interrelationship between NIRS measurements of cerebral cytochrome-c-oxidase and systemic changes indicates injury severity in neonatal encephalopathy" *Brain 2015 Vancouver, Canada*
- **Oral Presentation** "A new broadband NIRS system for in-vivo measurements of cerebral cytochrome-c-oxidase changes in neonatal brain injury" *fNIRS 2014 Montreal, Canada*
- **Oral Presentation** "In-Vivo Measurements of Cerebral Changes in Cytochrome-c-Oxidase using Broadband Near-Infrared Spectroscopy in Neonates" *ISOTT 2014 London, UK*
- **Poster Presentation** "In-Vivo Measurements of Cerebral Changes in Cytochrome-c-Oxidase using Broadband Near-Infrared Spectroscopy in Perinatal Hypoxic-Ischaemic Encephalopathy" *OSA Biomed 2014 Miami, USA*
- **Oral Presentation** "NIRS detection of cerebral autocorrelation impairment during anaesthesia in the newborn piglet" *ISOTT 2013 Hannover, USA*

Prizes

- ISOTT **Duane F Bruley Award** July 2015
- UCL Provost's **Engineering Engager of the Year** May 2015
- Medical Physics **PhD Showcase Presentation Award** April 2015
- International Society for Cerebral Blood Flow and Metabolism **Young Investigator Travel Bursary** March 2015
- Medical Physics **PhD Prize** October 2014

- Photonics Centre for Doctoral Training **Presentation of the Year** June 2014
- OSA Biomed **Student Poster Finalist** April 2014
- UCL Graduate School **Travel Fund** April 2014
- ISOTT **Duane F Bruley Award** June 2013
- UCL Graduate School **Travel Fund** June 2013

Contents

List of Figures

List of Tables

List of Abbreviations

ADP	adenosine diphosphate
aEEG	amplitude integrated electroencephalogram
APD	avalanche photodiode
ASL	arterial spin labelling
ATP	adenosine triphosphate
AUC	area under the curve
BBB	blood-brain barrier
BP	blood pressure
CAD	computer aided design
CBF	cerebral blood flow
CBV	cerebral blood volume
CCA	canonical correlation analysis
CCD	charge coupled device
CCO	cytochrome-c-oxidase
CFM	cerebral function monitor
$CMRO_2$	cerebral metabolic rate of oxygen
CNS	central nervous system
CO_2	carbon dioxide
CPP	cerebral perfusion pressure
CSF	cerebrospinal fluid
CuA	copper A
CW	continuous wave
CYRIL	cytochrome research instrument and application
DCS	diffuse correlation spectroscopy
DPF	differential pathlength factor
ECG	electrocardiogram
ECT	extracerebral tissue
EEG	electroencephalogram
ETC	electron transport chain
FAD	flavin adenine dinucleotide

FD	frequency domain
FiO_2	fraction of inspired oxygen
fMRI	functional magnetic resonance imaging
fNIRS	functional near-infrared spectroscopy
FTOE	tissue oxygen extraction factor
GA	gestational age
GM	grey matter
GUI	graphical user interface
HbD	haemoglobin difference
HbO_2	oxygenated-haemoglobin
HbT	total haemoglobin
HHb	deoxygenated-haemoglobin
HR	heart rate
HRF	haemodynamic response function
HVx	correlation between MABP and HbT
Lac	lactate
LED	light emitting diode
MABP	mean arterial blood pressure
$MABP_{OPT}$	optimum mean arterial blood pressure
MBLL	modified Beer Lambert law
MD	multi-distance
MR	magnetic resonance
MRI	magnetic resonance imaging
MRS	magnetic resonance spectroscopy
μ_a	absorption coefficient
μ_s	scattering coefficient
μ_s'	transport scattering coefficient
NA	numerical aperture
NAA	n acetyl aspatate
NAD+	nicotinamide adenine dinucleotide
NADH	nicotinamide adenine dinucleotide hydride
NICU	neonatal intensive care unit
NIR	near-infrared
NIRS	near-infrared spectroscopy
NMR	neonatal mortality rate
O_2	oxygen
oxCCO	oxidised cytochrome-c-oxidase
$PaCO_2$	partial pressure of carbon dioxide
PaO_2	partial pressure of oxygen

PCA	principle component analysis
PMT	photomultiplier tube
PNS	peripheral nervous system
RMS	root mean square
ROI	region of interest
RR	respiratory rate
RTE	radiative transport equation
SaO_2	arterial oxygen saturation
SpO_2	arterial oxygen saturation measured by pulse oximetry
SRS	spatially resolved spectroscopy
SvO_2	venous oxygen saturation
TCA	tricarboxylic acid cycle
TCD	transcranial Doppler ultrasound
TH	therapeutic hypothermia
TOBY Xe	total body hypothermia plus xenon
TOI	tissue oxygenation index
TR	time resolved
UCLn	UCL algorithm with n wavelengths
Vmca	velocity of the middle cerebral artery
WM	white matter

Chapter 1

Introduction

This chapter introduces the motivations behind this thesis and outlines its key aspects. The main clinical motivation emerges from a severe disorder in newborn babies called hypoxic-ischaemic encephalopathy (HIE) and the need for a brain tissue physiological monitor to assess the illness and its progression to guide treatment. This chapter gives an overview of HIE and outlines the key specifications of a monitoring instrument that uses broadband near infrared spectroscopy (NIRS) to quantify a unique marker of cellular metabolism, cytochrome-c-oxidase (CCO). The final sections give a summary of the subsequent chapters in this thesis and outlines my part in the work.

1.1 Motivation and Aims

This thesis is part of a collaboration between two teams at University College London (UCL): the Multimodal Spectroscopy Group based in the Biomedical Optics Research Laboratory (BORL) and researchers from the Institute of Women's Health who are part of the Baby Brain Study based at University College London Hospitals (UCLH). The Baby Brain Study was set-up to assess the relation between magnetic resonance (MR) measurements of brain intracellular pH and brain perfusion, and NIRS derived measurement of CCO in infants with acute brain injury, in particular those with neonatal encephalopathy at term. The goal of the Multimodal Spectroscopy Group, led by Dr Ilias Tachtsidis, is to develop clinically useful brain monitors, in particular focussed on the measurement of CCO to inform on cellular metabolism. The ethos of the group is that the combination of physiological monitors will paint a more accurate picture and give a better assessment of brain health.

In recent years, a collaboration between Professor Nikki Robertson at the Institute of Women's Health and the Multimodal Spectroscopy Group has led to the use of NIRS in a piglet model of HIE. Striking results have found that the CCO signal has a strong relationship with MR spectroscopy (MRS) measured biomarkers of cellular metabolism, and have also found that the CCO signal is significantly related to subject survival [12].

There is a long history of NIRS research in the UCLH neonatal intensive care unit (NICU). As early as 1988, Edwards et al. [69] used NIRS to monitor critically ill babies, and over the next 27 years this

research has continued, for example on HIE babies [70, 71], as well as preterm infants [72].

This PhD thesis brings together and expands these previous works with the use of a broadband NIRS system to measure CCO in the NICU for the first time. The focus of this PhD is to develop a novel NIRS system capable of measuring CCO within a clinical environment on infants suffering from HIE; and further, to investigate the hypothesis that the relation of the CCO signal to other physiological changes will identify the severity of injury, which will aid clinical diagnosis and treatment in the first days of life.

More specifically, the objectives of this PhD are:

- To design and build a broadband NIRS system with the capability to monitor changes in the oxidation state of CCO specifically for neonates.
- To demonstrate the use of the system in the NICU on babies with brain injury.
- To assess the capacity of the system to measure accurately the changes in metabolic CCO independently of the haemoglobin signals.
- To develop and test analysis techniques to assess the ability of CCO to provide information on neonatal brain injury.
- To gain insight into the potential of CCO as a useful biomarker of brain injury.

1.2 Clinical Introduction

Hypoxic-ischaemic (HI) injury occurs around the time of birth, however the injury can progress and evolve for days afterwards. The best outcome biomarker following HIE is currently from magnetic resonance spectroscopy (MRS) but this is only available after five days or longer following the acute brain injury, and gives only a snapshot of the cerebral injury at a particular time and location. However, MRS technology is only available in high-end clinics as it is very expensive to run. Electroencephalography (EEG) is the most commonly used monitor to assess HIE, and it is a reliable predictor of outcome 6 hours of age, however there is a reduction in its predictive ability at 48 hours [5]. Therefore there is an urgent need for an early biomarker of brain tissue injury severity in the first days of life, to fill the gap between EEG and MRS. Chapter 2 gives more detail on the injury, its progression, treatment and current clinical monitors.

1.3 Near-Infrared Spectroscopy Introduction

In 1977, Franz Jobsis discovered an optical window into living tissue in the near-infrared (NIR) spectrum; light in the region of 650-1000nm travels through tissue and therefore it is possible to interrogate absorbing compounds within the tissue. The strongest absorbers in this region are also clinically interesting; haemoglobin in both oxygenated and deoxygenated (HbO_2 and HHb) forms, and CCO.

NIRS systems are relatively simple: they essentially consist of a light source, which illuminates tissue, and a detector, to record light that has travelled through and exits the tissue (the light can either travel

through back-reflection or transmission across the tissue). The monitored changes in light attenuation from the tissue are related to the changes in concentration of the absorbers within the tissue. It is possible to calculate these changes by comparing them to the known absorption spectra of the absorbers, this is done using the modified Beer-Lambert law (which is discussed in section 3.1). This technique allows real insight into the haemodynamic and metabolic changes within tissue, such as the brain and muscle, in a non-invasive, non-ionising, relatively inexpensive, portable manner.

Most commercial NIRS systems use 2-4 wavelengths of light to interrogate the tissue and resolve changes in the concentrations of HbO_2 and HHb. However, in order to accurately measure changes in CCO, a compound that exists in much lower concentrations in-vivo, many more wavelengths are needed. Broadband NIRS, which is defined here as a NIRS system using more than 100 wavelengths of light, has therefore been used to record changes in this metabolic marker. Broadband NIRS requires a broadband light source and spectrometer to detect the changes in attenuation across the entire NIR spectrum. A clinical broadband NIRS system to monitor CCO has yet to be developed commercially and, although many in-house systems exist, has never been used to monitor infants within an intensive care unit. This challenge is addressed by this PhD.

Terminology

Note that in this thesis the term 'NIRS' will be used to describe the technique when HbO_2 and HHb are derived from 2-4 discrete wavelengths of light and 'broadband NIRS' will be used to describe the measurement of HbO_2, HHb and CCO using over one hundred wavelengths of light.

1.4 Cytochrome-C-Oxidase Introduction

NIRS measurements of CCO have the potential to yield crucial information about cerebral metabolism and tissue oxygenation at the baby's cotside. CCO is the terminal electron acceptor in the electron transport chain, the final stage of oxidative metabolism. The CCO signal does not arise from changes in concentration of CCO itself (the concentration of CCO is stable over a measurement period) but rather from changes in its oxidation state. A unique copper dimer in the enzyme has an absorption peak around 835nm in its oxidised form, but not in its reduced state. Therefore broadband NIRS is able to resolve changes in the oxidation state using the difference spectrum between the oxidised and reduced species to obtain an indicator of the changes in the CCO redox state. A change in the redox state represents a change in oxidative cellular metabolism which is dependent on tissue oxygen and glucose availability, along with other factors such as cellular injury. Therefore monitoring the CCO redox state changes gives an indication of changes in tissue oxygenation and metabolism at a cellular level.

A full literature review summarising the state of the art clinical measurements of CCO using NIRS is provided in Chapter 4.

Terminology

Previous publications, both pre-clinical and clinical, have referred to this signal as CytOx, aa_3, CuA, CCO and oxCCO. For clarity, in this thesis the term oxCCO is used to describe the NIRS measurement of changes in the concentration of the oxidation state of cytochrome-c-oxidase, which arise from the redox state-dependent changes in the NIR spectrum. Although the dominant chromophore in the NIR is the CuA centre, other cytochrome redox centres and oxygen intermediates can contribute to this signal.

1.5 Thesis Overview

The thesis has eleven subsequent chapters. Briefly, the next three chapters cover the background to the work, followed by two chapters which describe the instrumentation development and the experimental design, then there are four results chapters and the thesis finishes with a discussion of further work and a conclusion.

For the background chapters, Chapter 2 contains a medical background including an introduction to the brain, its circulation, metabolism, and development, and HIE, from the aetiology to the treatment and monitoring of the illness. In Chapter 3, a summary of NIRS is presented, including the fundamentals of the technique, and the instrumentation and measurements involved. This chapter concludes with a literature review of NIRS studies of HIE. A full literature review of the clinical NIRS-measured CCO signal is given in Chapter 4. This covers the history of the measurement and the methods used to obtain the signal, an evaluation of these methods and a full review of the neonatal and adult studies to date.

Chapter 5 covers the development of the new broadband NIRS system called CYRIL (CYtochrome-c-oxidase Research Instrument and appLication), from the design considerations to the hardware and software. The specification of the system is presented with some preliminary testing. Chapter 6 describes the use of the CYRIL system in the NICU and the experimental design considerations. Also presented in this chapter are details of the patients included in the studies.

The results chapters begin with Chapter 7 in which analysis of the broadband NIRS data recorded in the NICU is performed to ensure a robust oxCCO signal. The depth sensitivity of the signal is investigated. Assessment of the capacity of the multi-distance measurements possible with CYRIL is also performed. Chapters 8 and 9 investigate the effect of spontaneous hypoxia on the cerebral NIRS signals. This is done firstly by looking at the magnitude of the change of the signals for many events, and then by assessing the physiology behind the dynamics of the changes. The final results chapter, Chapter 10, looks at the relationship between each cerebral NIRS signal and the systemic physiology as a whole, using a multivariate statistical technique.

The thesis closes with a brief overview of work currently in progress, and a discussion of the future for this work in Chapter 11, and Chapter 12, which comprises a summary of the thesis and a discussion of the results.

1.6 Personal Statement

The work presented in this thesis can be separated into three parts:

1. The development of a broadband NIRS system to monitor changes in CCO in a clinical environment.
2. The demonstration of this system combined with multimodal monitors in the NICU to monitor infants with acute brain injury.
3. The analysis of multimodal data using (three) different approaches to understand the CCO signal in relation to brain injury severity.

Some of the work involved in this project is a collaboration by a number of individuals, therefore it is important to acknowledge those involved and to highlight the work I carried out.

The first part was mainly carried out by myself, with the guidance of my colleagues in BORL. This involved the selection and modification of optical components, bringing together the components to form a system suitable for the clinic, the design of optical fibres and holders, the development of LabVIEW software and preliminary testing and characterisation of the system.

The data collection in the neonatal intensive care unit (NICU) was mostly carried out by myself and Dr Subhabrata Mitra, a neonatal registrar undertaking a PhD. Dr Mitra and I, with guidance from our supervisors (Dr Ilias Tachtsidis, Dr Judith Meek and Professor Nikki Robertson), designed and set-up the experiments, which involved integrating the NIRS system into the NICU environment, and collecting systemic data. This work was supported by staff in NICU, particularly Dr Cristina Uria, Dr Giles Kendall and Mary Dinan, who were involved in approaching parents for informed consent and helping with the data collection. As well as data collection, I was responsible for maintenance and updates of the system, ensuring good quality optical data collection, evaluation of optical data, synchronising the NIRS and systemic data, creating a data processing procedure, and saving back-ups of the data securely.

I also provided technical support for other analysis, mainly involving designing Matlab programmes to be used by other members of the team. My analysis initially focussed on spontaneous hypoxia events and the CCO response to them (Chapters 8 and 9). The analysis was then expanded to examine the effect of all systemic changes on the cerebral NIRS signals simultaneously using multidimensional statistical analysis (Chapter 10). The entire team was involved in the discussion of the physiological implication of our results.

Some of this thesis has been published in peer-reviewed journals. I have written three papers from work directly produced for this thesis, and another which was carried out during this PhD, but is not relevant here; this paper covers the analysis of data from a piglet study which was performed to assess cerebral autoregulation impairment during anaesthesia. These publications are shown in Appendix B. Dr Mitra is first author on another three papers from the neonatal data recorded.

Chapter 2

The Neonatal Brain and Hypoxic-Ischaemic Encephalopathy

In order to understand neonatal brain injury one must first understand the brain under normal conditions, in particular, its energy supply and energy usage. Then it is possible to understand the brain in context of neonatal development and finally, neonatal brain injury. Accordingly, this chapter begins with an overview of cerebral anatomy and, importantly, the cerebral circulation and cell metabolism. Finally, we will look at brain development in-utero and perinatal brain injury; specifically hypoxic-ischaemic encephalopathy, its causes, treatment and assessment.

2.1 Anatomy and Physiology of the Brain

2.1.1 The Nervous System

The human nervous system is the most complex achievement of the process of evolution. The anatomy and physiology of some aspects of neural function are well understood, while others are the subject of research in both the basic and clinical sciences.

The basic structural and functional unit of the nervous system is the neuron (or nerve cell or neurone) and the human nervous system is estimated to contain 10^{10} neurons [73]. The function of the neuron to respond to stimuli, transmit the resulting excitations to neurons or effector organs (e.g. muscle cells or glandular cells) with the goal of conveying and receiving information. Neuron shape and size is diverse but all neuron cells have a few characteristics in common: a cell body; with branching receptors known as dendrites; a long nerve fibre, or axon; which carries information away from the cell body and which may split into several branches, collaterals; and at the end of the axon specialisations called terminal boutons occur, which transfer information to the dendrites of other neurons [73]. Figure 2.1 shows a schematic representation of the basic structure of the neuron.

Neurons code information through changes in electrical energy. The neuron possesses a resting potential across its membrane (between 60 and 70mV), the inside is negative with respect to the outside.

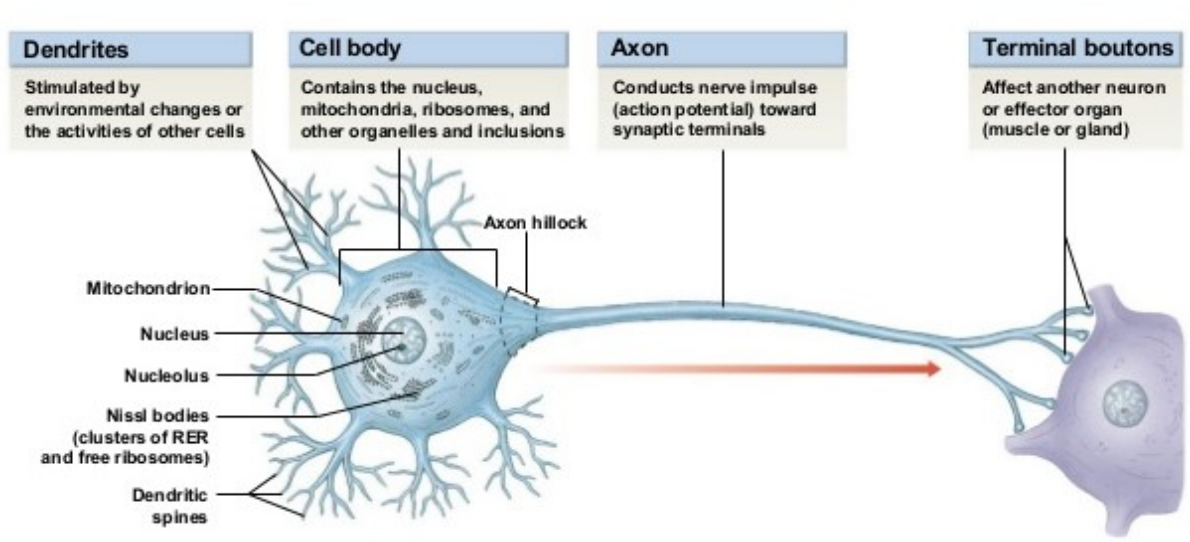

Figure 2.1: Schematic of neuron structure (Pearson Education, 2012).

When a neuron is stimulated above a certain threshold level, there is a brief reversal of polarity, known as the action potential. Action potentials propagate down the axon into the terminals. Transmission of the potential between two neurons is chemical rather than electrical; the action potential releases neurotransmitters from synaptic vesicles in the terminals, the neurotransmitters travel across the synapse to bind to receptors on the dendrites of the next neuron. When the neurotransmitters bind to the receptors they bring about a change in membrane potential which will either depolarise, to move towards the action potential, or hyperpolarise to stabilise the cell.

The other major cellular components of the nervous system are neuroglia (or glial) cells which outnumber neurons by an order of magnitude. Neuroglia perform a range of different ancillary functions essential for the functioning of neurons. The three main types of glial cells are:

- Oligodendrocytes which form the myelin sheath that surrounds many neuronal axons to increase the conduction rate of action potentials.
- Astrocytes are involved with the neuronal connection to the cerebral vasculature. Some astrocytes form 'perivascular feet' upon the walls of capillaries and mediate the transfer of chemicals between the circulatory and nervous systems.
- Microglia which have a protective role in response to nervous system damage.

The nervous system is divided into the central nervous system (CNS), comprising the brain encapsulated by the skull, and the spinal cord at the centre of the vertebral column, and the peripheral nervous system (PNS), which consists of the nerves connecting the CNS to the rest of the body. The CNS is a heterogeneous structure in terms of the distribution of nerve cell bodies and their processes. In the brain, the grey matter (GM) is enriched with neuronal cell bodies while the white matter (WM) contains mostly axons (which are myelinated, hence the term white matter) [73]. The nerve cell bodies are grouped by

their anatomical connections and functions (e.g. motor neurons connected to a group of related muscles) and hence share common pathways or tracts.

2.1.2 Anatomy of the Brain

The brain is divided into the cerebrum, brain stem and cerebellum. The cerebrum is split into two cerebral hemispheres and the diencephalon; the brain stem comprises the mid-brain, pons and the medulla (see Figure 2.2).

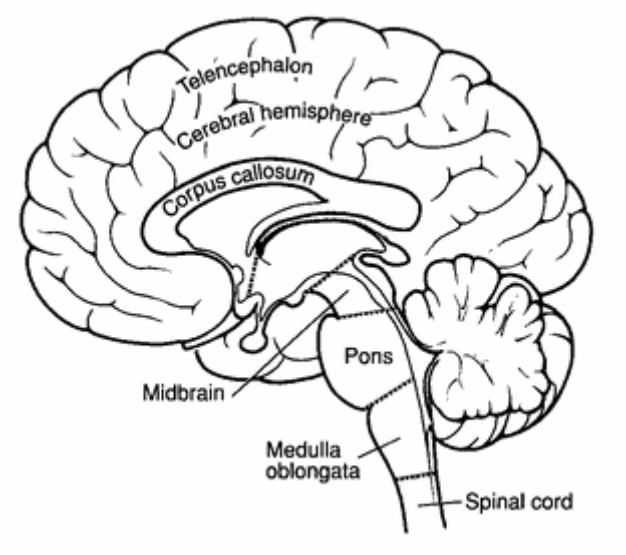

Figure 2.2: Major subdivisons of the brain viewed in sagittal section [1].

The brain stem sits on top of the spinal cord and, although it forms a small proportion of the entire brain, it is crucially important [73]. Its centres control vital functions such as respiration, the cardiovascular system and the level of consciousness.

The cerebellum is attached behind the brain stem by a large mass of fibres that connect the two parts together. It has an outer cortex of grey matter with inner white matter. The cerebellum is primarily concerned with the coordination of movement and operates at an entirely unconscious level.

The cerebrum (or forebrain) dominates the brain and is divided into two hemispheres which are, to a large extent physically separate, although cross-connections do exist. The diencephalon lies above the brain stem and comprises four parts, of which the thalumus is the largest. The thalumus plays a large part in sensory, motor and cognitive functions and is connected extensively with the cerebral cortex. Another important part of the diencephalon is the hypothalamus which is involved with the autonomic nervous system, the limbic system and the neuro-endocrine system.

The large cerebral hemispheres have an outer cortex made of grey matter with underlying regions of white matter like the cerebellum [1]. In addition to the cortex, buried in the white matter are several subcortical masses of cell bodies (i.e. grey matter) collectively referred to as the basal ganglia. The two halves of the cortex are separated by a deep midline cleft referred to as the great longitudinal fissure. The outer cortex is folded into a complex series of ridges and fissures, known as gyri and sulci respectively,

which increase the cerebral surface area. Some sulci are used as landmarks that divide each hemisphere in four lobes; the frontal lobe, the parietal lobe, the occipital lobe and the temporal lobe (see Figure 2.3). Certain areas of the cortex perform specific sensory or motor functions, for example: in the frontal lobe, the gyrus immediately in front of the central sulcus contains the primary motor cortex which controls movement at the highest level; on the other side of the central sulcus in the parietal lobe lies the primary somatosensory cortex which is the terminal site for pathways carrying modalities of touch, pain and temperature; the visual cortex is located in the occipital lobe; in the temporal lobe lies the auditory cortex; and in the prefrontal cortex (at the front of the frontal lobe) cognitive functions of a high order such as judgement and intellect are situated.

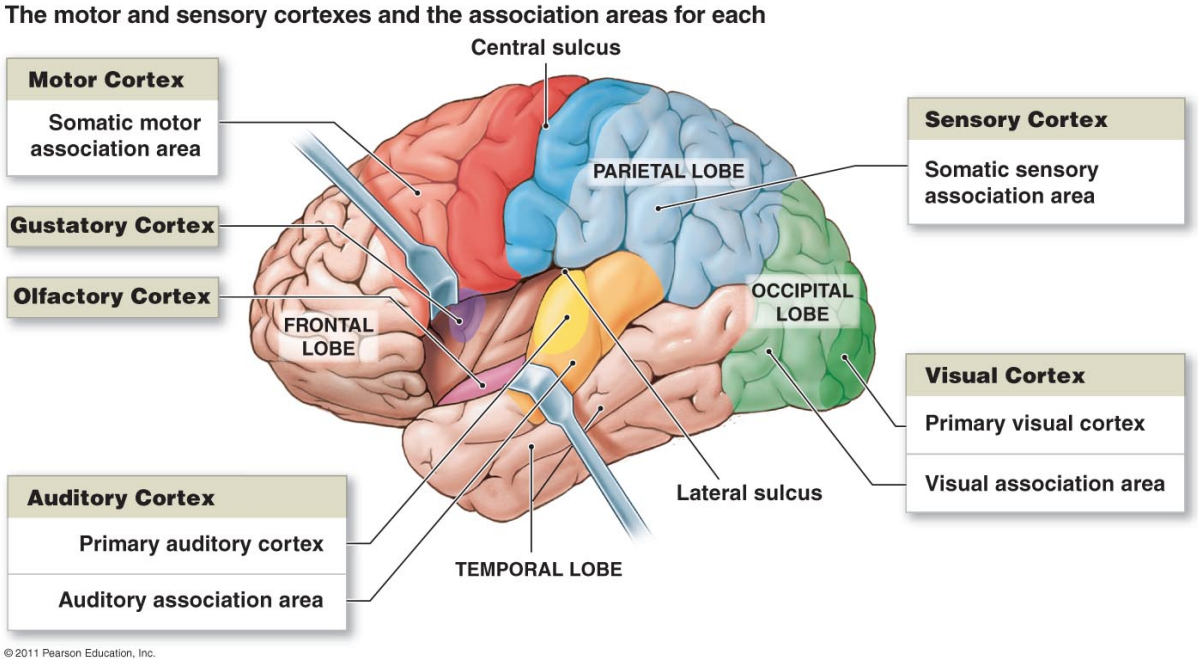

Figure 2.3: Diagram showing the functional regions of the brain (Pearson Education, 2011).

2.1.3 Extracerebral Tissue

Covering the brain are supportive and protective layers of bone and membrane. The brain lies within the cranial cavity of the skull which provides protection from physical injury. The floor of the cranial cavity consists of three fossae (holes) which accommodate particular parts of the brain and contains foramina (small holes or channels) through which cranial nerves and blood vessels enter and leave [73].

Within the skull, the brain is covered with three layers of concentric membranes, the meninges, which are (from outer to inner): dura mater, arachnoid mater and pia mater. Between the arachnoid and pia mater exists the subarachnoid space through which cerebrospinal fluid (CSF) circulates. Figure 2.4 shows an illustration of a section through the extracerebral tissue and the brain.

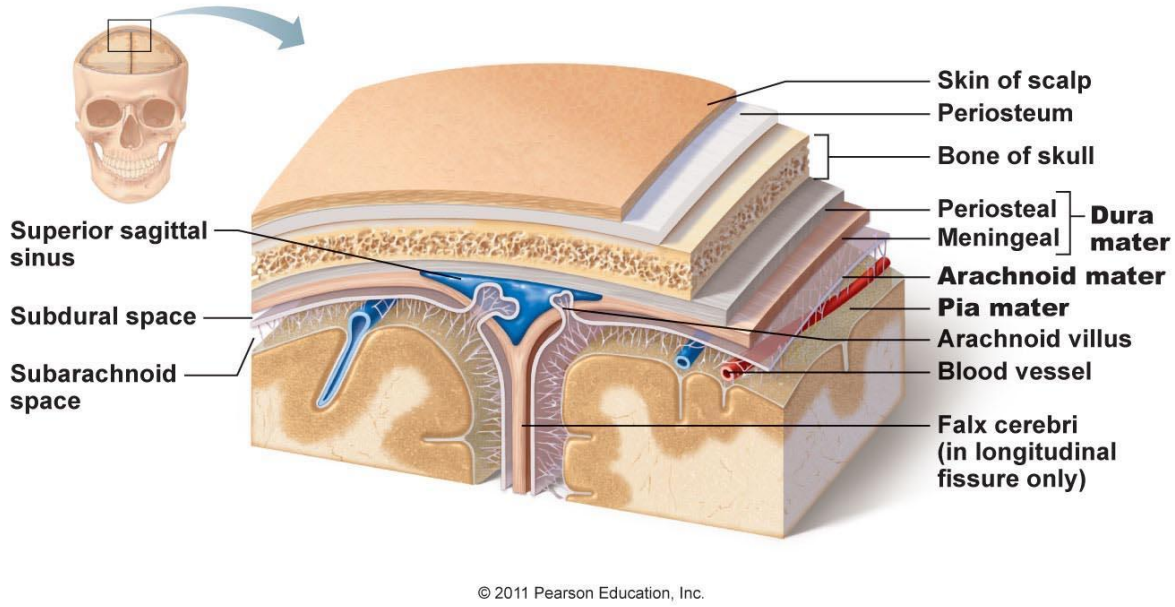

Figure 2.4: Section through the skull, meninges and brain (Pearson Education, 2011).

2.1.4 Ventricular System

The brain contains an elaborate system of ventricles through which CSF flows; the brain is submerged in this fluid [73]. It is produced in the chlorid plexus, which hangs from the roof of each ventricle, and flows through the ventricles and finally into the subarachnoid space where it is absorbed into the venous system. The CSF has a similar composition to blood plasma. It has many functions:

- The CSF allows the brain to exist in neutral buoyancy, which allows the brain to maintain a high density without being impaired by its own weight (which would cut off blood supply and kill neurons in the lower sections).
- The CSF cushions the brain and provides protection from sudden movements.
- The CSF is continually being produced and absorbed into the blood supply so it is able to carry waste products from metabolism out of the brain. Recently, it has been discovered that the CSF also penetrates along the blood vessels of the brain in order to remove the metabolic waste, this has been coined the 'glymphatic system' in reference to its similarity to the lymphatic system and the involvement of glia cells [74].

2.2 Cerebral Circulation

The brain is always active and therefore requires a large and reliable blood supply. Although accounting for only ∼2% of the body's weight, the brain receives ∼20% of arterial blood from the heart and generates ∼20% of bodily energy [1]. A constant flow of blood is needed as the brain does not store much oxygen or glucose; it derives its energy almost entirely from the aerobic metabolism of glucose delivered by the

blood.

2.2.1 Cerebral Vasculature

Arteries transport blood away from the heart, veins carry blood back to the heart and capillaries take the blood to and from the exchange sites in the tissue. Blood is supplied to the brain through the pairs of internal carotid and vertebral arteries, which are the sources for the anterior and posterior circulations respectively. The anterior and posterior cerebral circulations are interconnected via the Circle of Willis which acts as a safety valve to ensure blood supply to the entire brain if one of the arteries is occluded (see Figure 2.5). Tree-like arteries that branch off the Circle of Willis deliver blood to the surrounding tissues.

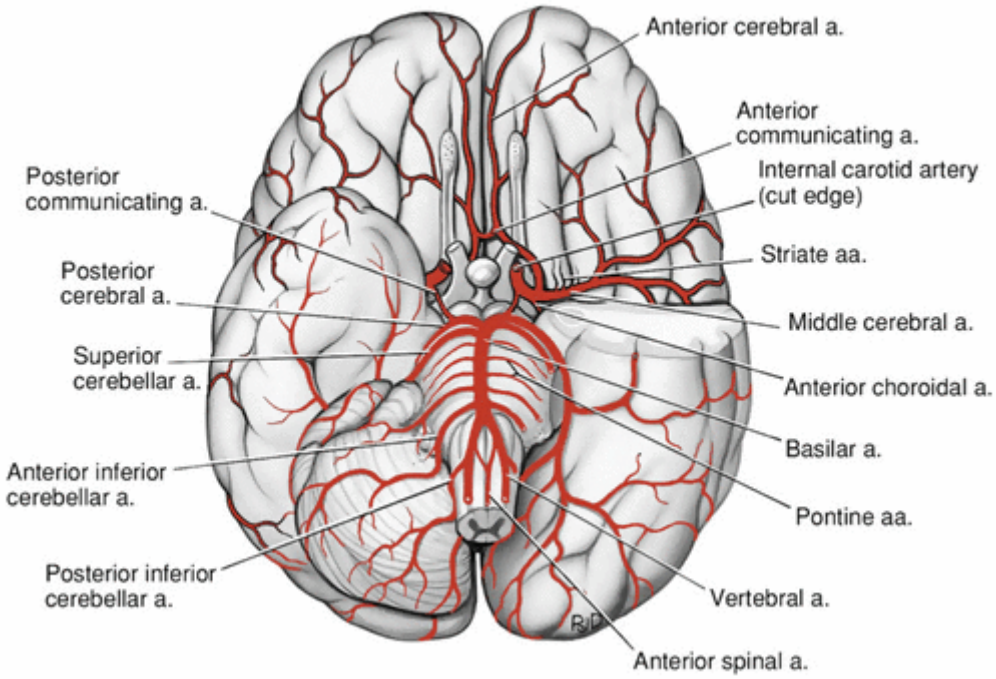

Figure 2.5: Major arterial supply to the brain viewed from below. The anterior circulation is shown in dark red and the posterior circulation in light red. The Circle of Willis comprises the anterior communicating artery (a.), the paired anterior cerebral, internal carotid, posterior communicating and posterior cerebral arteries. Taken from [1].

The venous drainage of the brain stem and cerebellum roughly follows the arterial pattern to these structures and can be separated into the superficial and deep subdivisions. The superficial system is composed of dural venous sinuses, which have walls composed of dura mater as opposed to a vein. Therefore the dural sinuses are located on the surface of the cerebrum. The deep venous drainage is primarily composed of traditional veins inside the deep structures of the brain. Most of the blood ultimately leaves the brain via the internal jugular veins at the base of the skull.

2.2.2 Blood-Brain Barrier

Neural signalling within the central nervous system (CNS) requires a highly controlled environment [75]. The blood-brain barrier (BBB) protects the brain from harmful substances in the blood via a specialised system of capillary endothelial cells. Unlike peripheral capillaries that allow relatively free exchange of substance across the cell wall, the BBB strictly limits transport into the brain. The BBB ensures that the brain is supplied with the required nutrients for proper function; glucose, essential amino acids, and some electrolytes move passively through the endothelial cell membranes. Blood-borne metabolic wastes, such as urea and creatinine, as well as proteins, certain toxins and most drugs are prevented from entering brain tissue. The barrier is ineffective against fats, fatty acids, oxygen, carbon dioxide, and other fat soluble molecules that diffuse easily through all plasma membranes; this explains why alcohol, nicotine, and anaesthetics can affect the brain. The BBB can be disrupted in cases of brain injury such as HIE, during sepsis or in prematurity [76].

2.2.3 Cerebral Autoregulation

In order to maintain a constant supply of essential nutrients to the brain at all times, autoregulation, the ability to maintain its required blood flow despite fluctuations in blood pressure, is tightly controlled in the brain. While all organs perform some degree of autoregulation, the brain is particularly sensitive to over- and under-perfusion. Cerebral autoregulation is a homoeostatic mechanism that minimises deviations in cerebral blood flow (CBF) when cerebral perfusion pressure changes [77]. Cerebral autoregulation acts through vasomotor effectors that control cerebrovascular resistance. There is controversy over the mechanisms governing cerebral autoregulation; the three main hypotheses regarding the mechanism are:

- The myogenic hypothesis suggests that the smooth muscle cells of cerebral vessels detect changes in pressure across the inside and outside of the vessel walls, and respond by contracting or dilating the vessel wall [78].
- The metabolic hypothesis is that the high neuronal activity causing variations in concentrations of oxygen, carbon dioxide and other metabolites (such as adenosine) induce an increase in CBF [79].
- The neurogenic hypothesis states that blood vessel walls are controlled by nerves connected to them [78].

Cerebral autoregulation can be assessed by comparing measurements of arterial blood pressure and CBF. This has informed research in brain injuries, including those resulting from hypoxic-ischaemia (see section 2.5), which have been shown to impair cerebral autoregulation [2, 72]. The normal autoregulatory range will vary between infants and adults, healthy and injured brains [80]; Figure 2.6 depicts the autoregulatory range in a preterm infant.

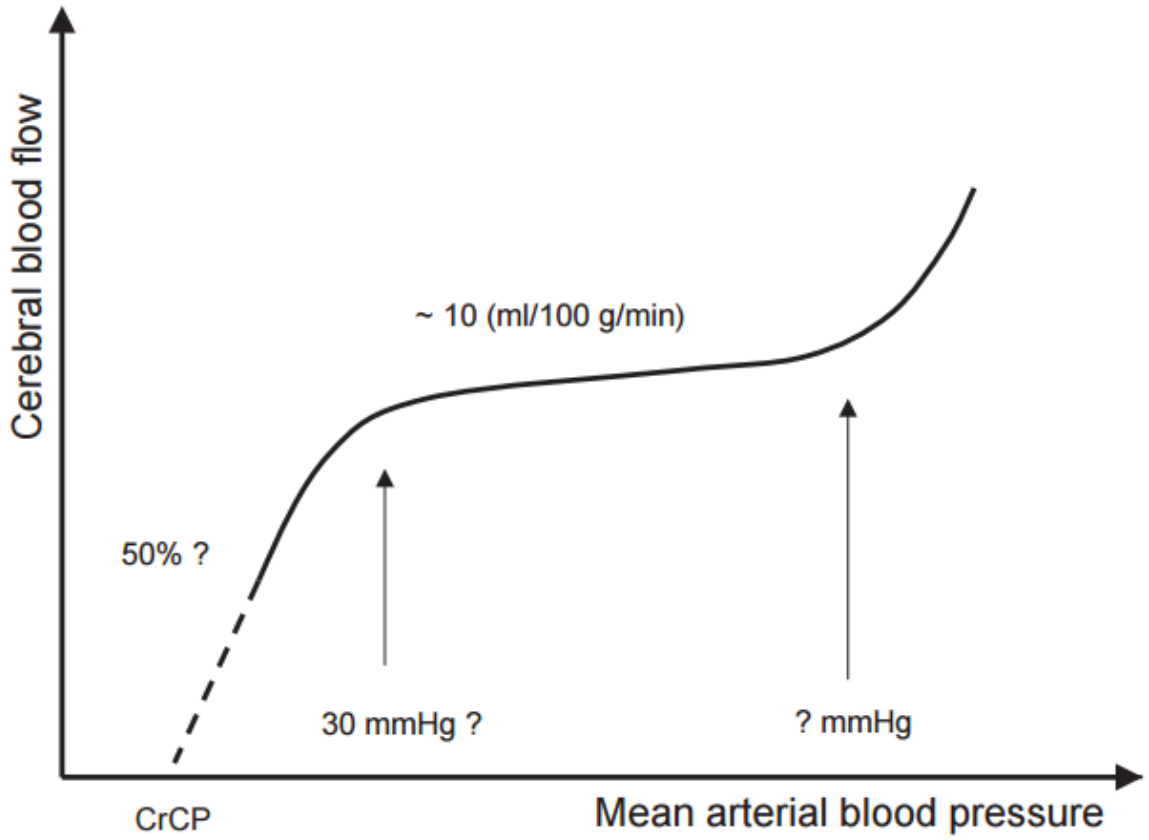

Figure 2.6: A schematic drawing of the CBF against the mean arterial blood pressure in the normal cerebral circulation in the preterm newborn baby. The flat portion represents the autoregulatory plateau where the slope is near zero. Below the lower threshold, blood flow falls more than in proportion to pressure. The critical closing pressure (CrCP) depends on the intracranial pressure and on arterial elasticity. The lower threshold is 30mmHg or less. There are no good estimates of the upper threshold. It is reasonable to assume that the ischaemic threshold is around 50% of resting blood flow. Taken from [2].

2.2.4 Blood Gases and Cerebral Blood Flow

Carbon Dioxide

Carbon dioxide (CO_2) has a profound effect on CBF; hypercapnoea causes dilation of cerebral arteries and arterioles and increases CBF, whereas hypocapnoea causes constriction and decreases CBF [81]. It has been demonstrated that in humans 5% CO_2 inhalation causes a CBF increase of 50%, and 7% CO_2 inhalation causes a 100% increase in CBF [81]. Although several mechanisms involved in hypercapnic vasodilation have been proposed, the major mechanism appears to be related to a direct effect of extracellular protons on vascular smooth muscle [82].

Oxygen

The brain has the highest metabolic demand of all the organs and so acute hypoxia is a dilator of blood vessels that produces marked increases in CBF [83]. Acute hypoxia causes an increase in CBF via direct effects on vascular cells of cerebral arteries and arterioles. Hypoxia-induced drop in adenosine triphosphate (ATP) levels causes hyperpolarisation and vasodilation [84]. In addition, hypoxia rapidly increases nitric oxide and adenosine production locally, also promoting vasodilation [85].

2.3 Cell Metabolism

Cells produce and consume ATP for energy in the mitochondria which is the cell's energy 'powerhouse'. Respiration is the production of ATP from glucose and oxygen, with carbon dioxide and water as by-products. The cell produces energy when ATP is converted to adenosine diphosphate (ADP), releasing energy. The entire process of respiration is carried out in three major states: glycolysis, the tricarboxylic acid cycle (TCA, also known as the Kreb's cycle or citric acid cycle) and oxidative phosphorylation (of which the electron transport chain (ETC) is a part). The entire process is illustrated in Figure 2.7.

A mitochondrion is a double-membraned organelle that exists within most cells to produce ATP. The organelle is composed of compartments that carry out specialised functions. These compartments include the outer membrane, the intermembrane space, the inner membrane, the cristae and the matrix (see Figure 2.7 for an illustration). The number of mitochondria within a cell varies between species and cell type, for example red blood cells have no mitochondria whereas a neuron has a high density of mitochondria as it requires a lot more energy.

2.3.1 Glycolysis

Glycolysis literally means the breaking down of glucose. Over a series of several steps, glycolysis breaks down one molecule of glucose into two molecules of pyruvate. These reactions occur in the cytosol within the cell cytoplasm.

$$glucose + 2Pi + 2ADP + 2NAD^{+} \rightarrow 2pyruvate + 2ATP + 2NADH \tag{2.1}$$

where Pi is inorganic phosphate, and NAD^{+} and NADH are the oxidised and reduced forms of nicotinamide adenine dinucleotide, respectively. During the sequence of reactions, some of the free energy released is conserved in the form of ATP and NADH which is used in the subsequent processess.

2.3.2 Tricarboxylic Acid Cycle

There is a short step in between glycolysis and the TCA cycle: pyruvate is transformed into acetyl CoA:

$$pyruvate + NAD^{+} \rightarrow acetylCoA + CO_2 + NADH. \tag{2.2}$$

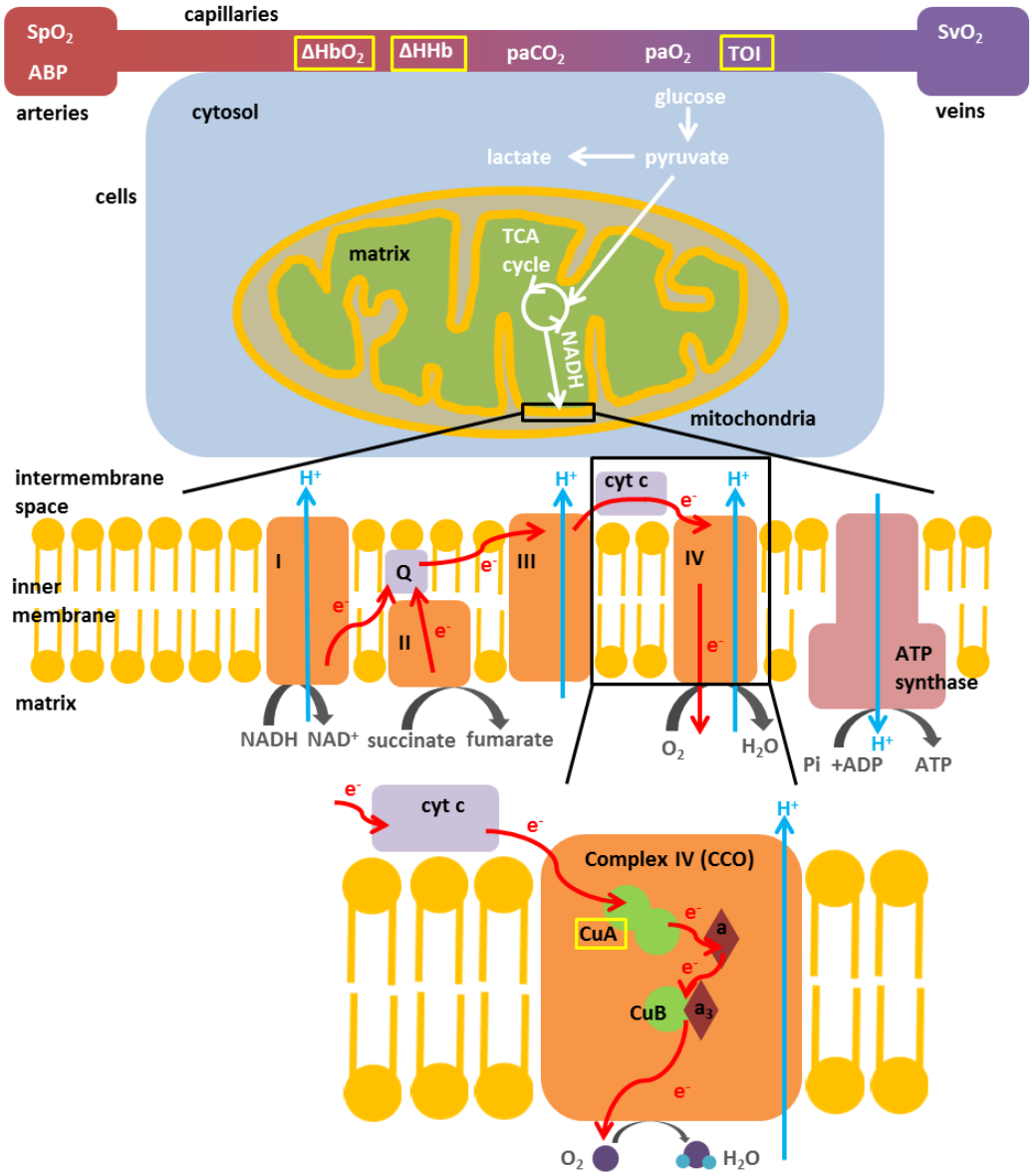

Figure 2.7: Schematic of cellular metabolism with the electron transport chain and CCO expanded. CCO is represented as complex IV. This diagram is limited to the carbohydrate metabolism (from glucose); fat metabolism, also aerobic, is ignored. Chromophores that are measured by NIRS are highlighted in yellow boxes.

The purpose of the TCA cycle is to release the energy shuttle molecules, NADH and $FADH_2$ (the hydroquinone form of flavin adenine dinucleotide (FAD)), from the free energy of pyruvate. The energy shuttles can transport high energy electrons to the electron transport chain. To start the cycle, acetyl CoA fuses with oxaloacetate to form citric acid. There is a series of further reactions, catalysed by enzymes, that rearrange the carbon atoms in citric acid until oxaloacetate is formed again (hence *cycle*). During these reactions energy is released to produce the electron shuttles, NADH and $FADH_2$.

The overall reaction that occurs during the TCA cycle is:

$$pyruvate + 4NAD^{+} + FAD + GDP + Pi \rightarrow 3CO_2 + 4NADH + FADH_2 + GTP \tag{2.3}$$

where GTP is guanosine triphosphate and GDP is guanosine diphosphate.

2.3.3 Oxidative Phosphorylation

Oxidative phosphorylation is the process where energy is harnessed through a series of protein complexes (known as complexes I - V) embedded in the inner-membrane of mitochondria to create ATP. Figure 2.7 shows the position of these complexes within the inner-membrane. Oxidative phosphorylation can be broken down into two parts: oxidation of NADH and $FADH_2$ via complexes I - IV, known as the electron transport chain (ETC), and phosphorylation, the production of ATP, at complex V.

Oxidative phosphorylation begins with the arrival of free electron carriers, NAD and $FADH_2$, from the TCA cycle which transfer electrons to Complex I and II. These electrons are passed to another membrane-bound electron carrier called ubiquinol (Q) producing ubiquinone (QH_2). QH_2 is oxidised by complex III and then to another electron carrier, cytochrome c (not to be confused with cytochrome-c-oxidase which is also known as complex IV), which takes electrons to complex IV. Complex IV interacts with oxygen, the final electron acceptor, and water is formed as oxygen receives the electrons. In other words, cytochrome-c-oxidase is the enzyme that oxidises the substrate, cytochrome c, to complete the electron transport chain:

$$4cyt\ c(Fe^{2+}) + 4H^{+} + O_2 \rightarrow 4cyt\ c(Fe^{3+}) + 2H_2O. \tag{2.4}$$

The process of oxidation at each of the complexes I, III and IV results in the pumping of protons across the membrane from the matrix to the inner-membrane space. This creates a high concentration of protons outside of the matrix and therefore an electrochemical gradient across the membrane. When the concentration of protons is high then the protons are pushed through complex V, also called ATP synthase, which causes ATP synthase to bind ADP to Pi, producing ATP.

2.3.4 Anaerobic Respiration

The processes described above depend on oxygen being present to oxidise pyruvate and receive electrons from complex IV. If oxygen is not present then fermentation occurs. Fermentation starts after glycolysis, replacing the TCA cycle and oxidative phosphorylation. The pyruvate is converted to lactate which forms lactic acid. This is less efficient than aerobic respiration, in which 32 molecules of ATP are produced from a single glucose molecule, as only 2 molecules of ATP are formed during glycolysis and before fermentation. Further, the lactic acid needs to be removed from the cells and broken down which is inefficient.

2.3.5 Cerebral Metabolic Rate of Oxygen

The rate of cerebral oxygen metabolism ($CMRO_2$) can be quantified by the difference between the rate of flow of oxygen into the brain and out of the brain. This give a relationship with CBF which is derived from Fick's law:

$$CMRO_2 = CBF([O_2]_a - [O_2]_v) \tag{2.5}$$

where $[O_2]_a$ and $[O_2]_v$ are the oxygen concentrations within the arteries and veins entering and leaving the brain, respectively [86].

2.4 Brain Development

In order to understand injury in the neonatal brain, one must first understand the state of the brain at birth. Brain maturation involves a complex sequence of functional, morphological and organisational changes. In the period between 24 weeks gestation and full-term (between 37 and 42 weeks gestational age(GA)) there are dramatic changes in the structure and physiology in the brain [3]. Therefore a baby born preterm, or prematurely, between 24 to 37 weeks GA, will be at a very different state of neurodevelopment to a term baby, and this will affect how the brain responds to both injury and treatment.

The largest and most obvious change in the brain between 24 and 37 weeks is the overall increase in size [3]. The cortical layers form from the inside of brain moving outwards. The layers are formed by neuronal migration along radial glial cells; this process is typically completed by 24 weeks GA. Between 29 weeks GA and term, the grey matter volume increases from approximately 60ml to 160ml [87]. As well as the increase in size, there is also an increase in the number of cortical folds which eventually make up the gyri and sulci (as can be seen in Figure 2.8); initially the brain is smooth in appearance but as growth proceeds the folding pattern of the cortex develops allowing a considerable increase in the surface area of the brain [3]. At 24 and 25 weeks GA white matter can be found; the origins of myelination of the white matter cannot be observed until 35 weeks GA.

The cerebral circulation develops alongside these structural changes. The blood vessel density increases with GA from 16 to 40 weeks with the most rapid increase between 28 to 36 weeks [88]. At 36-40 weeks GA, the grey matter has a similar vessel density to that of an adult brain which suggests that cerebral vasculature in term infants is approaching maturity. Low vascularity in the preterm infant may increase the propensity for brain injury.

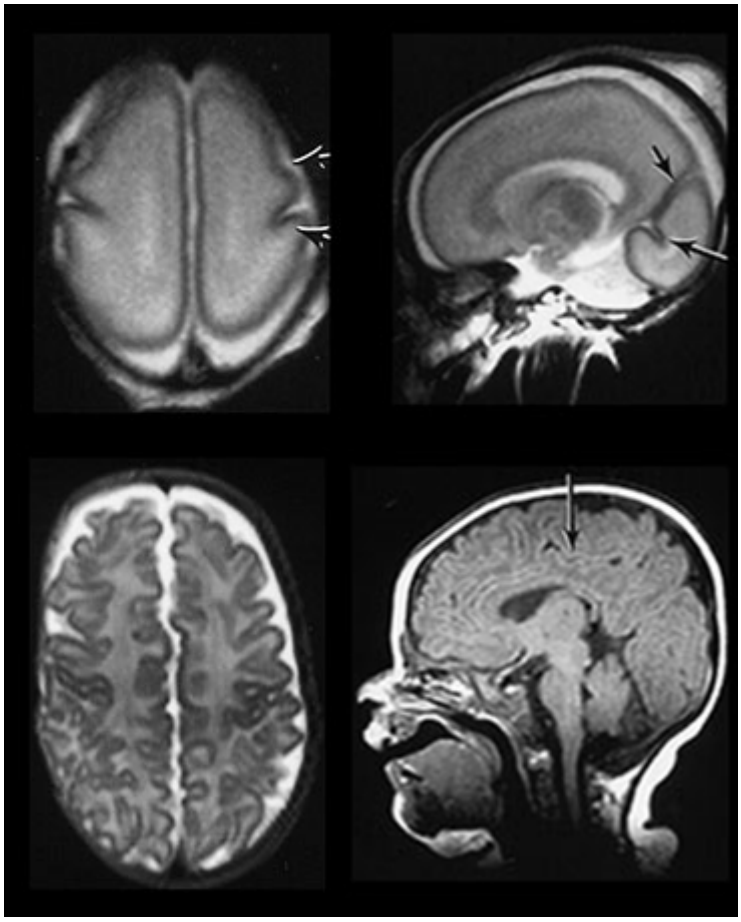

Figure 2.8: Magnetic resonance imaging (MRI) picture of cortical folding at 26 weeks GA (above) and term (below) in the transverse (left) and sagittal (right) planes. Taken from [3].

2.5 Neonatal Brain Injury: Hypoxic-Ischaemic Encephalopathy

Neurological injury can be caused by many different disorders, including extrinsic disorders caused by pressure on a part of the nervous system, intrinsic disorders which are primarily disorders of the nervous system, systemic disorders that originate at another organ, and vascular disorders resulting from damage to brain circulation. The damage from vascular disorders is usually caused by infarction (death of tissue) due to a restriction in the blood supply, or haemorrhage (bleeding into nervous tissue). This section discusses a form of acute neonatal brain injury that is the clinical focus of this thesis: hypoxic-ischaemic encephalopathy (HIE).

2.5.1 Definition and Incidence

Neonatal brain injury caused by a HI event (perinatal asphyxia) is known as HIE. It is the result of events during or before birth causing a reduction of oxygenation (hypoxia) and/or perfusion (ischaemia) in the brain.

It is difficult to establish the incidence of HIE as different definitions are used in the literature. In developed countries the incidence of HIE has been estimated to be 1.5 per 1000 live births [89]. A single

centre study in UK revealed a fall in the incidence of HIE in term infants (1.9 vs. 4.6 per 1000 total live births) over a 21 year study period alongside the fall in neonatal mortality rate (NMR) [90]. The incidence in preterm infants is much higher [91] as is the incidence in developing countries [92].

HIE can lead to severe neurodevelopmental problems or to death. It accounts for 15-28% of cases of cerebral palsy [93] and is responsible for a quarter of global infant mortality [92].

2.5.2 Aetiology

A baby in-utero has oxygen, necessary nutrition and life support from the mother delivered from the placenta via the blood vessels in the umbilical cord. Waste products and CO_2 from the foetus are sent back through the umbilical cord to the mother's circulation to be disposed of. The foetal circulation is different to that of a newborn; blood does not need to flow through the liver or lungs for oxygenation and metabolism as the mother provides these functions. The foetal heart acts as a one-way pump with shunts called the foramen ovale and ductus arteriosus that bypass the lungs, and another shunt called the ductus venosus to bypass the liver (see Figure 2.9). After birth, the neonate no longer receives oxygen or nutrients from the umbilical cord. As the baby takes its first breaths, the lungs begin to expand and clear of fluid. This creates changes in blood pressure that close the shunts which are no longer needed and the heart becomes a two-way pump.

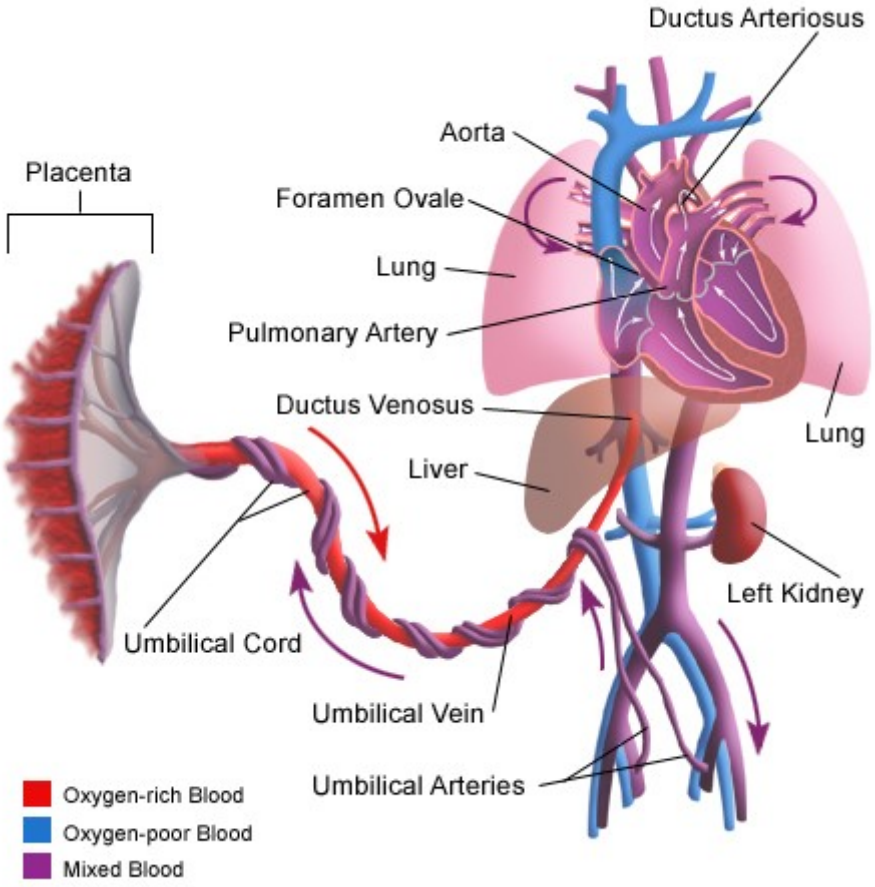

Figure 2.9: Schematic of foetal circulation. Taken from [1].

During labour and the huge subsequent physiological changes, problems can occur that lead to asphyxia. During normal labour, uterine contractions will apply some degree of pressure to the umbilical cord resulting in reduced blood flow to the foetus. Other factors during childbirth such as maternal hyper- or hypoventilation, dehydration and a higher oxygen consumption from both mother and baby can lead to a reduced oxygen delivery to the brain. If the mother has a pre-existing condition, such as pre-eclampsia, or there is a complication during the birth, a cord accident for example, then dangerous levels of asphyxia can be reached [94].

Ninety percent of asphyxia insults occur just before or during birth due to placental insufficiency; the remainder happen postpartum, usually secondary to pulmonary, cardiovascular or neurological insufficiency. Intrauterine growth restriction and breech presentation are both associated with increased incidence of asphyxia [94]. In the term infant, the most common mechanism of hypoxic injury is intrauterine asphyxia brought on by circulatory problems, such as clotting of placental arteries or placental abruption, or inflammatory processes. These result in perinatal depression leading to diminished exchange of O_2 and CO_2, and severe lactic acidosis [91].

During a hypoxic-ischaemic insult the brain is more easily damaged than other organs; neurons are so specialised that most are incapable of reproducing themselves and they lose viability if in a hypoxic environment for more than a few minutes [1]. Neurons do not build an oxygen debt like other cells so cannot survive anaerobically. The brain will lose functionality if the oxygen supply is cut off for more than a few minutes. The most susceptible sites for injury are: basal ganglia, thalamus, cortex, subcortical white matter and the brain stem. These areas have increased metabolic rates, increased glutamate receptors and are actively myelinating which increases their propensity to damage [3]. The effects of hypoxia and ischaemia are not identical but they are difficult to separate clinically [95].

2.5.3 Clinical Presentation

All of the following must be present for the designation of perinatal asphyxia severe enough to result in acute neurological injury (guidelines from the American Academy of Paediatrics and American College of Obstetrics and Gynaecology, 1996):

- Profound metabolic or mixed acidemia (pH<7) in an umbilical artery blood sample.
- Persistence of an Apgar score (a scale determined by evaluating the newborn baby on five simple criteria on a scale from zero to two, then summing up the five values) of 0-3 for longer than 5 minutes.
- Neonatal neurological sequelae (e.g. seizures, coma, hypotonia).
- Multiple organ involvement (e.g. kidney, lungs, liver, heart, intestines).

HIE can be categorised into three severities of injury, these are outlined in Table 2.1.

HIE is commonly presented with multi-organ dysfunction including heart, lungs, renal, liver and haematologic.

Mild HIE	**Moderate HIE**	**Severe HIE**
Muscle tone may be slightly increased and deep tendon reflexes may be brisk during the first few days.	The infant is lethargic, with significant hypotonia and diminished deep tendon reflexes.	Stupor or coma is typical. The infant may not respond to any physical stimulus.
Transient behavioural abnormalities, such as poor feeding, irritability, or excessive crying or sleepiness may be observed.	The grasping, Moro (response to a sudden loss of support), and sucking reflexes may be sluggish or absent.	Breathing may be irregular, and the infant often requires ventilatory support.
Typically resolves in less than 24 hours.	The infant may experience occasional periods of apnoea.	Generalised hypotonia and depressed deep tendon reflexes are common.
	Seizures typically occur early within the first 24 hours after birth.	Neonatal reflexes (eg, sucking, swallowing, grasping, Moro) are absent.
	An initial period of well-being or mild HIE may be followed by sudden deterioration, suggesting ongoing brain cell dysfunction, injury, and death during this period, seizure intensity might increase.	Disturbances of ocular motion may be revealed by cranial nerve examination.
		Pupils may be dilated, fixed, or poorly reactive to light.
		Seizures are delayed, can be severe and may be initially resistant to conventional treatments. The seizures are usually generalised, and their frequency may increase during the 24-48 hours after onset, correlating with the phase of reperfusion injury. As the injury progresses, seizures subside and the EEG becomes isoelectric (flat) or shows a burst suppression pattern. At that time, wakefulness may deteriorate further, and the fontanelle may bulge, suggesting increasing cerebral edema.
		Irregularities of heart rate and blood pressure are common during the period of reperfusion injury, as is death from cardiorespiratory failure.

Table 2.1: The clinical presentation of HIE split into three injury severities. The definitions of HIE injury severity are taken from [67].

2.5.4 Progression

HIE is not a single event; it is an evolving process. There is an evolution of a delayed cascade of molecular events triggered by the initial insult which is reflected in the clinical signs. Magnetic resonance imaging (MRI) studies have shown progression of lesion size over the first few days after injury [91]; typically starting as small lesions, and usually progressing over the days to involve larger portions of the brain. Magnetic resonance spectroscopy (MRS) shows a similar pattern of progression, with an increase in lactic acid (Lac), produced in anerobic metabolism, and a reduction of N-acetyl-aspartate (NAA), suggesting neuronal loss, over the first few days after initial insult.

Research suggests the concept of a brief 'therapeutic window' between the time of insult and the occurrence of cell death due to a cascade of molecular events [94]. (However, it is difficult to recognise the onset of cerebral insult, and the diagnosis of asphyxia can be delayed; these problems restrict this window of time.) HIE presents a biphasic pattern of cerebral energy failure; the first phase occurs during the insult, primary energy failure, which is followed by re-perfusion and a period of cerebral recovery. After a latent period of up to 24 hours, a secondary energy failure may occur which can cause severe cell death and injury. Figure 2.10 shows a schematic of this process. During this latent phase there is the potential for clinical intervention, however it is difficult to assess the severity of the initial injury.

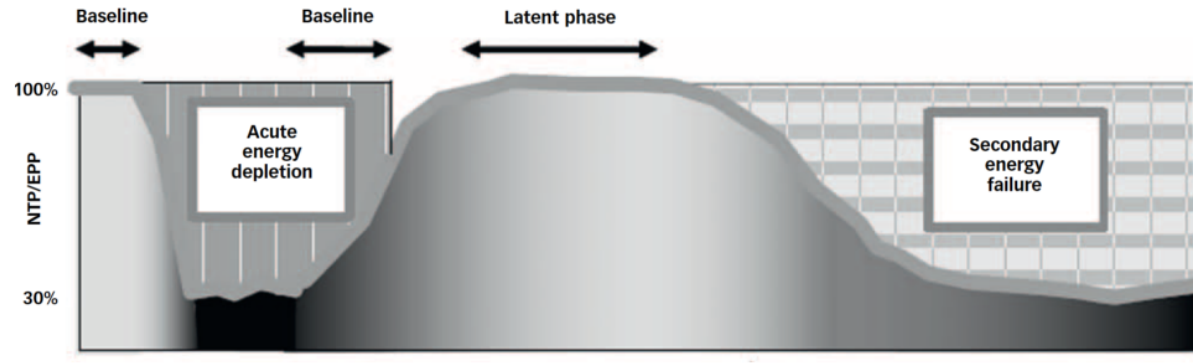

Figure 2.10: Schematic of theorised changes in cerebral energy metabolism during HIE. Taken from [4].

The cascade of metabolic events during the initial phase of HI begins with a rapid depletion of ATP leading to the failure of the cell ion pump and depolarisation of the cell. This causes severe cell swelling and cytoplasmic calcium ion accumulation, leading to necrosis and activation of multiple cascades that eventually lead to more cell death. In general, the form of cell death depends on the severity of ischaemic injury. Necrosis predominates in more severe cases, whereas apoptosis occurs in areas with milder ischaemic injury, often days after the initial insult [91].

Injury from HI is usually localised to particular regions or groups of structures within the brain as opposed to manifesting as a global injury to cerebral tissue [96]. Predominant neural patterns of injury have been discovered through analysis from primate studies and post-mortem neonatal studies. These include: basal ganglia and thalamic injury, with possible hippocampal and brain stem involvement; watershed predominant pattern of injury, affecting cortical regions related to anteriormiddle cerebral artery and posteriormiddle cerebral artery (the vascular watershed zones); and less commonly, injury to

the subcortical white matter and cortex [97]. There are several other patterns each relating to the original localisation of brain injury. It is more likely that the pattern of regional cerebral injury is governed by intrinsic properties of vulnerable neurones due to their positioning within the maturing excitatory neural circuitry, rather than the pattern of vascular supply in the brain or cerebral blood flow [98].

2.5.5 Management

After identification of HIE from the presentation, the severity of the injury will be graded as mild, moderate or severe with the Sarnat score (a staging system used to classify severity of HIE) which combines clinical and EEG findings (although not necessarily EEG). There is an urgent need for a clinical biomarker of brain injury to identify not only infants at risk, but also infants with an injury that might evolve and thus might benefit from additional treatment [99].

A newborn presenting with HIE will be cared for in a Neonatal Intensive Care Unit (NICU). The management of HIE focuses on maintaining homoeostasis with respect to temperature, perfusion, ventilation, glucose levels, fluids, etc. in order to maintain a normal metabolic state, brain pH and cerebral blood flow [95]. Oxygen levels should be kept within a normal range by monitoring arterial partial pressure of oxygen (PaO_2) or oxygen saturation (SpO_2) by pulse oximetry and treating hypoxia with oxygen or ventilation. Likewise, CO_2 should be kept to normal levels by continuous monitoring to prevent vasodilation or vasoconstriction from hypercapnoea or hypocapneoa respectively. In order to maintain a constant cerebral perfusion pressure (CPP), the arterial blood pressure (BP) needs to be tightly controlled, this is usually measured with an arterial line. In HIE infants it is likely that the cerebral autoregulatory mechanisms have been impaired so CPP will entirely reflect arterial BP. A CPP that is too high can cause haemorrhage in areas of damaged blood vessels and a low CPP can lead to ischaemic injury. Blood glucose levels should be controlled to provide adequate substrate for brain metabolism. High levels may lead to elevation of brain lactate and hypoglycemia can lead to seizures.

If the baby is experiencing seizures, anticonvulsants (such as phenobarbitone) must be given as seizures may cause further damage so need to be controlled effectively [95]. Seizures may be associated with increased cerebral metabolic rate. A rise in BP during seizures may contribute towards cerebral haemorrhage. Continuous EEG is used to monitor electrical activity.

Clinical trials are under way to test new treatments, such as inhaled xenon gas, and preclinical studies are under-way looking at future neuroprotective agents. Currently the only treatment that has been proved to be successful is therapeutic hypothermia (TH) which involves cooling the infant to 33.5°C for the first 72 hours after birth. This has been shown to reduce adverse outcome so is now standard practice in the UK [100]. TH must be administered within 6 hours of birth to be effective; clinical trails have shown that the earlier the cooling is commenced, the better the outcome. TH reduces cerebral metabolism and protects mitochondrial function [101].

Premature infants have different neuroanatomy and neurophysiology which will affect how the infant responds to injury and treatment. Most brain injury in the preterm infant occurs in the postnatal period which can make detection of the insult difficult [94]. Logitharajah et al. [102] found that the outcome for preterm infants with HIE is poorer than that expected for term HIE with only one-third of seventy

infants studied having normal outcomes at two years of age. Therapies used in the term population need to be evaluated thoroughly before being suggested for preterm HIE. TH is not currently used to treat preterm infants with HIE.

2.5.6 Monitors

The techniques currently used to monitor the injured neonatal brain during the first days of life in the NICU include EEG, cranial ultrasound and MRS. Here the benefits and limitations of these technologies are discussed.

Magnetic Resonance Scanning

MR monitoring has become the gold standard for the study of neonates with encephalopathy or suspected brain injury. The development of MR-compatible monitoring tools and incubators allow hospitals with MR scanners to study sick infants that need continuous intensive care. Additionally, dedicated neonatal coils have increased signal-to-noise ratio in these patients, producing high quality images and spectroscopic traces [103]. There are many different scan sequences and methods to study the newborn brain; those which are relevant to neonatal encephalopathy are discussed here. Movement artefacts are the biggest problem with this imaging modality and can render data uninterpretable [3].

In most clinical environments the MR scan will take place after the therapeutic hypothermia has been completed (from day 4 of life onwards) and before the second week of life. This is the major drawback of the technology as it only gives a snapshot of the injury at one time and it is not possible to monitor the brain in the crucial early days post-partum. Furthermore, the MR equipment is expensive both to purchase and operate.

Magnetic Resonance Imaging

Conventional anatomical T1 and T2 (so called due to the different relaxation times of protons) weighted MRI sequences performed between 5 and 8 days after birth can help identify the pattern of the injury which can predict outcome [3]. These sequences can show some of the causes of encephalopathy such as haemorrhage, infarction, or congenital malformations. HI injury to grey and white matter can be detected through T1 and T2 imaging depending on the time of imaging, the location of the injury, and the underlying cause of the injury.

From 24 hours onwards diffusion tensor imaging is the most sensitive sequence to detect early ischaemic lesions [3]. Diffusion tensor imaging exploits the random motion of water in the tissue; the diffusivity of the tissue is reduced in acute infarction. The localisation of the injury is best diagnosed using diffusion weighted MRI [97].

Magnetic Resonance Spectroscopy

Proton MRS (^{1}H MRS) is the most sensitive technique to identify brain injury in the first 24 hours of life [103]. In an injured brain, Lac levels will be elevated and NAA levels may be reduced (see Figure 2.11); a high Lac/NAA ratio indicates predicted poor outcome at 18 months (i.e. death or severe neurodevelopmental problems). The ^{1}H MRS Lac/NAA is currently the gold standard for predicting outcome as shown by the meta-analysis from Thayyil et al. [104]. The biggest drawback of MRS is that it is limited to a single voxel in the brain and so the spectroscopy result may not reflect the location of the greatest damage. MRS requires a dedicated team of physicists to collect and interpret the data, and as such, many NICUs do not have access to MRS gold standard measurements.

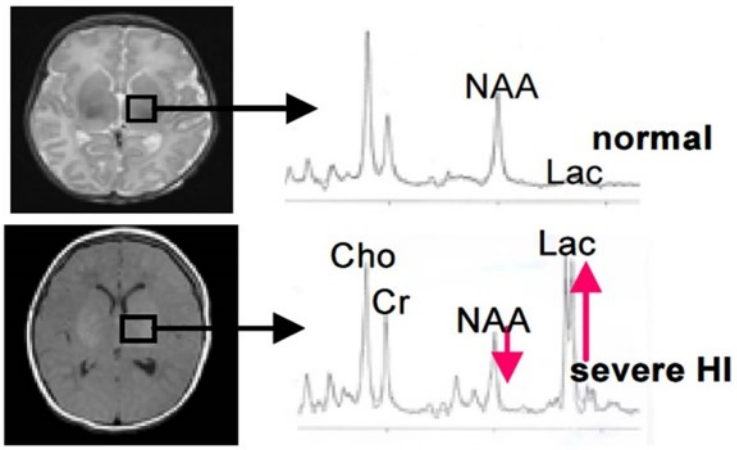

Figure 2.11: MRS Lac/NAA is the gold standard for identifying poor outcome after HIE.

Other MR Techniques

Recent advances in scan sequences have resulted in a technique called arterial spin labelling (ASL) which is able to measure CBF. ASL applies a magnetic label to the water molecules in flowing blood, as the magnetic label enters the imaging slice it exchanges with tissue water and slightly alters the image contrast. This gives a picture of the cerebral perfusion [105]. The Baby Brain Study is currently investigating the ASL technique to assess if CBF is related to brain injury severity.

Electroencephalography

EEG is used clinically to grade the severity of injury. EEG monitoring is performed from the first day of life after suspected brain injury. EEG uses multiple electrodes to record the brain's spontaneous electrical activity from the scalp. Serial EEG is a good indicator of outcome in the first 24 hours of life. A very inactive or depressed EEG beyond 8-12 hours indicates poor outcome. An active EEG, or an inactive EEG that recovers within the first 8 hours, are associated with good outcome [106] (see Figure 2.12).

Amplitude-integrated EEG (aEEG) is a valuable EEG technique for predicting long-term neurodevelopmental outcome [107]. It gives a quick assessment of the brain's function by displaying the cerebral

function monitor (CFM) trace. The CFM is created by filtering and compressing EEG to reflect the maximum and minimum EEG variations which shows long-term changes and trends in electrocortical background activity. aEEG is used clinically to predict outcome as it is available in most hospitals. It is more widely used than serial EEG as it is easier to apply (only 4 electrodes are required) and easier to interpret the data.

Figure 2.12: Example of EEG in an infant with mild HIE. Taken from [5]. A: Recording at 6 hours from birth with markedly suppressed amplitude and continuous discontinuity. B: Recording at 24 hours when EEG findings have recovered, discontinuity seen only during quiet sleep.

Cranial Ultrasound

Cranial ultrasound is a readily available bedside tool for the assessment of cerebral structures and can be repeated regularly as the HI injury evolves with time. It is a useful tool to exclude congenital anomalies and other causes of encephalopathy, and to determine the timing of insult. The different patterns of injury, whether the injury is specific to GM or WM, can also be identified using ultrasound and can contribute to outcome prediction [108]. The initial scan following HI can be normal but the cortical appearance can change as injury develops. It is relatively inexpensive, non-invasive, easy to operate and can be used repeatedly at the cotside, however it cannot assess cerebral oxygenation, metabolism or energetic state.

Doppler ultrasound measurements of resistive index (RI) of the middle cerebral arteries can add more information regarding the severity of HIE; severe HIE results in the loss of autoregulation resulting in haemodynamic disturbance, which can be monitored with RI [109].

Near-Infrared Spectroscopy

NIRS has the potential to monitor cerebral changes in haemodynamics and metabolism at the cotside, with an application process that is similar to EEG. This technique is non-ionising, easy to use, relatively inexpensive and does not require dedicated physicists for operation or interpretation of results. A full description of NIRS is covered in Chapter (3), including a literature review of the use of NIRS in HIE.

2.6 Summary

The brain is a very complex organ with high energy demand that needs to be constantly maintained; disturbance to the energy supply can cause irreversible injury. Energy is produced through metabolism which predominantly depends on a supply of glucose and oxygen which are delivered by the extensive vascular network. Perinatal HI injury can lead to HIE which is a relatively common and severe injury that can lead to death or life-long neurodevelopmental impairment, such as cerebral palsy. The injury develops over the first days of life. There is a clinical need for a viable monitor of cerebral metabolism and oxygenation during these crucial days to inform diagnosis and treatment.

Chapter 3

Broadband Near-Infrared Spectroscopy

NIRS was first demonstrated on human tissue by Jobsis almost 40 years ago [110] when he discovered the NIR translucency of tissue. It is a non-invasive, non-ionizing, portable medical technique that exploits the high penetration of NIR light through biological tissue to interrogate its components. The technique uses changes in the intensity of diffusely scattered NIR light through tissue to estimate the changes in its optical properties. A change of the concentration of optical absorbers, or chromophores, within the tissue results in a change of the optical properties of tissue. Thus it is possible to monitor changes in the concentrations of such compounds in the NIR spectrum; the most physiologically interesting are oxygenated- and deoxygenated-haemoglobin (HbO_2 and HHb) and cytochrome-c-oxidase (CCO). The fundamentals of the technique and its use in neonatal monitoring, in particular on infants with HIE, are discussed in this chapter.

3.1 Fundamentals of NIRS

3.1.1 Light Transport in Tissue

When light travels through tissue it is attenuated due to a combination of scattering and absorption. These effects depend upon the wavelength of light used, the absorbing compounds, or chromophores, present in the tissue, and scattering due to the tissue structure and particle size. To characterise attenuation one must understand all of these effects individually before combining their effects.

Absorption

Absorption, in the simplest case of light travelling a short distance through an absorbing medium, was characterised by Pierre Bouger in 1729. An absorbing medium has an absorption coefficient μ_a which is defined as the probability over an infinitesimal path that a photon will be absorbed and is typically expressed in cm^{-1}. Bouguer observed that the proportion of light absorbed by the medium was always

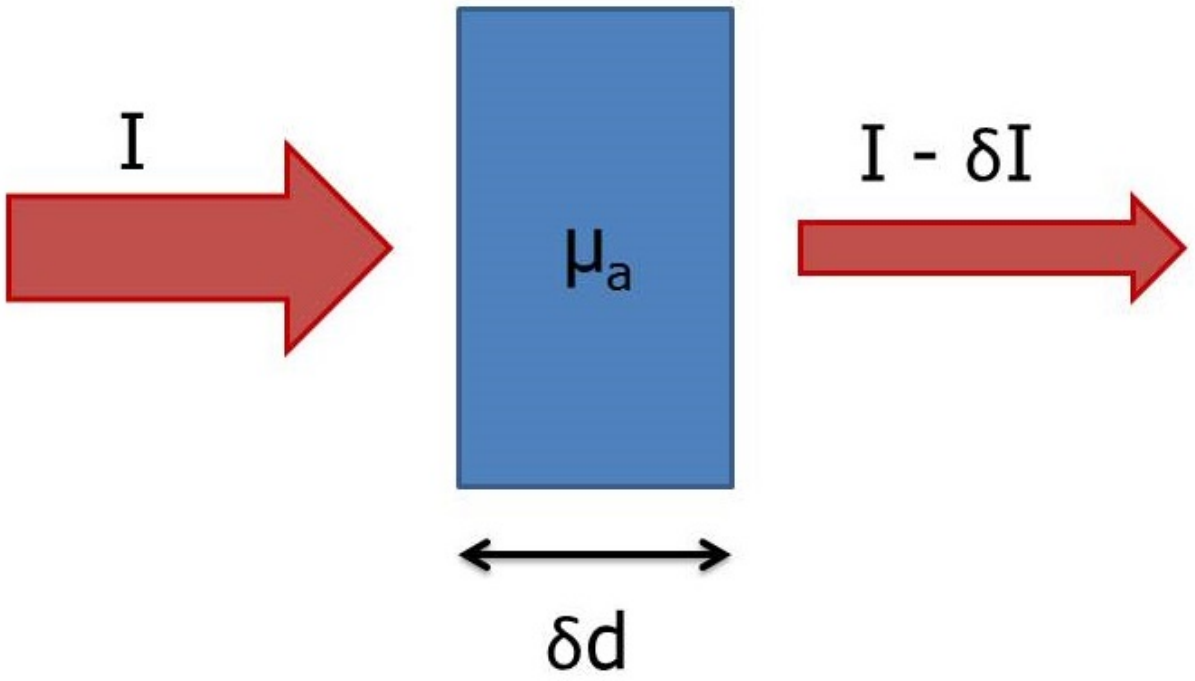

Figure 3.1: Attenuation of light through an absorbing medium.

the same, and in 1760 Johann Heinrich Lambert expressed it mathematically; for a medium of thickness δd and absorption coefficient μ_a light with incident intensity I will be attenuated by δI, see Figure 3.1. This is related via the following equation:

$$\delta I = -\mu_a \cdot \delta d \cdot I \tag{3.1}$$

which rearranges to

$$\frac{\delta I}{I} = -\mu_a \cdot \delta d. \tag{3.2}$$

If we assume that successive layers of material with thickness d absorb the same fraction of light, we can integrate this expression:

$$\ln I = -\mu_a \cdot d + constant \tag{3.3}$$

and also that when $d = 0, I = I_0$ (the incident intensity) so the transmitted intensity I is given by:

$$I = I_0 e^{-\mu_a \cdot d}. \tag{3.4}$$

This is the Lambert-Bouguer law. It can also be expressed in terms of $\log_{10}$ but this requires a change in terminology. In base 10 logs, k is the extinction coefficient (also with units of cm^{-1}):

$$I = I_0 10^{-k \cdot d} \tag{3.5}$$

and is related to μ_a by

$$\mu_a = k \ln 10. \tag{3.6}$$

Attenuation A is defined as the ratio of the the incident to transmitted intensity. Attenuation expresses the order of magnitude of the light loss and is dimensionless but has units of optical density (OD). In the case where attenuation is solely due to absorption, we are able to derive an equation for attenuation from 3.5:

$$A = \log_{10}(\frac{I_0}{I}) = k \cdot d. \tag{3.7}$$

In 1852 the Lambert-Bouguer law (3.4) was expanded by August Beer who found a link between the absorber concentration c (molar) and the absorption coefficient:

$$\mu_a = \alpha \cdot c \tag{3.8}$$

where α is the specific absorption coefficient (usually quoted in $molar^{-1}cm^{-1}$) which represents the probability of absorption for a unit concentration of a compound over the optical pathlength. Therefore the combination of the Lambert-Bouguer law and the Beer law results in the Beer-Lambert law (in natural logs):

$$I = I_0 e^{-\alpha \cdot c \cdot d} \tag{3.9}$$

which can be expressed in terms of the attenuation as:

$$A = \alpha \cdot c \cdot d. \tag{3.10}$$

The Beer-Lambert law can also be expressed in log base 10, but this requires another change in terminology:

$$I = I_0 10^{-\epsilon \cdot c \cdot d} \tag{3.11}$$

where ϵ is the specific extinction coefficient, expressed in base 10 logarithm units, and is related to α by:

$$\alpha = \epsilon \ln 10. \tag{3.12}$$

In terms of attenuation, this is:

$$A = \log_{10} \frac{I_0}{I} = \epsilon \cdot c \cdot d. \tag{3.13}$$

The Beer-Lambert law describes the attenuation of light travelling through a uniform medium containing an absorbing substance. It predicts that light attenuation decreases exponentially with distance. It is valid with many absorbing substances; each absorber contributes to the total absorption, this is represented as:

$$A = \epsilon_1 \cdot c_1 \cdot d + \epsilon_2 \cdot c_2 \cdot d + ... = \sum_i \epsilon_i \cdot c_i \cdot d. \tag{3.14}$$

Near-Infrared Window

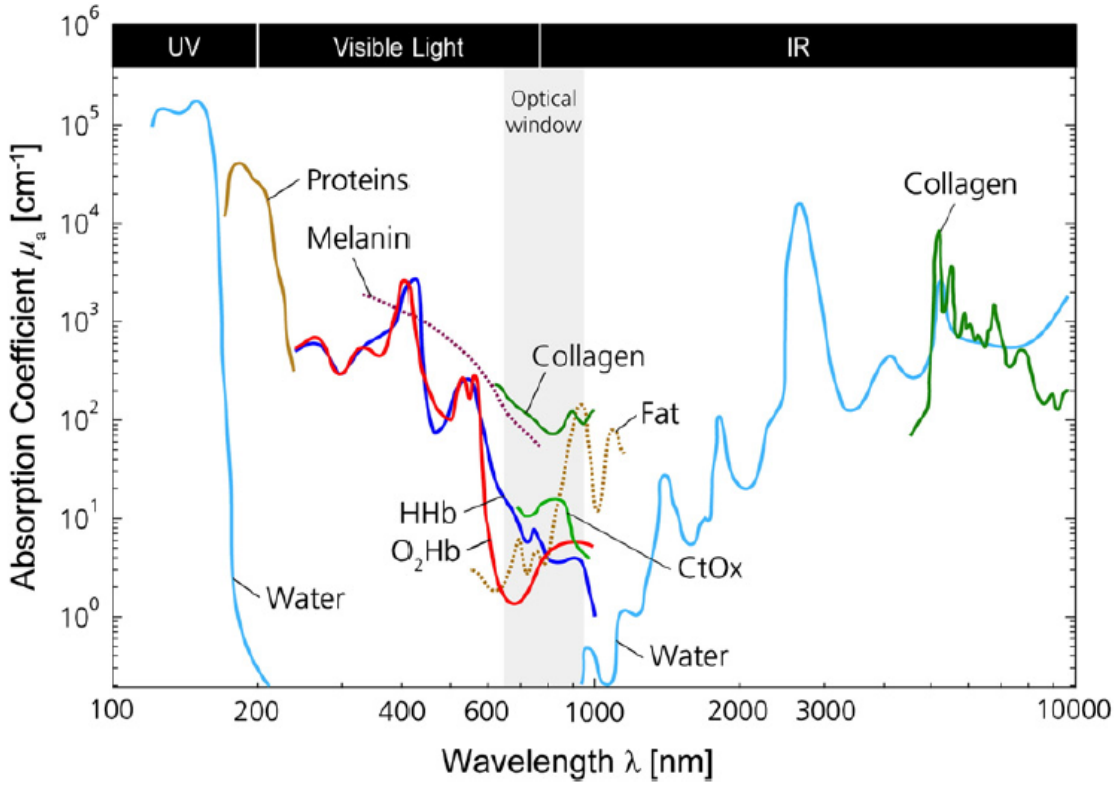

Figure 3.2: The NIR window in tissue. Taken from [6].

The attenuation of light in tissue is complex as it is due to the absorption of many different chromophores combined with multiple scattering events. In the absorption case, biological tissue can be approximated as a homogeneous mixture of compounds with an overall absorption that is dependent on the absorption coefficient and concentrations of those compounds.

In order to make measurements on tissue in-vivo and non-invasively, the light needs to penetrate the tissue with an optical pathlength long enough to reach deep, interesting tissues (e.g. brain or muscle) below the surface tissues and re-emerge to an external detector. Therefore we need to use a region of the electromagnetic spectrum in which there is low absorption in tissue, and this exists in the near-infrared (NIR) region. Water is a strong absorber in the ultraviolet (below 200nm) and far infrared regions (above 950nm) and light is strongly absorbed by haemoglobin below 650nm (see Figure 3.2); however within

650-950nm there is what is known as a 'NIR window'.

Near-Infrared Chromophores in Tissue

As biological tissue is made up of approximately 80% water, it is important to be aware of its absorption spectrum even within the 'NIR window'. Figure 3.3 shows the specific extinction coefficient for water across this window; between 650-900nm the extinction coefficient increases with wavelength but stays very low relative to other chromophores (note that in Figure 3.3 the water spectrum is increased by 6 orders of magnitude). It is fortunate that the water absorption spectrum allows us a view into the tissue, but we should be aware that the absorption of water in this region is neither negligible nor constant with wavelength.

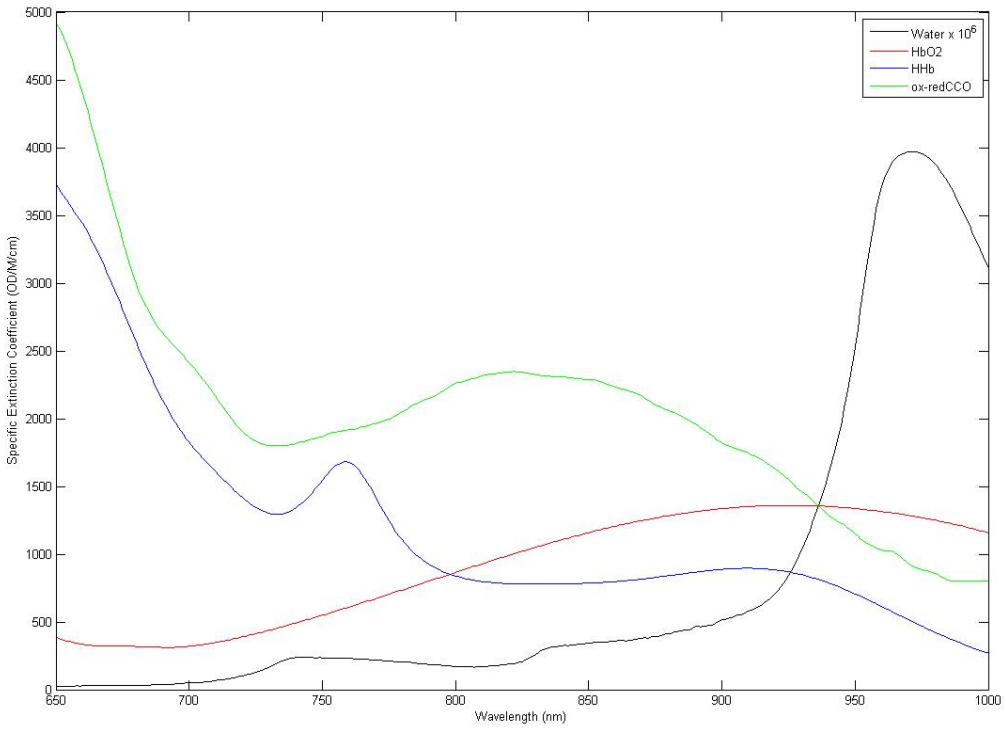

Figure 3.3: Extinction coefficient spectra for water, oxy-haemoglobin, deoxy-haemoglobin and oxidised - reduced cytochrome-c-oxidase. Note that the water spectrum is multiplied by 10^6 to be visible. Taken from [7].

The most interesting chromophores within this spectral range have absorption spectra that depend upon their oxidation state: these are haemoglobin and cytochrome-c-oxidase. Haemoglobin exists in the red blood cells and is the carrier of oxygen from the lungs to the rest of the body (i.e. tissues). It is a complex protein with four iron-containing haem sites that can bind to oxygen and transport it in the vascular system (this is discussed further in the next chapter). Its absorption spectra in the visible and infrared is dependent on whether oxygen is bound to the haem group. This is why oxygenated, arterial blood appears more red than the relatively more purple venous blood. Figure 3.4

shows the haemoglobin absorption spectrum when oxygen is bound (HbO_2) and without oxygen (HHb); the spectrum of haemoglobin in the NIR changes as the saturation of oxygen increases. Note the point at 800nm where the absorption does not change despite the saturation change; this is known as the isosbestic point and can be used to monitor total haemoglobin levels.

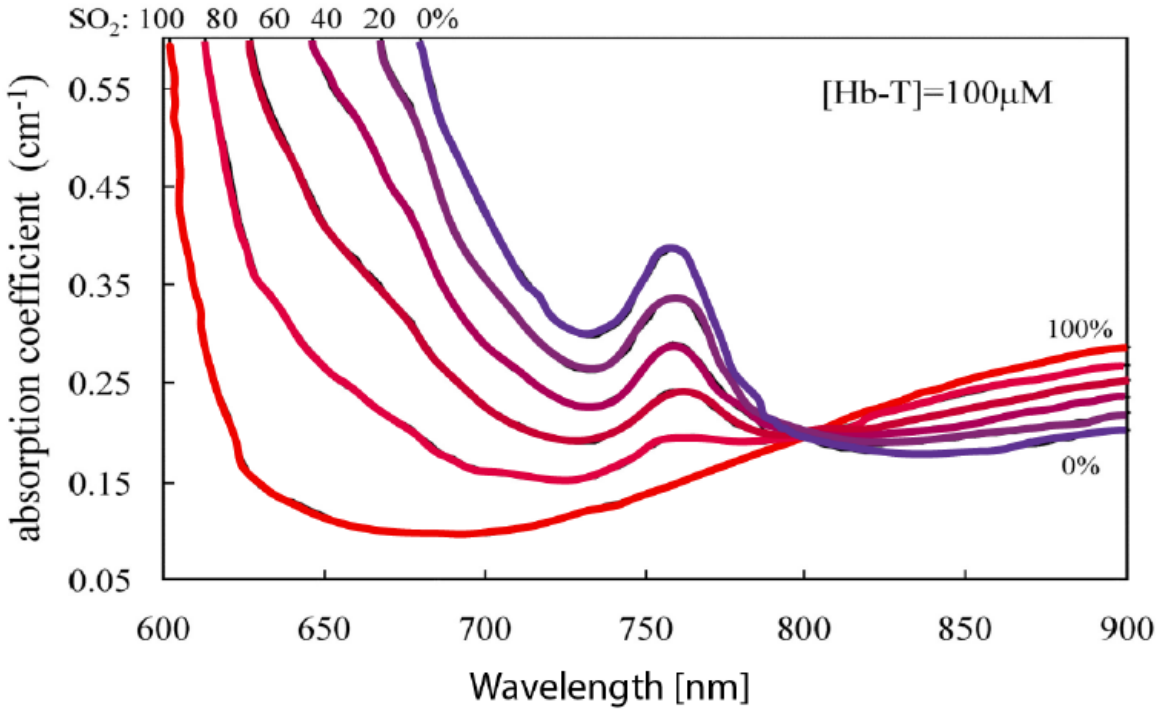

Figure 3.4: Absorption coefficient spectra for haemoglobin at different values of oxygen saturation. The curve for deoxy-haemoglobin corresponds to 0% whereas the curve for 100% corresponds to oxy-haemoglobin. Taken from [8].

The other interesting chromophore in the NIR is cytochrome-c-oxidase within the mitochondria. Mitochondria are described as the cell's 'powerhouse' because they generate most of a cell's energy supply, ATP, from glucose and oxygen. CCO participates towards the end of a chain of reactions to produce ATP; during the reaction its oxidation state is changed (i.e. it gains or loses an electron) as it transports an electron to oxygen (as part of the electron transport chain, see Chapter 2.3). This change in oxidation state is visible as a change in absorption spectrum (see Figure 3.3) but unlike haemoglobin the total concentration of CCO does not change within the time of a measurement (in the order of hours) so only the difference between the oxidised and reduced spectra is needed to monitor the oxidation state. Figure 3.3 shows the difference (oxidised - reduced) spectra of CCO in the NIR. The oxidation state of CCO (oxCCO) is a surrogate for tissue oxygen metabolism at the cellular level. A literature review of clinical measurements of cerebral oxCCO is included in the next chapter (4), including a discussion of the methods used to resolve the signal (section 4.3) and a summary of the work supporting the uniqueness of the signal (section 4.4).

There are many other chromophores in the NIR in tissue, such as melanin, fat, collagen, etc. but

these are assumed to remain stable during a monitoring period (in the order of hours of time). Their absorption spectra are shown in Figure 3.2. A chromophore specific to babies is bilirubin, which is the by-product of jaundice and is responsible for the yellow colour in jaundiced babies; bilirubin peaks around 450nm and has low absorption beyond ∼525nm so does not interfere with the NIR window [111].

Scattering

Scattering effects are the largest cause of attenuation in biological tissue. Tissue heterogeneity causes light to scatter, as scattering is caused by the mismatch of refractive indices at the boundaries between tissue types and small particles within tissues. The size and shape of the structure will determine the type of scattering event and the wavelength of light affected. Many factors such as the water concentration, and temperature will affect the scattering of light. Refraction and reflection occur at the boundaries between tissues, according to the ratio of the refractive indices of the tissues respectively.

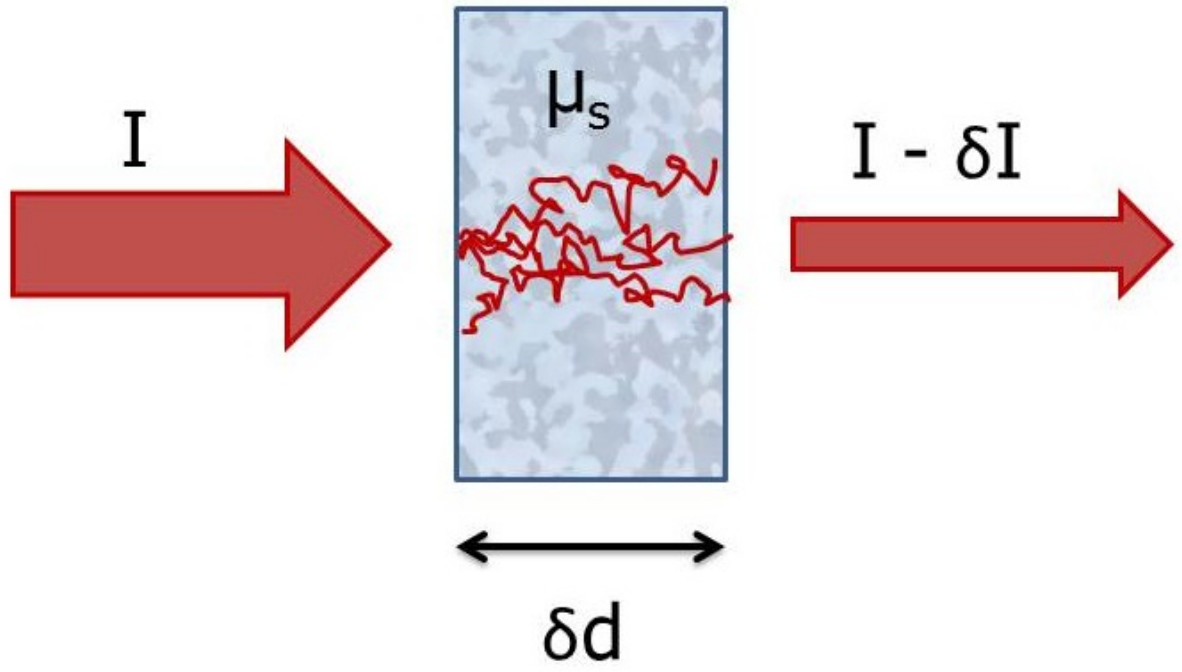

Figure 3.5: Attenuation of light through a scattering medium.

The attenuation of light due to scattering can be described similarly to absorption. If we make the same assumptions as with absorption (see Figure 3.5), then by analogy:

$$I = I_0 e^{-\mu_s \cdot d} \tag{3.15}$$

where μ_s is the scattering coefficient which is the probability per infinitesimal path that a photon will be scattered, and is typically expressed in $mm^{-}1$. The measured I is position, area and direction sensitive and only accounts for light that has not been scattered (i.e. when the scattering of the medium is sufficiently low to prevent the detection of multiply-scattered light).

A true description of light transport in tissue needs to take into account anisotropic scattering (i.e. scattering that is not equal in all directions), which is a very complex problem. The anisotropy is commonly characterised by the mean cosine of the scattering angle. This mean cosine of the scattering angle is known as the anisotropy factor g and provides a measure of the mean direction of scatter. Most tissues have a high g, which means that light scatters forward. When multiple scattering occurs (i.e. in diffuse media), light rapidly loses directionality. It is then often useful to assume isotropic scatter where the scattering coefficient has been reduced by a factor of $1 - g$. This modified scattering coefficient is called the transport scattering coefficient μ_s' which gives directionality and is defined as:

$$\mu_s' = \mu_s(1 - g). \tag{3.16}$$

3.1.2 Attenuation in Tissue

Tissue is a highly scattering medium [112]. By combining the effects of tissue absorption and multiple scattering events it is possible to make a modification to the Beer-Lambert law (3.14):

$$A = \sum_i \epsilon_1 \cdot c_i \cdot d \cdot B + G. \tag{3.17}$$

This equation is known as the Modified Beer-Lambert Law (MBLL). The scattering of light is taken into account with an unknown scattering loss term G, and B is the dimensionless differential pathlength factor (DPF) which is a multiplier to account for the increased optical pathlength within the tissue due to scattering [113].

The effective mean optical pathlength β is the product of the geometric distance and the DPF, and has units of length in cm:

$$\beta = B \cdot d. \tag{3.18}$$

The DPF is dependent on the wavelength of light as different wavelengths are scattered and absorbed differently in tissue. The DPF has been measured experimentally for different tissue types [114] and further the wavelength-dependency of the DPF has been quantified experimentally [115]. The DPF and optical pathlength estimation is discussed further in section 4.3.

3.1.3 Differential Spectroscopy

The modified Beer-Lambert law cannot be used to measure absolute chromophore concentrations from measured light attenuation because G is unknown. However, if it is assumed that G does not change throughout the measurement period then it is possible to determine a temporal change in concentration Δc from a measured change in attenuation ΔA.

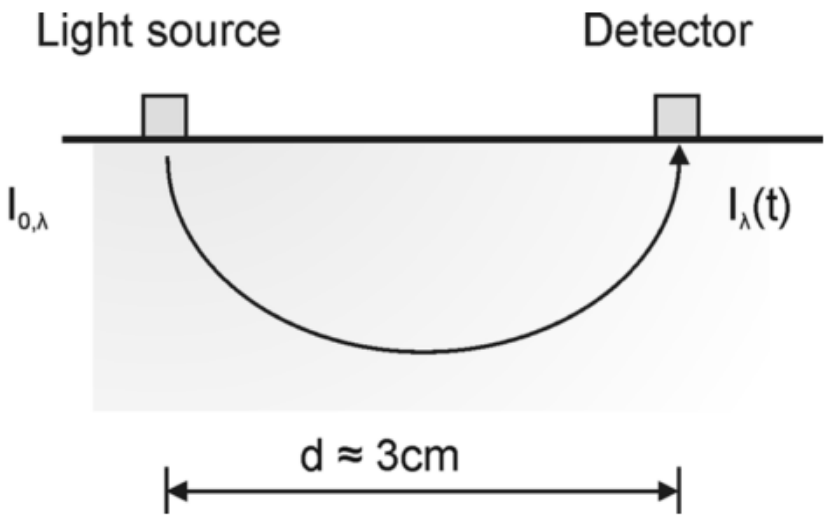

Figure 3.6: Schematic of a typical experimental set-up using differential spectroscopy. Taken from [9].

Figure 3.6 shows a typical measurement set-up to yield ΔA. For example for two chromophores, HbO_2 and HHb at one wavelength λ_j:

$$\begin{aligned} A_{\lambda_j} &= log_{10}\frac{I_{0,\lambda_j}}{I_{\lambda_j}} \\ &= \epsilon_{HHb,\lambda_j} \cdot c_{HHb} \cdot \beta + \epsilon_{HbO_2,\lambda_j} \cdot c_{HbO_2} \cdot \beta + G_{\lambda_j}. \end{aligned} \tag{3.19}$$

Measuring at two times, t_1 and t_2 to get $\Delta A_{\lambda_j} (= \Delta A_{\lambda_j}(t_2) - \Delta A_{\lambda_j}(t_1))$ gives:

$$\begin{aligned} \Delta A_{\lambda_j} &= log_{10}\frac{I_{0,\lambda_j}(t_2)}{I_{\lambda_j}(t_2)} - log_{10}\frac{I_{0,\lambda_j}(t_1)}{I_{\lambda_j}(t_1)} \\ &= \epsilon_{HHb,\lambda_j} \cdot \Delta c_{HHb} \cdot \beta + \epsilon_{HbO_2,\lambda_j} \cdot \Delta c_{HbO_2} \cdot \beta + G_{\lambda_j}(t_2) - G_{\lambda_j}(t_1). \end{aligned} \tag{3.20}$$

Assuming that there is no change in I_0 over time and that there are no changes in losses due to scattering effects (i.e. $G_{\lambda_j}(t_2) - G_{\lambda_j}(t_1) = 0$), the equation simplifies to:

$$\begin{aligned} \Delta A_{\lambda_j} &= log_{10}\frac{I_{\lambda_j}(t_1)}{I_{\lambda_j}(t_2)} \\ &= \epsilon_{HHb,\lambda_j} \cdot \Delta c_{HHb} \cdot \beta + \epsilon_{HbO_2,\lambda_j} \cdot \Delta c_{HbO_2} \cdot \beta, \end{aligned} \tag{3.21}$$

or in general terms [113]:

$$\Delta A_{\lambda_j} = \sum_{i,\lambda_j} \epsilon_{i,\lambda_j} \cdot \Delta c_{i,\lambda_j} \cdot \beta. \tag{3.22}$$

To solve for Δc for two chromophores, two wavelengths are needed:

$$\begin{bmatrix} \Delta A_{\lambda_1} \\ \Delta A_{\lambda_2} \end{bmatrix} = \begin{bmatrix} \epsilon_{HbO_2,\lambda_1} & \epsilon_{HHb,\lambda_1} \\ \epsilon_{HbO_2,\lambda_2} & \epsilon_{HHb,\lambda_2} \end{bmatrix} \begin{bmatrix} \Delta c_{HHb} \\ \Delta c_{HbO2} \end{bmatrix} \cdot \beta. \tag{3.23}$$

and the solution is:

$$\begin{bmatrix} \Delta c_{HbO_2} \\ \Delta c_{HHb} \end{bmatrix} = \frac{1}{\beta} \begin{bmatrix} \epsilon_{HbO_2,\lambda_1} & \epsilon_{HHb,\lambda_1} \\ \epsilon_{HbO_2,\lambda_2} & \epsilon_{HHb,\lambda_2} \end{bmatrix}^{-1} \begin{bmatrix} \Delta A_{\lambda_1} \\ \Delta A_{\lambda_2} \end{bmatrix}. \tag{3.24}$$

3.1.4 Broadband NIRS

To resolve changes in HbO_2 and HHb from the differential spectroscopy equation (3.24) it is sufficient to use just two wavelengths to solve for two unknowns. This is especially true if the wavelengths are chosen to distinguish between the chromophores e.g. chosen either side of the isosbestic point (see Figure 3.4). It is possible to use just two wavelengths because the differences between their absorption spectra are distinct and they exist in large concentrations within tissue. In theory, it should be possible to resolve for three chromophores (HbO_2, HHb and oxCCO) with just three wavelengths. However, the oxidised - reduced difference CCO spectrum has a relatively broad peak and further, CCO exists in tissue at a much lower concentration than haemoglobin. Hence, it is difficult to accurately resolve changes in oxCCO with only three wavelengths.

Broadband (or multi-wavelength) NIRS is therefore used to fully characterise the spectral attenuation due to haemoglobin *and* oxCCO. Matcher et al. demonstrated in 1995 that using multiple wavelengths improved the estimation of changes in oxCCO [48], and more recently this has been verified by many more studies using broadband NIRS [52, 60, 61]. This can be described with a matrix solution to equation 3.22:

$$\begin{bmatrix} \Delta c_{HbO_2} \\ \Delta c_{HHb} \\ \Delta c_{oxCCO} \end{bmatrix} = \frac{1}{\beta} \begin{bmatrix} \epsilon_{HbO_2,\lambda_1} & \epsilon_{HHb,\lambda_1} & \epsilon_{oxCCO,\lambda_1} \\ \epsilon_{HbO_2,\lambda_2} & \epsilon_{HHb,\lambda_2} & \epsilon_{oxCCO,\lambda_2} \\ \vdots & \vdots & \vdots \\ \epsilon_{HbO_2,\lambda_n} & \epsilon_{HHb,\lambda_n} & \epsilon_{oxCCO,\lambda_n} \end{bmatrix}^{-1} \begin{bmatrix} \Delta A_{\lambda_1} \\ \Delta A_{\lambda_2} \\ \vdots \\ \Delta A_{\lambda_n} \end{bmatrix} \tag{3.25}$$

See section 4.3 for more details regarding accurately resolving changes in oxCCO with broadband spectroscopy, and section 4.4 for an evaluation of the broadband NIRS-measured oxCCO signal.

3.1.5 Spatially Resolved Spectroscopy

Spatially resolved spectroscopy (SRS) is a technique to resolve absolute concentrations of chromophores using a solution to the diffusion equation which in itself is a special case of the radiative transfer equation. The technique uses multiple detectors to resolve the change in attenuation at different distances. This section begins with the derivation of, and solution to, the diffusion equation, and applies this to the SRS technique.

Derivation of the Diffusion Equation

A more fundamental description of light transport through tissue is given by the Boltzmann transport equation which describes the propagation of electromagnetic waves in scattering media. It is also known

as the radiative transfer equation (RTE) [9, 116]:

$$\frac{1}{c}\frac{\delta L(\mathbf{r},\hat{s},t)}{\delta t} + \nabla L(\mathbf{r},\hat{s},t)\hat{s} = -(\mu_s+\mu_a)L(\mathbf{r},\hat{s},t) + \mu_s \iint_{4\pi} L(\mathbf{r},\hat{s}',t) f(\hat{s}\cdot\hat{s}')d\Omega' + Q(\mathbf{r},\hat{s},t) \quad (3.26)$$

where c is the speed of light, $L(\mathbf{r},\hat{s},t)$ is the radiance (units W/m^2sr), $\hat{s}$ is a unit vector pointing in the direction of interest at the position vector $\mathbf{r}$ at time t, $Q(\mathbf{r},\hat{s},t)$ is the source term which represents the power injected into a unit volume, $d\Omega$ is the solid angle, and $f(\hat{s},\hat{s}')$ is the normalised differential scattering cross section which satisfies:

$$\iint_{4\pi} f(\hat{s}\cdot\hat{s}')d\Omega' = 1. \quad (3.27)$$

The photons are treated as billiard balls undergoing elastic collisions travelling at speed $c = (3.8\times 10^8 m/s)/n$ where n is the refractive index of the material. By integration over all solid angles and use of the definitions of the source term S, fluence rate ϕ and the flux $\mathbf{j}$ the equation becomes [9, 116]:

$$\frac{1}{c}\frac{\delta\phi(\mathbf{r},t)}{\delta t} + \nabla\cdot\mathbf{j}(\mathbf{r},t) = -\mu_a\phi(\mathbf{r},t) + S(\mathbf{r},t), \quad (3.28)$$

where

$$\begin{aligned} S(\mathbf{r},t) &= \iint_{4\pi} Q(\mathbf{r},\hat{s},t)d\Omega \\ \phi(\mathbf{r},t) &= \iint_{4\pi} L(\mathbf{r},\hat{s},t)d\Omega \\ \mathbf{j}(\mathbf{r},t) &= \iint_{4\pi} L(\mathbf{r},\hat{s},t)\hat{s}d\Omega. \end{aligned} \quad (3.29)$$

When scattering is much stronger than absorption ($\mu_s' \gg \mu_a$) i.e. a diffuse media, as it is in biological tissue, the radiance is nearly isotropic and can be approximated as a combination of an isotropic fluence rate plus a small directional flux [9, 116]:

$$L(\mathbf{r},\hat{s},t) = \frac{1}{4\pi}\phi(\mathbf{r},t) + \frac{3}{4\pi}\mathbf{j}(\mathbf{r},t)\cdot\hat{s}. \quad (3.30)$$

Substituting this approximation into equation 3.26 and multiplying by $\hat{s}$ and integrating over all solid angles yields:

$$\frac{1}{c}\frac{\delta\mathbf{j}(\mathbf{r},t)}{\delta t} = -\frac{1}{3}\nabla\phi(\mathbf{r},t) - \frac{1}{3D}\mathbf{j}(\mathbf{r},t), \quad (3.31)$$

where D is the diffusion coefficient and is given by:

$$D \equiv \frac{1}{3[(1-g)\mu_s+\mu_a]} \equiv \frac{1}{3[\mu_s'+\mu_a]}. \quad (3.32)$$

In a steady state (i.e. $\frac{\delta \mathbf{j}(\mathbf{r},t)}{\delta t} = 0$) equation 3.31 becomes

$$\mathbf{j}(\mathbf{r},t) = -D\nabla\phi(\mathbf{r},t) \tag{3.33}$$

which is analogous to Fick's law of diffusion [9, 116].

The two relations between the fluence rate and flux (equations 3.28 and 3.31) can be combined to give:

$$D\nabla^2\phi(\mathbf{r},t) - \mu_a\phi(\mathbf{r},t) = (1+3D\mu_a)\frac{1}{c}\frac{\delta\phi(\mathbf{r},t)}{\delta t} - S(\mathbf{r},t) + \frac{3D}{c^2}\frac{\delta^2\phi(\mathbf{r},t)}{\delta t^2} - \frac{3D}{c}\frac{\delta S(\mathbf{r},t)}{\delta t}. \tag{3.34}$$

As stated previously, in most biological tissues the scattering coefficient is much greater than the absorption coefficient hence both D and μ_a are small and therefore $3D\mu_a \ll 1$. If the source varies in time with frequencies of less than $\sim 1GHz$ then the last two terms can also be neglected [9, 116]. This leaves the diffusion equation:

$$D\nabla^2\phi(\mathbf{r},t) - \mu_a\phi(\mathbf{r},t) = \frac{1}{c}\frac{\delta\phi(\mathbf{r},t)}{\delta t} - S(\mathbf{r},t). \tag{3.35}$$

Solution to the Diffusion Equation

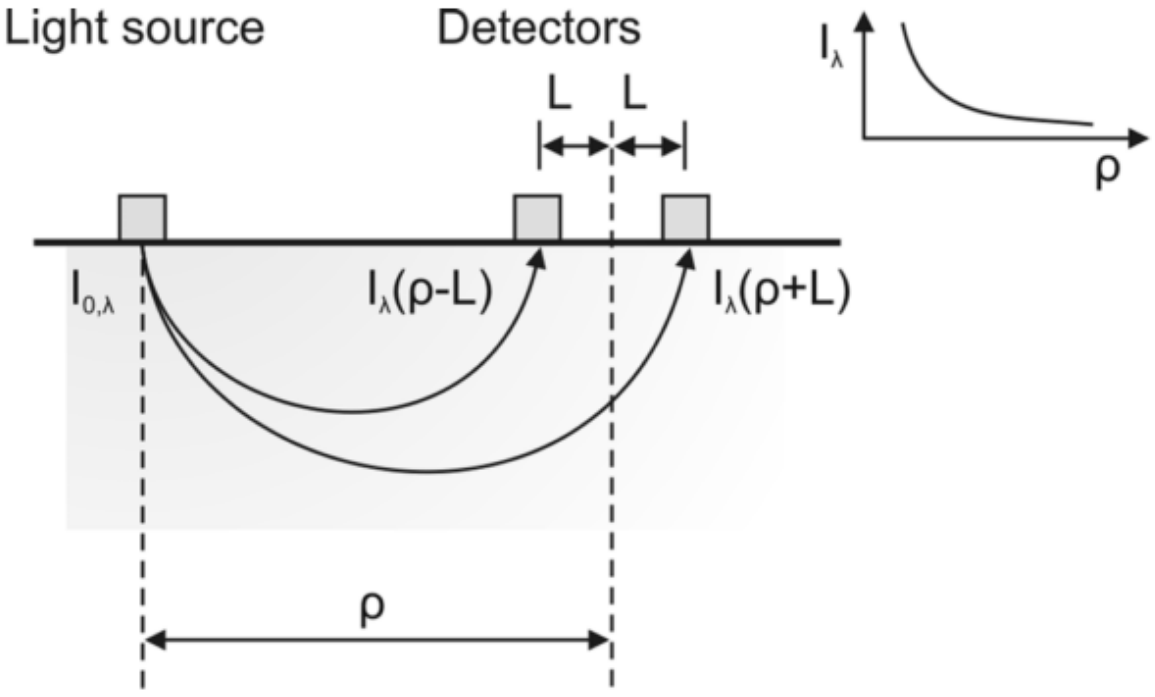

Figure 3.7: Schematic of experimental set-up using spatially resolved spectroscopy. Taken from [9].

For a Dirac pulse from an isotropic point source ($S(\mathbf{r},t) = \delta(0,0)$) the solution to the diffusion equation (equation 3.35) for an infinite and homogeneous medium is given by the Green's function

[9, 116]:

$$\phi(\mathbf{r},t) = c(4\pi Dct)^{3/2} exp(-\frac{|\mathbf{r}|^2}{4Dct} - \mu_a ct). \tag{3.36}$$

It is then possible to apply this solution to the experimental set-up for SRS as seen in Figure 3.7. From Fick's law, the reflectance at the surface R is:

$$R(\rho,t) = \left| -D\frac{\delta}{\delta z}\phi(\rho,0,t) \right| \tag{3.37}$$

which combined with equation 3.36 yields:

$$R(\rho,t) = (4\pi Dct)^{3/2}\frac{1}{\mu_s'} t^{(-5/2)} exp(-\frac{\rho^2 + \frac{1}{\mu_s'}^2}{4Dct} - \mu_a ct). \tag{3.38}$$

In the case of a continuous light source, such as in continuous wave NIRS,

$$R(\rho) = \int_{t=0}^{\infty} R(\rho,t)dt = \frac{1}{2\mu_s'\pi q^2}(\frac{1}{q} + \mu_{eff}) exp(-\mu_{eff} q) \tag{3.39}$$

where

$$\begin{aligned} q &= \sqrt{(\frac{1}{\mu_s'})^2 + \rho^2} \\ \mu_{eff} &= \sqrt{3\mu_a(\mu_a + \mu_s')}. \end{aligned} \tag{3.40}$$

If there is a large separation between the light source and detector then ρ is much greater than the transport mean free path ($z_0 = \frac{1}{\mu_s'}$), it is possible to simplify equation 3.39 [9, 116]:

$$R(\rho) = \frac{\mu_{eff}}{2\mu_s'\pi\rho^2} exp(-\mu_{eff}\rho). \tag{3.41}$$

Derivation of Equations for SRS

The attenuation in a semi-infinite slab geometry, as in Figure 3.7, is defined as:

$$A(\rho) = -\log_{10} R(\rho) = -\frac{1}{\ln(10)} \ln R(\rho). \tag{3.42}$$

Substituting the expression derived for $R(\rho)$ in equation 3.41 into equation 3.42, differentiating with respect to ρ and letting $\mu_s' \approx \mu_s' + \mu_a$ (from $\mu_s' \gg \mu_a$) gives:

$$\frac{\delta A}{\delta \rho} = \frac{1}{\ln(10)}(\sqrt{3\mu_a\mu_s'} + \frac{2}{\rho}). \tag{3.43}$$

Using the set-up in Figure 3.7, it is possible to experimentally measure ($\frac{\delta A}{\delta \rho}$). To achieve the relative magnitude of μ_a, an assumption regarding μ_s' is made:

$$\mu_s' = k(1 - h\lambda) \tag{3.44}$$

which relates μ_s' to wavelength via an unknown constant k and the slope of the wavelength dependency of μ_s' which is h and is set to $6.3 \times 10^{-4} nm^{-1}$ [117]. Combining 3.43 with 3.44 leads to

$$k\mu_a(\lambda) = \frac{1}{3(1 - h\lambda)}(\ln(10)\frac{\delta A(\lambda)}{\delta \rho} - \frac{2}{\rho})^2. \tag{3.45}$$

Combining equations 3.8 and 3.12 gives $\mu_a = \ln(10) \cdot \epsilon \cdot c$ and therefore from equation 3.45 can be used to solve for scaled concentrations of HHb and HbO_2 using two wavelengths:

$$\begin{bmatrix} kc_{HHb} \\ kc_{HbO_2} \end{bmatrix} = \frac{1}{\ln(10)} \begin{bmatrix} \epsilon_{HHb,\lambda_1} & \epsilon_{HbO_2,\lambda_1} \\ \epsilon_{HHb,\lambda_2} & \epsilon_{HbO_2,\lambda_2} \end{bmatrix}^{-1} \begin{bmatrix} k\mu_{a,\lambda_1} \\ k\mu_{a,\lambda_2} \end{bmatrix}. \tag{3.46}$$

To remove the unknown scaling factor k, we find the tissue oxygen saturation (also known as the tissue oxygenation index (TOI)) which is the average percentage of oxygenated blood in the brain and is related to oxygenation status, blood volume, flow changes and oxygen utilisation [9, 116, 117]:

$$TOI = \frac{kHbO_2}{k(HbO_2 + HHb)} \times 100\%. \tag{3.47}$$

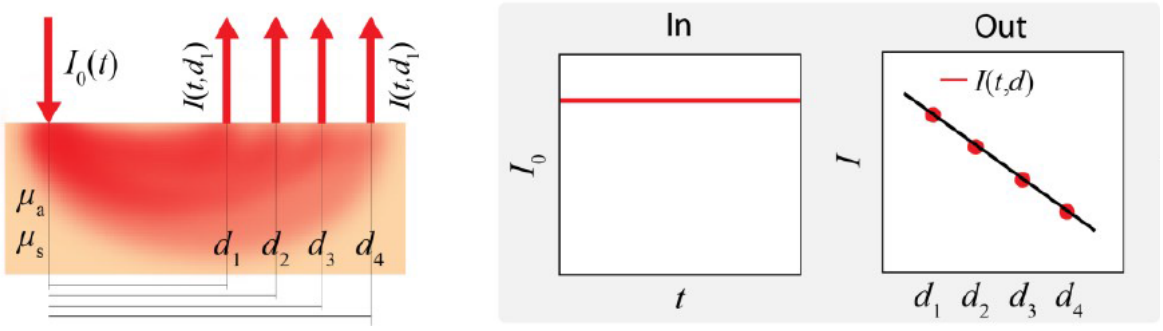

Figure 3.8: Schematic of SRS method. Taken from [10].

3.2 NIRS Instrumentation

There are many commercial and in-house built NIRS systems that are currently being used to monitor changes in the concentrations of HbO_2, HHb, and oxCCO, and/or TOI. These systems have many similarities in terms of the instrumentation but also many distinguishing features that allow for different applications. This section discusses those systems and also summarises the available commercial NIRS

systems for neonatal monitoring. Continuous wave NIRS is focussed on here, although frequency domain (FD) and time resolved (TR) NIRS are summarised briefly for completeness.

Essentially, a CW NIRS system consists of a continuous NIR light source coupled into tissue and a detector to receive the diffuse reflected light emerging from the tissue at a short distance from that source (see Figures 3.9 and 3.10 for illustrations). The three main components are therefore light sources, detectors and a means to connect these between the device and the tissue.

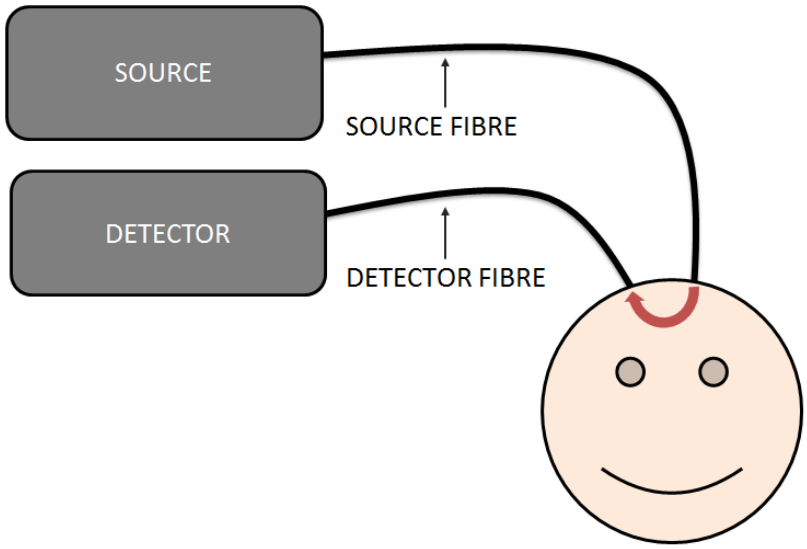

Figure 3.9: A simplified NIRS schematic.

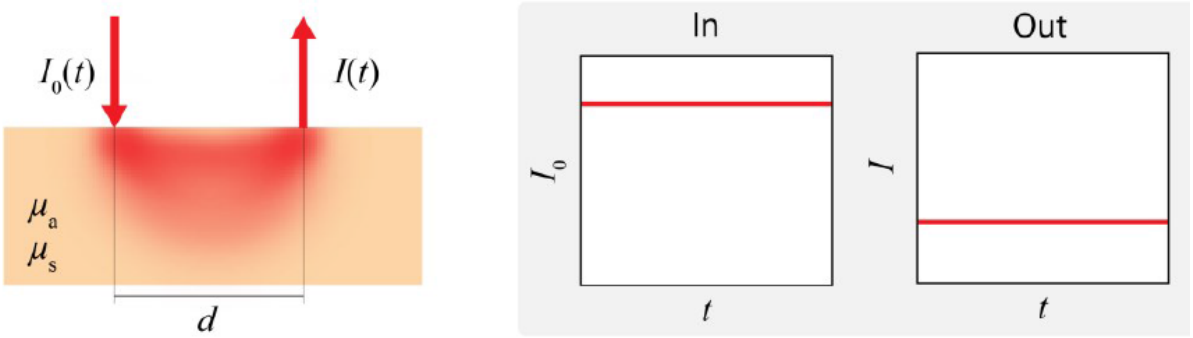

Figure 3.10: Schematic of continuous wave (CW) NIRS method. Taken from [10].

The key criteria when light sources are selected are illumination and stability. The radiated optical illumination should be chosen to maximise signal-to-noise received at the detector, but the power should not be so high so as to cause tissue heating which will distort the measurements but more importantly, may cause discomfort or damage to the subject. Tissue safety limits must be adhered to (the patients wear eye protection during monitoring so eye safety limits do not have to be adhered to). Stability of the light source is important for the integrity of the measurement. A source with intensity fluctuation will directly affect noise at the detector and temperature changes or emitter noise can lead to optical drift (i.e. changes in the intensity of a specific wavelength over time).

Most commercial NIRS systems use a small number of discrete wavelengths to evaluate changes in HHb and HbO_2 from the modified Beer-Lambert law 3.22 (see section 3.1). The different wavelengths are switched on in sequence so only one detector is required to identify the resulting intensity from the different wavelengths. The most widely used discrete light sources are laser diodes and light emitting diodes (LEDs) [6], both based on semiconductor technology, as they provide narrow radiation spectra. Laser diodes, based on stimulated emission, have a very narrow bandwidth (<1nm) so there is higher confidence of the wavelength used in the algorithm, and are coherent which make focussing into fibres simpler. However, laser diodes require large packing which is less suitable for miniaturisation. LEDs, based on spontaneous emission, have larger bandwidths (typically 10-50nm) but are able to be produced in smaller packaging and come in a wider range of wavelengths. In order to resolve oxCCO, a large number of wavelengths is needed to accurately quantify changes in the NIR spectra. Broadband light sources are therefore used in such systems, these are typically thermally-stable white light bulbs filtered to the NIR region using appropriate bandpass filters.

On the detector side, when discrete sources are used it is satisfactory to use photodetectors without spectrographs, however for broadband sources it is necessary to use spectrometers to record the entire absorption spectrum. Photodetectors are normally based on the photoelectric effect (i.e. photon generation of free-charge carriers which are detected as an electronic signal). The most common detectors in NIRS devices are photodiodes, photomultiplier tubes (PMTs), avalanche photodiodes (APDs) and charge-coupled devices (CCDs). Photodiodes have a high dynamic range, are small and easy to use as they do not require thermal or voltage stability, but have no internal signal amplification. APDs however, have moderate gains and dynamic range and also come in small packages. They require a stabilised power supply and temperature control. CCDs are commonly used in combination with a spectrograph for broadband NIRS as they provide spatial information (via an array of pixels) so can capture a spectrum of intensity across wavelengths. In a spectrometer, the light is passed through a system of lenses or mirrors and diffracted at a grating or prism, all of which reduce the resulting intensity received at the CCD; travelling through a spectrograph reduces the sensitivity, and therefore a high intensity source and careful system design are needed to achieve good light throughput. All photodetectors encounter three main types of noise [6]: shot noise, related to the quantum (discrete) nature of photons, is unavoidable and is proportional to the square root of the signal intensity, so is more important at low light levels; dark current, which is the current recorded when there are no photons from a statistical variation in the number of electrons thermally generated, it can be controlled by lowering the device temperature; and thermal noise, present in resistors internal and external to the detector due to the Brownian motion of electrons.

The sources and detectors are either placed directly on the tissue (for small devices e.g. LEDs and photodiodes) or the light is coupled to the tissue via fibre optics (for larger devices e.g. laser diodes and PMTs) depending on their size and weight. In the cases where the light needs to be transported to and/or from the tissue optical fibre bundles are used to guide the light. The fibres need to have a high numerical aperture (NA) to collect the diffuse light from a wide range of angles and large bundle diameter. Fibres have advantages in terms of safety as no electronic devices come into contact with the

skin, and good fibre design will allow the device and subject to be far apart (metres away) which is advantageous in clinical environments where bedsides can be crowded with monitors. However they can be bulky and restrictive due to the fragile nature of fibres and the weight of fibre bundles, and are also prone to coupling losses at junctions between the source/detector/tissue and the fibre. These losses are avoided with direct placement of sources and detectors on the tissue.

Coupling the sources and detectors to the tissue is one of the most challenging aspects of NIRS monitoring, especially in areas like the head where hair is a significant issue and in groups of patients, such as babies, where movement is difficult to avoid [118]. Probe, or optode, design is therefore a huge area of research [119] and it is important to design optodes and optode holders specifically for both the subject and environment. Hair is a strong absorber of NIR light so it must be removed from under the optode, one group has suggested fibre brushes to remove hair with the optode placement [120]. Changes in pressure can cause artefacts during the measurement so another solution is the use of spring-loaded optodes [121]. More typically, the optodes are attached with a supporting holder and double-sided tape, bandages over the probes, or via head caps in the case of NIR imaging [6, 119].

Commercial NIRS systems and series include NIRO (Hamamatsu, Japan), OxyMon (Artinis, Netherlands), ETG (Hitachi, Japan), NIRScout (NIRx, USA), NIRSOptix (TechEn, USA), NTS Optical Imaging System (Gowerlabs, UK), Imagent (ISS, USA), OEG (Spectratech, Japan), Brainsight (Rogue Research, Canada) and LABNIRS (Shimadzu, Japan) [6].

Cerebral oximetry systems have had success in clinical environments [122]. These systems monitor TOI and may not report changes in haemoglobin concentrations additionally. These systems use two or more source-detector separations to resolve TOI via changes in attenuation with distance (see section 3.1.5 for theory). This either entails two or more sources with a single detector, or vice-versa. Commercial oximeters include INVOS (Coridien, USA), CerOx (Ornim, USA), Equanox (Nonin, USA), and ForeSight (CASMED, USA).

FD and TR NIRS systems are more complex machines that are able to calculate μ_s' by measuring the light intensity phase change through tissue, in the case of FD NIRS, and μ_s' and μ_a from the time of flight of photons with TR NIRS. Figure 3.11 shows schematically the methodology behind each technique. Both domains require more advanced technology to measure phase and time of flight respectively so these systems are more expensive and less commonly used than CW NIRS.

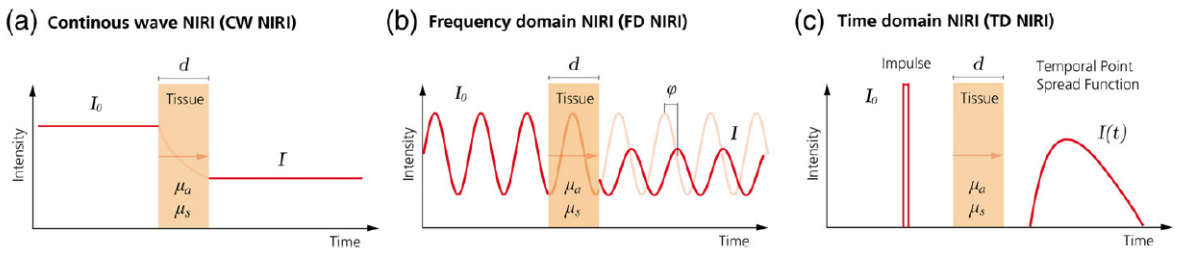

Figure 3.11: Different NIRS modalities. Taken from [6].

Broadband NIRS Instrumentation: Spectrographs

In order to perform broadband NIRS a spectrometer is required. A spectrometer fundamentally consists of an entrance slit for light input, collimating mirrors or lenses to reduce loss, a prism or diffraction grating, and focussing mirrors or lenses to direct light onto the detector. A dispersive prism disperses light into its wavelengths because the angle of refraction is dependent on the refractive index of a material which in turn is dependent on the wavelength of light that is travelling through it. This means that different wavelengths of light will travel at different speeds, and so the light will disperse into the colours of visible spectrum, with longer wavelengths being refracted less than shorter wavelengths. A diffraction grating diffracts light into its wavelengths through transmission or reflection of light through a series of parallel ruled lines (see Figure 3.12).

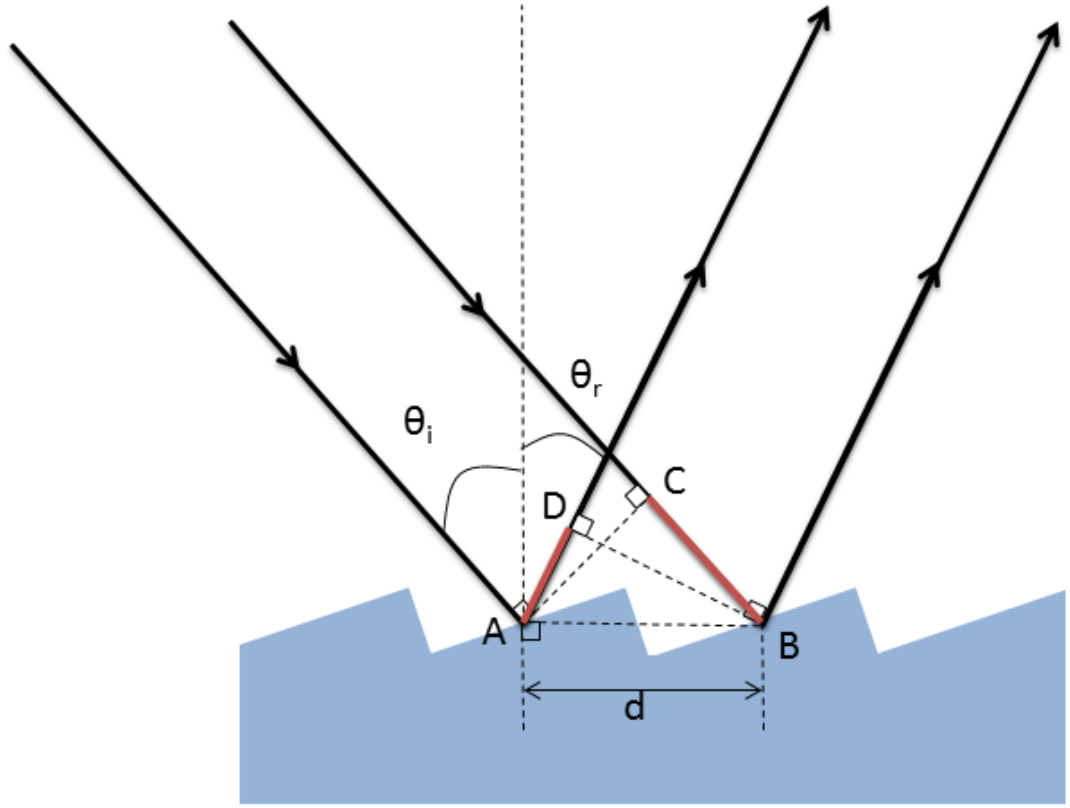

Figure 3.12: Diagram of diffraction grating showing the diffraction of incident light at an angle θ_i with reflected angle θ_r. Constructive interference occurs at the focus if the difference between the two pathlengths of light (marked in red) is equal to an integer number of wavelengths ($m\lambda$).

The light of the same wavelength will constructively interfere at the focus (convergence at infinity) when the difference between the pathlengths of light is equal to an integer number (m) of wavelengths (λ). Figure 3.12 shows that for light incident at an angle θ_i and reflected at θ_r, the pathlengths differ by the difference between the points CB and AD. These can be expressed in terms of the angles (note

that the angle formed by CAB is equal to θ_i and the angle ABD is equal to θ_r):

$$\begin{aligned} CB &= d\sin\theta_i \\ AD &= d\sin\theta_r. \end{aligned} \tag{3.48}$$

The difference between these must be equal to an integer number of wavelengths for constructive interference:

$$\begin{aligned} CB - AD &= m\lambda \\ d(\sin\theta_i - \sin\theta_r) &= m\lambda. \end{aligned} \tag{3.49}$$

A blazed grating is a special type of diffraction grating where the lines are separated by a sawtooth-shaped cross section which is tilted at a blaze angle. The blaze angle can be chosen to maximise the efficiency of a given diffraction order at a specific wavelength and therefore the grating achieves maximum efficiency around this wavelength.

There are many different spectrometer types, the most common being mirror-based Czerny-Turner designs which can be packaged into miniature spectrometers [123] (see Figure 3.13 for example system). Larger lens-based systems, such as the one used in this PhD project (see section 5.2), are less compact but have higher light throughput and a 2-dimensional optical plane which allows for multiple spectra from multiple light sources to be resolved simultaneously.

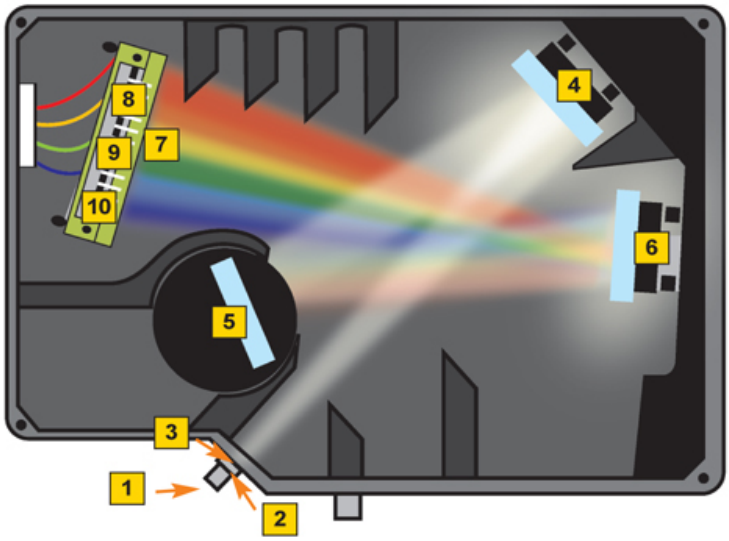

Figure 3.13: Ocean Optics HR2000+ miniature spectrometer with Czerny-Turner design. Internal components: 1) SMA connector 2) Slit 3) Filter 4) Collimating mirror 5) Grating and wavelength range 6) Focussing mirror 7) Data collection lenses 8-10) CCD detector. Taken from HR2000+ manual (Ocean Optics, USA).

Broadband NIRS Instrumentation: CCDs

A CCD is made up of an array of metal oxide semiconductor (MOS) capacitors (pixels) which are read out using the movement of electrical charge. Essentially, photons striking a silicon surface create free electrons through the photoelectric effect and an associated positive charge or 'hole' is generated as a consequence. If nothing else is done the hole and the electron will recombine and release energy in the form of heat. Small thermal fluctuations are very difficult to measure and it is thus preferable to gather electrons in the place they were generated and count them in some manner to create an image. This is accomplished by positively biasing discrete areas to attract electrons generated while the photons come onto the surface (this is shown in Figure 3.14). The substrate of a CCD is made of silicon, but photons coming from above the gate strike the epitaxial layer (which is essentially silicon with different elements doped into it) and generate photoelectrons. The gate is held at a positive charge in relation to the rest of the device, which attracts the electrons to it. Because of the insulating layer (essentially a layer of glass), the electrons cannot penetrate through to the gate, and are held in place by the positive charge above them, this creates a 'potential well'. The electrons build up in the potential well until the exposure is complete up to the maximum depth of the well. To read the number of electrons at each well (or pixel), the voltage (or potential) is shifted in one direction so that the electrons are moved along the wells until they reach the end of the array. At the end of the array the electrons are pulled in the other direction and read out by the camera electronics ('digitisation'). In this way the computer can build up a 2-dimensional intensity map (or image) of the incident light. Noise can be introduced by thermal effects, shot noise, dark current, digitisation and erroneous signals from the camera electronics.

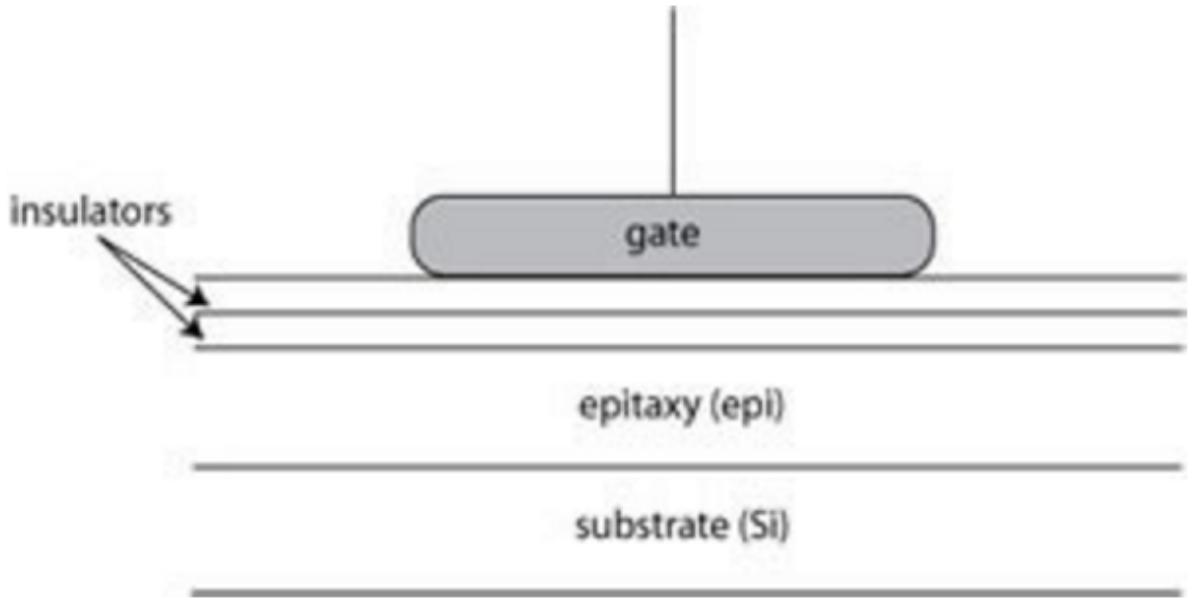

Figure 3.14: Simple diagram of a CCD pixel or MOS diode. In front-illuminated CCDs the light is incident from the top of the diagram.

3.2.1 NIRS Instrumentation for Neonates

Monitoring cerebral changes with NIRS on neonates is on one hand more challenging due to the the fragile nature of infants; on the other hand it is simpler because neonates have thinner scalps and skulls, so it is easier to transmit NIR light through to the cortex. Therefore the instrumentation at the optode end needs to be specially adapted for neonatal studies.

The biggest challenge in NIRS monitoring is achieving adequate source and detector contact to the tissue to ensure good light coupling. For adult devices contact can be improved by applying pressure to the probes; however, for neonatal studies this is not possible because a baby's head is very fragile, and if the probes make the baby uncomfortable then he or she will move, so probes have to be carefully designed to ensure effective light coupling without pressure. Furthermore, space on a baby's head is much more restricted as it is smaller.

Some commercial NIRS systems have optodes which have been developed specifically for use on neonates: Fore-sight (Casmed, USA), INVOS 5100 C (Somanetics, USA), NIMO (NIROX, Italy), NIRO 100 and 200 (Hamamatsu, Japan), O2 C (LEA, Germany), OM-220 (Shimadzu, Japan), T.Ox (ViOptix, USA) and TRS-20 (Hamamatsu, Japan) [124]. The neonatal probes are typically smaller, softer and lighter than adult versions. Figure 3.15 shows an example of a neonatal NIRS sensor on a baby (INVOS system).

Figure 3.15: INVOS probes on a neonate. Taken from INVOS Cerebral Oximetry Neonatal Sensor website (Medtronic, USA).

3.3 NIRS Measurements

3.3.1 Typical NIRS Measurements

There is a lot of work using NIRS in human neonates and adults. The intention of this section is not to review this work, but to briefly cover the use of NIRS in different environments and subjects to make the

connection between the measurement and the application. It also covers some typical forms of analysis of NIRS data. For more specific reviews of the literature, the use of NIRS in HIE neonates is covered in the next section (3.3.2), and the measurement of CCO with NIRS in human neonatal and adult studies is covered in sections 4.5 and 4.6, respectively.

NIRS measurements can be used in many different environments, subjects and areas of the body. There is a large body of work on skeletal muscle measurements using NIRS to understand the physiology of muscle oxygen consumption during exercise [125]. More relevant to this PhD are cerebral NIRS measurements which have been performed in both clinical and psychological experiments. There has been huge interest recently in functional NIRS (fNIRS) as an alternative to functional MRI (fMRI) [126]. This section describes how NIRS measured signals can inform on physiology.

Interpretation of NIRS Signals

The most commonly used NIRS signals are changes in concentration of HbO_2 and HHb. Changes in these signals are from an arbitrary zero at the beginning of a measurement but can still inform on responses to challenges or changes over time during pathophysiology. Furthermore, summing the two haemoglobin signals gives a measure of changes in the total haemoglobin concentration (HbT = HbO_2 + HHb) which gives an approximation of the change in blood volume. Similarly, finding the difference between the concentrations of the two oxygenation states of haemoglobin (HbD = HbO_2 - HHb) provides an estimation of the oxygen delivery to the tissue as it shows the mismatch between the oxygenated and deoxygenated blood. Therefore the absorption spectrum of haemoglobin can be exploited to quantify blood oxygen transport to tissues and further estimate the oxygen usage at the tissue.

These signals have been further exploited to quantify CBF and cerebral blood volume (CBV). It is possible to use HbO_2 as a tracer to calculate changes in flow from Fick's law [127]; Fick's law states that the change in concentration of a tracer in a volume (i.e. HbO_2 in the brain) is equal to the difference between the rate of flow into, and out of, the volume. Therefore using fast changes in SpO_2 by altering the inspired fraction of oxygen (FiO_2), it is possible to estimate CBF from the change in HbO_2 concentration in the brain. It is also possible to estimate changes in CBV using slower changes in SpO_2 [128].

oxCCO is a chromophore of interest because of its potential to be a direct oxygen sensor due to its position in the ETC and unique redox dependent absorption spectra [129]. It has the potential to provide direct information on the state of cellular metabolism which adds information to the vascular information from the haemoglobin species. The next chapter (Chapter 4) goes into detail about CCO measurements and the physiology behind the signal.

The TOI signal is a combination of the oxygen saturation in the blood and the brain. A 'normal' TOI in a healthy adult rests between 60-80% as it represents the average haemoglobin oxygenation across the arteries, veins, and capillaries. A hypothetical argument can explain this range: assuming that the total haemoglobin is made up of ∼25% arterial and ∼75% venous, and that at normal levels arterial saturation (SaO_2) is ∼98% and venous saturation (SvO_2) is ∼70% yields an approximate TOI of 77%. It can be shown by expanding equation 3.47 that the TOI is proportional to the arterial/venous volume ratio and oxygen consumption, and inversely proportional to CBF [130]. The TOI measurement has

the advantage that it is a percentage measure so it gives an assessment of tissue oxygenation that can be directly compared between subjects, whereas the other NIRS measurements rely on challenges (e.g. functional activation or changes in inspired gases) to provide context of the changes in concentration.

Functional NIRS

All of the cerebral measurements (HbO_2, HHb, HbT, HbD, CBF and CBV) inform about oxygenation and perfusion as well as oxygen consumption. This is particularly important in fNIRS which is looking for changes in cerebral perfusion due to neuronal activation. As neurons do not have an internal reserve of oxygen and glucose (required for metabolism) their firing causes a demand as neuronal excitation causes changes in oxidative metabolism (neuro-metabolic coupling) which is related to neuro-vascular coupling (NVC): blood vessel dilation causes an increase in CBF and CBV. The vascular response overcompensates the metabolic demand and so there is an oversupply of oxygenated blood (functional hyperaemia) which causes an increase in NIRS measured HbO_2 and HbT, and HHb to decrease (as seen in Figure 3.16). This is known as the haemodynamic response function (HRF). fMRI uses the blood-oxygen-level-dependent (BOLD) contrast signal to observe the relative change in blood oxygenation (essentially via changes in HHb) but cannot differentiate between the individual species as NIRS can.

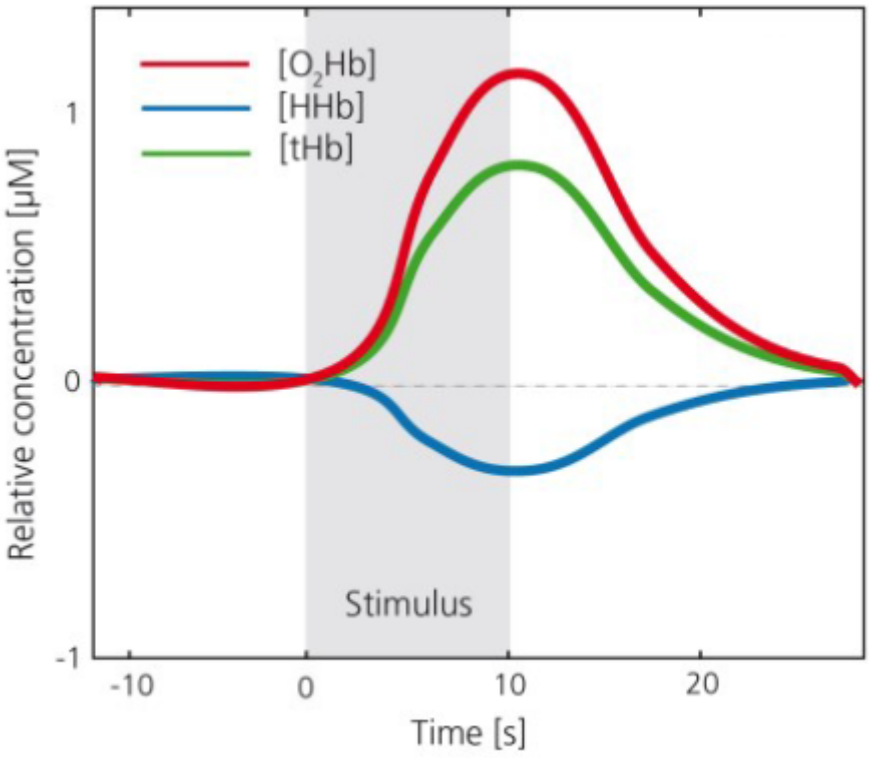

Figure 3.16: Sketch of typical changes measured by fNIRS during a functional activation task. Taken from [10].

Neonatal NIRS

Despite the functional response being well understood in adults, the HRF in neonates has not been fully characterised [126]. Both increases and decreases in HHb have been observed in fMRI and fNIRS studies in neonates [11]. A longitudinal study of the HRF in rat pups until adulthood has shown that the HRF evolves with age (see Figure 3.17). It was also observed that the neonatal HbT response correlated with blood pressure but this was not observed in adults; this suggests immature cerebral autoregulation in the neonatal brain impacts the cortical blood flow. The nature and cause of the inverted neonatal functional response is still being debated. It has also been suggested that there may be superfluous synaptic connections in younger infants which may play a role [131]. Nevertheless, it is important to be aware of brain maturity when observing haemodynamic and metabolic responses in neonates.

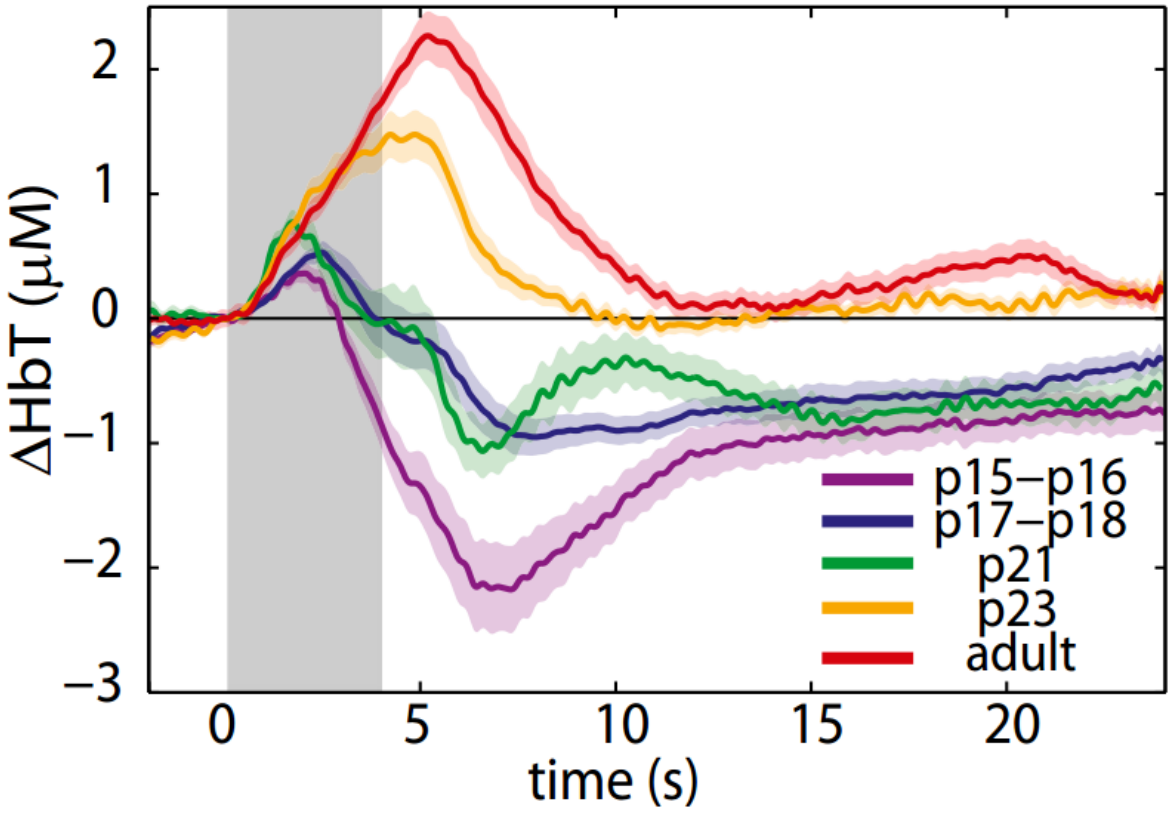

Figure 3.17: Evolution of the HbT response to fore-paw stimulus in rats progressing from neonatal response to adult response. Stimuli occur in the shaded region, p = postnatal day. Taken from [11].

Cerebral oximetry has become a popular technique in neonatal intensive care research [6, 124, 132]. Using the SRS method gives percentage assessment of cerebral tissue oxygenation so it has the potential to be used in a way analogous to pulse oximetry, i.e. a defined limit in the tissue saturation, at which clinical intervention is required (typically ∼85% in NICUs). A recent multi-centre randomised clinical trial, SafeBoosC, in preterm infants has found that using NIRS-monitored cerebral oxygenation to guide treatment, reduces the fraction of time that the infant is exposed to hypoxia [133], although it has not been shown to improve the results from early biomarkers of brain injury [134].

Optical tomography and topography techniques can provide information regarding the function and health of the entire brain, and work on these techniques (particularly tomography) has focussed on the neonatal brain due it its preferable optical properties and geometry. Optical topography produces 2-dimensional images of activated regions on the surface of the brain [135], while optical tomography produces 3-dimensional images of the whole head, and therefore can identify changes occurring in deeper tissues. Both techniques are performed using multiple sources and detectors to obtain data from multiple light paths across the head. Whole-head optical tomography has been performed on neonates during functional challenges [136], as well as in blood volume and oxygenation changes [137, 138]. Spontaneous events, such as seizures, have been studied using optical tomography [139] and topography [140] in neonatal populations.

NIRS Depth Sensitivity

Cerebral NIRS depends upon at least some of the NIR light both reaching the cerebral cortex and returning to the surface from there, otherwise the measurements will only reflect scalp physiology. The source-detector separation is key to ensure brain penetration. However it is not possible to measure the signal depth experimentally. Therefore, light propagation models have been used to estimate the sensitivity of NIRS measurements to the brain in the adult [141–143] and neonate [68, 144, 145] at different source-detector separations. Due to the different geometries and tissue densities in adults and neonates, there are differences in the propagation of light [68]. The cerebrospinal fluid has a large positive impact on the sensitivity of absorption change in the brain [141] whereas the skull thickness has a negative impact [142]. The thin skull and CSF layers in the neonate allow for more penetration of light into the cortex [68, 145]. Monte-Carlo simulations of light transport through realistic adult head models (including scalp, skull, CSF, grey and white matter) have found that 6% of the signal has travelled through grey matter at a source-detector separation of 2cm [143]. In addition, computational modelling work from Fukui et al. [68] suggests that while the white matter sensitivity in adults is almost negligible, even for large (50mm) source-detector separations, the neonatal model shows high white matter sensitivity at as low as 10mm separation. Another Monte Carlo-based simulation on anatomically accurate head models has shown that source-detector distances greater than 8.4mm for adults, and 2.15mm for neonates, have brain sensitivity greater than 5% [145]. Typical source-detector separations in adults and neonates are 3-4cm and 2-3cm respectively, so the simulation results suggest that these are sufficiently sensitive to the brain, particularly the neonatal brain.

3.3.2 Clinical NIRS Monitoring of HIE

This section contains a literature review of NIRS monitoring of HIE. Table 3.1 presents a summary of the literature covered in this section.

The first study to continuously monitor neonates with HIE using NIRS was performed in 1993 [21]. Babies with adverse outcome showed a decrease in CBV and oxCCO with age, whereas oxCCO remained stable in healthy and good outcome HIE babies. A later study conversely saw that CBV and CBF increased with age, especially in those with worse injury [71]. This is supported by the study by Grant

et al. [146] who observed increased CBV and $CMRO_2$ associated with brain injury. It is suggested that the increased cerebral perfusion is due to increased brain activity [146] or impaired control of cerebral haemodynamics [71]. However, lower CBF was seen in HIE neonates compared to controls [147] and in more severe injury [148]. There is little consistency between results of studies of HIE with CBV and CBF.

There is also no consistency across the cerebral oximetry studies of HIE. Five studies have found that infants with an adverse outcome after HIE have higher TOI [149–152] or increasing TOI [153] (note that infants were not treated with therapeutic hypothermia in this study) compared to those with normal outcome; some studies saw lower TOI in those with adverse outcome [147, 148] or in infants with HIE compared to age-matched healthy controls [154] (note that infants were not treated with therapeutic hypothermia in this study); and two studies found no significant difference between infants with adverse and normal outcomes [155] or in infants with HIE compared to age-matched healthy controls [146]. This suggests that cerebral oxygenation is not related to injury severity in a consistent way and this may be due to the heterogeneity of HIE injury, patients and treatment.

Therapeutic hypothermia (see section 2.5) is an important consideration in studies; cooling is known to reduce optically measured $CMRO_2$ and CBF [156] and so can confound conclusions reached about HIE. As TH is standard treatment in the UK and many other western countries, analysis of NIRS measurements during HIE must consider the effects of TH.

A study of HIE infants during inhaled oxygen challenges found the NIRS measured HbO_2 and TOI increased significantly less than in healthy controls (without TH) [154]. Further HHb declined to lower levels in the HIE group. The authors suggest that due to hypoxia in the HIE group, more HHb was oxidised during the challenge, but because flow is slower, more oxygen is released from the blood so the increase in HbO_2 is not as great.

There has only been one fNIRS study of HIE infants [157]; auditory stimuli were given to 22 HIE infants in the first 3 days of life. The infants typically showed a decrease of HbO_2 and HbT which is not the expected response but has been observed in healthy neonates (see previous section 3.3). The authors suggest this could be due to a 'stealing of blood flow' from the activated region if the probes are not placed directly above the activation, or inhibitory synaptic activity.

A recent trend of neonatal NIRS monitoring is cerebral autoregulation assessment, and this is true in HIE studies [158–162]. These studies typically measure cerebral autoregulatory vasoreactivity with the haemoglobin volume index (HVx) which is the correlation between mean arterial blood pressure and HbT and use this to identify optimum autoregulatory mean blood pressures ($MABP_{OPT}$). Children with long-term neurological impairments tend to deviate from $MABP_{OPT}$ more than those without impairments [158, 159].

Table 3.1: Table of literature review of NIRS monitoring of HIE in the NICU.

First Author (Date) Title	**Keywords**	**Methods**	**Results and Conclusion**
Van Bel (1993) Changes in cerebral haemodynamics and oxygenation in the first 24 hours of life following birth asphyxia [21]	NIRS, cytochrome c oxidase, birth asphyxia	18 neonates with HIE and 13 healthy neonates studied with NIRS including CCO measurement (4 wavelengths).	Babies with adverse outcome showed a decrease in CBV. CCO decreased from baseline with age in infants with adverse outcome, remained stable in healthy and good outcome HIE babies. In first 12 hours: CCO and $tcpO_2$ were positively correlated in HIE (but not in healthy) babies. CCO and MABP were inversely correlated in HIE infants. MABP and CBV were positively correlated only in HIE babies. From 12 to 24 hours: $tcpO_2$ and MABP positively correlated in HIE babies. No other correlations found. This suggests that in the first 12 hours of life there is a decrease in cerebral perfusion and oxygenation.

Meek (1999) Abnormal cerebral haemodynamics in perinatally asphyxiated neonates related to outcome [71]	Perinatal asphyxia, cerebral haemodynamics	27 term neonates with HIE were studied within 24 hours of birth. Used change in inspired O_2 and Ficks Law to calculate CBV/F and CBV response.	CBV and CBF highest in more severe injury. CBV and CBF both increased in first 24 hours, especially in those with greater severity. This suggests that there is an abnormal control of cerebral haemodynamics/loss of autoregulation in HIE.
Chen (2002) Auditory-evoked cerebral oxygenation changes in hypoxic-ischaemic encephalopathy of newborn infants monitored by near infrared spectroscopy [157]	Asphyxia, CBF, development, neuronal activity, oxygen metabolism	This study looks at auditory functional response in 22 HIE infants (age 1-3 days) with NIRO 500.	Normal newborns show similar functional response to auditory stimulus to adults. HIE infants typically showed decrease of HbO_2 and HbT. Could be due to stealing of blood flow from activated region (if activated region injured) or inhibitory synaptic activity. May show that HIE, aged and degenerated brain have similar neuronal responses. However, stimulating the injured brain may cause damage.

Huang (2004) Assessment of the hypoxic-ischaemic encephalopathy in neonates using non-invasive near-infrared spectroscopy [154]	NIRS, cerebral oxygenation, infant, inhaling oxygen stimulation	Healthy (n=25) vs. HIE (n=16) neonates studied during sleep and during oxygen inhalation on day ∼2 of life. Monitored SpO_2 and regional oxygen saturation (rSO_2) during both.	Significantly lower rSO_2 in HIE group during sleep, no difference in systemic SpO_2. The HIE infants were not cooled so this may explain differences with other papers. After inhaling oxygen, HbO_2 and rSO_2 increased in both groups but were significantly higher in healthy group. HHb declined to lower values in HIE group. The authors suggest that due to hypoxia in the HIE group, more HHb was oxidised but because flow is slower, more oxygen is released from the blood so increase in HbO_2 is not as great.
Toet (2006) Cerebral oxygenation and electrical activity after birth asphyxia: their relation to outcome [153]	Birth asphyxia, cerebral oxygen saturation, fraction cerebral oxygen extraction, aEEG, neurodevelopmental outcome	aEEG and NIRS recorded for 48 hours in 18 infants with HIE (no hypothermia) and survivors followed up in clinics up to 5 years of age.	rSO_2 normal and stable in infants with normal outcome but increased after 24 hours in those with adverse outcome. Tissue oxygen extraction factor (FTOE) decreased after 24 hours in those with adverse outcome and was significantly lower than in those with favourable outcome. May indicate vasoparalysis of the resistance vessels of the arterial cerebral vascular bed, or neuronal cell death with a consequential decrease in oxygen uptake. The increase in rSO_2 may indicate secondary energy failure.

Ancora (2009) Changes in cerebral haemodynamics and amplitude integrated EEG in an asphyxiated newborn during and after cool cap treatment	HIE, NIRS, aEEG, brain cooling [163]	Case report for one HIE infant before and during hypothermia and rewarming monitored with NIRO 200 and aEEG.	TOI and tissue haemoglobin index (THI) significantly increased when cooling started. TOI remained stable during rewarming. THI decreased during cooling and then increased again after rewarming. This suggests that the brain metabolism was reduced which explains the stable oxygenation despite changes in blood volume.
Grant (2009) Increased CBV and oxygen consumption in neonatal brain injury [146]	NIRS, hypoxic ischaemic injury (HIE), stroke, neonate, CBV, $CMRO_2$	Do FD NIRS measurements such as SO_2, CBV and $CMRO_2$ have the potential to distinguish brain injury from those with non-brain issues and healthy controls? Measurements were acquired from up to 4 different regions of the head for 8 seconds (repeated 3 times) in 43 neonates (14 with evidence of brain injury).	SO_2 not a sensitive marker for brain injury development, but useful during injury. Increased CBV and $CMRO_2$ associated with brain injury. Increased cerebral perfusion due to increased neuronal activity - may not be seen on EEG if unsynchronised.

Gucuyener (2012) Use of aEEG and NIRS finding in neonates with asphyxia during selective head cooling [164]	Perinatal asphyxia, aEEG, hypothermia treatment, NIRS	10 neonates with moderate or severe HIE were studied with NIRO 200. Measurements were taken before cooling at 36.5°C, at 34°C during cooling and at 36.5°C after rewarming. TOI and FTOE were measured. Subjects were evaluated up to 24 months of age.	Low TOI and high FTOE before cooling was indicative of seizures. During cooling these parameters were within a normal range which could be due to a reduction in brain metabolism and CBF because of hypothermia. There was no relationship between TOI and FTOE levels during or after cooling.
Ancora (2013) Early predictors of short term neurodevelopmental outcome in asphyxiated cooled infants. A combined brain amplitude integrated electroencephalography and near infrared spectroscopy study [149]	HIE, aEEG, NIRS, hypothermia, TOI	12 neonates with HIE were studied during cooling with NIRO 200 and aEEG. TOI average calculated at 6, 12 and 24 hours.	TOI at 12 hours significantly higher in infants with adverse outcomes than in those with normal outcome. TOI was also higher at 6 and 24 hours but not significantly. Probably due to luxury perfusion or secondary energy failure which causes a reduction in consumption. Abnormal aEEG was prognostic at all times.

Massaro (2013) Brain perfusion in encephalopathic newborns after therapeutic hypothermia [147]	Brain, HIE, newborns, hypothermia, NIRS	ASL-MRI was performed in the second week of life on term HIE neonates and healthy controls. A subset was studied with NIRS during and after hypothermia.	MRI showed lower CBF in thalamus in HIE patients than those without injury. Lower tissue oxygen fraction from NIRS was observed in infants with long-term damage (injury observed on MRI) and may be due to pseudonormalised metabolic demand after irreversible brain injury. 4 days of cooling decreased tissue oxygen fraction.
Wintermark (2013) NIRS versus MRI to study brain perfusion in newborns with HIE treated with hypothermia [148]	Brain, HIE, MRI, newborn, NIRS, perfusion	This study aims to determine the correlation between measurements of brain perfusion by ASL-MRI and NIRS in 7 term neonates with HIE. 2 NIRS sensors were placed over each side of the frontal lobe (on the newborns forehead) and recorded continuous SO_2 data during hypothermia and re-warming. Newborns underwent MRI 1-2 times within the first 72 hours of life. $CMRO_2$ estimated from NIRS and MRI.	Strong correlation was found between SO_2 (NIRS) and CBF (ASL-MRI). No difference between SO_2 in the groups. Newborns with severe HIE had lower CBF and extracted less oxygen (lower oxygen demand likely) than infants with moderate HIE. NIRS and ASL-MRI used in conjunction have the potential to help tailor neuroprotective strategies.

Lemmers (2013) Cerebral oxygenation and brain activity after perinatal asphyxia: does hypothermia change their prognostic value? [150]	NIRS, HIE, hypothermia, $rScO_2$	Evaluates predictive value of NIRS during hypothermia. 39 infants with HIE studied from birth (before TH) until rewarming completed at 84 hours of life. Infants grouped into favourable and adverse outcomes to assess predictive power of NIRS.	Both groups had similar regional cerebral oxygen saturation ($rScO_2$) before hypothermia and $rScO_2$ increased with postnatal age in both groups. $rScO_2$ was significantly higher in groups with adverse outcome. FTOE was lower in adverse group. aEEG better at predicting outcome than $rScO_2$ but combined aEEG and NIRS gives best prediction. Prediction was good at 12, 24 and 36 hours of life. $rScO_2$ tended to increase to levels of normal neonates between 12-24 hours which may be due to mild hypothermia keeping metabolism low.
Howlett (2013) Cerbrovascular autoregulation and neurologic injury in neonatal HIE [165]		HVx used to identify $MABP_{OPT}$ from rTHb (INVOS) and MABP in 24 HIE neonates from TH to normothermia.	Significant relationship between time spent below $MABP_{OPT}$ and brain injury: MABP within or above $MABP_{OPT}$ was associated with decreased injuries (as measured by diffusion tensor MRI). HVx monitoring shows potential to target optimal haemodynamic ranges to support autoregulation and prevent secondary injury.

Shellhaas (2013) Limited short-term prognostic utility of cerebral NIRS during neonatal therapeutic hypothermia [166]	aEEG, HIE, NIRS, TOI	18 neonates with HIE were monitored with NIRS and aEEG during hypothermia, rewarming and normothermia. Subjects were scored for severity of injury based on MRI scan and neurological exam on day 4.	Cerebral rSO_2 values at any stage did not predict short term injury severity. The variability (standard deviation) of systemic rSO_2 was only predictor of short term outcome (low variability predicts worse outcome). aEEG combined with systemic rSO_2 variability was the best predictive model.
Shellhaas (2015) An Evaluation of Cerebral and Systemic Predictors of 18-Month Outcomes for Neonates with HIE [155]	HIE, aEEG, NIRS, acute kidney injury, developmental outcome	Evaluates aEEG, NIRS and acute kidney injury as predictors of HIE outcome. 18 infants were monitored for first 72 hours of life. NIRS placed bilaterally over parietal regions.	Presence of acute kidney injury did not predict outcome. aEEG was predictive of outcome. rSO_2 not different between the groups.
Dehaes (2014) Cerebral oxygen metabolism in neonatal hypoxic-ischaemic encephalopathy during and after therapeutic hypothermia [156]	Cerebral blood circulation, SO_2, $CMRO_2$, NIRS, neonatal HIE, therapeutic hypothermia	10 neonates with HIE and 17 healthy controls were studied for the first days of life. The HIE infants were studied during hypothermia, rewarming and after normothermia. $CMRO_2$, CBF, CBV and SO_2 were measured with FD NIRS and DCS.	$CMRO_2$ and CBF were lower during hypothermia than post-hypothermia and in the controls. CBV and SO_2 were higher during hypothermia.

Peng (2014) Does NIRS identify asphyxiated newborns at risk of developing brain injury during hypothermia treatment? [151]	Birth asphyxia, HIE, MRI, metabolism, NIRS, newborn brain, perfusion	18 neonates, monitored rSO_2 during cooling, rewarming and afterwards, sensitivity/specificity analysis to assess predictive power.	Higher rSO_2 during first 10 hours in severe injuries, more sensitive and specific than aEEG at predicting adverse outcome. No change in oxygenation during rewarming. rSO_2 increased during first 2 days of life then stabilised in both groups (adverse/normal outcome). Higher rSO_2 in adverse outcome may be due to decrease in utilisation of dead tissue or 'luxury perfusion'.
Tekes (2014) Apparent diffusion coefficient scalars correlate with NIRS markers of cerebrovascular autoregulation in neonates cooled for perinatal HIE [158]	NIRS, HIE, cerebral autoregulation, correlation analysis, diffusion tensor imaging (DTI), MRI	31 neonates monitored with INVOS NIRS after HIE. Continuous moving correlation of HbT vs. MABP calculated (HVx) to monitor autoregulation. Found optimum MABP from most negative HVx. Time with below optimum MABP was noted as a percentage of monitoring time, deviation below MABP and area under curve were also recorded. This was compared with results from DTI (decreased diffusion associated with severe HIE).	DTI did not correlate with time below $MABP_{OPT}$, deviation from $MABP_{OPT}$ or area under curve. During cooling in babies with MRI on day<10 all correlated with DTI scalars in posterior centrum semiovale. Reflects complex nature of HIE and perils of only measuring one region of brain (i.e. MRS).

Nakamura (2015) Simultaneous measurement of cerebral haemoglobin oxygen saturation and blood volume in asphyxiated neonates by NIR TRS [152]		11 neonates with HIE were monitored with TRS-10(Hamamatsu, Japan). 5 were treated with TH, 6 were not.	High ScO_2 and CBV in infants with adverse outcome at 24 and 48 hours after birth. Infants treated with TH showed lower CBV at 24 hours and higher ScO_2 at 24 hours.
Burton (2015) A pilot cohort study of cerebral autoregulation and 2-year neurodevelopmental outcomes in neonates with hypoxic-ischaemic encephalopathy who received therapeutic hypothermia [159]	autoregulation, NIRS, HIE, TH, neurodevelopmental outcomes	28 neonates with HIE monitored with INVOS - measured HVx (MABP vs. rTHb) to find $MABP_{OPT}$ and rSO_2 during TH, rewarming and normothemia. Cognitive and motor development was assessed in 19 children at 21-32 months of age.	MABP deviation below $MABP_{OPT}$ during rewarming was associated with greater impairment. rSO_2 was not associated with neurodevlopmental outcome.

Massaro (2015) Impaired cerebral autoregulation and brain injury in newborns with HIE treated with TH	HIE, CBF, MRI, newborn [161]	NIRO 200 monitoring of TOI and MABP during TH to normothermia in 38 infants with HIE. Pressure passivity index (PPI) was assessed via spectral coherence between MABP and HbD.	Higher PPI in the right hemisphere was associated with adverse outcome (death or brain injury detectable by MRI).
Govindan (2015) A novel technique for quantitative bedside monitoring of NVC [167]	EEG, NIRS, NVC, spectral coherence, HIE	Spectral coherence between EEG and NIRO 200-measured HbD to assess NVC in 4 infants with HIE (2 with good outcome, 2 died).	Able to follow NVC evolution with time but no significant relationship with injury severity, although trend for lower NVC in adverse outcome.
Chalak (2015) Cerebral haemodynamics in asphyxiated newborns undergoing TH: pilot findings using a multiple-time-scale analysis [168]	Neonate, HIE, TH, cerebral haemodynamics, NIRS	Moving window correlation between MABP and ScO_2 (INVOS) in 10 HIE infants was compared with Bayley developmental test scores (5 abnormal). Study performed in the first 72 hours of life.	Infants with abnormal outcome had a high correlation between MABP and ScO_2.

3.3.3 Neonatal NIRS Study Design and Considerations

Review papers [124, 169, 170] highlight the advantages and challenges of using NIRS monitoring on neonates. The advantages are central to the principles of NIRS; the measurement is non-ionising and non-invasive, relatively simple compared with MR scanning, and is easy to apply to small infants at the cotside. The articles raise concerns over the low precision of the measurements and the large inter- and intra-patient variability. However, the authors agree that NIRS used as a trend-monitor for the individual patient can yield important clinical information that could guide clinical treatment, especially when combined with other parameters such as EEG and blood pressure. Wolf et al. [124] have noted that the changes in chromophores from an arbitrary baseline are not useful clinically unless they are combined with other physiological parameters or challenges.

The range of devices and parameters available can lead to confusion that prevents expansion of the use of NIRS in clinical care; it is important that different NIRS devices produce similar results if NIRS is to be adopted into routine use in neonatal intensive care. Dix et al.[171] performed comparison studies on a population of over 500 neonatal subjects with different devices (and sensors) to investigate the similarities or differences between $rScO_2$ values. They concluded that although the $rScO_2$ values were similar in the majority of cases, there were occasional significant differences which would complicate clinical application as it would compromise the possibility of using NIRS values as threshold markers to direct neonatal care. Further work should be done to compare not only devices but the parameters themselves to provide a uniform understanding of NIRS measurements across devices.

As well as variation in the parameters measured, the measurement time period varies from paper to paper. Some studies have continuous monitoring lasting for several days whereas others use acquisitions of less than a minute per measurement. Short measurement times reduce the possibility of movement artefacts; NIRS systems have intrinsic problems with movement and ambient light artefacts due to their high sensitivity [172]. Movement of the head or optodes cause changes in the light coupling to the tissue, and high ambient light intensity levels can reach the photodetectors. Long studies lasting several hours have the advantage of recording data over different stages of care and can look at specific events occurring in that time; however the data quality may be restricted. The Centre for Biomedical Imaging at Massachusetts General Hospital (MGH) uses multiple optical methods, such as frequency-domain NIRS with diffuse correlation spectroscopy (DCS), to give a measure of the cerebral metabolic rate of oxygen ($CMRO_2$) [156, 173, 174]. Studies from MGH ([146, 156, 173–176]) monitor short periods of time (10-16 seconds), whereas other studies ([147, 148]) record continuously over several hours. While the short monitoring periods are not likely to be subject to optical drift or movement artefacts, the short monitoring period may miss vital events which change the physiological status.

NIRS is used in conjunction with MR scanning in two papers: Massaro et al. correlate NIRS data with CBF measured by ASL-MRI [147], Wintermark et al. found a correlation between the NIRS and MRI measured markers of CBF [148]; and both studies found a lower CBF in patients with HIE. Massaro et al. also saw a lower tissue oxygenation fraction in the infants with long term injuries as measured by MRI.

Two studies have investigated the variation in NIRS measured signals with respect to the position of

the infant. Lin et al. [173] found hemispheric asymmetry was not influenced by the side of presentation (the side that infant was lying on, left or right). Bembich et al. [177] determined that the prone position gave a higher CBF than the supine position. These results are vital for ensuring proper design of experiments and comparison between studies.

3.4 Summary

NIRS is a non-invasive monitor of brain haemodynamics and oxygenation that can be performed at the patient bedside. The use of NIRS in neonatal medicine research has increased in recent years, particularly in the measurement of cerebral oxygenation, although the heterogeneity between different instrument measurements has prevented the technique entering routine clinical practice [170]. Broadband NIRS has the ability to monitor changes in the redox state of CCO which can give a complimentary measurement of metabolic activity. This thesis describes the investigation of broadband NIRS-monitored CCO in neonatal brain injury and its potential to give clinical insight.

Chapter 4

Review of Clinical NIRS Measurements of Cerebral Cytochrome-C-Oxidase

NIRS measurements of cytochrome-c-oxidase have the potential to yield crucial information about cerebral metabolism at the patient bedside. Developments in instrumentation and the analytical methods used to resolve changes in CCO have led to many novel clinical applications of the measurement since its first demonstration in 1977 by Jobsis [110]. There is a substantial literature of work on measures of CCO in animal and in-vitro studies, however this chapter focusses on translational studies. Almost forty years from the advent of the first measurement of CCO using NIRS, this signal continues to hold significant interest in our understanding of the human brain in health and disease. This chapter discusses methodologies for obtaining NIRS measurements of CCO in the clinic and reviews studies in neonates and adults.

4.1 Introduction

A patient's health is in great danger when there is a prolonged lack of oxygen delivery that is insufficient to meet the metabolic demand of the tissue; for example in traumatic brain injury (TBI) where derangements of cerebral oxygen delivery and utilisation often occur, rendering the brain susceptible to secondary, or additional, injury processes. Secondary injury can also occur in neonatal encephalopathy, secondary to perinatal hypoxia-ischaemia. Clinicians currently cannot monitor the biochemical status of the injured brain continuously and non-invasively at the patient bedside. There is an urgent need for real time in-vivo measurements of brain tissue oxygenation and biochemistry in the clinic; as well as a bedside sensor of brain tissue cellular oxygen utilisation that can improve diagnostic information.

Since 1977, when Franz Jobsis reported a new optical method in a seminal Science article [110], near-infrared spectroscopy has been seen as the technique which could deliver a solution to this clinical

need. NIRS was to become an established research and clinical tool for measuring changes in cerebral oxygenation, in particular changes in oxygenated and deoxygenated haemoglobin (HbO_2 and HHb) concentration. However, Jobsis's intention was to develop an optical technique to measure in-vivo changes in CCO, an enzyme in the mitochondria, and hence monitor tissue metabolism. Jobsis discovered that near-infrared light penetrates deep into living tissue and this optical window could be used to monitor changes in the concentrations of absorbing compounds inside the tissue.

There has been a significant amount of work on measuring haemoglobin concentration changes with NIRS since 1977 (see the recent reviews by Wolf et al. [135] and Scholkmann et al. [6]). A typical commercially available NIRS system is a non-invasive, inexpensive, portable, bedside monitor that can measure, at multiple sites, the changes in HbO_2 and HHb, and from those derive estimations of changes in oxygen delivery (via haemoglobin difference, HbD) and changes in total blood volume (via total haemoglobin, HbT). In addition, from technical developments in the late 1990s, we now have clinical NIRS cerebral oximeters that measure absolute tissue saturation using techniques such as spatially resolved spectroscopy [117, 133]. However, these measurements do not monitor metabolism at a cellular level unlike a measurement of the redox state of CCO, which has the potential to yield an in-vivo indication of cellular energy metabolism. Simultaneous measurement of the CCO signal and haemoglobin signals can therefore provide complimentary information on haemodynamics, oxygenation and metabolism. Monitoring of CCO with NIRS has been shown to be consistent with other measures of metabolism; including those from more invasive techniques, such as microdialysis in humans [52], or more expensive and less portable techniques, such as MRS in animal studies [12, 66, 178, 179]. Furthermore, the concentration of CCO is much higher in the brain than in extracerebral tissues, so it is a more brain-specific signal that is hence less prone to scalp and skull contamination than the haemoglobin signals [60, 61].

Pre-clinical and in-vitro studies have contributed enormously to the understanding of the optical issues surrounding the NIRS measurement of CCO, its role as marker of cellular metabolism, and its potential as a clinically relevant measure. This was a focus for several research groups in the 1980s and 1990s [180–186]. More recently, from the Multimodal Spectroscopy Group and Institute for Women's Health collaboration here at UCL, a study in a piglet model of HI brain injury has demonstrated the specificity of the broadband NIRS-measured oxCCO signal as a marker of tissue metabolism [12]. In this study the percentage recovery of CCO after HI to baseline levels was highly correlated with percentage recovery of phosphorus (^{31}P) MRS measures of cellular metabolism (see Figure 4.1). Furthermore, this study demonstrates the potential for CCO measures to identify outcome after injury. However, in this chapter the focus is on the translational clinical and human cerebral studies that have been ongoing since 1985 [16].

Figure 4.2 shows how the number of publications on, and the populations studied by, NIRS-measured CCO has varied over the years. Between 1977 and 1997, there was a gradual increase in the number of papers published, varying in subject and research group (Duke University, University College London (UCL), Hokkaido University, Sapporo and Keele University were home to the main groups involved). After 1997, the interest in the CCO measurement gradually declined due to both some controversy over

the optical instrumentation, methods and algorithms used to resolve it [49], and a shift of clinical interest due to the emergence of the absolute tissue saturation measurement with NIRS [117]. In the 2000s, efforts were made to optimise NIRS instrumentation and methods specifically for the measurement of CCO [62, 187] and studies were performed in healthy volunteers and patients to characterised the behaviour of the CCO signal as a marker of cerebral cellular oxygen metabolism [52, 60]. A resurgence in the number of papers published over the last few years reflects the continued clinical desire for in-vivo measures of metabolism and a renewed interest in the CCO signal following the demonstration of new technological and analytical methods.

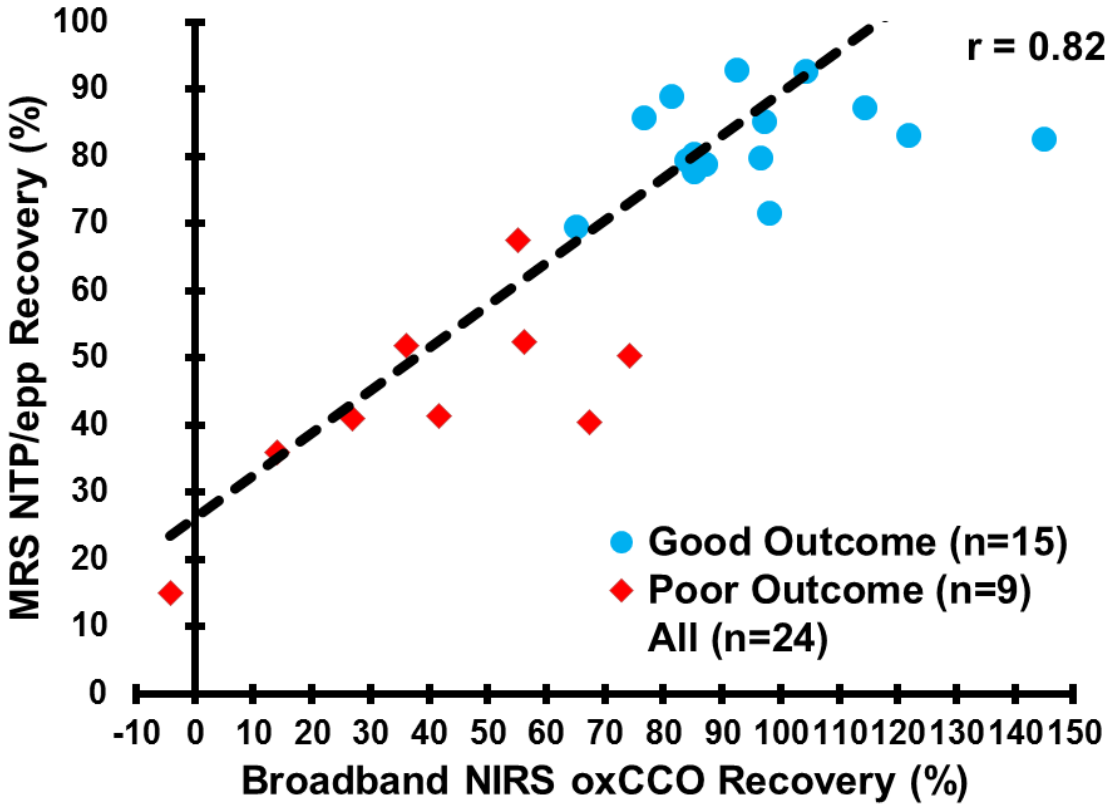

Figure 4.1: Measured changes in the oxidation state of CCO (oxCCO) following HI in a piglet model. Each data point represents the recovery fraction of the broadband NIRS oxCCO signal and the ^{31}P MRS NTP/epp (a surrogate marker of ATP). The broadband oxCCO measurements show a strong association (Pearson correlation, r = 0.82) with the MRS metabolic measurements and provide a good indication of outcome (good outcome refers to piglets that survived for more than 24h following HI). The figure has been produced from data presented by Bainbridge et al. [12].

The focus in this chapter is on measurements in patients and healthy volunteers, however in order to fully understand the chronology and advances made in the methodology, some important pre-clinical work is also discussed. While there is extensive work on the measurement of CCO changes in the visual part of the light spectrum (see the review by LaManna for a historical perspective [188]); here I have

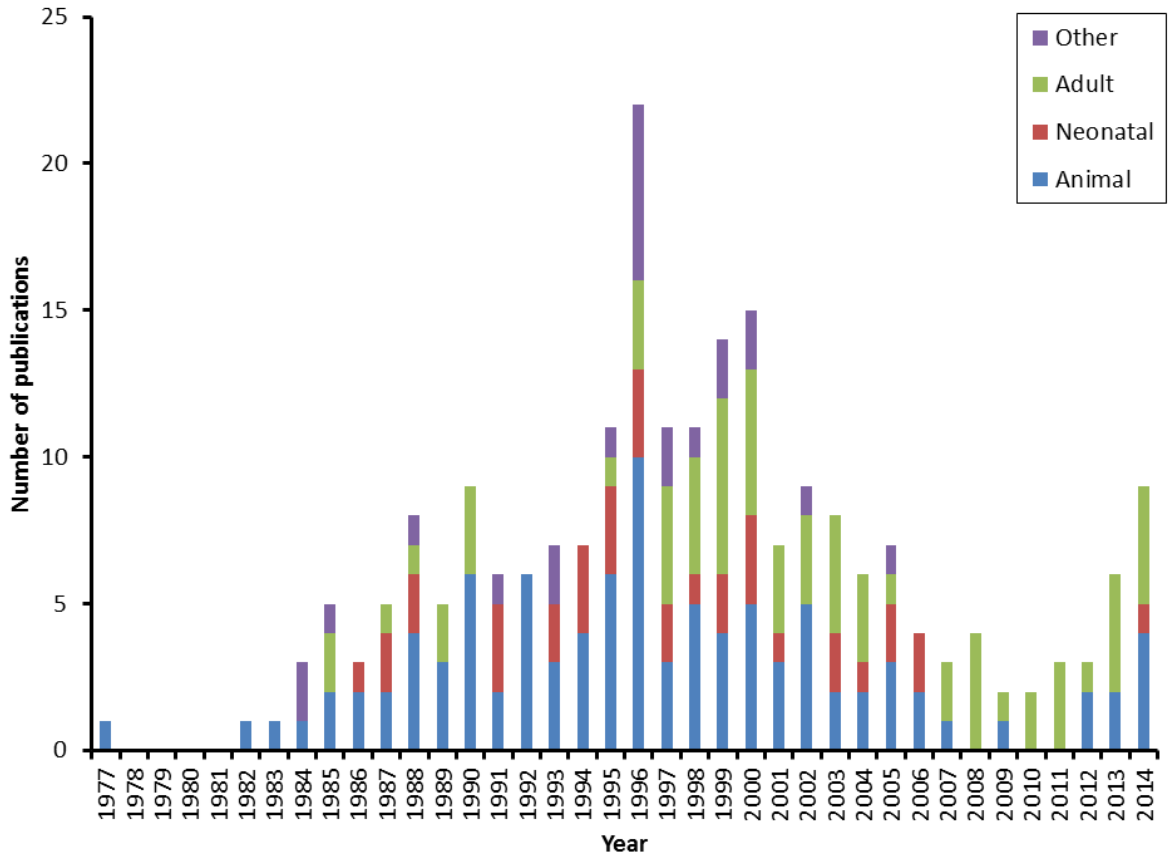

Figure 4.2: Number of papers published per year on the subject of cerebral NIRS measurements of CCO. The data were taken from the PubMed results for 'cytochrome oxidase infrared spectroscopy brain' (with the addition of the 1977 Jobsis paper). There are a total of 223 papers split into categories based on the subject: adults 67 papers (green), neonates 36 papers (red), animals 98 papers (blue) and other 23 papers (purple, including reviews of the subject, in-vitro work and computational simulations).

focused on the measurements with near-infrared light (650-1000nm). This chapter provides a description of the biochemistry of the enzyme to understand the origins of the optical signal; the methods, algorithms and instrumentation used to study it; a discussion of the issues with the methodology; a summary of the applications of cerebral NIRS measurements of CCO in neonatal and adult studies; and a forward perspective on the future of the technique. Almost forty years from the advent of the first measurement of CCO using NIRS, this signal continues to hold significant interest in the understanding of the human brain in health and disease.

Note

This Chapter has been modified and presented as a review article which has recently been published in the Journal of Biomedical Optics.

4.2 Biochemistry and Spectral Features of Cytochrome-C-Oxidase

In order to fully understand the CCO NIRS signal, one must understand the biochemistry from which the signal stems. CCO is a small but important part of the aerobic metabolism of glucose. Glycolysis converts glucose into pyruvate and in the process generates ATP and NADH. After glycolysis, pyruvate is transported into the mitochondria and converted to acetyl CoA, which then enters the tricarboxylic acid (TCA) cycle. During the TCA cycle additional ATP and NADH are produced. NADH is an electron donor; electrons from NADH can be used to, ultimately, convert oxygen to water, releasing useful chemical free energy in the process. The mitochondrial electron transfer chain (ETC) mediates this transfer, in the process converting ADP to ATP. The consequent change in ATP/ADP ratio provides usable energy to drive a wide variety of cellular processes.

Figure 2.7 (in Chapter 2.3) shows the mitochondrial protein complexes involved in this oxidative phosphorylation. Oxidative phosphorylation is the process where energy is harnessed through a series of protein complexes (known as complexes I V) embedded in the inner-membrane of mitochondria to create ATP. Oxidative phosphorylation can be broken down into two parts: oxidation of NADH (and other electron donors) in the ETC via complexes I - IV, and phosphorylation, the production of ATP, at complex V. Complex I accepts electrons from NADH and transfers them to the soluble membrane-bound electron carrier ubiquinol (Q), producing ubiquinone (QH_2). QH_2 is oxidised by complex III, in the process reducing the soluble electron transport protein, cytochrome c. Cytochrome c is then oxidised by the terminal electron acceptor cytochrome-c-oxidase (also known as complex IV), the electrons ultimately being used to reduce oxygen to water. The redox potential drop in the electron transfer processes in complex I, III and IV is converted to a proton electrochemical potential, which ultimately drives mitochondrial ATP synthesis via the mitochondrial ATP synthase (sometimes known as complex V).

The transfer of electrons within the mitochondrial ETC complexes occurs via a number of protein bound redox factors. Of particular interest in this literature review, CCO contains 4 redox centres: 2 haems (known collectively as aa3) and 2 copper sites. The electrons pass between these centres in a series of redox reactions. All of these redox changes have associated optical transitions. In the NIR region one of the copper sites, the Cu-Cu dimer copper A (CuA), dominates the absorption spectrum, with a strong peak in the oxidised form centred - in mammalian enzymes - around 830-840nm (see Figure 4.3). For a recent detailed discussion of the relative contributions of CCO chromophores to the NIR spectrum see [189] and references therein.

The difference between these absorption spectra (oxidised-reduced CCO) can be used to monitor changes in the redox states of the mitochondrial proteins. Note that the total cytochrome-c-oxidase concentration does not change over a short time period (hours), therefore for analytical purposes, it is only necessary to use the difference spectrum between the oxidised and reduced species to obtain an indicator of the changes in the CCO redox state.

The UCL group has shown that using the oxidised-reduced difference spectrum resolves changes in oxidised CCO (and conversely, using the reduced-oxidised difference spectrum resolves changes in reduced CCO). The proof uses the modified Beer-Lambert law and involves two scenarios. In Scenario

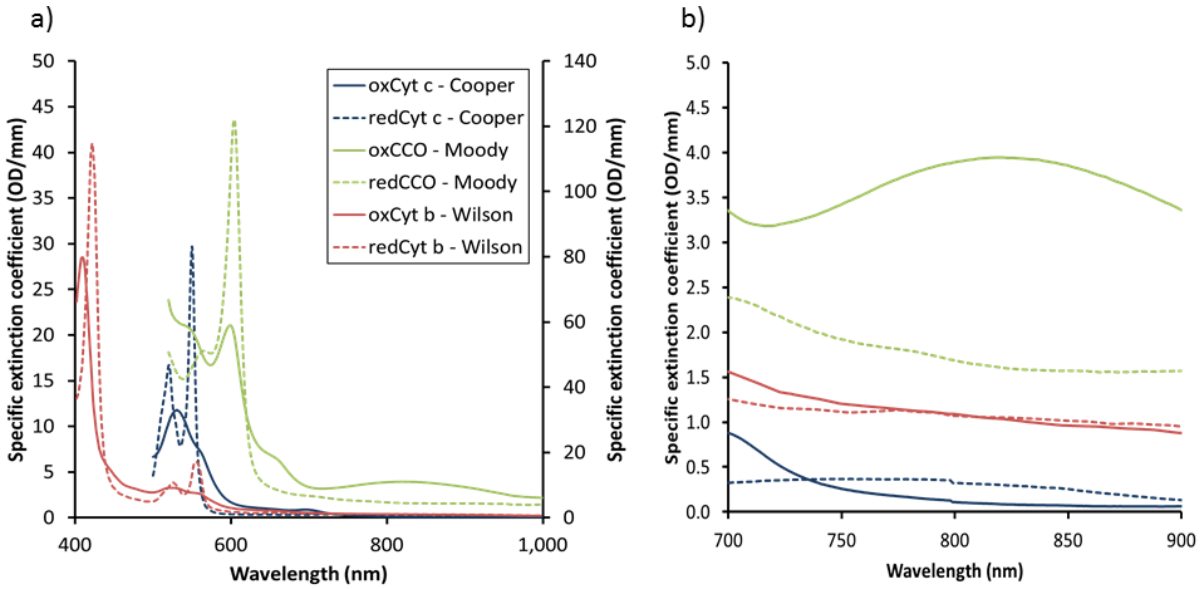

Figure 4.3: The extinction spectra of the absorbing cytochromes in the electron transport chain in the visible and NIR. a) Displayed between 400-1000nm, note that the cytochrome b spectra are plotted on a secondary axis, and b) zoomed into the near-infrared region of 700-900nm. Oxidised and reduced spectra of cytochrome c (oxCyt c and redCyt c respectively) measured by Chris Cooper at the University of Essex in the porcine heart. Oxidised and reduced spectra of CCO (oxCCO and redCCO) measured by John Moody at the University of Plymouth in the bovine heart. Oxidised and reduced spectra of cytochrome b (oxCyt b and redCyt b) measured by Mike Wilson at the University of Essex. All data were taken from the UCL Biomedical Optics Research Laboratory (BORL) website: http://www.ucl.ac.uk/medphys/research/borl/intro/spectra

1 (equations 4.1 - 4.5), CCO is fully oxidised (ox) at the initial time (t_0) and so the Beer-Lambert law states the attenuation (A) due to CCO is related only to the concentration (c) of oxidised CCO, its extinction coefficient (ϵ) and the optical pathlength of light (l):

$$A(t_0) = l \cdot \epsilon_{oxCCO} \cdot c_{oxCCO}(t_0). \tag{4.1}$$

At a later time (t_1) CCO is not fully oxidised so the attenuation is related to both oxidised and reduced (red) forms of the enzyme:

$$A(t_1) = l \cdot [\epsilon_{oxCCO} \cdot c_{oxCCO}(t_1) + \epsilon_{redCCO} \cdot c_{redCCO}(t_1)]. \tag{4.2}$$

Assuming that the total CCO concentration does not change, the initial concentration of fully oxidised CCO is equal to the sum of the oxidised and reduced forms at the later time:

$$c_{oxCCO}(t_0) = c_{oxCCO}(t_1) + c_{redCCO}(t_1). \tag{4.3}$$

Therefore it is possible to substitute the equations above into the difference measurement of the attenuation:

$$\begin{aligned}\Delta A &= A(t_1) - A(t_0) \\ &= l \cdot [\epsilon_{oxCCO} \cdot (c_{oxCCO}(t_1) - c_{oxCCO}(t_0)) + \epsilon_{redCCO} \cdot c_{redCCO}(t_1)] \\ &= l \cdot [\epsilon_{oxCCO} \cdot (c_{oxCCO}(t_1) - c_{oxCCO}(t_0)) + \epsilon_{redCCO}(c_{oxCCO}(t_1) - c_{oxCCO}(t_0))] \\ &= l \cdot (\epsilon_{oxCCO} - \epsilon_{redCCO})\Delta c_{oxCCO}.\end{aligned} \tag{4.4}$$

The oxidised-reduced difference ($diff$) extinction spectrum ($\epsilon_{diffCCO} = \epsilon_{oxCCO} - \epsilon_{redCCO}$) gives rise to equation 4.5, which expresses the change in attenuation due to a change in the concentration of oxidised CCO from the difference extinction spectra:

$$\Delta A = l \cdot \epsilon_{diff} \cdot \Delta c_{oxCCO}. \tag{4.5}$$

In a Scenario 2 (equations 4.6 - 4.10) where CCO is not fully oxidised initially (i.e. CCO exists in both oxidised and reduced forms), the same expression can be achieved. The initial and later equations are:

$$A(t_0) = l \cdot [\epsilon_{oxCCO} \cdot c_{oxCCO}(t_0) + \epsilon_{redCCO} \cdot c_{redCCO}(t_0)]. \tag{4.6}$$

$$A(t_1) = l \cdot [\epsilon_{oxCCO} \cdot c_{oxCCO}(t_1) + \epsilon_{redCCO} \cdot c_{redCCO}(t_1)]. \tag{4.7}$$

Assuming again that the total CCO concentration does not change:

$$c_{oxCCO}(t_0) + c_{redCCO}(t_0) = c_{oxCCO}(t_1) + c_{redCCO}(t_1). \tag{4.8}$$

Therefore:

$$\begin{aligned}\Delta A &= A(t_1) - A(t_0) \\ &= l \cdot [\epsilon_{oxCCO} \cdot (c_{oxCCO}(t_1) - c_{oxCCO}(t_0)) + \epsilon_{redCCO} \cdot (c_{redCCO}(t_1) - c_{redCCO}(t_0))] \\ &= l \cdot [\epsilon_{oxCCO} \cdot (c_{oxCCO}(t_1) - c_{oxCCO}(t_0)) + \epsilon_{redCCO}(c_{oxCCO}(t_1) - c_{oxCCO}(t_0))] \\ &= l \cdot (\epsilon_{oxCCO} - \epsilon_{redCCO})\Delta c_{oxCCO}\end{aligned} \tag{4.9}$$

which gives rise to the same expression as equation4.5:

$$\Delta A = l \cdot \epsilon_{diff} \cdot \Delta c_{oxCCO}. \tag{4.10}$$

These proofs show that the oxidised-reduced difference spectrum can be used to resolve changes in the concentration of oxidised CCO. An increase in the oxCCO signal therefore reports an increase in oxidised

CCO and an equivalent decrease in reduced CCO. Note that if the sign of the measured signal is changed it represents reduced CCO not oxidised CCO. The oxCCO term does not imply that we are only sensitive to the oxidised species. Nevertheless oxCCO is the term used to describe the measured changes from the difference spectra in this thesis.

To understand what a change in oxCCO means physiologically we need to know what the concentration of oxidised and reduced CCO is dependent on and how it can be affected in-vivo. The redox state is dependent on both the availability of oxygen in the cells and the supply of electrons entering the ETC. The review by Cooper and colleagues [190] gives an overview of the influencing factors on the CCO redox state. In the purified isolated enzyme these include changes in the 3 substrates (protons (pH), reduced cytochrome c, and oxygen tension), as well as a range of terminal inhibitors (such as nitric oxide and cyanide) and electrochemical potential. The complex interplay between these factors in the mitochondrial ETC has been investigated mathematically by Banaji [191]. This informs on clinical in-vivo measurements. Possible factors that might increase oxCCO in-vivo include: increase in oxygen tension, increased ATP turnover, decrease in proton electrochemical gradient, decrease in pH, or decrease in supply of reducing equivalents (substrates i.e. NADH) to the ETC, these factors have been discussed by Heekeren and colleagues [56].

The oxCCO concentration can readily be decreased in animal models, either by large drops in oxygen tension or the addition of inhibitors that act at the oxygen reduction site [181]. There have, though, been questions regarding how easy it is to increase the oxCCO signal in-vivo, but animal models have shown that there is the capacity to increase the oxidation state at normoxia [182, 192] as well as adult volunteer studies in hyperoxia and hypercapnia [60, 193], and functional activation [56, 61]. I acknowledge that there are some differences in the CCO response between the pre-clinical and clinical work, in particular when compared to results from non-anaesthetised human adults; it is not the intention in this chapter to discuss those physiological differences.

The CCO concentration in the brain is likely to change with maturity. Rodent studies have shown that there is an increase in the number of mitochondria per cell, as well as an increase in mitochondrial proteins and respiratory enzymes per mitochondrion in the first postnatal days [194]. Additionally there is a difference in energy metabolism and functional activity in the rodent brain during postnatal development compared with the adult, and so this must be taken into consideration when monitoring CCO with NIRS.

4.3 Methods of Cytochrome-C-Oxidase Measurements

CCO is one of the most abundant enzymes in mammalian systems. However, its relatively low concentration compared to the haemoglobin chromophores presents some challenges for NIRS techniques. The absolute concentration of CCO in the human brain is unknown, but optical methods have obtained values of 5.5 and 4.5 μ M in the adult rat [195, 196]. This should be considered an upper limit for the human CCO concentration as rats have a significantly higher cerebral metabolic rate of oxygen than humans [190]. The contribution of CCO to overall absorption in tissue is considerably less than that

of haemoglobin because of its lower concentration, despite a higher specific extinction spectrum in the NIR region. Although the detectable absolute concentrations may vary with species, age and optical set-up, it is clear that the overall maximal signal from CCO should be 5-10% of that from haemoglobin. Therefore light attenuation changes due to CCO can easily be masked by the much larger attenuation changes due to HbO_2 and HHb; this can result in cross-talk. I define cross-talk as a genuine change in one chromophore concentration inducing a spurious measured concentration change in another. Specific instrumentation and algorithms are necessary to be able to resolve these concentration changes without cross-talk; cross-talk is discussed later in this section and 4.4.

The principles of NIRS (only CW is considered here) are based on calculating changes in concentration from the changes in the measured light attenuation in tissue. In order to do this, an algorithm and instrumentation must be chosen, along with the selection of other variables such as the pathlength that the light has travelled, the absorption spectrum of the chromophore, and a set of measurement wavelengths. It is important that the algorithm and the other variables do not unknowingly induce artefacts. The factors that make up the algorithm and its variables have been the subject of discussion for many years. The choices to be made are:

- The algorithm
- The determination of the chromophore absorption spectra
- How the optical pathlength is estimated
- The number and choice of wavelengths

Calculating and validating changes in haemoglobin in both of its oxygenation states is simpler because its concentration in tissue is high. It is also relatively simple to isolate the molecule to produce an absorption spectra in-vitro. The absorption spectra have defined features in the near-infrared (see Figure 4.4) such as a peak at 750-760nm in HHb and the isosbestic point at 800nm. The CCO difference absorption spectrum, once identified, has a broad peak which is significantly different to that of the haemoglobin chromophores. However, the broad nature of the three chromophore peaks throughout the NIR region confounds simple deconvolution via standard optical techniques such as dual wavelength or derivative spectroscopy. Therefore to successfully separate the CCO signal from the larger haemoglobin signals requires careful selection of the algorithm, wavelengths and extinction spectra used. One of the biggest problems for the oxCCO signal is that there is no gold standard with which to compare and validate the NIRS signal experimentally. Although, the same problem exists for NIRS detectable haemoglobins, in this case there are at least invasive measurements that can be assumed to report on similar parameters (such as tissue oxygen, blood volume and arterial/venous oxygen saturation). This lack of external comparators is a problem in assessing which criteria produce the most physiologically accurate oxCCO signal. Yet, there have been a range of in-vitro and in-vivo controlled studies that inform on the success of the optical separation of the cellular oxCCO signal from changes in the haemoglobin signals. Additionally, integrated mathematical models of the biochemistry and physiology can aid the interpretation of results [197–199].

4.3.1 Algorithm

Various algorithms have been developed by different groups, and these were assessed and described fully in 1995 by Matcher et al. [48]. The algorithms can be reduced to those developed at Duke University (Duke), University College London (UCL), Hokkaido University, Sapporo (Sapporo) and Keele University (Keele).

The UCL algorithm is a generalised algorithm based on the modified Beer-Lambert law and the concentrations are derived using multilinear regression [113]. The modified Beer-Lambert law forms the mathematical basis of spectroscopic algorithms that relate wavelength-dependent optical attenuation signals to changes in chromophore concentrations. The generalised form of this algorithm for n wavelengths (termed UCLn) is equation 3.25 [48].

The algorithm assumes that tissue scattering and pathlength remain constant throughout the measurement period and is therefore suitable for all geometries and optical systems. It ignores, however, the multiple scattering effects including the non-linear relationship between absorption and attenuation [7], this is discussed later in section 4.3.3. A three wavelength version of this algorithm was also developed by researchers at Keele using different extinction spectra [200].

The algorithm developed in Sapporo is a four wavelength algorithm which uses attenuation differences between three measuring wavelengths and a fourth reference wavelength [201]. The reference wavelength was selected in a region in which, the authors claim, has zero attenuation from CCO. The algorithm was developed specifically for the intact rat head through a vertical plane from the roof of the mouth to the top of the skull and the coefficients used (not shown here but presented in [48, 202]) contain optical instrumentation factors so are only specific to one instrument. Their algorithm does not attempt to quantify the concentration changes in haemoglobins and oxCCO and thus measurements are expressed in relative terms [202]. The authors claim their algorithm to be robust to changes in scattering and optical pathlength changes during the measurement period [202].

The Duke algorithm uses 4 wavelengths and specific extinction spectra determined in-vivo from the intact cat brain to determine concentration changes [203]. The algorithm is not displayed here but can be found in [48] where it is also discussed.

4.3.2 Chromophore Absorption Spectra

The difference between the oxidised and reduced form of CCO can be determined in many different environments such as the isolated enzyme, in mitochondria and in-vivo. The first NIRS measurement used difference spectra that were taken through animal heads during anoxic challenges [110]. These spectra showed clear differences between oxidised and reduced CCO states. Later authors replaced blood with optically clear oxygen carrying perflurocarbon solutions in an attempt to produce haemoglobin free CCO spectra [183, 186, 204]. In addition, later studies were able to remove this contribution completely in rats [205, 206], cats [207], and piglets [181].

The use of perflurocarbon perfused blood-free animals has been key to the development of algorithms to detect oxCCO. In some cases these spectra were themselves used to generate the algorithms; in others

they were used to validate the use of in-vitro spectra. The latter was the case for the UCL algorithms.

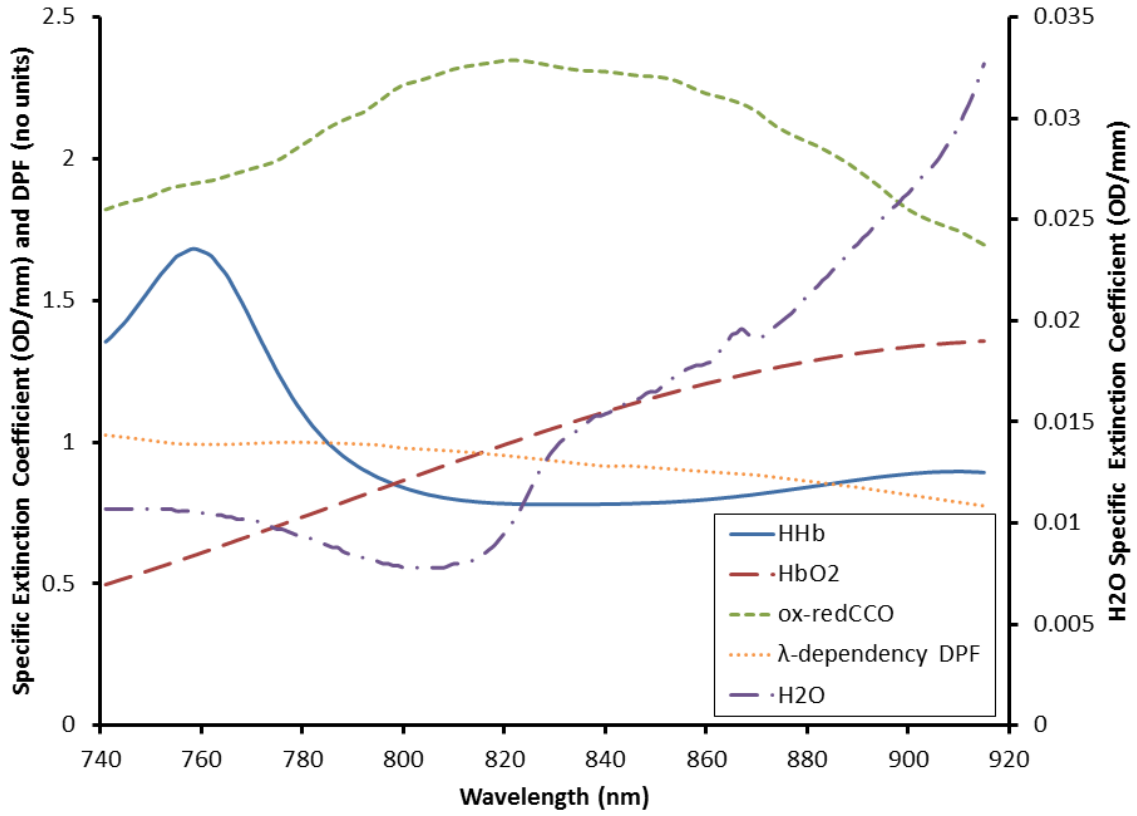

Figure 4.4: Specific extinction coefficients measured by Mark Cope (Cope 1991). The ox-redCCO spectra are not the same as the difference between the CCO spectra presented in Figure 4.3. Data taken from the UCL BORL website: http://www.ucl.ac.uk/medphys/research/borl/intro/spectra

Cope found that there is no appreciable difference between the spectra measured in-vivo and in-vitro [7]. Matcher et al. found similar results when using the 4-wavelength UCL algorithm, which uses in-vitro extinction spectra, and the 3-wavelength Keele algorithm, which uses in-vitro spectra but with whole blood, not purified haemoglobin, to resolve concentration changes from the same attenuation data [48]. Chromophore absorption spectra used at UCL are displayed in Figure 4.4.

4.3.3 Optical Pathlength

The estimation of optical pathlength is the one of the most notable challenges for the calculation of changes in oxCCO as it was thought that erroneous changes resolved in oxCCO (i.e. cross-talk) could be due to pathlength changes causing insufficient chromophore separation [49, 181]. As mentioned earlier in this section (4.3.1) the modified Beer-Lambert law does not account for tissue scattering and assumes that the reduced scattering coefficient (μ_s') is constant throughout a measurement period. The optical pathlength term is the only consideration of scattering in the equation so it must be estimated sufficiently to produce physiologically accurate representations of chromophore changes in-vivo.

The first attempts at optical pathlength estimation assumed a constant pathlength, equal to the product of the distance between the source and detector optodes and the differential pathlength (DPF) factor, an experimentally determined factor to account for the increased pathlength of light due to all forms of scattering [113]. The DPF can be calculated using FD or TR NIRS which estimate the optical pathlength [112–114]. In addition, to monitor the changes in pathlength in real-time with CW NIRS, Matcher and colleagues at UCL developed a method to resolve the pathlength using the water absorption spectrum and the measured broadband attenuation [208]; features in the second differential of the water absorption spectra around 740nm and 820nm can be combined with an assumed concentration of water in the tissue to estimate pathlength.

In 1993, the modified Beer-Lambert law algorithm was updated to account for the wavelength-dependency of the DPF which allowed for the decreasing scattering effects at increasing wavelengths in tissue [115]. DPF varies with wavelength through another attenuation mechanism; high absorption of light at a specific wavelength decreases the likelihood that light at that wavelength will reach the detector.

A few experiments have been set-up specifically to test whether changes in pathlength are responsible for cross-talk in the oxCCO measurement; none of these studies found significant changes in the pathlength during events where changes in oxCCO were observed, such as hypoxemia [52] or functional activation [59, 61]. Skov and Greisen suggest that the wavelength-dependent DPF is a solution to the cross-talk problems; they observed a linear relationship between HbT and oxCCO during hypoxemia when using a constant DPF, but not when using wavelength-dependent DPF [23].

There are physiological factors that will affect tissue scattering. For example, glucose levels affect the refractive index of extracellular fluid which contributes to the reduced scattering coefficient, therefore changes in the glucose concentration may affect the overall scattering of the tissue [209]. Swelling of the brain or oedema, which is common in HIE, is likely to change cerebral scattering properties. There is therefore a need to understand the influence of changing tissue scattering properties on the calculation of chromophore concentrations, or to measure scattering during the measurement period, particularly in cases such as brain injury.

4.3.4 Wavelength Selection

In theory, to extract information for three chromophores requires measurements at three wavelengths. Yet this approach is prone to noise and cross-talk artefacts that may lead to inaccurate quantification of changes in concentrations and misinterpretation of data. When measurements at a larger number of wavelengths are used in spectroscopic algorithms, any detrimental effects of cross-talk and noise are expected to diminish.

Due to the broad spectral peak in the oxidised-reduced CCO spectra and its relatively low concentration in-vivo, the choice of selection of the specific wavelengths and number of wavelengths used for spectroscopy is a big factor. This is also relevant for the haemoglobin chromophores. Matcher et al. [48] performed analysis to assess the separation of the oxCCO signal from the haemoglobin signals with different number of wavelengths (4, 6, and ‘n’ or 112) in a range of data: rat head, piglet head, adult

forearm, and a simulated data set. The results showed that the higher number of wavelengths used produced more accurate simulations, and improved the in-vivo measurements. Despite this, pre-clinical studies showed that limiting broadband measurements to 780-900nm improves the resolution of oxCCO as exclusion of shorter wavelengths lessens the contribution of HHb which has a large peak at 760nm [181]. Figure 4.5 shows graphically the selection of wavelengths used in the clinical papers mentioned in this chapter.

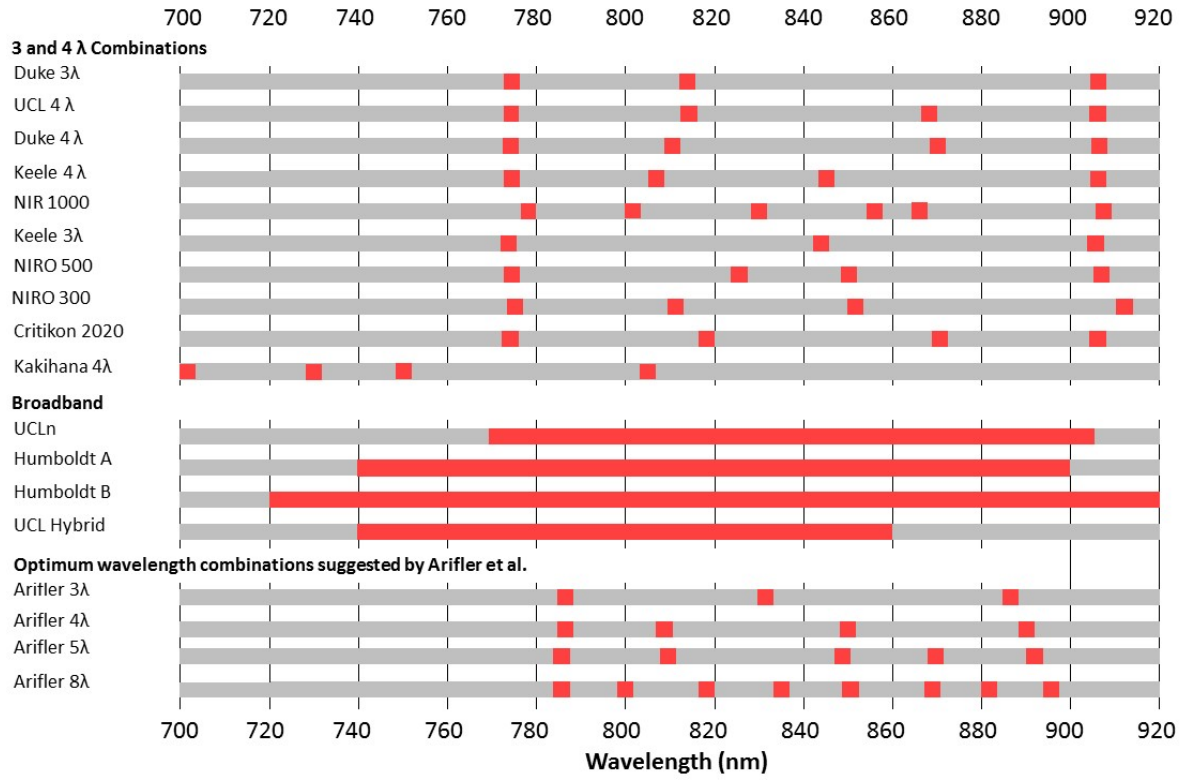

Figure 4.5: Chart of wavelengths used in NIRS systems from all clinical publications mentioned in this chapter. Systems are listed in chronological order from their first publication in this review and are separated into 3 and 4 wavelength combinations and broadband spectra. The suggested wavelengths determined by Arifler et al. are also shown [13]. Clinical papers using the wavelengths are: Duke 3λ [14–16], UCL 4λ [17], Duke 4λ [18–20], Keele 4λ [21–24], NIR 1000 [25–28], Keele 3λ [29, 30], NIRO 500 [31–38], NIRO 300 [39–46], Critikon 2020 [47], UCLn [48–54], Humboldt A [55, 56], Humboldt B [57, 58], UCL Hybrid [59, 59–62].

Broadband spectroscopy, offering a full range of measurement wavelengths, can be difficult to incorporate into wireless and multi-channel systems. A recent study has used a genetic algorithm method to assess the minimum number of wavelengths needed to resolve oxCCO accurately (compared to the current gold-standard of a broadband NIRS system across 780-900nm at 1nm wavelength resolution) [13, 210]. The results show that the optimal combination of wavelengths is a set that almost evenly spans the spectral range (see Figure 4.5). The error against the gold-standard reduces as number of wavelengths increases; increasing to 4, 5 and 8 wavelengths from 3 wavelengths leads to a 2-, 3- and 7-fold improvement in the reduction of errors. The wavelengths selected need to be spread across this

range in order to resolve the shape of the ox-redCCO spectra and disentangle it from the other chromophores; Arifler et al. found that the optimum 8 wavelengths were 784, 800, 818, 835, 851, 868, 881 and 894nm (displayed in Figure 4.5).

4.3.5 Optical Instrumentation

Advances in optical systems have allowed further development of the instrumentation, as well as the algorithm, which have contributed to the increased robustness of the measured oxCCO signal with NIRS.

Initially, NIRS instrumentation for the measurement of oxCCO was performed using 3 or 4 narrowband lasers at specific wavelengths between 740nm and 905nm [16] (see Figure 4.5 for more examples) using a PMT for detection. Commercial systems were developed to measure oxCCO using 4 discrete wavelengths using lasers and either photodiode detectors or PMTs (NIRO 300 and NIRO 500 respectively, Hamamatsu, Japan) [35, 39].

In UCL, systems have increasingly been developed in-house and focused on broadband spectroscopy with the aim of obtaining a more robust oxCCO signal [48], (see section 4.3.1). These systems typically use a broadband white light source (i.e. a tungsten halogen bulb) with a spectrograph and CCD using optical fibres to transmit light both to and from the tissue [12, 54, 65]. The UCL broadband NIRS systems include (i) a broadband instrument developed in the 1990s by Springett and colleagues [65]; (ii) a multi-distance hybrid broadband and FD domain system developed by Tachtsidis and colleagues in 2010 (called Hybrid Optical Spectrometer or pHOS) [62]; and (iii) in 2014 two variations of that system without the FD component developed by Bale and colleagues to be used in neonates (called Cytochrome Research Instrument and appLication or CYRIL) [54] and Phan and colleagues with the capacity to do imaging [63]. All UCL developed systems are broadband instruments with the capacity to apply the UCLn algorithm in real-time and I explicitly mention them in the reported studies below.

Miniaturisation is a trend seen in all forms of technology and NIRS is no exception. The trend towards making devices smaller, more portable and cheaper has pushed broadband spectroscopy towards miniature spectrometers [211] and discrete wavelength systems towards wireless NIRS [212]. For wireless devices, in which there is a need to eliminate heavy fibre optics, LEDs and laser diodes can be applied directly to the head with wireless transmitters to send the data to a nearby computer. Versions of both of these technologies are in development with the aim of incorporating a measurement of oxCCO [213].

In 2000, a combined CW and FD NIRS system was developed to use measurements of μ_s' and μ_a to inform the calculation of absolute chromophore concentrations [214]. This was further developed by UCL to the pHOS system that attempted to measure oxCCO using the UCL hybrid algorithm [62]. These hybrid devices use broadband CW systems and several lasers in the frequency domain (7 [214] and 4 [62] wavelengths) to achieve this. By resolving for both absorption and scattering it may be possible to measure absolute concentrations of the chromophores.

4.4 Analysis of Broadband Cytochrome-C-Oxidase Measurements

Here the clinical experiments that assess the oxCCO signal for robustness and independence from other chromophores (i.e. cross-talk) are discussed. This chapter focusses mainly on clinical papers that use many wavelengths (broadband NIRS) and use the wavelength-dependent DPF, methods which are required to minimised cross-talk. There is a strong weight of evidence against cross-talk if enough wavelengths are utilised.

The simplest way to assess cross-talk is to compare the oxCCO signals with the HbO_2 and HHb, and this has been done in many different experiments. In the assessment of the low frequency oscillations during visual stimuli, there was a phase shift between the haemodynamics and the oxCCO signal [55]. Additionally, the authors noted that the oxCCO recordings were "remarkably stable...compared to the changes in the haemoglobins, making a simple cross-talk rather improbable". Another functional activation study also showed differences in the oxCCO directional changes despite normal haemodynamic response functions [61]. Further, the same study confirmed that there was no relationship between oxCCO and the measured systemic changes. During blood pressure changes in orthostatic hypotension patients, oxCCO dropped despite different HbT directional responses [46]. During spontaneous desaturation events in infants with HIE, different directional changes were seen for oxCCO despite consistent decreases in HbO_2 and increase in HHb [54]. As discussed in the section 4.3.3, in no study where oxCCO and pathlength have been measured simultaneously has a correlation been found between their changes.

Uludag and colleagues found from simulations that incorrect estimation of the wavelength-dependency of partial pathlengths can contribute to cross-talk in chromophores with low concentration [57]. However, when this was investigated experimentally by studies in healthy adult volunteers using the Humboldt B broadband NIRS system they found that the majority of oxCCO changes could not be explained by this effect [187].

Wolf et al. investigated the changes in oxCCO in 22 preterm infants during slow arterial oxygen saturation changes caused by inspired O_2 changes [47]. Changes in the concentrations of HbO_2, HHb and HbT, induced by small and slow O_2 changes, were inversely correlated to the measured changes in the oxidation state of oxCCO with a 4-wavelength Critikon 2020. This is a surprising result and the authors suggest that, although there has been some evidence of oxCCO increases during hypoxia in animal [66, 184], their oxCCO measurement is probably erroneous; the small number of wavelengths used (4) to resolve oxCCO might be the explanation for this.

The most compelling evidence of a unique metabolic signal comes from human studies in which simultaneously measured changes in metabolism have been made using other modalities. Increases in oxCCO during hyperoxia correspond with decreases in microdialysis measures of lactate/pyruvate ratio which is a marker of anaerobic metabolism [52]. Tisdall et al. saw a linear relationship between oxCCO and estimated oxygen delivery (measured via pulse oximetry and TCD ultrasound) during hypoxemia in healthy adult volunteers, this relationship was not seen between HbD and oxygen delivery [50].

Residual analysis enables an observation of the goodness of fit of the chromophore spectra to the measured attenuation. To see if the CCO difference spectrum is necessary to explain the measured

attenuation, 2- and 3-chromophore fits can be performed with and without CCO. Heekeren et al. found that using the 3-chromophore fit explains in-vivo data better than the 2-component [56]. The residuals for 2-component fit have the same shape as oxCCO which suggests that a chromophore with a similar shape to oxCCO is needed to fully explain the spectra. Above 760nm, the 3-component fit residuals were random. This result was also found in other broadband adult studies [53, 61] and a neonatal study [54].

4.5 Neonatal Studies

In this section NIRS measures of oxCCO in neonates are reviewed in different clinical environments: during spontaneous changes in systemic physiology (e.g. periods of hypoxia, increases in blood pressure, etc.), during surgery, with neonatal drug administration, and during functional activation.

4.5.1 Hypoxia and Other Spontaneous Systemic Changes

In 1985 Jobsis's group published the first NIRS study on newborn infants [16]. They observed a decrease in oxCCO during spontaneous oxygen desaturations in three preterm infants using the Duke 3-wavelength system. Further, the timing and magnitude of the oxCCO decrease depended on the preceding oxygenation state, the depth and length of desaturation event and presence of circulatory disorder. Another study in which eight preterm infants were monitored with the NIRO 1000 (Hamamatsu, Japan) showed that small SpO_2 changes did not alter oxCCO [70]. To add to the heterogeneity of the oxCCO response, Wickramasinghe et al. saw an inconsistent (increases and decreases) and insignificant change in oxCCO in seven infants during the reduction of inspired oxygen fraction (FiO_2) (SpO_2 change $\sim$10%) using a 3-wavelength Keele system [215]. A study of infants during repetitive apnoeas found a consistent trend of reduced oxCCO during the breathing cycle [33]. More recently, a UCL broadband NIRS study (with CYRIL) of over 200 oxygen desaturation events in six term infants with HIE saw changes in the concentration of oxCCO in both directions, but with a decrease in oxCCO on average [54]. The heterogeneous response to these hypoxias may be a reflection of the level of brain injury, prematurity, previous oxygenation levels or influence of systemic pathophysiology. Animal work during anoxic swings in piglets has shown that as the oxygen delivery rate is reduced, there is a linear decrease in HbO_2, but a biphasic elbow in oxCCO reduction [65]. A reduction in oxCCO may be a signal of impending damage, and this has also been previously suggested by Cooper et al. [190]. The heterogeneity of the oxCCO response to hypoxia has also been seen in a piglet study of increasingly severe episodes of hypoxia [66]. At lower severities of hypoxia (8 and 12% FiO_2) there were small increases in oxCCO while at higher degrees of hypoxia (6, 4 and 0% FiO_2) oxCCO decreased with severity; consistent decreases in HbO_2 and corresponding increase in HHb were observed in all hypoxic episodes. In 1985, Brazy called for an investigation into the degree of CCO reduction that causes brain injury in order to protect those at risk of injury [16], thirty years later there is still no answer but there is renewed effort to find it [54].

Following from the hypoxia work, the effect of respiratory changes, which cause a subsequent change in $PaCO_2$, on the cerebral metabolism was investigated in neonates. The 1985 infant study from Brazy et al. saw oxCCO increase during hyperventilation; this was the first human study to suggest that oxCCO

is not maximally oxidised in-vivo at normoxia and can be increased by hyperventilation [16]. The ability to increase oxCCO from normoxia is supported by another investigation where an increase in oxCCO was observed during an increase in $PaCO_2$ [24]. Edwards et al. suggest that the strong relationship between $PaCO_2$ and oxCCO is either due to cerebral haemodynamic changes caused by vasodilation due to CO_2, or CO_2 decreasing the pH in cells [70]. However, not all studies have seen this strong correlation; a study of $PaCO_2$ changes in 24 ventilated preterm infants observed changes in cerebral blood flow and volume, but not in oxCCO (4-wavelength Keele NIRS system) [24]. Brazy et al. reported the effects of crying on oxCCO and found different responses when lung disease was present and at different ages of infant [15]. An insignificant small decrease was observed in oxCCO during endotracheal suctioning of 15 preterm infants in the presence of marked decrease in HbO_2 and increase in HHb, monitored with the NIRO 500 [35].

Another early NIRS experiment examined changes in oxCCO during alterations in mean arterial blood pressure [14]. This study showed that increases in MABP were accompanied by increases in HbT and HHb, and a decrease in oxCCO as measured by a 3-wavelength Duke system. Infants whose clinical condition did not improve over the study duration showed larger changes in HbT and oxCCO. This area has potential for further investigation, especially in terms of cerebral autoregulatory effects on tissue metabolism.

The effects of changing intracranial pressure (ICP) was investigated during lumbar puncture [28] in six infants with posthaemorrhagic ventricular dilation with the NIR 1000: three infants had an increase in ICP which was accompanied by an increase in oxCCO, the other three had no change in either ICP nor oxCCO: this is the only study to link oxCCO to ICP. In a 2004 study of 12 infants with intraventricular haemorrhage (IVH), removal of CSF which is expected to cause a reduction of ICP, did not produce a change in oxCCO measured with the NIRO 500 [36].

4.5.2 Surgery and Anaesthesia

Concern for cerebral health during major surgery such as cardiopulmonary bypass (CPB) brought the introduction of NIRS to the operating room. The first use of oxCCO monitoring during neonatal surgery was to monitor cerebral metabolism throughout cardiac surgery. In 1991, 15 children were monitored during CPB at Duke with a 4-wavelength system [18] and a decrease of oxCCO was observed at onset of bypass with hypothermia and reduced further when rewarming began. In 1995, 63 infants were monitored during CPB and hypothermia, and interestingly oxCCO decreases were observed despite HbO_2 increases measured by the NIRO 500 [38]. Recovery of oxCCO was delayed despite HbO_2 recovery to above baseline levels. Larger and more rapid decreases were seen in oxCCO in older (>14 days) infants and those infants had worse recovery. The divergence in intravascular and mitochondrial oxygenation suggest an abnormal response, which the authors suggested could be due to: hypothermic temperature, effects of pH on the ETC, a disturbance in oxygen delivery to the mitochondria, disturbed perfusion, or decreased HbO_2 dissociation. The delay in recovery suggests mitochondrial dysfunction. Changes in haemodynamics and oxCCO measured by a 4-wavelength Keele system were seen in 5 out of 14 children who were hypoxemic during cardiopulmonary bypass for congenital heart disease [23]. Some recent studies with the NIRO 300

during repair of coarctation of aorta (without CPB) [40] and cardiac surgery [216] showed no significant change in oxCCO throughout either procedure.

Other stresses during surgery such as the use of therapeutic hypothermia and anaesthesia will have effects on cerebral metabolism and such effects are interesting and important to understand if NIRS monitoring of metabolism is to become clinically relevant. However, as du Plessis et al. note, it is difficult to disentangle the effects of hypothermia on oxCCO from the pathology or the stress of surgery [38]. The effects of the anaesthetic propofol during CPB in children (n=11) and CPB controls without propofol administration (n=13) was studied in 2000 [34]. A decrease in oxCCO was observed during CPB and a lower decrease was seen in those with propofol.

4.5.3 Effects of Drugs on the Neonatal Brain

The oxCCO response to other neonatal drugs, such as aminophylline have been monitored. A NIR 1000 was used to assess aminophylline delivery to 13 preterm infants in order to wean off ventilators [27]. A decrease in oxCCO was seen after administration, which the authors suggest could be mediated by reduction in perfusion of CO_2. A later similar study using a NIRO 300 on the effects of aminophylline and caffeine for treatment of apnoeas in preterm infants [42] found that neither drug made a significant change to oxCCO.

Measures of oxCCO have been used to identify cerebral metabolic changes caused by indomethacin for the treatment of patent ductus arteriosus. Despite using different NIRS systems, three separate studies recorded decreases in oxCCO, HbO_2, CBV and CBF with increases in HHb when indomethacin was administered [22, 26, 30]. This result, combined with other evidence from changes in CBF, have provided evidence against the use of the drug due to its reduction in CBF and cerebral oxygen consumption, in favour of other drugs, such as ibuprofen, which do not have such a cerebral metabolic effect [217].

4.5.4 Neonatal Brain Injury

In 1997, a review by Cooper and Springett [49] highlighted the potential for NIRS-measured oxCCO to monitor the progression of neonatal hypoxic-ischaemic brain injury. The management strategy of HIE could be improved with additional information regarding the cerebral metabolic state, as the development of the injury progresses over time and can lead to a secondary energy failure (SEF). There have been a handful of clinical studies of HIE with oxCCO which have promising results. A study of 11 infants with HIE showed that increases of SpO_2 and $PaCO_2$ increased oxCCO (measured with the UCL4 algorithm) which is a normal response and does not suggest pathophysiology [218]. van Bel et al. [21] saw a CBV and oxCCO (using the Keele 4-wavelength algorithm) decrease in first 12 hours after birth in severe HIE, but stable changes in mild HIE and controls; this could suggest the delayed neuronal cell death as predicted by the animal models. They also saw a positive relationship between $PaCO_2$ and oxCCO in all HIE infants.

Recently, the relationship between the UCLn NIRS-measured oxCCO and oxygen delivery (HbD) was investigated in 6 HIE infants and found that an increased affinity between cerebral metabolism and

oxygenation indicated brain injury [54]. Analysis of the rewarming data after therapeutic hypothermia from this cohort provides more evidence that the relationship between the multimodal signals is indicative of brain injury [219]. Further analysis of these data with a multivariate statistical technique showed that a strong relationship between oxCCO and the systemic physiology indicated more severe brain injury (as measured by ^{31}P MRS) [220]. This suggests that the importance of the oxCCO measurement may not lie in the signal itself, but in its relationship with oxygenation or systemic physiology which can inform about the delicate equilibrium in pathology. However, most of this study occurred during therapeutic hypothermia, now a routine treatment for HIE, so it is difficult to compare with other earlier studies.

Further, therapeutic hypothermia may make it difficult to observe SEF and cause unusual metabolic responses as mentioned before [38]. As previously discussed, there need to be more studies of the oxCCO response during cooling.

Recent animal studies of HIE have shown promising results. The UCL group demonstrated a relationship between broadband NIRS-measured oxCCO recovery fraction and HIE outcome in a piglet model [12].

The oxCCO signal has recently been observed during neonatal stroke in a term infant for the first time [219]. Repeated transient decreases in cerebral HbT, HbD and oxCCO were noted on both cerebral hemispheres without significant changes in the monitored systemic physiology. A clear asymmetry was noted in the degree of change between the two sides of the brain. Cerebral oxygenation (measured with HbD) and oxCCO were only highly coupled on the injured side of the brain.

4.5.5 Functional Activation

There has been a huge wealth of work in fNIRS using HbO_2 and HHb as indicators of the haemodynamic response to neuronal activity since it was first presented in 1993 [221]. We have an opportunity with the oxCCO signal to inform directly on cerebral metabolism during neurovascular coupling; there is no other non-invasive in-vivo modality that can assess oxygen consumption during functional tasks. Concerns have been raised regarding the likelihood of measuring 'false positives or negatives' in the haemodynamic response using fNIRS from haemodynamic signals that do not originate from neurovascular coupling [222]. Given that the oxCCO signal is more brain-specific than the haemodynamic signals, it could prove to be a very valuable addition to the fNIRS toolbox [60, 61].

There has only been one functional activation study involving infants and oxCCO and this used the NIRO 300. 19 newborns were given auditory stimulus and no significant oxCCO change was observed despite a normal haemodynamic response [39]. The expected response of oxCCO during functional activation is unknown, although an increase is often seen in adult studies of functional activation (see section 4.6.2). Differences between the mature and neonatal brain are supported by the NIRS study during cardiac surgery by du Plessis et al. where different oxCCO responses were seen at different ages, which could either reflect greater mitochondrial hypoxic tolerance in younger infants or differences in the concentration of CCO at different ages [38].

4.6 Adult Studies

In order to characterised measured changes in the oxCCO signal, an increasing number of studies on adults have been performed over the past 10 years. These studies fall into three categories: volunteer studies with controlled inspired gas challenges to investigate the oxCCO response to systemic physiology, functional activation studies on healthy volunteers, and clinical studies.

4.6.1 Volunteer Studies: Systemic Challenges

The first NIRS studies on adult volunteers were performed in the early 1990s at Duke University. Hypoxic challenges were used to assess the changes in oxCCO in the adult brain at normocapnoea [19] and hyper- and hypocapnoea [20] with 4-wavelength Duke NIRS systems. This work demonstrated a reduction of oxCCO during hypoxia at all levels of $PaCO_2$.

More recently, the UCL group has performed hypoxemia studies (SpO_2 to 80%) during normocapnoea in healthy volunteers using the UCLn algorithm to estimate oxCCO [50, 53]. The hypothesis was that in non-anaesthetised humans a significant decrease in oxygen saturation should reduce oxCCO; this was confirmed in the study. There was a linear correlation between oxygen delivery (estimated from the measurement of the velocity of the middle cerebral artery (Vmca) an indicator of changes in CBF as monitored with TCD ultrasound) and oxCCO. A temporal delay between the HbD drop and oxCCO of ∼5s was also observed. A later study using the pHOS and the UCLn algorithm confirmed the decrease in oxCCO during hypoxia [60].

Conversely, in hyperoxia the oxCCO signal has been found to increase [60, 193]. Tachtsidis et al. found that the oxCCO signal as measured with the UCLn algorithm was correlated with TOI (measured with the NIRO 300), as well as Vmca [193]. Later, Kolyva et al. repeated this study using the pHOS and also showed that the magnitude of the oxCCO decrease during hypoxia was dependent on the distance between the source and the detector [60].

The oxCCO response to changes in $PaCO_2$ was investigated first in 2009 [193]. During hypercapnoea, Tachtsidis and colleagues increased inspired CO_2 and saw a significant increase in oxCCO (estimated with the UCLn algorithm) and Vmca from baseline. There was no correlation between oxCCO and Vmca, but there were correlations with oxCCO and TOI (as measured with the NIRO 300). More recently, Kolyva et al. confirmed the increase in oxCCO during hypercapnoea when monitored with the UCL pHOS system [60]. They also performed hypocapnoea and saw a decrease in oxCCO. Increased CO_2 in the blood has a vasodilatory effect which can increase CBF, but it also decreases the pH which can reduce oxCCO. The authors suggested that the increases in blood flow from hypercapnoea outweigh the potential damage to the respiratory chain from acidosis. In these studies, the oxCCO signal had a different trend to changes in HbT but oxCCO showed a similar trend to TOI. A hyperventilation experiment from a different group also showed minor decreases in oxCCO with the NIRO 500 [31].

As well as answering physiological questions, the study by Kolyva and colleagues (Kolyva et al. 2014) was also designed to address scattering issues and brain-specificity questions using the UCL pHOS system. The magnitude of the oxCCO response increased with detector distance, which was not true

for the haemoglobin signals. This oxCCO depth dependence shows that the signal is more brain specific which is due to the higher CCO concentration in the brain, so the signal is less prone to extracerebral contamination than HbO_2 and HHb. Neither this study [60] nor the previous one [50] saw any changes in pathlength during any of these physiological challenges.

4.6.2 Volunteer Studies: Functional Activation

Functional activation in adults has been studied with fNIRS since 1993 (see section 4.5.5). Visual stimulation of the occipital cortex provides a robust stimulation method and there have been a few studies in this area to evaluate transient changes in the cellular energy metabolism that occur during changes in neuronal activity. Heekeren et al. saw an oxCCO increase during functional activation with a broadband NIRS (Humboldt A system), and they speculate that the cause of the increased oxCCO is not due to increase in oxygen as it would imply that the tissue is in a low PaO_2 state normally, but due to decreases in proton electrochemical gradient increasing the rate of electron flow [56]. This phenomenon was also seen by the same group in later papers with the Humboldt B broadband system [58, 187]. Fourier analysis of the frequencies showed that oxCCO and HHb signals have the same frequency as the stimulation, whereas HbO_2 has other peaks which can be due to other factors [58].

Significant heterogeneous oxCCO responses were seen in an anagram-solving working memory study using the UCL pHOS system [59, 61]. No group significant change in oxCCO was seen during anagram-solving task but there were significant increases and decreases seen in different subjects. In some subjects a significant decrease in oxCCO was seen in the presence of a typical haemodynamic response (increase in HbO_2 and decrease in HHb) [59, 61]. It is hard to predict or model the effect of functional activation on oxCCO; the authors suggested that the NADH oxidation and proton motive force can affect oxCCO without affecting haemodynamics, which may provide an explanation as to the heterogeneity of the oxCCO response despite a consistent homogeneous haemodynamic reaction. This would support the theory of [56] regarding their visual stimuli data.

Different depths give different oxCCO responses, which could be explained by spatial distribution of CCO which is more highly concentrated in the brain than in the extracerebral tissue [61]. A recent UCL working-memory study with CYRIL at multiple source-detector distances showed that the increase in oxCCO observed in the longer channels was not present in the short separation channels, despite a typical haemodynamic response in all channels [223]. The addition of the measurement of a brain-specific oxCCO signal in fNIRS functional studies could potentially reduce 'false positives and negatives'.

4.6.3 Clinical Studies

Monitoring cerebral dysfunction in a clinical setting is important both in cases where the brain is at risk of injury (e.g. cardiac surgery) or where brain injury has already occurred (e.g. TBI). There have been an increasing number of clinical NIRS studies in adults for pathologies such as obstructive sleep apnoea (OSA), cardiac surgery and hypotension, as well as brain injury itself.

The first investigation of cerebral oxCCO with NIRS during surgery occurred in 1995 due to con-

cerns regarding cerebral stress of cardiac surgery causing post-operative neuropsychological damage. A NIRO 500 study of 41 patients undergoing cardiac surgery with CPB found that patients who suffered from neurological defects after surgery had lower minimum oxCCO values during surgery compared to those without defects [224]. The oxCCO and venous saturation were inversely correlated during CPB suggesting that increase in oxygen saturation may not be representative of an increase in tissue oxygenation. Kakihana et al. [225] using the Sapporo algorithm and instrument saw that their measurement of oxCCO was a good predictor of postoperative cerebral outcome in a group of 66 patients who underwent thoracic aortic surgery; the recovery fraction of broadband NIRS-measured oxCCO following the surgery was predictive of neurological outcome.

Further to cardiac surgery, investigators recorded changes in oxCCO with the NIRO 300 during implantation of subpectoral implantable cardioverter defibrillators under general anaesthesia [44]. A random change in both directions was seen in oxCCO (measured with the NIRO 300) during implantable cardioverter defibrillator testing, despite consistent decrease in HbO_2 and increase in HHb. This suggests that the availability of oxygen at mitochondrial level was not affected by short term lack of oxygen delivery and that mitochondrial function may be able to identify cerebral abnormalities in this group of patients that haemodynamic changes do not reveal.

A case study of an adult woman with a long term neurological disorder examined the oxCCO response to seizures with the NIRO 500 [32]. Prior to seizure activity, a gradual increase in HbO_2 and HbT was observed with a simultaneous reduction in oxCCO. Throughout the seizure there was an increase in oxCCO, and HHb; seizures caused increased metabolic demand and the increase in oxCCO corroborates this.

To investigate the response to hyperoxia in cases of brain injury, eight patients with TBI undertook a hyperoxia challenge (60% and 100% FiO_2) [52]. The concentration of oxCCO measured with the UCLn algorithm increased during hyperoxia and correlated with brain tissue oxygen tension as measured by microdialysis [52]; there was a negative correlation between oxCCO and lactate/pyruvate ratio which shows that the oxCCO NIRS changes are related to cellular metabolism. Another investigation of 6 patients with TBI showed a mean increase in oxCCO during hypercapnoea, but not in all individuals (4 increase, 2 decrease) despite increases in Vmca this could be due to heterogeneity of TBI [51]. This study did not find an association between oxCCO and the lactate/pyruvate ratio, the authors suggest that this may be due to more complex changes induced by CO_2, such as pH, nitric oxide (NO) and cerebral metabolic rate of oxygen ($CMRO_2$) changes [51].

Bed tilts were performed in patients with primary autonomic failure to assess cerebral oxCCO during hypotension measured with the NIRO 300 [46]. There was a range of NIRS-measured oxCCO responses during large decrease in HbD and HbT. In patients where a significant decrease in oxCCO was observed, there was a threshold in HbD and HbT reduction before that occurred. A similar threshold has been seen in piglet studies of anoxia ([65] and it may indicate the point at which damage to the cells due to hypoxia and/or ischaemia occurs.

Another population at risk of hypoxic injury is obstructive sleep apnoea (OSA) patients and these have been studied with the NIRO 300. The first study looked at OSA patients during daytime naps with

NIRS monitoring, polysomnography and laser Doppler, end tidal CO_2 and SpO_2 were also monitored [43]. Correlations were seen during spontaneous hypoxias between changes in oxCCO and changes in: TOI, CBF, SpO_2 and MABP, there was a weak negative correlation between oxCCO and CO_2. The oxCCO signal was in phase with TOI but not HbO_2 or HHb. These results suggest that OSA hypoxias cause anaerobic metabolism or CO_2 changes to reduce CCO. In another study of 62 sleep apnoea patients, 6 had deep apnoeas (TOI drop of >10%) and oxCCO dropped for all of these deep apnoeas [45].

4.7 Discussion

NIRS-measured oxCCO has been studied in many clinical environments. For neonates this has included term and preterm infants, infants studied on neonatal intensive care units and during cardiac surgery. The results from the neonatal cohort are not consistent but that is largely due to the heterogeneity of the populations studied and differences between the protocols. A shining example of the application of oxCCO in neonates is the indomethacin work which has shown that the oxCCO signal can provide clinically important information [22, 26, 30]. The most recent work on neonatal HIE has shown that the relationship between cerebral oxCCO and oxygenation is indicative of the level of brain injury as measured by a ^{31}P MRS biomarker of outcome [54], so oxCCO has potential clinical importance as a cotside marker of cerebral well-being.

The adult literature also covers a wide range of clinical environments. The large study by Kakihana et al. is an excellent example of the potential of oxCCO to be a clinical tool that is predictive of neurological outcome after surgery [225]. Further, there is a great potential for the oxCCO measurement to be used in fNIRS studies for a deeper understanding of oxygen metabolism during neurovascular coupling, and for its brain-specificity [61].

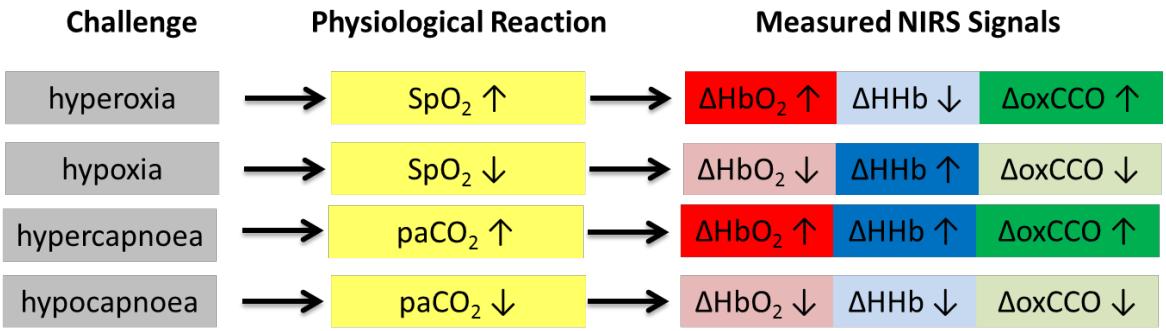

Figure 4.6: hysiological stimuli and predicted NIRS-measured haemoglobin oxygenation and oxCCO changes based on findings from this review chapter for the healthy adult brain.

The adult work also covers a portfolio of volunteer studies which have been used to deepen the knowledge of the oxCCO signal in humans. The behaviour of the oxidation state of CCO is not fully understood as there is no gold standard for the measurement in-vivo. However from the summary of the results found in this review chapter, it is possible to summarise the changes in its behaviour from challenges performed on healthy adult volunteers. The results are limited to the adult brain as it is

not possible to obtain such controlled data on neonates. Quantification of a normal oxCCO response in a healthy brain will allow the identification of abnormal, and perhaps pathophysiological, cerebral responses. The generalised trends of the three NIRS chromophores are summarised in Figure 4.6.

Interpretation of a change in the oxidation state of CCO is complex because it represents a change in equilibrium which may reflect fluctuations in any of several factors and the balance between them including: O_2 supply, glucose or other substrate supply, pH, temperature, and other ETC rates. Understanding the CCO signal is sometimes challenging as there are many different factors that can cause increased oxidation or reduction of the enzyme. This complexity can be dealt with by using computer modelling of the physiology [34].

The UCL group has developed a mathematical model of the physiology of brain metabolism and circulation to aid the interpretation of the measurable cerebral signals [197–199, 226]. The first version of the model was an elaborate representation of the adult brain [226] and was extended to simulate changes in the NIRS variables, in particular changes in oxCCO [197]. The model has been used with NIRS-based adult studies [197] and, after modification for the piglet brain [198], has been used in controlled pre-clinical studies of HIE [199].

4.8 Future Directions

Measuring a real-time, bedside marker of brain tissue metabolism is an active area of NIRS research. Many biomedical optics groups are measuring cerebral $CMRO_2$ with combined NIRS and diffuse correlation spectroscopy (DCS) [156, 174, 175, 227] and others are combining MRI and NIRS to measure $CMRO_2$ [148] confirming the need for a non-invasive measurement of tissue metabolism. NIRS-measured oxCCO changes could be an alternative and/or complimentary measurement to these other monitors of cerebral metabolism.

Near-infrared imaging (NIRI) or diffuse optical tomography (DOT) is under continuous development [6]. Recent work by Phan et al. demonstrated the first oxCCO images, acquired using a multi-channel broadband spectroscopy system (Figure 4.7) [63]. Topographical images with oxCCO in addition to HbO_2 and HHb will allow investigation of regional changes in cerebral oxygenation and oxygen consumption in the healthy and injured brain.

The most challenging but exciting foreseeable development for CCO would be an absolute measurement. To resolve changes in the oxidised concentration with respect to the reduced concentration of CCO would be revolutionary as it would allow more easy comparison between patients or volunteers and give a better understanding of the state of tissue metabolism. The UCL group is working towards methods to do this, both in new hardware and algorithms. The group has recently developed a multi-wavelength TR spectrometer to quantify absolute changes in absorption and scattering with a view to measuring absolute CCO redox changes [228].

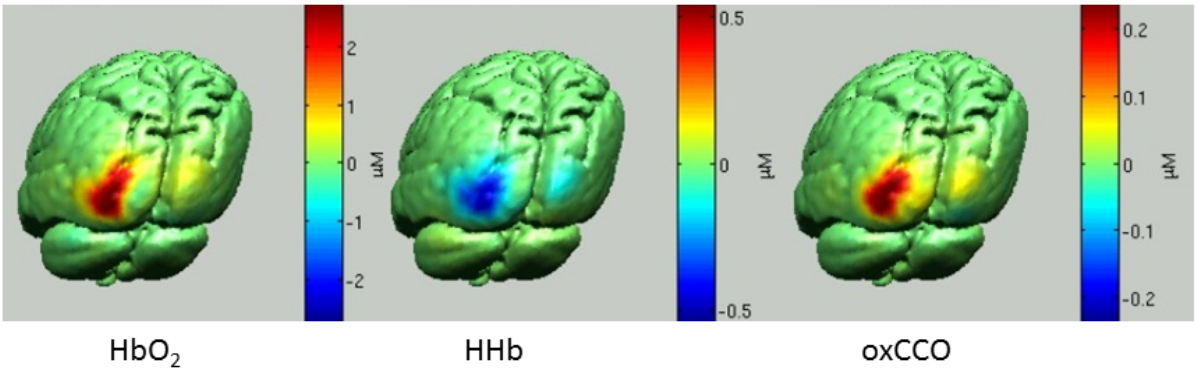

Figure 4.7: Images of block-averaged concentration changes over the occipital lobe from HbO_2, HHb and oxCCO for one subject shown during half-field chequerboard visual stimulation, demonstrating spatial distribution of responses [63]. There is an increase in HbO_2 and oxCCO on the contralateral hemisphere during activation and a decrease in HHb. There are spatial differences between the haemoglobin and oxCCO images as assessed by centre of gravity analysis.

4.9 Summary

This review chapter described the rationale, methods and analysis behind NIRS measures of oxCCO. The range of human brain studies (in healthy volunteers and patients) was summarised from those first performed by the Jobsis group, as early as 1985, to the present day. I found 103 papers published on cerebral oxCCO NIRS measurements in humans, 65% of the studies are on adults and the remainder on neonates. The need for a low-cost, bedside and non-invasive monitor of cerebral oxygen metabolism remains an important and relevant clinical goal. This unmet clinical need has driven continued advances to deliver NIRS instrumentation and methodologies which are optimised specifically for CCO measures. With this comes renewed focus on defining the role of these measures in a range of clinical scenarios, and fulfilling Jobsis's vision for this optically derived metabolic marker.

Chapter 5

Development of a Novel Broadband NIRS System: CYRIL

This chapter describes the design, development and preliminary testing of a novel broadband NIRS system to monitor changes in cerebral cytochrome-c-oxidase in the neonatal intensive care unit.

5.1 Introduction

The biggest challenge in designing an optical system for use in a neonatal intensive care unit is the environment. The system needs to be robust, adaptable, compact, easy to use and minimally invasive. The key to undertaking studies within a high pressure clinical environment is ensuring that the device does not interfere with clinical care and is simple enough for use by non-physicists. This chapter describes the design considerations required to develop a monitor for the NICU and the development of such a system.

Note

Some of the work described in this chapter and Chapter 6 has been published in Biomedical Optics Express [54]. A copy of the paper is shown in Appendix B.

5.1.1 Design Considerations

The neonatal intensive care unit is a high pressure environment. The neonatal unit at UCLH has 25 intensive care/high-dependency cots, with four cots in each room. Each room has two specialist nurses at all times, plus any number of doctors, support staff and family members. Acutely ill and premature babies are treated in the NICU; conditions include respiratory problems, jaundice, anaemia, sepsis, as well as all forms of brain injury. At UCLH there is a high turnover of infants (in February 2016: 85 infants were admitted, 87 infants were discharged and 27 infants were transferred). This is a challenging environment to bring a new machine into, so the system was designed with this in mind (see Table 5.1).

Table 5.1: CYRIL design specifications.

	Specification	**Necessity**	**Solution**
Safety	Light intensity within safety levels and does not cause heating	Essential	Low and high-pass filters block light from either side of NIR region (610-950nm) to minimise heat deposition
	Electrically safe on patient end	Essential	Fibres applied so no electrical device at patient side
	Electrically safe on device end	Essential	Isolation transformer to protect from mains supply
Optics	Sensitive to low light levels	Essential	Lens-based spectrometer for high throughput
	Measures oxCCO	Essential	Broadband, UCLn algorithm and high signal-to-noise from spectrometer
	Measures TOI	Desirable	Multiple source-detector distances
	Measures both hemispheres of brain	Desirable	Dual light source and multiple fibres
	Insensitive to ambient light	Essential	Blackout fabric placed over probe holder
	Stable measurement over long periods	Essential	Cooling at CCD and thermally stable light source
	1Hz sample frequency	Desirable	Need high intensity from 1s exposure: high NA and bundle fibres, high light throughput in spectrometer
	Flexible detection	Desirable	Fibre configuration not fixed so can change set-up via 3D printing
Clinical Practicalities	Probes suitable for neonate	Essential	Light and small plastic fibres and holders custom built
	Probes stay on for long studies	Essential	Fibres attached by double-sided tape
	Compact and portable	Essential	All components fit on trolley
	Device does not interfere with patient care	Essential	Long 3m fibres allow device to be placed far from cotside and optodes placed on forehead (not used)
	MRI safe	Desirable	Magnetically safe plastic fibres (can be made up to 10m)
	Stable and reproducible data acquisition	Essential	Device has no motorised parts - all operation is done via software
	Easy to use	Essential	LabVIEW GUI user friendly, being used by medical doctors
Data Storage	Stores data in event of system crash	Essential	Data saved on hard drive in real-time
	Continues running in event of power cut	Essential	Universal power supply
	Simultaneous recording of systemic monitor data	Essential	ixTrend software installed on laptop to record systemic data with same time-stamp

5.2 CYRIL Hardware

As discussed in section 3.2, a broadband NIRS system is made up of a broadband light source, fibres to transmit the light to and detect from the tissue and a spectrometer. The system developed for this PhD is no different. However, the system is specifically designed to be flexible and robust enough to perform optical measurements within the NICU with minimal adjustments and the fibres are uniquely designed to be comfortable for the neonatal head. In order to achieve the requirements set out in Table 5.1, the components were carefully selected and designed; these components are described in this section.

The system is named CYRIL which stands for the CYtochrome-c-oxidase Research Instrument and appLication (this name was chosen to reflect the key purpose of the system, to measure oxCCO) but also to be a friendly name that would be accepted in the NICU. Figure 5.1 shows a schematic of the core system components and a photograph of the CYRIL system in the NICU is shown in Figure 5.2. Light is coupled into the dual source fibre bundle and carried to the tissue where the fibres are attached with optode holders. Back-reflected light is collected by the eight detector fibres and transported to the spectrometer where each channel is diffracted into its wavelengths and detected separately on a 2-dimensional CCD camera. The camera is controlled by, and records data in, a program created in LabVIEW. These intensity spectra are converted into changes in chromophore concentrations via the modified Beer-Lambert law 3.25 and displayed in real-time.

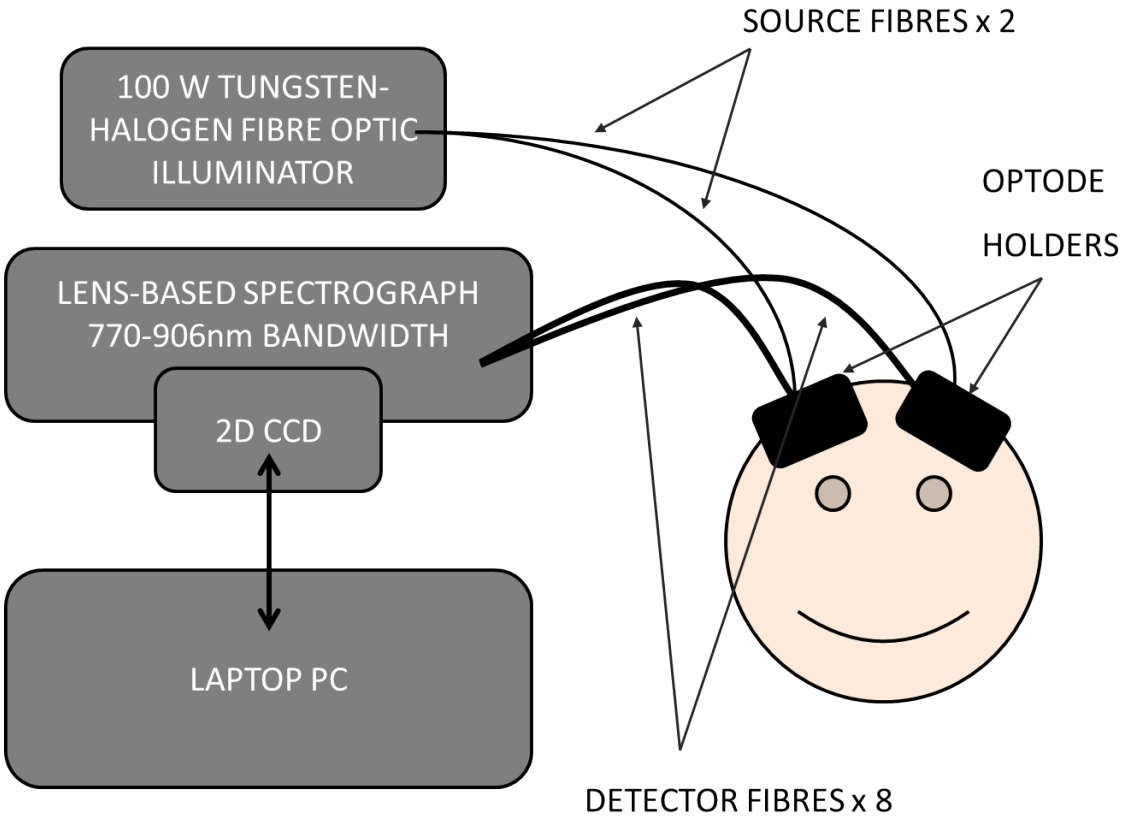

Figure 5.1: Schematic of CYRIL in the NICU. a) The portable instrument. b) The optodes and optode holders on an infant.

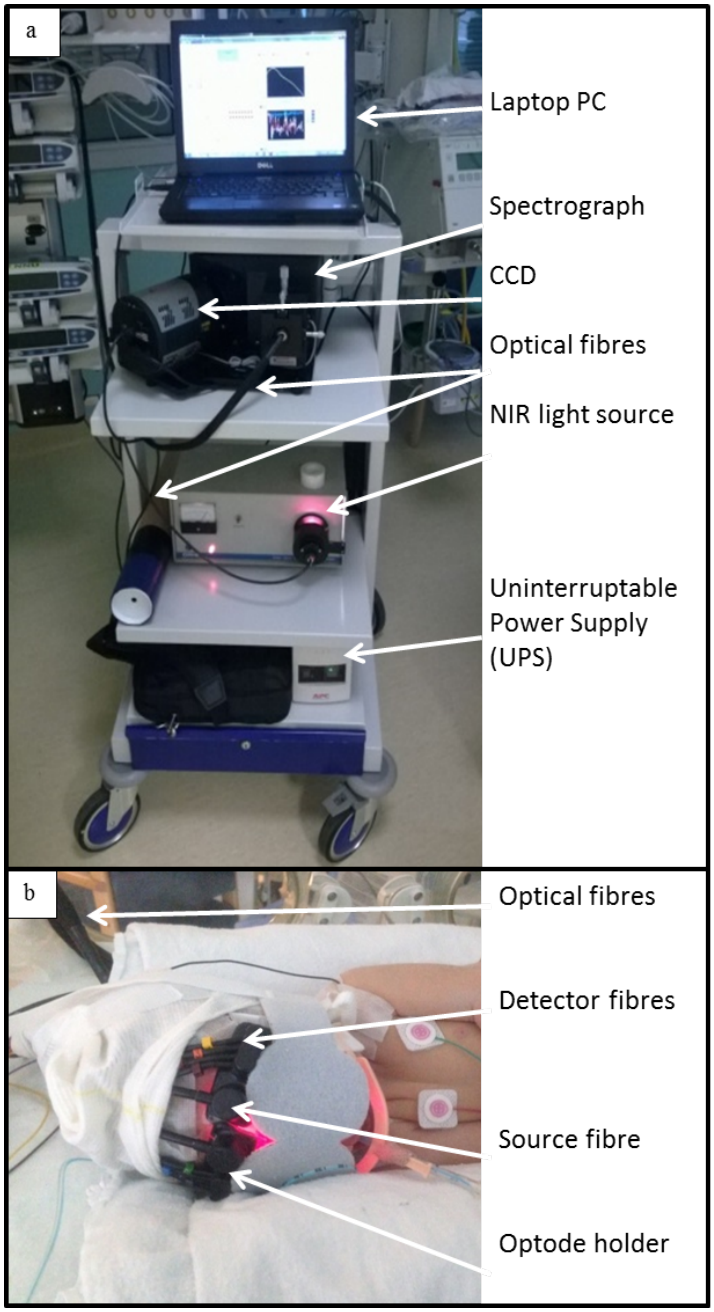

Figure 5.2: CYRIL in NICU.

5.2.1 Broadband Light Source

A broadband light source was chosen to be thermally stable with high output intensity over the NIR region. The ORIEL Fibre Optic Illuminator 77501 produces a thermally stable broadband white light source with a high intensity in the NIR region to illuminate the tissue. The bulb is a 100W quartz tungsten halogen lamp with an axial filament. The lamp output is collimated with an aspheric lens and focussed onto the fibre input to ensure good coupling into the fibre bundle (see Figure 5.3). A shutter and iris can be used to block or limit the light entering the fibre. To minimise the heat deposition on the subject's head, a 610nm long-pass filter and 950nm short-pass filter were placed in the collimated

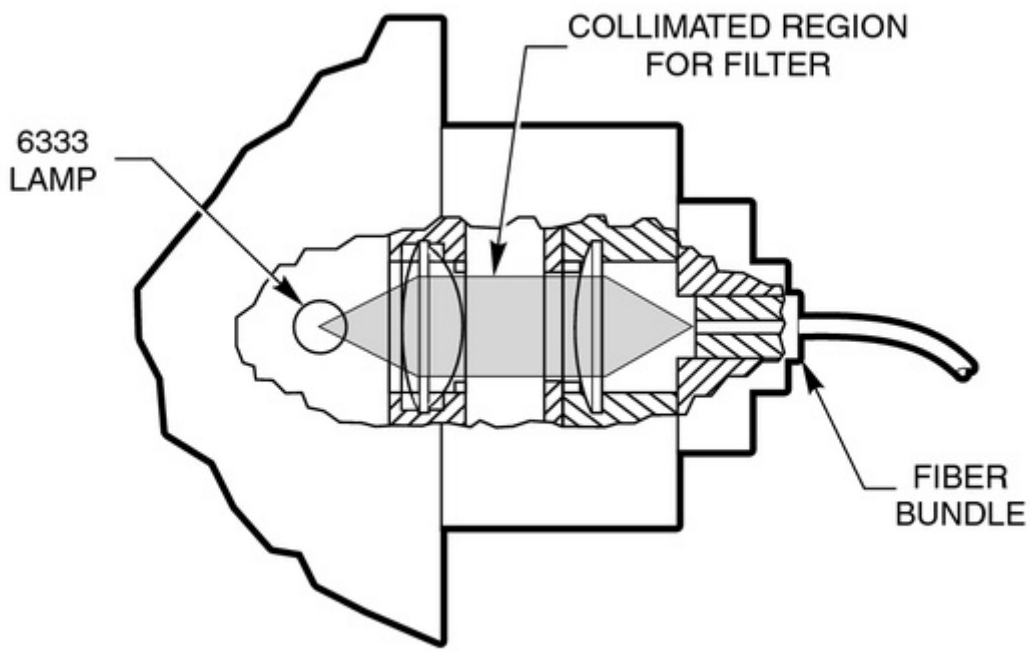

Figure 5.3: Optical configuration of the ORIEL fibre optic illuminator 77501. Taken from 77501 manual (ORIEL, USA).

region between the lamp and the fibre. The resulting spectrum is shown in Figure 5.4, measured with the QE65 miniature spectrometer (Ocean Optics), and Figure 5.5, measured by CYRIL.

The effects of elevated skin temperature caused by the probe and the illuminating beam of the light source were measured by Sonya Mahony in her MSc thesis [64] on a phantom (Figure 5.6) and human arm (Figure 5.7). The biggest rise in temperature is due to placing probes on the arm with no change in temperature caused by turning the light on. In the studies described in this thesis, no thermal effects or damage to the tissue has been observed in any use of the system.

5.2.2 Spectrograph

The spectrograph was primarily selected for its ability to maximise the light throughput in the NIR region. The Acton LS785 by Princeton Instruments (USA) is a lens-based spectrograph; lens-based systems have a higher effectiveness than mirror-based spectrometers with respect to the throughput of light (over 99% transmission throughout the entire working range of the spectrograph). The lenses have anti-reflection coatings to provide high throughput in the NIR (specifically 740-1050nm). This system uses fast lenses (f/2) to maximise the light gathering power. The lenses provide a flat 2D focal plane that is 8 x 27mm. The LS785 is f-matched to a high NA input which is essential for minimising loss. The light input is through a fibre adapted entrance and a variable slit which prevents overexposure. The

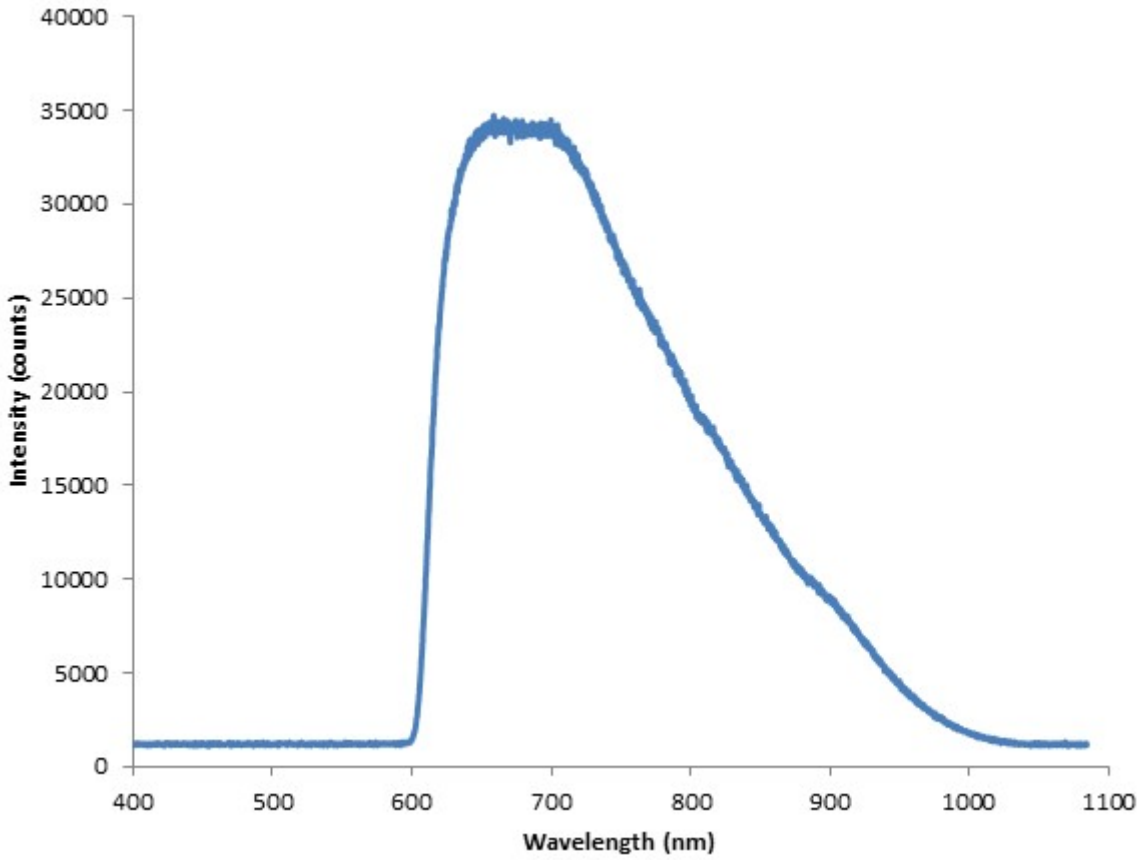

Figure 5.4: Intensity spectrum of the ORIEL 77501 fibre optic illuminator with a 610nm long-pass filter over 400-1100nm as measured with the QE65 spectrometer.

slit size was chosen to be 20μm for the CYRIL set-up as it allows good throughput but also maintains a high spectral resolution (see section 5.5). The light is collimated to reduce loss by a series of lenses and then is incident upon a gold-coated diffraction grating (see Figure 5.10). The grating is blazed at 1000nm and has 830 grooves/mm (each groove is 0.7nm) which gives a 136nm bandwidth. The grating is mounted on a rotating platform so it is possible to select the range of wavelengths that are recorded with a micrometer control gauge; as oxCCO is a strong absorber at 830nm, the 770nm-906nm range was selected (see section 4.3 for further details, previous in-house systems built to measure oxCCO have used the 780-900nm range successfully [61]). After diffraction at the grating, the light is focussed onto the CCD detector (discussed in the next section) with an f/2 focussing lens; focussing the light in the y-direction reduces cross-talk between the detector channels. Figures 5.8 and 5.9 show the spectrograph components described here. There are no motorised parts in the LS785 which makes it stable and reproducible which is ideal for the clinical environment.

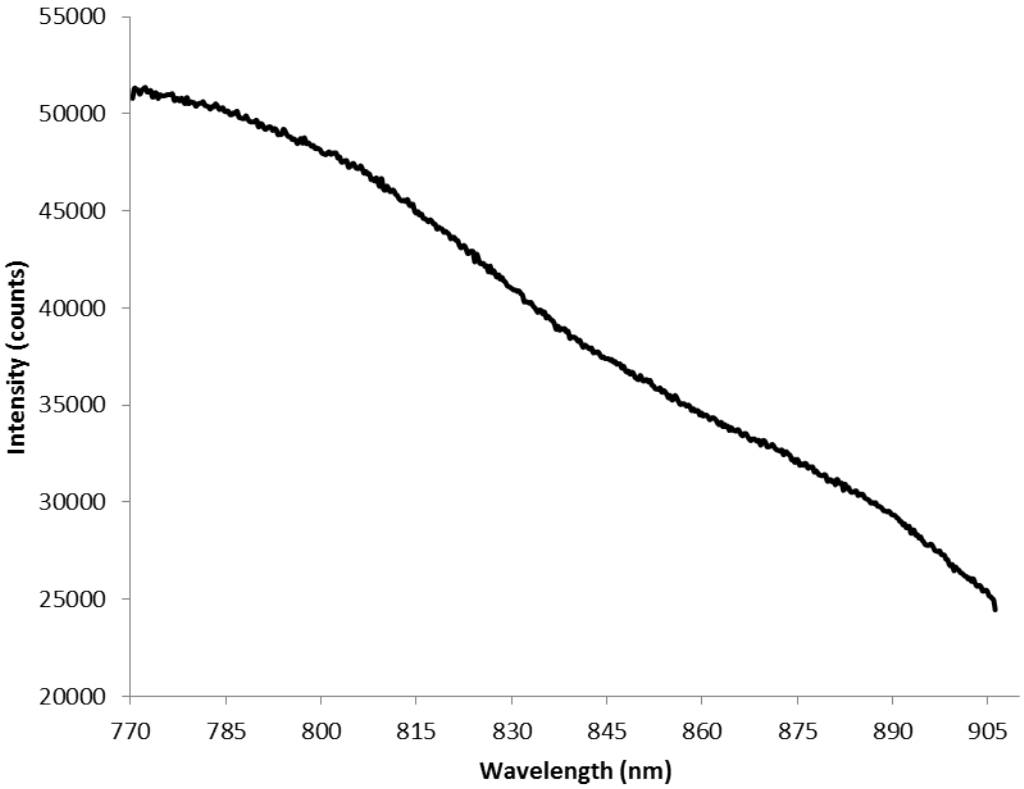

Figure 5.5: Output spectrum of the ORIEL fibre optic illuminator 77501 over 770-906nm as measured with CYRIL.

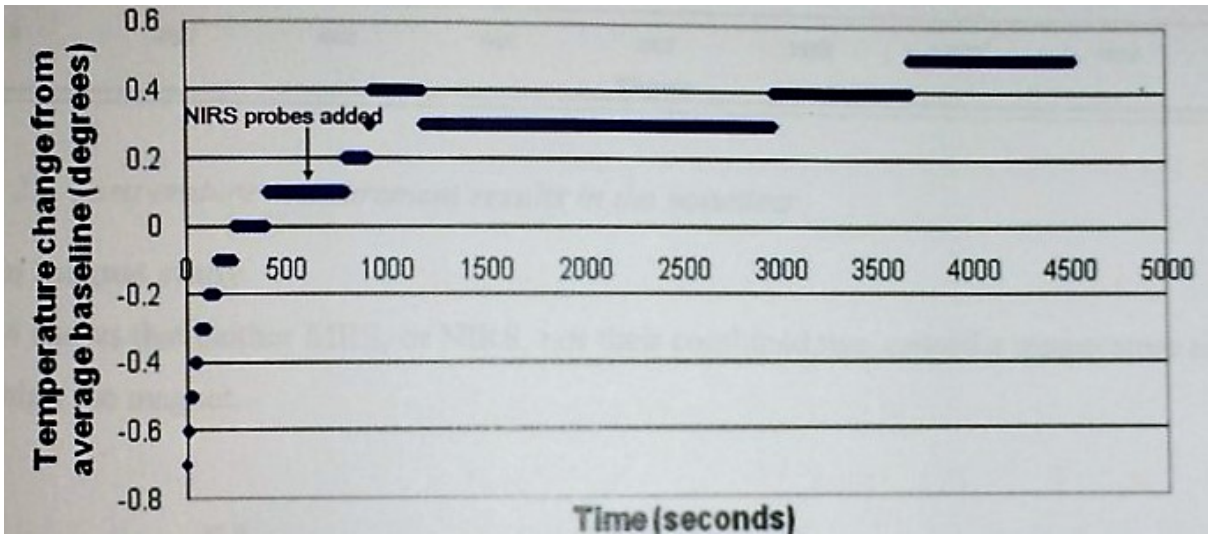

Figure 5.6: Thermal changes on a phantom to test the heating effect of the ORIEL 77501 light source. The source was turned on when placed on the phantom. Taken from [64].

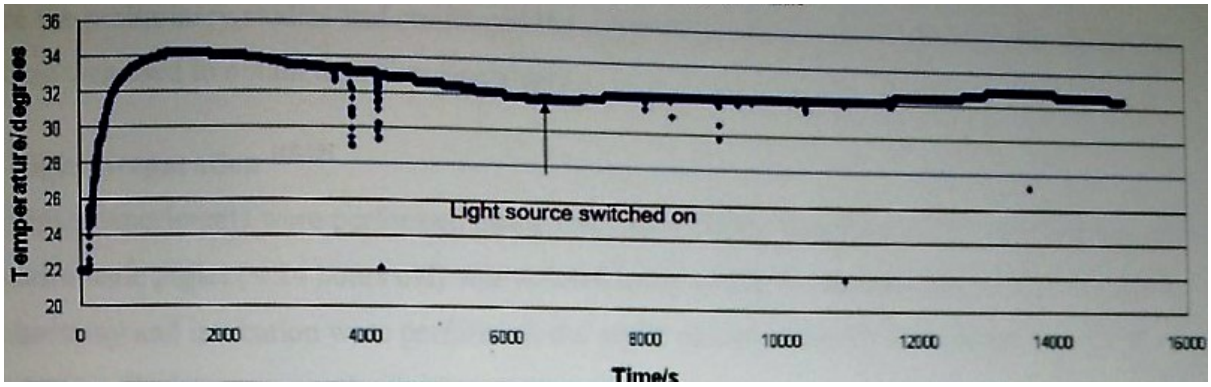

Figure 5.7: Thermal changes on a human arm to test the heating effect of the ORIEL 77501 light source. Taken from [64].

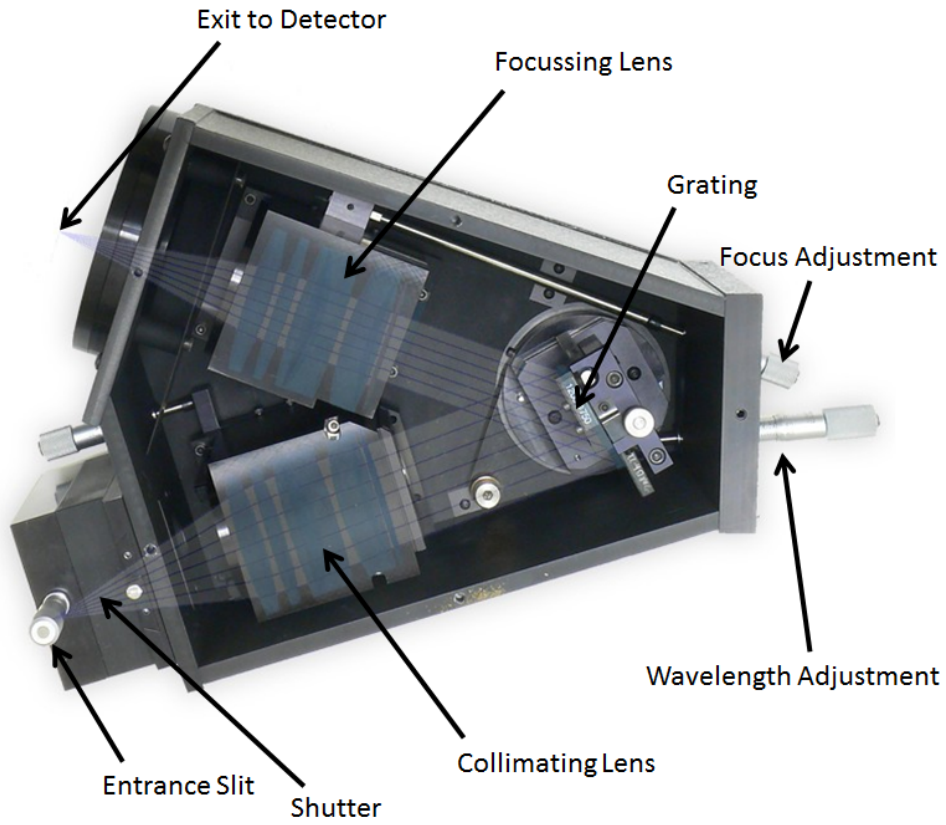

Figure 5.8: Internal view from above of Acton LS785 Spectrograph. Taken from LS785 manual (Princeton Instruments, USA).

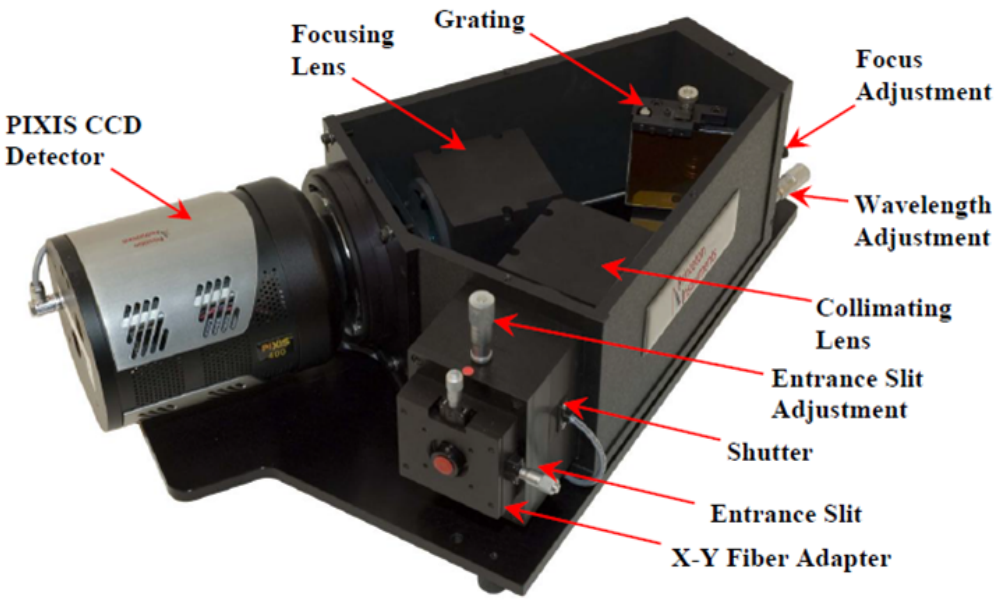

Figure 5.9: External view of Acton LS785 Spectrograph. Taken from LS785 manual (Princeton Instruments, USA).

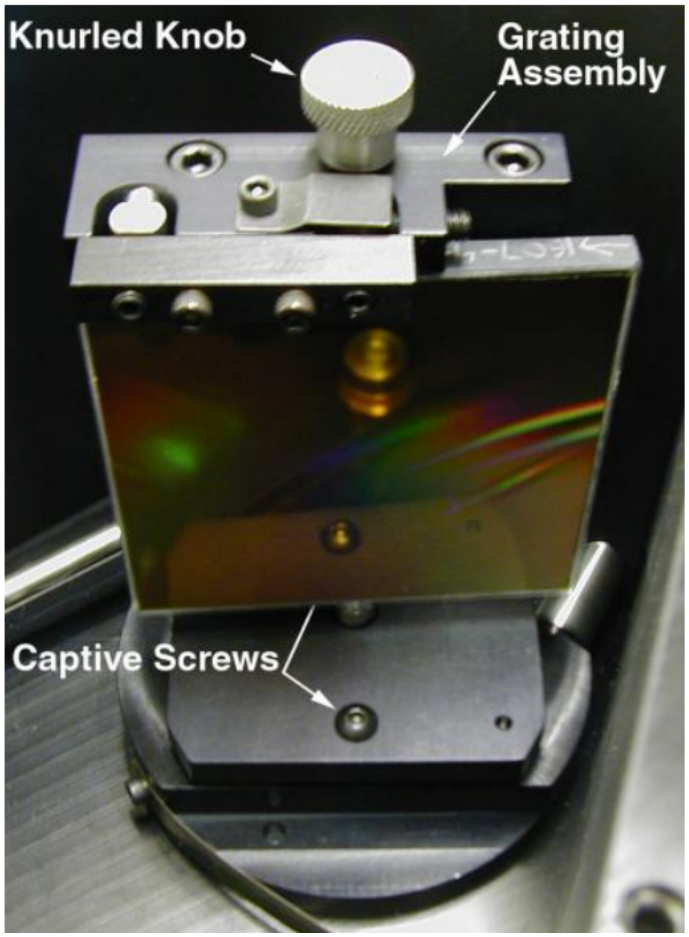

Figure 5.10: Princeton Instruments Acton LS785 Spectrograph grating. Taken from LS785 manual (Princeton Instruments, USA).

5.2.3 CCD Camera

The PIXIS 512f CCD camera (Princeton Instruments, see Figure 5.11) was chosen to detect light from the spectrograph because of its large detector array and high dynamic range. It has a two-dimensional array of 512 by 512 detector pixels (each 24μm by 24μm) on a 12.3mm by 12.3mm chip with 16-bit dynamic range (i.e. 65536 levels). It is a front-illuminated CCD which is good for the moderate to low light levels of NIRS, and the peak quantum efficiency lies within the NIR region (see Figure 5.12). The CCD is cooled to -70°C (thermally stable to ±0.05°C) during operation to reduce thermal noise and dark count; at this temperature the dark current is 0.002 electrons per pixel per second. The low dark noise allows the detection of faint signals which is ideal for the low light intensities in NIRS. The CCD read noise at 1000kHz is 5 electrons root mean square (RMS). The CCD has a USB 2.0 data interface for control and acquisition with a laptop (see section 5.3 below).

The 2-dimensional CCD chip is able to record data from the eight detector fibres simultaneously by binning different regions of interest as seen in Figure 5.13 (this is explained further in section 5.3). Binning effectively increases the pixel size to increase the light collection while retaining the selectivity for each detector fibre.

Figure 5.11: PIXIS 512f CCD camera. Taken from PIXIS 512f manual (Princeton Instruments, USA).

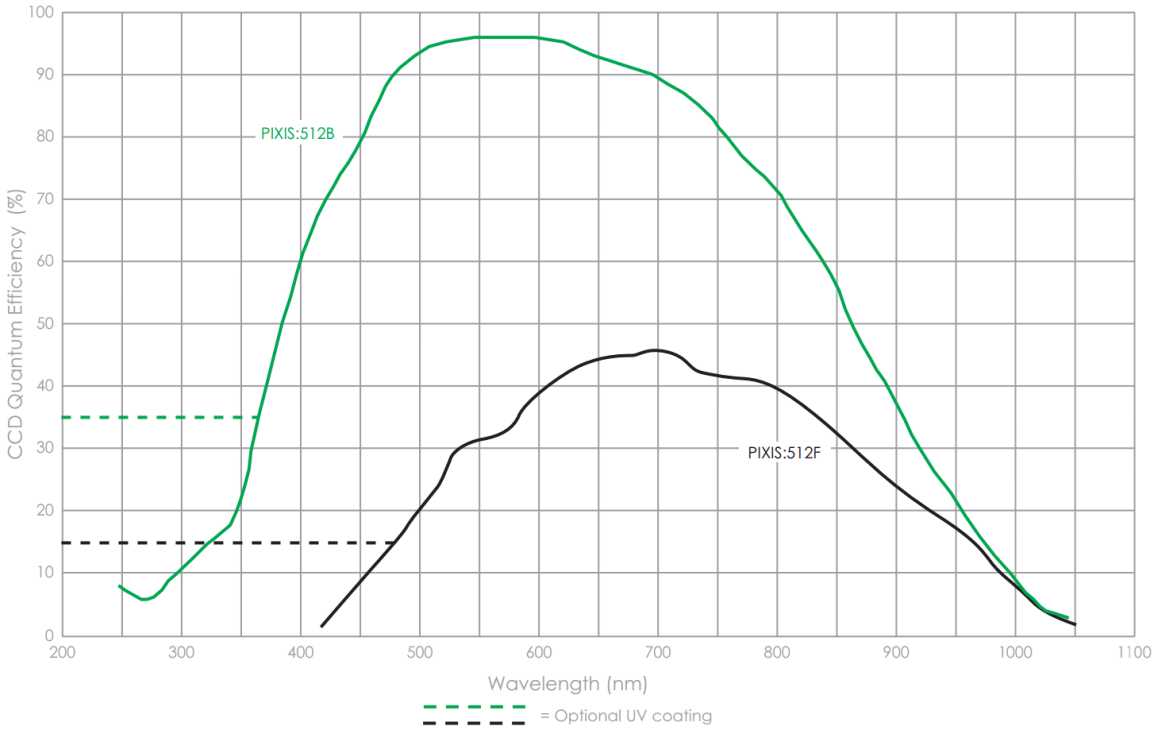

Figure 5.12: Quantum efficiency of the CCD chip (solid black line). Taken from PIXIS 512f manual (Princeton Instruments, USA).

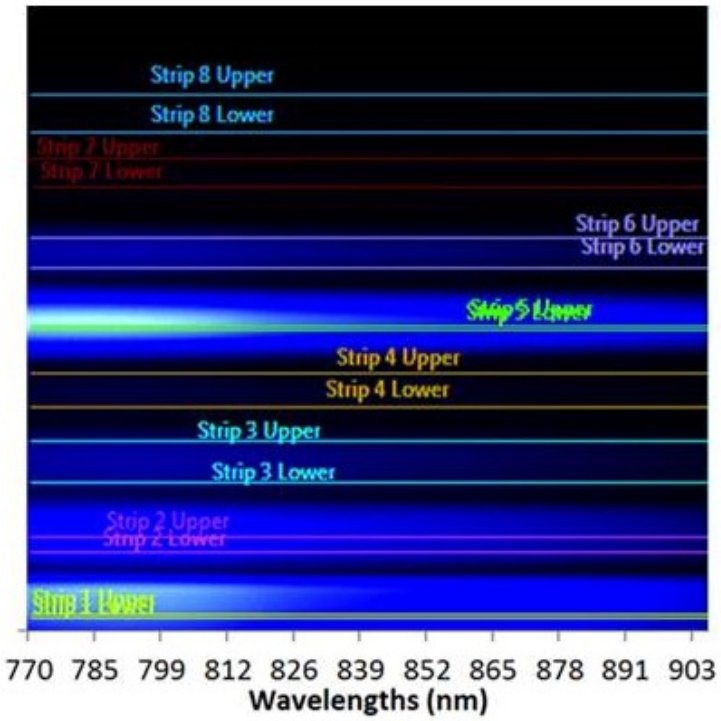

Figure 5.13: Intensity map on the CCD camera and the bins selected when using 8 detector fibres as displayed in the LabVIEW program. The lines (labelled 'Strips') are used to define the region of interest for all of the input fibres, see Figure 5.23 for more details.

5.2.4 Optical Fibres and Holders

Optical fibres (optodes) and corresponding optode holders were designed to connect between the light source and the tissue and the tissue and the spectrograph. Two channels with four detectors each were used. This was possible with a single spectrograph and camera by using the 2-dimensional camera chip which allows the individual detection of multiple fibres simultaneously (see Figure 5.20). The fibres were custom built by Loptek (Germany) to fit the source and spectrometer at the system end, and to be as light and small as possible at the patient end to maximise comfort.

The light source fibre bundle branches into two fibre heads to give two source channels; a bundle of high NA optical fibres takes light from the source lamp, after 2.5m the fibres split into two parts each with diameter of 2.8mm for 0.5m. The optical heads are made of magnet-compatible plastic to ensure that they are light but also MR scanner compatible (see Figures 5.16 and 5.17).

The detector fibres consist of eight individual fibres with high NA that have a 1mm diameter. Each fibre has an individual head (see Figure 5.17) of diameter 5mm which detects light on the tissue surface. The fibres bundled into one cable and are arranged vertically into a ferrule that inputs the light to the spectrometer (see Figure 5.20) which enables the spectrum from each fibre to be detected individually and simultaneously.

Optode holders were designed using AutoDesk Inventor, 3-dimensional computer aided design (CAD) software, and 3D printed with the Objet500 Connex in a rubber-like black material (TangoBlack FLX973) that is combined with a more rigid material (VeroWhitePlus) to increase stiffness. The design holds the source optode next to the four detector optodes with a gap of 1.5cm between the source and the first fibre, and 0.5cm between the centres of the other fibres (see Figures 5.15 and 5.18); this gives source-detector distances of 1.5cm, 2.0cm, 2.5cm and 3.0cm (see Figure 5.14). The holders were designed to be small and flexible to reduce the footprint on the head and to allow for curvature; several different combinations of the rubber-like black material and rigid white material were trialled to find the balance between flexibility and durability (the rubber-like black material has a tendency to tear). As there are two sets of optodes, the two optode holders are mirror-images of each other so that the fibres can lead from the same direction (typically up away from the head). For babies with smaller head circumferences, another optode holder was designed that uses a single source but with four detectors each side (see Figure 5.18). This will allow the measurement of two hemispheres but with a smaller footprint on the head.

A double-sided tape that is safe for human use (Tape Range Distributors, UK) is used to apply the optodes to the skin. The tape is placed on the underside of the optode holder (as in Figure 5.2) and then placed on the head. This method holds the optical fibres to the skin securely which reduces the number of movement artefacts and optical drift from a changing position. It also does not involve applying pressure to the skull to maintain optode contact to the tissue which can result in pressure sores. There is a possibility that some light may propagate directly from the source to the detector via the thin layer of tape between the probe and the skin (known as light piping). If this is true, then the light piping should remain constant throughout a measurement and thus is is unlikely to have a significant effect on the measurement of *changes* in light attenuation, and therefore should have a negligible effect on the *changes* in chromophore concentrations.

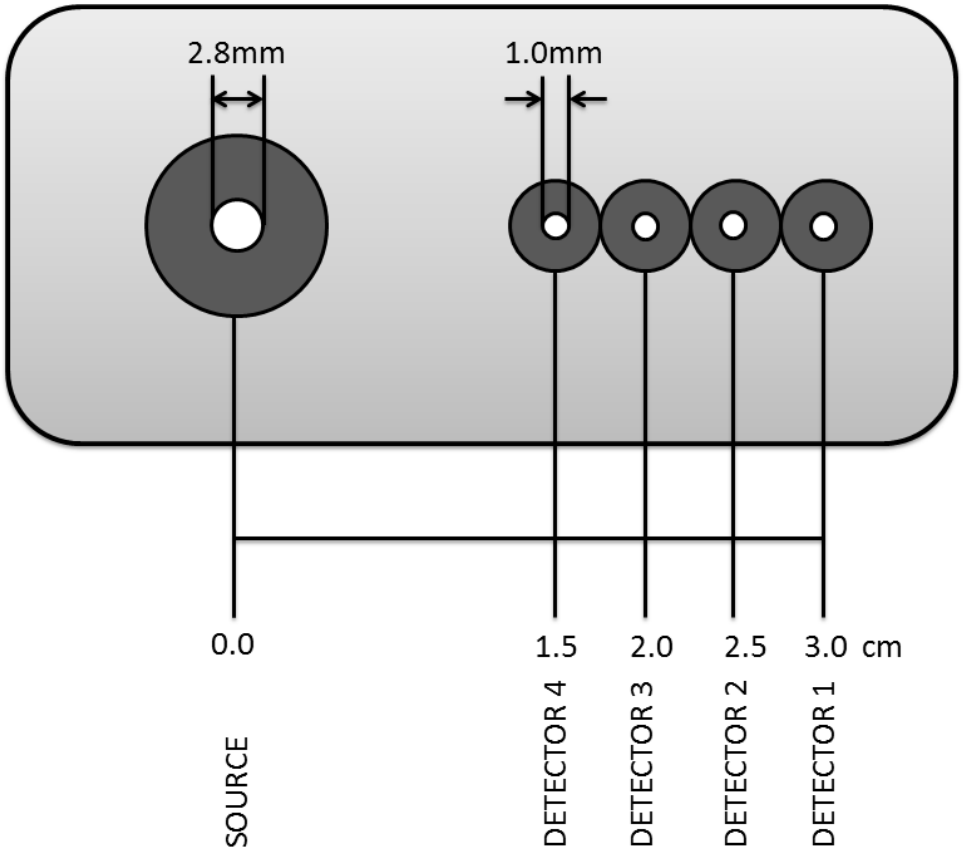

Figure 5.14: Diagram of optode holder design.

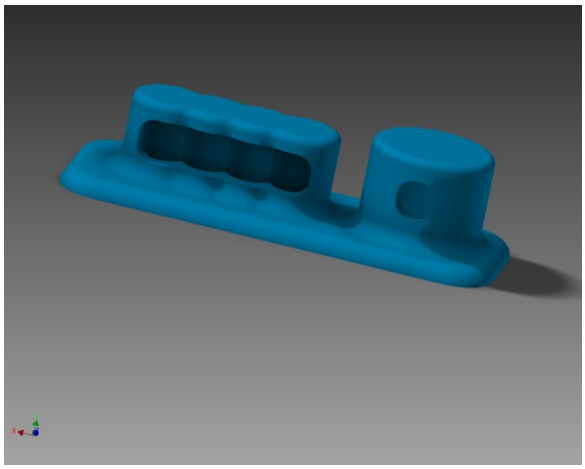

Figure 5.15: CAD design of an optode holder with 1 source and 4 detectors (for left side of head) with same dimensions as Figure 5.14.

Figure 5.16: Patient end of optical fibre detectors shown in and out of optode holder (from CAD design in Figure 5.15).

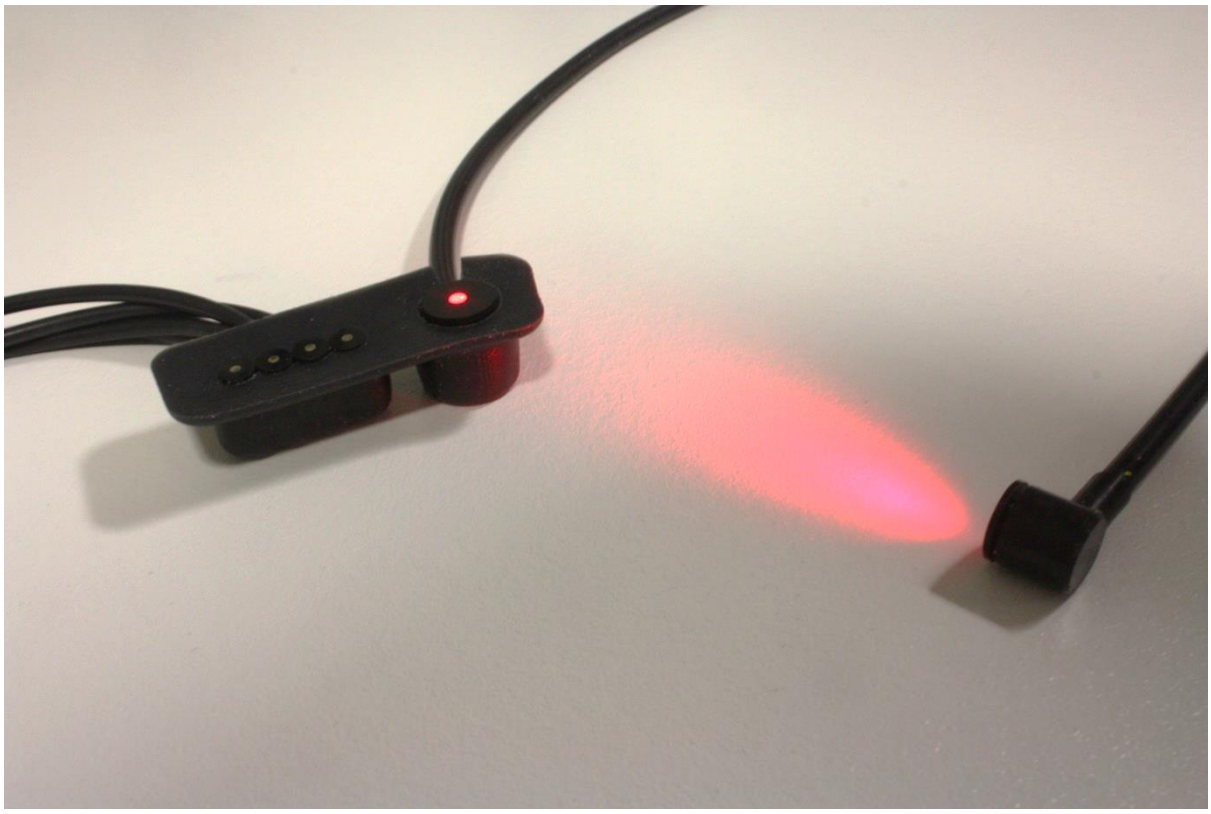

Figure 5.17: Optical fibre source and detectors in optode holder (left) and source fibre head (right).

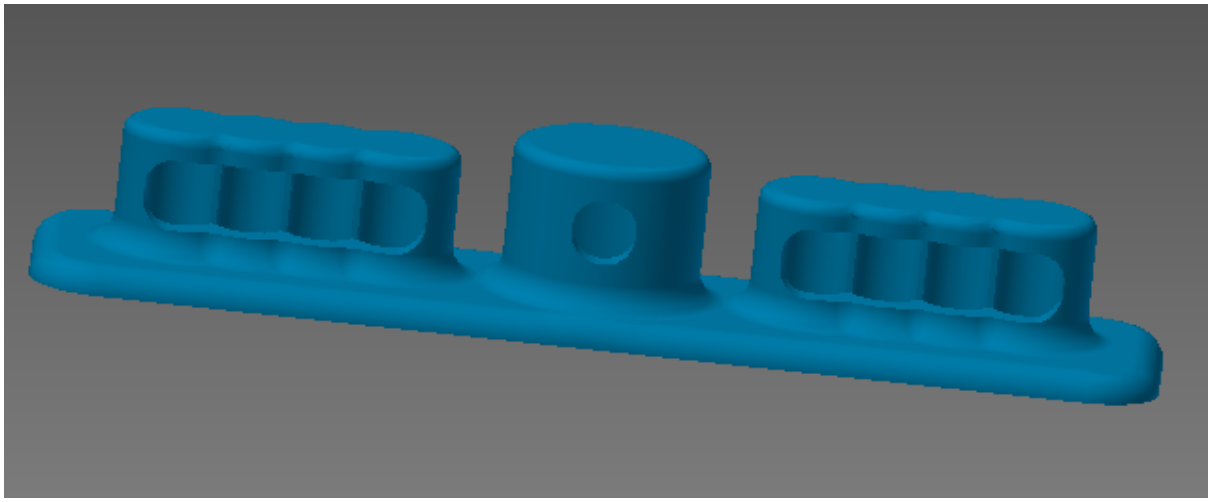

Figure 5.18: CAD design of an optode holder with 1 source and 8 detectors.

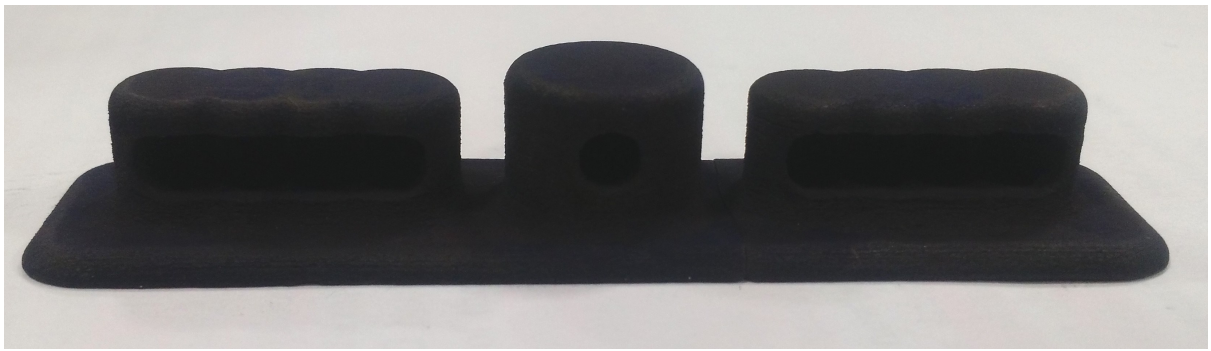

Figure 5.19: Optode holder with one source and 8 detectors from CAD design in Figure 5.18.

Figure 5.20: Input ferrule of the detector fibres at the spectrometer end.

5.3 CYRIL Software

A program was created in LabVIEW to control the CCD, collect the raw intensity data and calculate, display and save the corresponding concentrations. Two versions of this program have been created and are discussed in this section.

5.3.1 Version 1

Version 1 of the software was finalised in October 2013. Figure 5.21 is a flowchart which shows the main functions of the first version of the program. The program is essentially structured in three sections (as illustrated by different colours on Figure 5.21). The first section contains all of the settings for the camera and GUI. Once the settings have been confirmed, the user presses 'Start' and the second section initialises. The second and third sections are designed as 'producer-consumer' pair. The producer's job is to generate a piece of data, and place it into a fixed-sided buffer which is used as a queue. The consumer then removes the data from the queue and processes it. This ensures that the producer can generate data at regular intervals without having to wait for the consumer to process it. In this program, the producer collects intensity data from the CCD and displays it, while the consumer calculates the changes in chromophore concentrations and then displays and saves all of the data. The intensity and concentration data are each saved in separate files for each detector channel along with a time log file. This section describes the different parts of the graphical user interface (GUI) functions in more detail.

Settings

The 'Settings' tab on the left-hand side of the GUI is shown in Figure 5.22. The user can choose the exposure time, the shutter settings and the temperature of the CCD. Variables for the calculation of the concentration changes such as the optode distance, DPF and interpolation method are also available to select in this tab. Further the user can specify the file name and folder to save the data.

Warning levels for low or high intensities in each channel can be set; these trigger a warning if any part of the spectrum exceeds the saturation limit or drops below the noise level. The warning is placed in the time log file so the user can identify periods of camera saturation or low light levels without looking at the raw data. When a warning level is triggered this also appears on the GUI by illuminating an icon. At saturation, the green icons labelled 'S1-8' for each detector will illuminate and at low intensities red icons labelled 'N1-8' will illuminate. The user is also able to enter comments into the time log file (e.g. about the subject's status, a movement artefact or a medical event, etc.) using the 'Comment' box.

Figure 5.23 shows the CCD binning functionality of the GUI. The user can take and display an intensity weighted image of the CCD pixel array and subsequently choose the region of interest (ROI) for each horizontal strip to bin (see Figure 5.13 for a larger view). Each strip is related to one of the detector fibres that are input into the spectrometer via the ferrule as in Figure 5.20. The strips can be adjusted for each subject to maximise the intensity spectra at each channel without saturation.

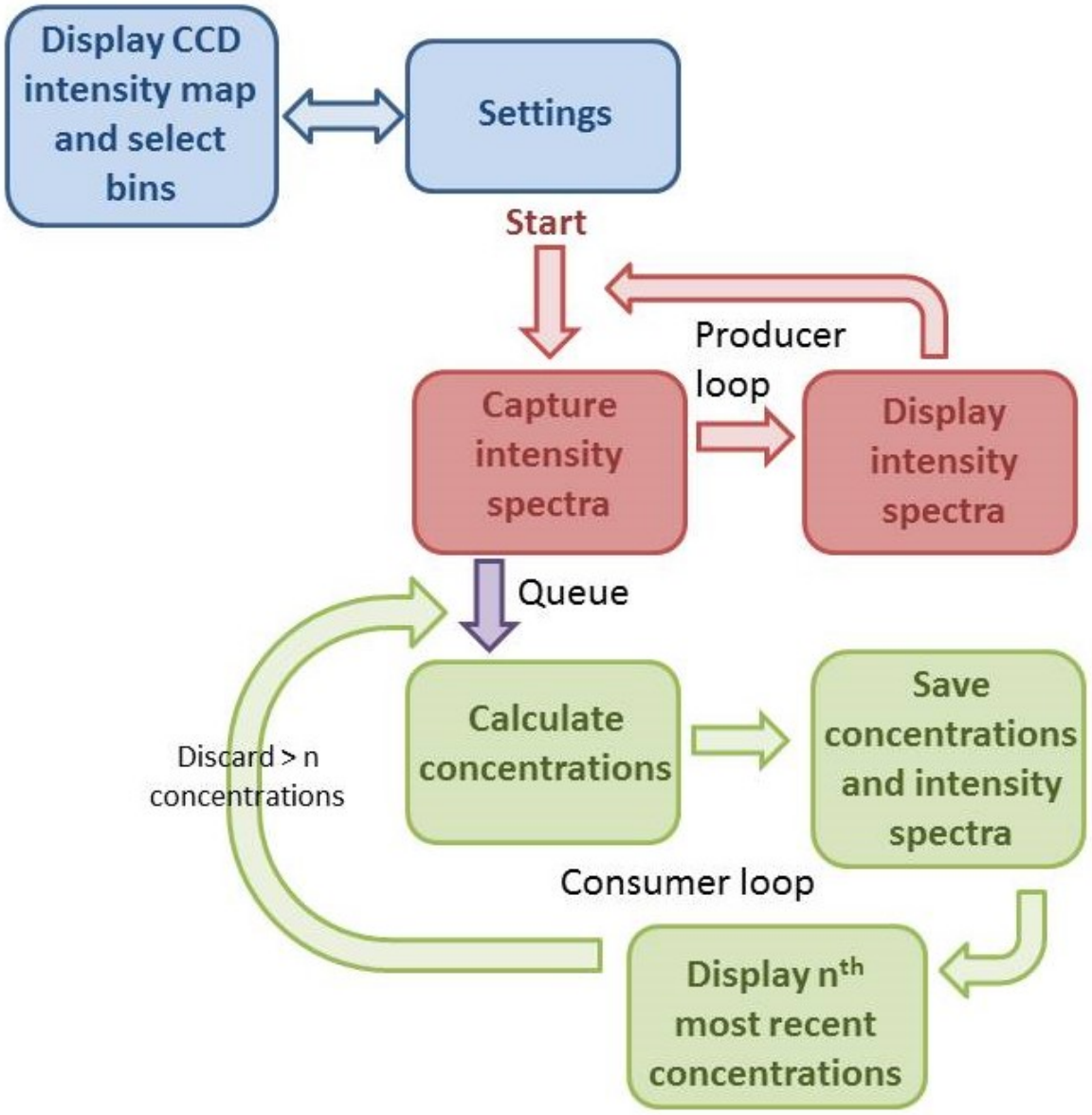

Figure 5.21: Block diagram of the main functions of the LabVIEW program - version 1. The colours represent the three different sections within the program.

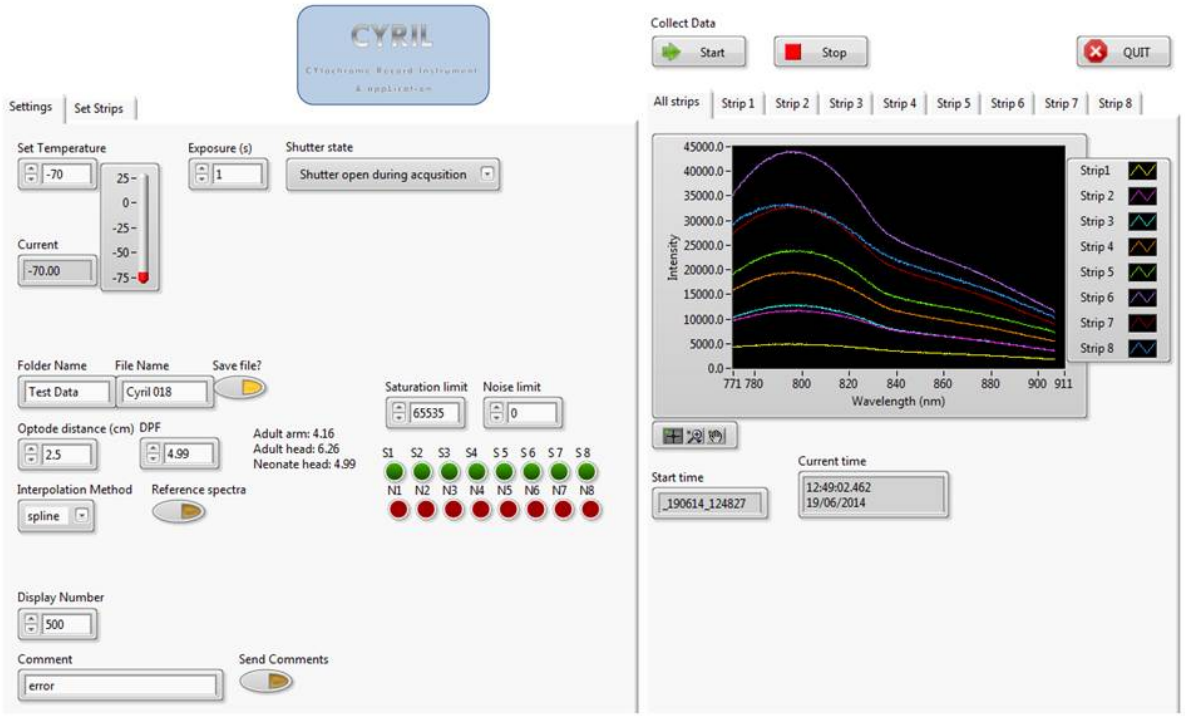

Figure 5.22: CYRIL software version 1 - Settings tab. On the left side from top to bottom: the user can set and view the CCD temperature, exposure time, and shutter state; adjust the file saving settings; enter the optode distance and DPF; select the interpolation method to down-sample the spectra to every wavelength; choose the number of concentration data points displayed, and send comments to the time file. The warning icons also appear on the left side. On the right side the recorded spectra for all ROIs are displayed with the start time and current time. The user can begin/end the data collection by pressing the Start/Stop buttons above the tabs.

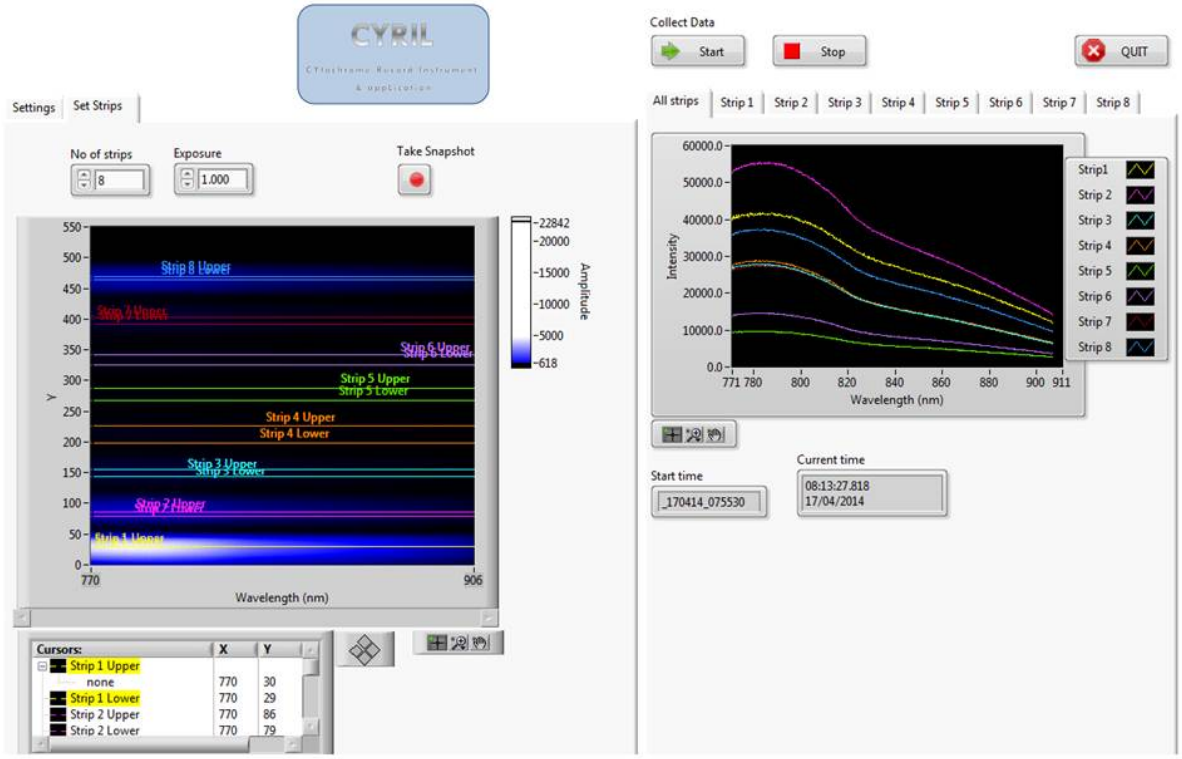

Figure 5.23: CYRIL software version 1 - bin settings. The left side displays the CCD intensity map and the user can take an image of the map using the Take Snapshot button and set the ROIs by moving the strip boundaries. The right side is the same as in the previous figure.

Intensity Data Acquisition

When the user selects 'Start' the CCD is programmed to acquire data per the settings using LabVIEW drivers for the PIXIS 512f CCD (Scientific Imaging Tool Kit, R Cubed Software). The CCD collects data separately from the ROIs and bins the data by wavelength. The intensity spectra for each ROI are displayed on the upper right-hand side of the GUI and the user can move between the tabs to view each detector ROI separately.

Chromophore Calculation

The intensity spectra are processed using the UCLn algorithm (equation 3.22) to give differential concentrations from an arbitrary baseline [48]. The changes in chromophore concentrations were calculated from the measured changes in broadband NIR light attenuation using the modified Beer-Lambert law as applied with the UCLn algorithm (illustrated in Figure 5.25). The UCLn algorithm in matrix form (equation 3.25) is a least-squares fitting procedure based on multiple regression analysis, using the Beer-Lambert law to determine the best fit of the chromophore extinction coefficients.

The change in attenuation is calculated (from equation 3.13) and interpolated to the nearest nanometre across 770-906 nm using a spline interpolation (or the form of interpolation that the user selects in the 'Settings' tab). The UCLn algorithm was applied to solve for changes in the concentrations of HbO_2, HHb and oxCCO across these 136 wavelengths. The specific extinction coefficient spectra used are displayed in Figure 4.4. The optical pathlength was derived from the product of the distance between the optodes and the DPF, which was has been previously measured as 4.99 ± 0.45 on the head of a newborn infant [114], corrected for the wavelength-dependency of the DPF (also plotted in Figure 4.4). The changes in concentration are displayed in real-time for each channel in the tabs on the right side of the GUI.

Data Saving

The raw data (intensity spectra), processed data (differential concentrations) and time log for each detector are saved as comma-separated value (.csv) files in real-time immediately after the data has been processed for each measurement. Each new measurement is appended to the .csv file to ensure that the data are saved in real-time which will prevent loss of data in the event of system failure. The time log contains the time and date of each measurement, elapsed time from the beginning of the measurement and warnings or comments which are encountered or entered at each time point.

Changes in concentrations of the chromophores are displayed in real-time on the lower right-hand side of the GUI. The number of data points that are displayed can be adjusted in the 'Settings' tab. However, in order to minimise the amount of data kept in random access memory (RAM) and therefore reduce the processing time, it is advised to limit the number of measurements displayed.

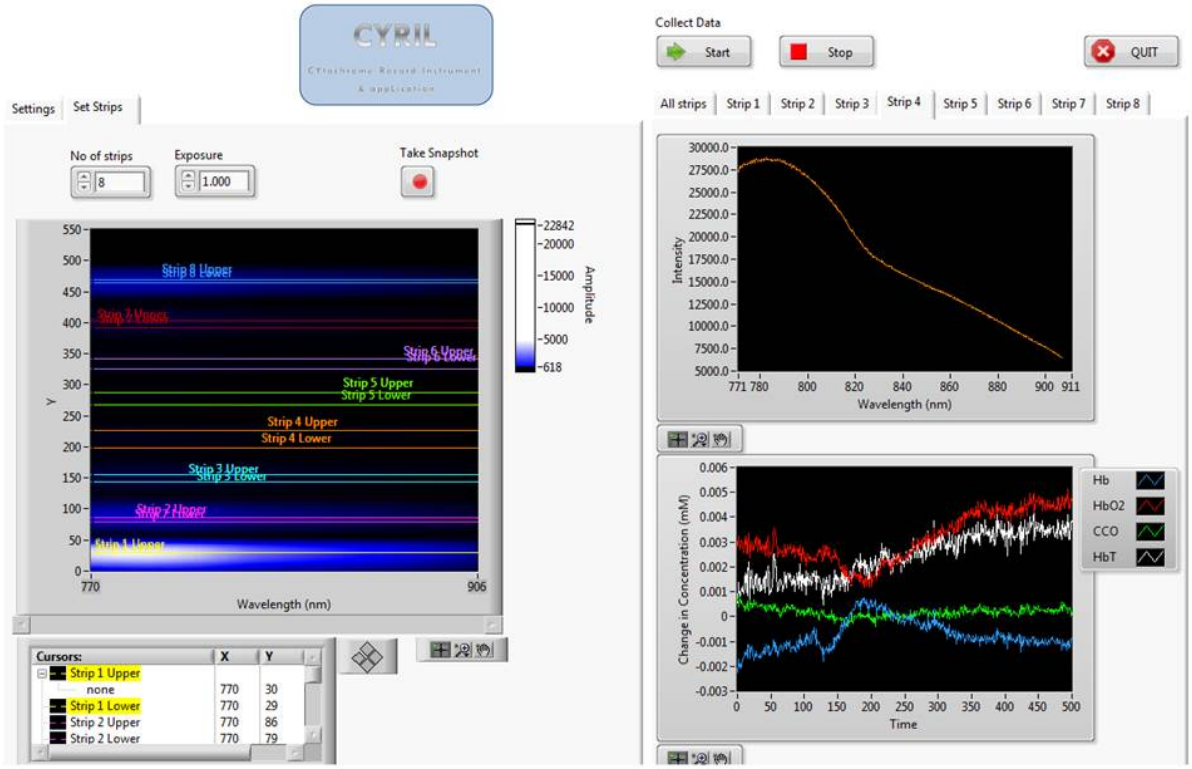

Figure 5.24: CYRIL software version 1 - displaying concentrations of chromophores in real-time. Each tab on the right side shows the intensity spectra (above) and changes in chromophore concentration (below) from a different source-detector channel, set by the ROIs.

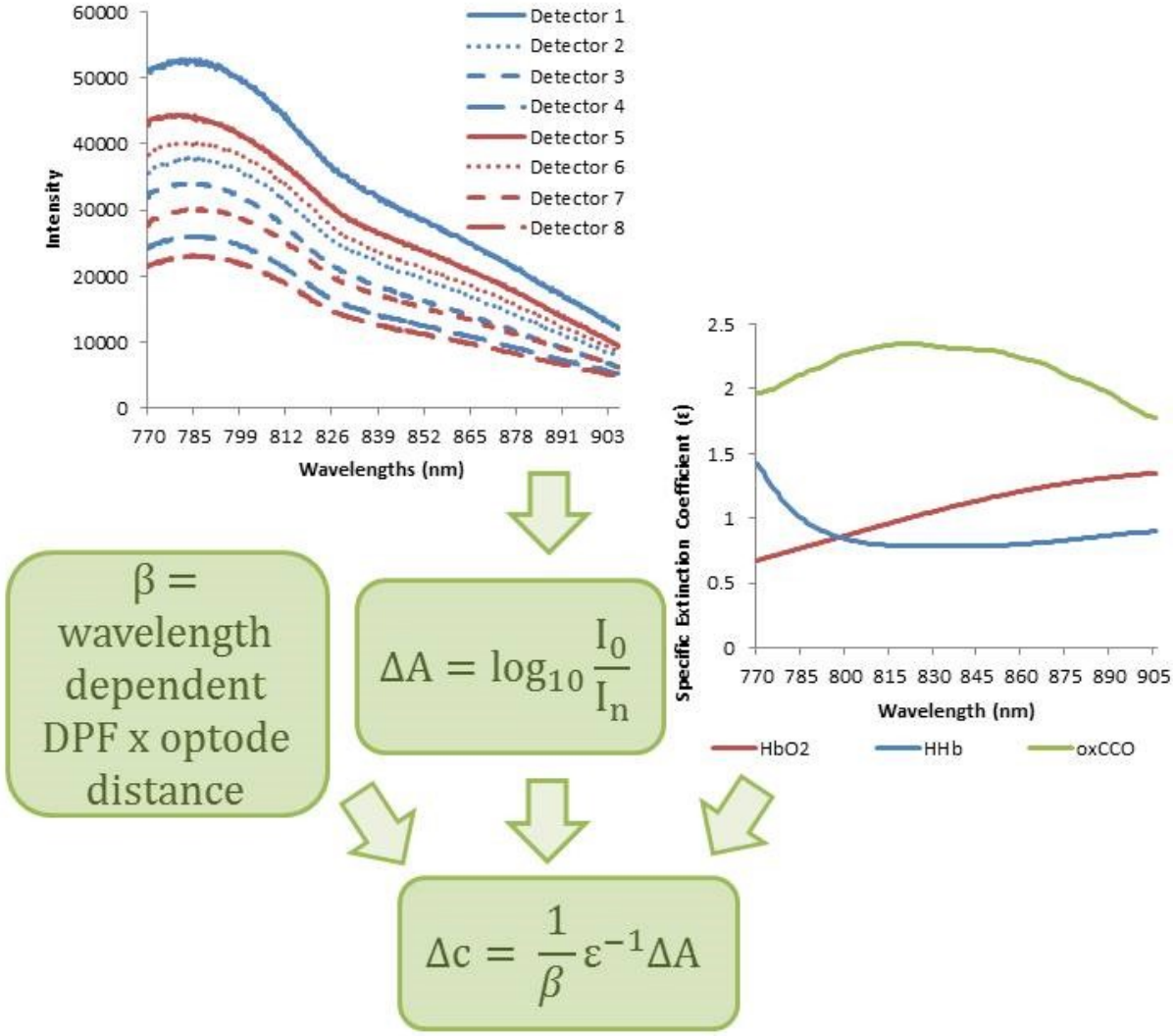

Figure 5.25: Schematic showing modified Beer-Lambert law and the input variables. Intensity spectra, I, are recorded simultaneously at all detectors (red = channel 1, blue = channel 2). The intensity spectra are converted to change in attenuation ΔA and the change in concentration Δc are calculated using the UCLn algorithm with the specific extinction coefficient of the chromophores ϵ and the pathlength β.

5.3.2 Version 2

The software was updated in October 2014 after the first year of use to be more user friendly and also to calculate the TOI in real-time (prior to this the TOI was calculated offline in data pre-processing). Figure 5.26 shows the major new additions to the software structure added to the version 1 flowchart (Figure 5.21).

Settings

The new 'Settings' tab (Figure 5.27) has the same functionality as version 1 but it also includes a diagram of the optode positions and the option to record a reference spectra (this was previously done manually). To record a reference spectra the user selects 'Reference spectra' and then chooses the channels that they are recording (either left side channels 1-4 (labelled '1234') or right side channels 5-8 ('5678')). One spectrum is captured for each of the four channels selected and this is saved as a single reference file which can be loaded in the TOI tab (see the next section).

The new tab for the binning settings (Figure 5.28) has not changed apart from the intensity map which has been made larger to allow more precise strip selection.

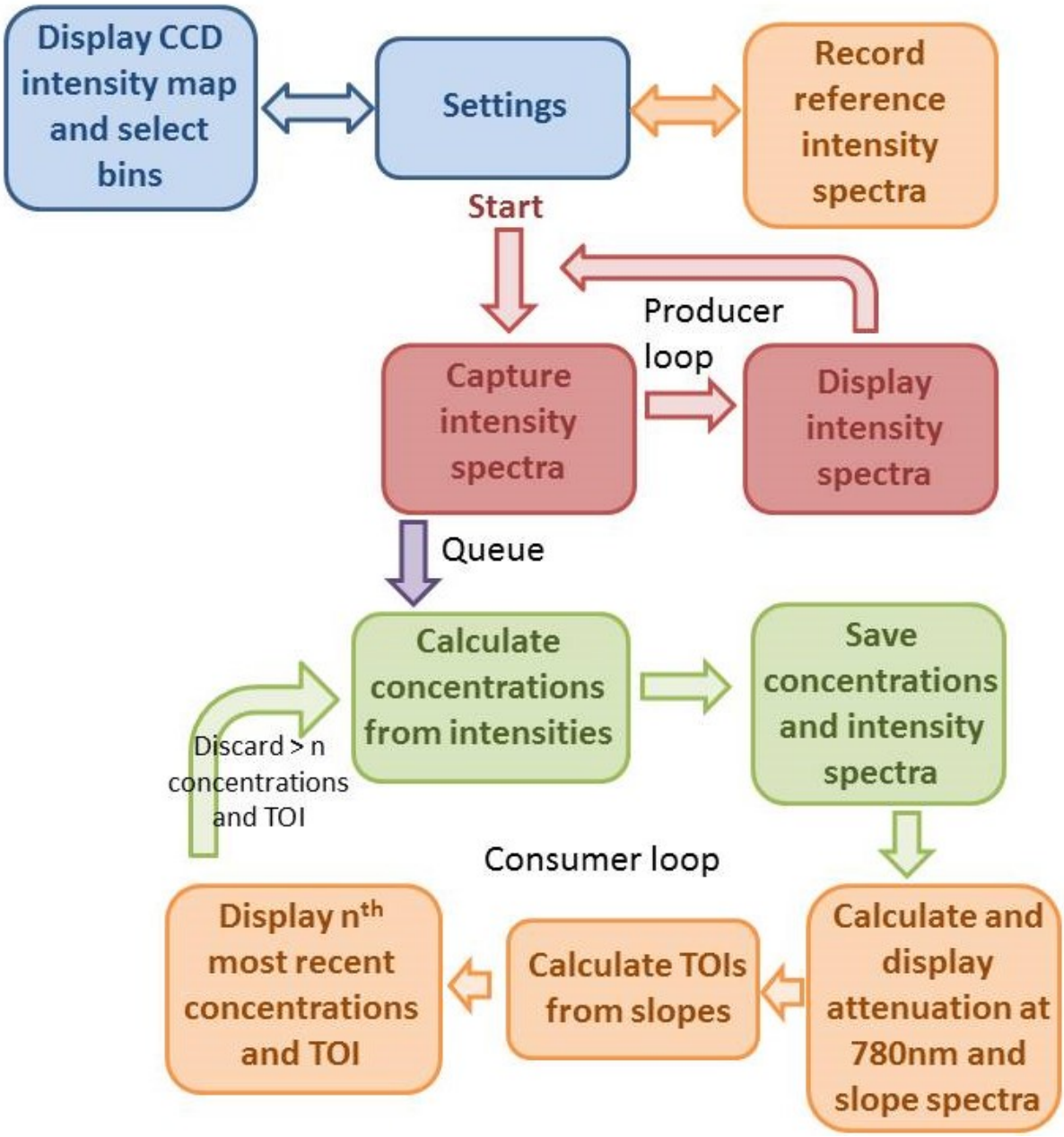

Figure 5.26: Block diagram of the main functions of the LabVIEW program - version 2. The orange coloured boxes represent the addition to the previous version.

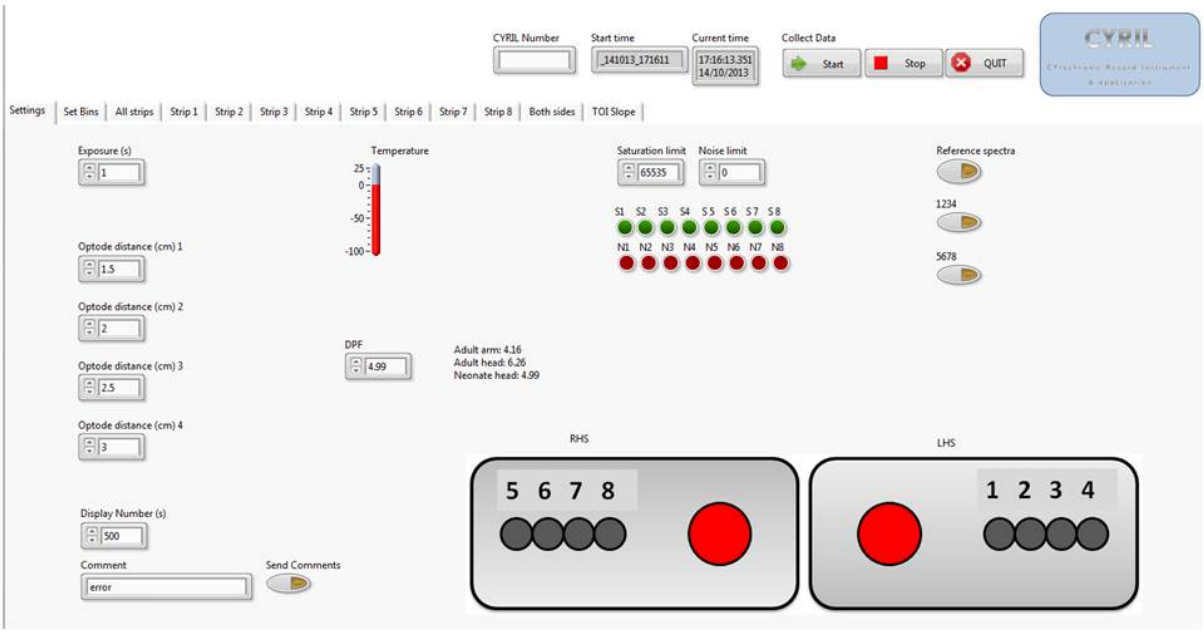

Figure 5.27: CYRIL software version 2 - settings. In this tab the user can set the exposure, optode distances, DPF, and number of concentration data points displayed; send comments to the time file; view the warning icons; and decide to record a reference spectra. The position of each channel in the optode holder is illustrated in the bottom right corner for ease of use. Above the tab, the user must enter the name of the file and can begin/end he data collection by pressing Start/Stop.

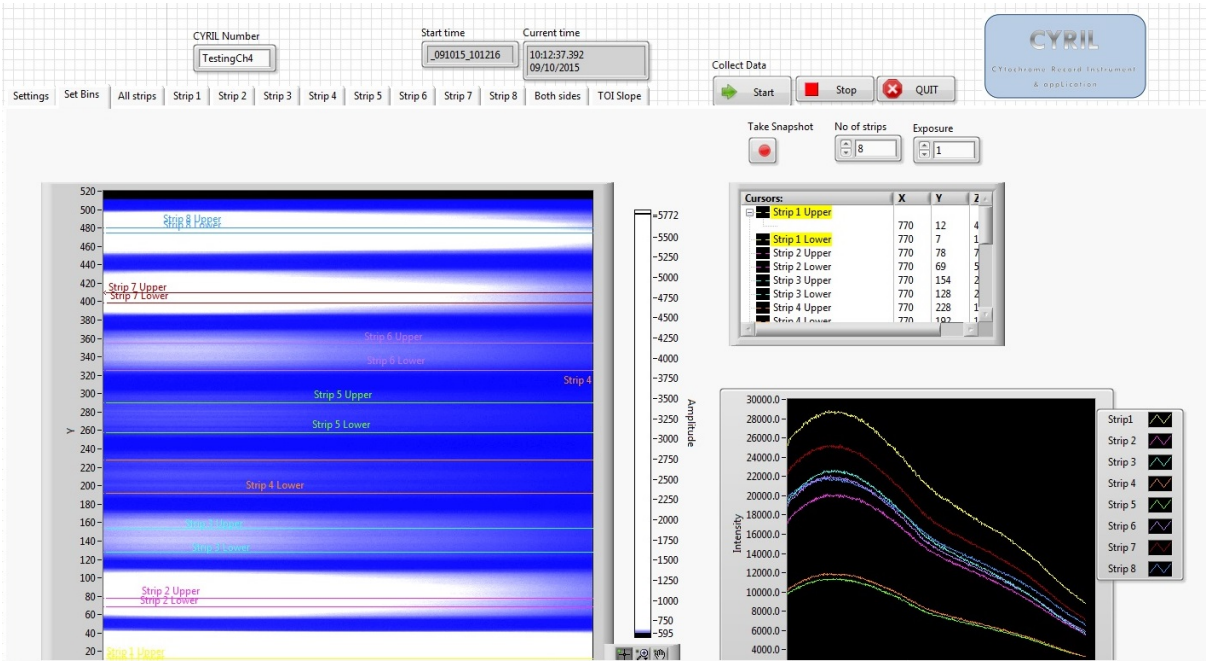

Figure 5.28: CYRIL software version 2 - bin settings. The bin settings tab is the same as in Figure 5.23 but made larger for ease of use.

Detector Displays

To see the full spectra of all channels in high resolution, a new tab was created (Figure 5.29). Further each detector channel tab has been changed to a full screen width to allow the user a larger view of the intensity spectra and chromophore concentrations (Figure 5.30). There is also a new tab that displays the channels with the longest source-detector distances from both right and left sides of the head as well as the TOI from each side (Figure 5.31); this allows the clinicians to see all of the most relevant clinical information on one screen.

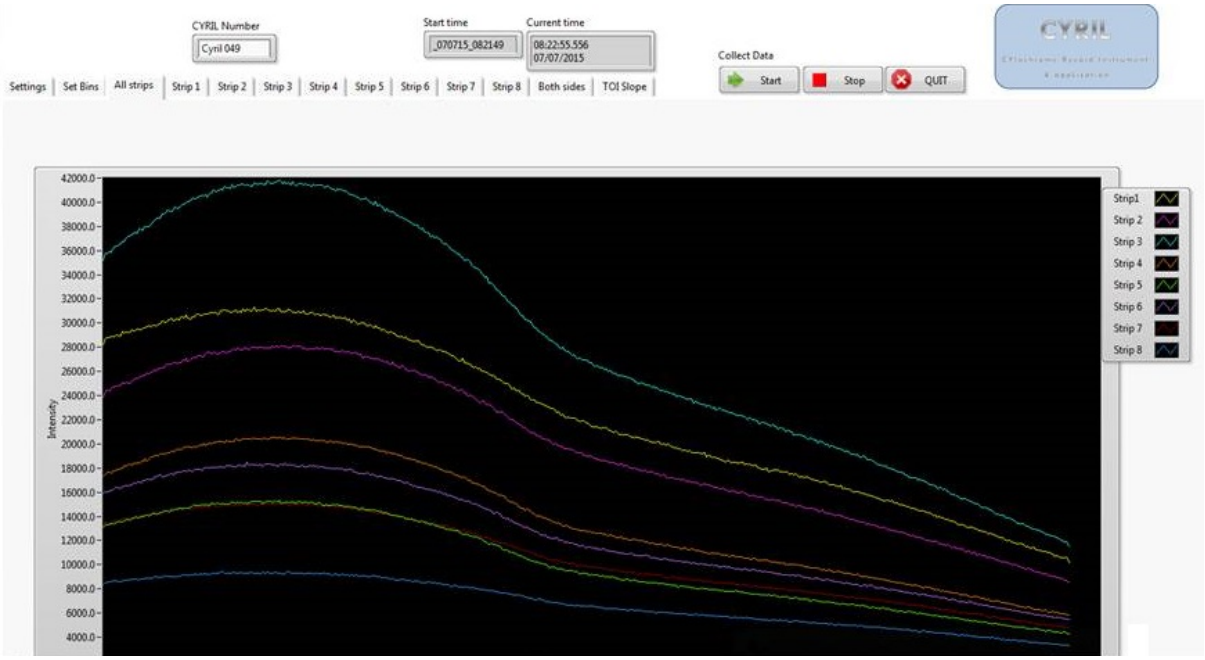

Figure 5.29: CYRIL software version 2 - displaying all intensity spectra.

TOI Calculation

The TOI is calculated in real-time within the consumer loop (discussed in section 5.3.1) - this process is illustrated in Figure 5.32. The software calculates the gradient of the attenuation against the distance (known as the 'slope') at every wavelength. This is fed into equation 3.45 and subsequently equation 3.46 to find the scaled concentrations of HHb and HbO_2. From those the TOI is calculated with equation 3.47.

There is a new tab in the GUI that assists in this measurement (Figure 5.33). The user can load the reference spectra (needed to calculate the absolute attenuation) and also decide to run the program without TOI (for example if the reference spectrum has not yet been recorded). The GUI also displays the plot of attenuation against distance at a single wavelength (780nm) so that the user can adjust the optodes if there is not a linear relationship. The slope at every wavelength is also displayed to check for normality. The TOI for both sides of the head is also displayed in real-time.

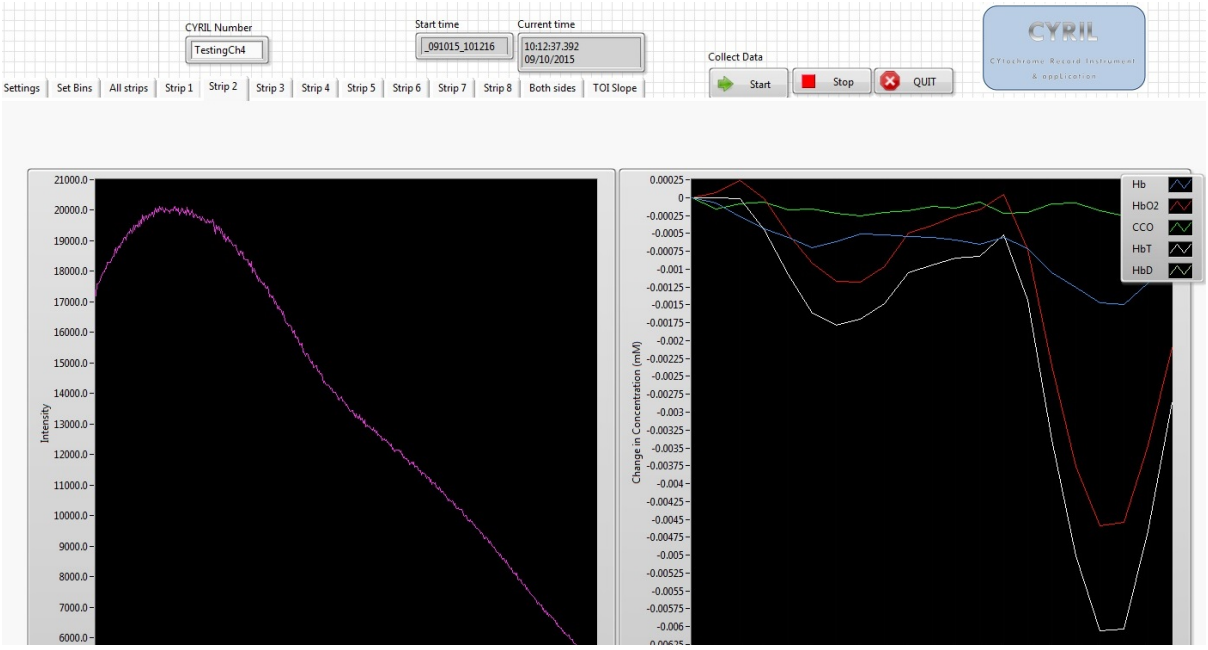

Figure 5.30: CYRIL software version 2 - displaying concentrations of chromophores in real-time. Each tab displays the data for a different channel as before but is larger for ease of use.

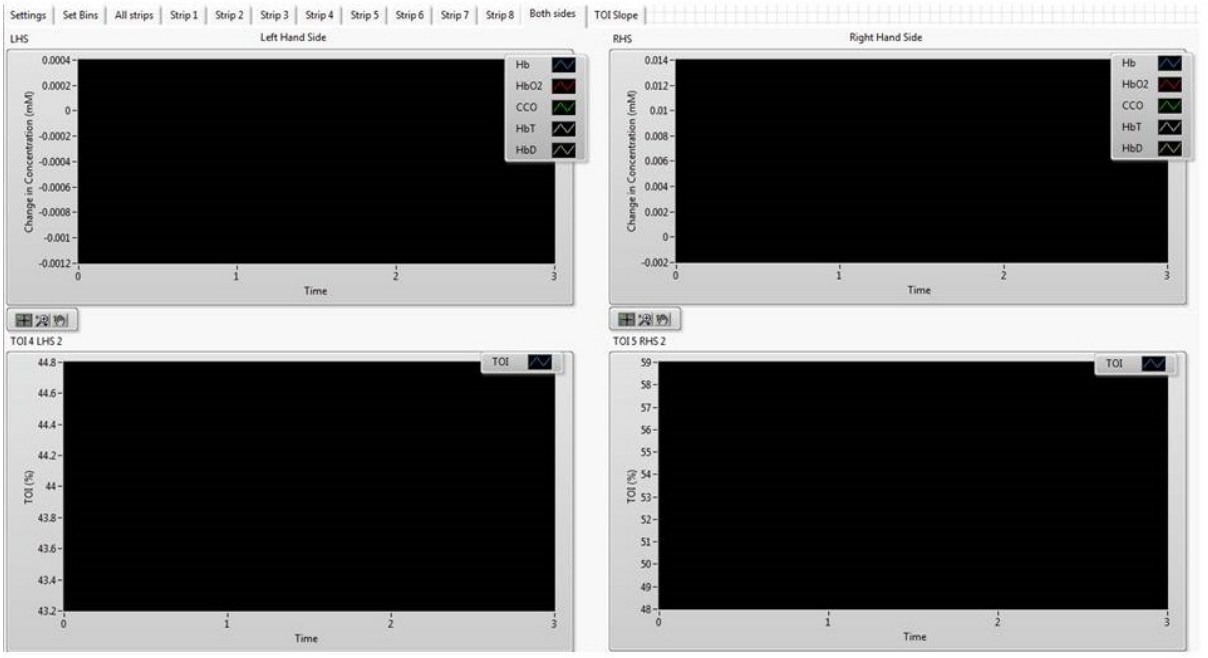

Figure 5.31: CYRIL software version 2 - summary of data collection tab. This tab gives the user a summary of the most important clinical data collected. The changes in concentration for the left and right side of the head (longest source-detector separation) are displayed at the top and the TOI for both sides of the head are displayed below. This is the recommended tab for viewing the data in real-time.

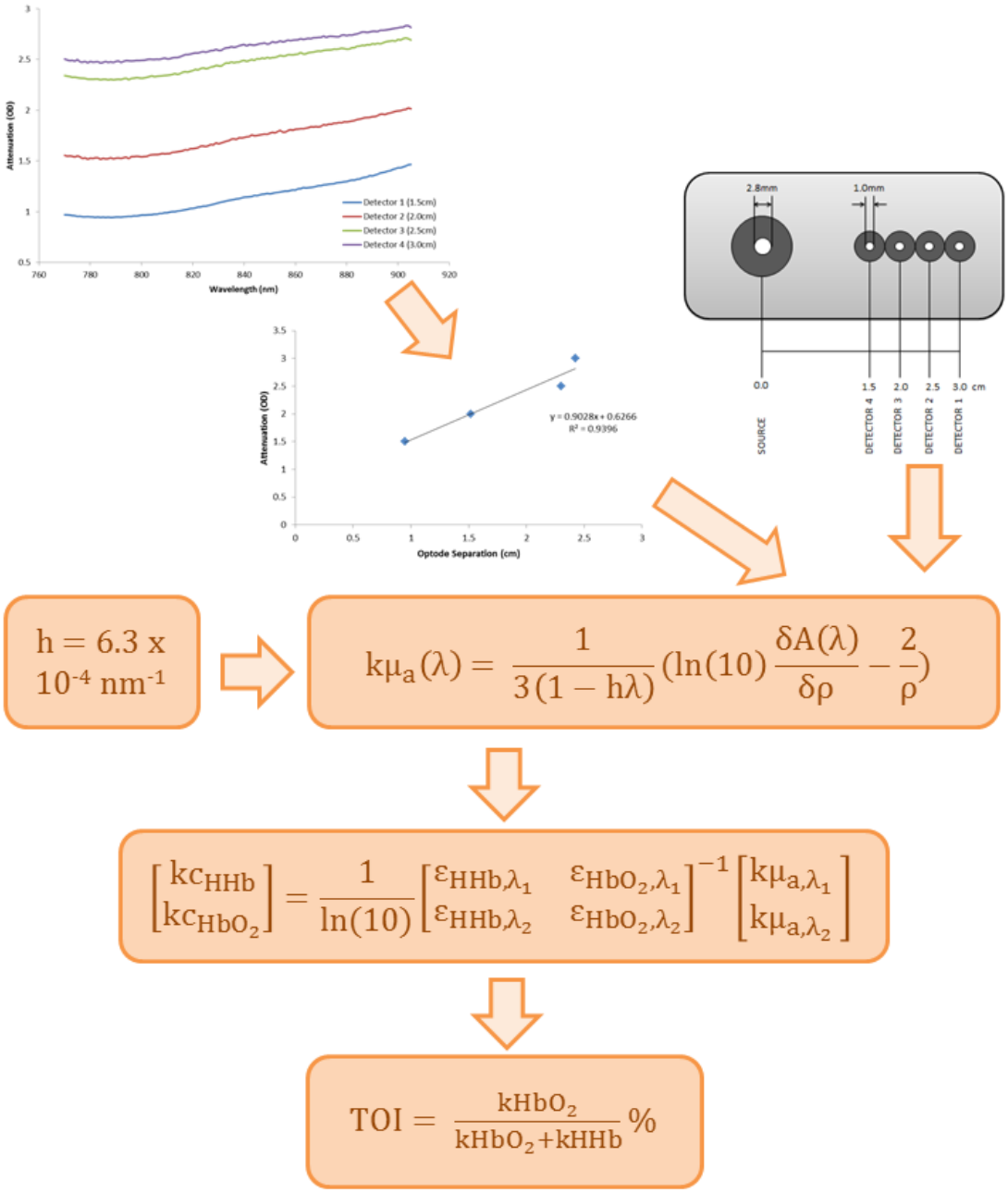

Figure 5.32: Flowchart of TOI calculation in LabVIEW software.

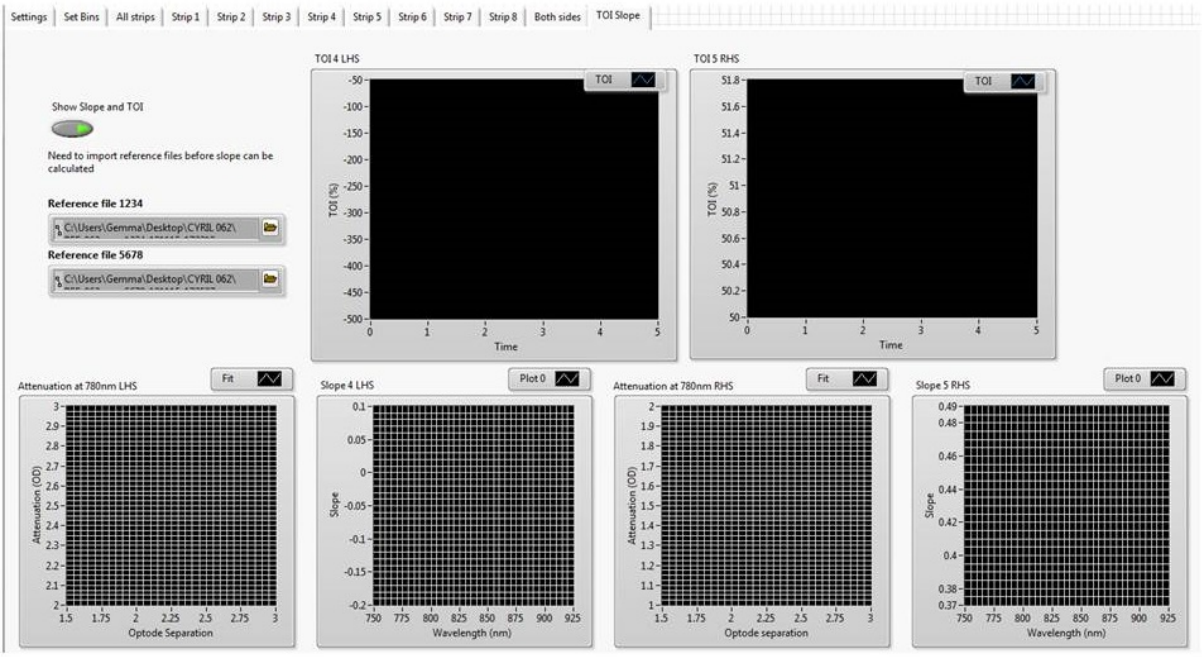

Figure 5.33: CYRIL software version 2 - TOI tab. This tab allows the user to set the reference spectra (required for TOI measurements) and view the TOI data. The plots at the top display the TOI for left and right sides, while the plots below show the attenuation per distance for one wavelength (780nm) and the slope across all wavelengths for both sides.

5.4 Calibrations

5.4.1 Wavelength Calibration

Every pixel on the CCD chip of the CYRIL system corresponds to a certain wavelength in the x-direction. The relationship between pixel and wavelength thus has to be determined through calibration. Each pixel in the x-direction is calibrated to its corresponding wavelength using the LightField (Princeton Instruments, USA) acquisition software with the IntelliCal calibration package. A neon-argon lamp with multiple emission lines across the NIR spectrum (see Figure 5.34) was used to illuminate the CCD for the IntelliCal calibration routine. The entrance slit width was set to 1μm. The spectrum was recorded (see Figure 5.35) and then the pixels were matched to a wavelength by a non-linear least squares regression refinement algorithm that minimises the intensity space residual with respect to a theoretical model of the spectrometer. This was done for multiple wavelength ranges which were changed by rotating the grating in the spectrograph. Therefore the system is calibrated for multiple wavelength ranges and the user can select the range by turning the micrometer and selecting the corresponding wavelength calibration file. The wavelength range of CYRIL is normally set to 770-906nm. The CCD resolution error after calibration is 0.27nm.

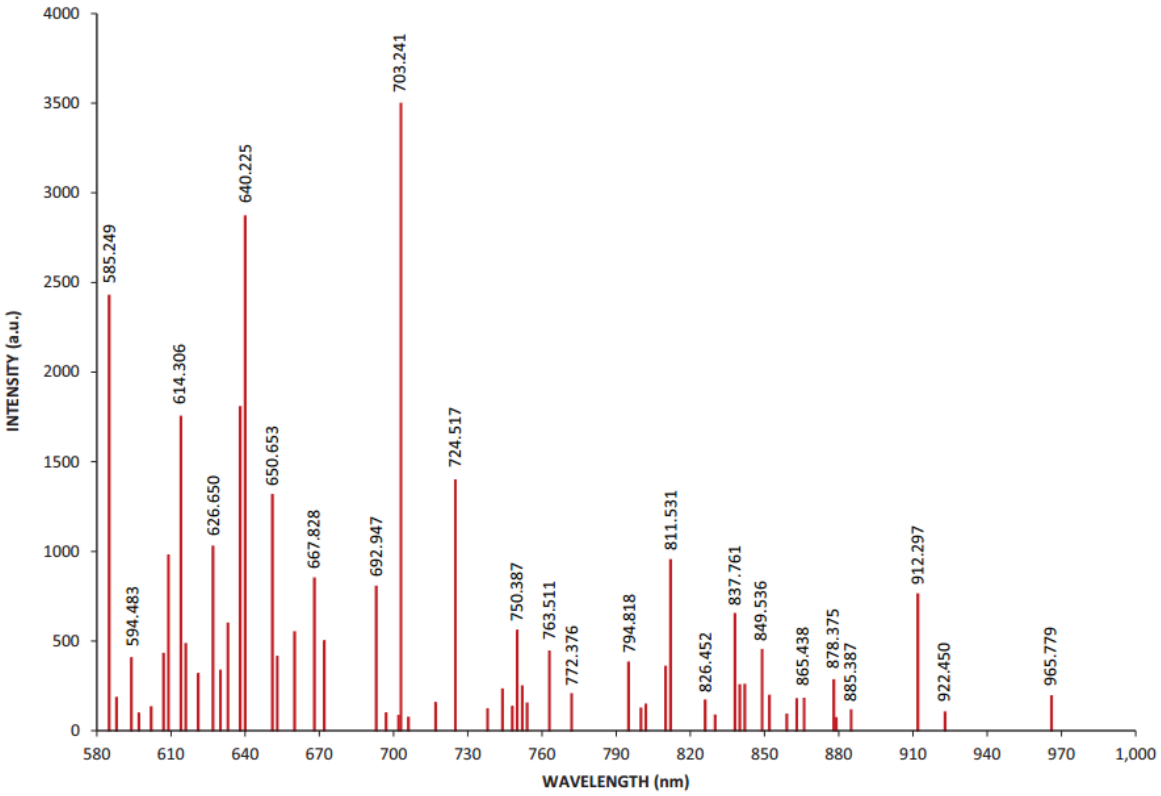

Figure 5.34: Neon-Argon lamp used for wavelength calibration. Taken from Hg and Ne/Ar USB Dual Light Source User Manual (Princeton Instruments, USA).

The wavelength resolution of the spectrometer alone was assessed during wavelength calibration. The peaks in the calibration source spectra can be used to measure the resolution by testing the minimum

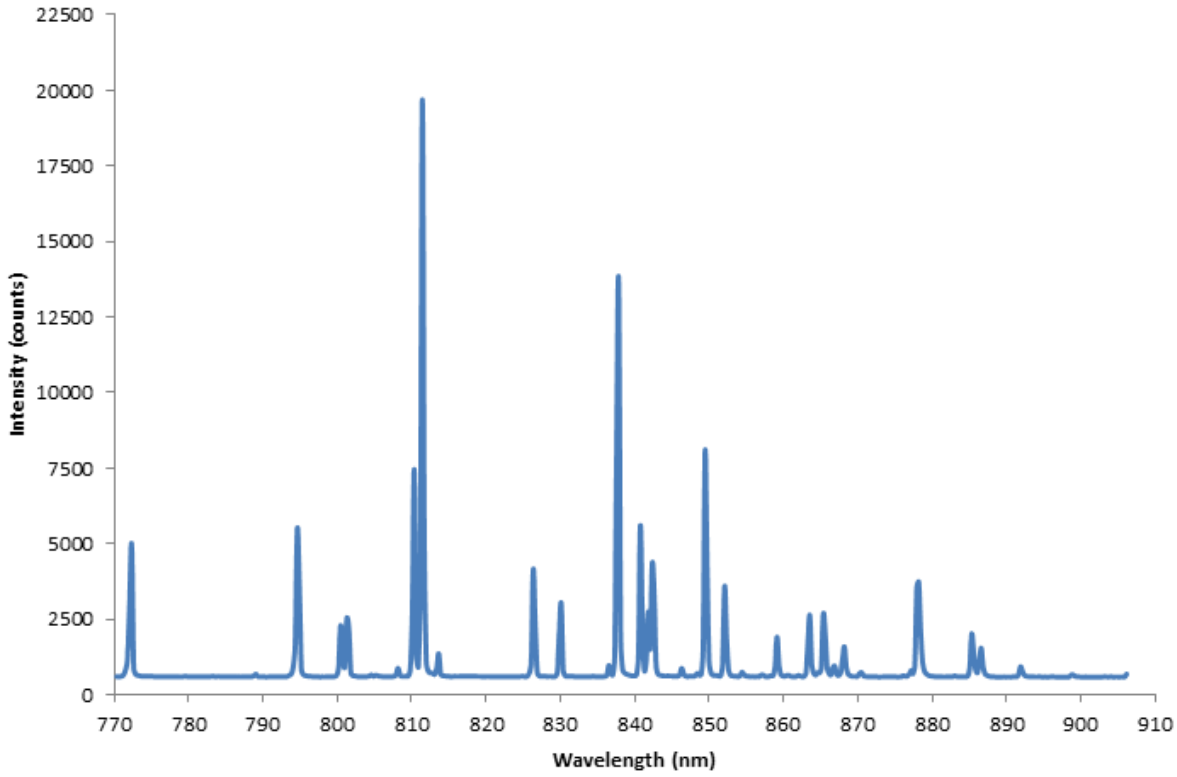

Figure 5.35: Wavelength calibration spectra recorded with CYRIL.

peak-to-peak separation that one can resolve. Figure 5.36 shows two peaks in the spectrum 1.7nm apart, therefore the resolution of the spectrometer is at least 1.7nm.

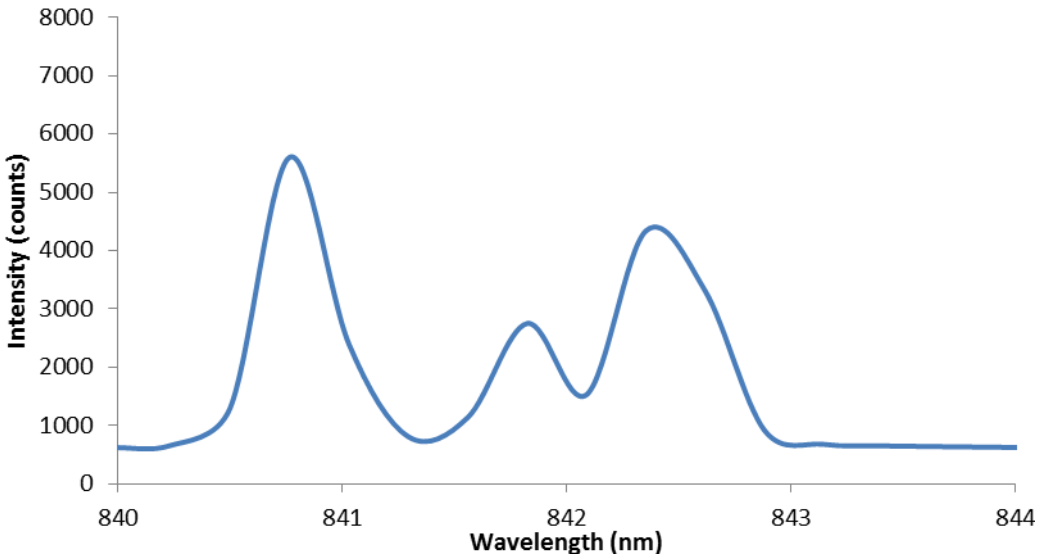

Figure 5.36: Wavelength calibration spectra recorded with CYRIL (shown in full in Figure 5.35) across 840-844nm to show resolution. The peaks at 840.7nm and 842.4nm are visible and distinct which confirms that the resolution is at least 1.7nm.

5.4.2 Intensity Calibration

The multiple detectors have different bin widths on the CCD and therefore require an intensity calibration due to the different intensity proportions of the eight detector fibres. Usually a dark room is used to record the intensity of the light source through free space with no absorbing medium. However, in a clinical environment there are no dark rooms therefore a poster tube lined with blackout rubberised fabric is used to collect the spectra. To ensure equal illumination of the four detector fibres the latter are placed at the other end of the tube from the light source fibre as illustrated in 5.37. The spectra of this set-up can then be acquired with the LabVIEW real-time program and saved as reference spectra in an .csv file which is loaded when the program is started. Figure 5.38 shows an example of the reference intensity spectrum recorded.

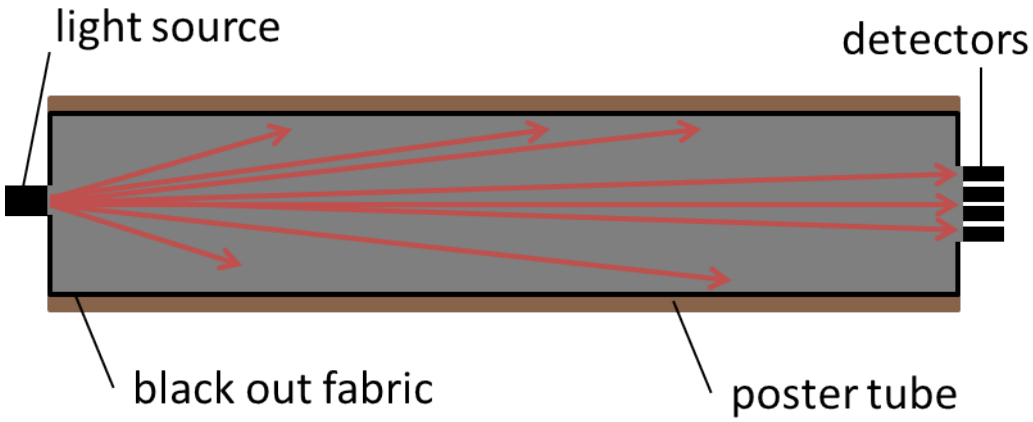

Figure 5.37: Reference intensity set-up in customised poster tube.

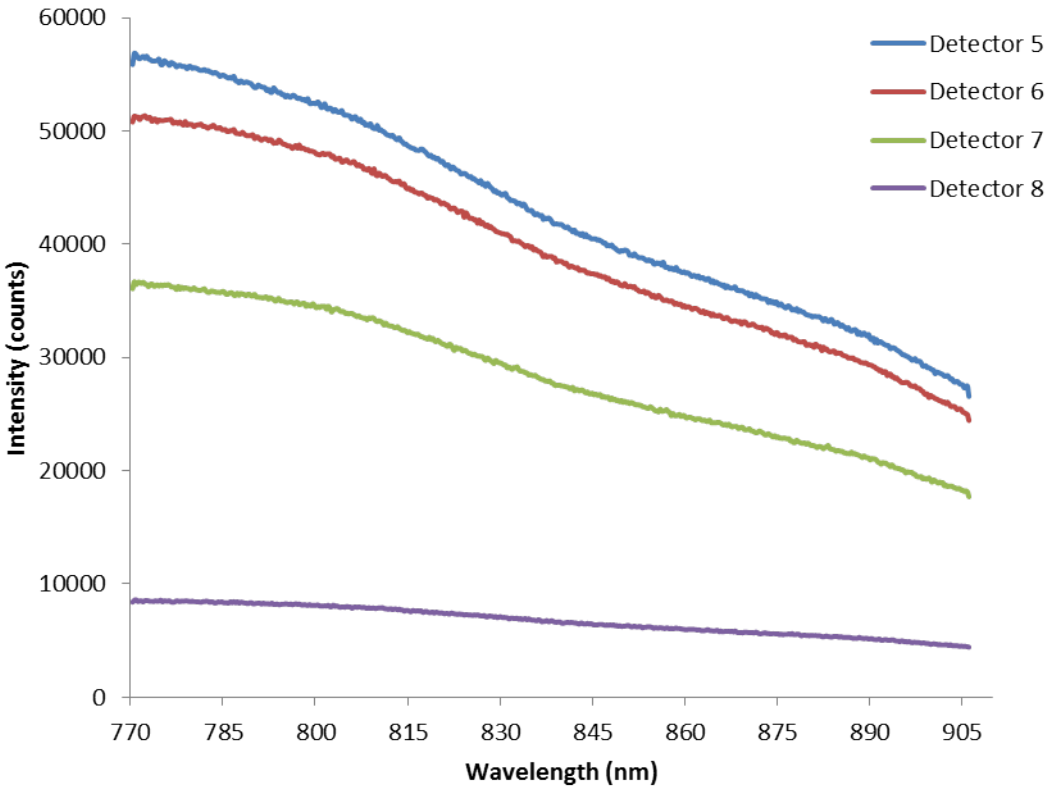

Figure 5.38: Reference intensity captured in poster tube for right side channels.

5.5 CYRIL Specification

The CYRIL system has been characterised and Table 5.2 details the specification of the system. This section described the processes to determine the specification.

Table 5.2: CYRIL specifications.

Requirement	**Specification**
Light throughput	99.4%
Bandwidth	136nm
Spectral range	770-905nm
Spectral resolution	4.48nm
CCD chip size	12.3mm x 12.3mm
CCD pixels	512 x 512
CCD Temperature	-70°C
Dark current	0.002 e^-/p/s
Dark count	∼400 counts per second
Read noise	5e^- RMS
Power output	1.62mW/mm^-2

5.5.1 Optical Bandwidth

The wavelength range of an instrument is referred to as its optical bandwidth. In CYRIL it is limited by the dimension of the CCD chip and the spectrograph grating groove density. The sensitivity of the CCD chip would also limit the bandwidth but in this case the CCD was chosen specifically to have a high quantum efficiency across the NIR (see Figure 5.12) so this does not limit it. The optical bandwidth is thus defined by the groove density of the grating and the size of the CCD chip. The optical bandwidth in this system has been measured to be 136nm. The range was selected to be 770-905nm

5.5.2 Optical Resolution

For broadband NIRS measurement of oxCCO an optical resolution of at least 5nm is required to characterise the broad peak around 835nm in the CCO difference extinction spectrum [53]. The wavelength resolution is dependent on the diffracting grating groove density, the entrance slit width of the spectro-

graph and the size of the CCD pixels:

$$\begin{aligned}
\text{Dispersion} &= \frac{\text{Spectral Range}}{\text{Number of detector elements}} \\
&= \frac{136nm}{512pixels} \\
&= 0.27nm/pixel \\
\text{Resolution} &= \text{Slit Width} \times \text{Grating groove density} \\
&= 20\mu m \times 830lines/mm \\
&= 16.6pixels \\
\text{Optical Resolution} &= \text{Dispersion} \times \text{Resolution} \\
&= 0.27nm/pixel \times 16.6pixels \\
&= 4.48nm
\end{aligned} \tag{5.1}$$

Therefore the optical resolution of the spectrometer is 4.48nm which is sufficient for resolving changes in oxCCO. This is larger than the resolution measured with the calibration source (section 5.4) because the slit is wider.

5.5.3 Power Output

The power at the end of the source fibre was measured to ensure that it conforms with safety standards and is not causing tissue heating that would be uncomfortable and potentially harmful to the patient. At 850nm the average power was measured with a power meter to be 10.03 ± 0.08mW. UK safety standards for tissue states that the maximum power should not exceed 2mW per square millimetre. The diameter of the source fibres is 2.80mm so the area is 6.15mm^2 thus the power per square millimetre is 1.62mW, which lies within safety limits.

5.5.4 Noise

The CYRIL system is not limited by noise under normal operation. The dark count was measured to be ∼400 counts per wavelength bin per second at -70°C.

Binning Dependence

Potential disadvantages of using a lens-based spectrograph instead of a set of separate spectrometers is the crosstalk among channels and/or reduction in the sensitivity. This issue of crosstalk between the detectors is resolved by proper focussing of the light onto the detector with the focussing lens and careful selection of pixels to be binned in the y-direction. The cross-talk was tested by blocking channels during a measurement on a solid tissue-like phantom. The crosstalk effect was not observed between binning regions. Figure 5.39 shows an image of the of the CCD chip where all detectors have been blocked except the top (channel 8, at 1.5cm source-detector separation). This shows that although there is excess light

outside of the binned ROI for that detector, the light does not affect the nearest binned ROI; there is no significant cross-talk effect observed.

Sensitivity

The sensitivity of the system is controlled by the wavelength binning of the pixels on the CCD and the dynamic range. The bin size ranges from 3 to 33 pixels. These ranges are comparable to micro-spectrometers which range from 1 pixel (Avantes Ava Spec Mini) up to 64 pixels (Ocean Optics QE64000) in the y-direction. The system has 16 bit digitisation for each ROI.

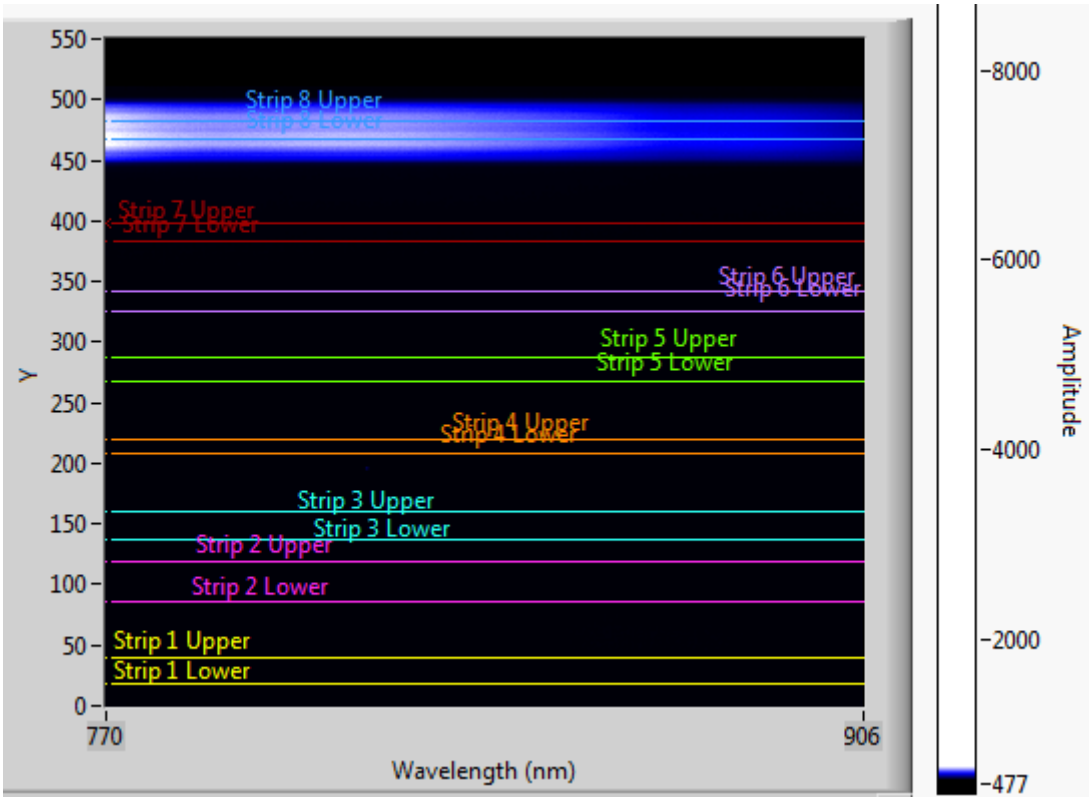

Figure 5.39: Intensity map of the CCD chip when all detectors have been blocked except the uppermost (detector 8). There is no cross-talk between the detector binning regions (coloured lines). Amplitude is measured in counts per pixel.

5.6 Preliminary Testing

CYRIL is able to successfully record data continuously at 1Hz for long periods (>90 hours) without error. CYRIL is a compact and portable system that can be moved to the cotside without hindering access to other equipment or the cot itself. The long (3m) fibres allow the system to be stored further from the cot as space is limited. This also enables access to the baby for essential medical and nursing care, which is especially vital in an emergency.

5.6.1 Phantoms

In order to test the stability of the system over time, studies on solid phantoms with tissue-like optical properties [229] were performed. Figure 5.40 shows the resolved changes in chromophore concentration on a stable phantom showing negligible changes (on the order of nM) with time.

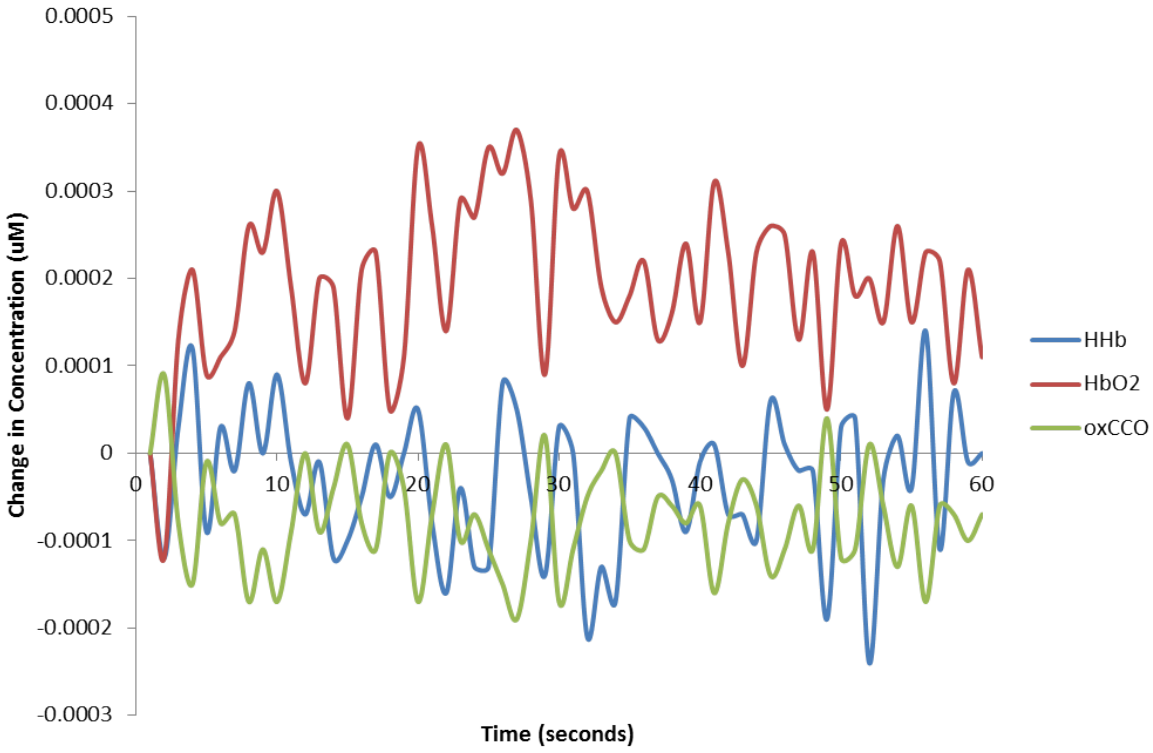

Figure 5.40: Changes in concentrations resolved from phantom study. Note that the scale is on the order of nM.

5.6.2 Cuff Occlusions

To test that the system is able to measure chromophore concentration changes in-vivo, cuff occlusion studies were performed on 5 healthy adult volunteers. Optodes were placed over the forearm muscle. A baseline was recorded and then a blood pressure cuff on the upper arm was inflated to 60mmHg to occlude the vein. After a period the cuff was deflated and the subject was given a rest. The cuff was then inflated to 200mmHg to occlude both the artery and the vein, followed by a rest.

Figure 5.41 shows examples of the intensity spectra recorded during the three events (baseline, venous occlusion and arterial occlusion).

The changes in the shape of the spectra reflect the different levels of chromophore concentrations during each period. In the venous occlusion there is a normal supply of HbO_2 but no way to remove the HHb from the tissue, hence the concentration of both increases; the spectra is reduced in intensity due to the increase in absorber concentration but does not change shape. However, during the arterial occlusion a difference in the shape of the spectra is observed (shift of the peak from ~770nm to ~788nm

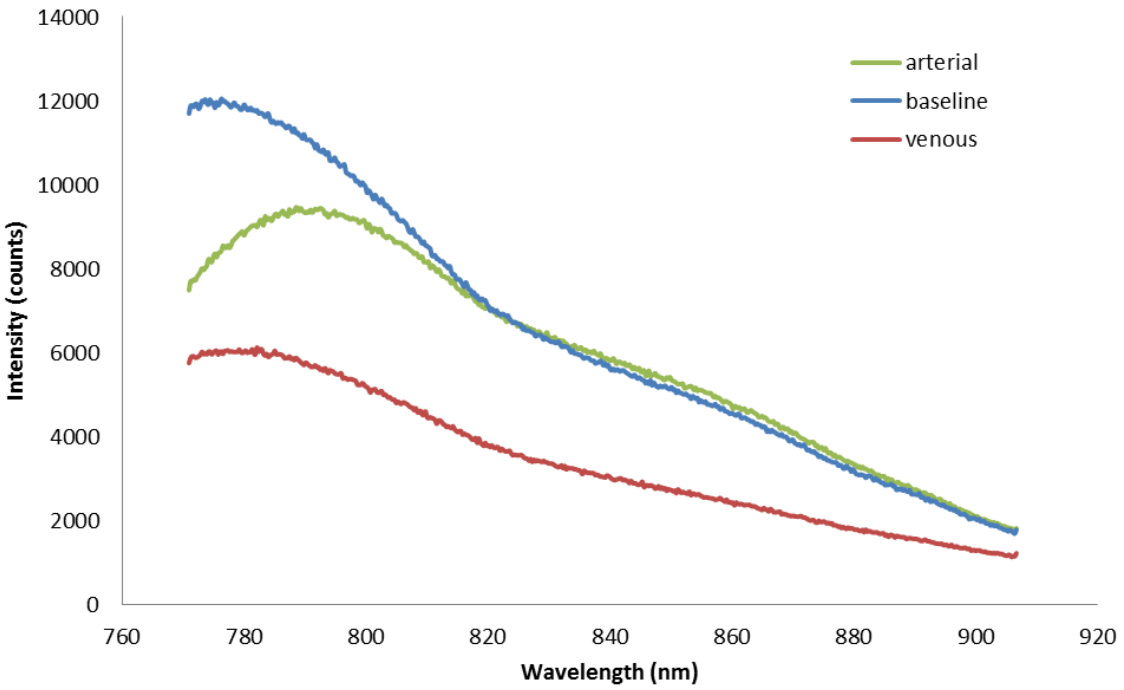

Figure 5.41: Intensity spectra through arm during baseline (blue), venous occlusion (red) and arterial occlusion (green) showing differences in spectra shapes in response to the change in chromophore concentrations.

and increase in the ~845nm 'shoulder') due to the decrease in HbO_2 as it is converted to HHb. The concentrations resolved from this study is shown in Figure 5.42. The oxCCO signal shows a small decline throughout the occlusion which suggests that CCO becomes more reduced as the oxygenation lowers which makes physiological sense. The gradient of the increase in HHb appears equal and opposite to the slope of the decrease in HbO_2 which corresponds with the physiological events. The stability of the HbT signal confirms that the system is measuring the events of an arterial occlusion accurately. This result was reproduced in all 5 subjects.

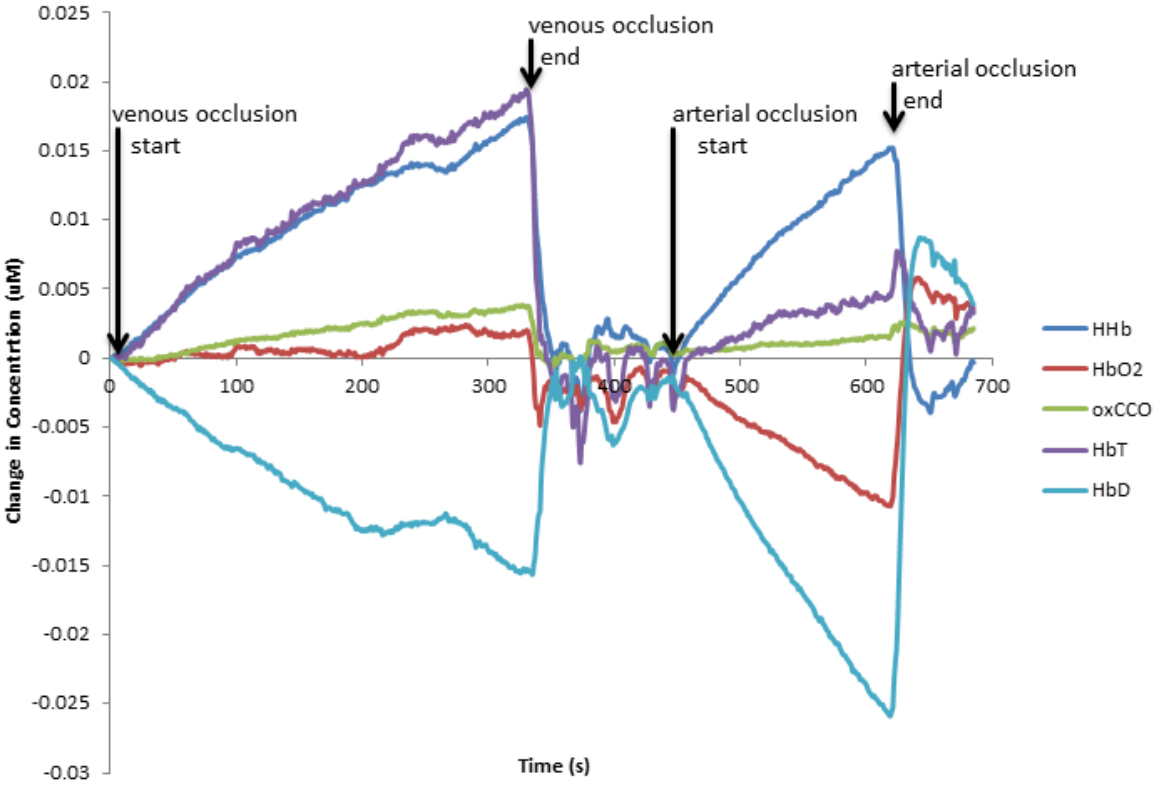

Figure 5.42: Change in concentration during venous and arterial cuff occlusion on forearm.

Chapter 6

Monitoring Cerebral Cytochrome-C-Oxidase in Infants with HIE

The design and testing of the broadband NIRS system, CYRIL, was described in the previous chapter; in this chapter the design of the studies of newborn infants with HIE is discussed. Infants with HIE were monitored at the cotside throughout the first week of life with CYRIL. The CYRIL broadband NIRS system was designed specifically for monitoring cerebral metabolism at the cotside in the NICU. However, there are many challenges faced when performing studies in this environment. This chapter describes those challenges and their solutions, and outlines the experimental protocol and data processing performed.

6.1 Objectives and Challenges

This is the first time broadband NIRS has been used to observe cerebral changes in oxCCO after HI injury in human newborns, and the second time oxCCO has been measured on this population [21]. The objective for this study was to:

1. Demonstrate the measurement of cerebral changes in oxCCO with broadband NIRS at the NICU cotside on HIE infants in the first days of life
2. Use the measurement of cerebral oxCCO in combination with multimodal data to assess brain injury severity after HIE

As the studies are to be undertaken in the first days of life, they are performed in the NICU while HIE is managed in an intensive environment (see section 2.5). This presents challenges and this chapter describes how these were dealt with.

6.2 Monitoring Set-Up

Ethical approval for the Baby Brain Study at University College London Hospital (UCLH), London was obtained from the North West Research Ethics Centre (REC reference: 13/LO/0106) and research and development (R&D) approval was obtained from the UCLH Trust. The NIRS study is part of the Baby Brain Study which aims to assess the relationship between brain intracellular pH (pHi), brain perfusion and oxCCO during neuroprotection therapies. The study is currently ongoing. Parents of term and preterm infants born at or transferred to UCLH for treatment of acute brain injury were approached for this project; only babies without congenital malformations are considered. Informed parental consent was obtained before inclusion in the study. The focus of this work is on term infants with HIE but also assesses the cerebral haemodynamic and metabolic changes in other term and preterm infants who have developed or at risk of developing neonatal encephalopathy from other aetiologies (e.g. neonatal stroke or seizures). The study details, parent information and consent forms are presented in Appendix A.

All infants were monitored continuously with 10 channel EEG using Nicolet monitors (Natus Medical Incorporated, USA) which also presents aEEG data. Systemic data from the Intellivue Monitors (Philips Healthcare, UK) were collected simultaneously using an application called ixTrend (ixellence GmbH, Germany). Signals recorded include oxygen saturation (SpO_2) measured by pulse oximetry on the foot or hand, heart rate (HR) by electrocardiograph (ECG), respiratory rate (RR), mean arterial blood pressure (MABP) from an intra-arterial catheter, and the partial pressures of O_2 and CO_2 measured transcutaneously. The babies spent one hour in the MR scanner after rewarming. They are not known to effect Lac/NAA.MR scans included a measurement of Lac/NAA with hydrogen (^1H) MRS. The babies were sedated with either morphine (intravenous) or chloral hydrate (oral); neither sedative is known to affect the Lac/NAA. See Figure 6.1 for schematic of monitoring time line, Figure 6.2 for diagram of monitors and Figures 6.3 to 6.6 for photographs of the study.

The CYRIL NIRS optodes are placed on each side of the forehead (as seen in Figures 6.5 and 6.6) which is free from EEG electrodes and hair. The optodes and holders are affixed to the head with double-sided tape which holds the optodes in place without applying pressure to the head. Each source-detector pairing is positioned over one hemisphere of the brain (4 channels either side). The sources are applied when the light shutter is closed for eye-safety reasons. The optodes are tucked underneath the EEG cap and a piece of black-out fabric is held between the cap and the optodes to reduce interference from ambient light. The infants were positioned in the supine position for the duration of the study.

All measurements were taken bilaterally on the forehead over the frontal lobe. NIRS measurements began as soon as consent was granted from the parents, with a view to acquiring data as close to birth as possible. Final NIRS measurements were performed immediately before and/or after the MR scan. The CYRIL NIRS measurements were collected continuously over periods from 1 to 24 hours during the first days of life at a sampling frequency of 1Hz. The aim was to record data for 4-6 hours each day during therapeutic hypothermia and rewarming (days 1-4 of life), and 0.5-1 hour pre- and post-MR scan. The protocol is fully described below.

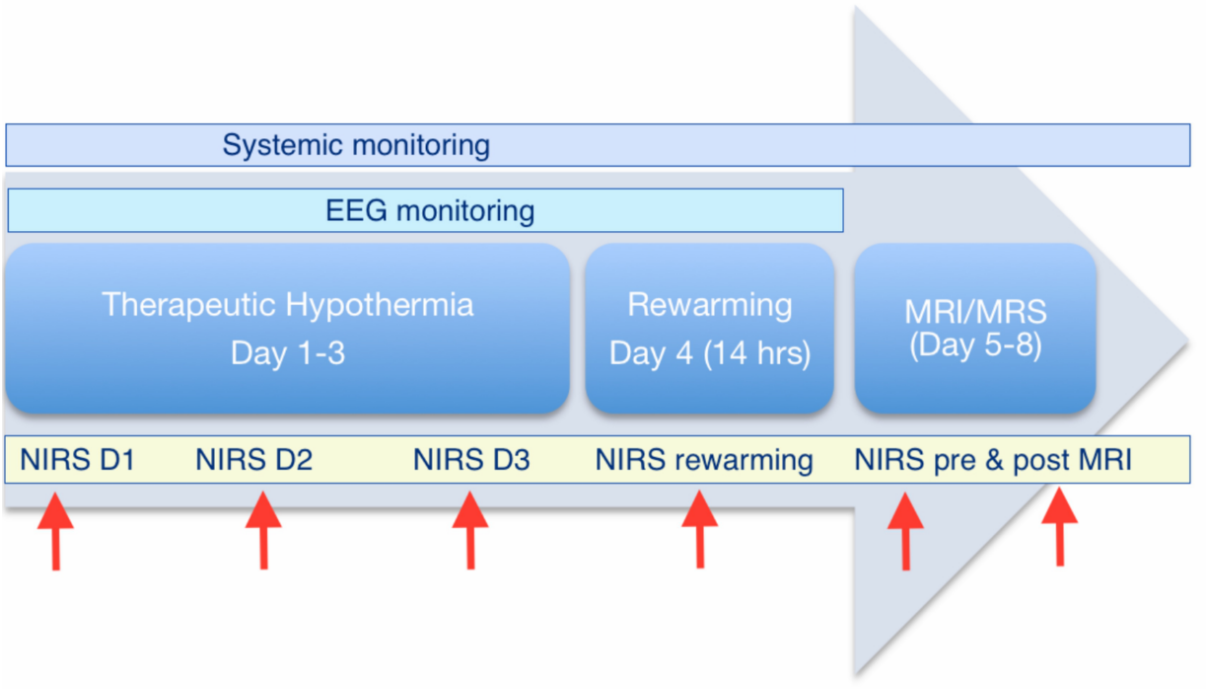

Figure 6.1: Typical time line of treatment and monitoring from birth to day 7 of life. Cooling starts as soon as possible after birth for 72 hours. NIRS starts as early as possible once parental consent is obtained. MR scan (MRI and ^{1}H MRS) occurs for 1 hour between days 4 and 15 of life.

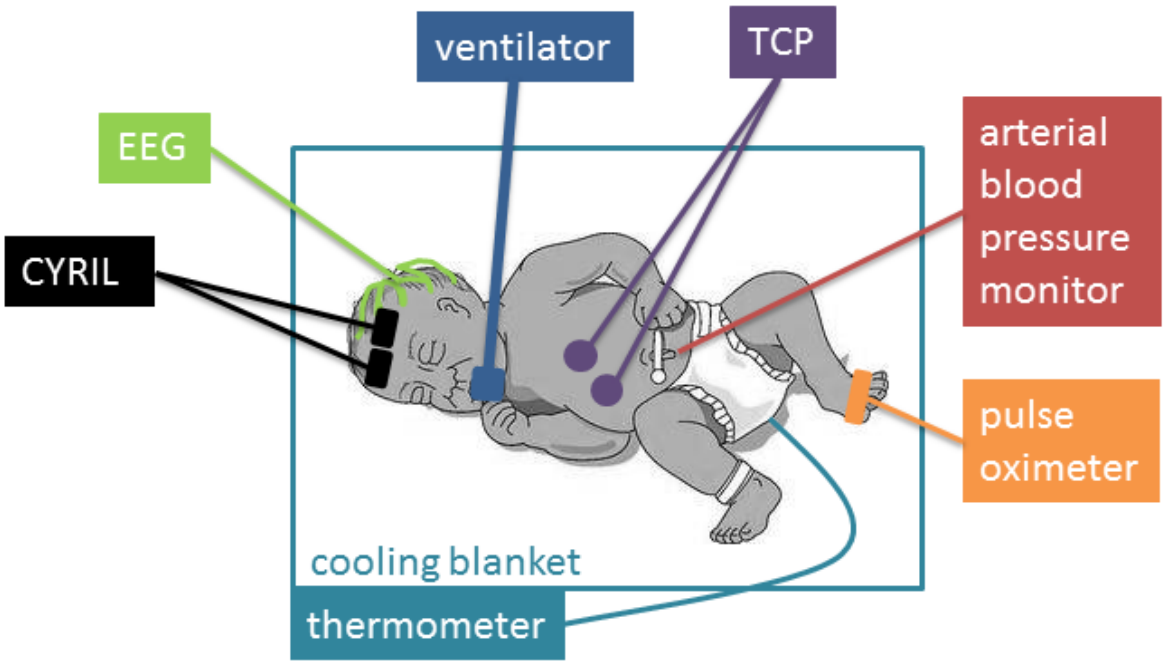

Figure 6.2: Monitors in the NICU on a HIE infant during the study.

Figure 6.3: CYRIL in the NICU.

Figure 6.4: CYRIL in the NICU on a HIE infant.

6.2.1 Problems Encountered

The studies began in November 2013; over the first few months of the studies several problems and challenges were encountered. Table 6.1 outlines these problems and describes the solutions implemented to solve them.

Table 6.1: Problems encountered during study set-up and solutions implemented.

	Problem	**Solution**
Patients	Having optode holders attached to forehead for long periods of time (>24 hours) caused minor dermatological abrasions on a small number of infants (these all resolved quickly)	Experiment protocol was changed from long (up to 4 days) studies to studies of 4-6 hours per day
	Some infants have very small foreheads and not enough space for 2 sets of optodes	A single source, double ended optode holder was designed and built to fit on a smaller forehead without compromising the measurement
Optics	Ambient light causing artefacts in signals	Black-out fabric placed over optode holders
	Examination lamps (halogen bulbs) caused artefacts in signals when moved	Medical staff were asked to refrain from using halogen lamps and to use phototherapy lamps (which have less interference with our recordings as they emit in the blue-end of the visible spectrum, see Figure 6.8) for examinations
	SRS measurements of TOI were not producing 'reasonable' values	Software updated to display the 'slope' at one wavelength (780nm), the spectrum of the 'slopes' across wavelengths and the TOI in real-time to allow adjustments (this problem has not yet been solved, see section 7.3)
Clinical Practicalities	LabVIEW and ixTrend software difficult to use for medical staff	LabVIEW software was modified to be more user friendly (see section 5.3) and a detailed user guide was drawn up
	Infection control is an important issue in the NICU	The neonatal infection control team advised us the appropriate cleaning methods for the broadband NIRS instrument (see section 6.2.3)
Data collection	ixTrend software would terminate recording if there were connection errors so we were unable to record for long periods of time (> 4 hours)	Liaised with ixellence developers and arranged for new version of the software that continues recording despite connection errors

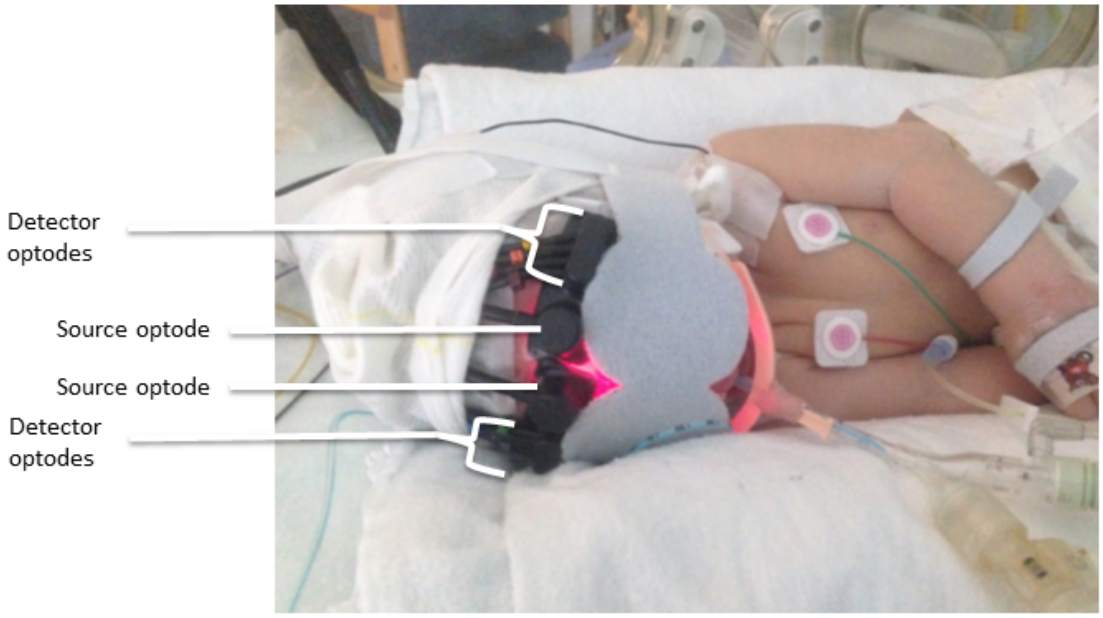

Figure 6.5: Optodes and holders on a subject.

Figure 6.6: Optodes and holders on a subject after MRI.

6.2.2 Final Protocol

Once the problems encountered in the initial studies were solved the final protocol was finalised. The study protocol is as follows:

1. Obtain informed consent from parent(s).
2. Clean and disinfect optodes and cables using anti-bacterial wipes (e.g. Clinell detergent wipes).
3. Switch on CYRIL system: plug in and turn on all devices (UPS, light source, spectrometer, laptop).
4. Use the shutter to shut off light in fibres (keep light on so it can stabilise but protect eyes from fibres while unattached).
5. Check the focus and wavelength adjustment micrometres at the back of the spectrometer and adjust if necessary.

6. Open the LabVIEW software on the laptop. Press the 'Run' arrow and enter the CYRIL subject number.

7. If the binning settings have changed, take a reference spectra:

   (a) Place a source fibre at one end of the poster tube.

   (b) Open the light source shutter and check that the light is visible at the other end of the poster tube.

   (c) For the first detector set ('1234' or '5678') place the detector optodes at the other end of the tube.

   (d) Set the LabVIEW program up to record a reference spectrum ('Settings' tab → 'Select Reference Spectra' and '1234' or '5678').

   (e) Record a reference spectrum (press 'Start') and ensure first measurement is not saturating in any channel.

   (f) Import the reference spectra into the LabVIEW software ('TOI Slope' tab → 'Reference File' and '1234'/'5678') and set this as default (right click → 'Data Operations' → 'Set current value as default').

   (g) Repeat for the other set of detectors.

   (h) Close shutter light source and remove fibres from poster tube.

   (i) set-up the LabVIEW program for normal data collection (remove 'Select Reference Spectra').

8. Start ixTrend software on the laptop and connect the laptop to the Philips Intellivue monitor.

9. Select patient (new or existing) and collect SpO_2, ABP, HR, RR, $tcpCO_2$, $tcpO_2$, pulse, ECG data using the ixTrend software.

10. Place the optodes through the cot and securely onto the infant's forehead with the double-sided tape and tuck under EEG cap.

11. Shield the optodes by tucking black-out fabric under the EEG cap and above the optodes.

12. Open the light source iris and shutter fully.

13. Take a short set of data to check the set-up (press 'Start').

14. Check the intensity spectra. Each channel should be >10000 counts and not saturating. Each channel needs to have a smooth spectrum free of peaks from ambient light sources. If the spectra are too low, increase the binning size for that channel (and ensure to take a reference spectra after the measurement). If there are peaks from ambient light improve the detector shielding or reduce ambient lighting if possible.

15. If recording TOI, check the TOI slope ('TOI Slope' tab). If not positive and linear then try adjusting the optode contact to the skin.

16. Press 'Stop'.
17. Check the EEG timing and adjust CYRIL clock to match the EEG if necessary.
18. Begin data collection: press 'Start'.
19. Aim to record data for 4-6 hours each day during therapeutic hypothermia and rewarming, and 0.5-1 hour pre- and post-MR scan.
20. When the study is finished, stop data collection (press 'Stop', data are saved automatically), turn off all devices and carefully remove optodes from patient's head using adhesive removal wipes.
21. Clean and disinfect optodes and cables using anti-bacterial wipes (e.g. Clinell detergent wipes).

6.2.3 Infection Control

Infection control is an important issue in NICU because neonates are immune compromised (especially preterm babies). Further, antibiotics are widely used which can lead to resistant organisms that must not be spread from one patient to another. The neonatal infection control team advised us on the appropriate cleaning methods for the broadband NIRS instrument. They are as follows:

1. Hands must be thoroughly washed before entering the unit and before touching the patient.
2. Clean and disinfect probes and cabling thoroughly using detergent wipes (e.g. Clinell detergent wipes). Thoroughly disinfect all areas of the optodes and the length of the cabling using 70% isopropyl alcohol wipes (e.g. PDI Sani-cloth 70).
3. The other areas of the equipment and trolley should also be cleaned and disinfected in the same manner before and after use.
4. Cover the equipment and store it in a clean and dry environment.

6.3 Subjects

At time of writing, 63 babies have been monitored with CYRIL under the Baby Brain Study between November 2013 and December 2015. The experimental work for this PhD was completed in May 2015 when 38 babies had been studied (31 of whom were diagnosed with HIE). Table 6.2 shows the clinical condition of each subject including the ^{1}H MRS Lac/NAA results and Table 6.3 shows the timings of the NIRS recordings across the days of life. All of the HIE babies were treated with TH. Some were included in a randomised clinical trial assessing the therapeutic effects of inhaled xenon (TOBY Xe); these babies were given xenon for 24 hours within the 72 hour cooling period [230]. data were recorded continuously from 0.2 hours up to 77.5 hours (i.e. 3.6 days).

Table 6.2: Clinical details of subjects studied. Abbreviations: enrolled in TOBY Xe study - yes (Y), parenchymal venous infarct (PVI), intraventricular haemorrhage (IVH), head trauma (HT), persistent pulmonary hypertension (PPHN), date of birth (DOB) and time of birth (TOB), gestational age (GA), male (M), female (F).

CYRIL	Condition	Gender	DOB	TOB	GA (weeks+days)	Birth Weight (g)	Lac/NAA	TOBY Xe
1	Ex preterm	M	22.09.2013		24+2			
2	HIE	F	25.11.2013	08:00	38+0	1770	0.87	Y
3	HIE	F	02.12.2013	14:28	41+0	3800	0.2	Y
4	HIE	M	10.12.2013	19:04	40+1	3310	0.16	
5	Stroke	M	16.12.2013	12:08	40+6	3370		
6	HIE	M	01.01.2014	06:35	40+2	3110	0.39	Y
7	HIE	M	05.01.2014	04:50	39+5	3640	1.32	Y
8	HIE	F	12.01.2014	07:35	41+6	3498	0.17	Y
9	HIE	M	12.02.2014	08:56	38+6	2850	0.16	
10	HIE	F	23.02.2014	02:39	40+2	3020	0.15	
11	HIE	F	01.04.2014	01:47	40+4	3580	0.08	Y
12	HIE	M	13.04.2014	11:40	39+0	2250	1.8	Y
13	HIE	M	29.04.2014	22:06	39+1	3060	0.76	Y
14	HIE	M	13.05.2014	03:57	37+5	3750	0.25	
15	HIE	F	15.05.2014	05:08	39+4	3240	0.15	Y
16	HIE	M	18.05.2014	06:01	40+0	3770		Y
17	HIE	F	11.06.2014	13:09	37+3	3160	0.35	
18	HIE+seizures	F	14.06.2014	06:20	38+2	3034	0.28	
19	HIE	F	15.06.2014	03:54	39+3	3700	0.16	
20	HIE	M	17.06.2014	08:16	40+6	3190	0.11	
21	HIE	M	24.06.2014	01:39	36+3	2440	0.2	
22	HIE	M	17.09.2014	13:23	41+4	3910	0.2	
23	HIE+PVI	F	14.10.2014	02:47	40+1	2996		
24	HIE	M	29.10.2014					
25	HIE	M	22.11.2014	08:02	41+6	4940	0.4	
26	HIE	M	21.11.2014	17:39	39+3	2811	0.52	
27	Preterm	F	24.11.2014	18:40	27+3	1220		
28	HIE+PPHN	M	27.11.2014	14:22	39+6	3200	0.16	
29	HIE+HT+seizures	M	07.12.2014	11:26	42+1	4280		
30	HIE	M	09.12.2014	03:50	40+0	3000	0.17	
31	HIE	M	13.12.2014	02:13	41+1	3145	1	
32	Stroke	F	04.02.2015	09:19	40+2	3610		
33	HIE	F	15.02.2015	00:45	38+3	2900	0.43	
34	Seizures	M	17.02.2015	02:28	41+1	3790		
35	HIE	F	22.02.2015	21:55	38+5	3150	0.14	
36	Seizures	M	21.02.2015	09:11	40+6	3325		
37	HIE	F	02.03.2015	10:04	39+3	3330	0.2	
38	IVH	M	04.03.2015	07:21	34+2	1999	2.11	

Table 6.3: Hours of data recorded per day of life for all subjects.

CYRIL	Day 1	Day 2	Day 3	Day 4	Day 5	Day 6	Day 7	Day 8	Day 9	Day 10
1	Test									
2		2.6	6.9,7.7	4.7,6.7,0.4						
3	2.3,6.6	0.2,8.5,6.9	7.5,7.6	7.6						
4	2.8,0.8	1.4,3.9	3.3,3.6,6.5	5.4						
5			3.4							
6			4.3,3.1,6.6	7.3,7.8	7.9,8.2					
7			6.3,2.9	7.5,8.0	0.2					
8	4.31	8.8	2.4,3.2,3.3	4.8	0.4,7.4					
9	3.8,5.9,4.4	5.9,3.4	4.7	7.1		0.6	1.2			
10		4.0,14.9	4.9,11.4	9.8,6.7	1.1					
11	9.4	24	24	20.1						0.8,2.2
12			7.8	1.0,0.6,1.1	2.6					
13	0.6,21.9	15.3	26.73				4.0,0.7,0.8			
14	3.4	12.6	7.9	7.0						
15	15.5		10.6	10.2						
16	8.2									
17	7.7	10.8	11.3	20.4						
18	0.2			31.3		0.8,1.5				
19	12.5	16.4				0.7,2.6				
20		15.1	16.0	17.6						
21		10.2	10.1,20.8							
22	No systemic data									
23	No data									
24	No data									
25			2.2	5.2,0.8	1.3					
26			6.1	0.6						
27			1.3,1.5	1.3						
28	2.4	1.6								
29		3.0								
30			2.5							
31			0.9	0.8,1.2						
32			0.9,4.1							
33	5.5		3.8	4.9	0.4,0.9					
34		3.6,3.4								
35	3.6	4.8	3.6					0.2		
36			3.4							
37	4.6	2.7		2.9						
38		5.6								

6.4 Data Processing

To ensure that the NIRS data being analysed is free from system noise and artefacts, the data has to be processed. This section describes the decisions made regarding processing and the protocol followed.

6.4.1 Synchronisation

Automatic synchronisation of the NIRS data with the systemic and EEG data was performed with a program which was written in MATLAB (MathWorks, USA) to interpolate both the NIRS data and the systemic data to the same time frame and frequency via spline interpolation. Therefore systemic data were down-sampled to 1Hz. The data are put together into one Excel file (.xlsx) which allows easy data sharing with the clinical team. This allows NIRS signals to be analysed in relation to the systemic physiology.

6.4.2 Artefact Identification and Correction

Before the data can be analysed, light and movement artefacts have to be carefully identified and removed. This is not a trivial task. Although we have strived to ensure good coupling of the optical fibres to the scalp, movement of the head of the subject (normally by the clinical team as the infants are sedated) will cause motion between each optical fibre and the scalp. This motion will cause a shift in the optical coupling between the fibre and the scalp, which usually results in a period of high-frequency noise in the recorded NIRS data. Even after the motion has subsided, the optical coupling is often altered, causing a shift in the baseline measurements of the NIRS chromophores (see example in Figure 6.7). Because the magnitude of this motion-induced noise is typically far greater than the changes associated with tissue haemodynamics, any changes in haemoglobin concentrations in the cerebral cortex which coincide with motion artefacts are usually so heavily contaminated that they are indiscernible.

Artefacts from changes in ambient lighting cause similar high-frequency shifts in the NIRS data. If the lighting change is temporary and returns to its original state there will not be a shift in the baseline of the measurement. However, a permanent change in the ambient light will cause an overall shift. To characterise light artefacts in the NICU environment of this study they were deliberately induced to help identification and prevention. Figure 6.8 shows the changes in concentration caused by changes in the ambient lighting from the main fluorescent room light and moveable lights (phototherapy lamp and halogen torch) that are attached to the cot itself for clinical purposes. Concentration changes induced from turning the main room lights on were not significant. The lights on the cotside caused large artefacts when held close to the neonate's head, but the halogen lamp also caused noticeable changes when simply turned on. Therefore, clinicians and nurses were asked to use the phototherapy lamp when examining patients, rather than the halogen lamp as this will reduce the number of ambient light artefacts.

It was not possible for the clinical research team to provide cover to mark events when the baby's head was moved or when ambient light was changes so identification of artefacts was performed after the measurement. In general, identification of artefacts can be performed manually through visual inspection of the data, or automatically using an artefact removal algorithm [231]. There are many different

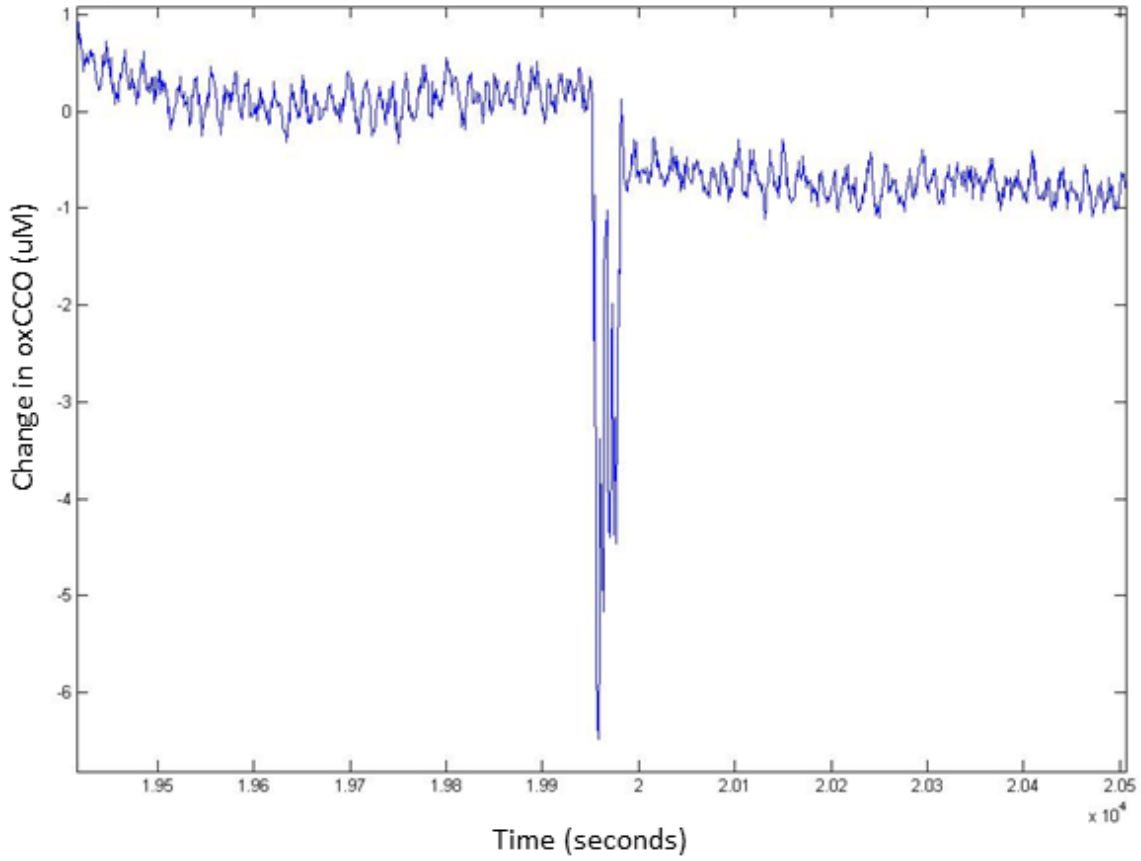

Figure 6.7: Concentration change in oxCCO measured by CYRIL on an infant in the NICU during movement artefact showing large spike and baseline shift.

approaches to automatic identification, some of which use another signal, such as an accelerometer [232] or a reference NIRS channel [233], but there are also many approaches that can be applied to a standard NIRS data set, like the one recorded with CYRIL. In NIRS studies where there are reproducible stimuli (such as in fNIRS), one approach is to perform enough trials to minimised the average impact of the artefacts or simply to remove any stimulus trials that coincide with identified artefacts. However, in this study there are no reproducible stimuli therefore each data set is unique and cannot be averaged out or rejected so simply. Correction of artefacts is, therefore, required to preserve these data. There have been several approaches to artefact correction such as principle component analysis (PCA) [234], spline interpolation [172], filtering based on wavelet transforms [235] and Kalman filtering [236]. Cooper et al. [231] performed a comparison of these four different approaches using real NIRS data sets and found that spline interpolation produces the largest average reduction in the mean-squared error while wavelet analysis produces the highest average increase in contrast-to-noise ratio. On the basis of this analysis, they recommended the routine application of motion correction techniques (particularly spline interpolation or wavelet analysis) to minimise the impact of motion artefacts on NIRS data.

Heeding this advice, the spline interpolation method was trialled with the neonatal data recorded with CYRIL. The movement artefact reduction algorithm (MARA) suggested by Scholkmann et al. [172]

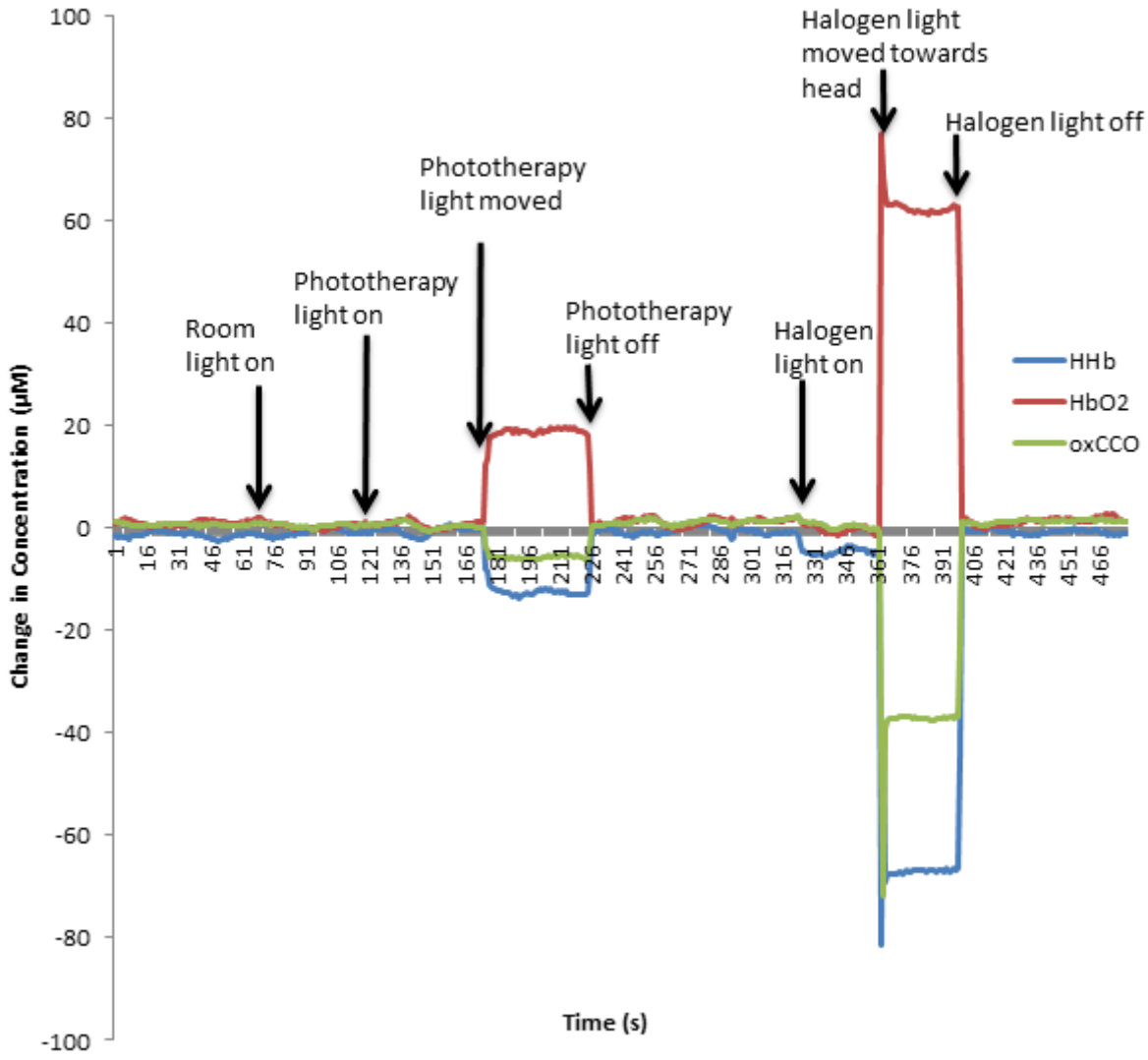

Figure 6.8: Concentration changes measured by CYRIL on an infant in the NICU during ambient light changes. The NICU has several different light sources, main fluorescent lights for the whole room, a phototherapy light attached to the cot and a halogen torch lamp also attached to the cot.

is based on moving standard deviation to identify the artefacts and spline interpolation for correction. This method also corrects shifts in the baseline due to artefact. MARA was applied to our data, an example is shown in Figure 6.9. However, due to the nature of our data, namely long (several hours) data sets with random fluctuations caused by spontaneous changes in physiology, MARA struggled to separate artefacts from real changes as they have similar changes in standard deviation (see Figure 6.10). Using the systemic data to add additional information to the artefact identification allowed this insight.

Therefore, a new approach to use the extra information from the systemic physiology to inform a manual artefact identification method was determined. A NIRS signal was displayed (for better visibility the data are normalised) with the MABP and SpO_2 and the artefacts are identified by visual inspection; if there is a correlation between the suspected NIRS artefact and the systemic signal that indicates that the NIRS signal is physiological. Removal of the artefacts is performed by destroying the signal within

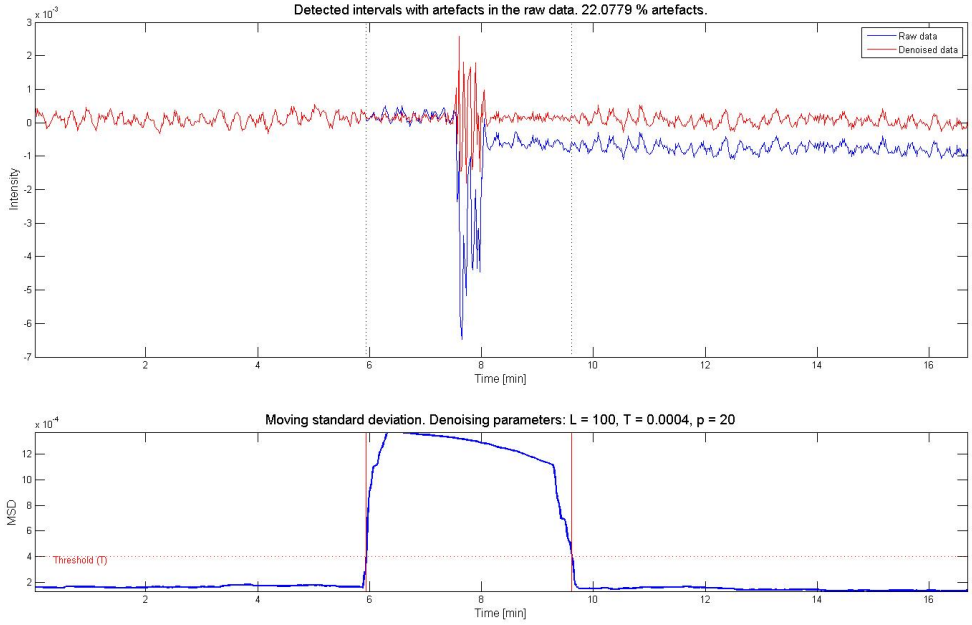

Figure 6.9: Changes in oxCCO measured by CYRIL during movement artefact. Upper graph shows signal before and after MARA. Lower graph shows moving standard deviation with threshold used to identify artefact.

the identified artefact period, shifting the baseline and interpolating across the period of artefact. Figure 6.11 shows the results from this procedure. The baseline shift is very simplistic as the baseline is moved manually to the point at which the start of the artefact was identified. The method could be improved by using a time-averaged signal either side of the artefact section and adding simulated noise to the artefact period.

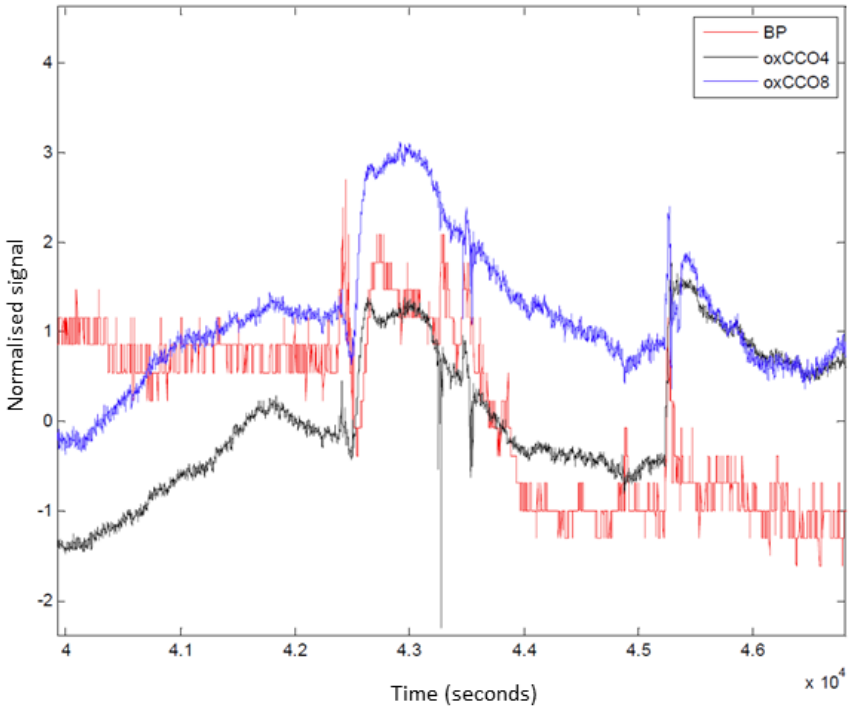

Figure 6.10: Changes in concentration of oxCCO (both right '8' and left '4' channels) measured with CYRIL showing two real rapid changes (around 4260s and 4530s) that MARA could not distinguish from motion artefact. The MABP is also displayed to show that the changes identified were actually real and caused by a physiological change.

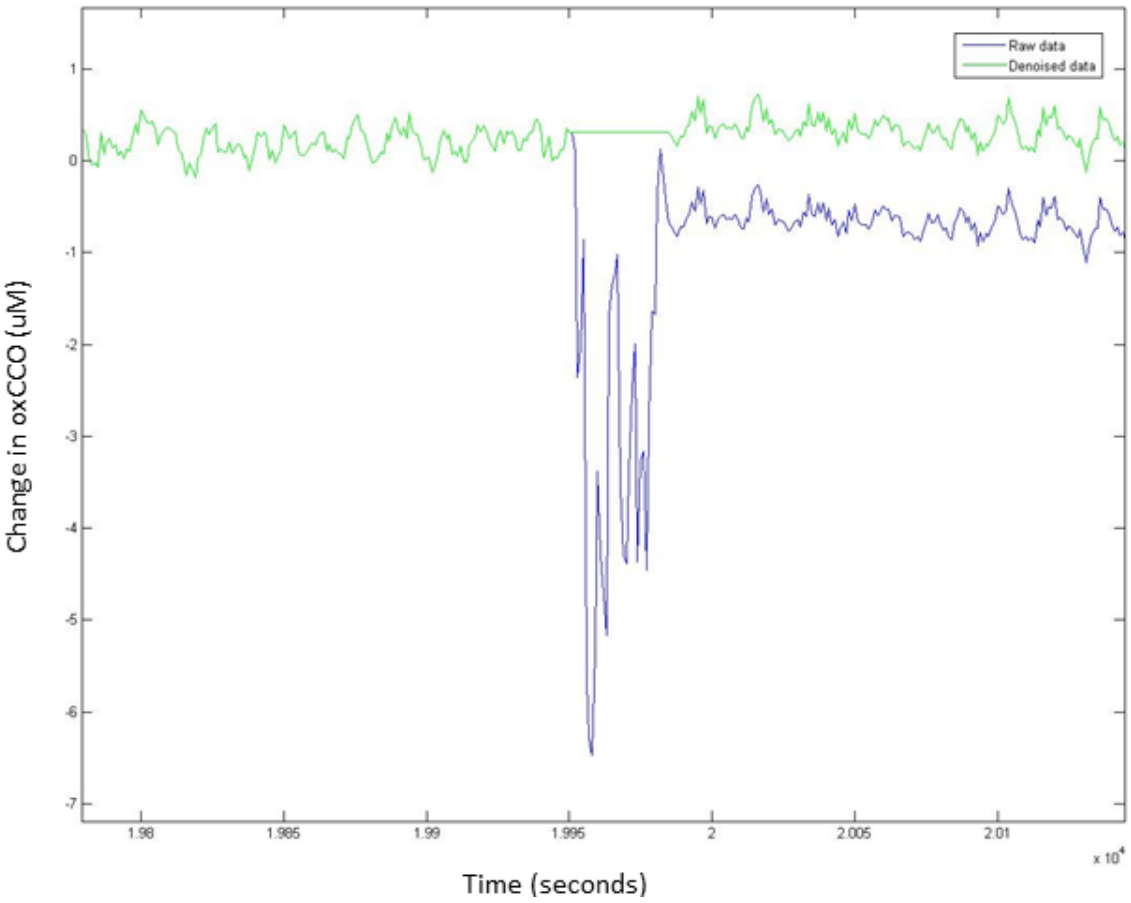

Figure 6.11: Concentration changes measured by CYRIL on an infant in the NICU before and after artefact removal.

6.4.3 Filtering

After artefact removal, NIRS data were processed with an automatic wavelet de-noising function which reduces the high frequency noise but maintains the trend information [237]. The function *wden* from MATLAB was used with a 4-level wavelet decomposition, using a Daubechies 4 as mother wavelet, hard thresholding to remove noisy coefficients, and the noise level was found using a heuristic approach to the Stein's unbiased risk estimate. Figure 6.12 shows an example of this process.

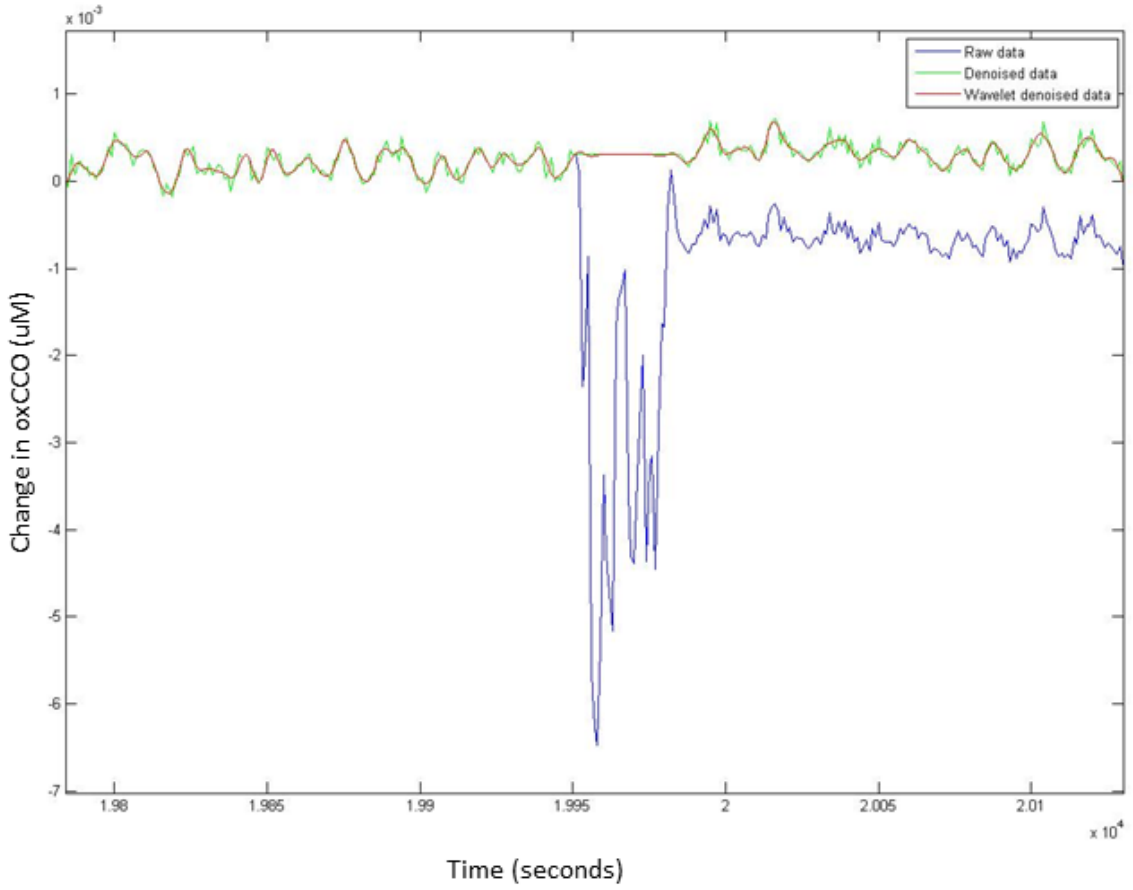

Figure 6.12: Concentration changes measured by CYRIL on an infant in the NICU before and after artefact removal and wavelet de-noising.

6.4.4 Data Post-Processing Protocol

All data post-processing as described above has been automated in Matlab code. The protocol is as follows:

1. Save NIRS and systemic data onto internal server (FileZilla) and back-up hard drive. All data are stored anonymously under CYRIL numbers.

2. Synchronise the NIRS and systemic data at 1Hz using 'synchALL.m' Matlab code and save Excel files on the server.

3. Artefact identification and removal using 'cutInterpShift.m' Matlab code.

4. Wavelet de-noising using 'wdenPlot.m' Matlab code.

6.5 Examples of Data

This section shows some examples of data recorded in the study. The CYRIL data are displayed with the systemic physiology data. Large changes in the systemic physiology will impact upon cerebral haemodynamics and metabolism. Figure 6.13 shows data from a HIE infant with a predicted poor outcome: a decrease in arterial oxygenation with a corresponding increase in blood pressure, respiratory rate and partial pressure of CO_2, and the resulting cerebral signals; an increase in HHb, a decrease in HbO_2 and oxCCO.

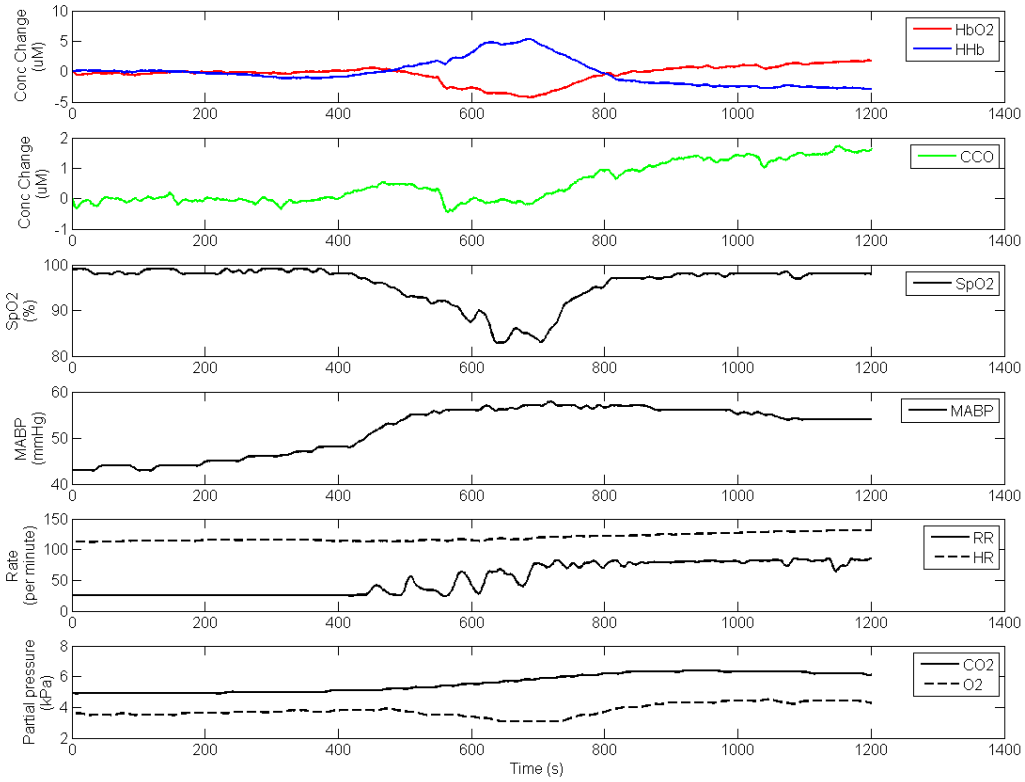

Figure 6.13: Signals recorded on 26/11/13 20:06:04 on infant 2 during a multitude of changes in systemic physiology.

Another example of data from a HIE infant with predicted poor outcome is shown in Figure 6.14. There is a decrease in arterial saturation, blood pressure, and heart rate which corresponding with decrease in cerebral oxygenation and metabolism.

A peak in blood pressure precedes a large arterial desaturation in Figure 6.15 in a HIE infant with predicted good outcome. The blood pressure increases is visible in HbO_2 and oxCCO signals and the

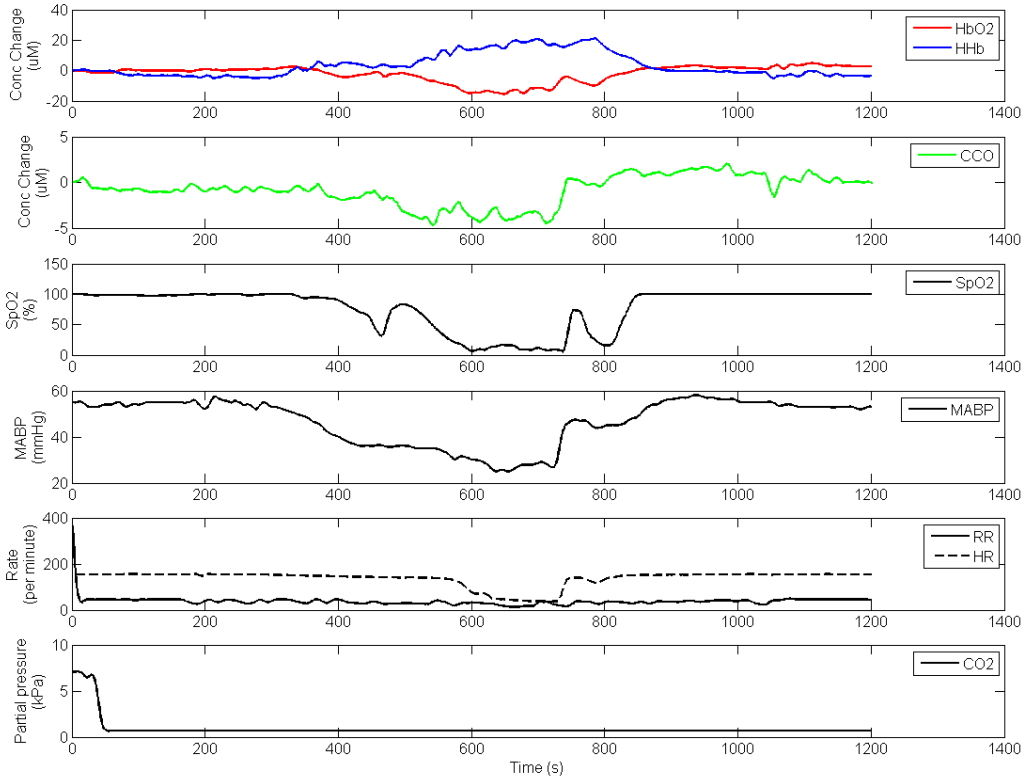

Figure 6.14: Signals recorded on 03/01/14 08:38:47 on infant 6 during arterial desaturation with blood pressure changes.

arterial desaturation correlates with a reduction in HbO_2 and oxCCO, and an increase in HHb.

These examples give a glimpse into the data recorded in the study, observing changes in the cerebral haemodynamics and metabolism due to spontaneous systemic changes. It is obvious that the data are complex and there is no simple relationship between the multimodal signals. However, the hypothesis of this thesis is that the relationship between the spontaneous systemic changes and the cerebral response will give an indication of cerebral injury severity. The proceeding chapters will investigate this hypothesis.

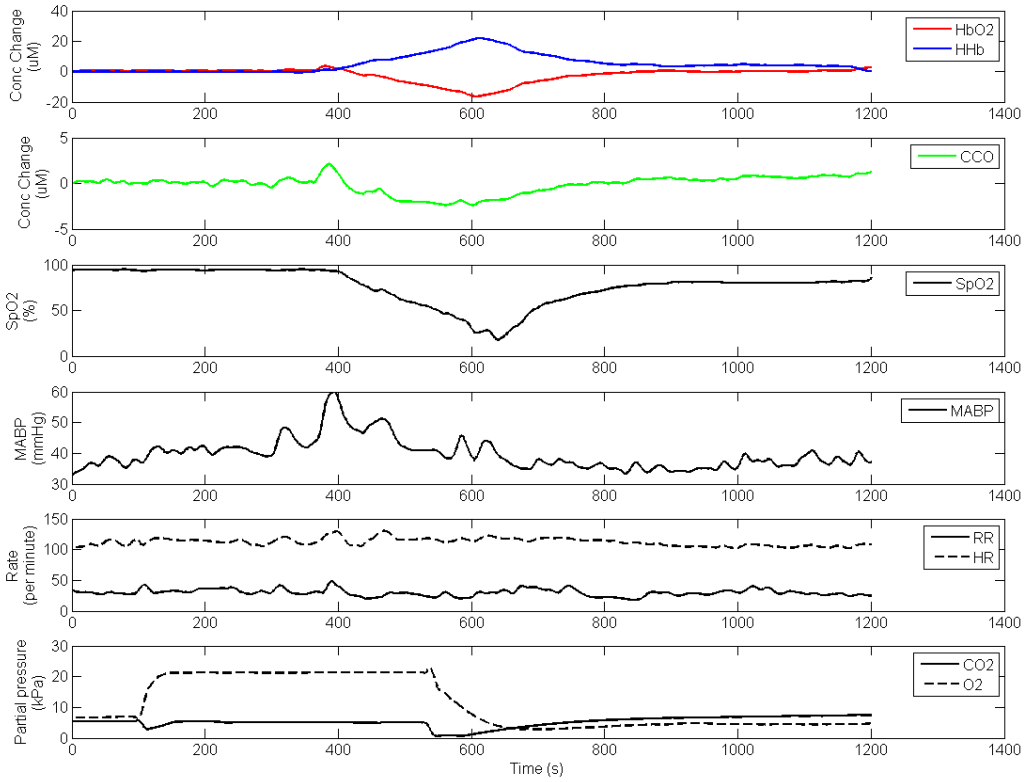

Figure 6.15: Signals recorded on 15/05/14 17:18:23 on infant 15 during desaturation (with blood pressure changes).

Chapter 7

Evaluation of Clinical Broadband NIRS Measurements

To my knowledge this is the first time that the in-vivo oxidation changes of brain tissue CCO have been recorded with broadband NIRS in HIE infants in the NICU. The use of CYRIL in the NICU for continuous periods over the first week of life has been demonstrated; recording from ∼1 hour up to 24 hours per day, to simultaneously measure changes in cerebral oxygenation, haemodynamics and metabolism in 38 newborn infants. In order to assess the data from the CYRIL system during its use, optical analysis was performed on the data recorded in the NICU as described in the previous chapter. This chapter describes the validation of the optical data recorded before the concentration data are used for physiological analysis.

7.1 Measurements of oxCCO

The literature has shown that there is concern over the uniqueness of the oxCCO measurement (see section 4.3). The oxCCO signal as measured by CYRIL was assessed to ensure that there is no cross-talk from the haemoglobin signals. First, the direction of the signal was observed in relation to the haemoglobin chromophores and then the residuals from the back-calculated attenuation changes were investigated.

7.1.1 Examples of oxCCO Changes with Haemoglobin Changes

The most simple test to see if the oxCCO is independent of HHb and HbO_2 is by observing changes in the signals and visually assessing for similarities. Figures 7.1 and 7.2 show two different examples of the oxCCO signal changing in the same direction as HbO_2, HHb and neither respectively. Additionally, Figures 6.13 to 6.15, and 11.4 show examples of oxCCO changing both with and against HbO_2.

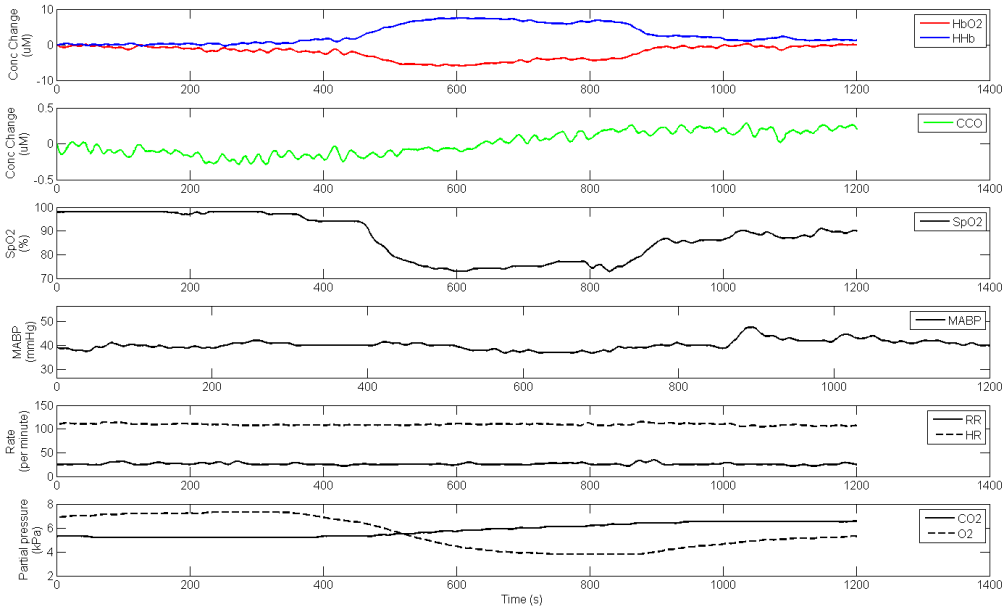

Figure 7.1: Data recorded on infant 21 at 25/06/14 09:29:41 showing changes in oxCCO that are different to the haemoglobin signals response during spontaneous hypoxia.

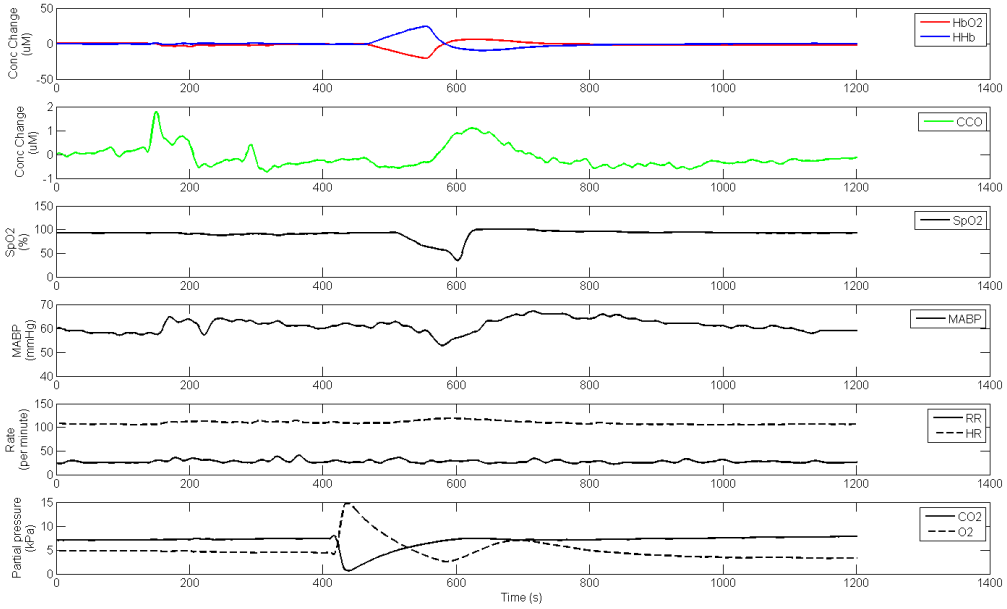

Figure 7.2: Signals recorded on infant 20 on 18/06/14 16:48:33 showing changes in oxCCO that are different to the haemoglobin signals response during spontaneous hypoxia.

7.1.2 Residual Analysis

The change in the shape of the intensity spectrum reflects the change in the levels of chromophore concentration in the tissue; Figure 7.3 shows the intensity spectra before and during a SpO_2 desaturation. The peak of the spectra shifts from ~780nm to ~785nm due to the decrease in HbO_2 and oxCCO, and the increase in HHb. The resulting attenuation is shown in Figure 7.4, with the associated changes in chromophore concentration in the legend.

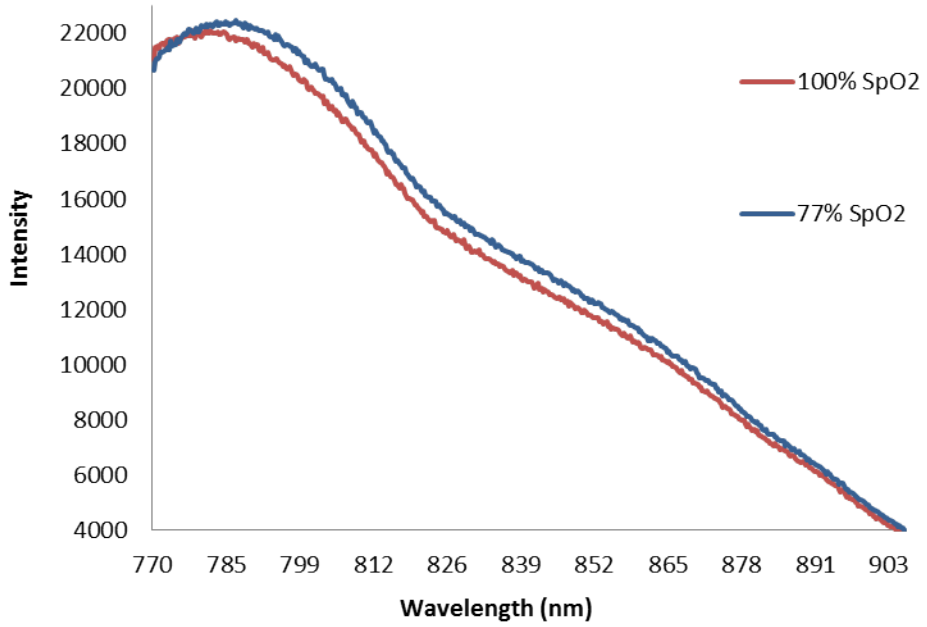

Figure 7.3: Example of intensity spectra before desaturation (SpO_2= 100%) and at the nadir of desaturation (SpO_2 = 77%) in subject 003, channel 1 from the longest source-detector distance. A shift in the peak of the spectrum is observed.

To investigate the spectral changes due to the oxCCO chromophore, the UCLn algorithm was also used to derive changes in chromophore concentrations when solving only for the other two chromophores (HbO_2 and HHb). Attenuation-change spectra were then back-calculated from these concentration changes and the differences between the 2- and 3-chromophore fits were studied. If all of the chromophores that explain the spectra are fitted then the residual error between the two sets should not have a defined shape, it should be randomly fluctuating around zero. However, if there is a shape to the spectra then this would suggest that there is a chromophore that is unaccounted for. Two examples of this process are shown in Figures 7.5 and 7.6 for two different infants during spontaneous hypoxia. The resulting residual fits have a similar shape to the oxCCO spectra which suggest that a change in all three chromophores is necessary to explain the attenuation change.

The back-calculated attenuation-change spectra from the furthest detector in a selection of infants are shown in Figure 7.7 as the difference between the 3- and the 2-chromophore fit for 6 subjects during their largest desaturation. It is noted that the spectrum presented for each subject is an average spectrum,

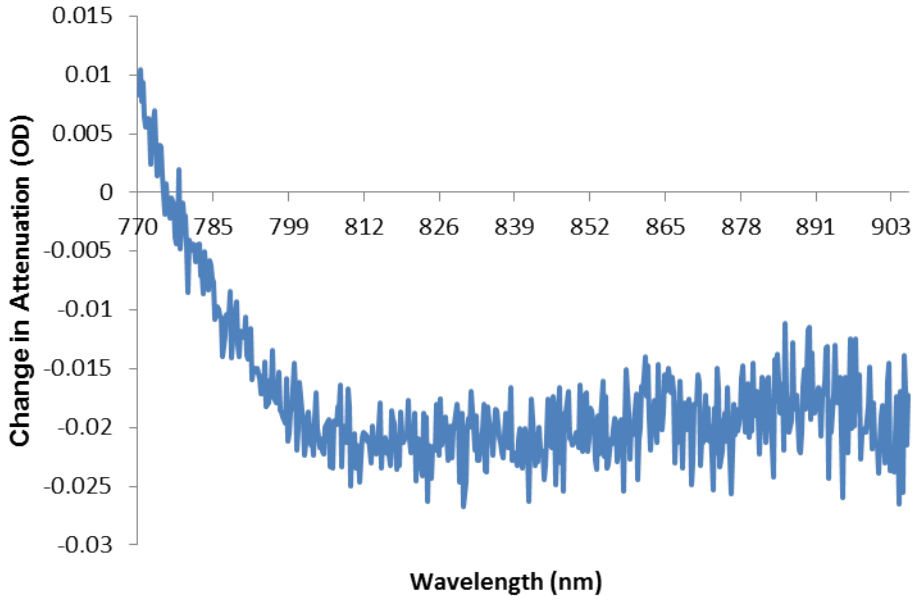

Figure 7.4: Change in attenuation between intensities shown in Figure 7.3 this relates to $\Delta[HbO_2]$ = ∼-6μM, $\Delta[HHb]$ = ∼3μM and $\Delta[oxCCO]$ = ∼-1.5μM.

derived from all individual spectra corresponding to the largest desaturation event in that subject. The spectra do not have an arbitrary distribution around y = 0, but appear to show a shape approximating the oxidised minus reduced CCO spectrum (see Figure 7.7), featuring a broad peak at approximately 830 nm. This suggests that fitting the measured changes in near-infrared attenuation only for HHb and HbO_2 would leave a chromophore with the spectral features of oxCCO unaccounted for. Based on these findings, only results from the 3-chromophore fit are discussed throughout this study.

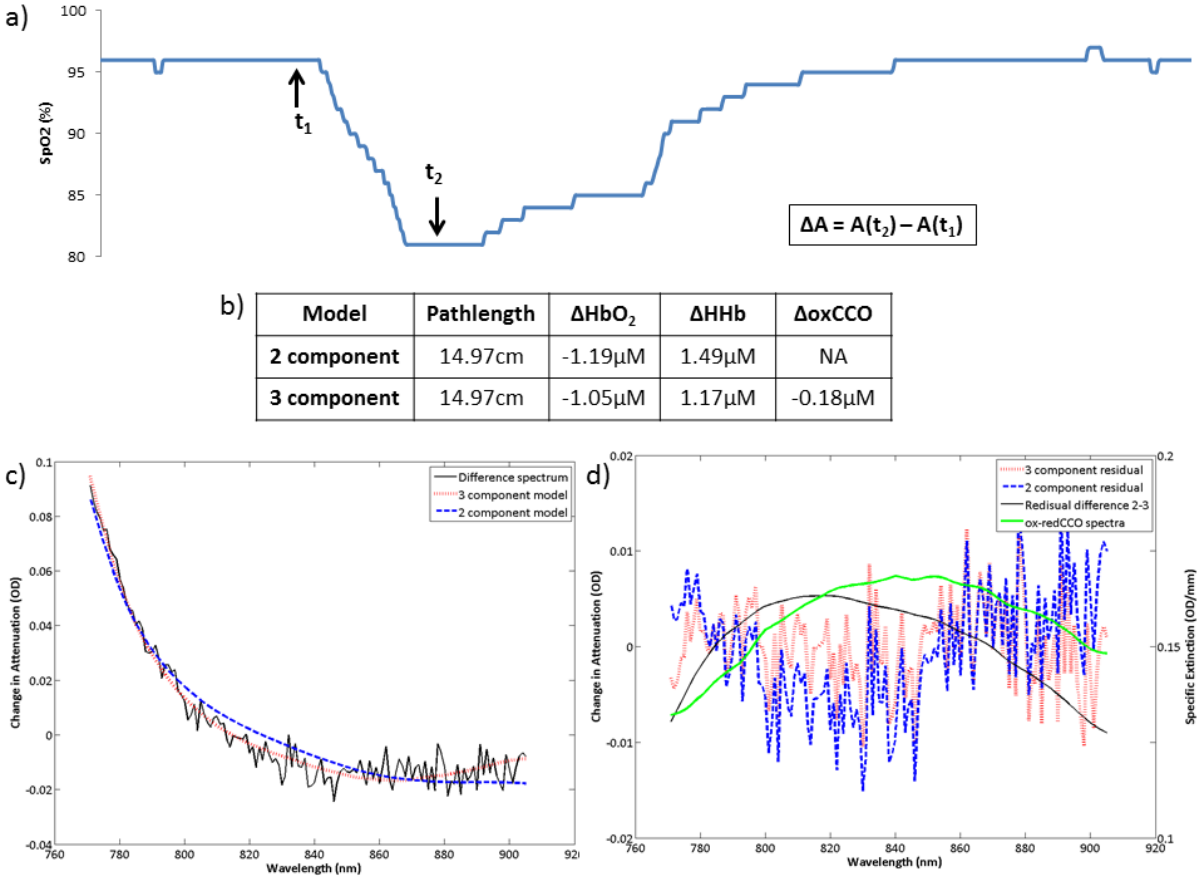

Model	Pathlength	ΔHbO$_2$	ΔHHb	ΔoxCCO
2 component	14.97cm	-1.19μM	1.49μM	NA
3 component	14.97cm	-1.05μM	1.17μM	-0.18μM

Figure 7.5: Example of residual analysis of NIRS data from the neonatal study. a) SpO_2 spontaneous decrease showing 2 time points, before and during hypoxia, from which the change in attenuation is calculated. b) Concentration results from fitting change in attenuation spectra to 2-(HHb and HbO_2) and 3-(HHb, HbO_2 and ox-redCCO) component models. c) Attenuation measured and attenuation fit back-calculated from 2- and 3- chromophore fits. d) Residual differences between real attenuation and back-calculated attenuations, and the difference between them; note the shape of the difference between the residuals for the 2- and 3-chromophore fits is similar to the ox-redCCO spectra (also plotted for comparison on a separate scale).

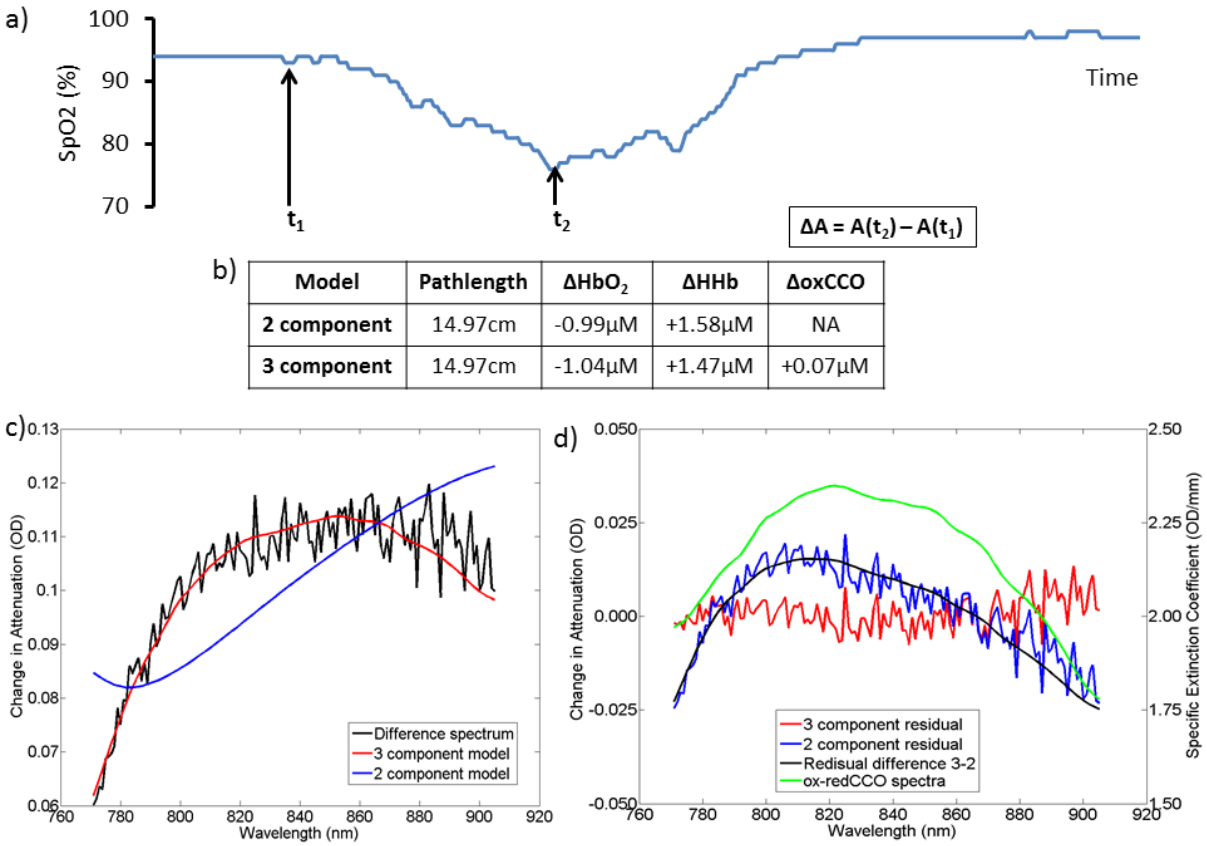

Model	Pathlength	ΔHbO_2	ΔHHb	ΔoxCCO
2 component	14.97cm	-0.99μM	+1.58μM	NA
3 component	14.97cm	-1.04μM	+1.47μM	+0.07μM

Figure 7.6: Another example of residual analysis of NIRS data from the neonatal study. a) SpO_2 spontaneous decrease showing 2 time points, before and during hypoxia, from which the change in attenuation is calculated. b) Concentration results from fitting change in attenuation spectra to 2-(HHb and HbO_2) and 3-(HHb, HbO_2 and ox-redCCO) component models. c) Attenuation measured and attenuation fit back-calculated from 2- and 3- chromophore fits. d) Residual differences between real attenuation and back-calculated attenuations, and the difference between them; note the shape of the difference between the residuals for the 2- and 3-chromophore fits is similar to the ox-redCCO spectra (also plotted for comparison on a separate scale).

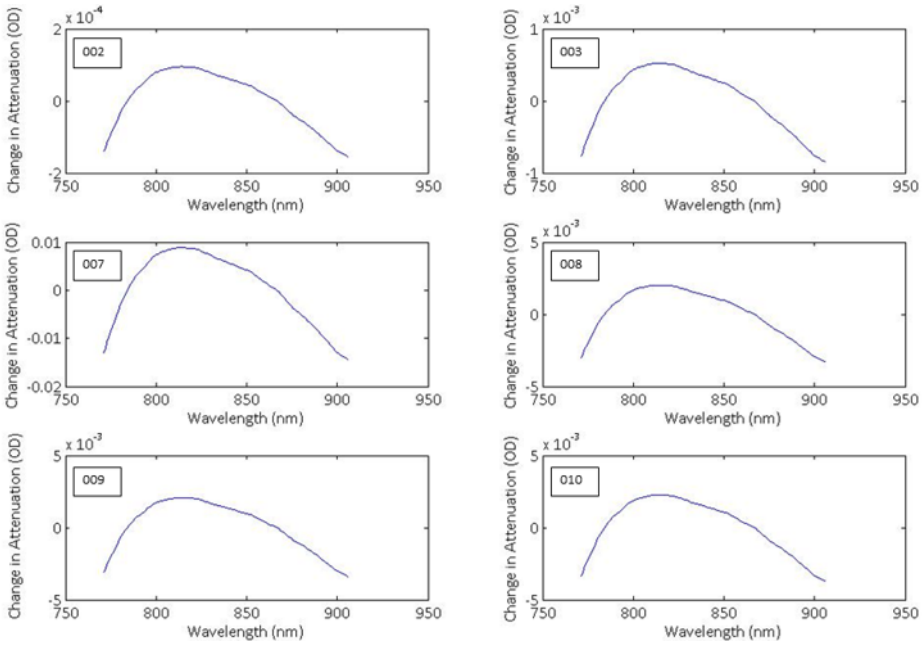

Figure 7.7: Difference between the 2- and 3-chromophore residual fits during a spontaneous hypoxia event in 6 different infants: 2, 5, 7, 8, 9 and 10. Attenuation-change spectra back-calculated from the calculated concentration changes during the largest SpO_2 desaturation observed in each subject. The presented spectra are the average of all spectra during the desaturation.

7.2 Depth Sensitivity

Previous NIRS studies have suggested that a source-detector separation of between 1.0 and 2.5cm will probe depths of ∼1cm which is sufficient to monitor cerebral activity [174]. In this section, the depth sensitivity of CYRIL is not estimated, however, its ability to resolve changes from the cerebral cortex is assessed.

7.2.1 Experimental Data

Using different source-detector distances it is possible to investigate the differences in the chromophore concentration changes at different tissue depths. In theory, light travelling between the longer source-detector separations will have travelled deeper into tissue (see Fig 3.8 for illustration) and so will be more likely to interrogate the brain. Therefore, if there is a cortex specific change occurring in the NIRS chromophores, the longer source-detector separation should resolve larger concentration changes. This has been shown in adult functional activation studies [61] as discussed in section 4.6.

As the density of mitochondria, and therefore CCO, is much higher in brain tissue than in the extracerebral tissue (ECT) it is expected that a change in oxCCO would be higher in this region. Therefore, a longer-source detector separation would resolve larger changes in oxCCO. This would not be as noticeable in the haemoglobin signals as the contrast between ECT and brain tissue vessel density is less stark. An example of this is shown in Figure 7.8 taken from subject 17 during spontaneous hypoxia. It can be seen that the haemoglobin signals have similar changes at all source-detectors distances, although the change in oxCCO decreases much more in the longest separation (∼2μM) compared to the shortest separation (∼0μM). This suggests that the light recorded at the longest source-detector separation is travelling through more mitochondria dense tissue, most likely the cortex, than the shortest separation.

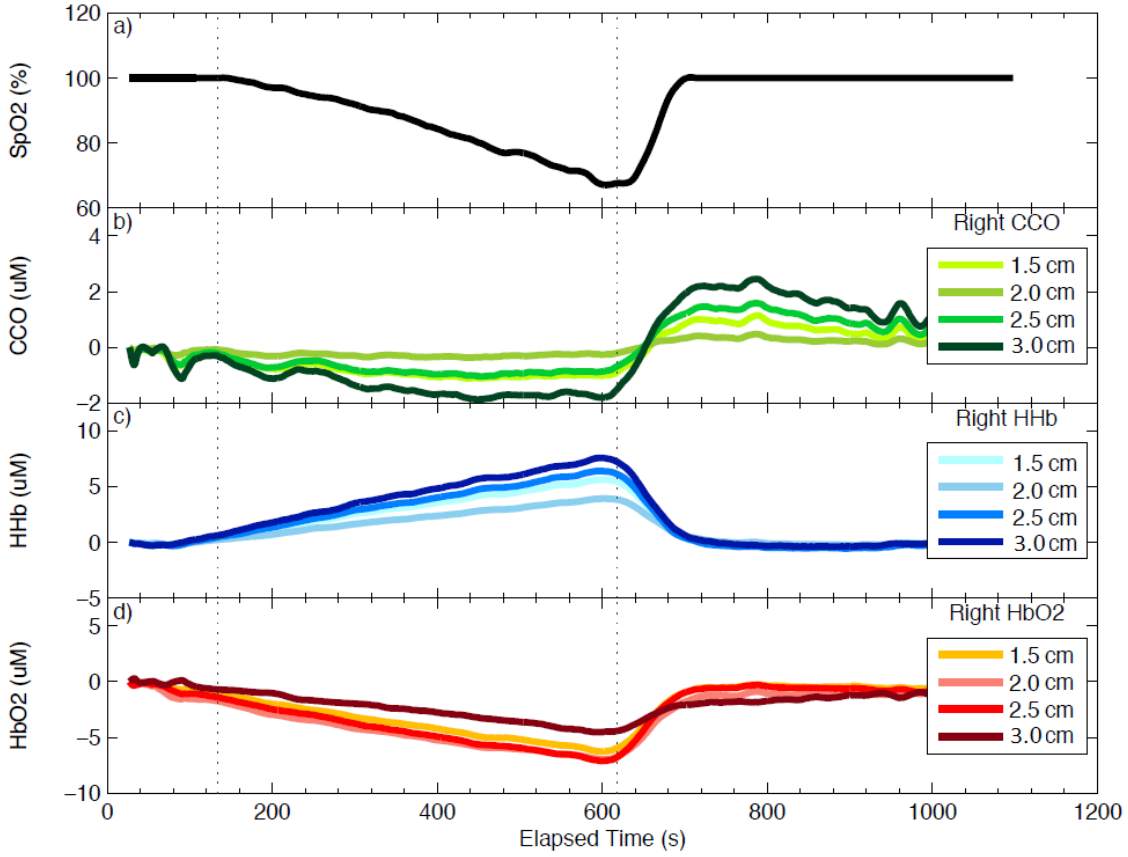

Figure 7.8: Changes in concentration on subject 17 from different source-detector distances during an arterial oxygenation decrease.

7.2.2 Simulations of Light Transport

A simulation based on work by Brigadoi and Cooper [145] was designed at UCL specifically for the CYRIL hardware to investigate the propagation of light at the multi-distance channels and to estimate the depth of light penetration. A neonatal head model of 40 weeks GA was used for the simulation. This atlas model was based on 324 newborn scans [145]. The different layers of the head were segmented into ECT, CSF, grey matter (GM) and white matter (WM). Due to the lack of MRI contrast in the newborn head, the scalp and skull layers were modelled as one layer referred to as the ECT. Each layer was modelled with different absorption and scattering coefficients; these optical properties are shown in Table 7.1. The simulation was run at 800 nm as the optical properties for the entire wavelength range 770 nm - 906 nm as used in CYRIL are not known. This creates a challenge for simulation studies of the broadband system.

In order to apply the model, an estimate of the probe positioning on the head was made (see Figure 7.9) and simulations were run for the source-detector separations of 1.5, 2.0, 2.5 and 3.0cm. The Monte Carlo simulation was performed with $1x10^8$ photons simulated as a source. The photon distribution at the different source-detector separations in the neonatal head can be seen in Figures 7.10 and 7.11 for a close-up of the longest source-detector distance. It can be seen that even the 1.5cm channel is sensitive

Table 7.1: Optical properties used for simulation of light propagation in neonatal head (data from Fukui et al. [68]).

Layer	**Transport Scattering Coefficient (mm^{-1})**	**Absorption Coefficient (mm^{-1})**
Scalp	1.9	0.018
Skull	1.6	0.016
CSF	0.25	0.004
Grey Matter	0.5	0.048
White Matter	1.0	0.037

to brain tissue with the furthest 3.0cm channel displaying the largest sensitivity to brain tissue. Table 7.2 shows the results from the simulation.

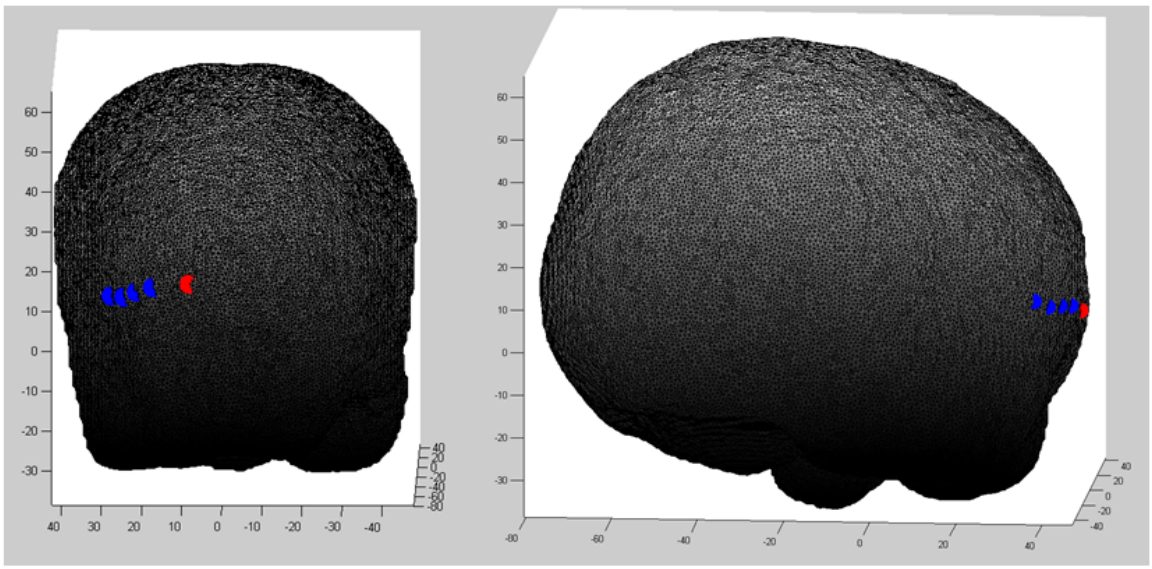

Figure 7.9: Position of CYRIL optodes on brain atlas used for simulations (right side only).

This analysis suggests that the CYRIL set-up is sensitive to brain (both GM and WM) at all source-detector separations on a term infant. This agrees with analysis on a generic set-up on a range of infants at different GA which found that channels with separations of 2.15mm or greater have brain sensitivity greater than 5% [145]. It is not possible to check this experimentally without performing a challenge which is specific to the brain (i.e. a functional task).

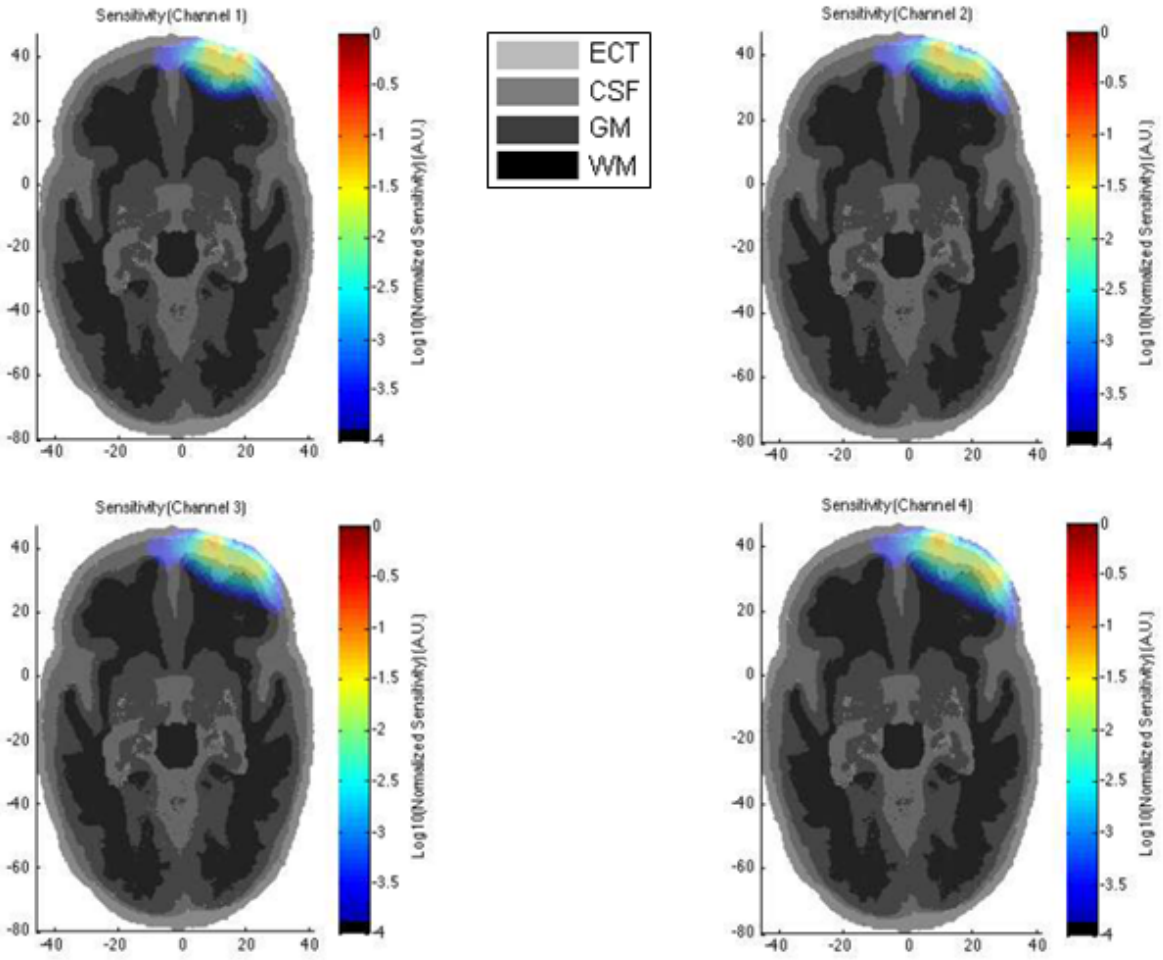

Figure 7.10: CYRIL sensitivity to 40 weeks GA brain from all source-detector separations (channel 1: 1.5cm, 2: 2.0cm, 3: 2.5cm, 4: 3.0cm).

Table 7.2: Results from Monte Carlo simulation.

Optode distance (cm)	**1.5**	**2**	**2.5**	**3**
Number of photons detected	2691	2110	1500	993
Absolute attenuation	4.6	4.7	4.8	5.0
Pathlength (cm)	10.0	11.2	12.3	15.2
DPF	6.7	5.6	5.0	5.1
Percent of pathlength through WM (%)	15	16	17	19
Percent of pathlength through GM (%)	20	20	19	21
Percent of pathlength through CSF (%)	36	36	37	35
Percent of pathlength through ECT (%)	29	27	27	24

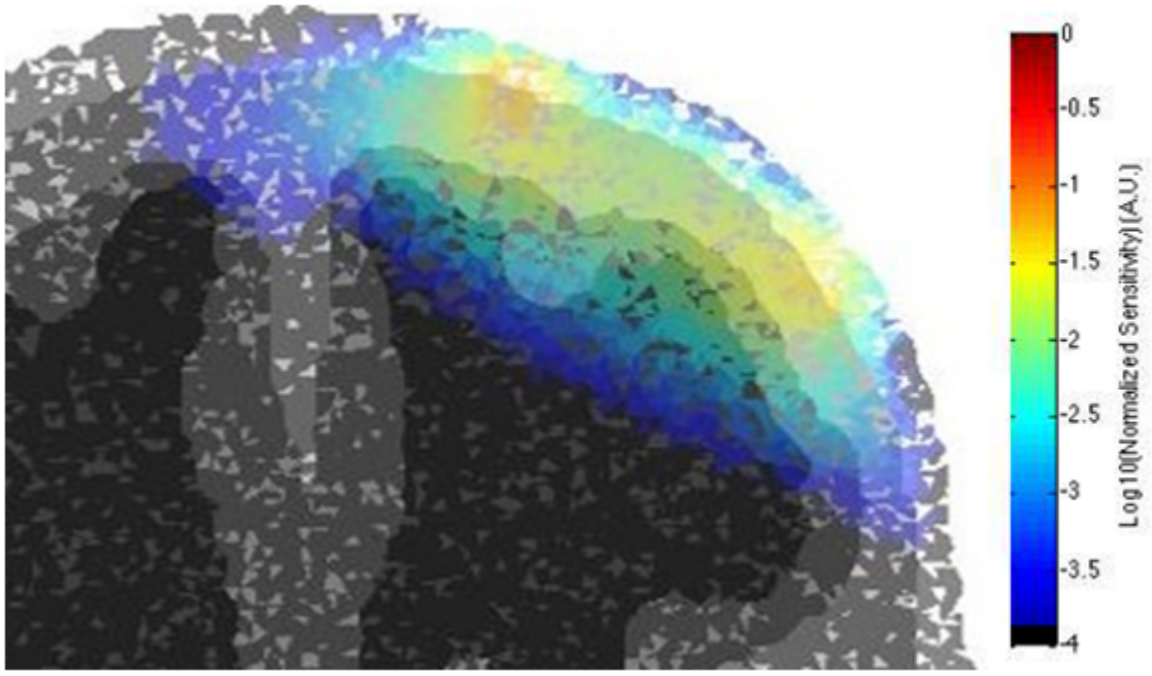

Figure 7.11: Close up of CYRIL sensitivity to 40 weeks GA brain from 3.0cm source-detector separation (channel 4).

7.3 TOI Measurements

The CYRIL system has the capability to record multi-distance (MD) measurements of attenuation so, in theory, it should be able to use the SRS method to resolve TOI. The TOI is an absolute measurement of cerebral oxygenation and is commonly used in clinical neonatal research so is of great interest. It would be particularly interesting to observe oxCCO activity with TOI; the knowledge of tissue saturation would inform on the absolute oxygen levels within the tissue, which would help explain the changes in the oxygen-dependent CCO redox state. However, there are many problems with the methodology and the precision and variability of TOI [238].

The SRS algorithm, as described in section 3.1.5, has been applied to the CYRIL data (see section 5.3) but there are many problems with the TOI results. In some instances the TOI calculated is negative or greater than 100% which is not physiologically possible as the TOI represents the fraction of haemoglobin which is oxygenated. An example of a data set from subject 27 where both of these cases occurs is shown, as well as some periods of TOI within a 'reasonable' range (i.e. between 0 and 100%) in Figure 7.12. To investigate the difference between these measurements the 'slopes' ($\frac{\delta A}{\delta \rho}$) at one wavelength for the three different periods are plotted in Figure 7.13. All three slopes have very strong correlations (R^2=0.97-0.99) and it is observed that a very small change in the slope (from 0.055 to 0.059) changes whether the TOI calculated is 'reasonable' or not. In this case the change in the slope is mostly likely due to poor optode to skin contact as there appear to be large motion artefacts between the different periods.

The theory behind SRS assumes that the tissue is a homogeneous semi-infinite medium (see section 3.1.5) but in actuality the head is a complex layered structure with vastly different optical properties between each layer (see Table 7.1). The SRS method was developed for the adult head and used a source-detector distance of ∼5cm. Therefore, to ascertain whether the neonatal head anatomy could be the source of the TOI problems, for example, if the change in attention with distance is not linear in the CYRIL geometry on a neonatal head, the model described in the previous section 7.2 was used to calculate the slope in an idealised situation (i.e. no optode contact losses). Figure 7.14 presents the results from the Monte Carlo simulation which show that there is a strong linear relationship (R^2=0.99). The slope from the simulated data are an order of magnitude higher than that of the experimental data which may allude to the problem. However, it is not possible to calculate a TOI from the simulated data as more than one wavelength is required (see equation 3.46).

It is obvious that the calculation of TOI needs a significant amount of work but the measurement of TOI is not the focus of this thesis, so this project has been moved to 'Further Work' (Chapter 11). TOI measurements will not be used in the analysis, as the issues with the measurement mean that it is unreliable even when it appears 'reasonable'.

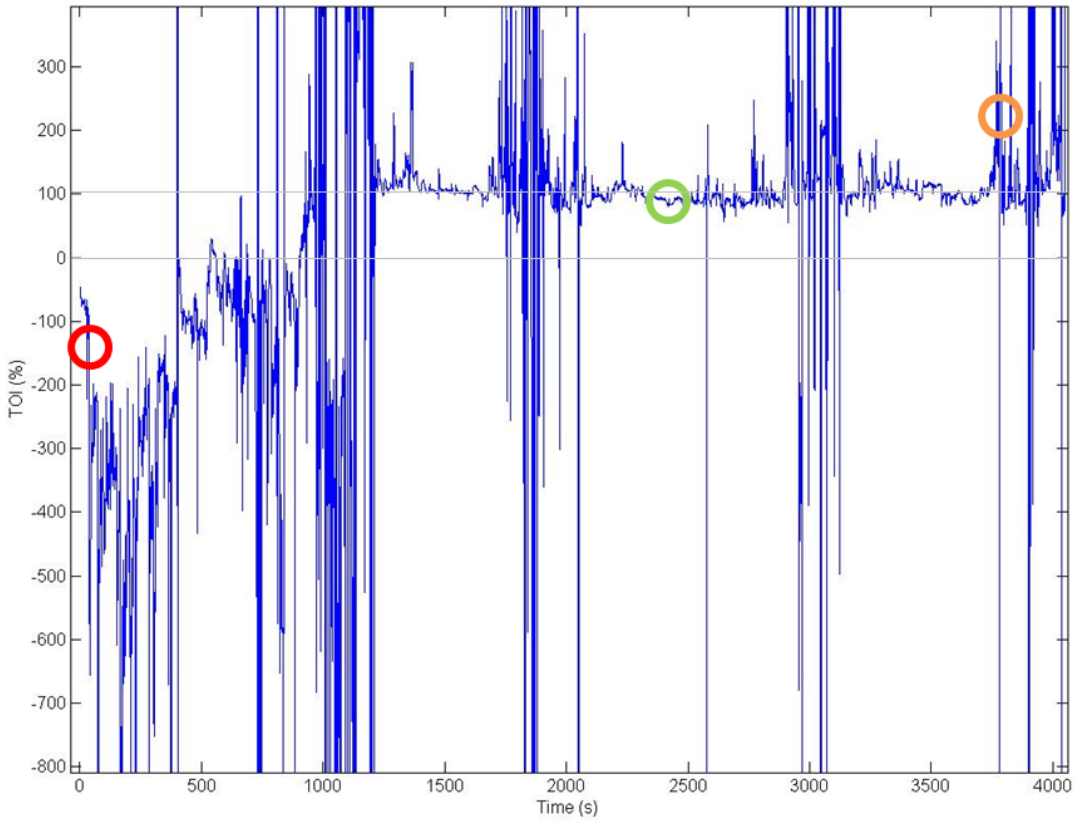

Figure 7.12: TOI recorded from infant 27. Points highlighted at three different cases (red: negative TOI, green: TOI between 0 and 100%, amber: TOI greater than 100%). The slope at each point is presented in Figure 7.13.

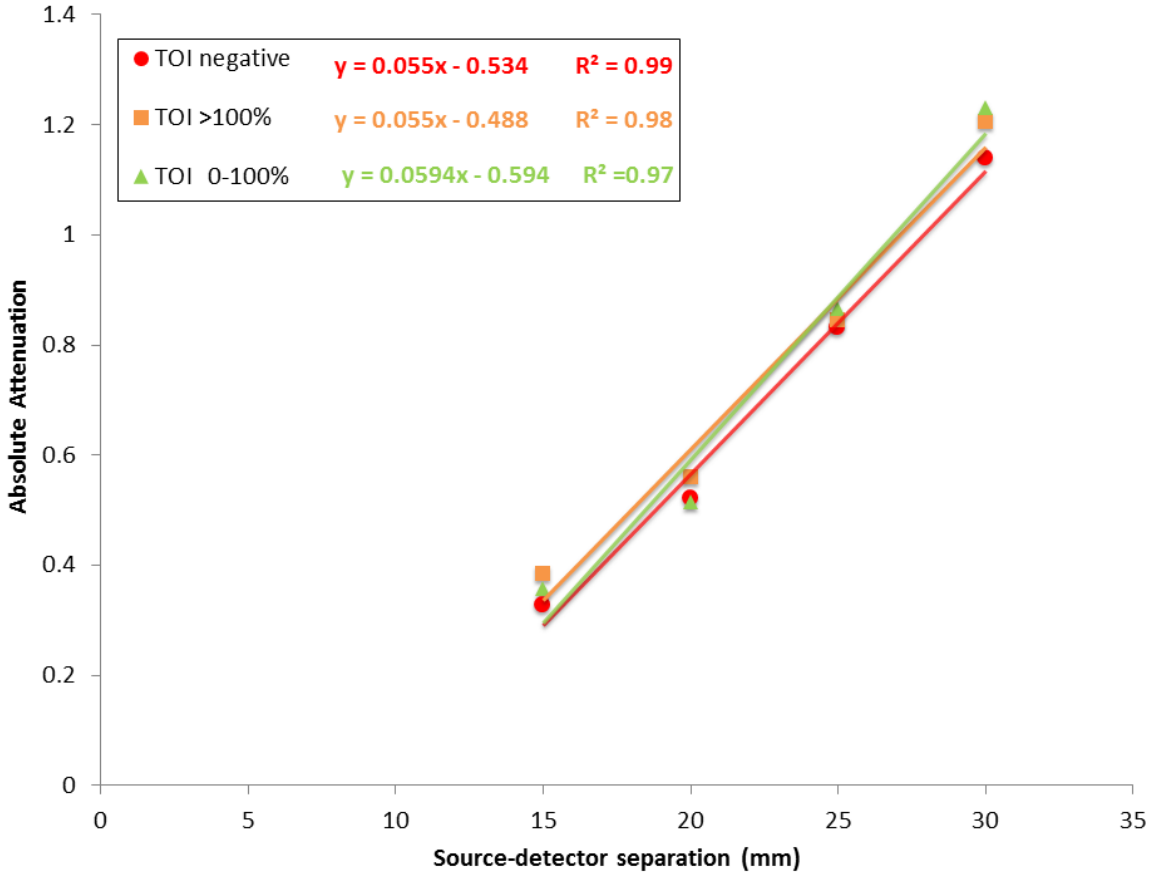

Figure 7.13: Slopes at 800nm from points highlighted in Figure 7.12.

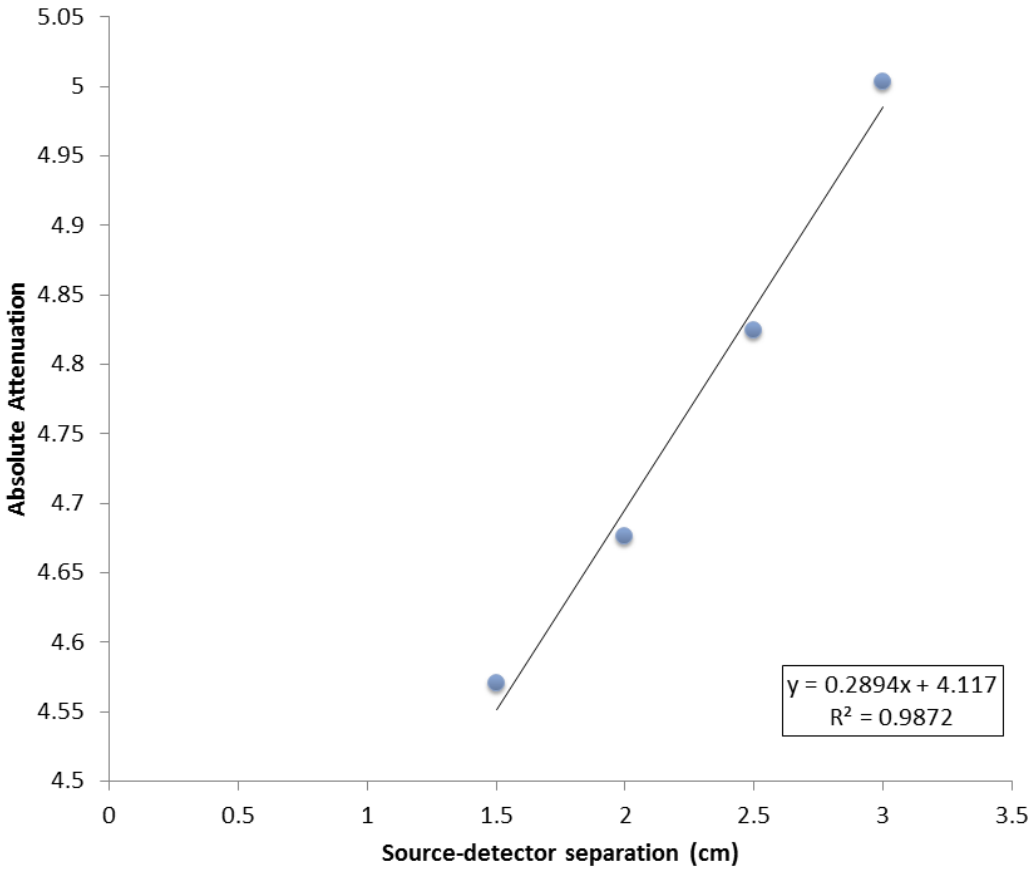

Figure 7.14: Slope at 800nm from simulated data in previous section.

7.4 Summary

The CYRIL system has been demonstrated within the NICU and the oxCCO signals recorded have been shown to be independent of the larger haemoglobin signals. Therefore this machine is capable of monitoring changes in cellular metabolic activity, in addition to haemodynamics and oxyegnation. CYRIL is sensitive to the neonatal cortex, both grey and white matter, in its current configuration. Despite the capacity to record multi-distance data for SRS, the calculation of a reliable and reasonable TOI was not possible and requires further work.

Chapter 8

Cerebral Oxygenation and Cytochrome-C-Oxidase Changes in Response to Spontaneous Hypoxia in HIE Infants

Analysis of the data collected with respect to the underlying physiology begins in this Chapter and continues in Chapters 9 and 10. The goal of broadband NIRS in intensive care is to provide a useful measure of brain metabolism at the cotside. As CYRIL uses differential spectroscopy to determine *changes* in concentration, it is not possible to use absolute measurements of chromophores to diagnose brain tissue health. Therefore, in order to compare the signals across different infants, it is necessary to assess the changes in response to external stimuli. Such stimuli include changes in the systemic variables measured, the temperature, a change in clinical care (e.g. beginning of treatment) or with age. This chapter uses spontaneous drops in arterial oxygenation as stimuli and examines the response in the cerebral NIRS signals.

8.1 Introduction

A transient arterial saturation decrease could be caused by a wide range of events including, but not limited to, apnoea, bradycardia (slowing of the heart rate), immaturity of the baby's nervous system, seizures, infection, acid reflux, high or low body temperature (note that HIE infants will be treated with hypothermia over the first 3 days of life), obstructed ventilation, and decreased ventilatory drive (caused by decreased mental status). Desaturation events are relatively common in HIE infants over the first week of life, and most of this cohort have experienced several arterial desaturations during the monitoring period. It is interesting to understand how they affect cerebral haemoglobins, oxygenation and metabolism. In particular, it is most interesting to know if the level of brain injury affects the

cerebral response to hypoxia and whether the response is related to the outcome as predicted by MRS.

Infant studies of oxCCO during hypoxia have found conflicting results, see section 4.5 for more details. Brazy and Jobsis observed a decrease in oxCCO during spontaneous oxygen desaturations in three preterm infants in the first NIRS study of neonates [16]. A preterm study showed that small SpO_2 changes did not alter oxCCO [70]. Wickramasinghe et al. saw an inconsistent (increases and decreases) and insignificant change in oxCCO during the reduction of FiO_2 (SpO_2 change ∼10%) in neonates [215]. A study of infants during repetitive apnoeas found a consistent trend of reduced oxCCO during the breathing cycle [33]. The heterogeneity of the response to these hypoxias may be a reflection of the level of brain injury, prematurity, previous oxygenation levels or influence of systemic pathophysiology.

Adult studies of hypoxia during normocapnoea in healthy volunteers have consistently found a decrease in oxCCO [50, 53]; there was a linear correlation between oxygen delivery (estimated from the measurement of the Vmca) and oxCCO. A temporal delay between the HbD drop and oxCCO of ∼5s was also observed. A later study confirmed the decrease in oxCCO during hypoxia [60].

Broadband NIRS studies of piglet models of HIE have found a strong link between the oxCCO signal and MRS markers of cerebral metabolism during the HI insult [12]. Another piglet study found that during anoxic swings a reduction in oxygen delivery caused a linear decrease in HbO_2, but a biphasic change in oxCCO [65] (shown in Figure 8.1). A reduction in oxCCO may be a signal of impending damage and this has also been previously suggested by Cooper et al. [190]. The heterogeneity of the oxCCO response to hypoxia has also been seen in a study of 4-week old piglets undergoing increasingly severe episodes of hypoxia [66]. At lower severities of hypoxia (8 and 12% FiO_2) there were small increases in oxCCO, while at higher degrees of hypoxia (6, 4 and 0% FiO_2) oxCCO decreased further with severity; consistent decreases in HbO_2 and corresponding increases in HHb were observed in all hypoxic episodes (see Figure 8.2). It is possible that the influence of the anaesthetic may cause the unexpected increase in oxCCO during hypoxia, although not many studies have investigated the influence of anaesthesia alone on CCO. A study of infants undergoing surgery with and without propofol, an anaesthetic, observed a larger decrease in oxCCO during surgery with propofol than without [34]. This suggests that anaesthesia does affect metabolism, but it is difficult to untangle the effects of anaesthesia on CCO in studies without a non-anaesthesia control group [38].

8.1.1 Aim

The hypothesis is that the relationship between oxygenation and cerebral metabolism during hypoxia will depend on the level of brain injury. To test this hypothesis, the cerebral NIRS signals will be analysed during spontaneous hypoxias, which are common in this cohort in the days proceeding birth. The analysis will compare with the MRS-measured Lac/NAA biomarker of injury severity.

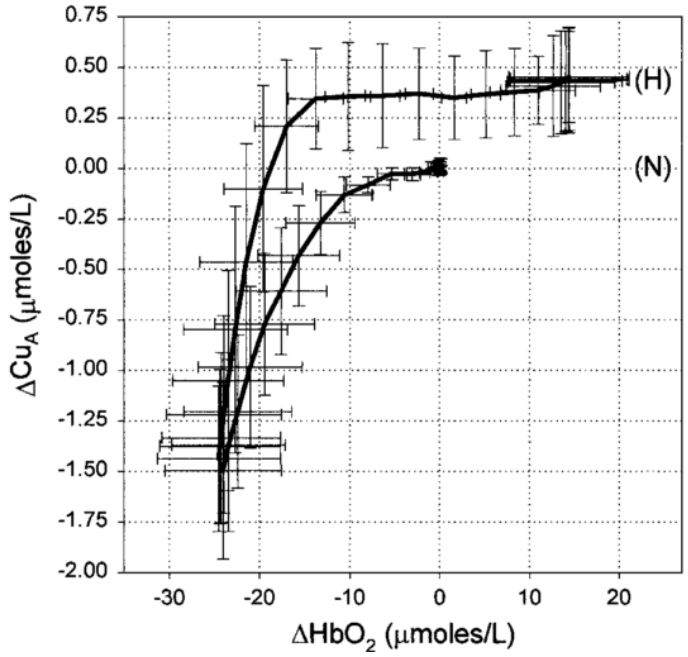

Figure 8.1: Changes in oxCCO (represented here as the Cu_A redox state) plotted against HbO_2 at both normocapnia (N) and hypercapnia (H) during the onset of anoxia. The results are shown as mean±SD (n=7 piglets). Taken from [65].

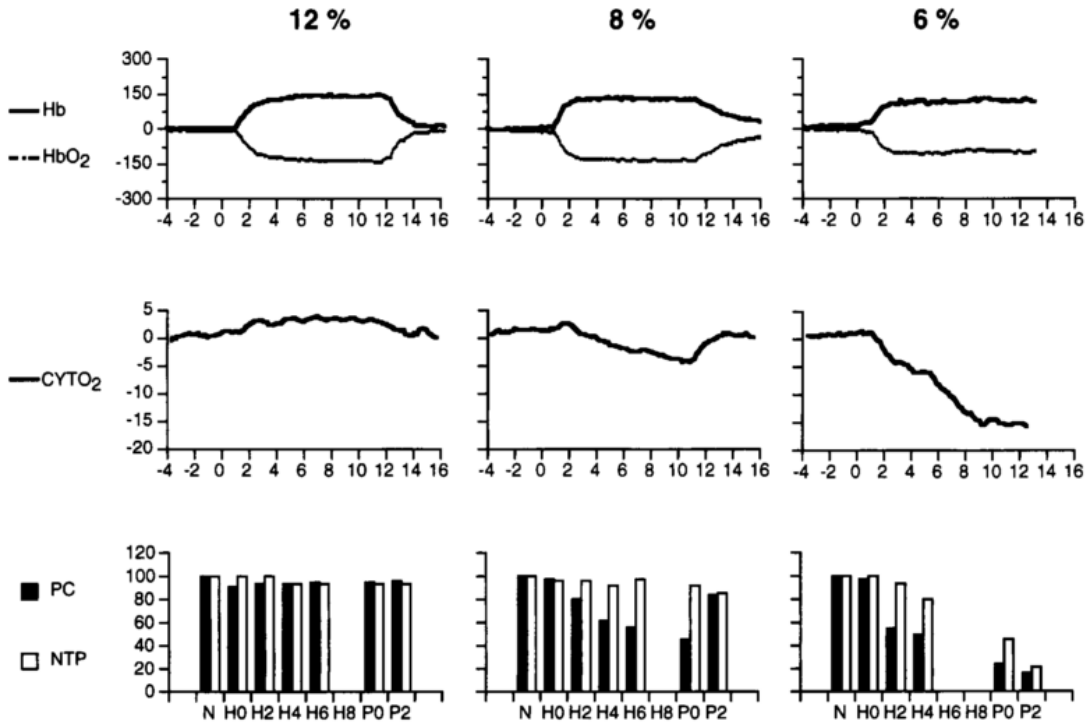

Figure 8.2: Temporal association of NIRS and MRS variables during different levels of FiO_2 in one piglet (taken from [66]). The x-axes are time in minutes. Hypoxia starts at time 0 (HO) and extends to time 10 (PO). NIRS changes are expressed in μM times DPF. Decreases in oxCCO (shown here as $CYTO_2$), temporally correspond to decreases in PCr as measured by MRS. More severe reduction of oxCCO, is accompanied by decreases in both PCr (shown here as PC) and NTP. PCr and NTP loss are not temporally associated with HbO_2 (shown here as HbO), and HHb (shown here as Hb) changes.

8.2 Method

data were collected and pre-processed as outlined in Chapter 6. Only infants diagnosed with HIE were included in this analysis.

8.2.1 Data Analysis

data were analysed according to decreases in SpO_2. For each SpO_2 desaturation with a decrease of 5% or greater, chosen as smaller changes may not be clinically significant, the magnitude of change in the cerebral NIRS variables was recorded. The SpO_2 signal was inspected and each desaturation start and nadir was identified and selected manually; these time points were then used to calculate the changes in HbD, HbT and oxCCO over the event. See Figure 8.3 for a schematic of this process. The surrogate markers of cerebral oxygen delivery and blood volume changes were used (i.e. HbD and HbT) as they are more intuitive representations of the physiology. Magnitude changes in HbD, HbT and oxCCO were recorded for both NIRS channels above the frontal lobes of the right and left hemispheres, and then these changes were averaged. The mean change in the NIRS signals were averaged per infant. The change of MABP, HR and CO_2 tension in the period between SpO_2 desaturation start and nadir were also recorded with their standard deviations.

8.2.2 Statistical Analysis

All statistical analysis was carried out in MATLAB (Mathworks, USA), in which scripts were written to semi-automate the procedure. The coefficients of determination R^2 (sometimes r^2) were calculated between the magnitudes of each SpO_2 saturation changes and the corresponding changes in HbD, HbT and oxCCO for each subject across all days of life. This tests how well the data fit to a linear model. R^2 was also calculated for oxCCO against HbD and HbT. Figure 8.7 shows 4 examples of this process. These coefficients were then correlated with the Lac/NAA measurement for each subject to identify trends between the relationships between SpO_2 and/or the NIRS measured values and the severity of injury. A p-value of less than 0.05 was considered statistically significant. If a subject had less than 5 desaturation events recorded, it was not eligible for this study as 4 data points were determined to be too few to observe a significant correlation across.

8.3 Results

Examples of NIRS data recorded, alongside systemic measurements (MABP, arterial SpO_2, heart rate, respiratory rate, and arterial CO_2 and O_2 tension), are shown in section 6.5 and in Figure 8.3.

There were a total of 29 HIE subjects for which full data were recorded, of which 8 infants were rejected from the analysis as there were less than 5 desaturation events recorded. Of the 21 eligible for this analysis, 8 infants had severe injury and 12 were female. The mean birth weight was 3.2±0.5kg and the mean GA was 39±1 weeks.

538 desaturations from the 21 subjects were identified. There was no relationship found between the number of desaturation events observed within an infant and the severity of injury. Desaturations occurred over periods from a few seconds up to ∼40 minutes and the mean desaturation magnitude was 11.8±3.5%. On average the MABP increased by 1.9±6.2mmHg (recorded in 16 of the 21 subjects analysed), the HR increased by 0.4±3.6 beats per minute, and the CO_2 decreased by 0.2±1.0kPa (recorded in 16 of the 21 subjects studied). The mean change in each variable is displayed per infant in Table 8.1. There were no significant correlations between the magnitude of change in any of the systemic variables and injury, as defined by Lac/NAA.

Across all subjects there was a consistent negative change in the HbD and oxCCO measurements: mean decreases were 3.8±4.3μM and 0.5±1.2μM; and a positive change in the HbT measurements: mean increase was 1.3±2.5μM. The individual mean changes are displayed in Figures 8.4 to 8.6. There were no significant correlations between changes in any of the NIRS variables and injury, as defined by Lac/NAA.

Table 8.2 presents the R^2 between the magnitudes of each SpO_2 change and the corresponding change in HbD, HbT and oxCCO, and for oxCCO against HbD and HbT. These coefficients were correlated with the corresponding Lac/NAA measurement across all subjects; these are displayed in Figures 8.8 to 8.12. Only the correlation coefficients between HbD and oxCCO has a statistically significant (p=0.018) correlation with the MRS-measured Lac/NAA values.

Table 8.1: Mean changes in systemic and broadband NIRS changes during oxygen desaturation events per patient. Haemoglobin changes are coloured to illustrate the direction of change: negative changes (<-0.5μM) are red, positive changes (>-0.5μM) are blue and no change (between -0.05 and 0.05μM) are green. For oxCCO these limits are reduced by 10% to reflect the smaller changes in this chromophore.

CYRIL	**SpO_2 Mean (%)**	**SpO_2 SD (%)**	**MABP Mean (mmHg)**	**MABP SD (mmHg)**	**$PaCO_2$ Mean (kPa)**	**$PaCO_2$ SD (kPa)**	**HR Mean (bpm)**	**HR SD (bpm)**	**HbT Mean (uM)**	**HbT SD (uM)**	**HbD Mean (uM)**	**HbD SD (uM)**	**oxCCO Mean (uM)**	**oxCCO SD (uM)**
2	-13.00	11.00	1.20	0.90	-0.61	0.57	0.09	1.27	0.45	3.40	-2.40	6.60	-0.02	0.63
3	-17.00	19.00	-2.60	6.00	0.41	0.17	0.58	5.70	1.40	3.50	-6.50	10.50	-0.37	1.10
6	-14.04	14.05	-2.11	6.94	-0.26	3.43	-0.91	3.43	-0.91	8.88	-3.30	13.44	0.59	7.11
7	-9.60	3.80	ND	ND	-2.80	1.80	-0.37	0.97	0.30	1.20	-1.30	3.30	-0.22	0.33
8	-9.40	9.60	ND	ND	0.23	0.09	4.33	6.92	0.94	3.70	-2.00	3.40	-0.18	1.10
9	-11.00	5.00	-1.30	2.20	0.03	0.24	4.79	11.16	1.80	1.90	-2.30	6.20	-0.29	0.50
10	-10.00	5.00	ND	ND	0.12	0.08	-1.60	6.38	0.21	3.30	-3.50	4.40	-0.28	1.10
11	-12.74	11.41	0.49	12.07	-0.56	7.82	0.50	7.82	2.20	3.41	-9.20	15.58	0.23	2.03
12	-16.50	10.87	-2.50	4.50	ND	ND	3.75	6.50	2.98	2.51	-1.06	6.68	-0.25	1.20
13	-6.57	1.76	-8.71	8.07	-0.85	12.94	-10.43	12.94	-6.32	7.30	-10.49	10.18	-4.45	4.06
14	-7.31	2.46	-0.85	2.74	0.05	4.79	-2.38	4.79	0.46	2.26	-3.37	4.48	-1.92	2.75
15	-16.35	19.78	-3.58	5.69	0.64	9.13	1.72	9.13	3.54	20.79	-11.47	29.93	-0.42	7.12
17	-16.65	17.36	0.38	3.03	0.19	14.69	1.17	14.69	2.50	4.47	-9.78	14.24	-2.29	4.09
18	-7.62	1.94	0.85	4.69	0.26	5.27	-2.62	5.27	0.12	1.55	-1.64	2.28	-0.17	1.67
19	-12.92	11.82	3.39	5.72	0.46	16.23	2.26	16.23	-0.97	3.85	-2.36	4.24	-0.23	1.51
20	-16.61	14.08	-2.03	5.58	-0.54	5.54	1.06	5.54	1.40	4.21	3.26	21.68	0.40	0.85
21	-9.89	6.86	ND	ND	0.10	6.82	1.11	6.82	1.39	3.41	-4.62	4.48	0.24	0.91
30	-6.33	2.13	ND	ND	ND	ND	-4.83	3.53	3.80	5.39	-0.21	5.53	0.61	1.37
33	-11.00	6.32	-0.09	2.75	ND	ND	2.30	2.83	1.64	1.02	-6.09	6.73	-0.06	0.39
35	-11.10	9.05	0.30	4.34	ND	ND	-0.90	6.25	7.35	18.52	5.74	24.30	-1.61	6.08
37	-11.80	10.85	-2.20	3.54	ND	ND	-0.20	7.68	2.91	1.85	-7.23	13.08	-0.04	2.35
Mean	-11.78		-1.21		-0.20		-0.03		1.29		-3.80		-0.51	
SD	3.38		2.60		0.79		3.25		2.48		4.23		1.14	
n increase									13		2		5	
n decrease									3		18		14	
n no change									5		1		2	

Table 8.2: R^2 of linear relationship between changes in SpO_2 and/or NIRS variables during spontaneous hypoxia per infant.

CYRIL	**SpO_2 vs. HbD R^2**	**SpO_2 vs. HbT R^2**	**SpO_2 vs. oxCCO R^2**	**HbT vs. oxCCO R^2**	**HbD vs. oxCCO R^2**	**No. of desaturations**	**HIE**	**Lac/NAA**
2	0.854	0.147	0.011	0.160	0.002	33	Severe	0.87
3	0.858	0.223	0.265	0.063	0.305	70	Moderate	0.2
4						<5	Mild	0.16
5							Stroke	
6	0.184	0.104	0.103	0.230	0.258	28	Severe	0.39
7	0.350	0.243	0.202	0.450	0.801	7	Severe	1.32
8	0.003	0.038	0.021	0.475	0.225	30	Mild	0.17
9	0.384	0.185	0.120	0.332	0.010	25	Moderate	0.16
10	0.016	0.011	0.033	0.541	0.025	71	Mild	0.15
11	0.742	0.226	0.128	0.074	0.291	54	Moderate	0.08
12	0.001	0.000	0.397	0.148	0.569	4	Severe	1.8
13	0.371	0.149	0.025	0.366	0.624	7	Severe	0.76
14	0.035	0.006	0.000	0.071	0.013	44	Mild	0.25
15	0.813	0.608	0.077	0.236	0.205	20	Mild	0.15
16						<5	Severe (died)	
17	0.607	0.600	0.142	0.017	0.103	26		0.35
18	0.050	0.031	0.296	0.012	0.005	13		0.28
19	0.209	0.013	0.106	0.074	0.110	37		0.16
20	0.281	0.030	0.382	0.004	0.271	18		0.11
21	0.625	0.085	0.151	0.023	0.054	19		0.2
22							No data	0.2
23							No data	
24							No data	
25						<5		0.4
26						<5		0.52
27							Preterm	
28						<5		0.16
29								No MRS
30	0.008	0.028	0.127	0.006	0.139	6		0.17
31						<5		1
32							Stroke	
33	0.842	0.666	0.033	0.000	0.139	11		0.43
34							Seizures	
35	0.097	0.017	0.043	0.805	0.805	10		0.14
36							Seizures	
37	0.929	0.010	0.035	0.044	0.000	5		0.2
38							IVH	2.11
vs. Lac/NAA	**-0.10**	**-0.01**	**0.34**	**0.08**	**0.51**	**538**		

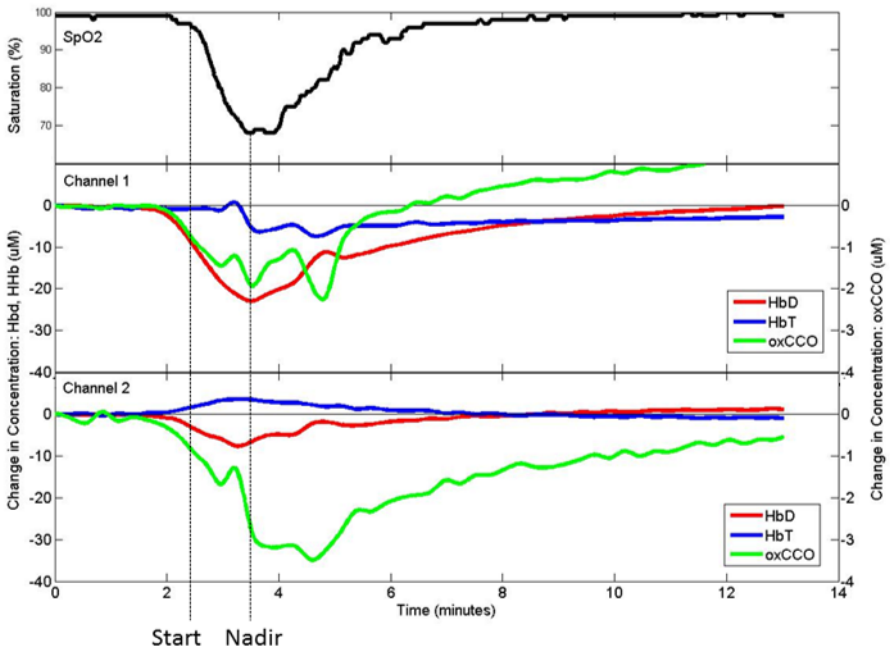

Figure 8.3: Example of SpO_2 desaturation from channels 1 and 2 (right and left side respectively) on subject 003 (mild injury) with start and nadir of desaturation marked for SpO_2 and corresponding position in the NIRS signals.

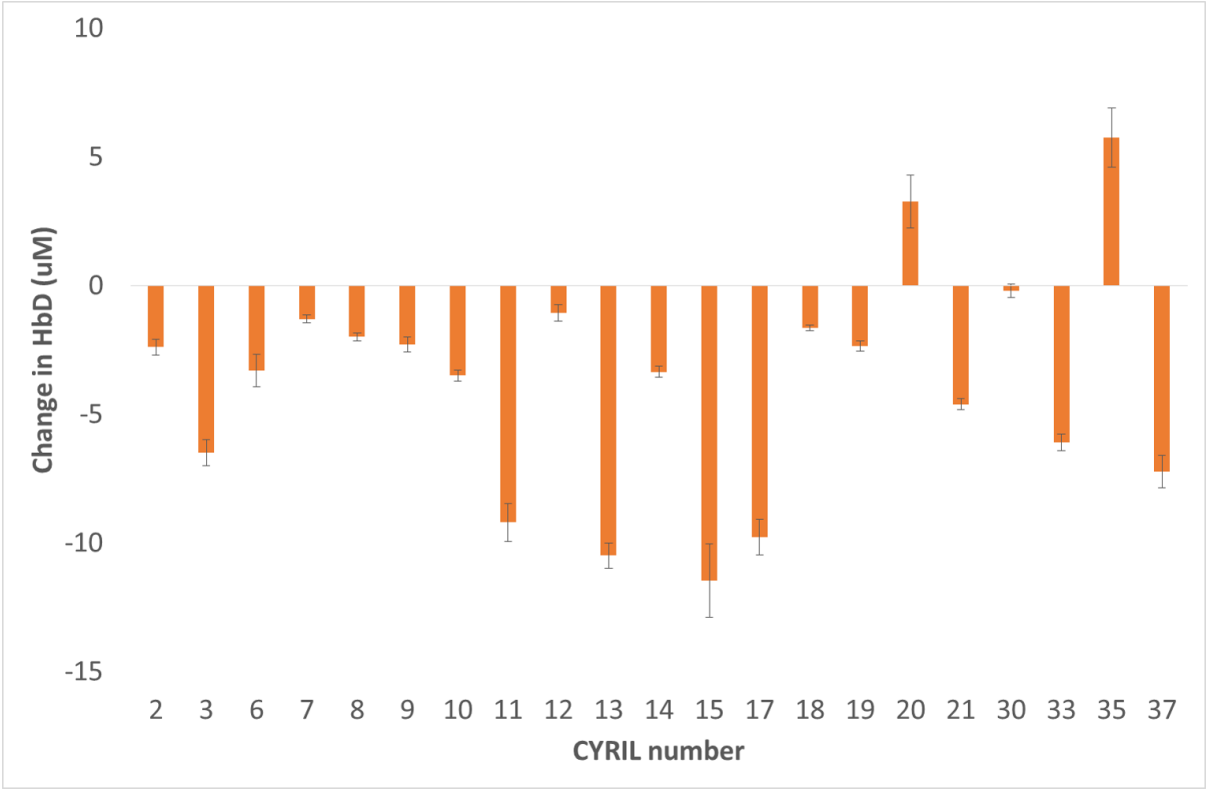

Figure 8.4: Mean change in HbD per infant during spontaneous desaturations.

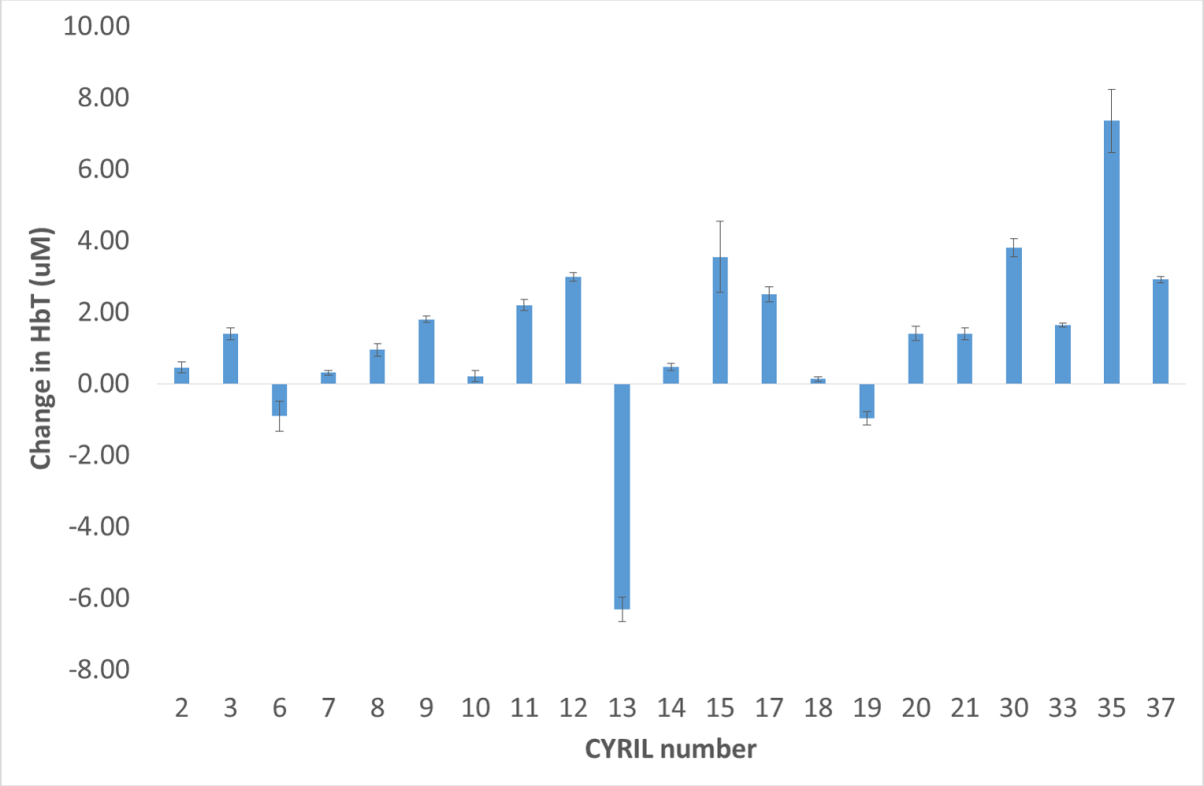

Figure 8.5: Mean change in HbT per infant during spontaneous desaturations.

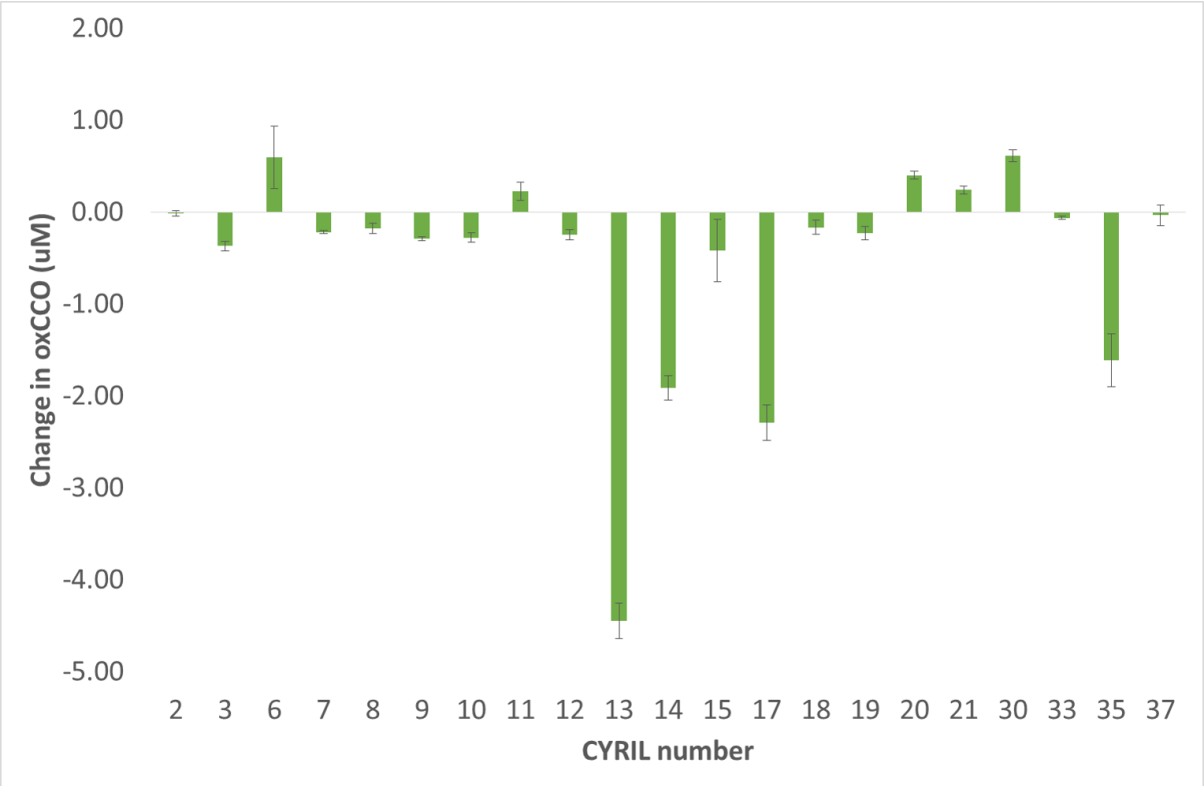

Figure 8.6: Mean change in oxCCO per infant during spontaneous desaturations.

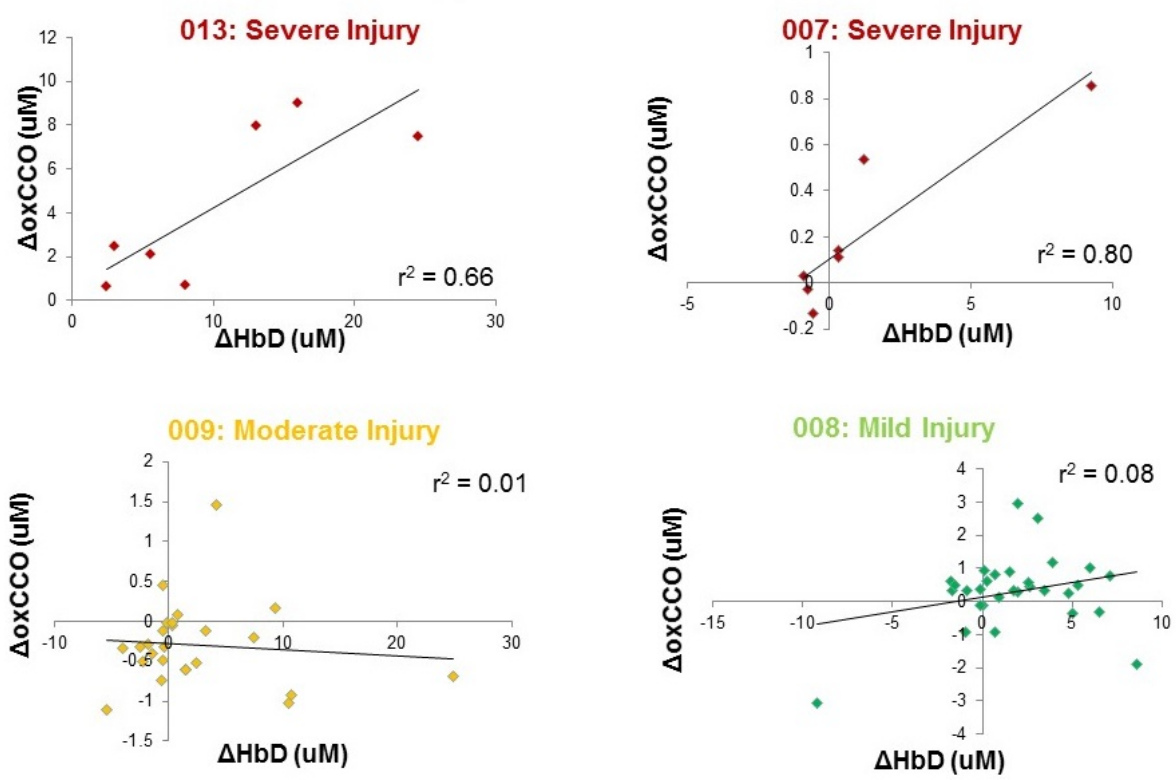

Figure 8.7: Examples of the magnitude of changes in HbD and oxCCO during desaturation events for four infants. Each point represents a single desaturation event. Notice that the severely injured infants (7 and 13) have strong correlations, whereas the infants with mild and moderate injury show no correlation.

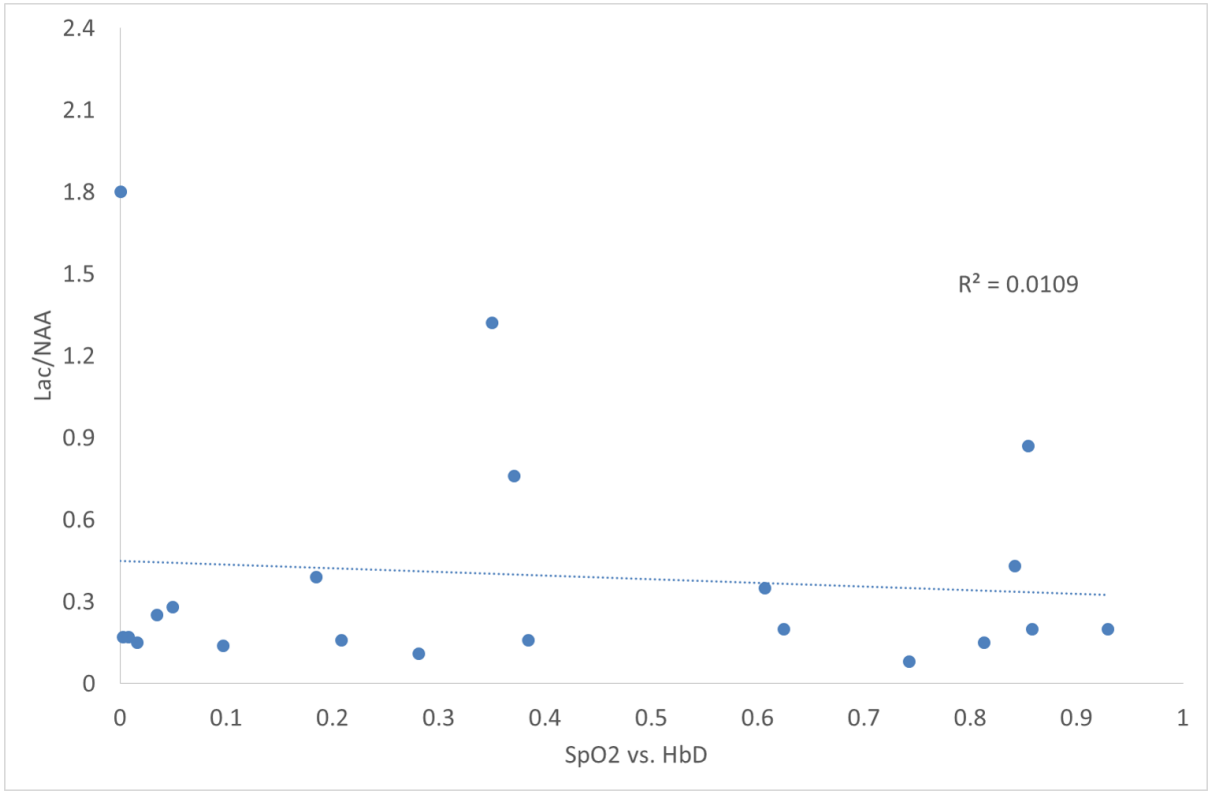

Figure 8.8: R^2 for Lac/NAA against SpO_2 versus HbD. Each point represents an infant.

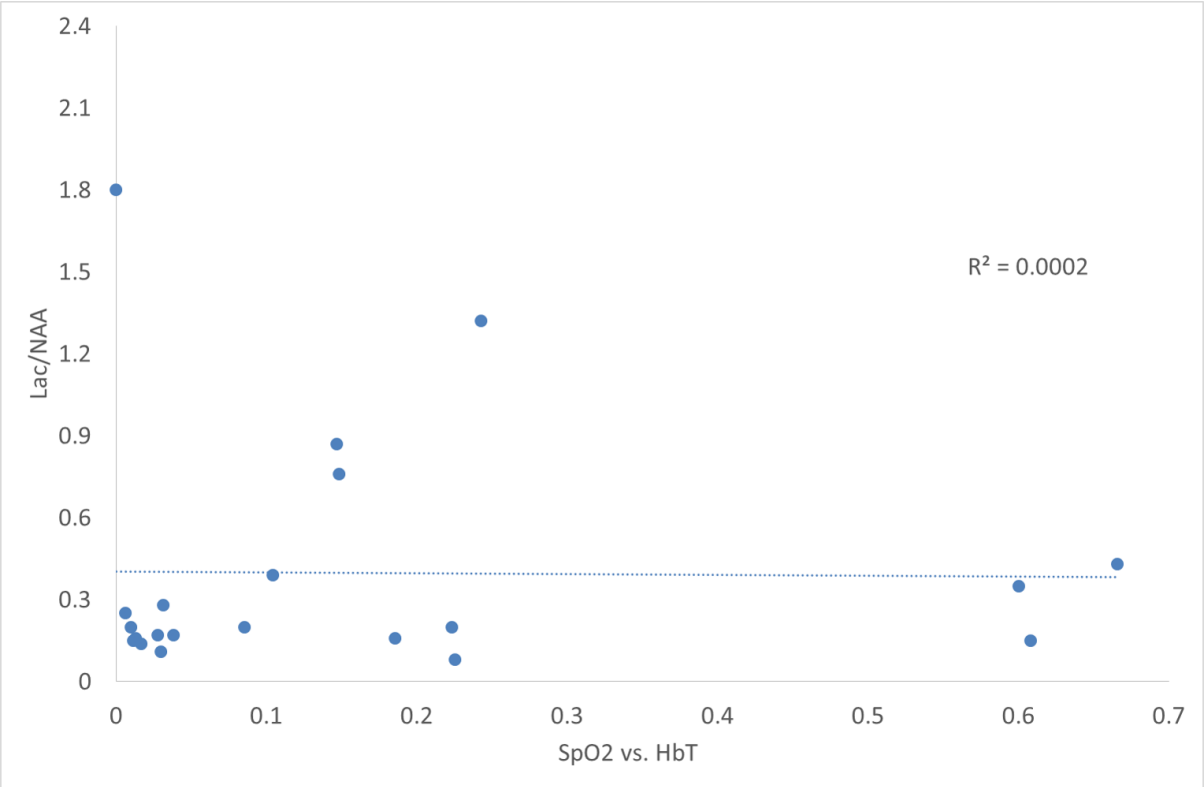

Figure 8.9: R^2 for Lac/NAA against SpO_2 versus HbT. Each point represents an infant.

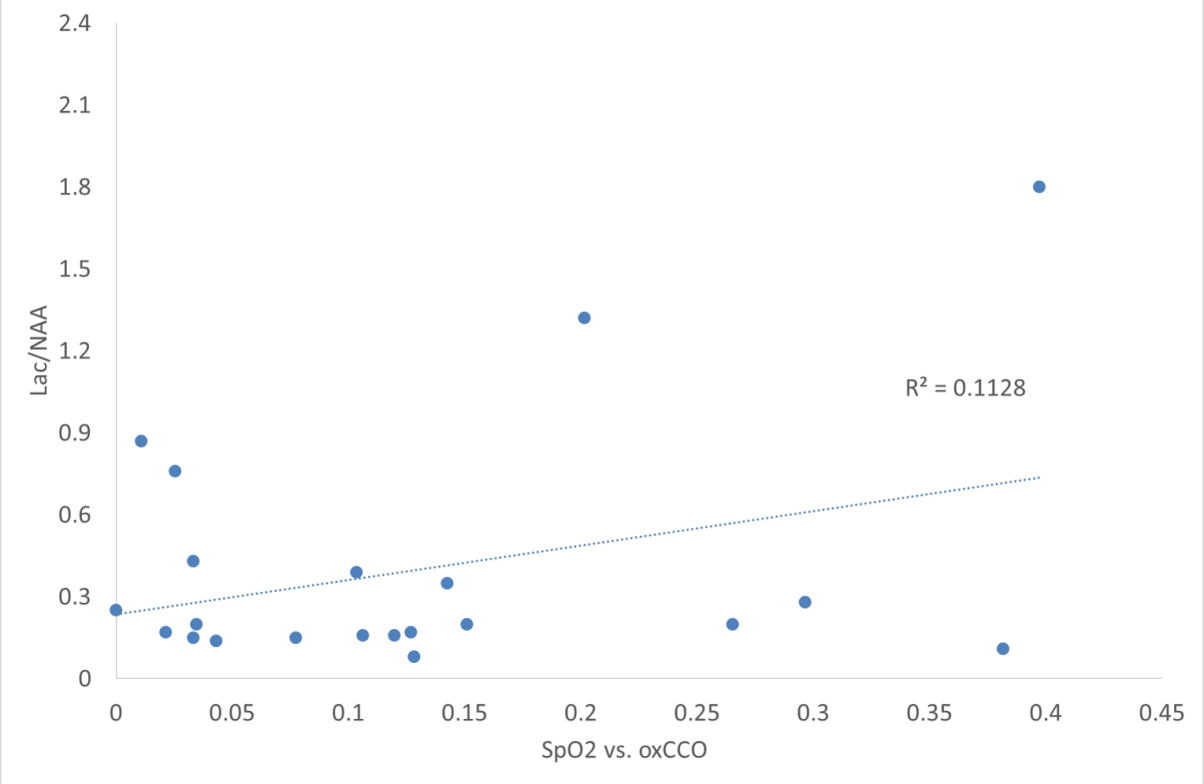

Figure 8.10: R^2 for Lac/NAA against SpO_2 versus oxCCO. Each point represents an infant.

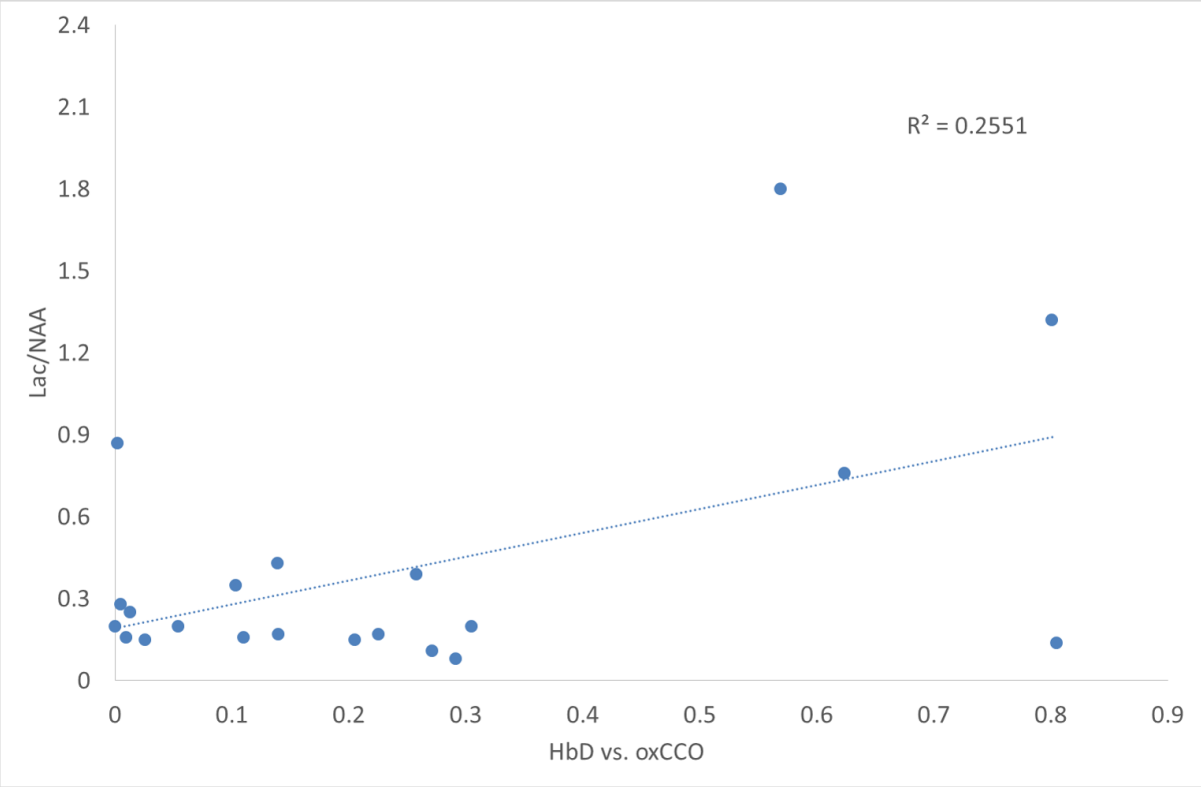

Figure 8.11: R^2 for Lac/NAA against HbD versus oxCCO. Each point represents an infant. The linear correlation is statistically significant, p = 0.018.

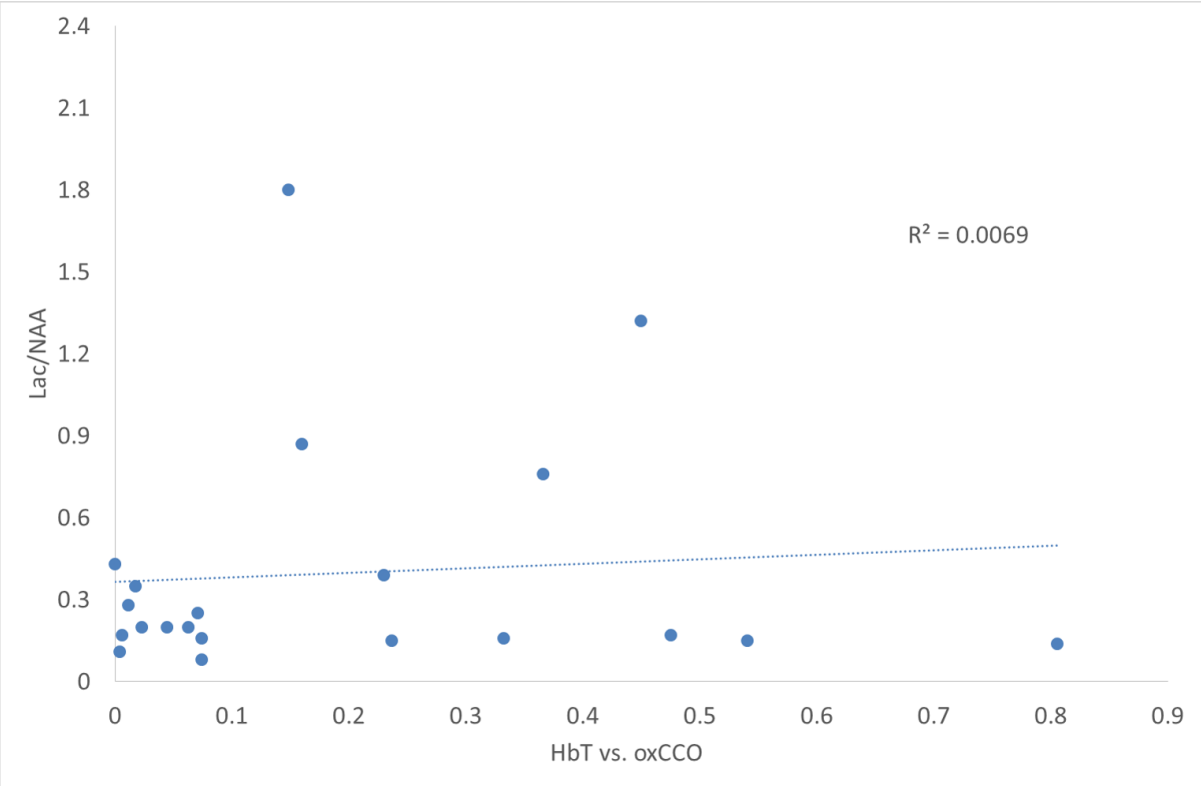

Figure 8.12: R^2 for Lac/NAA against HbT versus oxCCO. Each point represents an infant.

8.4 Discussion

This analysis of multiple spontaneous hypoxias was successfully performed on 21 out of 28 HIE infants to assess the clinical significance of the cerebral haemodynamic and metabolic information changes monitored by CYRIL. A significant association has been found between known biomarkers of HIE outcome as measured by ^{1}H MRS. This confirms the hypothesis that the relationship between cerebral metabolism and oxygenation are related to brain injury severity.

While there is, in general, a mean decrease in cerebral oxygenation per baby (HbD decrease in 19 out of 21 infants) and increase in total haemoglobin (HbT increase in 18 out of 21 infants) during spontaneous desaturation, the oxCCO response is less predictable with a decrease in 13, increase in 5 and no change in 3 infants (see Figures 8.4, 8.5, and 8.6). The haemoglobin changes are as would be expected in a healthy brain [60]; the reduction in cerebral oxygenation (via the surrogate, HbD) is a direct response to the reduction in arterial saturation, while an increase in total blood volume (via the surrogate, HbT) is an indirect response from cerebral autoregulation. In a healthy adult brain, a decrease in oxCCO has been recorded [53, 60], and is expected because there is a reduction in available oxygen, the final electron acceptor in the ETC, so CCO will be unable to pass electrons to it and thus will remain reduced (retaining electrons). However, this assumes that the substrate flow is maintained throughout the hypoxia; this will not be the case if the hypoxia is accompanied by ischaemia. Ischaemia will reduce glucose delivery to the other end of the metabolic system and hence the supply of free electrons to the ETC will decrease, leaving CCO oxidised (without electrons). Accordingly, it is sometimes difficult to interpret changes in the concentration of oxCCO, but work in a piglet model of HI has shown strong evidence that reduction in oxCCO represents the decline in ETC activity [12]. The unusual response of an increase in oxCCO has been seen in anaesthetised rodent models at small FiO_2 decreases [66] and may be caused by abnormal physiology caused by anaesthesia, or perhaps in this case, injury to the brain. However, there was no correlation between thalamic Lac/NAA and changes in oxCCO during hypoxia. This may be due to the difference in the measurement location of the separate monitors (i.e. MRS voxel placed in the thalamus and oxCCO measured over the frontal lobe) and the potential localisation of the HI injury. HI injury to the immature foetal brain are usually localised to particular regions or groups of structures within the brain as opposed to manifesting as a global injury to cerebral tissue [96].

One might expect that the correlation between the changes in oxCCO and cerebral oxygenation (via HbD) would be similar to that of oxCCO and systemic oxygenation (SpO_2); however this is not the case as the strength of the relationship differs on a subject level (e.g. subject 13 had an insignificant r^2 for SpO_2 against oxCCO, but a strong r^2 for HbD against oxCCO). This perhaps emphasises the fact that systemic arterial oxygenation at certain instances is not a good indicator of regional brain tissue oxygenation. The HbD and oxCCO r^2 values are significantly associated with the thalamic Lac/NAA ratio (p=0.018) which suggests that a highly coupled cerebral oxygenation and metabolism is indicative of a more severe brain injury. The data show that in more severely injured neonates the magnitude of the drop in oxCCO correlates highly with the magnitude of the HbD drop during systemic oxygen desaturations. This suggests a tight coupling between the oxygen delivery and oxygen utilisation in brain

injury.

It is interesting that the relationship between cerebral oxygenation and metabolism is related to brain injury severity while their individual changes are not. This might be because the change in the NIRS signals is from an arbitrary baseline (i.e. the initial oxygenation/oxidation state of the haemoglobin/CCO is unknown). Furthermore, the lack of relationship between the haemoglobin signals suggests that cerebral autoregulation impairment does not differ between the mild and severe injury levels as blood oxygen delivery is not changing with injury. Therefore, the metabolic CCO signal gives a better indication of the level of brain injury.

Edwards et al. studied oxCCO during spontaneous desaturations in newborn infants with no evidence of brain injury and found no relationship between oxCCO and SpO_2 over small (3-11%) changes in SpO_2 [70]. They concluded that cerebral haemodynamic changes more readily affect oxCCO than systemic oxygenation which agrees with our findings. The UCL group has recorded NIRS-measured oxCCO in controlled preclinical animal models of NE [12]. The recovery of the oxCCO signal after HIE was shown to correlate with the nucleotide triphosphate to exchangeable phosphate pool ratio (NTP/epp) which is a phosphorus (^{31}P) MRS-measured biomarker of HIE and is related to Lac/NAA. This feasibility study suggests that this finding is translatable from the piglet model to the human neonate.

There have been a few recent studies of HIE with NIRS [148, 156] (see also section 3.3.2). Dehaes et al. found that $CMRO_2$ and CBF were significantly lower in neonates during TH compared with post-TH and age-matched controls. This finding agrees with Wintermark et al. who reported that newborns with severe HIE had lower CBF and seemed to extract less oxygen. The reduction in metabolic rate in the most severely asphyxiated newborns may reflect mechanisms to minimise further injury. This could either be a manifestation or the cause of the underlying severity of HIE. Both of these studies noticed elevated tissue oxygen saturation in newborns with more severe HIE which suggest that they were extracting less oxygen.

8.4.1 Study Limitations

It should be noted that the NIRS measurements were taken from above the frontal lobe, whereas the MRS-measured Lac/NAA was from the thalamus. Thalamic Lac/NAA was used as our marker of HIE severity however it does not give the complete picture of the brain injury as the pathology is not always global, so a subject with injury localised in the cortical grey matter may not present a high Lac/NAA ratio in the uninjured thalamus. The cohort of survivors will be given a quantitative developmental assessment at regular intervals up to 2 years of age as part of the UCLH follow-up programme. The results of this test will provide a more accurate assessment of the clinical outcome than the Lac/NAA measurement, so the results of this analysis should be compared with the test results when they are available.

The spontaneous desaturations will have occurred for a variety of reasons (as discussed in earlier in section 8.1). The changes in cerebral oxygenation and oxygen utilisation recorded will vary depending on the cause of the desaturation, and other physiological changes such as CO_2, HR and MABP which were not corrected for in this study, but were generally of low values during the desaturations. CO_2, HR and

MABP have a large effect on the cerebral oxygenation and metabolism [197]. In Chapter 10, a method that considers multiple systemic variables, canonical correlation analysis [239], is used to assess the data. Monitoring changes in the other systemic measurements aids our understanding of the desaturations, yet there is still heterogeneity across and within subjects. As a controlled challenge could not be performed on these patients for ethical reasons, we are limited to focussing on spontaneously occurring events, of which spontaneous hypoxias are the most common.

One of the largest limitations of the data is the heterogeneity of the patients' injury, clinical treatment and response to treatment. Patients receive different sedatives and medication (dependent on their clinical needs) which may affect cerebral metabolism and blood flow. The different days of life over which this analysis is performed may be a confounding factor as the brain response to hypoxia will change as the injury evolves, matures and is treated. These factors can confuse the results regarding the relationship between brain injury and cerebral haemodynamic and metabolic changes. Future analyses should try to limit the number of differing variables in order to eliminate some of these confounding factors. The differences between the days of measurements and treatments (i.e. during or post-TH) should also be investigated as the relationship may alter as injury and treatment progress.

The method of assessing the desaturation based on magnitude change may not be representative of the data. A physiological lag might be expected between the arterial oxygenation changes and the cerebral oxygenation and metabolic changes. This analysis does not account for this and could be misleading, especially for oxCCO changes; a delay between an arterial reduction of oxygen and cerebral oxCCO decrease would be predicted as cerebral tissue oxygenation must reduce before it will impact upon metabolism. Perhaps those infants who show the largest changes in oxCCO are already at oxygen-limited states, so small changes in oxygen cause quicker and larger reductions of the oxCCO. This may also explain why the strongest relationship came from oxCCO and HbD as it could be expected that there is less temporal difference between cerebral oxygenation and cerebral metabolism, as opposed to arterial oxygenation and cerebral metabolism.

8.5 Summary

The relationship between cerebral oxygenation and metabolism was found to be stronger in infants with more severe HIE injury. This suggests that more severe injury is more dependent on oxygen, or that it has less capacity to buffer changes in oxygenation. The relationship between arterial oxygenation and metabolism was not significant, which suggests that arterial oxygenation may not be an ideal monitor of oxygen levels in the brain.

Chapter 9

Cerebral Oxygenation and Cytochrome-C-Oxidase Dynamics in Spontaneous Hypoxia in HIE Infants

This Chapter expands upon the work of the previous chapter to investigate the haemodynamic and metabolic cerebral response to spontaneous hypoxia in more depth. In Chapter 8 a correlation was found between severe brain injury and a tight coupling between cerebral oxygen and metabolism. In order to investigate the cerebral NIRS signals in more detail, the dynamics of the changes during hypoxia are examined in this chapter.

9.1 Introduction

The results in the previous chapter suggests that the way that the cerebral metabolism reacts to changes in oxygenation can indicate injury severity. The analysis looked at the magnitude of the cerebral changes but did not examine the relationship throughout hypoxia which is also interesting and could inform on cerebral injury. Furthermore, there is concern from doctors in neonatal intensive care over the safety of low oxygen saturation levels [240] but there is little evidence to give guidance over where the threshold saturation level lies. Cerebral broadband NIRS-measured oxCCO can provide an indication of changes in tissue oxygen availability. At the point where there is no oxygen available, CCO will be completely reduced, therefore, there should be a threshold at which oxCCO will reduce no further, indicating complete tissue hypoxia. The opportunity to study tissue hypoxia arises during spontaneous desaturations; particularly the dynamics of the changes during desaturation are observed in order to understand the nature of oxygenation within the brain. The relationship between vascular oxygen delivery and tissue oxygen consumption may provide light on the limits of safe oxygen saturations i.e. answering the question 'What is a safe systemic saturation level for babies with HIE?'.

Adult studies of hypoxemia have not seen a threshold in the oxCCO relationship with oxygen satura-

tion (see Figure 9.1) [60]. One study reported a linear correlation between oxCCO and cerebral oxygen delivery during the oxygen desaturations, but did not find a relationship between oxCCO and HbD [50]. It is possible that the lack of threshold observed is because the saturation cannot be safely and ethically brought low enough to reach full CCO reduction in volunteers.

A biphasic relationship in oxCCO change with ATP production has been seen in a piglet model of HI [12] (see Figure 9.2). The authors interpret the decreased oxCCO as impairment of the ETC, which in turn results in failure of ATP production through ATP synthase (see section 4.2 for background). The threshold point in the double-linear fit of the data has been interpreted as the point at which ATP manufacture is almost completely suppressed. Furthermore, at this point over 60% of the eventual reduction of oxCCO has occurred suggesting that the majority of the reduction in oxCCO occurs during the period where ATP manufacture via ATP synthase declines.

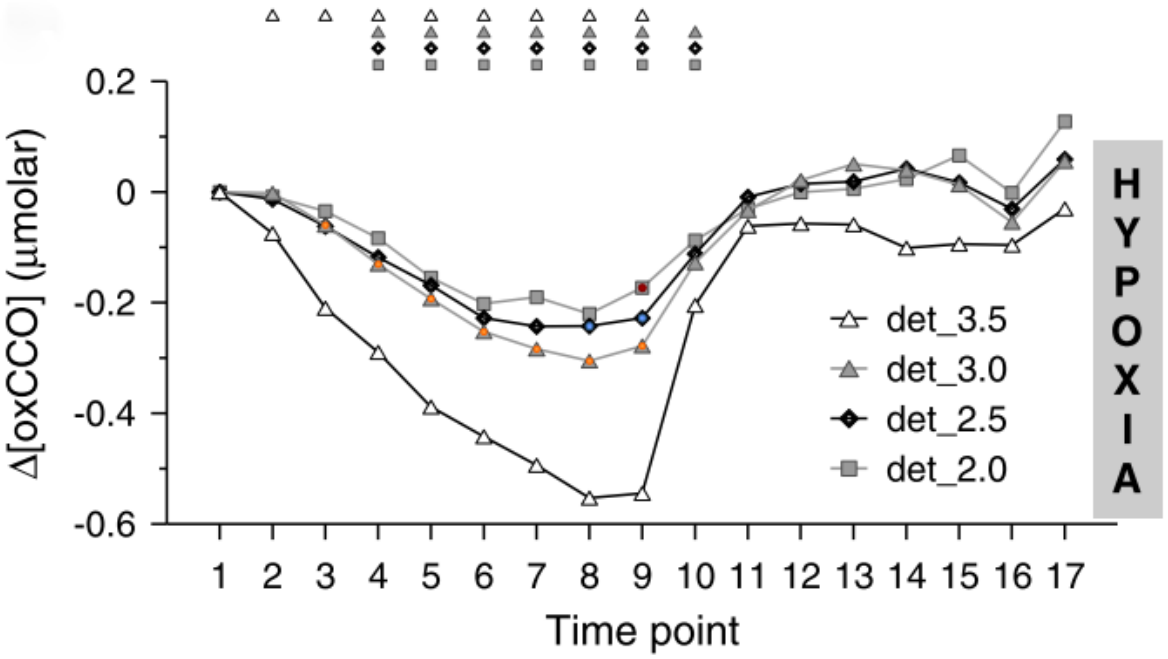

Figure 9.1: Group data of the time courses of oxCCO measured by the detectors 2.0, 2.5, 3.0 and 3.5cm away from the light source denoted, respectively, as det 2.0, det 2.5, det 3.0, and det 3.5. The averages are based on the 15 volunteers that participated in a hypoxia challenge. Taken from [60].

Another porcine study of hypoxia has shown a threshold in the oxCCO response (see Figure 8.1) in that as HbO_2 decreases initially there is no change in oxCCO, but there is then a point at which the redox state suddenly reduces. The authors postulate that this change is caused when metabolism becomes oxygen limited.

Banaji et al. predicted how the oxCCO signal should respond during an oxygen desaturation using a mathematical model of brain circulation and energy metabolism [197]. During hypoxia in a healthy, 'normal' brain there is an approximately linear relationship with HbO_2. When the metabolic rate and cerebral blood flow is lowered, however, the relationship becomes biphasic. This work shows that the

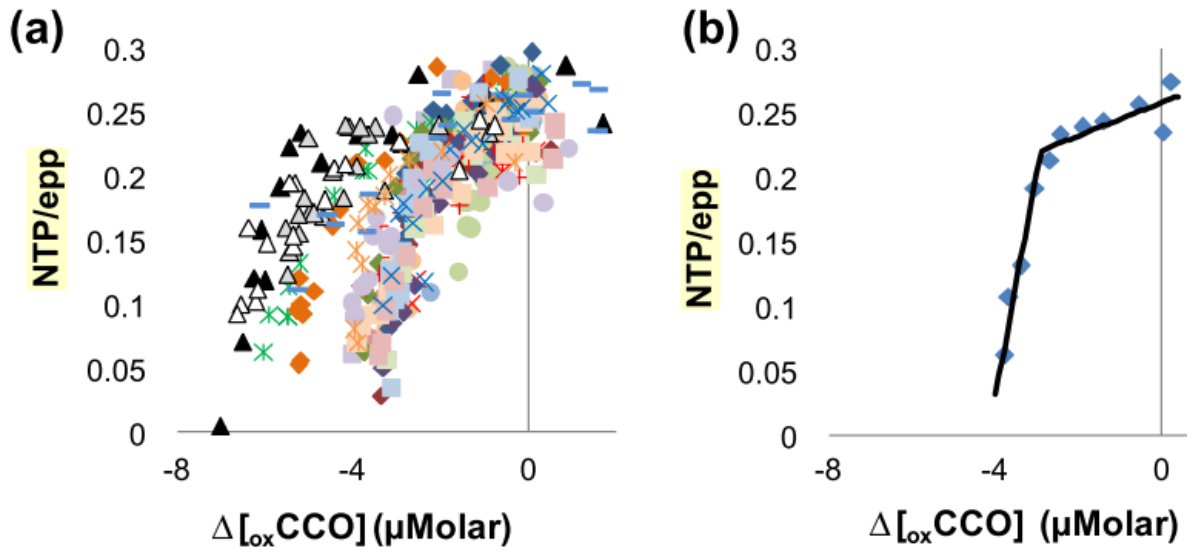

Figure 9.2: (a) NTP/epp plotted against change in oxCCO during HI (different symbols for individual piglets). The relationship between NTP/epp and oxCCO is similar for all piglets but for low NTP/epp the oxCCO distribution clearly separates. (b) An example of a double-linear fit of an individual piglet. A large proportion of NTP comes from ATP so it can be assumed the the changes in NTP/epp here predominantly reflect ATP. Taken from [12].

relationship between oxCCO and HbD could depend on the neurological health of the brain; a biphasic change in oxCCO during hypoxia has been hypothesised and observed in animal models.

9.1.1 Aim

The hypothesis is that the cerebral metabolism will have a different (i.e. non-linear) response to that of the haemoglobin signals (i.e. linear) during hypoxia. Specifically, this study investigates whether this is true in the injured neonatal brain. The aim of this section is to answer the questions: 'What is the oxCCO response to hypoxia?' and 'Is the oxCCO response dependent on the level of brain injury?'

9.2 Method

9.2.1 Data Analysis

Data were collected per Chapter 6. For this study, only data sections which had full systemic data recorded (SpO_2, MABP, $PaCO_2$, PaO_2, RR and HR) were considered to ensure that there was full information of the systemic physiology during the event. All data processing was done in MATLAB 2013b (Mathworks, USA) with a custom built, semi-automated script. The data recorded for each infant was scrutinised and any drop in arterial oxygen saturation from 'normal' levels (defined as 95% or above) to below 85% was selected as an hypoxic 'event'. This criteria is more well defined than that in the previous chapter (Chapter 8) to improve consistency across the events (ensuring they begin at normoxia) and to ensure that the events are causing cerebral hypoxia (dropping to below 85% which

is the saturation at which clinical intervention is required). If there were no desaturations fitting this description across the data recorded in an infant, then that infant was removed from this analysis.

For each hypoxic event the start time and nadir time were selected manually from the SpO_2 data (see example in Figure 9.3); the start time was defined as the time at which the SpO_2 decreased from baseline and the nadir time was first time during the desaturation that the SpO_2 reached a minimum stationary point. The NIRS variables were normalised to $0\mu M$ at the start time. As each event has a different duration from the start of desaturation to the minimum point, the time between start time and nadir time was split into ten epochs. The mean value of each of the systemic and cerebral NIRS variables was found across each epoch until the nadir time. The mean baseline was calculated across the 10 seconds preceding the desaturation start time.

9.2.2 Statistical Analysis

The desaturation events were grouped into babies with mild and severe injury based on the Lac/NAA ratio from the MRS scan; Lac/NAA of 0.3 or greater was considered a severe injury. The mean and standard error across the groups were calculated for each variable at each epoch. The epochs are split as such: epoch 1 = 10 seconds baseline, epoch 2 = start of desaturation, epochs 3-12 = desaturation period, epoch 13 = nadir of desaturation. NIRS data are normalised to 0μM at the start of the desaturation (epoch 2). The significance of the difference between the group NIRS variables and baseline was assessed using a paired Student's t-test for each epoch during the desaturation (epochs 3-13) for both mild and severe groups. A t-test (unpaired) was also performed to test the difference between the mild and severe groups at each epoch for all variables. A p-value of 0.05 or less was considered statistically significant. The data were also grouped per day of life to assess the changing relationship with the progression of injury and treatment.

The relationship between the SpO_2 and each of the NIRS variables between baseline and nadir was plotted for each group. The oxCCO signals were also plotted against the cerebral haemoglobin signals to assess the relationship between the oxygenation and metabolism in the brain.

9.3 Results

Table 9.1 shows the infants included in this analysis (and the reason why an infant was not included, if not), the number of events recorded per infant and the day of life on which those events were recorded. An eligible desaturation event was identified in 17 out of 29 subjects with full data recorded, of these 7 infants had severe injury and 10 were female. The mean birth weight was 3.3±0.7kg and the mean GA was 39±1 weeks.

A total of 48 events were identified (see examples of such events in section 6.5): 15 from the severe injury group and 33 from the mild injury group. The average desaturation period occurred over 152±94 seconds, with a range from 22 to 455 seconds. The events were recorded from days 1, 2, 3, 4 and 5 of life.

An example, from subject 15, is shown in Figure 9.3 (a) where a large fall in arterial oxygen induces

Table 9.1: Table of subjects analysed with this method, as described in section 9.2.

CYRIL	**Injury**	**Analysis Performed?**	**No. of Events**	**Day (No. of Events)**
2	HIE	Y	1	2(1)
3	HIE	Y	9	1(1),3(5),4(3)
4	HIE	no desats	-	-
5	Stroke	not HIE	-	-
6	HIE	Y	3	3(3)
7	HIE	Y	3	3(2),4(1)
8	HIE	Y	2	3(1),4(1)
9	HIE	Y	6	2(5),4(1)
10	HIE	no MABP	-	-
11	HIE	Y	1	1(1)
12	HIE	Y	1	5(1)
13	HIE	no desats >10%	-	-
14	HIE	Y	2	1(1),3(1)
15	HIE	Y	3	1(1),3(1),4(1)
16	HIE	no desats >10%	-	-
17	HIE	Y	5	1(1),2(1),4(3)
18	HIE	no desats >10%	-	-
19	HIE	Y	1	1(1)
20	HIE	Y	3	2(1),3(1),4(1)
21	HIE	no desats >10%	3	2(2),3(1)
22	HIE (no data)	no data	-	-
23	HIE (no data)	no data	-	-
24	HIE (no data)	no data	-	-
25	HIE	Y	1	4(1)
26	HIE	no desats >10%	-	-
27	Preterm	not HIE	-	-
28	HIE+PPHN	no desats >10%	-	-
29	HIE+head trauma+seizures	no MRS	-	-
30	HIE	no MABP	-	-
31	HIE	no desats >10%	-	-
32	Stroke	not HIE	-	-
33	HIE	Y	1	4(1)
34	Seizures	not HIE	-	-
35	HIE	Y	1	1(1)
36	Seizures	not HIE	-	-
37	HIE	Y	2	1(2)
38	IVH	not HIE	-	-
- TOTAL	**HIE = 28**	**17**	**48**	-

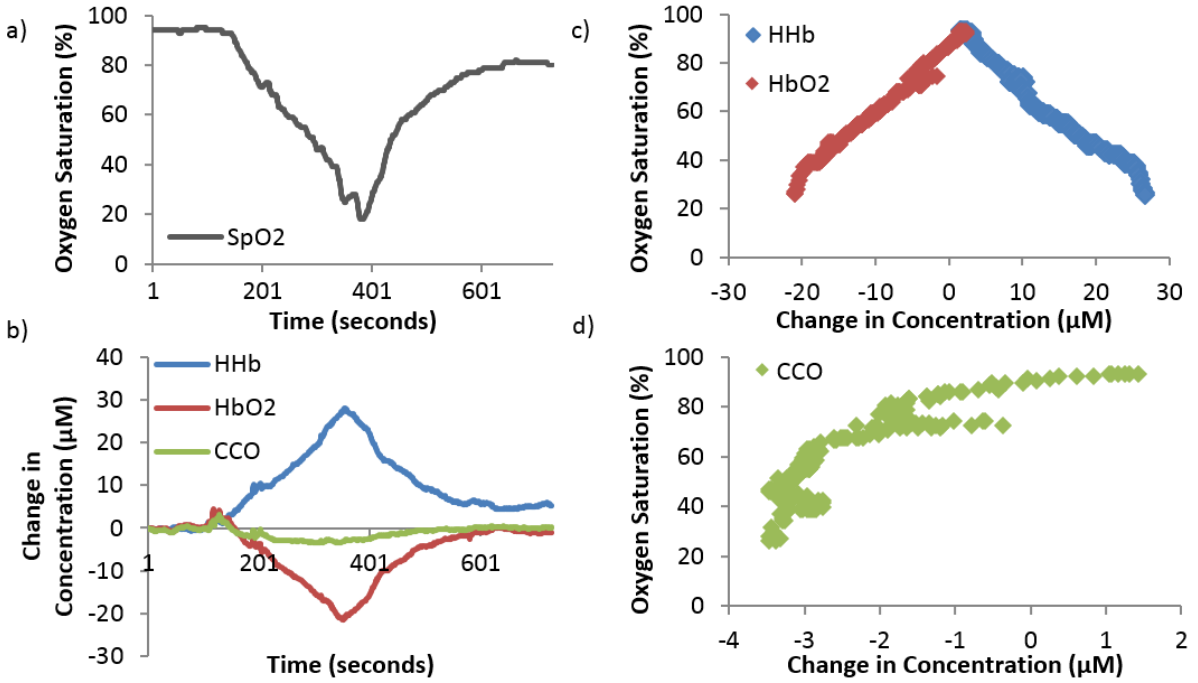

Figure 9.3: Example of an SpO_2 desaturation from subject 15 (a) and corresponding changes in NIRS chromophores (b). The change in HbO_2 and HHb with SpO_2 is linear (c) whereas the change in oxCCO shows a biphasic relationship (d).

a decrease in HbO_2 and corresponding increase in HHb (Figure 9.3 (b)). When plotted against SpO_2 in Figure 9.3 (c) it is clear that this is a linear response between SpO_2 and the haemoglobin signals. However, the oxCCO drops rapidly but then reaches a threshold; here CCO has a biphasic relationship with SpO_2 (Figure 9.3 (d)).

The group mean arterial saturation changes of the mild and severe groups split into epochs are shown in Figure 9.4, the mean changes in each group appear similar and there were no statistical differences between them. The mean nadir of SpO_2 was 62.8±23.4%.

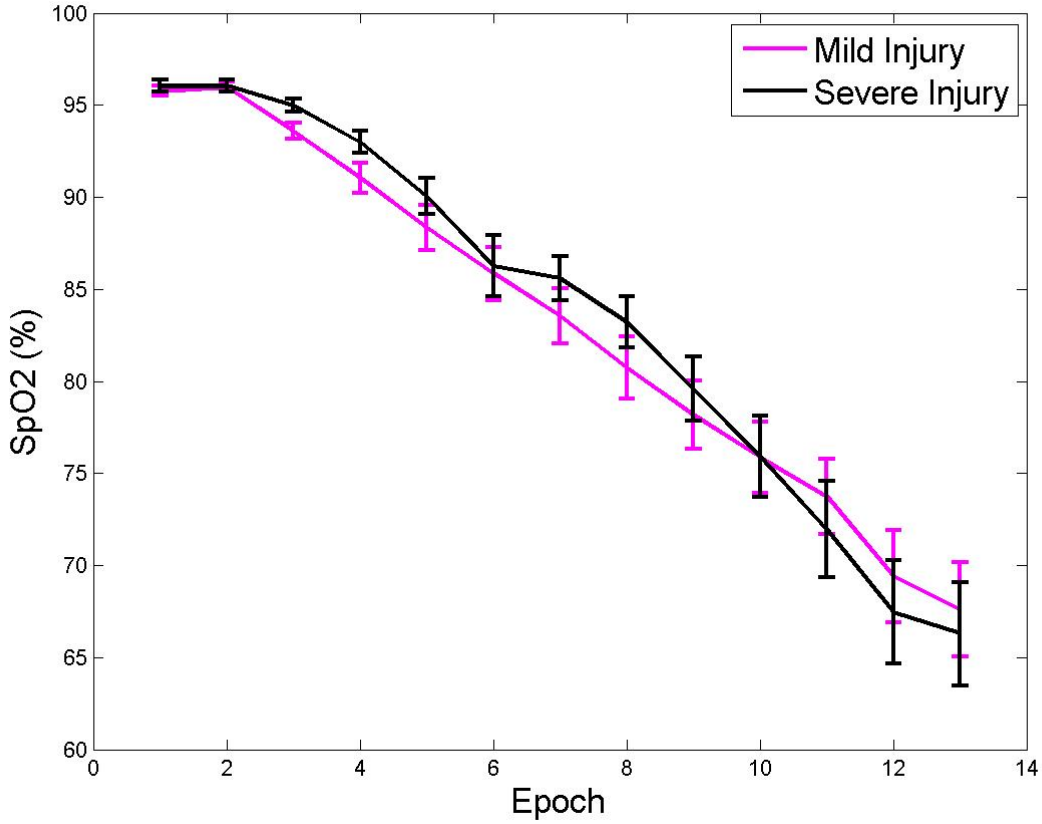

Figure 9.4: Mean desaturation for mild and severe groups in epochs. Error bars show the standard error of the mean. There were no statistical differences between the group means at each epoch.

9.3.1 Systemic Variation

The changes in each of the measured systemic variables during the SpO_2 desaturation are shown in Figures 9.5, 9.6, 9.7, 9.8 and 9.9. In order to ensure that the events are as close to pure hypoxia as possible, only events in which the other measurements remained stable were chosen, hence, there were almost no variation in these measurements; the only statistically significant change from the start of desaturation occurred in the $PaCO_2$ signal in the mild injury group.

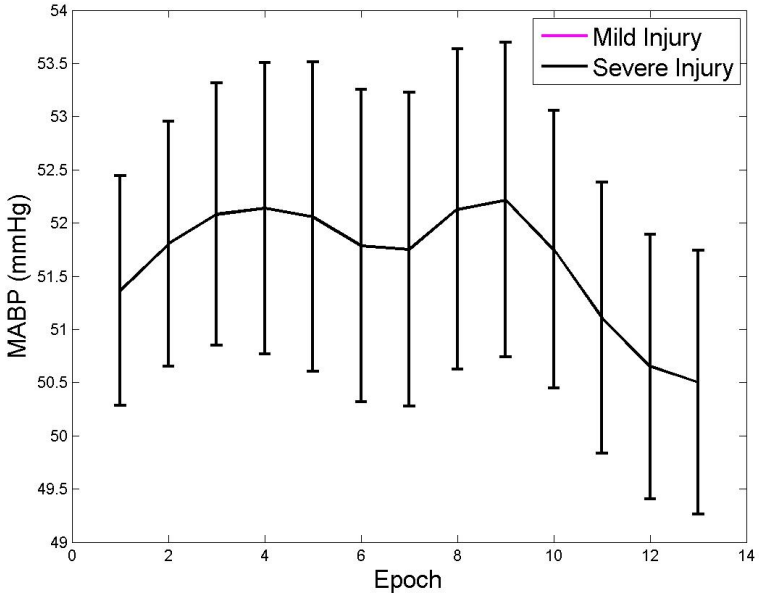

Figure 9.5: Mean change in MABP during desaturation for mild and severe groups in epochs. Error bars show the standard error of the mean. There were no statistically significant changes from start of desaturation. There were no statistical differences between the group means at each epoch.

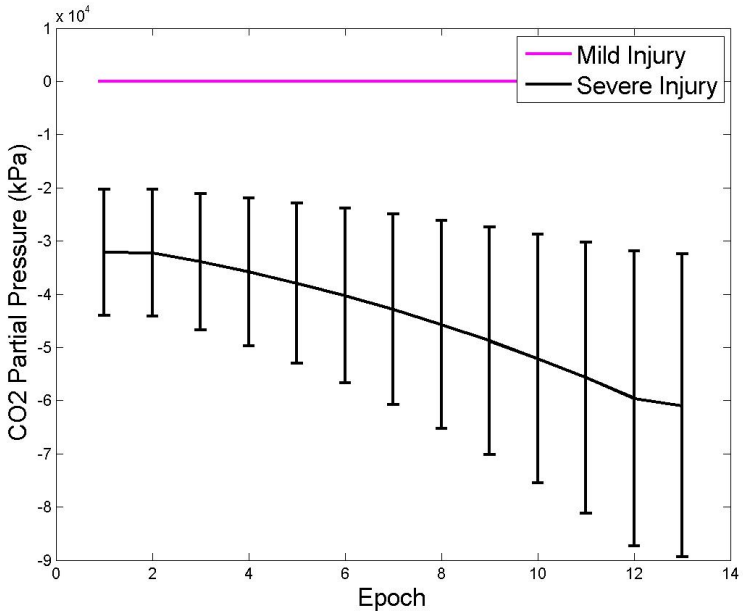

Figure 9.6: Mean change in $PaCO_2$ during desaturation for mild and severe groups split into tenths either side of nadir. Error bars show the standard error of the mean. The statistically significant changes from the start of desaturation are displayed as asterisks. There were no statistical differences between the group means at each epoch.

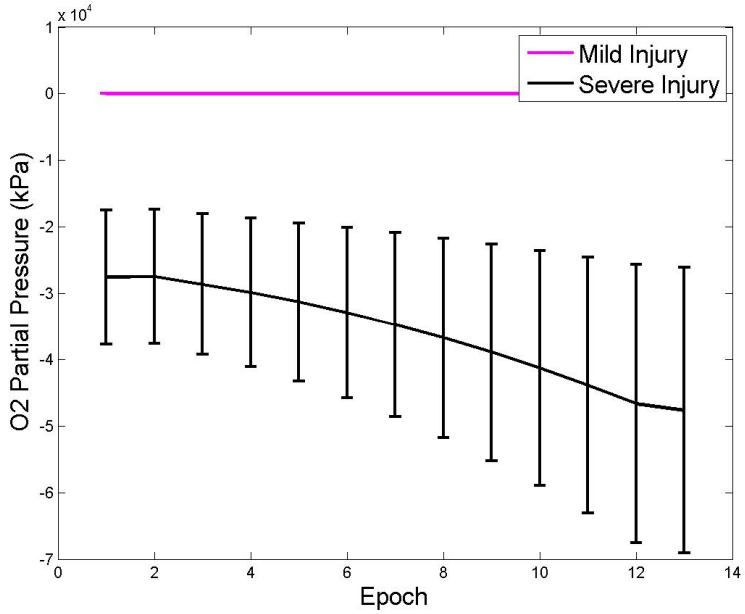

Figure 9.7: Mean change in PaO_2 during desaturation for mild and severe groups in epochs. Error bars show the standard error of the mean. There were no significant changes from start of desaturation. There were no statistical differences between the group means at each epoch.

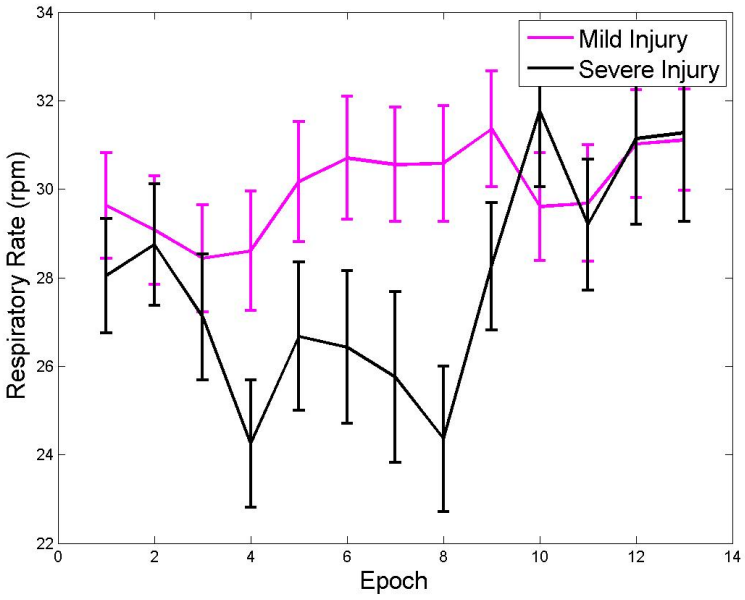

Figure 9.8: Mean change in RR during desaturation for mild and severe groups split in epochs. Error bars show the standard error of the mean. There were no significant changes from start of desaturation nor statistical difference between the group means at each epoch.

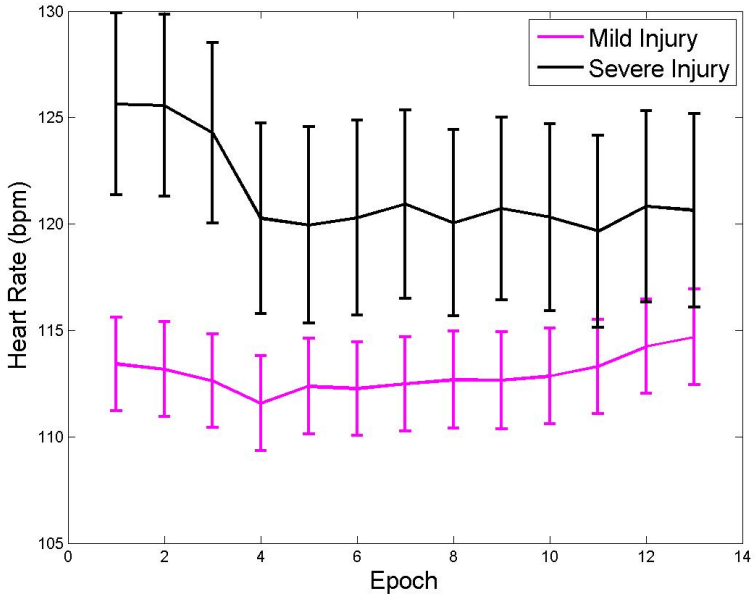

Figure 9.9: Mean change in HR during desaturation for mild and severe groups split in epochs. Error bars show the standard error of the mean. No significant change from start of desaturation nor statistical difference between the group means at each epoch.

9.3.2 Group NIRS Changes during Desaturation

The mean changes in the NIRS variables during the desaturation are shown in Figures 9.10, 9.11, 9.12 and 9.13. The increase in HHb and decrease in HbD were significantly different from the baseline immediately (by the first epoch from the start) in both groups and both hemispheres. The HbO_2 decrease was significant immediately in the mild injury group (both hemispheres) but was slightly delayed in the severe injury group. The HbT change was immediate in both groups on the right side of the brain, but very delayed in the left. The oxCCO decrease from baseline has a different pattern to the haemoglobins; in the mild injury group there were less epoch with statistically significant reduction from the baseline.

There was no difference between the injury groups per epoch in the haemoglobin signals, but there was difference in the oxCCO signals between the two injury severity groups from the ninth epoch until the nadir.

The mean changes in the NIRS variables at the nadir of SpO_2 are: -4.2±4.8μM for HbO_2, 5.8±5.1μM for HHb, -10.1±9.5μM for HbD, 1.7±2.4μM for HbT and -0.4±1.2μM for oxCCO for the left side, and -3.4±4.4μM for HbO_2, 5.1±4.9μM for HHb, -8.6±8.8μM for HbD, 1.7±3.1μM for HbT and -0.5±1.5μM for oxCCO for the right side.

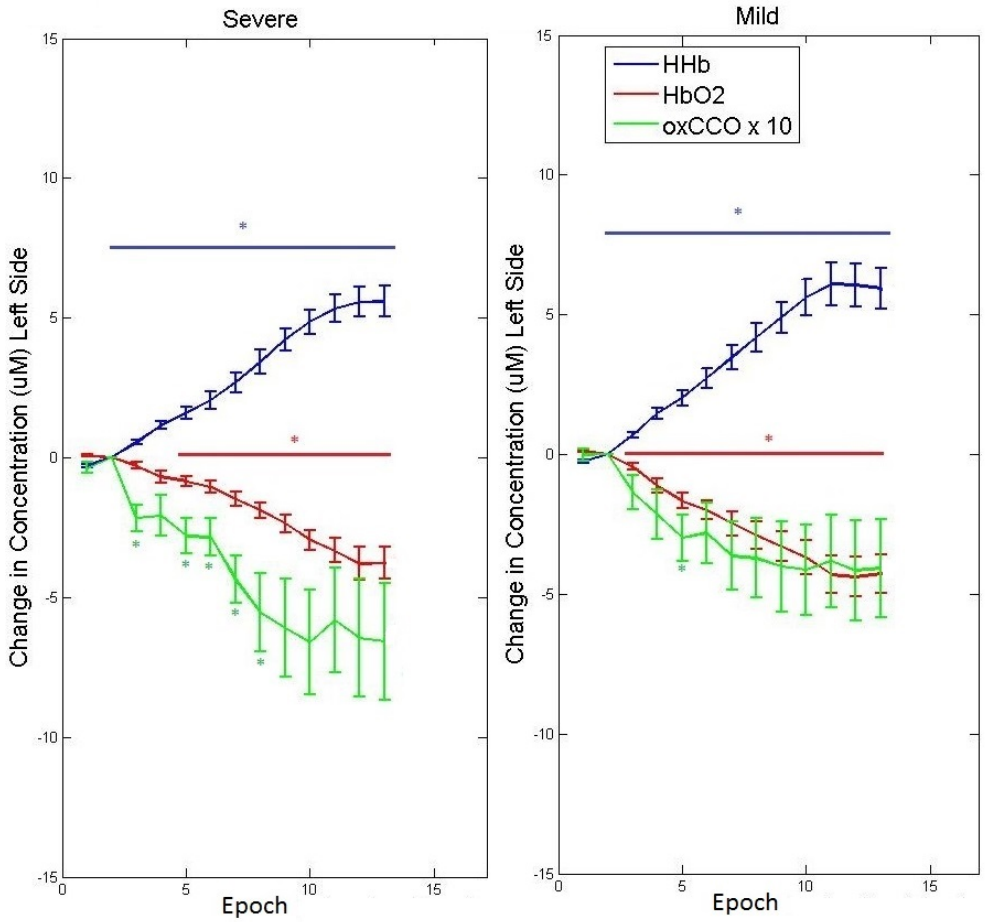

Figure 9.10: Mean cerebral response of left side to desaturation for mild and severe groups in epochs. Note that oxCCO signal is scaled by a factor of 10 for visibility. Error bars show the standard error of the mean. Asterisks represent statistical significance from the start of desaturation period (epoch 2) to the nadir (covering epochs 3-13). There were no statistical differences between the group means for any of the signals.

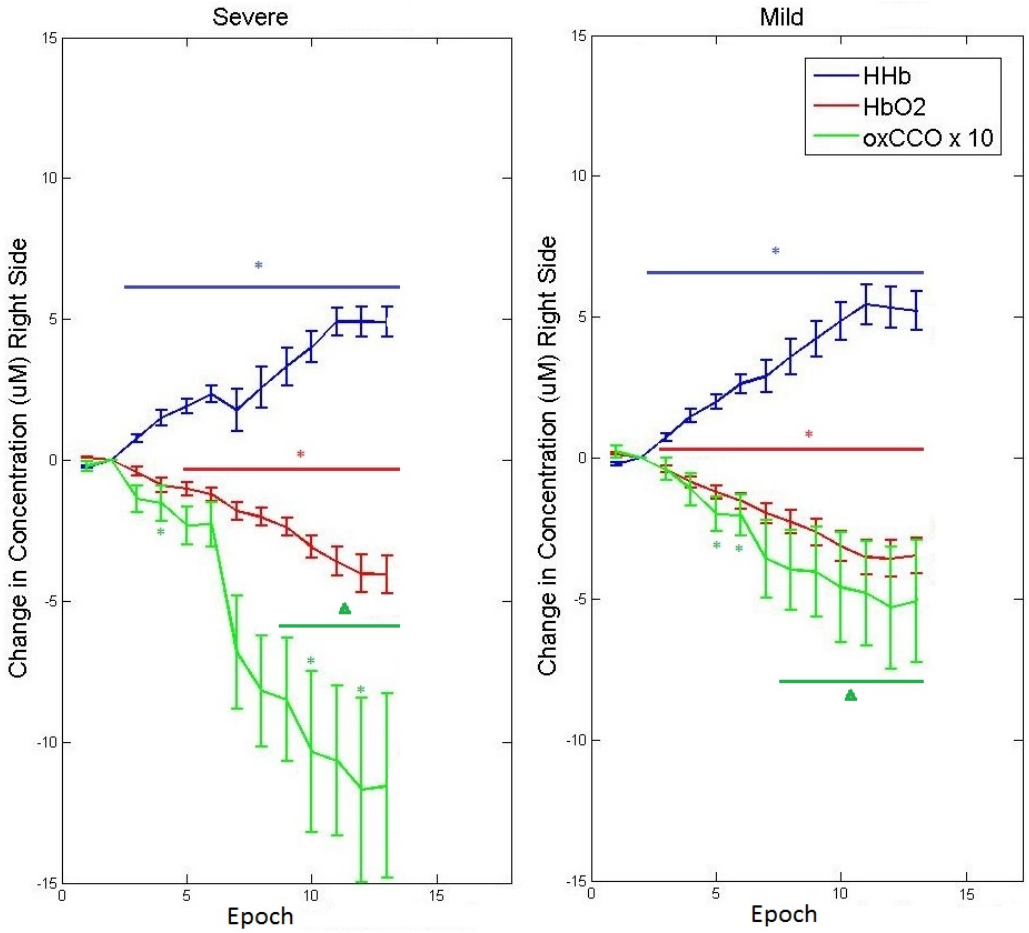

Figure 9.11: Mean cerebral response of right hand side desaturation for mild and severe groups in epochs. Note that oxCCO signal is scaled by a factor of 10 for visibility. Error bars show the standard error of the mean. Asterisks represent statistical significance from the start of desaturation period (epoch 2) to the nadir (covering epochs 3-13). Triangles represent statistical differences between the group means at each epoch; there was no statistical difference between the group means for the haemoglobin signals.

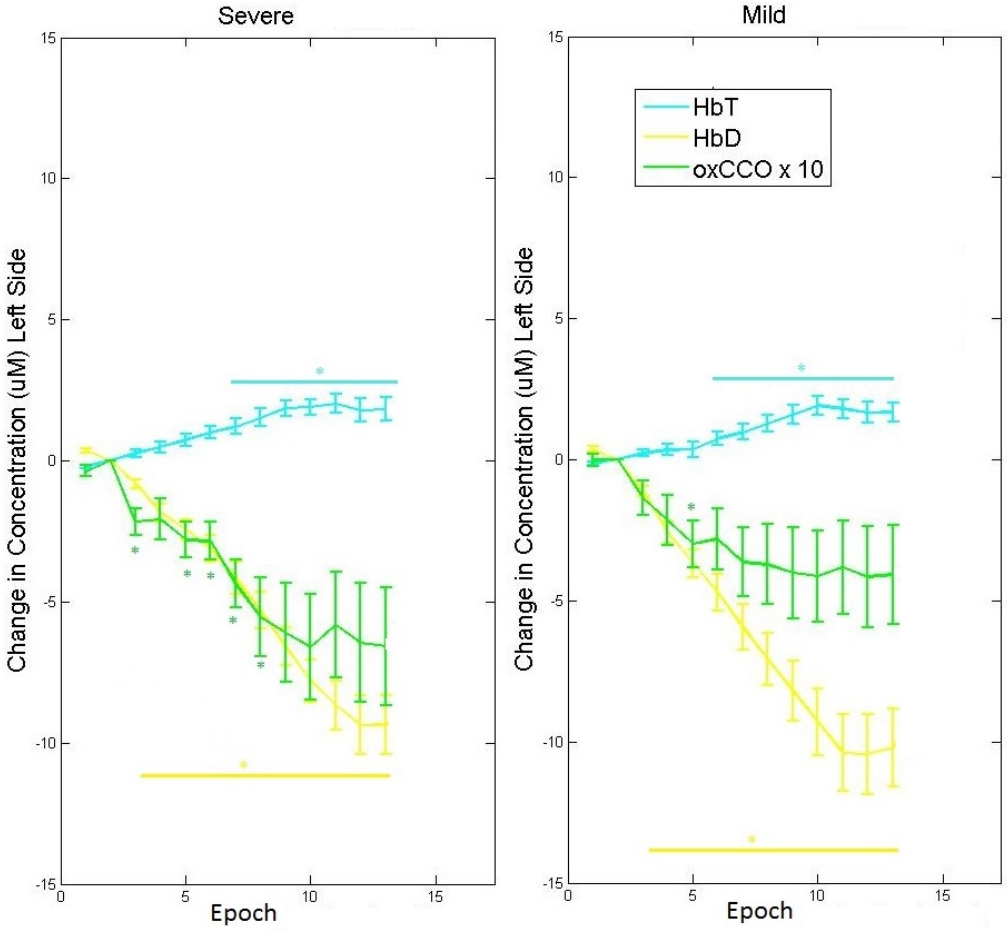

Figure 9.12: Mean cerebral response of left side to desaturation for mild and severe groups in epochs. Note that oxCCO signal is scaled by a factor of 10 for visibility. Error bars show the standard error of the mean. Asterisks represent statistical significance from the start of desaturation period (epoch 2) to the nadir (covering epochs 3-13). There were no statistical differences between the group means for any of the signals.

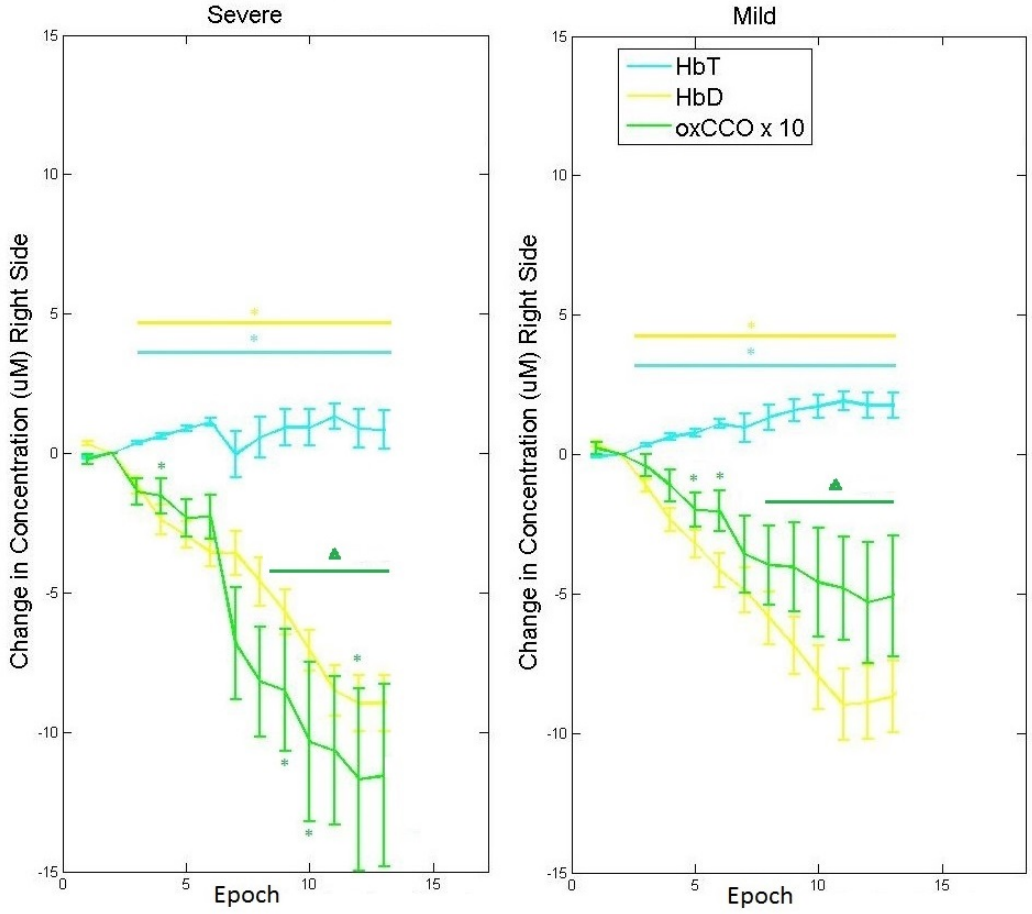

Figure 9.13: Mean cerebral response of right hand side desaturation for mild and severe groups in epochs. Note that oxCCO signal is scaled by a factor of 10 for visibility. Error bars show the standard error of the mean. Asterisks represent statistical significance from the start of desaturation period (epoch 2) to the nadir (covering epochs 3-13). Triangles represent statistical differences between the group means at each epoch; there was no statistical difference between the group means for the haemoglobin signals.

9.3.3 Relation of Cerebral Oxygenation and SpO_2

The cerebral broadband NIRS haemodynamic measurements are plotted against SpO_2 in Figures 9.14 to 9.21. The relationships between SpO_2 and each of the haemoglobin signals are linear and the magnitudes of change are similar on each side of the brain. There is no significant difference between the mild and severe groups.

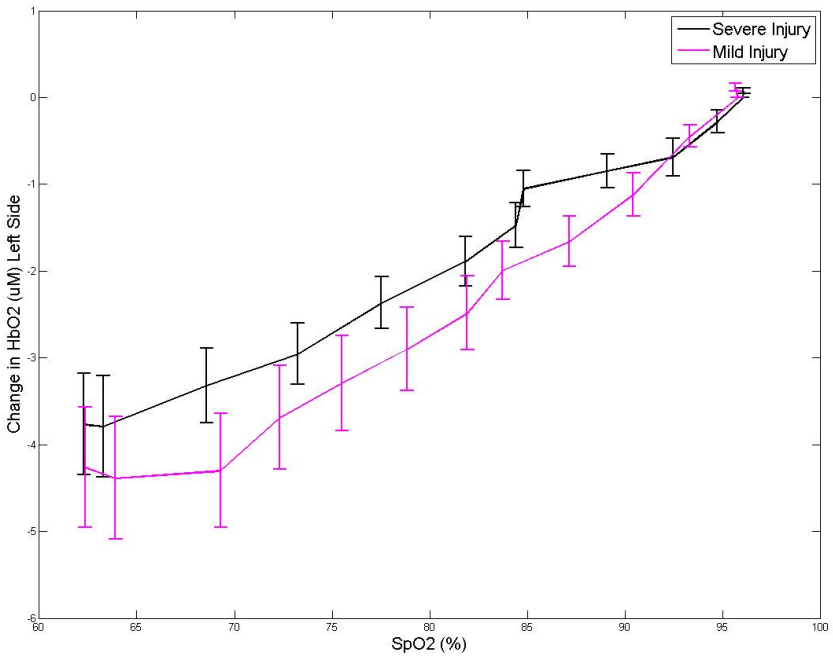

Figure 9.14: Changes in left mean HbO_2 against SpO_2 during desaturation for mild and severe groups in epochs. Error bars show the standard error of the mean.

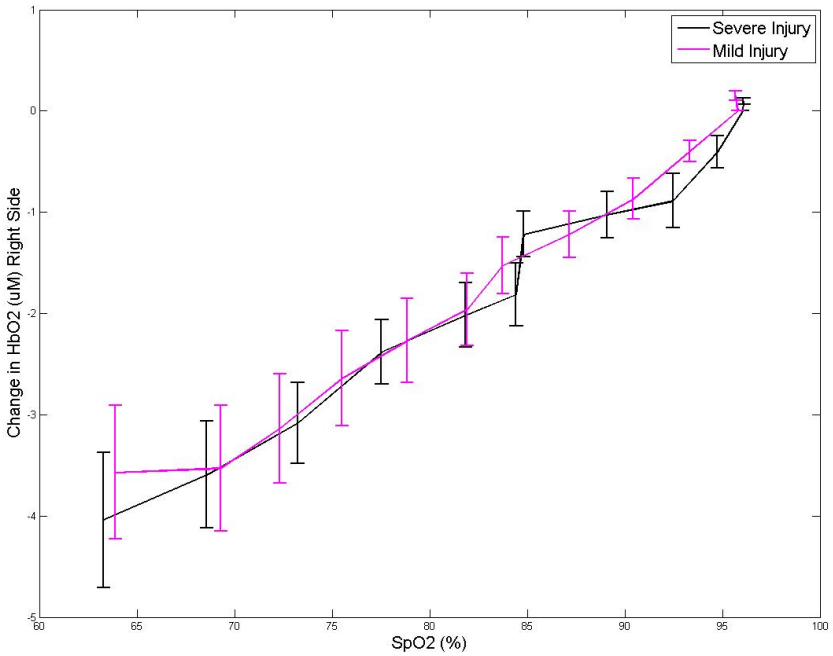

Figure 9.15: Changes in right mean HbO_2 against SpO_2 during desaturation for mild and severe groups in epochs. Error bars show the standard error of the mean.

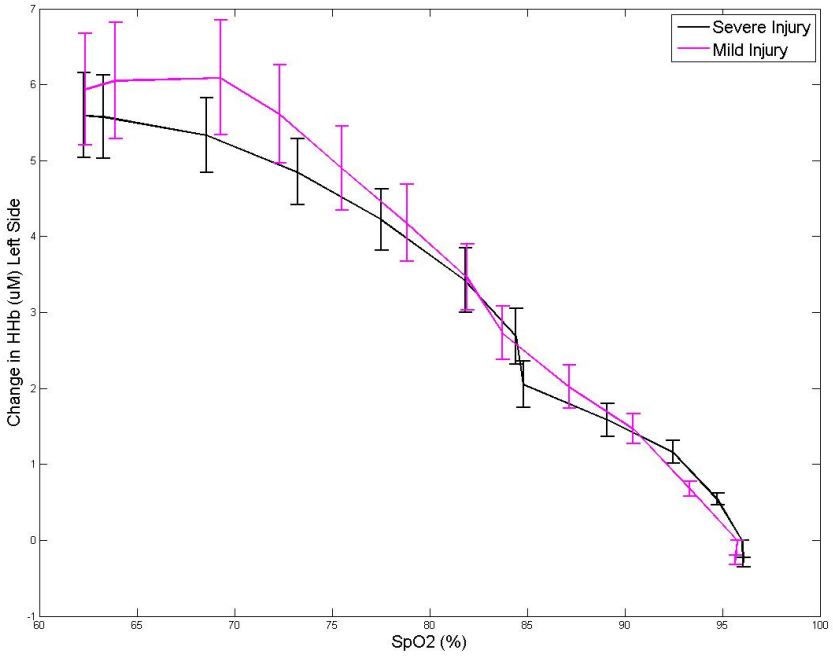

Figure 9.16: Changes in left mean HHb against SpO_2 during desaturation for mild and severe groups in epochs. Error bars show the standard error of the mean.

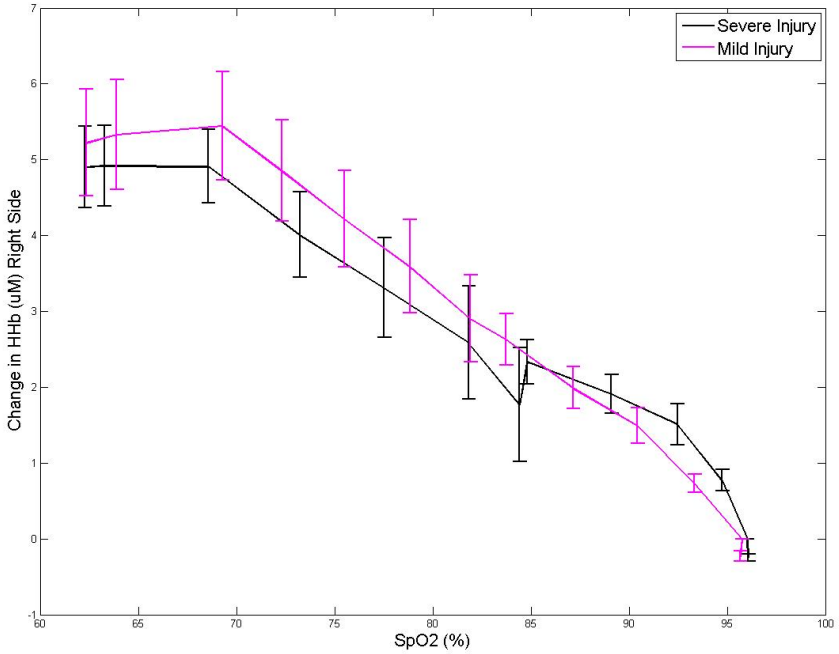

Figure 9.17: Changes in right mean HHb against SpO_2 during desaturation for mild and severe groups in epochs. Error bars show the standard error of the mean.

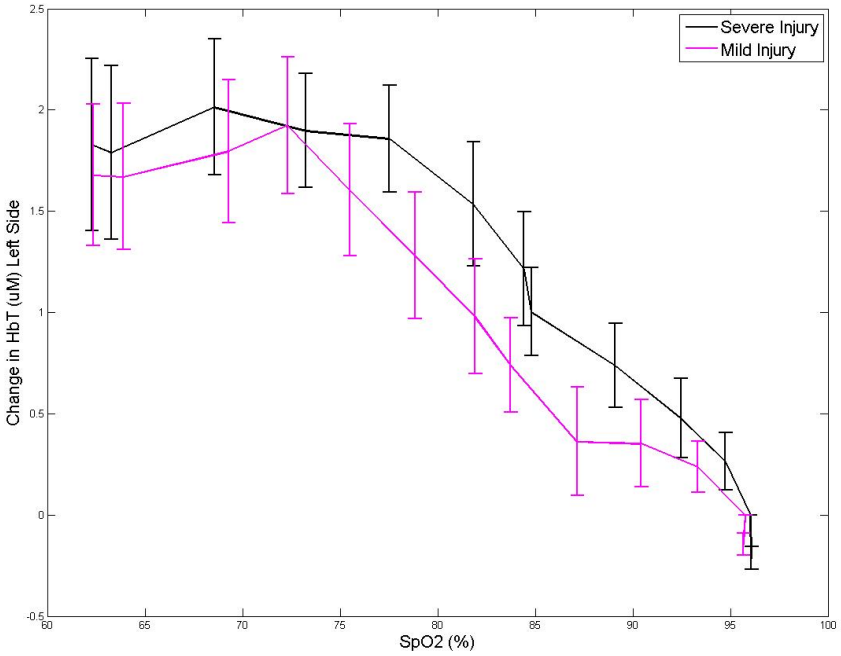

Figure 9.18: Changes in left mean HbT against SpO_2 during desaturation for mild and severe groups in epochs. Error bars show the standard error of the mean.

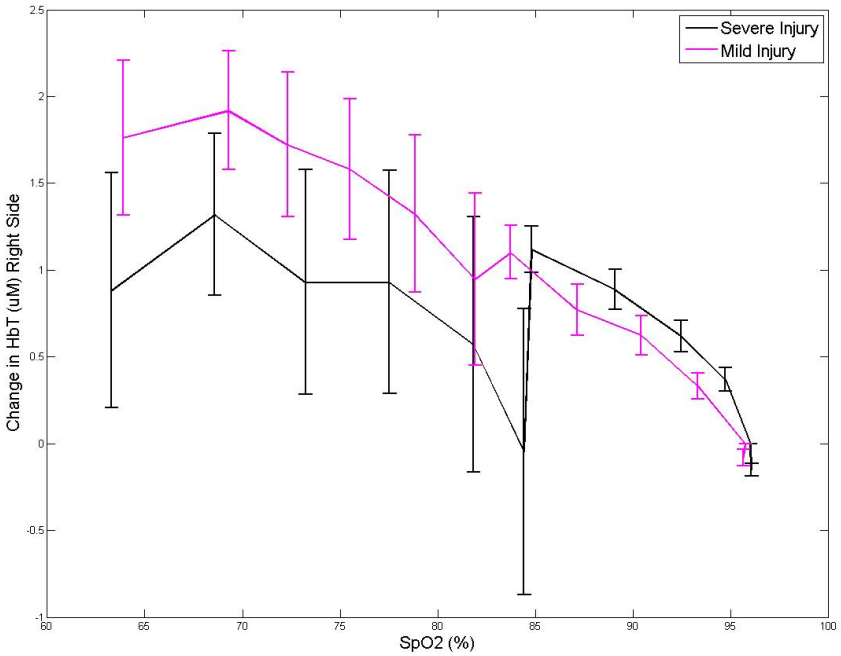

Figure 9.19: Changes in right mean HbT against SpO_2 during desaturation for mild and severe groups in epochs. Error bars show the standard error of the mean.

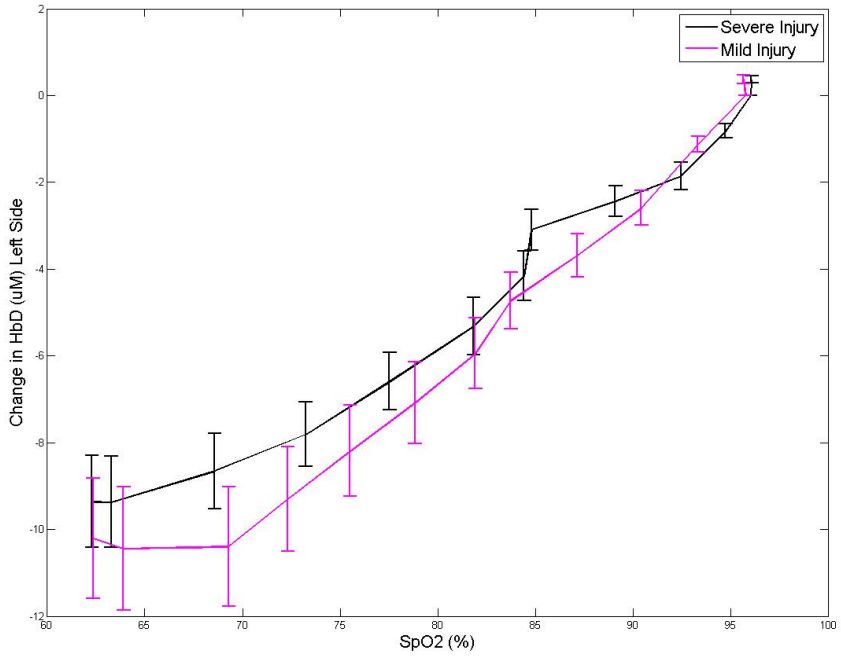

Figure 9.20: Changes in left mean HbD against SpO_2 during desaturation for mild and severe groups in epochs. Error bars show the standard error of the mean.

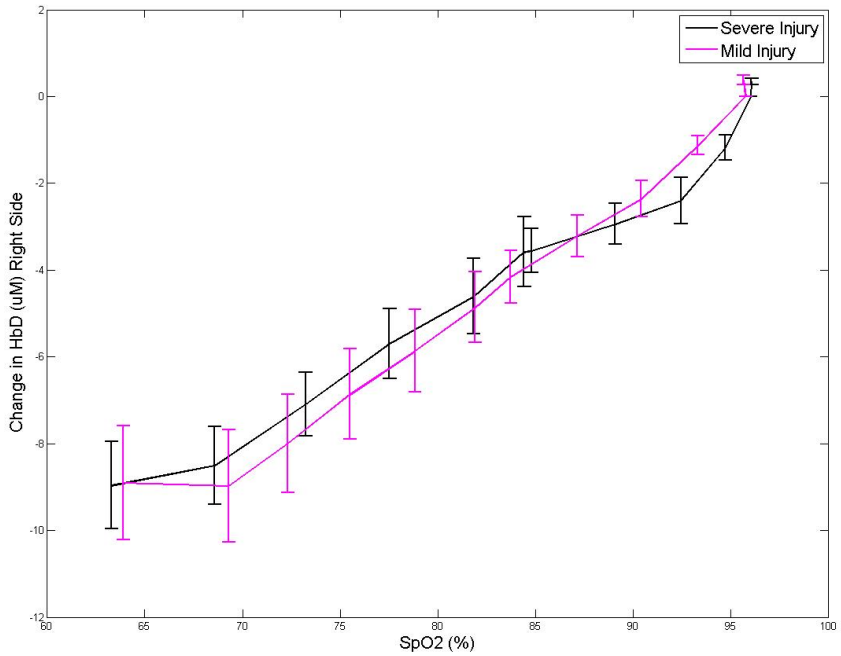

Figure 9.21: Changes in right mean HbD against SpO_2 during desaturation for mild and severe groups in epochs. Error bars show the standard error of the mean.

9.3.4 Relation of Cerebral Metabolism and SpO_2

The cerebral broadband NIRS metabolic measurements are plotted against SpO_2 in Figures 9.22 and 9.23. Unlike the relationships between SpO_2 and the haemoglobin signals, the oxCCO relationships are not linear and there is laterality between the hemispheres; there is a bigger decrease in the signal from the right hemisphere. The oxCCO signals dropped linearly with oxygenation initially and then reaches a plateau. The plateaus in oxCCO for the left side are $\sim$-0.3μM and $\sim$-0.6μM for the mild and severe groups, respectively; and for the right side are $\sim$-0.2μM and $\sim$-1μM for the mild and severe groups, respectively.

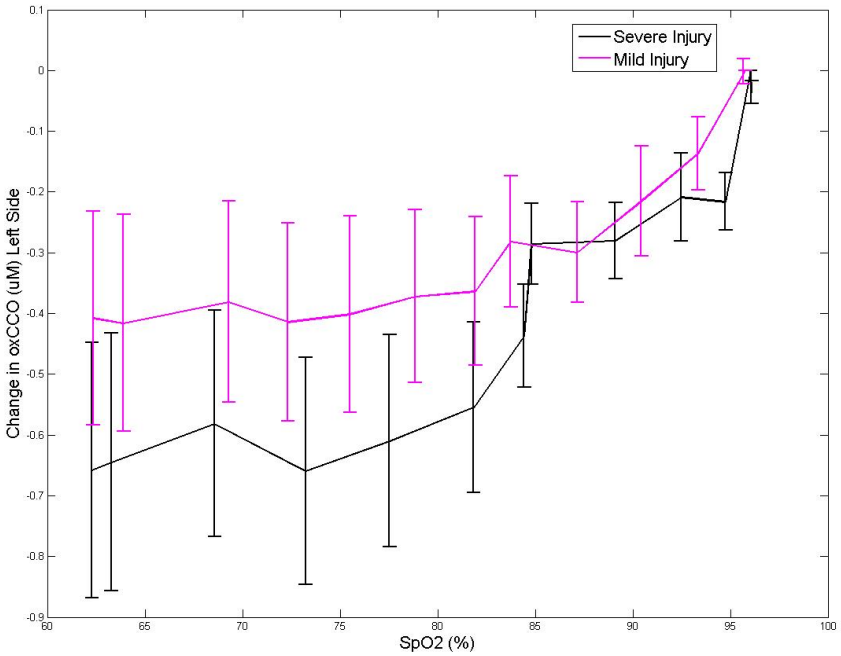

Figure 9.22: Changes in left mean oxCCO against SpO_2 during desaturation for mild and severe groups in epochs. Error bars show the standard error of the mean.

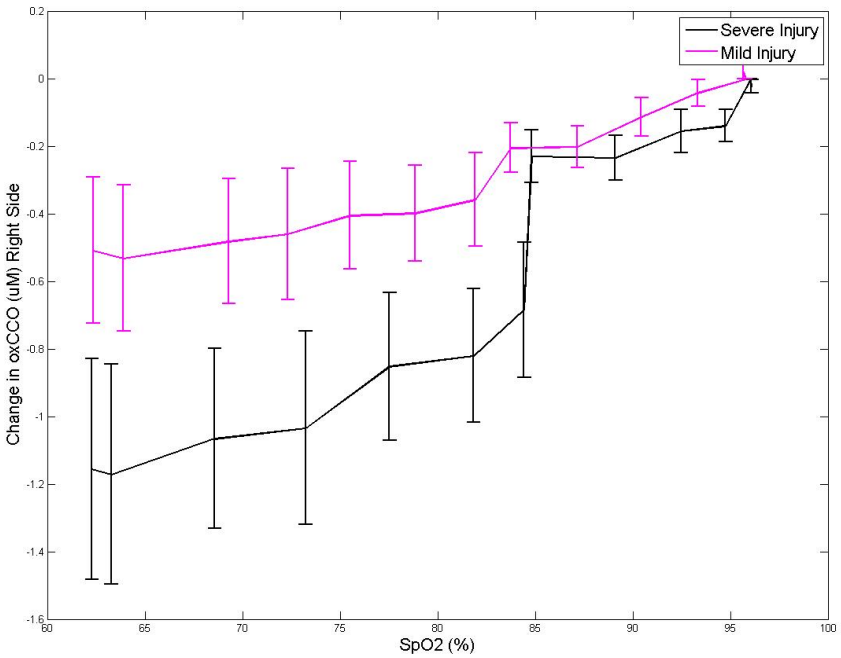

Figure 9.23: Changes in right mean oxCCO against SpO_2 during desaturation for mild and severe groups in epochs. Error bars show the standard error of the mean.

9.3.5 Relation of Cerebral Oxygenation and Metabolism

The relationships between the cerebral haemoglobins and oxCCO are presented in Figures 9.24 to 9.27 for the left side (the right side displays similar trends so the graphs are not presented here). The severe and mild groups both show approximately linear relationships between the oxCCO and the haemoglobins signals, but the gradients are steeper in the severe group for oxCCO against HbO_2, HHb, and HbD.

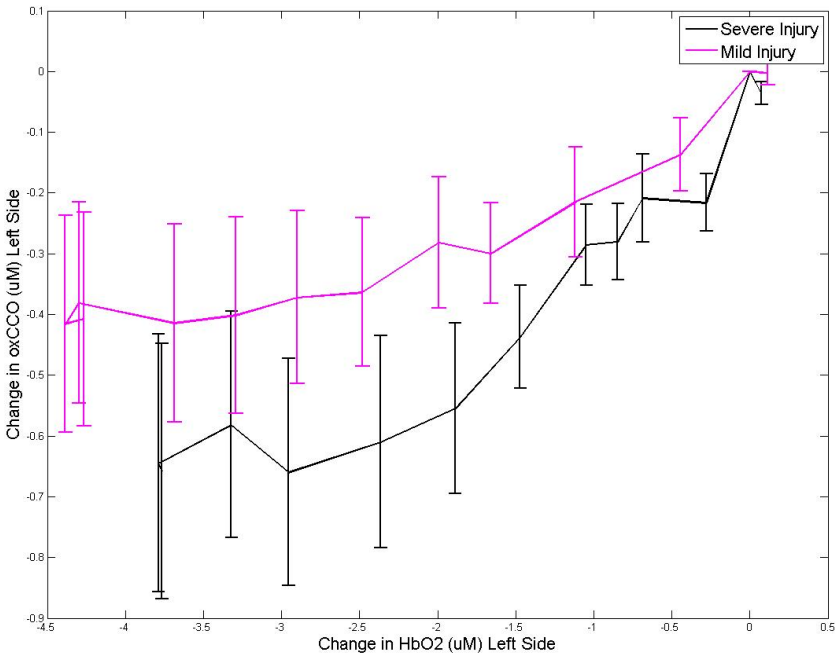

Figure 9.24: Mean left oxCCO against HbO_2 during desaturation for mild and severe groups in epochs. Error bars show the standard error of the mean.

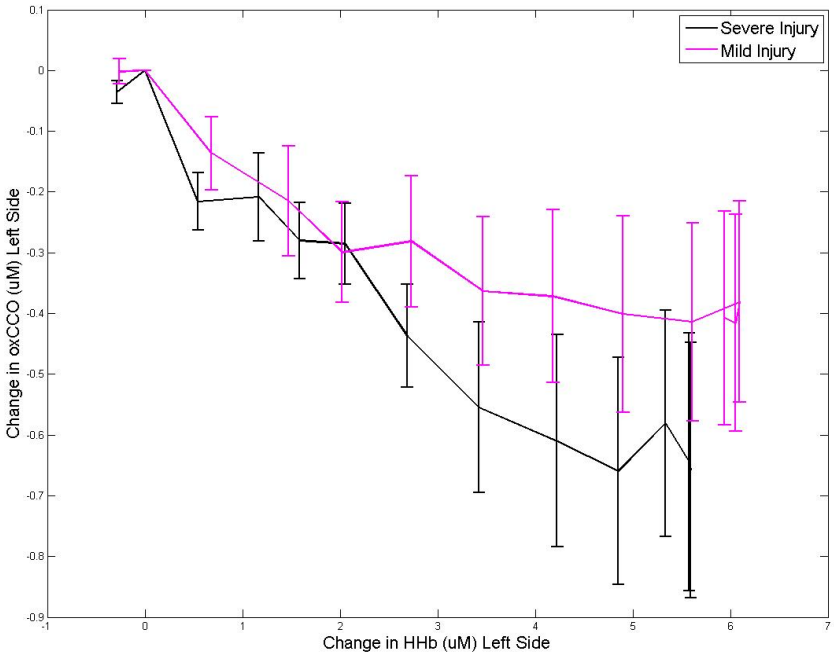

Figure 9.25: Mean left oxCCO against HHb during desaturation for mild and severe groups in epochs. Error bars show the standard error of the mean.

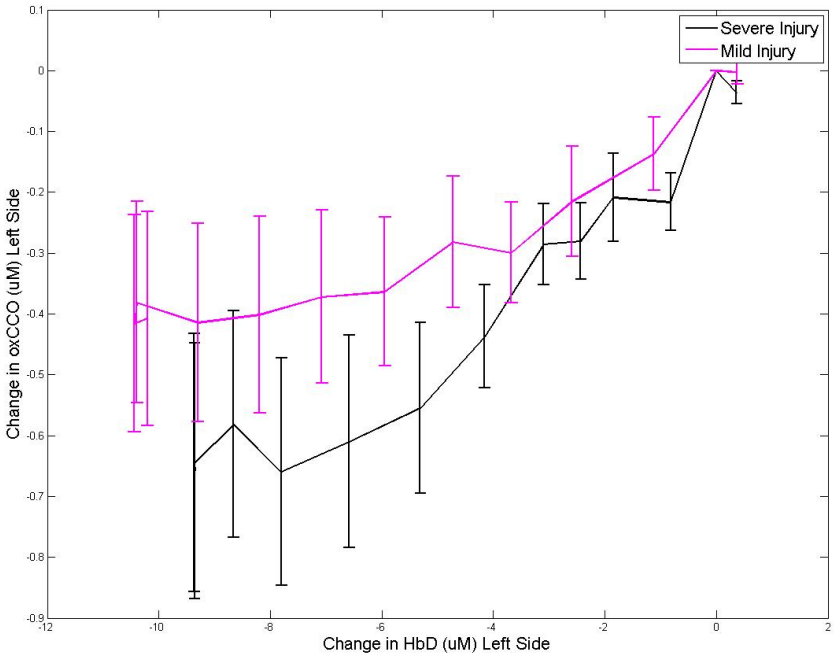

Figure 9.26: Mean left oxCCO against HbD during desaturation for mild and severe groups in epochs. Error bars show the standard error of the mean.

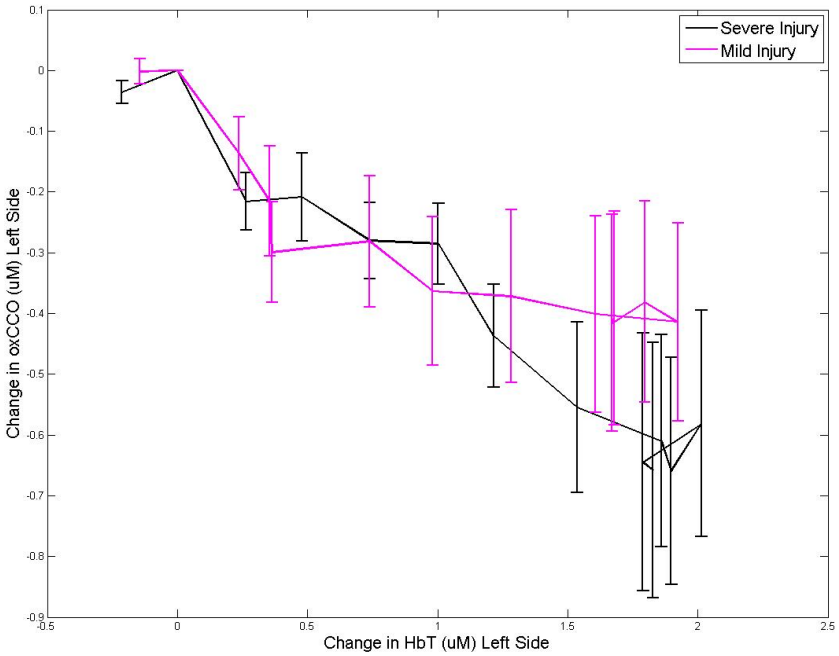

Figure 9.27: Mean left oxCCO against HbT during desaturation for mild and severe groups in epochs. Error bars show the standard error of the mean.

9.4 Discussion

The response of the haemoglobin signals to hypoxia in general was similar across both hemispheres and in both injury severities. This suggests that brain injury severity does not impact on the performance of the cerebral vasculature. Increases in HHb and HbT are expected during hypoxia, as are the decreases seen in HbO_2 and HbD [60]. The slopes of the haemodynamic changes were similar between the two injury groups so the oxygen delivery changes during the desaturation were not affected by injury. The linear changes with arterial saturation decrease shows that the arterial and cerebral oxygenation are directly linked, which is expected.

It was seen that there were more epochs with significant oxCCO reduction from baseline in the more severe injury babies and there was a statistically significant difference between the group oxCCO levels in the epochs at the lower end of desaturation. These results suggest that cellular metabolism in the more severe brain injury is more vulnerable to hypoxic events.

Measurements of oxCCO from the right hemisphere showed a larger drop in oxCCO than the left. No asymmetry was observed in the haemoglobin signals. Interestingly, a study of hemispheric laterality in term and preterm infants, with NIRS and DCS monitoring of rSO_2 and $CMRO_2$, found that there was no difference in cerebral oxygenation but the $CMRO_2$ was much higher on the right side [173]. This might suggest that the larger drop in the oxCCO signal represents a drop from a higher metabolic state.

Non-linear changes in the oxCCO signal were observed with desaturation, and there were differences in the responses between the injury severity groups, as suggested by the hypothesis. This was not seen

in the changes in haemoglobin concentrations, so this suggests that the injury severity causes differences at the metabolic level but not in the vascular response. On average, the oxCCO concentration decreased with SpO_2 initially before reaching a stable value. As there was a linear relationship between SpO_2 and the haemoglobin variables, the oxCCO relationship with haemoglobin is also non-linear.

However, this result does not match with those in the literature. An animal model of hypoxia saw the oxCCO stable at the start of desaturation and then drop at a threshold [65], which is opposite behaviour to these results. The difference may be due to differing physiology in the piglet, the influence of sedatives or general anaesthesia used in the animal model, and/or the severity of the hypoxia which was much more extreme in the animal model. Furthermore, the animal model was performed on an initially normal, healthy brain which was also more mature than these patients. A human adult study of hypoxemia to 80% SpO_2 did not see a plateau in the oxCCO signal [60]. The difference between these results could be from a different concentration of CCO in the adult brain [194], the lack of injury in the adults, altered physiology due sedation in the babies, or, most likely, that the adult studies did not reduce to a level of hypoxia needed to reach the threshold.

One theory is that the more injured brain may be at a lower energetic state so the CCO has less capacity to buffer changes in oxygen delivery. Therefore, the drop in oxCCO is larger. After more severe injury the infant undergoes secondary energy failure so the metabolic rate will be reduced. Dehaes et al. [156] and Wintermark et al. [148] both found, using different $CMRO_2$ measurement techniques, lower rates of metabolism in infants with HIE compared to healthy controls [156] and in severe HIE injury compared to infants with moderate injury as determined by aEEG. Lemmers et al. [150] observed a lower cerebral fractional tissue oxygen extraction in infants with adverse outcome. van Bel et al. [21] saw a decrease in oxCCO with time from birth in more severe injury; this suggests that the rate of metabolism is decreasing as the injury progresses. However, the patients in this study were not treated with hypothermia which will alter the metabolism, therefore it is not wise to simply compare their study result with the results in this chapter. These studies all give weight to the theory that there is a reduction in cerebral metabolism after severe HIE.

The SpO_2 level at which the oxCCO stabilises is significantly lower in the severe HIE group. Higher cerebral saturation has been observed in more severe HIE injury previously [150–152], so it is possible that in severe injury the reduction in arterial oxygenation does not lower cerebral oxygenation to a critical level as quickly as the mild cases. Alternatively, it may be that the metabolism takes longer to buffer the reduction in oxygen so, therefore, the threshold is noted at lower SpO_2 values. This argument is supported by the similar rates of oxCCO decrease on the left side in the first few percent SpO_2 decrease (see Figure 9.28), and the steeper gradient in the severe group oxCCO on the right side (see Figure 9.29).

9.5 Study Limitations and Further Work

There is more detail to be drawn from these data but a larger sample size is required before any conclusions can be made.

As in Chapter 8, the heterogeneity of the neonates' conditions, treatment and the cause of spontaneous

hypoxia are confounding factors in this analysis. However, the selection of the events was more controlled in this analysis to reduce the impact of the heterogeneity. Yet there are large differences in the NIRS responses, this is particularly evident in oxCCO with some increases in concentration across hypoxia, which are problematic for the grouping of data across infants.

The difference across days means that the group analysis using all days could be problematic. It might be wise to remove day 4 data from the grouped analysis, and only group data recorded during TH as hypothermia will have a large impact on cerebral metabolism. Furthermore, some infants included in this study were given xenon on day 1 so this may affect the cerebral oxygenation and metabolism. See below for preliminary analysis of the variations with postnatal age.

Also, the timing of the desaturation events is removed in this methodology; the events occurred over periods ranging from 22 to 455 seconds and the physiology will react differently depending on the speed of the desaturation. The wide variation in the timings is a confounding factor in this analysis.

Although every effort was taken to select events in which there was little or no change in other systemic variables, there were significant changes in the average $PaCO_2$ during the event period in the mild injury group. Changes in $PaCO_2$ will affect blood flow as it is a vasodilator. The data included could be re-assessed to remove events which have systemic changes greater than a threshold value to reduce their impact on the results.

The use of epochs to normalise the data has enabled analysis on heterogeneous hypoxia events, with different timings and oxygenation decreases. However, as suggested above, this approach is flawed. It might be more useful to bin the data in terms of the SpO_2 level, as in the method suggested by Tachtsidis et al. [46].

The differences in the recovery of the cerebral NIRS signals after desaturation is interesting but has not yet been investigated; more work is needed in this area.

9.5.1 Biphasic Fitting

A preliminary attempt at analysing the biphasic oxCCO response has been undertaken. A double-linear fit was applied to model any threshold change and the r^2 was found for each linear fit. The fits were of the following form:

$$\begin{aligned} y &= ax + b \quad : x < A \\ y &= cx + d \quad : x > A \end{aligned} \tag{9.1}$$

where y is the NIRS variable, x is the SpO_2 and A is the point of gradient change. In order to find the point of change, A was increased for each step in x from $x(4)$ to $x(8)$ (so that there were a minimum of 4 data points on each side of the threshold), and the A with the maximum mean of the r^2 was selected.

The fits are presented in Figures 9.28 and 9.29. The fits for the severe and mild group were best at different SpO_2 levels: the severe group SpO_2 turning point (A) was at 81.8%, whereas the mild group turning point was at 86.5%. More analysis is required to confirm the validity of this model.

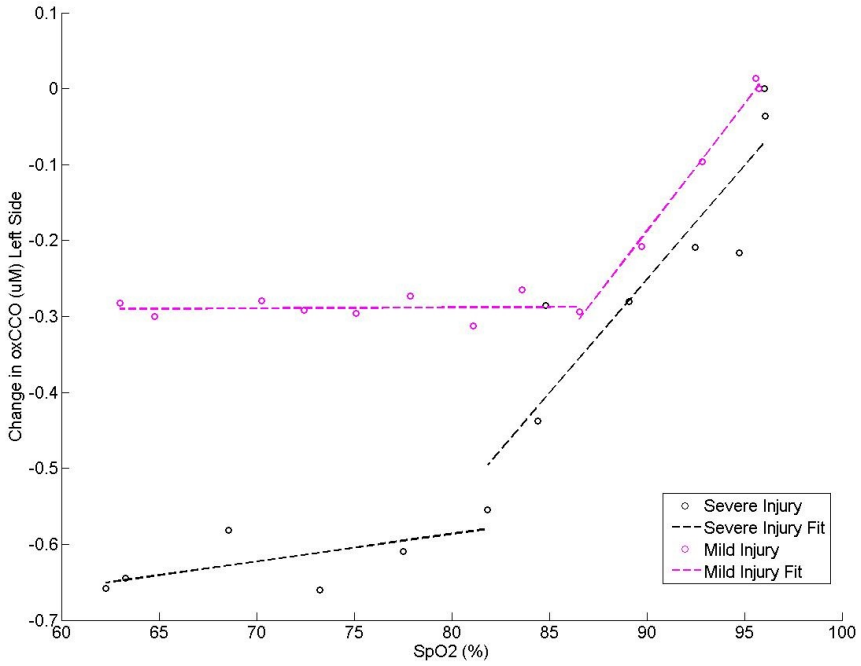

Figure 9.28: Changes in left mean oxCCO against SpO_2 during desaturation for mild and severe groups in epochs. Lines show two linear fits. Point of inflection is at 81.8% SpO_2 for the severe group and 86.5% for the mild group.

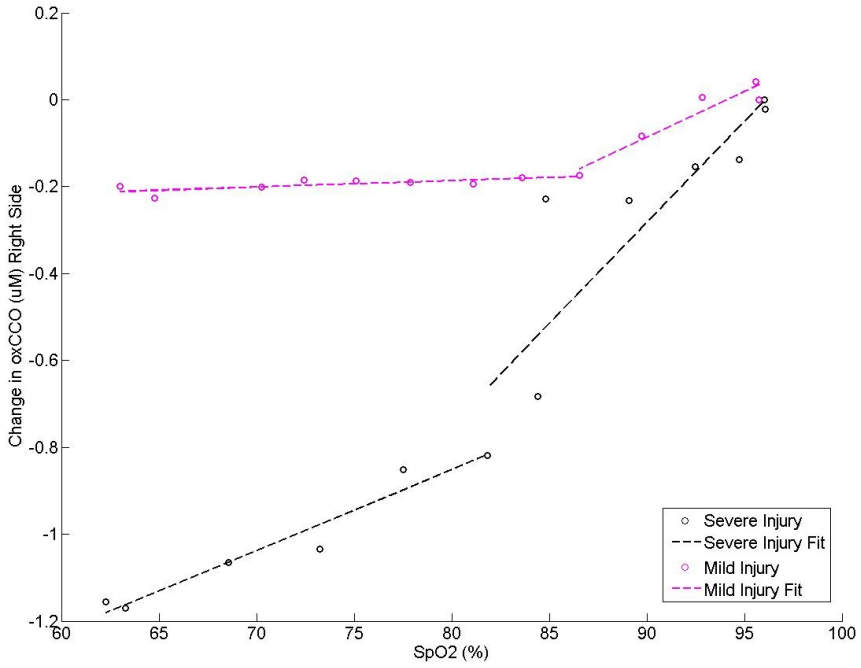

Figure 9.29: Changes in right mean oxCCO against SpO_2 during desaturation for mild and severe groups in epochs. Lines show two linear fits. Point of inflection is at 81.8% SpO_2 for the severe group and 86.5% for the mild group.

9.5.2 Variation of Cerebral Metabolism and Oxygenation with Postnatal Age

Another preliminary analysis into the changes in the relationship with age has been performed. The SpO_2 changes during the desaturation event per day from birth are shown in Figure 9.30. The relationship between the cerebral signals and SpO2 per day are shown in Figures 9.31 to 9.33, as well as the relationship between cerebral oxygenation and oxCCO in Figure 9.34.

There are differences in the haemoglobin and oxCCO responses to hypoxia on different days. The HbO_2 and HHb signals have the same shape but different magnitude changes across days. This is explained by the difference in the SpO_2 decreases (Figure 9.30). The oxCCO response is lowest on day 1 which might suggest that the brain is less able to buffer from a reduction in oxygenation in the early hours of injury. Day 2 appears to have no oxCCO change during the event; however, the average SpO_2 change is smallest on that day.

One important factor to consider is the use of hypothermia; TH occurs over days 1, 2 and 3 and the rewarming period begins on day 4. The SpO_2 change is lowest on day 4 but not significantly so. Due to the low number of subjects it is not possible to draw conclusions from the differences in the day-wise response, a larger sample is needed.

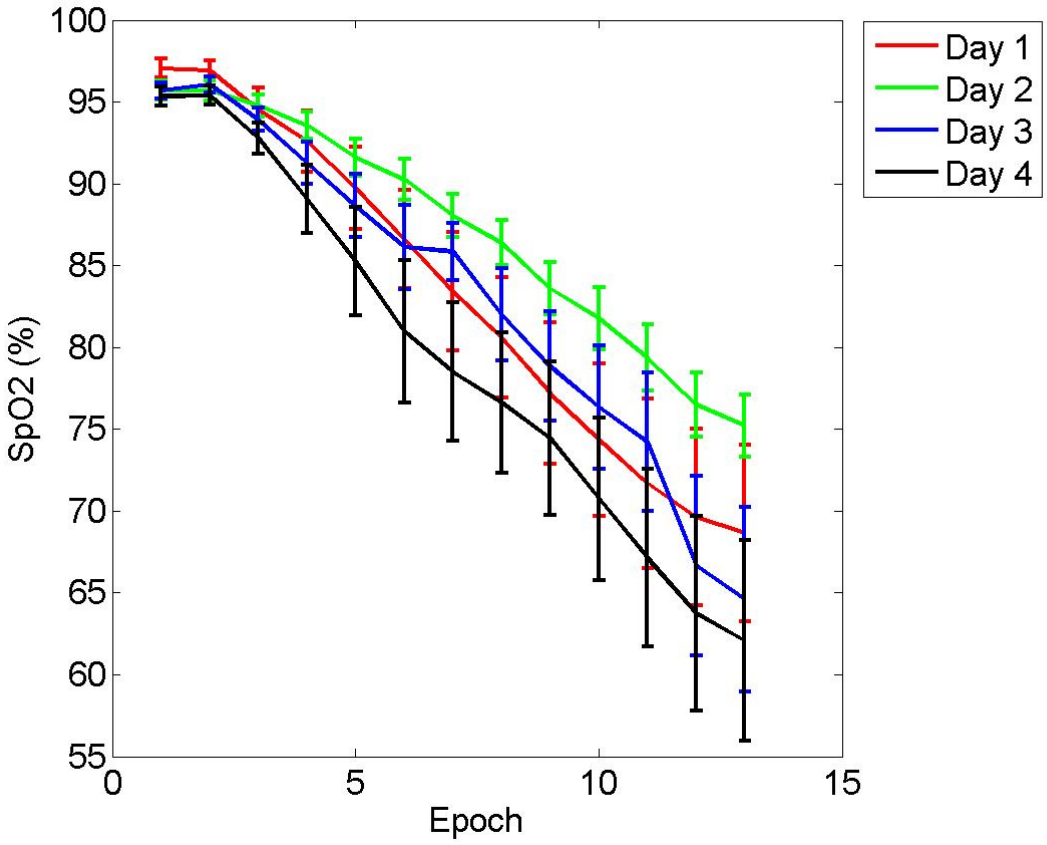

Figure 9.30: Mean SpO_2 during desaturation for each day of life in epochs. Error bars show the standard error of the mean.

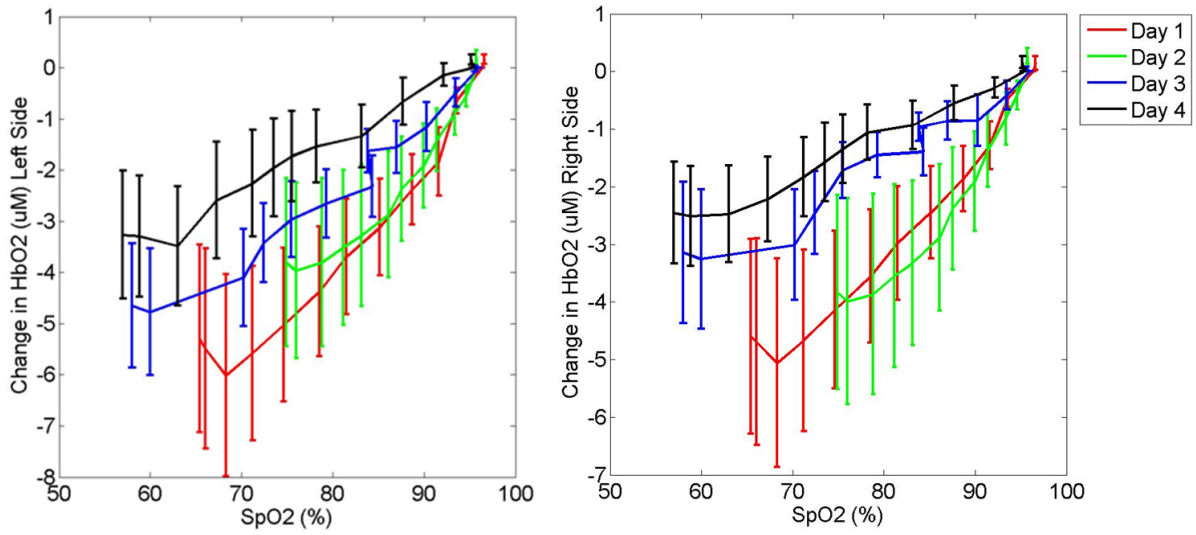

Figure 9.31: Mean HbO_2 against mean SpO_2 during desaturation for each day of life in epochs for left and right sides. Error bars show the standard error of the mean.

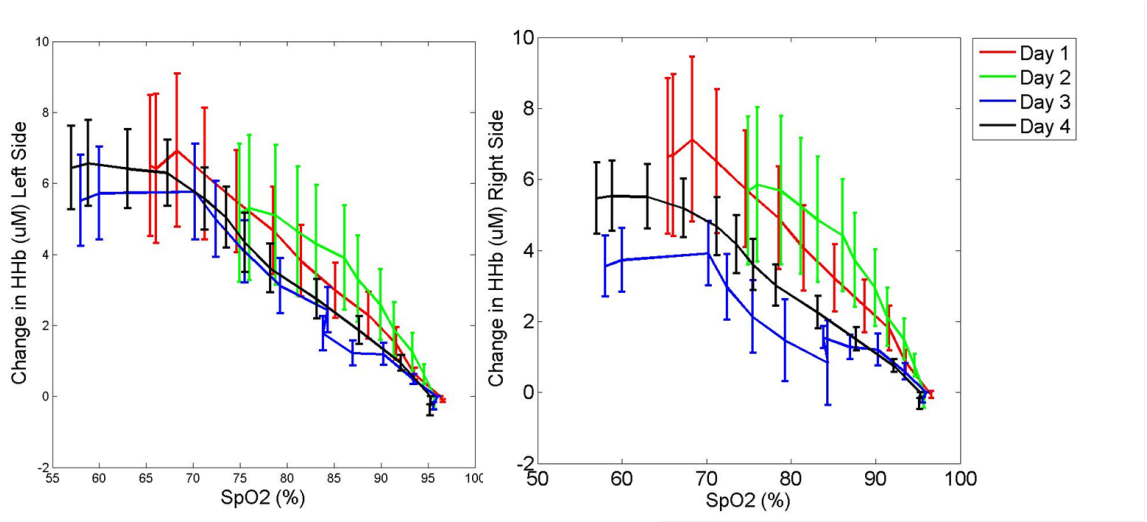

Figure 9.32: Mean HHb against mean SpO_2 during desaturation for each day of life in epochs for left and right sides. Error bars show the standard error of the mean.

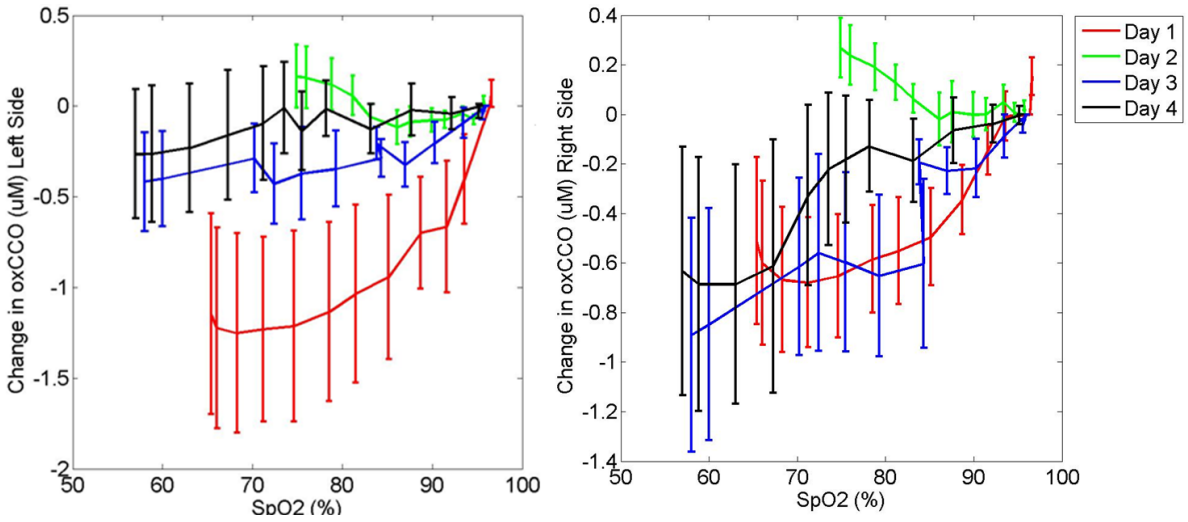

Figure 9.33: Mean oxCCO against mean SpO_2 during desaturation for each day of life in epochs for left and right sides. Error bars show the standard error of the mean.

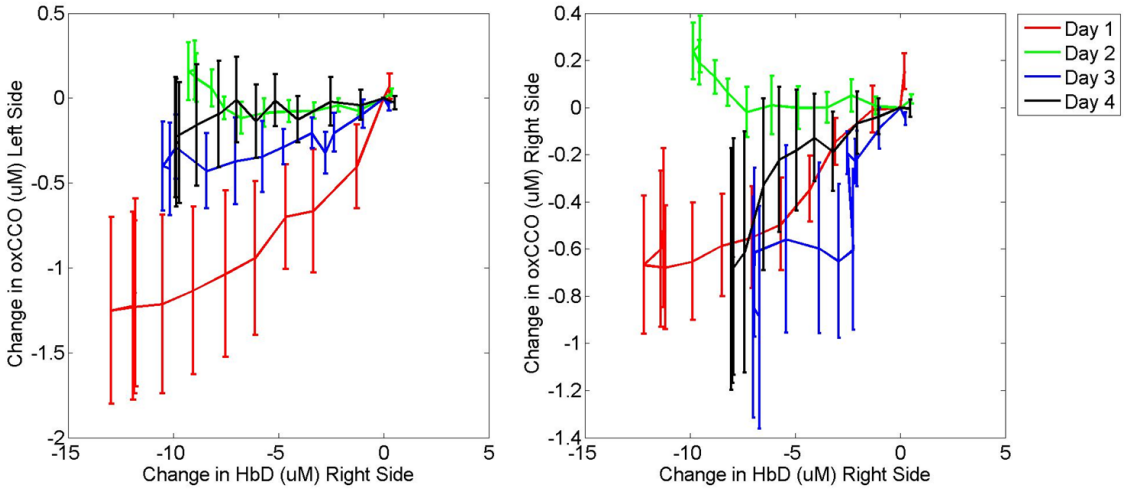

Figure 9.34: Mean oxCCO against mean HbD during desaturation for each day of life in epochs for left and right sides. Error bars show the standard error of the mean.

9.6 Summary

This analysis shows that the dependence of cerebral metabolism on SpO_2 is related to the level of brain injury, unlike the cerebral oxygenation; as in Chapter 8, the oxCCO appears more sensitive to the brain injury state. Larger decreases in oxCCO are related to more severe HIE injury. This is likely to be caused by lower cerebral metabolic rate in the more injured brain which is less able to buffer decreases in tissue oxygenation.

However, a larger sample size is needed to improve the current analysis. In the preliminary analysis, clear differences have emerged in the changes of NIRS variables during desaturation with age which must be taken into account for future analysis.

Chapter 10

Interrelationship Between Cerebral and Systemic Changes in HIE Infants

The previous two chapters have looked at the cerebral NIRS signals in response to spontaneous oxygen desaturations. This approach has shown that the relationship between cerebral oxygenation and metabolism is affected by the state of the brain injury. However, these spontaneous decreases in oxygen saturation have different causes and are usually accompanied by, or caused by, changes in other systemic physiology, such as arterial blood pressure or $PaCO_2$. In order to account for the combined effect of all of the systemic variables, this chapter presents the use of a multivariate statistical analysis technique.

10.1 Introduction

The relationship between systemic and cerebral changes after HI injury can give information regarding the status of cerebral autoregulation/vasoreactivity (see section 2.2). Cerebral autoregulation is typically evaluated by assessing the relationship between MABP and CBF, but CBF is difficult to measure continuously in the NICU. Surrogate NIRS measures of CBF have been used in practice. It has been shown that, under stable arterial saturation (SpO_2 changes of less than 5%), changes in TOI and HbD represent CBF changes [72]. Wong et al. found that cerebral autoregulation impairment, as measured by high coherence between cerebral TOI and blood pressure, was strongly associated with subsequent mortality in premature babies [72].

CYRIL provides an indication of cerebral metabolism (via oxCCO) as well as oxygenation, so in this chapter a multivariate statistical technique is used to assess the relationship between all of the cerebral variables and the systemic physiology in order to assess both cerebral autoregulation and the impact of systemic physiology on cerebral metabolism. The hypothesis is that more severe brain injury will be accompanied by an impairment of cerebral autoregulatory effects, so there will be a stronger correlation

between the cerebral and systemic signals.

10.1.1 Canonical Correlation Analysis

Canonical correlation analysis (CCA) is a multivariate statistical method that can draw relationships between multiple independent and multiple dependent variables. It can be considered an extension to multiple regression, which measures the ability of multiple independent variables to predict a single dependent variable using a linear combination of the independent variables. Canonical correlation predicts multiple dependent variables from multiple independent variables [241, 242].

The general form of canonical analysis is:

$$Y_1 + Y_2 + ... + Y_n = X_1 + X_2 + ... + X_n \tag{10.1}$$

which relates one group of variables, Y, to another, X [241]. The key terms to understand the concepts and terminology of CCA are described below.

Independent and Dependent Canonical Variates

CCA uses the linear combination of the independent and dependent variable sets (X and Y) to create the independent and dependent canonical *variates* (there is no mathematical difference between the independent and dependent data sets). These form a single canonical variate pair. The number of canonical variate pairs produced depends on the smallest number of variables in either set. For instance, if there were four independent variables and six dependent variables, four canonical variate pairs would be formed.

Canonical Weights

The canonical weights are a set of values that describe the contribution of each variable in a set to its respective canonical variate. These weights will vary for different canonical variate pairs so that the first set of weights maximises the correlation between the independent and dependent canonical variates in the first pair. The next set of canonical weights would then maximise the correlation between canonical variates in the second pair based on the residual variance not explained by the first variate pair and so on for the remaining variate pairs.

Canonical Correlation Coefficients

The independent and dependent canonical variate in a pair can be inter-correlated to produce the canonical correlation coefficient. This quantity is maximised by the canonical weights so that the first canonical variate pair will possess the most canonical correlation. Subsequent variate pairs will have lower canonical correlations as more variate pairs form.

CCA looks for a linear transformation of the variables in the independent and dependent data sets in such a way that the correlation between the generated canonical variates is maximised. This does not

imply that the canonical weights represent a measure of the influence on the dependent dataset of the corresponding variable in the independent dataset. In addition, the canonical correlation coefficients only measure the explained variability between canonical variates. Therefore, conclusions cannot be drawn based on these two parameters [243].

Independent and Dependent Loading Coefficients

Loading coefficients are expressed as a value between -1 and $+1$ as the linear correlation between a variable and its respective canonical variate on the same side, and should not be confused with canonical weight. For example, an independent loading coefficient is the linear correlation between an independent variable and an independent canonical variate.

Independent and Dependent Cross-Loading Coefficients

The independent and dependent canonical variates can also be used to draw linear correlations with individual variables of the opposite set, also expressed as values between -1 and $+1$. For example, the first independent canonical variate can be correlated with any one of the dependent variables. The resulting linear correlation is called the first independent cross-loading coefficient. Likewise, a linear correlation between the first dependent canonical variate and with any one of the independent variables is the first dependent cross-loading coefficient.

The loading and cross-loading coefficients can be used in order to draw conclusion about the relationship between variables in the dependent and independent data sets [243].

Redundancy Indices and Sum of Redundancy Index

The redundancy index of a dependent canonical variate is the product of the squared canonical correlation and the mean squared dependent loading coefficients. This gives the proportion of variance in the dependent variable set that can be explained by a single independent canonical variate. To derive the proportion of variance in the dependent variable set that can be explained by the independent variable set, redundancy indices for all variate pairs are summed, producing the sum of redundancy index [241, 242]. Simply, the sum of the redundancy index gives a measure of how strongly the variables in the independent data set are related to the corresponding canonical variates in the dependent data set (analogous to r in Pearson correlation).

10.1.2 Aim

The hypothesis is that the nature of the changes in cerebral oxygenation and metabolism, measured by broadband NIRS, in response to systemic changes will indicate brain injury severity. Cerebral autoregulation has been shown to break down in cases of brain injury and become pressure-passive; therefore changes in systemic physiology will cause changes in the brain. To test this, CCA is used to estimate the strength of the relationship between the changes in the brain (cerebral NIRS signals) and the changes in the body (systemic signals).

Note

This Chapter contains work presented in a paper to be published in the Advances in Experimental Medicine and Biology (currently in press), which can be found in in Appendix B.

10.2 Method

10.2.1 Data Analysis

Data were collected and processed as described in Chapter 6. Data analysis was carried out in MATLAB (Mathworks, USA) and Excel (Microsoft, USA).

For consistency this analysis was applied to data sets recorded on postnatal day 3. Day 3 was chosen because the most data were recorded on this day (at the time of analysis, April 2014). Also it is the final day of hypothermia and so the therapeutic effects of cooling will have occurred, and the infants are normally stable throughout the day (unlike day 4 when rewarming occurs, as the infant will be in a different state at the beginning and end of the day). A period of 3 hours where the NIRS and systemic data are stable was selected for CCA. This period should contain no large events (e.g. spontaneous desaturations, BP decreases) or artefacts. The aim is to observe natural oscillations in the signals; events in one variable rather than another are likely to increase the dependency of the other data set on that variable. A time period of 3 hours was chosen as it is long enough to observe slow-wave oscillations, but it is short enough to avoid artefacts which are more likely to occur in longer segments of data [1]. Furthermore, if dynamic changes were occurring then CCA would need to be performed on a shorter time scale as the analysis over large changes will not be valid as large changes can disrupt the inherent nature of the relationships.

For the CCA analysis, the signals were grouped into 'cerebral' (HbO_2, HHb and oxCCO, for both left and right sides) and 'systemic' sets (MABP, SpO_2, HR, RR, $PaCO_2$ and PaO_2). Patients without complete systemic data sets were excluded from this analysis. The CCA was performed using the MATLAB function 'canoncorr'. The first step of CCA is to form linear combinations of the variables in each data set. Then the correlation between each group of variables is used to assess the dependency of the cerebral signals on the systemic signals. All CCA terms as described in section 10.1 were calculated and the results were compared with the severity of the injury which was assessed by MRS-measured Lac/NAA.

10.2.2 Statistical Analysis

The CCA scores for the sum of redundancies, first dependent and independent cross-loading coefficients of each variable per infant were plotted against Lac/NAA to assess the correlations with injury. This was

[1] This analysis decision was made in April 2014 when there were only 13 data sets recorded, at this point most studies occurred for many hours per day so a period of 3 hours was common. The studies from November 2014 were shorter because it was decided to collect data over 3-4 hours per day to reduce the time that the optodes are on the head (see Table 6.1). Hence it is more difficult to find a stable 3 hour period in these data.

done for each of the systemic variables as well as the NIRS variables, to find out whether their influence over the brain is related to brain injury. For the NIRS chromophores the mean of the left and right cross-loading coefficients was found. The Pearson's coefficient r was used to assess the linear correlation between cross-loading coefficients and Lac/NAA. The median of the dependent cross-loading coefficients was found for mild (Lac/NAA$<$0.3) and severe (Lac/NAA$\geqslant$0.3) injury groups. As the data were found not to be normally distributed, the median and Kruskal-Wallis tests were used to assess the significance of differences between the groups. The level of statistical significance was set at $p<0.05$. The sensitivity and specificity of the CCA scores to predict injury classification was also evaluated and plotted using receiver operating characteristic (ROC) curves. ROC curves are created by plotting the true positive rate against the false positive rate at various threshold settings.

10.3 Results

In 14 of the 29 patients with HIE, a period of 3 hours fitting the criteria was found and CCA was successfully performed. Figure 10.1 shows an example of the data recorded for one infant. Table 10.1 shows the babies that were included in this study. However, most of these 14 infants were treated with xenon in the first 72 hours (normally on day 1) so the other 3 were excluded from the analysis as the effects of xenon on the cerebral regulation is unknown and having a mix of those treated with and without xenon is likely to confound the results. Therefore, 11 infants remained in this analysis: severe injury n = 6, mild injury n = 5; female = 6, male = 5. All infants were born at term gestation (mean 39$\pm$1 weeks), and were of normal birth weight (mean 3.1$\pm$0.6 kg).

10.3.1 Sum of the Redundancy Index

The average sum of the redundancy index was 0.65$\pm$0.14. The individual sum of redundancy indices plotted against the Lac/NAA is shown in Figure 10.2. There is no relationship between the sum of the redundancy indices and the level of injury as measured by Lac/NAA.

Table 10.1: Table of infants eligible for CCA analysis and reasons for ineligibility. 'Y' means CCA analysis was performed, 'Y (xenon)' means that CCA analysis was performed but was excluded due to treatment with xenon, 'not 3 hours data' means that there was no data recorded that was clear of significant systemic events or had low number of artefacts for a continuous three hour period.

CYRIL	**Injury**	**CCA Analysis?**
2	HIE	Y
3	HIE	Y
4	HIE	Y (xenon)
5	Stroke	not HIE
6	HIE	Y
7	HIE	Y
8	HIE	Y
9	HIE	Y
10	HIE	missing systemic data
11	HIE	Y
12	HIE	Y
13	HIE	Y
14	HIE	Y (xenon)
15	HIE	Y
16	HIE	not 3 hours data
17	HIE	Y
18	HIE	not 3 hours data
19	HIE	not 3 hours data
20	HIE	Y (xenon)
21	HIE	missing systemic data
22	HIE (no data)	no systemic data
23	HIE (no data)	no data
24	HIE (no data)	no data
25	HIE	not 3 hours data
26	HIE	not 3 hours data
27	Preterm	not HIE
28	HIE+PPHN	not 3 hours data
29	HIE+head trauma+seizures	no MRS
30	HIE	not 3 hours data
31	HIE	missing systemic data
32	Stroke	not HIE
33	HIE	not 3 hours data
34	Seizures	not HIE
35	HIE	not 3 hours data
36	Seizures	not HIE
37	HIE	not 3 hours data
38	IVH	not HIE
TOTAL	**HIE = 28**	**11**

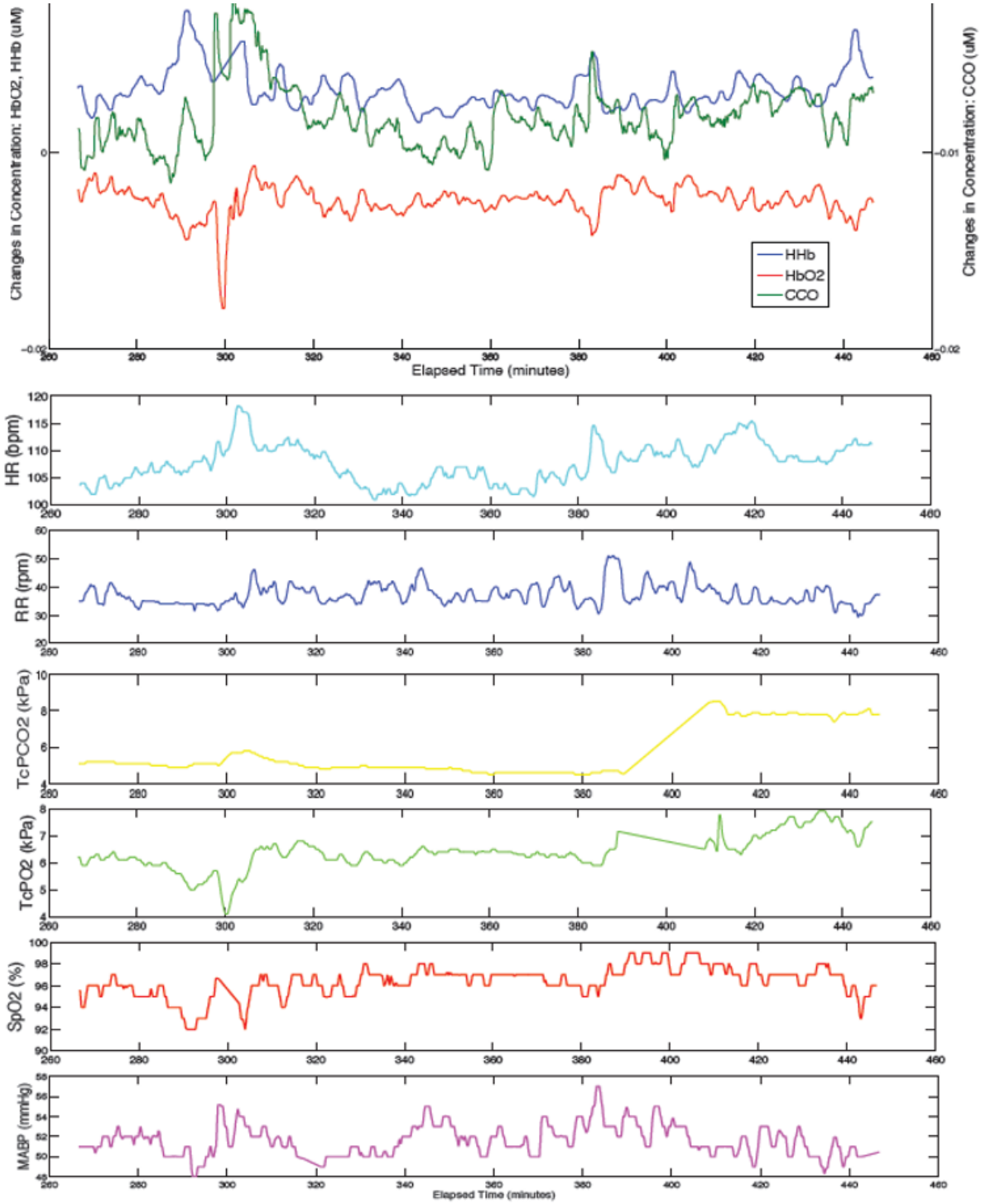

Figure 10.1: Example of cerebral and systemic signals measured on day 3 for infant 14.

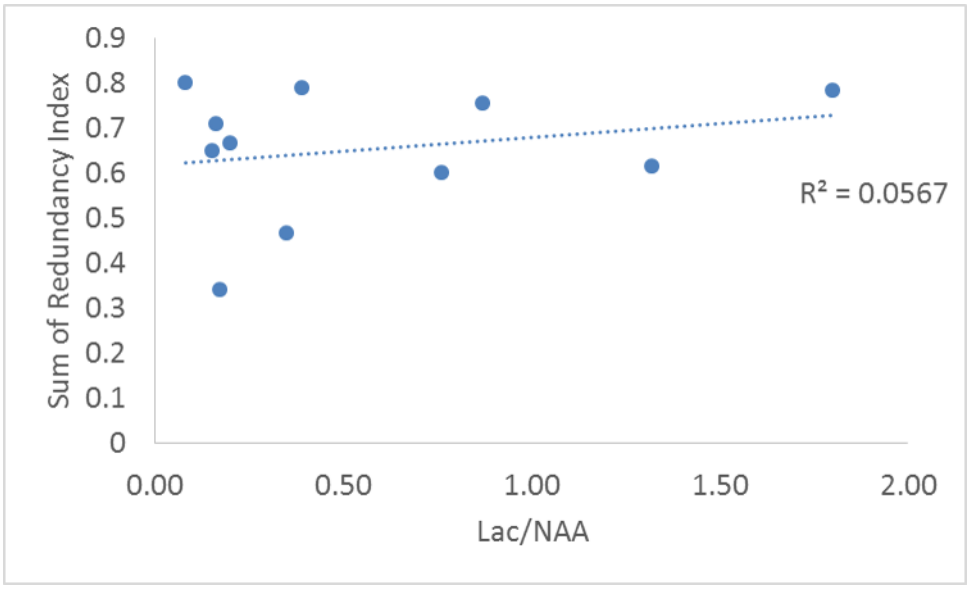

Figure 10.2: Sum of the redundancy indices against Lac/NAA as measured by MRS.

10.3.2 NIRS Cross-Loading Coefficients

The CCA analysis showed that each of the cerebral signals could be in part explained by the systemic physiological variations; the HbO_2 signal had a mean cross-loading coefficient of 0.55±0.20 which means that 55% of the HbO_2 signal could be explained by systemic variations, the HHb and oxCCO mean CCA scores were 0.59±0.23 and 0.58±0.18 respectively. The cross-loading coefficient scores for each cerebral variable were grouped into mild and severe injury categories and are shown in Figure 10.3. There is no statistical difference between the mild and severely injured groups in the dependency of either HbO_2 or HHb on the systemic signals (p = 0.62 and 0.32 respectively). However, the infants with severe injury showed significantly (p = 0.04) higher oxCCO dependency (median = 0.74) than those with mild injury (median = 0.49). Note that the outlier in the severe injury group dependency of oxCCO has a Lac/NAA of 0.35 which is the lowest of the severe group. Neurodevelopmental tests at 18 months will determine whether this infant did have a poor outcome as predicted by MRS.

The cerebral NIRS cross-loading coefficients are plotted against Lac/NAA in Figures 10.4 to 10.6. The cross-loading coefficients for HbO_2 and oxCCO have positive correlations with injury, but only the HbO_2 coefficients have a significant correlation (r=0.65, p=0.03). However, despite the linear correlation, the HbO_2 coefficients do not separate the mild and severe injuries (this is seen in Figure 10.3) whereas the oxCCO coefficients, which do not have a significant linear relationship (r = 0.58, p = 0.06), do discriminate for injury.

ROC curves for the ability of the NIRS cross-loading coefficients to predict injury category are presented in Figures 10.7 to 10.9. The area under the curve (AUC) for the ROC curves are: 0.67 for HbO_2 , 0.43 for HHb and 0.83 for oxCCO. An AUC of 1 is perfect and less than 0.5 is useless (i.e. odds of 50%). The best predictor of injury is oxCCO; the infants with severe injury were identified by an oxCCO cross-loading coefficient greater than 0.6 (sensitivity = 100%, specificity = 83%).

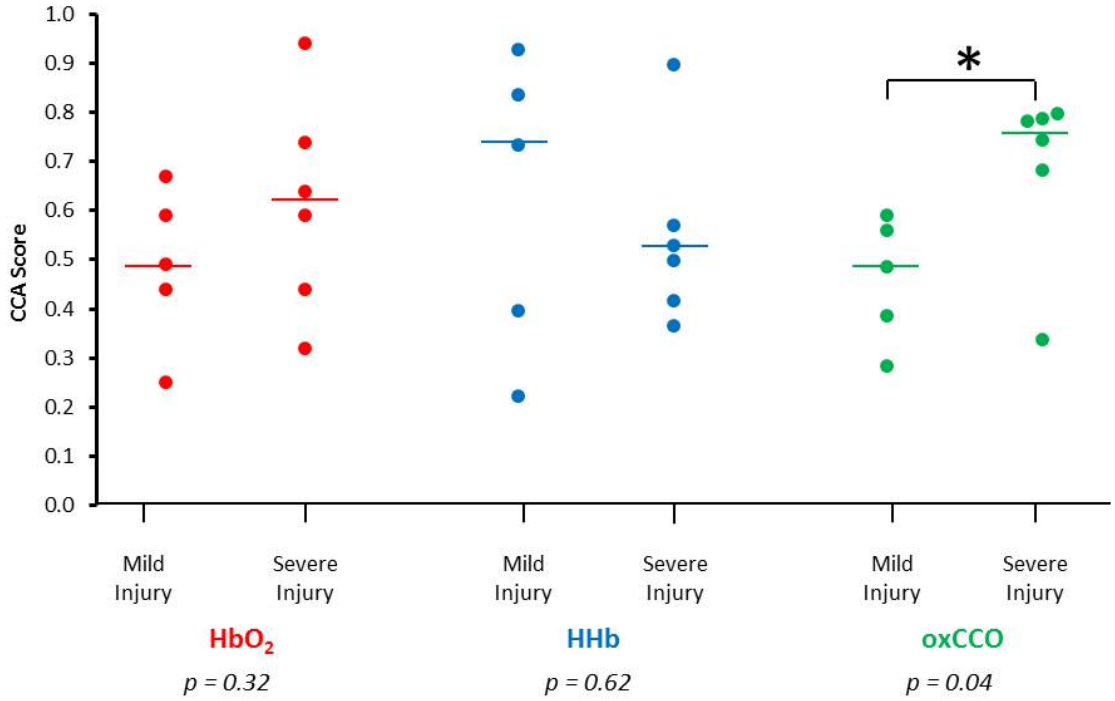

Figure 10.3: CCA scores (cross-loading coefficients) for mild (n = 5) and severe (n = 6) groups for each chromophore. Median score for each group is displayed as a line. Kruskal Wallis test found statistical significance between the groups for oxCCO only: HbO_2 p = 0.62, HHb p = 0.32 and oxCCO p = 0.04.

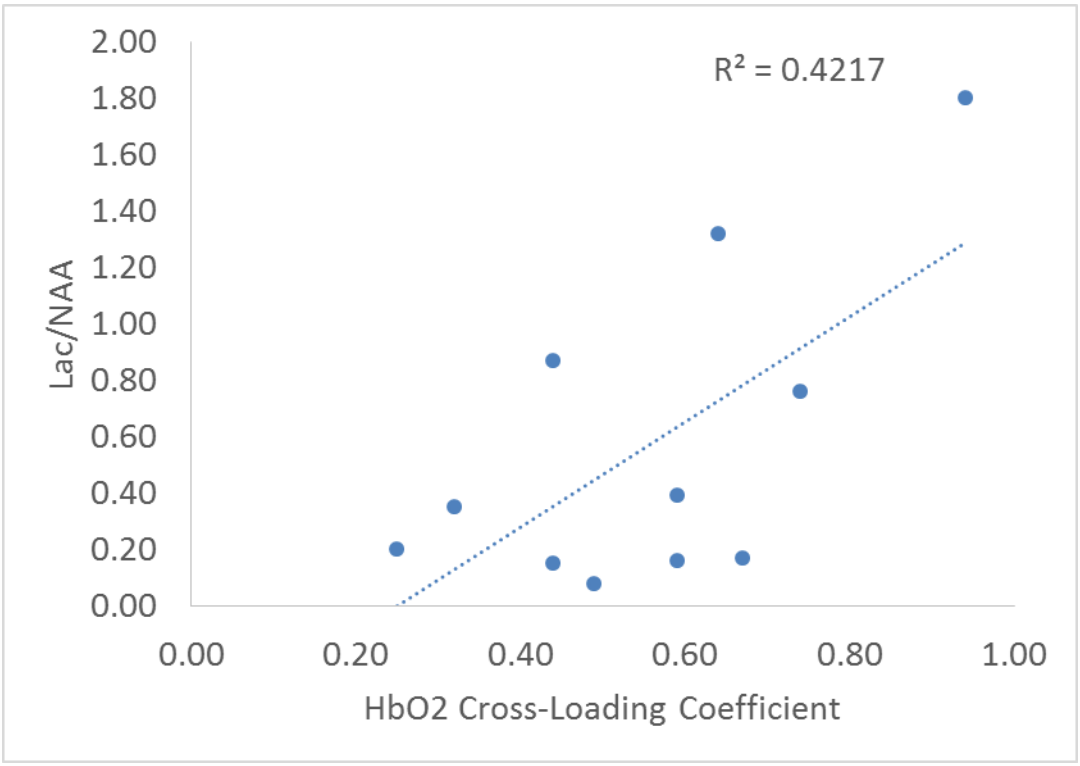

Figure 10.4: CCA scores for relationship between HbO_2 and systemic physiology against Lac/NAA as measured by MRS. There is a significant linear relationship (r = 0.65, p = 0.03).

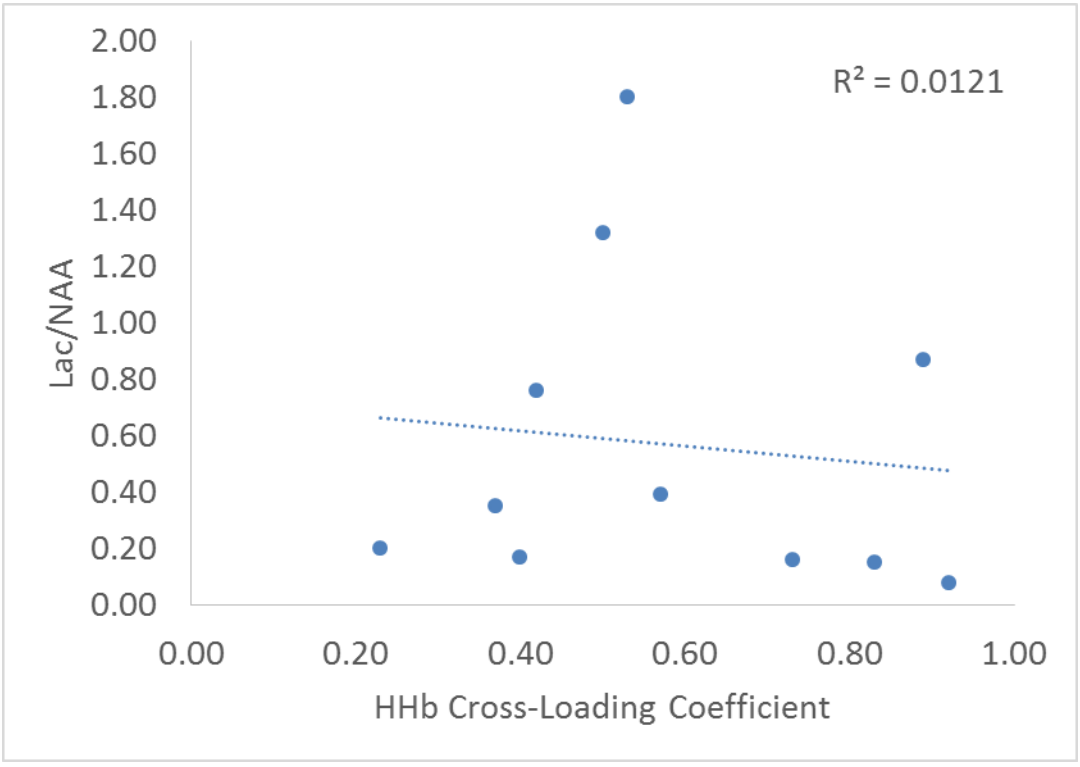

Figure 10.5: CCA scores for relationship between HHb and systemic physiology against Lac/NAA as measured by MRS. There is no significant linear relationship (r = -0.11, p = 0.97).

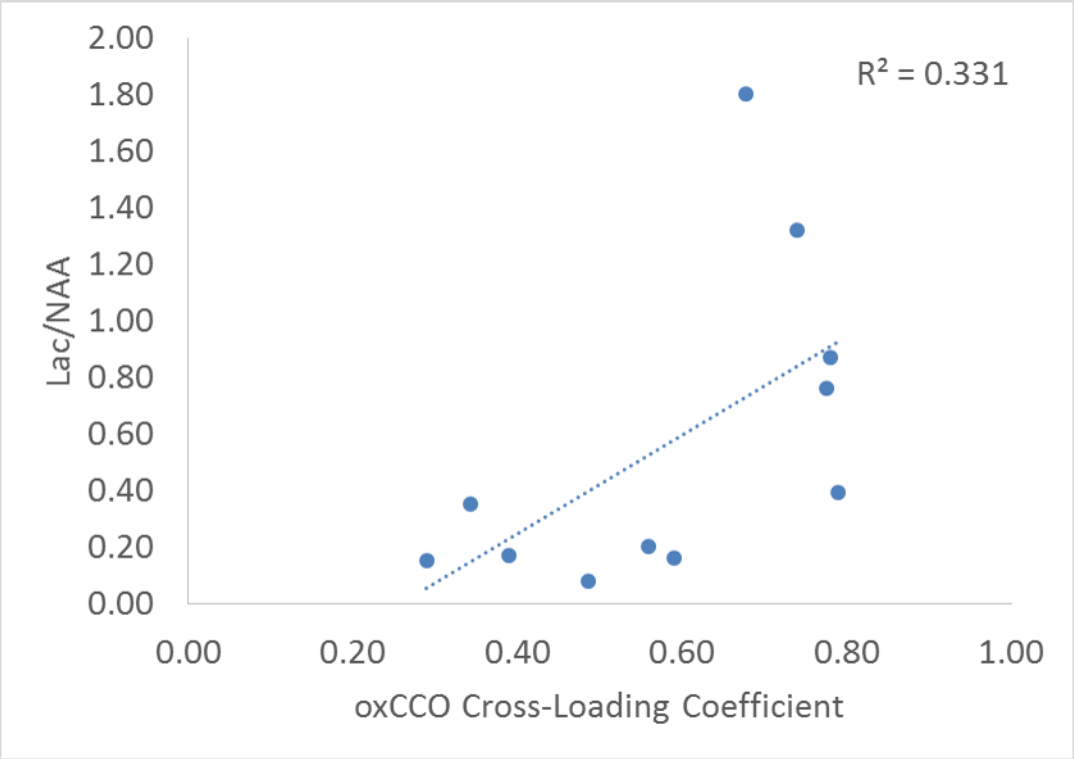

Figure 10.6: CCA scores for relationship between oxCCO and systemic physiology against Lac/NAA as measured by MRS. There is no significant linear relationship (r = 0.58, p = 0.06).

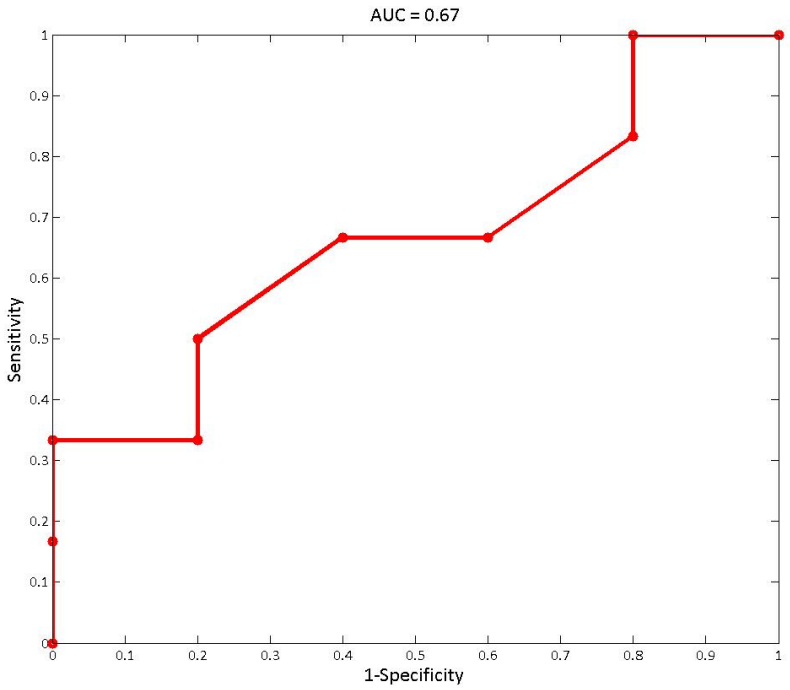

Figure 10.7: ROC curve for the HbO_2 cross-loading coefficient to predict injury classification. The area under the curve (AUC) is 0.67.

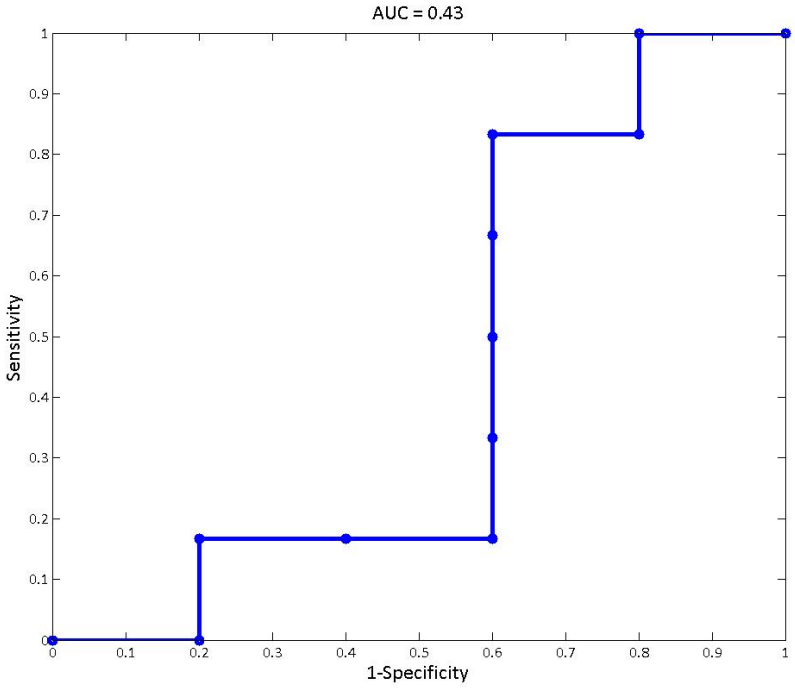

Figure 10.8: ROC curve for the HHb cross-loading coefficient to predict injury classification. The area under the curve (AUC) is 0.43.

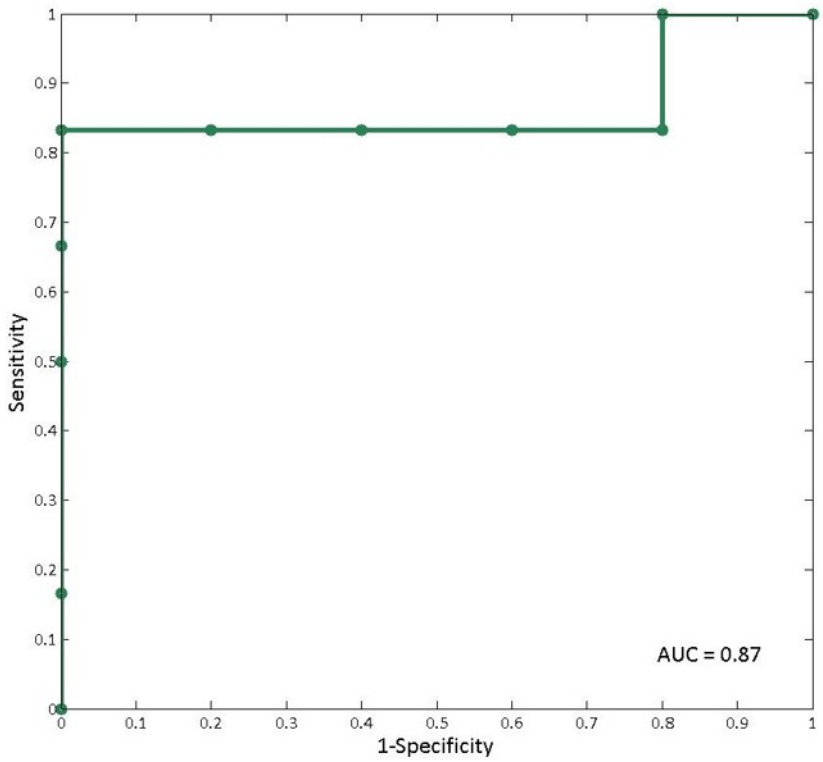

Figure 10.9: ROC curve for oxCCO cross-loading coefficient to predict injury classification. The area under the curve (AUC) is 0.87. For threshold of 0.6 there is a sensitivity of 100% and specificity of 83%.

10.3.3 Systemic Cross-Loading Coefficients

The systemic cross-loading coefficients are plotted against Lac/NAA in Figures 10.10 to 10.16. These assess whether the strength of the influence of each systemic variable on the brain is related to injury. There is a positive correlation between the heart rate cross-loading coefficient and injury as measured by MRS (r=0.62, p=0.04). The ROC curve is presented in Figure 10.13 and shows an AUC of 0.83. There were no significant correlations between injury and any other systemic cross-loading coefficients (p>0.05).

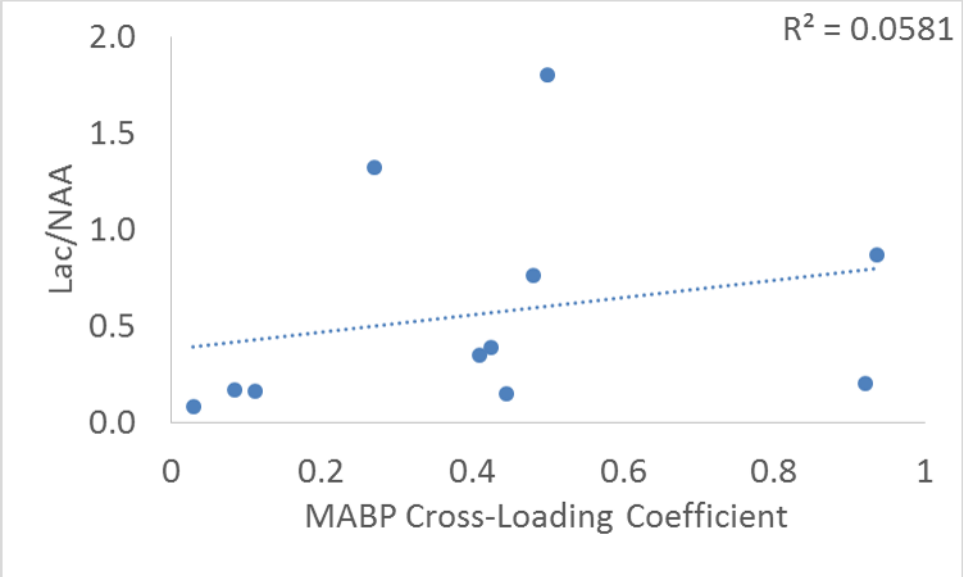

Figure 10.10: Lac/NAA against CCA scores for relationship between MABP and systemic physiology (given by the cross-loading coefficients).

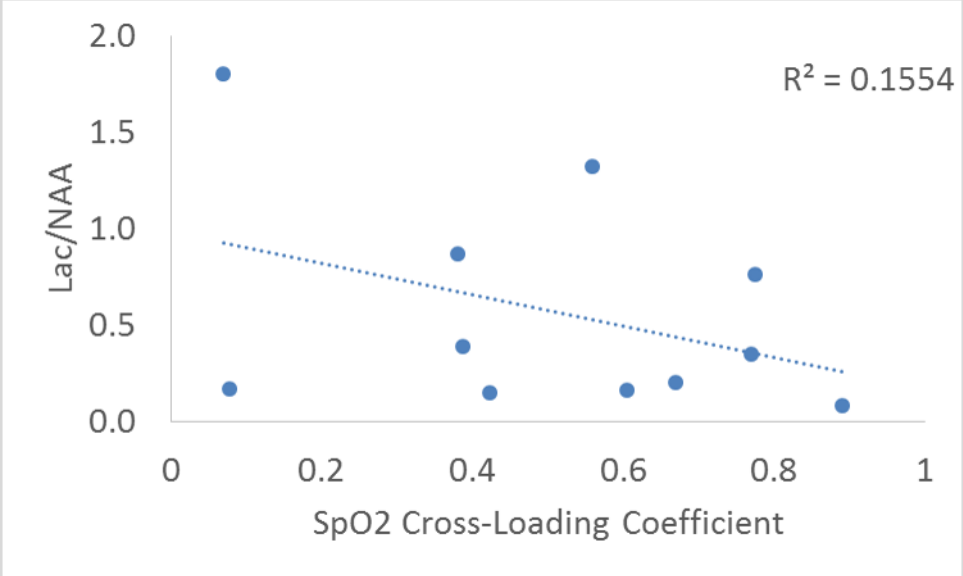

Figure 10.11: Lac/NAA against CCA scores for relationship between SpO_2 and systemic physiology (given by the cross-loading coefficients).

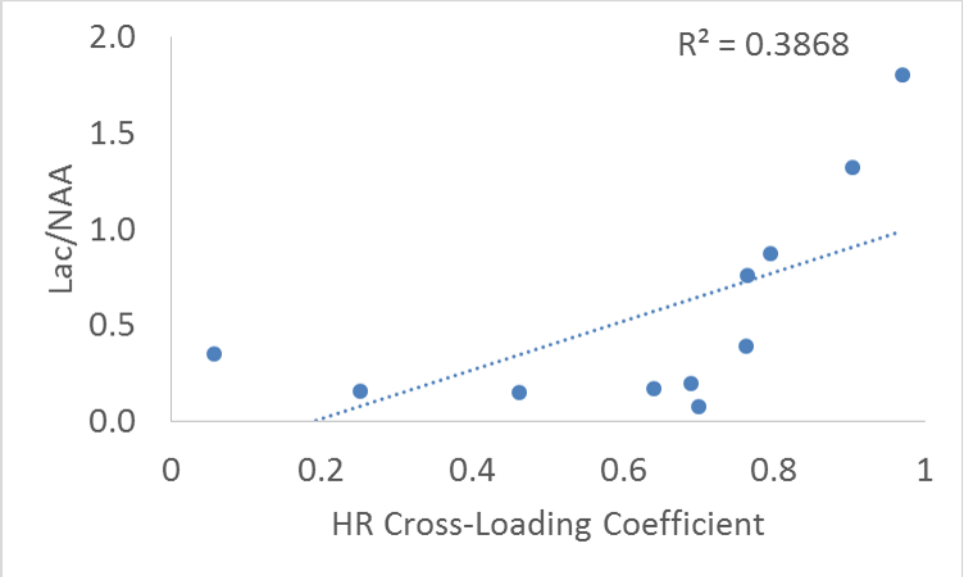

Figure 10.12: Lac/NAA against CCA scores for relationship between HR and systemic physiology (given by the cross-loading coefficients).There is a significant correlation (r = 0.62, p = 0.04).

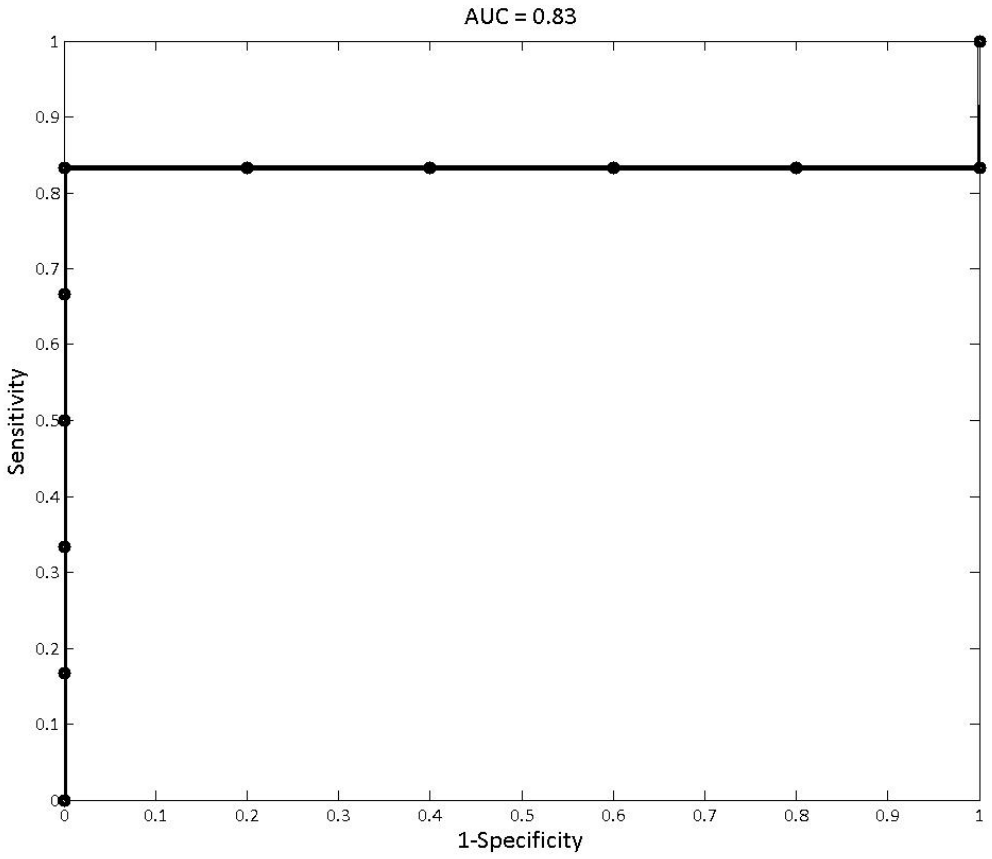

Figure 10.13: ROC curve for HR cross-loading coefficient to predict injury classification. The area under the curve (AUC) is 0.83. For a threshold of 0.75, there is a sensitivity of 83% and specificity of 100%.

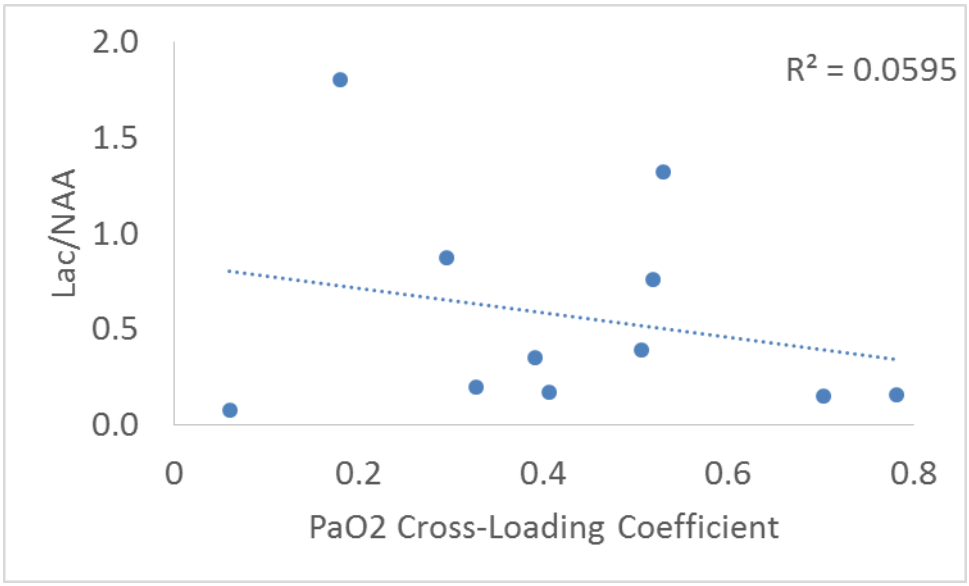

Figure 10.14: Lac/NAA against CCA scores for relationship between PaO_2 and systemic physiology (given by the cross-loading coefficients).

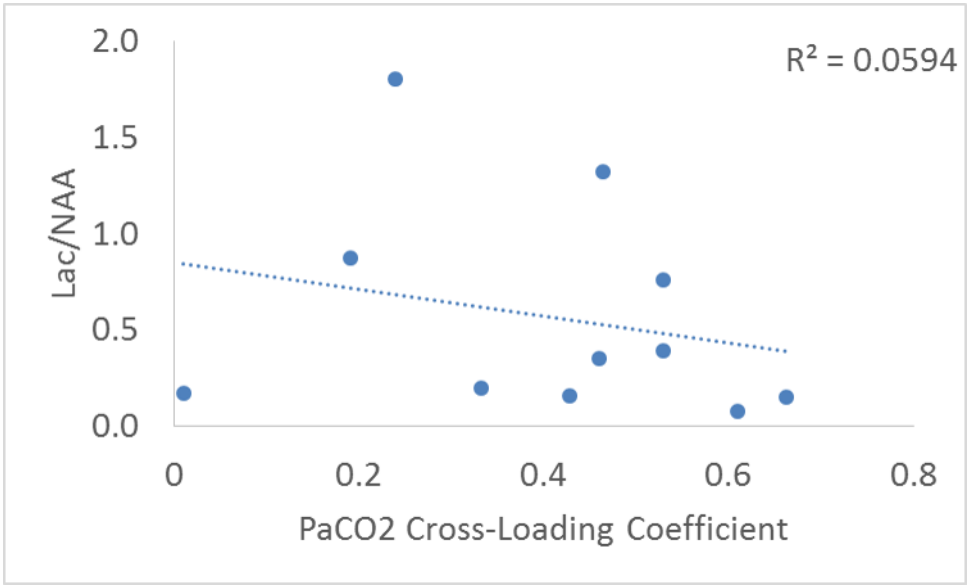

Figure 10.15: Lac/NAA against CCA scores for relationship between $PaCO_2$ and systemic physiology (given by the cross-loading coefficients).

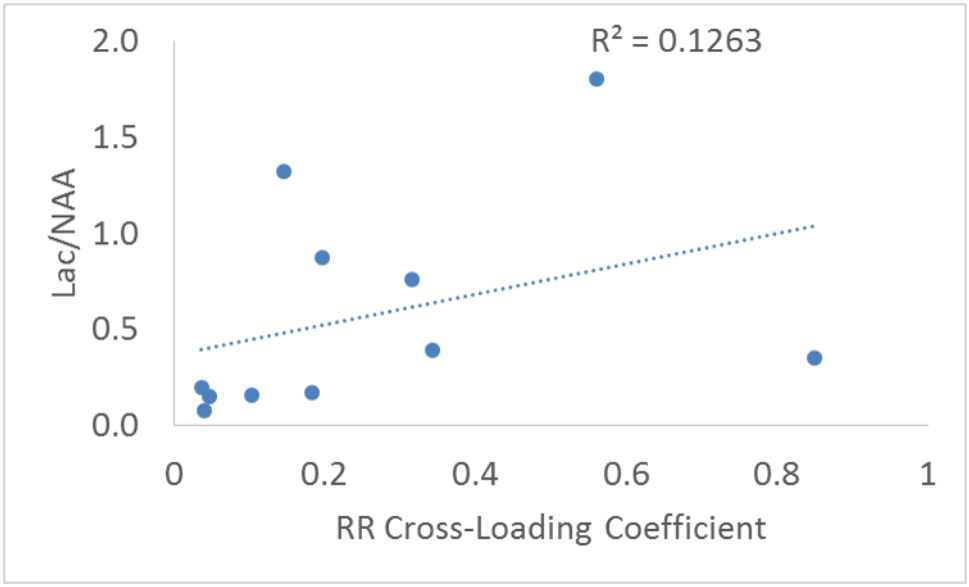

Figure 10.16: Lac/NAA against CCA scores for relationship between RR and systemic physiology (given by the cross-loading coefficients).

10.4 Discussion

CCA showed that broadband NIRS measured cerebral signals could be explained, in part, by changes in the systemic physiology. This is expected because the systemic physiology should influence the cerebral haemodynamics and metabolism even when cerebral autoregulation is unimpaired. Although the relationship between changes in HHb and systemic signals varied between the infants, the relationship was not indicative of injury as measured by Lac/NAA. The relationship between HbO_2 and systemic physiology (represented by the HbO_2 cross-loading coefficient) was linearly related to injury. This suggests that an increased dependence of cerebral oxygen delivery on cerebral changes indicates more severe brain injury. Cerebral autoregulation impairment could explain this result; a pressure-passive relationship will cause a stronger correlation between the cerebral HbO_2 and systemic physiology.

The oxCCO relationship with systemic physiology was able to predict injury, although there was not a significant linear relationship; a high oxCCO dependency on the systemic signals indicated a negative outcome. This difference from the HbO_2 signal could be explained by the difference between the cerebral vasculature and tissue oxygenation. A high vascular oxygenation dependency on systemic signals may highlight which infants have impaired autoregulation, whereas the tissue oxygenation dependency on systemic signals may indicate which infants are suffering at a cellular level from impaired autoregulation. Another theory is that lower cellular energetics in the more injured brain would mean that CCO has less capacity to buffer changes in oxygenation from systemic variations. It is possible that the differences in the metabolic responses are due to changes in the brain leading to, or after, SEF in the severely injured brain.

In Chapter 8, a strong linear correlation between changes in oxCCO and NIRS measured cerebral oxygenation was found during systemic desaturation events in infants with severe HIE. This relationship supports the findings in this study; in the more injured brain CCO is more readily affected by changes in oxygen delivery and, therefore, would be more disturbed by systemic variations.

There was a strong relationship between the cross-loading coefficient of the heart rate and injury (see Figure 10.12). There was a significant linear relationship but looking at the data there appears to be a biphasic relationship between the HR influence on the cerebral NIRS signals and injury. The ROC curve shows that the HR cross-loading coefficient is a good predictor of injury severity. In severe injury the cerebral NIRS signals were strongly dependent on the heart rate. This could suggest that there is an impairment of cerebral autoregulation (although not in the traditional sense of MABP relationship with CBF) in more severe injury, as cerebral oxygenation and metabolism is being strongly affected by changes in vascular output (from heart rate). It is interesting that there is no relationship between MABP cross-loading coefficient and injury as this suggests that cerebral autoregulation is not injury dependent. The systemic cross-loading coefficient results are clinically interesting; in situations where cerebral monitoring is not available it is important to know which systemic signals are linked to the brain to focus attention upon.

CCA has been performed in one other NIRS study [243], and shows promise as a useful tool that can decode complex physiological interrelationships that cannot be explained with more simple models.

However, the most significant relationships to be reported in this study have stemmed from the cross-loading coefficients between a single variable and a group variate. This case can be investigated with multiple linear regression which is less complex to understand and explain (which is important when trying to communicate results to an audience). Therefore, multiple linear regression should be explored as an alternative method to interpret the data.

10.4.1 Study Limitations

There are several limitations to this study to discuss. Firstly, this is a small sample size which is due to the requirement for a long period of stable physiology (3 hours). The sample size needs to be increased to draw any firm conclusions. Also, this analysis should be expanded to investigate the other days monitored after birth to see if and how the cerebral/systemic relationship changes with time. This is particularly important for postnatal day 1 when a prognosis is useful for deciding therapeutic options for neuroprotection.

Secondly, the Lac/NAA is measured in the thalamus and at a later day than the NIRS measurements which are from above the frontal lobe. The difference in location and timings mean that the Lac/NAA measurement is not an ideal outcome marker; the 2 year developmental outcome will be a more robust indicator to assess our results against.

Finally, the CCA technique assumes a linear relationship between all of the variables which may not be true in this complex system and, moreover, CCA examines the relationship over a long window of time (3 hours) during which the complex interrelationship between the systemic and cerebral physiologies might change. A moving CCA, which calculates the relationship between the cerebral and systemic signals over short windows of time, could be employed to examine changes in the relationships with time. This would be particularly important if there are any large spontaneous events analysed as these can change the relationships.

10.5 Summary

Using a multimodal statistical tool has allowed the use of all of the multimodal data to untangle the relationships between the systemic and cerebral physiology. This results show that the relationship between cerebral metabolism and systemic physiology is able to predict the level of injury; a strong systemic influence on the cerebral metabolic changes in the brain indicates severe injury. This result is most probably related to failed autoregulatory capacity, but only the metabolic oxCCO signal can discriminate brain injury. This is likely because an abnormal response caused by brain injury is located at the cellular level rather than in the vasculature. The CCA technique is suitable to use on every data set recorded and has the potential to be performed in real-time at the cotside.

Chapter 11

Further Work

This thesis has presented a lot of advances in bringing broadband NIRS into the clinical environment and represents a big step in using CCO as a biomarker of brain injury. However, there are many issues that need to be addressed and warrant further study. Additionally, from the broadband NIRS system design, clinical application and data analysis methods presented in this thesis, further areas of research have arisen. There are more general future prospects in the field of broadband NIRS. The further work following on from this thesis, some of which is already in progress, is briefly discussed in this chapter.

11.1 NIRS System Design

There are many upgrades that can be made to the CYRIL system, some in terms of the user experience, and others developing the data recorded.

11.1.1 CYRIL Software Updates

The CYRIL GUI, despite being used successfully by members of the clinical team, could be improved to be more user-friendly. Commercial NIRS instruments do not normally display the raw optical data, only the concentration changes calculated, which makes the instrument more simple to use. To come in-line with this, and reduce complexity of the understanding, a clinical version of the software will be designed. This could include warnings to alert the user when the optical spectrum is not optimal, for example, if the spectral intensity is low, the alert could be "signal low - improve optode contact", rather than expecting the user to observe a change in the spectrum and act appropriately. Furthermore, the spectral amplitude changes can give information regarding the optode contact with the tissue; large changes in the overall amplitude could be detected and inform the user that the optodes attachment might be weakening. These warnings regarding the optical data could be emailed in order to notify the user and allow relevant action to be taken.

Finally, the LabVIEW program can be removed from the LabVIEW environment and run as a standalone executable file. This has now been implemented and will make the software easier to use and also easier to transfer to different devices.

11.1.2 CYRIL Hardware Updates

CYRIL has recently (as of March 2016) had a hardware upgrade in order to record a larger portion of the NIR spectrum. The diffraction grating (previously 830 grooves/mm) has been replaced with a 600 grooves/mm grating which gives a larger bandwidth (consequentially sacrificing wavelength resolution). Furthermore, the CCD chip has been upgraded to one with 1340 pixels in the x-direction (previously 512 pixels) which also increases the bandwidth. The new CYRIL system, named CYRIL 2, has a bandwidth of 465nm (503 to 968nm). The wider bandwidth will allow investigation of CCO features in the lower wavelengths (see Figure 4.3 and this is discussed below in section 12.2), while still providing continued measurements within the previously used wavelength range.

A new version of the system has recently begun development (as of April 2016) and will have more channels (∼16 detectors) which will allow whole head coverage. Due to the clinical EEG electrodes covering the head, it was only possible to record data from the frontal lobe in this study. This is a limitation of CYRIL in its current form as HIE injury can be localised to specific areas of the brain. Therefore, in order to obtain data from above the whole cortex, the CYRIL optodes and optode holders need to be miniaturised and designed to integrate with the EEG. Having many sources and detectors over the whole head will allow for diffuse optical topography (DOT) which has been successfully performed and combined with EEG on neurologically compromised neonates before [140], but not with broadband NIRS. A broadband NIRS DOT study has recently been performed on adults [63] and has identified spatial differences in the occipital lobe on the oxCCO signal to the haemoglobins during optical stimulation. The oxCCO and haemoglobin signals have different origins (cellular and vascular, respectively) so it is possible that these early oxCCO DOT measurements are observing this phenomena. Images of the oxCCO signal may be important in both functional activation and brain injury studies to locate origins of neurological activity/damage.

CYRIL has been successful in the NICU but would benefit from having a smaller footprint. Space is precious at the babies' cotsides and a smaller system, one that could fit directly behind the cot, would make NIRS studies much easier and more acceptable for the clinical team. A new miniature version of CYRIL (named mini-CYRIL) has been developed in the Multimodal Spectroscopy Group using an 'off-the-shelf' micro spectrometer, the Ventana (Ocean Optics, USA). Figure 11.1 shows CYRIL and mini-CYRIL next to a model baby for size comparison. This miniature system will be packed into a small package and so will be truly portable and easily deployable in the clinical environment.

11.1.3 Additional Data Recovery

The raw attenuation data from broadband NIRS contains a lot more information about the chromophores within the tissue. For example, the optical pathlength can be estimated using attenuation due to water in the tissue [208]. The method exploits the fact that the differential pathlength exceeds the geometric pathlength (i.e. the optode separation) by a factor (i.e. the DPF) and so the amplitudes of any spectral features of absorbers present in the tissue will be enhanced by approximately the same amount. Since water is present in tissue in concentrations that are often known (with accuracies of a few percent)

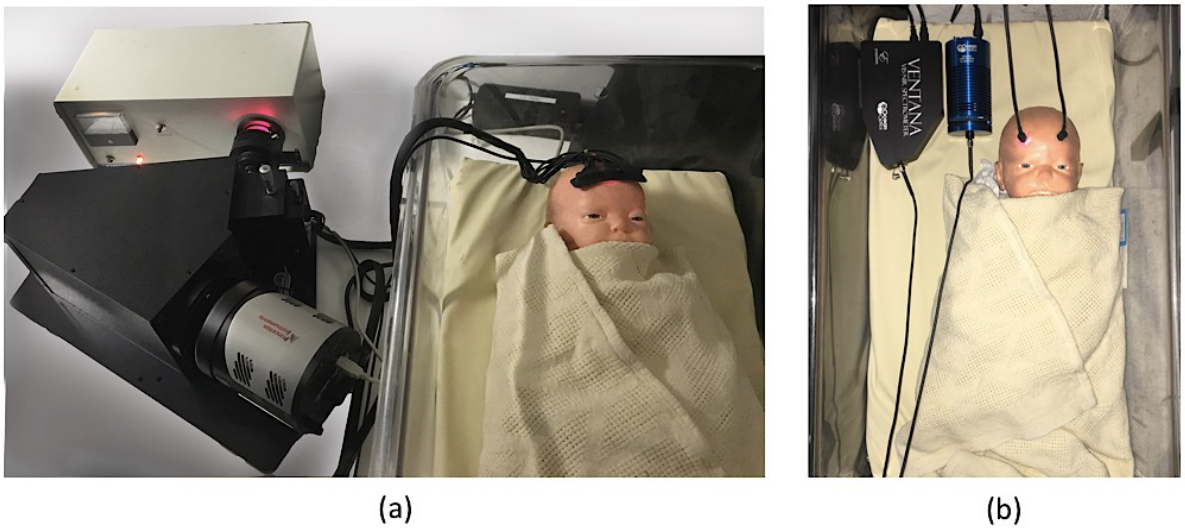

Figure 11.1: (a) CYRIL on a babys frontal cortex. (b) mini-CYRIL performing one-channel reflectance measurement on a babys frontal cortex; white light from HL2000 miniature light source(Ocean Optics, USA) is filtered and transmitted to the frontal cortex via an optical fibre. The reflected light is collected and focused into the Ventana through an identical detector fibre.

[244], and it has a weak absorption feature at 820nm, it is possible to calculate the water concentration from the amplitude of this spectral feature. When this is divided by the known water concentration, an estimate of the differential pathlength is obtained. This method can be, and has been, performed in post-processing using the second differential of the attenuation spectrum at 820nm, with the data collected by CYRIL and shows promise (see Figure 11.2), although it has not been verified fully. This method could be implemented in real-time to improve the estimation of chromophore concentrations using a changing pathlength. This will improve the accuracy of the changes in chromophore concentration which is especially important in babies with changing pathophysiology which may change the nature of the anatomy (e.g. through swelling or oedema) during the measurement period.

Additionally, the absolute concentration of HHb can also be calculated using a second differential method [245]. This method utilises peaks in the HHb spectra between 710-780nm so a larger bandwidth is necessary. This will be possible with CYRIL 2, described above, whose bandwidth is currently 503 to 968nm.

11.1.4 SRS Measurements of TOI

As discussed in section 7.3, the biggest problem that was not solved in this work was the recording of data suitable for SRS calculation of TOI. The primary goal of this PhD was to record in-vivo measurements of oxCCO so the calculation of TOI was beyond its scope. Work on TOI measurements with CYRIL is now in progress.

The challenges encountered and the first attempts to understand the problems are described in section 7.3. Many other trials and modifications to the algorithm have been performed to attempt to find a

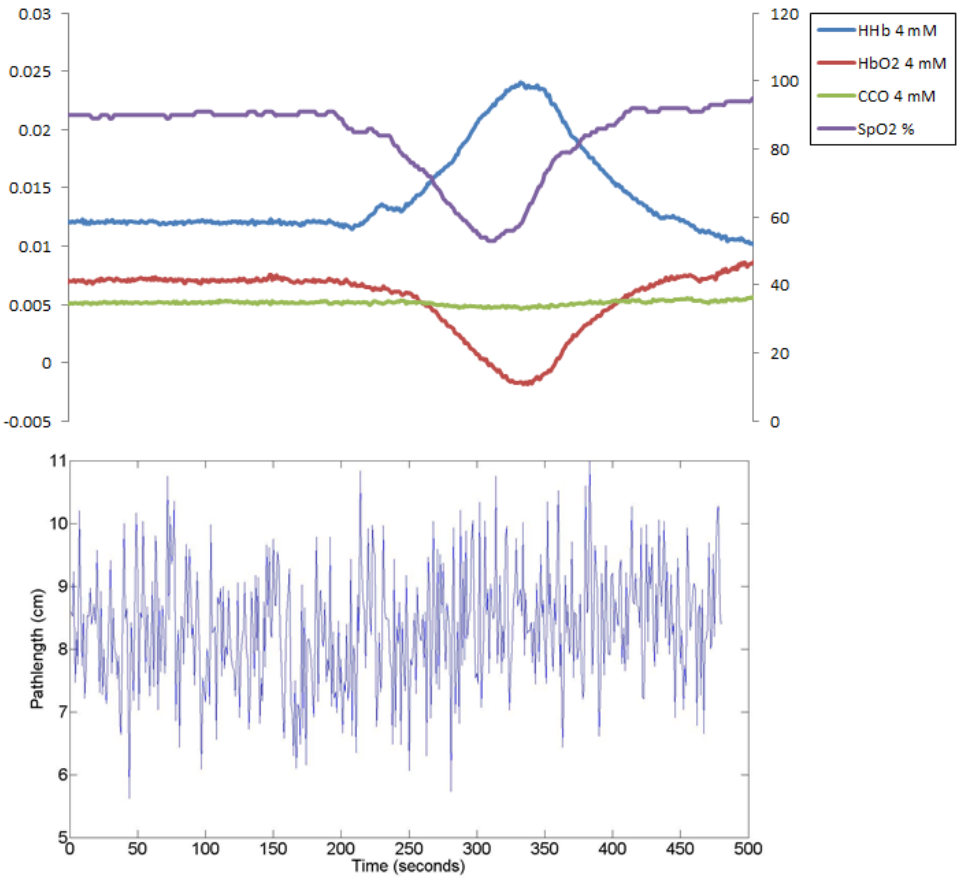

Figure 11.2: Chromophore concentration changes (above) and pathlength calculated from second differential of the water spectrum method (below) during a spontaneous hypoxia event in infant 59. The average DPF is 2.78 which is lower than the expected DPF (4.99).

solution to this problem including:

- Reducing the number and combination of wavelengths
- Reducing the number and combination of source-detector separations
- Altering the h scaling factor
- Using the water extinction coefficients to resolve for the concentration of water
- Adjusting the optodes to find a 'reasonable' TOI in real-time using the Version 2 of the LabVIEW software (section 5.3)
- Improving light shielding
- Designing new optode holders (see Figure 5.19) to improve optode contact with tissue
- Calculating TOI in all data sets in attempt to find a pattern.

Yet none of these have produced any enlightenment on the underlying problems or have produced a reliable TOI. It is most likely that poor/uneven optode-tissue contact is the source of the problem, but it is difficult to improve this as the neonates are very delicate. A solution to the problem is to modify the probe design to improve tissue-to-optode contact across all detectors and prevent the differences in attenuation caused by it. The fibres used to couple the broadband light in and out of the tissue have a high profile protruding from the tissue (9mm) which might result in poor contact as the height makes them unstable; new designs with a lower profile (5mm) are currently being developed with the fibre manufacturer (Loptek, Germany). It is also possible that light piping through the tape used to attach the optodes to the tissue could affect the absolute attenuation measurement; this should be investigated.

An absolute measurement of tissue saturation would be especially useful in aiding interpretation of the oxCCO signal. As discussed in section 9.4, the differences between the changes in the oxCCO signal with injury may be due to the initial CCO state being more highly oxidised in more severe injury. TOI would give insight to this problem as it will reveal the level of available oxygen in the tissue.

This analysis of TOI is important more generally and it will be beneficial to the NIRS community to understand the problems with broadband SRS, as they may be concealed in SRS methods with a few discrete wavelengths. This is vital as there are clinical trials occurring with this technology [133, 246], while there are still problems with inter- and intra-subject differences [247–249].

11.1.5 Absolute Measurement of CCO

The most ambitious but also most exciting future prospect is a measurement of the absolute redox state of CCO which would give information on the fraction of CCO that is oxidised/reduced. An absolute redox measurement would allow the assessment of metabolic function in real-time. To achieve this we need instruments and methodologies that can decouple light absorption and scattering from light attenuation, as well as measuring light absorption at multiple specific wavelengths.

The Multimodal Spectroscopy Group has recently developed a time resolved NIRS system which has 16 wavelengths [228, 250]. This instrument can measure the absolute optical properties (absorption and scattering) of the tissue at multiple wavelengths within 600nm and 1100nm and will, hence, be able to resolve absolute tissue concentrations of the brain tissue chromophores. Absolute measurements of CCO redox state have been performed in the visible region previously [251] but it will be a challenge to achieve this within the NIR window to interrogate deeper into tissue.

11.2 Clinical Broadband NIRS

11.2.1 Present Study

One of the biggest problems with the data discussed in the thesis is the low numbers of subjects so there is not enough statistical power to draw strong conclusions from the results. This is being rectified as the Baby Brain Study is continuing to study more infants with CYRIL, and now CYRIL 2. To date, 63 infants have been studied (of which 50 were diagnosed with HIE). The present methods of data analysis

will be expanded to include all of these, and future, subjects. To improve the statistical power of any results, the sample size must be increased by an order of magnitude [252]. The data recorded must be monitored to ensure that each of the first few days of life are equally sampled, and that infants studied have a spread of injury severities.

Another area of improvement would be to use the actual outcome of neurodevelopment (as opposed to the predictive marker, Lac/NAA). Collection of these data has begun; the developmental tests have begun for this cohort of infants so the results from those will be included into the data analysis. This will also reduce problems with injury localisation (as the Lac/NAA measurement is taken from a thalamic voxel whereas the NIRS measurement occurs over the frontal cortex).

The three analysis methods presented have a high infant rejection level: Chapter 8 includes 22/28 subjects, Chapter 9 includes 17/28 subjects and Chapter 10 includes 11/28 subjects. A method that does not depend on observing spontaneous events (such as hypoxias) or long periods of stability needs to be found. The CCA analysis method, as all analyses of slow-wave oscillations, has this potential as the window of time studied can be reduced to minimise rejection of data.

11.2.2 Analysis in Progress

There are three data analysis methods currently being performed on the data. The first is multiple linear regression a technique that is similar to the CCA analysis presented in Chapter 10. The results of CCA found that the relationship between the systemic and cerebral data as a whole was not injury-dependent. However, the individual cerebral signals' correlation with the systemic data were specific to injury. This case (one variable correlated to multiple variables) can be modelled with multiple linear regression analysis so this is currently being investigated.

The second project is to investigate differences between the left and right NIRS channels. In Chapter 9 it was noticed that the change in oxCCO was larger when measured over the right hemisphere. This hemispheric laterality is interesting and requires further investigation. Therefore, using a laterality index method (a technique commonly used in fMRI experiments to determine hemispheric dominance [253]) this is being investigated. It will be interesting to see if hemispheric asymmetry occurs in HIE and if it is dependent on injury, gender and/or age. Regional and hemispheric asymmetries have been observed in preterm and term newborns previously [173]. Laterality index analysis may facilitate early detection of abnormalities.

The aim of the third analysis is to use the spontaneous hypoxias observed to estimate CBF. The method is based on Fick's principle which states that the rate of accumulation of a tracer in an organ is equal to the difference between its rate of arrival and departure. If a substance is introduced into the arterial blood, and the time of measurement is less than the transit time through an organ, the tracer will not appear in the venous blood. Therefore, the flow can be measured as the ratio of tracer accumulated to the quantity of tracer introduced. It is possible to use a change in HbD as a tracer; when a sudden change in SpO_2 occurs, the change in HbD represents a change in tracer concentration and thus calculates CBF. So far the CBF has been calculated in 30 HIE infants. For some neonates the CBF was also measured with arterial spin labelling MRI and a strong positive correlation was found between

the NIRS- and MRI-measured CBF values (r^2 = 0.96, p = 0.04). For infants with severe injury there was an increase in CBF with age. The relationship between CBF and injury will be investigated further. Additionally, with the CBF and absolute haemoglobin measurement (discussed above) it is possible to calculate $CMRO_2$ [254]; it will be especially interesting to compare another marker of metabolism with injury and oxCCO.

11.2.3 Interesting Examples of Data

A couple of interesting phenomena that have been recorded are shown here. Analysis into these is necessary and ongoing. A strong systemic oscillation was seen in a HIE infant with predicted poor outcome by MRS and is shown in Figure 11.3. The large fluctuations in blood pressure are translated to big oscillations in the cerebral NIRS data. This suggest that the infant has impaired cerebral autoregulation and so the changes in MABP are directly affecting the CPP. Analysis of the relationship between HbD and MABP will allow an assessment of autoregulation impairment; this could be done through CCA, coherence analysis [72], HVx [165], or wavelet cross-correlation [255] to name a few methods.

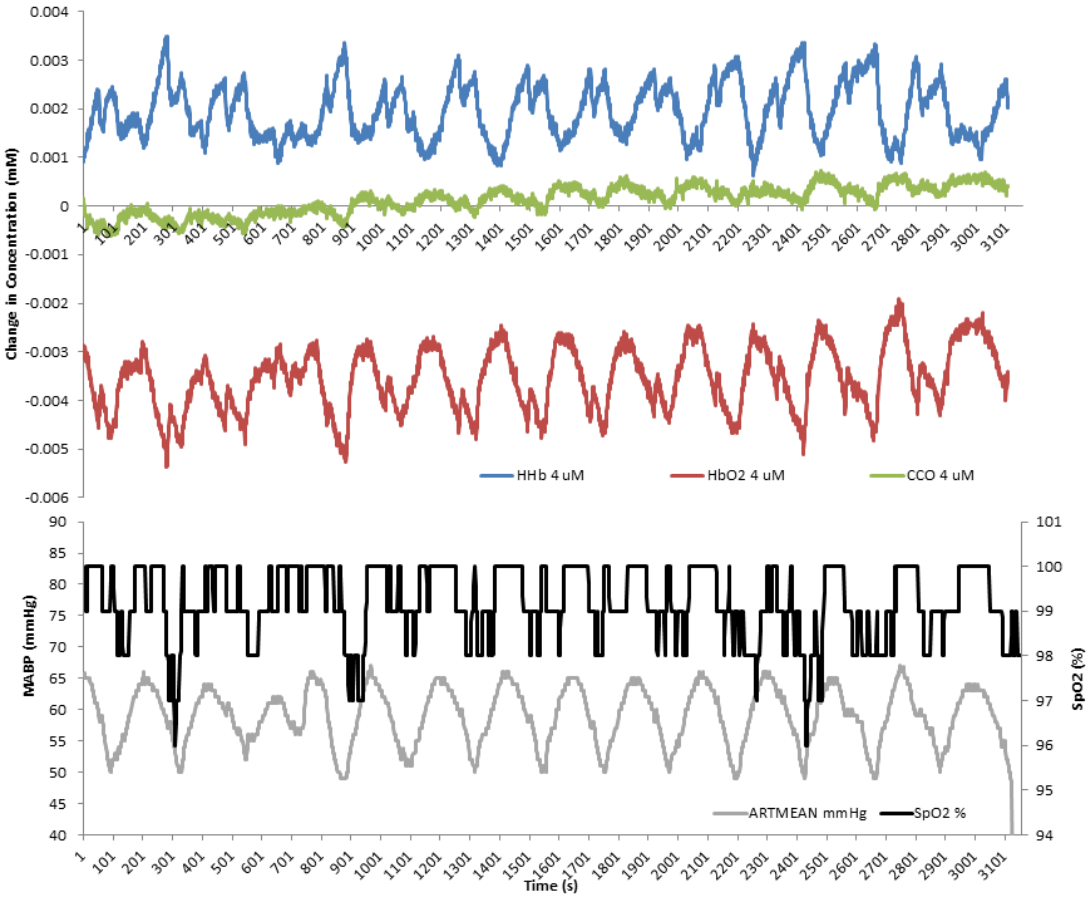

Figure 11.3: Signals recorded on 15/12/14 17:34:57 on infant 31 showing strong blood pressure oscillation.

A sequence of seizures was observed in an infant with severe HI injury during the rewarming phase. Figure 11.4 shows the aEEG trace and the corresponding systemic and cerebral changes. Interestingly, during the five periods of seizure activity there was an increase in the concentration of oxCCO suggesting

an increase in metabolism during the seizure. This is accompanied by a decrease in HbO_2, SpO_2 and an increase in HHb, MABP and HR. This observation is discussed fully in a paper written by Dr Subhabrata Mitra which is currently under review [256].

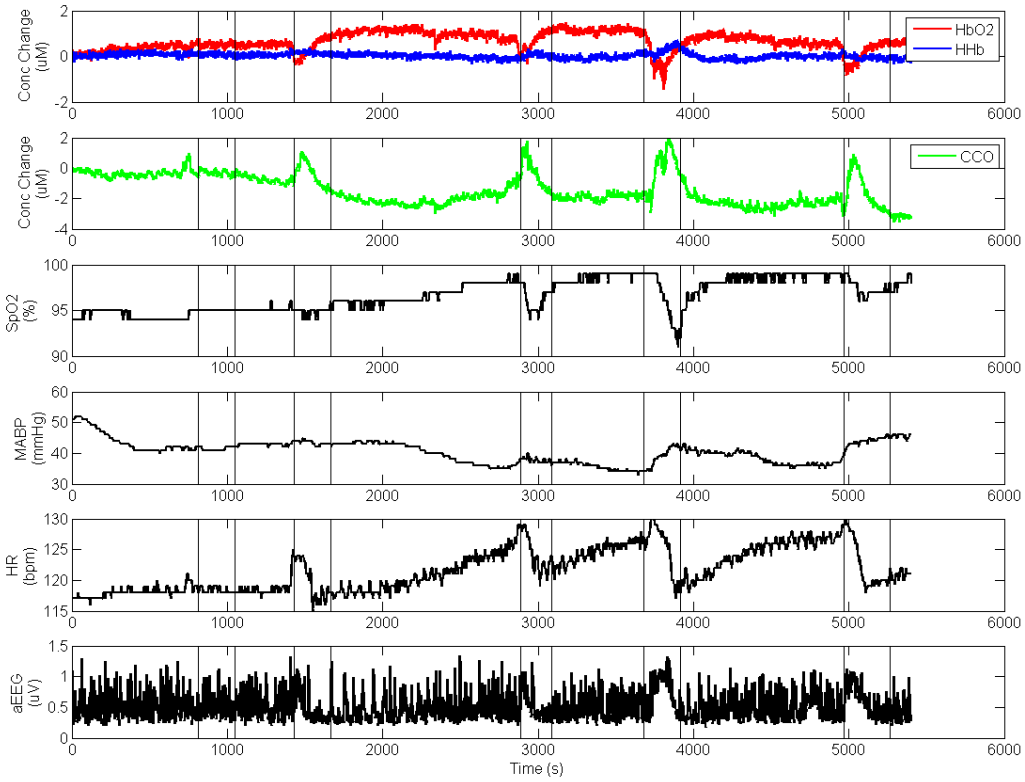

Figure 11.4: Signals recorded on infant 18 during a series of 5 seizures. Lines show start and end point of each seizure as identified from the aEEG by a clinician who was blind to the NIRS data.

11.2.4 Future Studies

In my opinion, the ideal study of HIE using broadband NIRS-measured oxCCO would have a repeatable controlled event (for example, a controlled change in inspired oxygen, or a functional challenge), age-matched healthy infants to get baseline data, and be performed over the entire head. A repeatable event would remove the current problem of the heterogeneity of the data. Functional activation studies have found differences in the haemodynamic response between different grades of HIE injury [157] and adult studies have seen a response from the oxCCO signal during activation [61]. Therefore, studying the oxCCO functional response in HIE could provide an assessment of brain health. Including healthy infants as controls will allow for a better assessment of our results so far. Although it is possible to assess the data based on grades of severity, there is a gap in the data as the oxCCO signal has not been studied in healthy babies before. These data are vital in the translation of oxCCO into the clinic. Whole head NIRS and DOT would add another dimension to the analysis; by examining the cerebral

haemodynamic and metabolic response over all areas of the cortex, it may be possible to identify areas of injury. This could provide data analogous to the EEG, ultrasound and MRI images which are the technologies currently used to identify lesions. Furthermore, comparison with more cerebral monitors, such as EEG, will help validate the measurement as well as advancing knowledge.

The work presented here has focussed on assessing the oxCCO signal in order to find a biomarker of injury; further work into the nature of the signal and its physiology is required to gain confidence. Historically, CCO has been studied in infants under clinical care (see section 4.5), adults, both clinical and healthy (see section 4.6), and animal models (see section 4.2). NIRS measurements of CCO have not been performed on a healthy human neonate, which means that CCO pathophysiology in HIE is difficult to separate from normal neonatal physiology. However, it is difficult to obtain oxCCO data on healthy neonates as evoked responses would be necessary.

Some of the questions regarding the underlying physiology behind oxCCO in HIE may not be able to be answered using human infants. Pre-clinical models of HIE (particularly piglet models) have been used successfully for clinical trials (notably for hypothermia therapy [257]) and in the assessment of changes in metabolites, including oxCCO [12]. Animal models of HIE that assess oxCCO in a translational manner, for example, by performing a challenge that is repeatable in humans, could bring answers to the physiological questions but also shed light on the usefulness of the measurement in the clinic.

The analysis performed has shown that the multimodal data analysis provides more information relating to injury than any single signal, this reflects the use of multiple monitors in the NICU. Doctors make their case for a diagnosis based on a number of parameters and, therefore, we should not be striving for a complete diagnosis from one biomarker; a marker that can give information on part of the clinical pathology is sufficient. It may be the relationship between cerebral metabolism (via oxCCO) and other variables provides the best assessment of cerebral health.

Chapter 12

Conclusion

This, the final, chapter summarises the work presented in this PhD thesis and discusses the various results obtained as a whole. Appendix B contains copies of the publications resulting from these analyses.

12.1 Summary

This PhD thesis describes the development and characterisation of a novel broadband NIRS system, its use in the NICU and methods to interpret the data recorded.

12.1.1 Instrumentation

This work provides new instrumentation and data analysis tools to investigate cerebral physiology, particularly oxygenation and metabolism, in neonatal brain injury. The use of the broadband NIRS instrument developed has been shown to be feasible in the NICU, and has been successfully used by physicists and clinicians alike.

The optical signals recorded on infants with HIE were analysed for cross-talk between the signals. The oxCCO signal was found to behave independently to the haemoglobin signals. This is of particular importance for the measurement of oxCCO as there is historical controversy over its independence. Furthermore, the results suggest that using broadband spectra to solve for the haemoglobin signals without the oxCCO component could be erroneous.

12.1.2 Biomarker Analysis

The system has been used successfully in the NICU on fragile infants suffering from HIE. This is, to my knowledge, the first time that oxCCO has been monitored with broadband NIRS on a neonatal population. The system was designed carefully to ensure that it can perform in the challenging NICU environment and collect data from neonates safely and comfortably for any length of time. However, the system has limitations and the biggest challenge faced was the recording of data suitable for SRS calculation of TOI.

Due to the nature of the experiment (i.e. observational without any stimulus) and the NIRS data (i.e. changes in concentration from an arbitrary baseline) it is not trivial to analyse the data to recover meaningful information. Therefore in this thesis, three different data analysis methods have been suggested and trialled. Two methods use spontaneous hypoxic events as stimuli and the other method applies multivariate statistical analysis over long periods of stable physiology to assess the link between the systemic and cerebral changes over time. All three methods have found a link with the oxCCO signal and injury. These tools have been written as code and so can be applied to further data and also for other studies.

The analysis has found some interesting results, however, the number of patients studied is low so conclusions are speculative. In general it was found that HHb and HbO_2 respond predictably despite different levels of brain injury. There is little difference between the haemoglobin response to arterial desaturation in mild and severe injury, which suggests that the vascular response is not affected by injury level. This has one exception from the CCA analysis where the strength of the HbO_2 dependency on systemic physiology had a positive linear relationship with injury. The oxCCO response is less understood but appears to be injury dependent:

- A strong linear oxCCO relationship with cerebral oxygenation (from HbD) during hypoxia was correlated with injury
- A larger decrease in oxCCO during hypoxia was observed in the severe brain injury
- A strong relationship between oxCCO and systemic physiology predicted severe injury

The results are not conclusive but, with the exception of HbO_2 in the CCA analysis, only oxCCO has significant relationships with injury. This is interesting but it is not surprising that relationships with injury were not found in the haemoglobins in general; as discussed in section 3.3.2, HIE has been studied with NIRS for the past 25 years and there has not been any strong evidence that changes in HbO_2 or HHb are related to injury. Therefore, the result that the metabolic marker, oxCCO, does have an injury-dependent response is promising. This suggests that, if the experimental paradigm and analysis are optimised, then CCO could be an early marker of brain injury in HIE and, potentially, other forms of brain injury.

Chapters 8 and 9 present slightly different conclusions. In the analysis of the magnitude of change across all desaturation events per baby (Chapter 8), there was a significant relationship between injury and a strong relationship between HbD and oxCCO; in the analysis of the dynamics of the hypoxia, the decrease in the oxCCO signals was larger in infants with more severe injury. There was no relationship found between the magnitude of the oxCCO change and injury found in Chapter 8. This is likely caused by the different selection processes; in Chapter 9 the hypoxic events were chosen to begin at normoxia and to decrease more than 10%. Starting from normoxia increases homogeneity amongst the events and the larger (10%) decrease is more likely to provoke a change in oxCCO.

The system and data recorded have also been used by medical doctors to answer other questions regarding the cerebral changes occurring during HIE. Although not described in this thesis, the CYRIL

data has been used to answer medical questions regarding the cerebral changes during stroke [219], rewarming after TH [258] and seizures [256].

12.2 The Future of CCO in the NICU

Thus far, NIRS, and in particular NIRS-measured oxCCO, has remained a research tool rather than a clinical one. There are many hurdles to overcome before oxCCO becomes a routine measurement, some of which are described in Chapter 11. In summary, the hardware needs to be easy to use (both in terms of the software and the application of the optodes), compact, and robust; the oxCCO signal needs to be better understood, particularly in the healthy newborn; and the experimental method needs to take into account the limitations of a differential measurement.

NIRS is relatively inexpensive so the cost is not an obstacle and also the signals are quite simple to understand, especially when compared to EEG, which have become routine measurements in the NICU. Therefore, providing this future work is undertaken, the broadband NIRS measurement of oxCCO has strong potential as a cerebral monitor in the NICU, with applications beyond HIE, such as in stroke or seizure monitoring.

12.3 Impact

Brain monitoring is a very important tool in critical intensive care as it can help guide diagnosis and direct treatment. In particular, in neonatal intensive care, the brain is one of the most important organs to protect because it is also the most vulnerable. An incremental improvement in clinical care could make a huge impact on the patient's quality of life, or in extreme cases, their chance of survival. Monitoring brain metabolism continuously at the cotside could provide a unique view into the cerebral well-being. The broadband NIRS measurement of oxCCO has the potential to provide this insight. This thesis has demonstrated that the use of a broadband NIRS device is feasible within the NICU, and further, that the oxCCO signal is linked to brain injury severity. CCO has promise as a biomarker of brain health after HI injury, and could improve the lives of many babies and their families. There is more research to be done but this body of work has shown that changes in oxCCO from broadband NIRS is a clinical measurement with a hopeful future.

Bibliography

[1] N. L. Strominger, R. J. Demarest, and L. B. Laemle, "Noback's Human Nervous System," *Humana Press*, vol. 7, 2012.

[2] G. Greisen, "Autoregulation of cerebral blood flow in newborn babies," *Early Human Development*, vol. 81, no. 5, pp. 423–428, 2005.

[3] L. Srinivasan and M. A. Rutherford, "MRI of the newborn brain," *Paediatrics and Child Health*, vol. 18, pp. 183–195, 2008.

[4] R. D. Sanders, H. J. Manning, N. J. Robertson, D. Ma, A. D. Edwards, H. Hagberg, and M. Maze, "Preconditioning and Postinsult Therapies for Perinatal HypoxicIschemic Injury at Term," *Anesthesiology*, vol. 113, no. 7, pp. 233–249, 2010.

[5] D. M. Murray, G. B. Boylan, C. A. Ryan, and S. Connolly, "Early EEG findings in hypoxic-ischemic encephalopathy predict outcomes at 2 years.," *Pediatrics*, vol. 124, no. 3, pp. 459–67, 2009.

[6] F. Scholkmann, S. Kleiser, A. J. Metz, R. Zimmermann, J. Mata Pavia, U. Wolf, and M. Wolf, "A review on continuous wave functional near-infrared spectroscopy and imaging instrumentation and methodology.," *NeuroImage*, vol. 85 Pt 1, pp. 6–27, 2014.

[7] M. Cope, "The application of near infrared spectroscopy to non invasive monitoring of cerebral oxygenation in the newborn infant," *PhD Thesis*, 1991.

[8] M. A. Franceschini, D. A. Boas, A. Zourabian, S. G. Diamond, S. Nadgir, D. W. Lin, J. B. Moore, and S. Fantini, "Near-infrared spiroximetry: noninvasive measurements of venous saturation in piglets and human subjects," *J Appl Physiol*, vol. 92, no. 1, pp. 372–384, 2002.

[9] M. Lindkvist, G. Granåsen, and C. Grönlund, "Coherent derivation of equations for differential spectroscopy and spatially resolved spectroscopy: an undergraduate tutorial," *Spectroscopy Letters*, vol. 7010, no. January 2016, 2013.

[10] F. Scholkmann, "Shedding light on human brain activity," *PhD Thesis*, 2014.

[11] M. Kozberg and B. Chen, "Resolving the transition from negative to positive blood oxygen level-dependent responses in the developing brain," *PNAS*, vol. 110, no. 11, pp. 4380–4385, 2013.

[12] A. Bainbridge, I. Tachtsidis, S. Faulkner, D. Price, T. Zhu, E. Baer, K. D. Broad, D. L. Thomas, E. B. Cady, N. J. Robertson, and X. Golay, "Brain mitochondrial oxidative metabolism during and after cerebral hypoxia-ischemia studied by simultaneous phosphorus magnetic-resonance and broadband near-infrared spectroscopy.," *NeuroImage*, vol. http://dx.doi.org/10.1016/j.neuroimage.2013.08.016, pp. 1–11, 2013.

[13] D. Arifler, T. Zhu, S. Madaan, and I. Tachtsidis, "Optimal wavelength combinations for near-infrared spectroscopic monitoring of changes in brain tissue hemoglobin and cytochrome c oxidase concentrations," *Biomedical Optics Express*, vol. 6, no. 3, p. 933, 2015.

[14] J. E. Brazy and D. V. Lewis, "Changes in cerebral blood volume and cytochrome aa3 during hypertensive peaks in preterm infants.," *The Journal of pediatrics*, vol. 108, no. 6, pp. 983–987, 1986.

[15] J. E. Brazy, "Effects of crying on cerebral blood volume and cytochrome aa3.," *The Journal of pediatrics*, vol. 112, pp. 457–461, 1988.

[16] J. Brazy, D. Lewis, M. Mitnick, and F. vander Vliet, "Noninvasive monitoring of cerebral oxygenation in preterm infants: preliminary observations," *Pediatrics*, vol. 75, no. 2, pp. 217–225, 1985.

[17] J. S. Wyatt, M. Cope, D. T. Delpy, S. Wray, and E. O. Reynolds, "Quantification of cerebral oxygenation and haemodynamics in sick newborn infants by near infrared spectrophotometry.," *Lancet*, vol. 2, no. 8515, pp. 1063–1066, 1986.

[18] W. J. Greeley, F. H. Kern, R. M. Ungerleider, J. L. d. Boyd, T. Quill, L. R. Smith, B. Baldwin, and J. G. Reves, "The effect of hypothermic cardiopulmonary bypass and total circulatory arrest on cerebral metabolism in neonates, infants, and children," *J Thorac Cardiovasc Surg*, vol. 101, no. 5, pp. 783–794, 1991.

[19] D. S. Bacon, M. S. Afifi, J. a. Griebel, and E. M. Camporesi, "Cerebrocortical oxygenation and ventilatory response during sustained hypoxia.," *Respiration physiology*, vol. 80, no. 2-3, pp. 245–57, 1990.

[20] N. B. Hampson, E. M. Camporesi, B. W. Stolp, R. E. Moon, J. E. Shook, J. A. Griebel, and C. A. Piantadosi, "Cerebral oxygen availability by NIR spectroscopy during transient hypoxia in humans.," *J Appl Physiol*, vol. 69, no. 3, pp. 907–913, 1990.

[21] F. van Bel, C. A. Dorrepaal, M. J. Benders, P. E. Zeeuwe, M. van de Bor, and H. M. Berger, "Changes in cerebral hemodynamics and oxygenation in the first 24 hours after birth asphyxia.," *Pediatrics*, vol. 92, no. 3, pp. 365–372, 1993.

[22] M. J. Benders, C. A. Dorrepaal, M. van de Bor, and F. van Bel, "Acute effects of indomethacin on cerebral hemodynamics and oxygenation," 1995.

[23] L. Skov and G. Greisen, "Apparent cerebral cytochrome aa 3 reduction during cardiopulmonary bypass in hypoxaemic children with congenital heart disease. A critical analysis of in vivo near-infrared spectrophotometric data," *Physiological Measurement*, vol. 15, no. 4, p. 447, 1994.

[24] O. Pryds, G. Greisen, L. L. Skov, and B. Friis-Hansen, "Carbon dioxide-related changes in cerebral blood volume and cerebral blood flow in mechanically ventilated preterm neonates: comparison of near infrared spectrophotometry and 133Xenon clearance.," *Pediatric research*, vol. 27, no. 5, pp. 445–9, 1990.

[25] A. Edwards, J. Wyatt, and C. Richardson, "Effects of indomethacin on cerebral haemodynamics in very preterm infants," *The Lancet*, vol. 335, pp. 1491–1495, 1990.

[26] D. C. McCormick, a. D. Edwards, G. C. Brown, J. S. Wyatt, a. Potter, M. Cope, D. T. Delpy, and E. O. Reynolds, "Effect of indomethacin on cerebral oxidized cytochrome oxidase in preterm infants.," *Pediatric research*, vol. 33, no. 6, pp. 603–608, 1993.

[27] H. U. Bucher, M. Wolf, M. Keel, K. von Siebenthal, and G. Duc, "Effect of aminophylline on cerebral haemodynamics and oxidative metabolism in premature infants," *European Journal of Pediatrics*, vol. 153, pp. 123–128, 1994.

[28] P. Casaer, K. von Siebenthal, A. van der Vlugt, L. Lagae, and H. Devlieger, "Cytochrome aa3 and intracranial pressure in newborn infants; a near infrared spectroscopy study.," *Neuropediatrics*, vol. 23, no. 2, p. 111, 1992.

[29] K. D. Liem, J. C. W. Hopman, B. Oeseburg, a. F. J. De Haan, and L. a. a. Kollée, "The effect of blood transfusion and haemodilution on cerebral oxygenation and haemodynamics in newborn infants investigated by near infrared spectrophotometry," *European Journal of Pediatrics*, vol. 156, no. 4, pp. 305–310, 1997.

[30] K. D. Liem, J. C. W. Hopman, L. a. a. Kolle, and B. Oeseburg, "Effects of repeated indomethacin administration on cerebral oxygenation and haemodynamics in preterm infants: combined near infrared spectropho- tometry and Doppler ultrasound study," *European Journal of Pediatrics*, vol. 153, no. 7, pp. 504–509, 1994.

[31] G. Grubhofer, W. Tonninger, P. Keznickl, P. Skyllouriotis, M. Ehrlich, M. Hiesmayr, and a. Lassnigg, "A comparison of the monitors INVOS 3100 and NIRO 500 in detecting changes in cerebral oxygenation.," *Acta anaesthesiologica Scandinavica*, vol. 43, no. 4, pp. 470–475, 1999.

[32] P. D. Adelson, E. Nemoto, M. Scheuer, M. Painter, J. Morgan, and H. Yonas, "Noninvasive Continuous Monitoring of Cerebral Oxygenation Periictally Using Near-Infrared Spectroscopy: A Preliminary Report," *Epilepsia*, vol. 40, no. 11, pp. 1484–1489, 1999.

[33] B. Urlesberger, G. Pichler, E. Gradnitzer, F. Reiterer, G. Zobel, and W. Müller, "Changes in cerebral blood volume and cerebral oxygenation during periodic breathing in term infants," *Neuropediatrics*, vol. 31, no. 2, pp. 75–81, 2000.

[34] J. G. LeBlanc, D. Blackstock, a. J. Macnab, F. Gagnon, R. Gagnon, J. Russell, and T. Ring, "Effects of propofol on cerebral oxygenation during cardiopulmonary bypass in children.," *Canadian journal of anaesthesia = Journal canadien d'anesthésie*, vol. 47, no. 11, pp. 1082–9, 2000.

[35] C. Kohlhauser, G. Bernert, M. Hermon, C. Popow, R. Seidl, and a. Pollak, "Effects of endotracheal suctioning in high-frequency oscillatory and conventionally ventilated low birth weight neonates on cerebral hemodynamics observed by near infrared spectroscopy (NIRS)," *Pediatric Pulmonology*, vol. 29, no. 4, pp. 270–275, 2000.

[36] J. S. Soul, E. Eichenwald, G. Walter, J. J. Volpe, and A. J. D. U. Plessis, "CSF Removal in Infantile Posthemorrhagic Hydrocephalus Results in Significant Improvement in Cerebral Hemodynamics," *Pediatric Research*, vol. 55, no. 5, pp. 872–876, 2004.

[37] G. Nollert, M. Nagashima, J. Bucerius, T. Shin'oka, and R. a. Jonas, "Oxygenation strategy and neurologic damage after deep hypothermic circulatory arrest. I. Gaseous microemboli," *Journal of Thoracic and Cardiovascular Surgery*, vol. 117, no. 6, pp. 1166–1171, 1999.

[38] A. J. Du Plessis, J. Newburger, R. a. Jonas, P. Hickey, H. Naruse, M. Tsuji, A. Walsh, G. Walter, D. Wypij, and J. J. Volpe, "Cerebral oxygen supply and utilization during infant cardiac surgery," *Annals of Neurology*, vol. 37, no. 4, pp. 488–497, 1995.

[39] P. Zaramella, F. Freato, A. Amigoni, S. Salvadori, P. Marangoni, A. Suppjei, B. Schiavo, and L. Chiandetti, "Brain Auditory Activation Measured by Near-Infrared Spectroscopy (NIRS) in Neonates," *Pediatric Research*, vol. 49, no. 2, pp. 213–219, 2001.

[40] A. Azakie, J. Muse, M. Gardner, K. L. Skidmore, S. P. Miller, T. R. Karl, and P. S. McQuillen, "Cerebral oxygen balance is impaired during repair of aortic coarctation in infants and children," *The Journal of thoracic and cardiovascular surgery*, vol. 130, no. 3, pp. 830–836, 2005.

[41] N. Nagdyman, T. P. K. Fleck, P. Ewert, M. Redlin, and P. E. Lange, "Cerebral oxygenation measured by near-infrared spectroscopy during circulatory arrest and cardiopulmonary resuscitation," *British Journal of Anaesthesia*, vol. 91, no. 3, pp. 438–442, 2003.

[42] C. Dani, G. Bertini, M. F. Reali, M. Tronchin, L. Wiechmann, E. Martelli, and F. F. Rubaltelli, "Brain hemodynamic changes in preterm infants after maintenance dose caffeine and aminophylline treatment.," *Biology of the neonate*, vol. 78, no. 1, pp. 27–32, 2000.

[43] A. McGown, H. Makker, C. Elwell, P. Al Rawi, a. Valipour, and S. Spiro, "Measurement of changes in cytochrome oxidase redox state during obstructive sleep apnea using near-infrared spectroscopy," *SLEEP*, vol. 26, no. 6, pp. 1–7, 2003.

[44] E. McNeill, R. E. Gagnon, J. E. Potts, J. A. Yeung-Lai-Wah, C. R. Kerr, and S. Sanatani, "Cerebral oxygenation during defibrillator threshold testing of implantable cardioverter defibrillators.," *Pacing and clinical electrophysiology : PACE*, vol. 28, no. 6, pp. 528–33, 2005.

[45] I. Tachtsidis, C. Cooper, A. D. McGown, H. Makker, D. T. Delpy, and C. E. Elwell, "Changes in cerebral total haemoglobin volume and cytochrome oxidase redox state during deep apnoeas in patients with obstructive sleep apnoea," *Biomedical Optics Express*, vol. OSA Biomed Meeting, pp. 1–3, 2004.

[46] I. Tachtsidis, M. Tisdall, T. S. Leung, C. E. Cooper, D. T. Delpy, M. Smith, and C. E. Elwell, "Investigation of in vivo measurement of cerebral cytochrome-c-oxidase redox changes using near-infrared spectroscopy in patients with orthostatic hypotension.," *Physiological measurement*, vol. 28, no. 2, pp. 199–211, 2007.

[47] M. Wolf, M. Keel, V. Dietz, K. von Siebenthal, H. Bucher, and O. Baenziger, "Do slow and small oxygen changes affect the cerebral cytochrome oxidase redox state measurement by near-infrared spectroscopy?," *Adv Exp Med Biol*, vol. 578, pp. 245–250, 2006.

[48] S. J. Matcher, C. E. Elwell, C. E. Cooper, M. Cope, and D. T. Delpy, "Performance comparison of several published tissue near-infrared spectroscopy algorithms.," *Analytical biochemistry*, vol. 227, pp. 54–68, 1995.

[49] C. E. Cooper and R. Springett, "Measurement of cytochrome oxidase and mitochondrial energetics by near-infrared spectroscopy.," *Philosophical transactions of the Royal Society of London. Series B, Biological sciences*, vol. 352, no. 1354, pp. 669–76, 1997.

[50] M. M. Tisdall, I. Tachtsidis, T. S. Leung, C. E. Elwell, and M. Smith, "Near-infrared spectroscopic quantification of changes in the concentration of oxidized cytochrome c oxidase in the healthy human brain during hypoxemia.," *Journal of biomedical optics*, vol. 12, no. 2, p. 024002, 2007.

[51] I. Tachtsidis, M. M. Tisdall, C. Pritchard, T. S. Leung, A. Ghosh, C. E. Elwell, and M. Smith, "Analysis of the changes in the oxidation of brain tissue cytochrome-c-oxidase in traumatic brain injury patients during hypercapnoea," *Advances in experimental medicine and biology*, vol. 701, pp. 9–14, 2011.

[52] M. M. Tisdall, I. Tachtsidis, T. S. Leung, C. E. Elwell, and M. Smith, "Increase in cerebral aerobic metabolism by normobaric hyperoxia after traumatic brain injury.," *Journal of neurosurgery*, vol. 109, no. 3, pp. 424–32, 2008.

[53] M. M. Tisdall, I. Tachtsidis, T. S. Leung, C. E. Elwell, and M. Smith, "Changes in the attenuation of near infrared spectra by the healthy adult brain during hypoxaemia cannot be accounted for solely by changes in the concentrations of oxy- and deoxy-haemoglobin.," *Advances in experimental medicine and biology*, vol. 614, pp. 217–25, 2008.

[54] G. Bale, S. Mitra, J. Meek, N. Robertson, and I. Tachtsidis, "A new broadband near-infrared spectroscopy system for in-vivo measurements of cerebral cytochrome-c-oxidase changes in neonatal brain injury.," *Biomedical optics express*, vol. 5, no. 10, pp. 3450–66, 2014.

[55] H. Obrig, M. Neufang, R. Wenzel, M. Kohl, J. Steinbrink, K. Einhäupl, and a. Villringer, "Spontaneous low frequency oscillations of cerebral hemodynamics and metabolism in human adults.," *NeuroImage*, vol. 12, no. 6, pp. 623–39, 2000.

[56] H. R. Heekeren, M. Kohl, H. Obrig, R. Wenzel, W. von Pannwitz, S. J. Matcher, U. Dirnagl, C. E. Cooper, and a. Villringer, "Noninvasive assessment of changes in cytochrome-c oxidase oxidation in human subjects during visual stimulation.," *Journal of cerebral blood flow and metabolism : official journal of the International Society of Cerebral Blood Flow and Metabolism*, vol. 19, no. 6, pp. 592–603, 1999.

[57] K. Uludag, M. Kohl, J. Steinbrink, H. Obrig, and a. Villringer, "Cross talk in the Lambert-Beer calculation for near-infrared wavelengths estimated by Monte Carlo simulations.," *Journal of biomedical optics*, vol. 7, no. 1, pp. 51–9, 2002.

[58] P. Wobst, R. Wenzel, M. Kohl, H. Obrig, and a. Villringer, "Linear aspects of changes in deoxygenated hemoglobin concentration and cytochrome oxidase oxidation during brain activation.," *NeuroImage*, vol. 13, no. 3, pp. 520–530, 2001.

[59] A. Ghosh, I. Tachtsidis, C. Kolyva, C. E. Cooper, M. Smith, and C. E. Elwell, "Use of a hybrid optical spectrometer for the measurement of changes in oxidized cytochrome c oxidase concentration and tissue scattering during functional activation.," *Advances in experimental medicine and biology*, vol. 737, pp. 119–24, 2012.

[60] C. Kolyva, A. Ghosh, I. Tachtsidis, D. Highton, C. E. Cooper, M. Smith, and C. E. Elwell, "Cytochrome c oxidase response to changes in cerebral oxygen delivery in the adult brain shows higher brain-specificity than haemoglobin," *NeuroImage*, vol. 85, pp. 234–244, 2014.

[61] C. Kolyva, I. Tachtsidis, A. Ghosh, T. Moroz, C. E. Cooper, M. Smith, and C. E. Elwell, "Systematic investigation of changes in oxidized cerebral cytochrome c oxidase concentration during frontal lobe activation in healthy adults.," *Biomedical optics express*, vol. 3, no. 10, pp. 2550–66, 2012.

[62] I. Tachtsidis, L. Gao, T. S. Leung, M. Kohl-Bareis, C. E. Cooper, and C. E. Elwell, "A hybrid multi-distance phase and broadband spatially resolved spectrometer and algorithm for resolving absolute concentrations of chromophores in the near-infrared light spectrum.," *Advances in experimental medicine and biology*, vol. 662, pp. 169–75, 2010.

[63] P. Phan, D. Highton, S. Brigadoi, I. Tachtsidis, M. Smith, and C. Elwell, "Spatial Distribution Of Changes In Oxidised Cytochrome C Oxidase During Visual Stimulation Using Broadband Near Infrared Spectroscopy Imaging," *Adv Exp Med Biol*, In press.

[64] S. Mahony, "Exploration of the Implementation of Combined Magnetic Resonance and Optical Methods for Assessment of Brain Metabolism and Haemodynamics," *MSc Thesis*, 2011.

[65] R. Springett, J. Newman, M. Cope, and D. T. Delpy, "Oxygen dependency and precision of cytochrome oxidase signal from full spectral NIRS of the piglet brain.," *American journal of physiology. Heart and circulatory physiology*, vol. 279, no. 5, pp. H2202–9, 2000.

[66] M. Tsuji, H. Naruse, J. Volpe, and D. Holtzman, "Reduction of cytochrome aa3 measured by near-infrared spectroscopy predicts cerebral energy loss in hypoxic piglets.," *Pediatric research*, vol. 37, no. 3, pp. 253–259, 1995.

[67] A. S. A. Zanelli, C. Editor, and T. Rosenkrantz, "Hypoxic Ischemic Encephalopathy Treatment & Management," *http://emedicine.medscape.com/article/973501-treatment-d7*, no. 2, pp. 1–9, 2016.

[68] Y. Fukui, Y. Ajichi, and E. Okada, "Monte Carlo Prediction of Near-Infrared Light Propagation in Realistic Adult and Neonatal Head Models," *Applied Optics*, vol. 42, no. 16, p. 2881, 2003.

[69] A. Edwards, C. Richardson, and M. Cope, "Cotside measurement of cerebral blood flow in ill newborn infants by near infrared spectroscopy," *The Lancet*, pp. 1977–1978, 1988.

[70] A. D. Edwards, G. C. Brown, M. Cope, J. S. Wyatt, D. C. McCormick, S. C. Roth, D. T. Delpy, and E. O. Reynolds, "Quantification of concentration changes in neonatal human cerebral oxidized cytochrome oxidase.," *Journal of applied physiology*, vol. 71, no. 5, pp. 1907–1913, 1991.

[71] J. Meek, C. Elwell, D. C. McCormick, A. D. Edwards, J. P. Townsend, A. L. Stewart, and J. S. Wyatt, "Abnormal cerebral haemodynamics in perinatally asphyxiated neonates related to outcome," *Arch Dis Child Fetal Neonatal Ed*, vol. 81, pp. 110–115, 1999.

[72] F. Y. Wong, T. S. Leung, T. Austin, M. Wilkinson, J. H. Meek, J. S. Wyatt, and A. M. Walker, "Impaired autoregulation in preterm infants identified by using spatially resolved spectroscopy.," *Pediatrics*, vol. 121, no. 3, pp. e604–11, 2008.

[73] J. J. Wyndaele, *Neuroanatomy: an illustrated colour text.*, vol. 49. 2011.

[74] N. A. Jessen, A. S. F. Munk, I. Lundgaard, and M. Nedergaard, "The Glymphatic System: A Beginner's Guide," *Neurochemical Research*, vol. 40, no. 12, pp. 2583–2599, 2015.

[75] N. J. Abbott, A. A. K. Patabendige, D. E. M. Dolman, S. R. Yusof, and D. J. Begley, "Structure and function of the blood-brain barrier," 2010.

[76] N. R. Saunders, S. A. Liddelow, and K. M. Dziegielewska, "Barrier mechanisms in the developing brain," *Frontiers in Pharmacology*, vol. 3, no. 46, pp. 1–18, 2012.

[77] R. Aaslid, K. F. Lindegaard, W. Sorteberg, and H. Nornes, "Cerebral autoregulation dynamics in humans," *Stroke; a journal of cerebral circulation*, vol. 20, no. 1, pp. 45–52, 1989.

[78] A. van Beek, J. Claassen, M. Olde Rikkert, and R. Jansen, "Cerebral autoregulation: an overview of current concepts and methodology with special focus on the elderly.," *Journal of cerebral blood flow and metabolism*, vol. 28, no. 6, pp. 1071–1085, 2008.

[79] P. C. Johnson, "Brief Review Autoregulation of Blood Flow," *Circulation Research*, pp. 483–495, 1986.

[80] L. Tyszczuk, J. Meek, C. Elwell, and J. S. Wyatt, "Cerebral Blood Flow Is Independent of Mean Arterial Blood Pressure in Preterm Infants Undergoing Intensive Care," *Pediatrics*, vol. 102, no. 2, pp. 337–341, 1998.

[81] S. S. Kety and C. F. Schmidt, "the Effects of Altered Arterial Tensions of Carbon Dioxide and Oxygen on Cerebral Blood Flow and Cerebral Oxygen Consumption of Normal Young Men 1," *Journal of Clinical Investigation*, vol. 27, no. 4, pp. 484–492, 1948.

[82] H. a. Kontos, a. J. Raper, and J. L. Patterson, "Analysis of vasoactivity of local pH, PCO2 and bicarbonate on pial vessels.," *Stroke; a journal of cerebral circulation*, vol. 8, no. 3, pp. 358–360, 1977.

[83] K. Masamoto and K. Tanishita, "Oxygen transport in brain tissue.," *Journal of biomechanical engineering*, vol. 131, no. 7, p. 074002, 2009.

[84] H. Taguchi, D. D. Heistad, T. Kitazono, and F. M. Faraci, "ATP-sensitive K+ channels mediate dilatation of cerebral arterioles during hypoxia.," *Circulation research*, vol. 74, no. 5, pp. 1005–8, 1994.

[85] E. V. Golanov and D. J. Reis, "A role for K(ATP)/+-channels in mediating the elevations of cerebral blood flow and arterial pressure by hypoxic stimulation of oxygen-sensitive neurons of rostral ventrolateral medulla," *Brain Research*, vol. 827, no. 1-2, pp. 210–214, 1999.

[86] K. M. Tichauer, D. Y. L. Wong, J. a. Hadway, R. J. Rylett, T. Y. Lee, and K. S. Lawrence, "Assessing the severity of perinatal hypoxia-ischemia in piglets using near-infrared spectroscopy to measure the cerebral metabolic rate of oxygen," *Pediatric Research*, vol. 65, no. 3, pp. 301–306, 2009.

[87] R. W. Cooke and L. J. Abernethy, "Cranial MRI and school performance in very low birth weight infants in adolescence," *Arch Dis Child Fetal Neonatal Ed*, vol. 81, pp. 116–121, 1999.

[88] P. Ballabh, A. Braun, and M. Nedergaard, "Anatomic analysis of blood vessels in germinal matrix, cerebral cortex, and white matter in developing infants.," *Pediatric research*, vol. 56, no. 1, pp. 117–24, 2004.

[89] N. N. Finer, C. M. Robertson, R. T. Richards, L. E. Pinnell, and K. L. Peters, "Hypoxic-ischemic encephalopathy in term neonates: perinatal factors and outcome.," *The Journal of pediatrics*, vol. 98, pp. 112–117, 1981.

[90] J. Smith, L. Wells, and K. Dodd, "The continuing fall in incidence of hypoxic-ischaemic encephalopathy in term infants.," *BJOG : an international journal of obstetrics and gynaecology*, vol. 107, no. 4, pp. 461–6, 2000.

[91] A. Fatemi, W. Mary Ann, and J. Michael V, "Hypoxic Ischemic Encephalopathy in the Term Infant," *Clinical Perinatology*, vol. 36, no. 4, pp. 835–vii, 2009.

[92] J. E. Lawn, M. Kinney, A. C. C. Lee, M. Chopra, F. Donnay, V. K. Paul, Z. A. Bhutta, M. Bateman, and G. L. Darmstadt, "Reducing intrapartum-related deaths and disability: Can the health system deliver?," in *International Journal of Gynecology and Obstetrics*, vol. 107, pp. 1–11, 2009.

[93] K. Himmelmann and G. Hagberg, "The changing panorama of cerebral palsy in Sweden. IX. Prevalence and origin in the birthyear period 19951998," *Acta Paediatrica*, vol. 94, pp. 287–294, 2005.

[94] A. J. du Plessis and J. J. Volpe, "Perinatal brain injury in the preterm and term newborn.," *Current opinion in neurology*, vol. 15, no. 2, pp. 151–7, 2002.

[95] J. P. Cloherty and A. R. Start, "Manual of Neonatal Care," *Lipponcott-Raven*, 1998.

[96] J. J. Volpe, "Brain injury in the premature infant: Neuropathology, clinical aspects, and pathogenesis," *Mental Retardation and Developmental Disabilities Research Reviews*, vol. 3, no. 1, pp. 3–12, 1997.

[97] L. S. De Vries and F. Groenendaal, "Patterns of neonatal hypoxic-ischaemic brain injury," *Neuroradiology*, vol. 52, no. 6, pp. 555–566, 2010.

[98] M. Johnston, "Hypoxic-Ischemic Encephalopathy.," *Current treatment options in neurology*, vol. 2, no. 2, pp. 109–116, 2000.

[99] D. M. Ferriero and S. L. Bonifacio, "The search for the elusive biomarkers of neonatal brain injury," *J Pediatr*, vol. 163, no. 3, pp. 438–440, 2014.

[100] A. D. Edwards, P. Brocklehurst, A. J. Gunn, H. Halliday, E. Juszczak, M. Levene, B. Strohm, M. Thoresen, A. Whitelaw, and D. Azzopardi, "Neurological outcomes at 18 months of age after moderate hypothermia for perinatal hypoxic ischaemic encephalopathy: synthesis and meta-analysis of trial data.," *BMJ (Clinical research ed.)*, vol. 340, p. c363, 2010.

[101] P. P. Drury, L. Bennet, and A. J. Gunn, "Mechanisms of hypothermic neuroprotection," *Seminars in Fetal and Neonatal Medicine*, vol. 15, no. 5, pp. 287–292, 2010.

[102] P. Logitharajah, M. a. Rutherford, and F. M. Cowan, "Hypoxic-ischemic encephalopathy in preterm infants: antecedent factors, brain imaging, and outcome.," *Pediatric research*, vol. 66, no. 2, pp. 222–9, 2009.

[103] A. J. Barkovich, "MR imaging of the neonatal brain.," *Neuroimaging clinics of North America*, vol. 16, no. 1, pp. 117–35, viii–ix, 2006.

[104] S. Thayyil, M. Chandrasekaran, A. Taylor, A. Bainbridge, E. B. Cady, W. K. K. Chong, S. Murad, R. Z. Omar, and N. J. Robertson, "Cerebral magnetic resonance biomarkers in neonatal encephalopathy: a meta-analysis.," *Pediatrics*, vol. 125, no. 2, pp. e382–e395, 2010.

[105] G. Brown, C. Clark, and T. Liu, "Measurement of cerebral perfusion with arterial spin labeling: Part 2. Applications," *Journal of the International Neuropsychology*, vol. 13, no. 3, pp. 526–538, 2007.

[106] R. M. Pressler, G. B. Boylan, M. Morton, C. D. Binnie, and J. M. Rennie, "Early serial EEG in hypoxic ischaemic encephalopathy," *Clinical Neurophysiology*, vol. 112, pp. 31–37, 2001.

[107] R. E. Spitzmiller, T. Phillips, J. Meinzen-Derr, and S. B. Hoath, "Amplitude-integrated EEG is useful in predicting neurodevelopmental outcome in full-term infants with hypoxic-ischemic encephalopathy: a meta-analysis.," *Journal of child neurology*, vol. 22, no. 9, pp. 1069–78, 2007.

[108] C. P. Chao, C. G. Zaleski, and A. C. Patton, "CENTRAL NERVOUS SYSTEM : STATE OF THE ART Neonatal Hypoxic- athy : Multimodality Imaging Findings 1," *Radiographics*, vol. 32224, pp. 159–173, 2006.

[109] J. Liu, H. Y. Cao, X. H. Huang, and Q. Wang, "The pattern and early diagnostic value of doppler ultrasound for neonatal hypoxic-ischemic encephalopathy," *Journal of Tropical Pediatrics*, vol. 53, no. 5, pp. 351–354, 2007.

[110] F. Jobsis, "Noninvasive, infrared monitoring of cerebral and myocardial oxygen sufficiency and circulatory parameters," *Science*, vol. 198, no. 4323, pp. 1264–1267, 1977.

[111] B. T. Doumas, T. W. Wu, and B. Jendrzejczak, "Delta bilirubin: absorption spectra, molar absorptivity, and reactivity in the diazo reaction.," *Clinical Chemistry*, vol. 33, no. 6, pp. 769–774, 1987.

[112] S. R. Arridge, M. Cope, and D. T. Delpy, "The theoretical basis for the determination of optical pathlengths in tissue: temporal and frequency analysis.," *Physics in medicine and biology*, vol. 37, no. 7, pp. 1531–60, 1992.

[113] D. Delpy and M. Cope, "Estimation of optical pathlength through tissue from direct time of flight measurement," *Physics in medicine and biology*, vol. 33, no. 12, pp. 1433–1442, 1988.

[114] A. Duncan, J. H. Meek, M. Clemence, C. E. Elwell, L. Tyszczuk, M. Cope, and D. T. Delpy, "Optical pathlength measurements on adult head, calf and forearm and the head of the newborn infant using phase resolved optical spectroscopy.," *Physics in medicine and biology*, vol. 40, no. 2, pp. 295–304, 1995.

[115] M. Essenpreis, C. E. Elwell, M. Cope, P. van der Zee, S. R. Arridge, and D. T. Delpy, "Spectral dependence of temporal point spread functions in human tissues.," *Applied optics*, vol. 32, no. 4, pp. 418–425, 1993.

[116] R. C. Haskell, L. O. Svaasand, T.-T. Tsay, T.-C. Feng, M. S. McAdams, and B. J. Tromberg, "Boundary conditions for the diffusion equation in radiative transfer," *J Opt Soc Am A*, vol. 11, no. 10, pp. 2727–2741, 1994.

[117] S. Suzuki, S. Takasaki, T. Ozaki, and Y. Kobayashi, "A Tissue Oxygenation Monitor using NIR Spatially Resolved Spectroscopy," *SPIE Proceedings*, vol. 3597, pp. 582–592, 1999.

[118] F. Scholkmann, A. J. Metz, and M. Wolf, "Measuring tissue hemodynamics and oxygenation by continuous-wave functional near-infrared spectroscopy - how robust are the different calculation methods against movement artifacts?," *Physiological Measurement*, vol. 35, no. 4, pp. 717–734, 2014.

[119] A. Kassab, J. L. Lan, P. Vannasing, and M. Sawan, "Functional near-infrared spectroscopy caps for brain activity monitoring : a review," *Applied Optics*, vol. 54, no. 3, pp. 576–586, 2015.

[120] B. Khan, C. Wildey, R. Francis, F. Tian, M. R. Delgado, H. Liu, D. Macfarlane, and G. Alexandrakis, "Improving optical contact for functional nearinfrared brain spectroscopy and imaging with brush optodes.," *Biomedical optics express*, vol. 3, no. 5, pp. 878–898, 2012.

[121] G. Strangman, D. A. Boas, and J. P. Sutton, "Non-invasive neuroimaging using near-infrared light," *Biological Psychiatry*, vol. 52, no. 7, pp. 679–693, 2002.

[122] E. A. M. Frost, "Cerebral oximetry: A replacement for pulse oximetry?," 2012.

[123] M. Diop, K. M. Tichauer, J. T. Elliott, M. Migueis, T.-Y. Lee, and K. St Lawrence, "Comparison of time-resolved and continuous-wave near-infrared techniques for measuring cerebral blood flow in piglets.," *Journal of biomedical optics*, vol. 15, no. 5, p. 057004, 2015.

[124] M. Wolf and G. Greisen, "Advances in near-infrared spectroscopy to study the brain of the preterm and term neonate.," *Clinics in perinatology*, vol. 36, no. 4, pp. 807–34, 2009.

[125] M. Ferrari, M. Muthalib, and V. Quaresima, "The use of near-infrared spectroscopy in understanding skeletal muscle physiology: recent developments," *Philosophical Transactions of the Royal Society A: Mathematical, Physical and Engineering Sciences*, vol. 369, no. 1955, pp. 4577–4590, 2011.

[126] S. Lloyd-Fox, A. Blasi, and C. E. Elwell, "Illuminating the developing brain: the past, present and future of functional near infrared spectroscopy.," *Neuroscience and biobehavioral reviews*, vol. 34, no. 3, pp. 269–84, 2010.

[127] H. Owen-Reece, C. E. Elwell, W. Harkness, J. Goldstone, D. T. Delpy, J. S. Wyatt, and M. Smith, "Use of near infrared spectroscopy to estimate cerebral blood flow in conscious and anaesthetized adult subjects.," *British journal of anaesthesia*, vol. 76, no. 1, pp. 43–48, 1996.

[128] H. Owen-Reece, C. E. Elwell, J. Wyatt, and D. T. Delpy, "The effect of scalp ischaemia on measurement of cerebral blood volume by near-infrared spectroscopy The effect of scalp ischaemia on measurement of cerebral blood volume by near-infrared spectroscopy," *Physiological Measurement*, vol. 17, pp. 279–286, 1996.

[129] D. A. Boas and M. A. Franceschini, "Haemoglobin oxygen saturation as a biomarker: the problem and a solution," 2011.

[130] I. Tachtsidis, "Experimental measurements of cerebral haemodynamics and oxygenation and comparisons with a computational model: a near-infrared spectroscopy," *PhD Thesis*, pp. 1–247, 2005.

[131] V. L. Marcar, A. E. Strässle, T. Loenneker, U. Schwarz, and E. Martin, "The influence of cortical maturation on the BOLD response: An fMRI study of visual cortex in children," *Pediatric Research*, vol. 56, no. 6, pp. 967–974, 2004.

[132] G. Greisen, T. Leung, and M. Wolf, "Has the time come to use near-infrared spectroscopy as a routine clinical tool in preterm infants undergoing intensive care?," *Philosophical transactions. Series A, Mathematical, physical, and engineering sciences*, vol. 369, no. 1955, pp. 4440–51, 2011.

[133] S. Hyttel-Sorensen, A. Pellicer, T. Alderliesten, T. Austin, F. van Bel, M. Benders, O. Claris, E. Dempsey, a. R. Franz, M. Fumagalli, C. Gluud, B. Grevstad, C. Hagmann, P. Lemmers, W. van Oeveren, G. Pichler, a. M. Plomgaard, J. Riera, L. Sanchez, P. Winkel, M. Wolf, and G. Greisen, "Cerebral near infrared spectroscopy oximetry in extremely preterm infants: phase II randomised clinical trial," *BMJ*, vol. 350, no. doi: 10.1136/bmj.g7635, pp. 1–11, 2015.

[134] A. M. Plomgaard, W. van Oeveren, T. H. Petersen, T. Alderliesten, T. Austin, F. van Bel, M. Benders, O. Claris, E. Dempsey, A. Franz, M. Fumagalli, C. Gluud, C. Hagmann, S. Hyttel-Sorensen, P. Lemmers, A. Pellicer, G. Pichler, P. Winkel, and G. Greisen, "The SafeBoosC II randomised trial: treatment guided by near-infrared spectroscopy reduces cerebral hypoxia without changing early biomarkers of brain injury," *Pediatric Research*, no. January, pp. 1–8, 2015.

[135] M. Wolf, M. Ferrari, and V. Quaresima, "Progress of near-infrared spectroscopy and topography for brain and muscle clinical applications.," *Journal of biomedical optics*, vol. 12, no. 6, p. 062104, 2007.

[136] A. P. Gibson, T. Austin, N. L. Everdell, M. Schweiger, S. R. Arridge, J. H. Meek, J. S. Wyatt, D. T. Delpy, and J. C. Hebden, "Three-dimensional whole-head optical tomography of passive motor evoked responses in the neonate," *NeuroImage*, vol. 30, no. 2, pp. 521–528, 2006.

[137] J. C. Hebden, A. Gibson, T. Austin, R. M. Yusof, N. Everdell, D. T. Delpy, S. R. Arridge, J. H. Meek, and J. S. Wyatt, "Imaging changes in blood volume and oxygenation in the newborn infant brain using three-dimensional optical tomography.," *Physics in medicine and biology*, vol. 49, no. 7, pp. 1117–1130, 2004.

[138] T. Austin, A. P. Gibson, G. Branco, R. M. Yusof, S. R. Arridge, J. H. Meek, J. S. Wyatt, D. T. Delpy, and J. C. Hebden, "Three dimensional optical imaging of blood volume and oxygenation in the neonatal brain," *NeuroImage*, vol. 31, no. 4, pp. 1426–1433, 2006.

[139] H. Singh, R. J. Cooper, C. Wai Lee, L. Dempsey, A. Edwards, S. Brigadoi, D. Airantzis, N. Everdell, A. Michell, D. Holder, J. C. Hebden, and T. Austin, "Mapping cortical haemodynamics during

neonatal seizures using diffuse optical tomography: A case study," *NeuroImage: Clinical*, vol. 5, pp. 256–265, 2014.

[140] R. J. Cooper, J. C. Hebden, H. O'Reilly, S. Mitra, a. W. Michell, N. L. Everdell, a. P. Gibson, and T. Austin, "Transient haemodynamic events in neurologically compromised infants: a simultaneous EEG and diffuse optical imaging study.," *NeuroImage*, vol. 55, no. 4, pp. 1610–6, 2011.

[141] E. Okada and D. T. Delpy, "Near-Infrared Light Propagation in an Adult Head Model. II. Effect of Superficial Tissue Thickness on the Sensitivity of the Near-Infrared Spectroscopy Signal," *Applied Optics*, vol. 42, no. 16, p. 2915, 2003.

[142] E. Okada and D. T. Delpy, "Near-Infrared Light Propagation in an Adult Head Model. I. Modeling of Low-Level Scattering in the Cerebrospinal Fluid Layer," *Applied Optics*, vol. 42, no. 16, p. 2906, 2003.

[143] G. E. Strangman, Q. Zhang, and Z. Li, "Scalp and skull influence on near infrared photon propagation in the Colin27 brain template," *NeuroImage*, vol. 85, pp. 136–149, 2014.

[144] M. Dehaes, P. E. Grant, D. D. Sliva, N. Roche-Labarbe, R. Pienaar, D. A. Boas, M. A. Franceschini, and J. Selb, "Assessment of the frequency-domain multi-distance method to evaluate the brain optical properties: Monte Carlo simulations from neonate to adult," *Biomedical optics express*, vol. 2, no. 3, pp. 552–67, 2011.

[145] S. Brigadoi and R. J. Cooper, "How short is short? Optimum source detector distance for short-separation channels in functional near-infrared spectroscopy distance for short-separation channels in functional near-infrared spectroscopy," *Neurophotonics*, vol. 2, no. 2, 2015.

[146] P. E. Grant, N. Roche-Labarbe, A. Surova, G. Themelis, J. Selb, E. K. Warren, K. S. Krishnamoorthy, D. a. Boas, and M. A. Franceschini, "Increased cerebral blood volume and oxygen consumption in neonatal brain injury.," *Journal of cerebral blood flow and metabolism : official journal of the International Society of Cerebral Blood Flow and Metabolism*, vol. 29, no. 10, pp. 1704–13, 2009.

[147] A. N. Massaro, M. Bouyssi-Kobar, T. Chang, L. G. Vezina, a. J. du Plessis, and C. Limperopoulos, "Brain perfusion in encephalopathic newborns after therapeutic hypothermia," *American Journal of Neuroradiology*, vol. 34, pp. 1–7, 2013.

[148] P. Wintermark, a. Hansen, S. K. Warfield, D. Dukhovny, and J. S. Soul, "Near-infrared spectroscopy versus magnetic resonance imaging to study brain perfusion in newborns with hypoxic-ischemic encephalopathy treated with hypothermia.," *NeuroImage*, vol. 85 Pt 1, pp. 287–93, 2014.

[149] G. Ancora, E. Maranella, S. Grandi, F. Sbravati, E. Coccolini, S. Savini, and G. Faldella, "Early predictors of short term neurodevelopmental outcome in asphyxiated cooled infants. A combined brain amplitude integrated electroencephalography and near infrared spectroscopy study," *Brain and Development*, vol. 35, no. 1, pp. 26–31, 2013.

[150] P. M. a. Lemmers, R. J. Zwanenburg, M. J. N. L. Benders, L. S. de Vries, F. Groenendaal, F. van Bel, and M. C. Toet, "Cerebral oxygenation and brain activity after perinatal asphyxia: does hypothermia change their prognostic value?," *Pediatric research*, vol. 74, no. 2, pp. 180–5, 2013.

[151] S. Peng, E. Boudes, X. Tan, M. Shevell, P. Wintermark, and C. Saint-martin, "Does Near-Infrared Spectroscopy Identify Asphyxiated Newborns at Risk of Developing Brain Injury During Hypothermia Treatment ?," *Am J Perinatol*, vol. 1, no. 212, pp. 1–9, 2014.

[152] S. Nakamura, K. Koyano, W. Jinnai, S. Hamano, S. Yasuda, Y. Konishi, T. Kuboi, K. Kanenishi, T. Nishida, and T. Kusaka, "Simultaneous measurement of cerebral hemoglobin oxygen saturation and blood volume in asphyxiated neonates by near-infrared time-resolved spectroscopy," *Brain and Development*, vol. http://dx.doi.org/10.1016/j.braindev.2015.04.002, pp. 1–8, 2015.

[153] M. C. Toet, P. M. a. Lemmers, L. J. van Schelven, and F. van Bel, "Cerebral oxygenation and electrical activity after birth asphyxia: their relation to outcome.," *Pediatrics*, vol. 117, no. 2, pp. 333–9, 2006.

[154] L. Huang, H. Ding, X. Hou, C. Zhou, G. Wang, and F. Tian, "Assessment of the hypoxic-ischemic encephalopathy in neonates using non-invasive near-infrared spectroscopy.," *Physiological measurement*, vol. 25, pp. 749–761, 2004.

[155] R. A. Shellhaas, J. S. Kushwaha, M. a. Plegue, D. T. Selewski, and J. D. E. Barks, "An Evaluation of Cerebral and Systemic Predictors of 18-Month Outcomes for Neonates With Hypoxic Ischemic Encephalopathy," *Journal of Child Neurology*, vol. 10.1177/0883073815573319, pp. 1–6, 2015.

[156] M. Dehaes, A. Aggarwal, P.-Y. Lin, C. Rosa Fortuno, A. Fenoglio, N. Roche-Labarbe, J. S. Soul, M. A. Franceschini, and P. E. Grant, "Cerebral oxygen metabolism in neonatal hypoxic ischemic encephalopathy during and after therapeutic hypothermia.," *Journal of cerebral blood flow and metabolism : official journal of the International Society of Cerebral Blood Flow and Metabolism*, vol. 34, no. 1, pp. 87–94, 2014.

[157] S. Chen, K. Sakatani, W. Lichty, P. Ning, S. Zhao, and H. Zuo, "Auditory-evoked cerebral oxygenation changes in hypoxic-ischemic encephalopathy of newborn infants monitored by near infrared spectroscopy," *Early Human Development*, vol. 67, pp. 113–121, 2002.

[158] A. Tekes, A. Poretti, M. M. Scheurkogel, T. A. G. M. Huisman, J. A. Howlett, E. Alqahtani, J.-H. K. Lee, C. Parkinson, K. Shapiro, S.-E. Chung, J. M. Jennings, M. M. Gilmore, C. W. Hogue, L. J. Martin, R. C. Koehler, F. J. Northington, and J.-H. K. Lee, "Apparent Diffusion Coefficient Scalars Correlate with Near-Infrared Spectroscopy Markers of Cerebrovascular Autoregulation in Neonates Cooled for Perinatal Hypoxic-Ischemic Injury.," *American journal of neuroradiology*, vol. http://dx.doi.org/10.3174/ajnr.A4083, pp. 1–6, 2014.

[159] V. J. Burton, G. Gerner, E. Cristofalo, S.-E. Chung, J. M. Jennings, C. Parkinson, R. C. Koehler, R. Chavez-Valdez, M. V. Johnston, F. J. Northington, and J. K. Lee, "A pilot cohort study

of cerebral autoregulation and 2-year neurodevelopmental outcomes in neonates with hypoxic-ischemic encephalopathy who received therapeutic hypothermia.," *BMC neurology*, vol. 15, no. 1, p. 209, 2015.

[160] C. A. C. Pardo, "Autoregulation in Infants with Neonatal Encephalopathy," *Pediatric neurology briefs*, vol. 29, no. 10, p. 2377148, 2015.

[161] A. N. Massaro, R. B. Govindan, G. Vezina, T. Chang, N. N. Andescavage, Y. Wang, T. Al-shargabi, M. Metzler, K. Harris, A. J. Plessis, Y. Wang, M. Metzler, K. Harris, and P. Aj, "Neurological Disease and Autonomic Dysfunction Impaired cerebral autoregulation and brain injury in newborns with hypoxic-ischemic encephalopathy treated with hypothermia," *J Neurophysiol*, vol. 114, pp. 818–824, 2015.

[162] F. Tian, T. Tarumi, H. Liu, R. Zhang, and L. Chalak, "Wavelet coherence analysis of dynamic cerebral autoregulation in neonatal hypoxicischemic encephalopathy," *NeuroImage: Clinical*, vol. 10.1016/j.nicl.2016.01.020, 2016.

[163] G. Ancora, E. Maranella, C. Locatelli, L. Pierantoni, and G. Faldella, "Changes in cerebral hemodynamics and amplitude integrated EEG in an asphyxiated newborn during and after cool cap treatment," *Brain and Development*, vol. 31, no. 6, pp. 442–444, 2009.

[164] K. Gucuyener, S. Beken, E. Ergenekon, S. Soysal, I. Hirfanoglu, O. Turan, S. Unal, N. Altuntas, E. Kazanci, F. Kulali, E. Koc, C. Turkyilmaz, E. Onal, and Y. Atalay, "Use of amplitude-integrated electroencephalography (aEEG) and near infrared spectroscopy findings in neonates with asphyxia during selective head cooling," *Brain and Development*, vol. 34, no. 4, pp. 280–286, 2012.

[165] J. A. Howlett, F. J. Northington, M. M. Gilmore, A. Tekes, T. A. Huisman, C. Parkinson, S.-E. Chung, J. M. Jennings, J. J. Jamrogowicz, A. C. Larson, C. U. Lehmann, E. Jackson, K. M. Brady, R. C. Koehler, and J. K. Lee, "Cerebrovascular autoregulation and neurologic injury in neonatal hypoxicischemic encephalopathy," *Pediatric Research*, vol. 74, no. 5, pp. 525–535, 2013.

[166] R. a. Shellhaas, B. J. Thelen, J. R. Bapuraj, J. W. Burns, A. W. Swenson, M. K. Christensen, S. a. Wiggins, and J. D. E. Barks, "Limited short-term prognostic utility of cerebral NIRS during neonatal therapeutic hypothermia," *Neurology*, vol. 81, no. 3, pp. 249–255, 2013.

[167] R. Govindan, A. Massaro, T. Chang, G. Vezina, and A. du Plessis, "A novel technique for quantitative bedside monitoring of neurovascular coupling," *Journal of Neuroscience Methods*, vol. 259, pp. 135–142, 2015.

[168] L. F. Chalak, F. Tian, D. Ph, T. Tarumi, D. Ph, R. Zhang, and D. Ph, "Cerebral Hemodynamics in Asphyxiated Newborns Undergoing Hypothermia Therapy: Pilot Findings Using a Multiple-Time-Scale Analysis," *Pediatric Neurology*, vol. 10.1016/j.pediatrneurol.2015.11.010, 2015.

[169] F. van Bel, P. Lemmers, and G. Naulaers, "Monitoring neonatal regional cerebral oxygen saturation in clinical practice: value and pitfalls.," *Neonatology*, vol. 94, no. 4, pp. 237–44, 2008.

[170] M. Wolf, G. Naulaers, F. van Bel, S. Kleiser, and G. Greisen, "A review of near infrared spectroscopy for term and preterm newborns," *J Near Infrared Spectrosc*, vol. 20, pp. 45–55, 2012.

[171] L. M. L. Dix, F. van Bel, W. Baerts, and P. M. a. Lemmers, "Comparing near-infrared spectroscopy devices and their sensors for monitoring regional cerebral oxygen saturation in the neonate.," *Pediatric Research*, vol. 74, pp. 557–563, 2013.

[172] F. Scholkmann, S. Spichtig, T. Muehlemann, and M. Wolf, "How to detect and reduce movement artifacts in near-infrared imaging using moving standard deviation and spline interpolation.," *Physiological measurement*, vol. 31, no. 5, pp. 649–62, 2010.

[173] P.-Y. Lin, N. Roche-Labarbe, M. Dehaes, A. Fenoglio, P. E. Grant, and M. A. Franceschini, "Regional and Hemispheric Asymmetries of Cerebral Hemodynamic and Oxygen Metabolism in Newborns.," *Cerebral cortex*, vol. doi:10.1093/cercor/bhs023, 2012.

[174] N. Roche-Labarbe, S. A. Carp, A. Surova, M. Patel, D. A. Boas, P. E. Grant, and M. A. Franceschini, "Noninvasive optical measures of CBV, StO2, CBF index, and rCMRO2 in human premature neonates' brains in the first six weeks of life.," *Human brain mapping*, vol. 31, no. 3, pp. 341–52, 2010.

[175] N. Roche-Labarbe, A. Fenoglio, A. Aggarwal, M. Dehaes, S. a. Carp, M. A. Franceschini, and P. E. Grant, "Near-infrared spectroscopy assessment of cerebral oxygen metabolism in the developing premature brain.," *Journal of cerebral blood flow and metabolism*, vol. 32, pp. 481–8, 2012.

[176] N. Roche-Labarbe, A. Fenoglio, H. Radhakrishnan, M. Kocienski-Filip, S. a. Carp, J. Dubb, D. a. Boas, P. E. Grant, and M. A. Franceschini, "Somatosensory evoked changes in cerebral oxygen consumption measured non-invasively in premature neonates.," *NeuroImage*, vol. http://dx.doi.org/10.1016/j.neuroimage.2013.01.035, pp. 1–8, 2013.

[177] S. Bembich, C. Oretti, L. Travan, A. Clarici, S. Massaccesi, and S. Demarini, "Effects of prone and supine position on cerebral blood flow in preterm infants.," *The Journal of pediatrics*, vol. 160, no. 1, pp. 162–4, 2012.

[178] T. Shin'oka, G. Nollert, D. Shum-Tim, a. du Plessis, and R. a. Jonas, "Utility of near-infrared spectroscopic measurements during deep hypothermic circulatory arrest.," *The Annals of thoracic surgery*, vol. 69, no. 2, pp. 578–583, 2000.

[179] C. Peeters-Scholte, E. Van Den Tweel, F. Groenendaal, and F. Van Bel, "Redox state of near infrared spectroscopy-measured cytochrome aa 3 correlates with delayed cerebral energy failure following perinatal hypoxia-ischaemia in the newborn pig," *Experimental Brain Research*, vol. 156, pp. 20–26, 2004.

[180] H. Matsumoto, T. Oda, M. A. Hossain, and N. Yoshimura, "Does the redox state of cytochrome aa3 reflect brain energy level during hypoxia? Simultaneous measurements by near infrared spectrophotometry and 31P nuclear magnetic resonance spectroscopy.," *Anesthesia and analgesia*, vol. 83, no. 3, pp. 513–8, 1996.

[181] C. E. Cooper, M. Cope, R. Springett, P. N. Amess, J. Penrice, L. Tyszczuk, S. Punwani, R. Ordidge, J. Wyatt, and D. T. Delpy, "Use of mitochondrial inhibitors to demonstrate that cytochrome oxidase near-infrared spectroscopy can measure mitochondrial dysfunction noninvasively in the brain," *Journal of Cerebral Blood Flow and Metabolism*, vol. 19, no. 1, pp. 27–38, 1999.

[182] V. Quaresima, R. Springett, M. Cope, J. T. Wyatt, D. T. Delpy, M. Ferrari, and C. E. Cooper, "Oxidation and reduction of cytochrome oxidase in the neonatal brain observed by in vivo near-infrared spectroscopy," *Biochimica et Biophysica Acta - Bioenergetics*, vol. 1366, no. 3, pp. 291–300, 1998.

[183] M. Ferrari, I. Giannini, A. Carpi, and P. Fasella, "Non-invasive near infrared spectroscopy of brain in fluorocarbon exchange-transfused rats," *Physiol. Chem. Phys. Med. NMR*, vol. 15, no. 2, pp. 107–113, 1983.

[184] Y. Hoshi, O. Hazeki, Y. Kakihana, and M. Tamura, "Redox behavior of cytochrome oxidase in the rat brain measured by near-infrared spectroscopy.," *Journal of applied physiology (Bethesda, Md. : 1985)*, vol. 83, no. 6, pp. 1842–1848, 1997.

[185] Y. Hoshi and M. Tamura, "Dynamic changes in cerebral oxygenation in chemically induced seizures in rats: study by near-infrared spectrophotometry," *Brain Res*, vol. 603, no. 2, pp. 215–221, 1993.

[186] C. a. Piantadosi and F. F. Jöbsis-Vandervliet, "Spectrophotometry of cerebral cytochrome a, a3 in bloodless rats.," *Brain research*, vol. 305, no. 1, pp. 89–94, 1984.

[187] K. Uluda, J. Steinbrink, M. Kohl-Bareis, R. Wenzel, A. Villringer, and H. Obrig, "Cytochrome-c-oxidase redox changes during visual stimulation measured by near-infrared spectroscopy cannot be explained by a mere cross talk artefact.," *NeuroImage*, vol. 22, no. 1, pp. 109–19, 2004.

[188] J. C. LaManna, "The redox state of cytochrome oxidase in brain in vivo: an historical perspective.," *Advances in experimental medicine and biology*, vol. 530, pp. 535–546, 2003.

[189] M. G. Mason, P. Nicholls, and C. E. Cooper, "Re-evaluation of the near infrared spectra of mitochondrial cytochrome c oxidase: Implications for non invasive in vivo monitoring of tissues.," *Biochimica et biophysica acta*, vol. 1837, no. 11, pp. 1882–91, 2014.

[190] C. E. Cooper, S. J. Matcher, J. S. Wyatt, M. Cope, G. C. Brown, E. M. Nemoto, and D. T. Delpy, "Near-infrared spectroscopy of the brain: relevance to cytochrome oxidase bioenergetics.," *Biochemical Society transactions*, vol. 22, no. 4, pp. 974–80, 1994.

[191] M. Banaji, "A generic model of electron transport in mitochondria," *Journal of Theoretical Biology*, vol. 243, no. 4, pp. 501–516, 2006.

[192] J. P. Newman, D. M. Peebles, S. R. Harding, R. Springett, and M. a. Hanson, "Hemodynamic and metabolic responses to moderate asphyxia in brain and skeletal muscle of late-gestation fetal sheep.," *Journal of applied physiology (Bethesda, Md. : 1985)*, vol. 88, no. 1, pp. 82–90, 2000.

[193] I. Tachtsidis, M. M. Tisdall, T. S. Leung, C. Pritchard, C. E. Cooper, M. Smith, and C. E. Elwell, "Relationship between brain tissue haemodynamics, oxygenation and metabolism in the healthy human adult brain during hyperoxia and hypercapnea.," *Advances in experimental medicine and biology*, vol. 645, pp. 315–20, 2009.

[194] K. Blomgren and H. Hagberg, "Free radicals, mitochondria, and hypoxia-ischemia in the developing brain," *Free Radical Biology and Medicine*, vol. 40, no. 3, pp. 388–397, 2006.

[195] G. C. Brown, M. Crompton, and S. Wray, "Cytochrome oxidase content of rat brain during development.," *Biochimica et biophysica acta*, vol. 1057, no. 2, pp. 273–5, 1991.

[196] C. Cooper, D. Delpy, and E. Nemoto, "The relationship of oxygen delivery to absolute haemoglobin oxygenation and mitochondrial cytochrome oxidase redox state in the adult brain: a near-infrared spectroscopy study," *Biochem. J*, vol. 632, pp. 627–632, 1998.

[197] M. Banaji, A. Mallet, C. E. Elwell, P. Nicholls, and C. E. Cooper, "A model of brain circulation and metabolism: NIRS signal changes during physiological challenges.," *PLoS computational biology*, vol. 4, no. 11, p. e1000212, 2008.

[198] T. Moroz, M. Banaji, N. J. Robertson, C. E. Cooper, and I. Tachtsidis, "Computational modelling of the piglet brain to simulate near-infrared spectroscopy and magnetic resonance spectroscopy data collected during oxygen deprivation.," *Journal of the Royal Society, Interface / the Royal Society*, vol. 9, no. 72, pp. 1499–509, 2012.

[199] M. Caldwell, T. Hapuarachchi, D. Highton, C. Elwell, M. Smith, and I. Tachtsidis, "BrainSignals Revisited: Simplifying a Computational Model of Cerebral Physiology.," *PloS one*, vol. 10, no. 5, p. e0126695, 2015.

[200] Y. a. Wickramasinghe, K. S. Palmer, R. Houston, S. a. Spencer, P. Rolfe, M. S. Thorniley, B. Oeseburg, and W. Colier, "Effect of fetal hemoglobin on the determination of neonatal cerebral oxygenation by near-infrared spectroscopy.," *Pediatric research*, vol. 34, no. 1, pp. 15–7, 1993.

[201] O. Hazeki and M. Tamura, "Quantitative analysis of hemoglobin oxygenation state of rat brain in situ by near-infrared spectrophotometry.," *Journal of applied physiology (Bethesda, Md. : 1985)*, vol. 64, pp. 796–802, 1988.

[202] Y. Kakihana, A. Matsunaga, T. Yasuda, T. Imabayashi, Y. Kanmura, and M. Tamura, "Brain oxymetry in the operating room: current status and future directions with particular regard to cytochrome oxidase.," *Journal of biomedical optics*, vol. 13, no. 3, p. 033001, 2008.

[203] C. A. Piantadosi, "Absorption spectroscopy for assessment of mitochondrial function," *Methods Toxicol*, vol. 2, pp. 107–126, 1993.

[204] H. Miyake, S. Nioka, a. Zaman, D. S. Smith, and B. Chance, "The detection of cytochrome oxidase heme iron and copper absorption in the blood-perfused and blood-free brain in normoxia and hypoxia," *Analytical Biochemistry*, vol. 192, no. 1, pp. 149–155, 1991.

[205] S. Wray, M. Cope, D. T. Delpy, J. S. Wyatt, and E. O. Reynolds, "Characterization of the near infrared absorption spectra of cytochrome aa3 and haemoglobin for the non-invasive monitoring of cerebral oxygenation.," *Biochimica et biophysica acta*, vol. 933, pp. 184–192, 1988.

[206] a. Matsunaga, Y. Nomura, S. Kuroda, M. Tamura, J. Nishihira, and N. Yoshimura, "Energy-dependent redox state of heme a + a3 and copper of cytochrome oxidase in perfused rat brain in situ.," *The American journal of physiology*, vol. 275, no. 4 Pt 1, pp. C1022–C1030, 1998.

[207] R. Stingele, B. Wagner, M. V. Kameneva, M. A. Williams, D. A. Wilson, N. V. Thakor, R. J. Traystman, and D. F. Hanley, "Reduction of cytochrome-c oxidase copper precedes failing cerebral O2 utilization in fluorocarbon-perfused cats.," *The American journal of physiology*, vol. 271, no. 2, pp. 0–587, 1996.

[208] S. J. Matcher, M. Cope, and D. T. Delpy, "Use of the water absorption spectrum to quantify tissue chromophore concentration changes in near-infrared spectroscopy.," *Physics in medicine and biology*, vol. 39, no. 1, pp. 177–96, 1994.

[209] J. S. Maier, S. a. Walker, S. Fantini, M. a. Franceschini, and E. Gratton, "Possible correlation between blood glucose concentration and the reduced scattering coefficient of tissues in the near infrared," *Optics Letters*, vol. 19, no. 24, pp. 2062–4, 1994.

[210] T. Zhu, S. Faulkner, T. Madaan, A. Bainbridge, D. Price, D. Thomas, N. Robertson, X. Golay, and I. Tachtsidis, "Optimal Wavelength Combinations for Resolving in-vivo Changes of Haemoglobin and Cytochrome-c-oxidase Concentrations with NIRS," *OSA Biomed Conference*, pp. 4–6, 2011.

[211] M. Diop, J. Kishimoto, V. Toronov, D. S. C. Lee, and K. S. Lawrence, "Development of a combined broadband near-infrared and diffusion correlation system for monitoring cerebral blood flow and oxidative metabolism in preterm infants," *Biomedical Optics Express*, vol. 2, no. 7, pp. 264–270, 2014.

[212] T. Muehlemann, D. Haensse, and M. Wolf, "Wireless miniaturized in-vivo near infrared imaging.," *Optics express*, vol. 16, no. 14, pp. 10323–30, 2008.

[213] D. Chitnis, D. Airantzis, D. Highton, R. Williams, P. Phan, V. Giagka, S. Powell, R. J. Cooper, I. Tachtsidis, C. E. Elwell, J. C. Hebden, and N. Everdell, "Towards a wearable near infrared spectroscopic probe for monitoring concentrations of multiple chromophores in biological tissue in vivo," *Under Review*.

[214] F. Bevilacqua, a. J. Berger, a. E. Cerussi, D. Jakubowski, and B. J. Tromberg, "Broadband absorption spectroscopy in turbid media by combined frequency-domain and steady-state methods.," *Applied optics*, vol. 39, no. 34, pp. 6498–6507, 2000.

[215] Y. a. Wickramasinghe, P. Rolfe, K. Palmer, and S. a. Spencer, "Investigation of neonatal brain cytochrome redox by NIRS.," *Brain research. Developmental brain research*, vol. 89, no. 2, pp. 307–308, 1995.

[216] N. Nagdyman, T. Fleck, S. Schubert, P. Ewert, B. Peters, P. E. Lange, and H. Abdul-Khaliq, "Comparison between cerebral tissue oxygenation index measured by near-infrared spectroscopy and venous jugular bulb saturation in children.," *Intensive care medicine*, vol. 31, no. 6, pp. 846–50, 2005.

[217] K. C. Sekar and K. E. Corff, "Treatment of patent ductus arteriosus: indomethacin or ibuprofen?," *Journal of perinatology : official journal of the California Perinatal Association*, vol. 28 Suppl 1, pp. S60–2, 2008.

[218] J. S. Wyatt, A. D. Edwards, D. Azzopardi, and E. O. Reynolds, "Magnetic resonance and near infrared spectroscopy for investigation of perinatal hypoxic-ischaemic brain injury.," *Archives of disease in childhood*, vol. 64, no. 7 Spec No, pp. 953–63, 1989.

[219] S. Mitra, G. Bale, J. Meek, N. Robertson, and I. Tachtsidis, "In vivo measurement of cerebralmitochondrial metabolism using broadbandnear infrared spectroscopy following neonatal stroke," *Adv Exp Med Biol*, vol. 876, pp. 493–499, 2016.

[220] G. Bale, S. Mitra, I. de Roever, M. Chan, A. Caicedo-Dorado, J. Meek, N. Robertson, and I. Tachtsidis, "Interrelationship between broadband NIRS measurements of cerebral cytochrome-c-oxidase and systemic changes indicates injury severity in neonatal encephalopathy," *Adv.Exp.Med.Biol*, vol. in press, 2016.

[221] A. Villringer, J. Planck, C. Hock, L. Schleinkofer, and U. Dirnagl, "Near infrared spectroscopy (NIRS): A new tool to study hemodynamic changes during activation of brain function in human adults," *Neuroscience Letters*, vol. 154, no. 1-2, pp. 101–104, 1993.

[222] I. Tachtsidis and F. Scholkmann, "False positives and false negatives in functional NIRS: 7 issues, challenges and the way forward," *Neurophotonics*, vol. 3, no. 3, p. 031405, 2016.

[223] I. de Roever, G. Bale, R. J. Cooper, and I. Tachtsidis, "Broadband NIRS Measured Cytochrome-C-Oxidase Shows Higher Brain-Specificity than Haemoglobin in Functional Activation," *OSA Biomed*, vol. in press, 2016.

[224] G. Nollert, T. Shin'oka, and R. Jonas, "Near-infrared spectrophotometry of the brain in cardiovascular surgery," 1998.

[225] Y. Kakihana, A. Matsunaga, K. Tobo, S. Isowaki, M. Kawakami, I. Tsuneyoshi, Y. Kanmura, and M. Tamura, "Redox behavior of cytochrome oxidase and neurological prognosis in 66 patients who underwent thoracic aortic surgery.," *European journal of cardio-thoracic surgery : official journal of the European Association for Cardio-thoracic Surgery*, vol. 21, no. 3, pp. 434–9, 2002.

[226] M. Banaji, I. Tachtsidis, D. Delpy, and S. Baigent, "A physiological model of cerebral blood flow control," *Mathematical Biosciences*, vol. 194, no. 2, pp. 125–173, 2005.

[227] K. M. Tichauer, J. T. Elliott, J. A. Hadway, D. S. Lee, T.-Y. Lee, and K. St Lawrence, "Using near-infrared spectroscopy to measure cerebral metabolic rate of oxygen under multiple levels of

arterial oxygenation in piglets.," *Journal of applied physiology (Bethesda, Md. : 1985)*, vol. 109, no. 3, pp. 878–85, 2010.

[228] L. Dunne, J. Hebden, and I. Tachtsidis, "Development of a Near Infrared Multi-Wavelength, Multi-Channel, Time-Resolved Spectrometer for Measuring Brain Tissue Haemodynamics and Metabolism," *Adv Exp Med Biol*, vol. 812, pp. 181–186, 2014.

[229] M. Firbank, M. Oda, and D. T. Delpy, "An improved design for a stable and reproducible phantom material for use in near-infrared spectroscopy and imaging.," *Physics in medicine and biology*, vol. 40, no. 5, pp. 955–961, 1995.

[230] D. Azzopardi, N. J. Robertson, A. Bainbridge, E. Cady, G. Charles-Edwards, A. Deierl, G. Fagiolo, N. P. Franks, J. Griffiths, J. Hajnal, E. Juszczak, B. Kapetanakis, L. Linsell, M. Maze, O. Omar, B. Strohm, N. Tusor, and A. D. Edwards, "Moderate hypothermia within 6 h of birth plus inhaled xenon versus moderate hypothermia alone after birth asphyxia (TOBY-Xe): A proof-of-concept, open-label, randomised controlled trial," *The Lancet Neurology*, pp. 145–153, 2015.

[231] R. J. Cooper, J. Selb, L. Gagnon, D. Phillip, H. W. Schytz, H. K. Iversen, M. Ashina, and D. a. Boas, "A systematic comparison of motion artifact correction techniques for functional near-infrared spectroscopy.," *Frontiers in neuroscience*, vol. 6, no. October, p. 147, 2012.

[232] A. Blasi, D. Phillips, S. Lloyd-Fox, P. H. Koh, and C. E. Elwell, "Automatic detection of motion artifacts in infant functional optical topography studies," in *Advances in Experimental Medicine and Biology*, vol. 662, pp. 279–284, 2010.

[233] F. Robertson, T. Douglas, and E. Meintjes, "Motion Artifact Removal for Functional Near Infrared Spectroscopy: A Comparison of Methods," *IEEE Transactions on Biomedical Engineering*, vol. 57, no. 6, pp. 1377–1387, 2010.

[234] Y. Zhang, D. H. Brooks, M. A. Franceschini, and D. a. Boas, "Eigenvector-based spatial filtering for reduction of physiological interference in diffuse optical imaging.," *Journal of biomedical optics*, vol. 10, no. 1, p. 11014, 2005.

[235] B. Molavi and G. A. Dumont, "Wavelet-based motion artifact removal for functional near-infrared spectroscopy.," *Physiological measurement*, vol. 33, no. 2, pp. 259–70, 2012.

[236] M. Izzetoglu, A. Devaraj, S. Bunce, and B. Onaral, "Motion artifact cancellation in NIR spectroscopy using Wiener filtering," *IEEE Transactions on Biomedical Engineering*, vol. 52, no. 5, pp. 934–938, 2005.

[237] A. Caicedo, C. Varon, B. Hunyadi, I. Tachtsidis, and S. V. Huffel, "Signal Decomposition Based on Wavelet Regression and Oblique Subspace Projections : Applications on Biomedical Signal Processing," *IEEE*, vol. 11, no. 4, pp. 1–14, 2012.

[238] F. van Bel, P. Lemmers, and G. Naulaers, "Monitoring neonatal regional cerebral oxygen saturation in clinical practice: value and pitfalls.," *Neonatology*, vol. 94, no. 4, pp. 237–44, 2008.

[239] A. Caicedo, M. D. Papademetriou, C. E. Elwell, A. Hoskote, M. J. Elliott, S. V. Huffel, and I. Tachtsidis, "Canonical Correlation Analysis in the Study of Cerebral and Peripheral Haemodynamics Interrelations with Systemic Variables in Neonates Supported on ECMO," vol. 765, pp. 23–29, 2013.

[240] A. Castillo, A. Sola, H. Baquero, F. Neira, R. Alvis, R. Deulofeut, and A. Critz, "Pulse Oxygen Saturation Levels and Arterial Oxygen Tension Values in Newborns Receiving Oxygen Therapy in the Neonatal Intensive Care Unit: Is 85% to 93% an Acceptable Range?," *Pediatrics*, vol. 121, no. 5, pp. 882–889, 2008.

[241] J. F. Hair, R. E. Anderson, R. L. Tatham, and W. C. Black, "Multivariate Data Analysis," *Prentice Hall, Inc*, vol. 5th Editio, p. Chapter 8: Canonical Correlation Analysis, 1998.

[242] B. Thompson, "Canonical correlation analysis: uses and interpretation," 1984.

[243] A. Caicedo, *Signal Processing for Monitoring Cerebral Hemodynamics in Neonates*. 2013.

[244] H. Q. Woodard and D. R. White, "The composition of body tissues," *British Journal of Radiology*, vol. 59, no. 708, pp. 1209–1218, 1986.

[245] S. J. Matcher and C. E. Cooper, "Absolute quantification of deoxyhaemoglobin concentration in tissue near infrared spectroscopy," *Physics in medicine and biology*, vol. 39, no. 8, pp. 1295–312, 1994.

[246] G. Pichler, B. Urlesberger, N. Baik, B. Schwaberger, C. Binder-Heschl, A. Avian, J. Pansy, P.-Y. Cheung, and G. M. Schmölzer, "Cerebral Oxygen Saturation to Guide Oxygen Delivery in Preterm Neonates for the Immediate Transition after Birth: A2-Center Randomized Controlled Pilot Feasibility Trial," *The Journal of Pediatrics*, 2015.

[247] S. Hyttel-Sorensen, S. Kleiser, M. Wolf, and G. Greisen, "Calibration of a prototype NIRS oximeter against two commercial devices on a blood-lipid phantom.," *Biomedical optics express*, vol. 4, no. 9, pp. 1662–72, 2013.

[248] S. J. Arri, T. Muehlemann, M. Biallas, H. U. Bucher, and M. Wolf, "Precision of cerebral oxygenation and hemoglobin concentration measurements in neonates measured by near-infrared spectroscopy.," *Journal of biomedical optics*, vol. 16, no. 4, p. 047005, 2011.

[249] L. C. Sorensen and G. Greisen, "Precision of measurement of cerebral tissue oxygenation index using near-infrared spectroscopy in preterm neonates.," *Journal of biomedical optics*, vol. 11, no. 5, p. 054005, 2014.

[250] L. Dunne, J. Hebden, and I. Tachtsidis, "Development of a Near Infrared Multi- Wavelength, Multi-Channel, Time-Resolved Spectrometer for Measuring Brain Tissue Haemodynamics and Metabolism," *Adv Exp Med Biol*, vol. 812, pp. 181–186, 2014.

[251] Y. Sakata, M. Abajian, M. O. Ripple, and R. Springett, "Measurement of the oxidation state of mitochondrial cytochrome c from the neocortex of the mammalian brain.," *Biomedical optics express*, vol. 3, pp. 1933–46, aug 2012.

[252] P. Kadam and S. Bhalerao, "Sample size calculation.," *International journal of Ayurveda research*, vol. 1, no. 1, pp. 55–57, 2010.

[253] M. L. Seghier, "Laterality index in functional MRI: methodological issues," *Magnetic Resonance Imaging*, vol. 26, no. 5, pp. 594–601, 2008.

[254] K. M. Tichauer, J. a. Hadway, T.-Y. Lee, and K. St Lawrence, "Measurement of cerebral oxidative metabolism with near-infrared spectroscopy: a validation study.," *Journal of cerebral blood flow and metabolism : official journal of the International Society of Cerebral Blood Flow and Metabolism*, vol. 26, pp. 722–730, 2006.

[255] A. B. Rowley, S. J. Payne, I. Tachtsidis, M. J. Ebden, J. P. Whiteley, D. J. Gavaghan, L. Tarassenko, M. Smith, C. E. Elwell, and D. T. Delpy, "Synchronization between arterial blood pressure and cerebral oxyhaemoglobin concentration investigated by wavelet cross-correlation.," *Physiological measurement*, vol. 28, no. 2, pp. 161–73, 2007.

[256] S. Mitra, G. Bale, J. Meek, N. Robertson, and I. Tachtsidis, "Changes in cerebral oxidative metabolism measured by broadband near infrared spectroscopy during neonatal seizures following hypoxic ischemic brain injury," Under Review.

[257] I. Juránek and L. Bačiak, "Cerebral hypoxia-ischemia: Focus on the use of magnetic resonance imaging and spectroscopy in research on animals," 2009.

[258] S. Mitra, G. Bale, J. Meek, N. Robertson, and I. Tachtsidis, "Relationship between cerebral oxygenation and metabolism during rewarming in newborn infants after therapeutic hypothermia following hypoxic-ischemic brain injury," *Adv Exp Med Biol*, In Press.

Appendix A

Ethics and Patient Data

The UCH Baby Brain Study: Near infrared monitoring and 3T MRI/MRS in Babies with Acute Brain Injury

Short title: UCH Baby Brain Study

Protocol v.4.0
24 January 2013

Sponsor: **UCL**
Sponsor reference number: **13/0013**

REC: **NW Research Ethics Centre**
REC Reference number: **13/LO/0225**

STUDY PERSONNEL AND CONTACT DETAILS

Sponsor: **University College London**
Contact name Dave Wilson
Database and Information Officer
Joint UCLH/UCL Biomedical Research (R&D) Unit
Rosenheim Wing, Ground Floor
25 Grafton Way
London WC1E 5DB

Chief investigator: **Professor Nicola Robertson**
Academic Division of Neonatology
Institute for Women's Health
Medical School Building
74 Huntley Street
London WC1E 6AU
Phone: 020 7679 6052
Fax: 020 7387 7429
Email: n.robertson@ucl.ac.uk

Co-investigators:

Dr. Cristina Uria-Avellanal
UCL Institute for Women's Health
Medical School Building (401 Rockefeller Building)
74 Huntley Street
London WC1E 6AU
Email: c.uria@ucl.ac.uk

Dr. Judith Meek
UCLH NHS Trust - Neonatal Unit
EGA Wing – level 2
25 Grafton Way
London WC1E 6DB
Tel: 02034478094 (Consultant's PA)
Email: judith.meek@uclh.nhs.uk

Magda Sokolska
UCL Institute of Neurology
Neuroimaging Analysis Centre
Queen Square 8-11
London WC1N 3BG
Tel: 02034483449
Email: m.sokolska@ucl.ac.uk

Dr. Giles Kendall
UCLH NHS Trust - Neonatal Unit
EGA Wing – level 2
25 Grafton Way
London WC1E 6DB
Email: g.kendall@ucl.ac.uk

Professor Neil Marlow
UCL EGA Institute for Women's Health
74 Huntley Street
London WC1E 6AU
Tel: +44 (0) 20 7679 0834 (PA)
Fax: +44 (0) 20 3108 2036
Email: n.marlow@ucl.ac.uk

Professor Sebastian Ourselin,
Centre for Medical Image Computing
Malet Place, UCL
E mail: s.ourselin@ucl.ac.uk

Ernest Cady
UCLH NHS Trust– Dept Medical Physics and Bioengineering - EGA Wing, level -2
235 Euston Road
London NW1 2BU
Tel: 02034472321
Fax 02034472185
Email: ernest.cady@uclh.nhs.uk

Dr. Ilias Tachtsidis
UCL- Biomedical Optics Research Laboratory
Dept Medical Physics and Bioengineering
Malet Place Engineering Building
London WC1E 6BT
Email: i.tachtsidis@ucl.ac.uk

Gemma Bale
UCL- Biomedical Optics Research Laboratory
Dept Medical Physics and Bioengineering
Malet Place Engineering Building
London WC1E 6BT
Email: gemma.bale.11@ucl.ac.uk

Professor Xavier Golay
UCL Institute of Neurology
Queen Square 8-11
London WC1N 3BG
Tel: 020 7676 2198
Email: x.golay@ion.ucl.ac.uk

SYNOPSIS

Title	**The UCH Baby Brain Study: Near infrared monitoring and 3T MRI/MRS in Babies with Acute Brain Injury**
Acronym	Baby Brain Study
Chief Investigator	Nicola J Robertson, Professor of Perinatal Neuroscience and Honorary Consultant Neonatologist, University College London
Objectives	In term and preterm infants with acute brain injury 1.What is the predictive value of intracellular brain pH (pHi) for 2-year outcome? (primary outcome) 2. How does the bedside near Infrared spectroscopy (NIRS) derived measurement of cytochrome oxidase relate to: • brain pHi, • brain lactate/N-acetyl aspartate ratio(Lac/NAA), • brain perfusion using arterial spin labelling, and • venous oxygenation using T2-relaxation-uder-spin-tagging (TRUST)? 3. How does brain 31P-MRS pHi relate to pHi measured by Chemical saturation transfer (CEST) ? 4. How does pHi relate to other measures obtained by MR spectroscopy? 5. What are the predictive values of cytochrome oxidase and MRS measures for information processing and short term memory over the first postnatal year
Study Configuration	Prospective cohort study
Setting	Neonatal unit and outpatient clinics
Sample size estimate	Prospective cohort study of 70 newborn babies born preterm and term with acute brain injury
Number of participants	70 babies
Eligibility criteria	All term and preterm babies born at UCH or transferred to UCH for treatment of acute brain injury without life threatening congenital malformations and considered likely to survive

Description of interventions	Alongside routine continuous EEG, babies will be monitored using NIRS, and receive 1 MRI scan at 5-14 days. This MRI scan is carried out routinely in babies with acute brain injury and lasts 45-50 minutes. In those infants who remain stable, we will continue the acquisition of sequences for a total scanning time of 90 mins. A range of neurobehavioural tests will be undertaken over the first 2 years after discharge home
Duration of study	5 years from February 2013
Outcome measures	• NIRS cytochrome oxidase measurement • EEG background activity and seizures • Brain intracellular pHi and metabolite ratios on phosphorus-31 (31P) and proton (1H) MR Spectroscopy • Structural MRI scan • Brain perfusion using arterial spin labelling • Brain venous oxygenation using T2-relaxation-uder-spin-tagging (TRUST) • Brain pHi measured using Chemical saturation transfer (CEST) imaging • Neurodevelopmental assessment Bayley Scale of Infant and Toddler Development -3rd edition (BSID-III)
Statistical methods	Data will be compared between subgroups and over time using appropriate categorical or continuous statistical methods. Linear regression will be used to adjust associations for confounding variables. Two statistical software packages will be used, SPSS and Stata in their most up to date version at the completion of the study.

Neuro-monitoring and 3T MRI/MRS in Babies with Acute Brain Injury

BACKGROUND

Neonatal encephalopathy

Neonatal encephalopathy (NE) occurs in 1-2 per 1000 live term births in the UK – with a term birth rate of 750,000 births in the UK, the number of affected infants is estimated to be 750-1125 infants annually in the UK. There is an unmet need for objective, quantitative cerebral magnetic resonance (MR) markers of perinatal brain injury for clinical trials of neuroprotection; such markers will improve our understanding of the tissue response to injury and may expedite clinical translation of novel neuroprotectants.

As adjunct neuroprotective therapies evolve, we need more accurate MR biomarkers that can detect earlier and more subtle changes in brain structure and function than before. We believe that phosphorus MR spectroscopy (31P MRS) combined with the other state-of the art imaging techniques (e.g. Chemical Exchange Saturation Transfer (CEST) imaging and brain perfusion) developed by the co-applicants will provide the detail needed to enhance our care of infants undergoing neuroprotection.

Magnetic resonance imaging and spectroscopy

UCL has been a world leader in cerebral MRS for over 30 years. The first ever “in man” 31P MR brain spectrum was obtained by Prof Reynolds and Mr Ernest Cady (co-applicant) at UCL in 1982 in an infant with NE (1); this and later studies (2,3) were significant landmarks in the understanding of neuroprotection for the newborn and demonstrating the existence of a therapeutic window after hypoxia-ischaemia (see Figure 1). In 2010, the National Institute of Health and Clinical Excellence (NICE) endorsed therapeutic hypothermia as standard care for infants with moderate to severe encephalopathy (4). Currently with this treatment, for every 7 infants treated with cooling, one will escape an adverse outcome (5). More work is on-going at UCL and elsewhere to develop adjunct therapies that can further improve outcomes.

Surrogate outcome measures or biomarkers are important as their use can expedite the translation of new therapies to the clinic. In 2002, Robertson et al., demonstrated that brain intracellular pH (pHi) was alkaline following perinatal hypoxia-ischaemia and the extent of the alkalosis was associated with neurodevelopmental outcome and brain injury severity on conventional MR imaging (MRI) (6). Dr Kendall (co-applicant) demonstrated the importance of brain pHi in the rodent brain (7) and Prof Robertson has shown that manipulation of brain pHi with amiloride is neuroprotective in the newborn piglet (8). Brain pHi is thus likely to be an important marker of injury, but no studies have been done in babies since the work done by Robertson et al in 2002 (6).

An exciting development is that now we have the opportunity to develop and validate 31P MRS brain biomarkers relative to other sophisticated MR imaging techniques developed by Prof Golay. Recently Prof Golay has developed a novel MRI method, called GlucoCEST, currently in press in Nature Medicine (9). This method uses the principles of chemical exchange to provide information on glucose uptake. We here propose to adapt this technique to the measurement of pHi, through the base-catalyzed chemical exchange between amide protons and surrounding water in the brain (10). This new MRI technique is safe, as it is similar to conventional magnetization transfer MRI, but has never been used in newborns.

UCLH is a regional referral centre for term NE, recruiting around 45 infants per year; all infants undergo MRI and proton MRS aged 5-10 days. We have a very successful MRI

service (led by Dr Giles Kendall and Prof N Robertson) using a Philips 3T multinuclear (i.e. including 31P) MR scanner.

Near infrared spectroscopy

Another very exciting technique for neuromonitoring is NIRS. It is portable and NIR light is safe. It can therefore be used to monitor critically ill patients who cannot be moved out of an intensive care environment. NIRS is highly sensitive to both haemoglobin concentration, oxygenation and oxygen utilisation and can therefore provide information of brain tissue function. Such a system is ideally suited to monitor the brain of patients both adults and neonates.

The MultiModal Spectroscopy (MMS) group in the Biomedical Optics Research Laboratory (BORL) at UCL, lead by Dr. Ilias Tachtsidis, has developed novel optical instrumentation and methods to investigate brain oxygen utilisation and regulation, during systemic provocations in infants (11) and adults. Ilias has recently developed equipment and methodologies that allow simultaneous NIRS and MRI/MRS measurements (12) hence providing novel data on brain tissue haemodynamic patterns, oxygenation and mitochondrial metabolism (redox state of cytochrome-c-oxidase).

Between 2004 and 2008 Dr Tachtsidis has used NIRS systems to characterise cerebral oxygen delivery and oxygen utilisation in different groups of adult patients. The study in eight TBI patients with traumatic brain injury (TBI) has demonstrated, for the first time, a correlation between the NIRS monitored oxCCO and the cerebral lactate pyruvate ratio (measured invasively with cerebral microdialysis) (13). This study confirms that oxCCO may be used as a surrogate marker of cellular oxygen metabolism and help identify treatment strategies in brain injured patients (such as hyperoxygenation).

Recently Dr Tachtsidis have completed studies in over 50 volunteers in order to explore the applicability of NIRS to monitor brain tissue physiology and metabolism, suggesting that physiological challenges (such as hypercapnia and hyperoxia) can be used to increase cerebral oxygen metabolism (14,15). In a separate study, during controlled isocapnic hypoxia in healthy adults, estimated cerebral oxygen delivery and oxCCO were linearly correlated (16). Clearly the combination of brain tissue measurements of changes in haemoglobin concentration and intracellular oxCCO can identify relationships between brain tissue haemodynamics and tissue oxygen utilisation, which can be used to understand the coupling between tissue oxygenation and cell metabolism; while also helping us define thresholds for brain wellbeing.

Dr Tachtsidis group in collaboration with Prof Nicola Robertson and Prof Xavier Golay have recently developed a novel methodology that combines spectroscopic data from broadband NIRS and magnetic resonance spectroscopy (MRS) that provides information on the brain vasculature haemodynamics, brain tissue oxygenation, brain tissue biochemistry and importantly mitochondrial metabolism. They completed a set of experiments investigating in a neonatal preclinical model brain metabolism during and following hypoxic-ischemia (HI) and demonstrated for the first time through the synchronous measurements of oxCCO (by broadband NIRS) and Lac/NAA (by ^{1}H MRS) mitochondrial impairment following hypoxic-ischemia (12). It therefore is a potential clinical marker of the balance between mitochondrial oxygen delivery and utilization.

Outcome following neonatal encephalopathy

Despite improvements in care for babies with encephalopathy and the introduction of therapeutic hypothermia, up to 40% of babies with moderate or severe encephalopathy will still die or have serious impairment at follow up. For survivors it is critically important that we identify babies who will develop disability in neuromotor or cognitive domains, as these are the two commonest outcomes. We currently use a structured neurological examination and assessment of General Movements at term and 3 months of age to support early diagnosis, but there are no early indicators of cognitive impairments other than routine clinical developmental assessment, which is poorly predictive.

Over the past year we have developed a range of infant assessment protocols for very preterm children over the first year (UCH Preterm Development Project [Funding SPARKS; Sponsor UCL 10/0312; REC approval NW London REC 2 10/H0720/80]). We would like now to extend these investigations to include this high-risk group using the same protocol at the same ages (preterms are assessed at post-term age equivalents). This includes 3 visits at 3, 6 and 12 months timed to coincide with routine follow up evaluations.

PLAN OF INVESTIGATION

We will recruit a cohort of term and preterm infants at risk of acute brain injury. These infants might have a diagnosis of neonatal encephalopathy, seizures or require a clinical MRI study for any indication.

These children will be recruited into a longitudinal follow-up study with routine neurodevelopmental assessment using the Bayley Scale of Infants and Toddler Development – 3rd edition (BSID – III) at 2 years.

Term and preterm babies at risk of acute neurological injury admitted to the neonatal unit will be assessed by the clinical team. A member of the neuro-clinical research team will approach the parents for consent for entry into the extended neuromonitoring and neuroimaging study within the first 24h.

It is routine for babies at risk of acute neurological injury to undergo EEG monitoring immediately after admission and stabilisation. Following the EEG application we will request consent for extended neuromonitoring using NIRS. This will involve an additional probe to be gently fixed to the side of the scalp and another small machine (NIRS system) to be beside the baby's cot. The NIRS monitoring will continue for up to 5 days and can be done intermittently if the baby requires moving or during routine cranial ultrasound scanning. This technique is safe for the newborn as far as we know. The application of the probes on the scalp is similar to the EEG electrodes – part of the clinical care.

Some infants who, after assessment with EEG, are eligible for entry into the TOBY Xenon study will have a further consent for entry into this study. We will make it clear that the MR imaging and spectroscopy (MRI/MRS) study is a routine part of the care of the baby whether he or she is eligible or ineligible for the TOBY Xenon study. What we are requesting in the extended neuromonitoring and neuroimaging study is a slightly longer period in the MRI scanner when the scan is done between day 5-14.

During the time the baby is in the neonatal intensive care unit, there will be a close contact between the nursing, clinical and research staff and the parents. Cranial ultrasound imaging and continuous EEG will occur as part of the routine care of the baby. The NIRS monitoring will continue alongside these routine investigations.

One to two days before the MRI/MRS scan the clinical research team will discuss the consent for the extended imaging study. We will explain again that the routine scan time for both clinical or Toby Xenon scans is 45-50min and only if the baby remains settled and stable will be acquire more sequences up to 90 minutes time in the magnet.

MRI/MRS assessment is routinely carried out on day 5-14 after birth in infants at risk of acute brain injury. At least one hour before the scan, a paediatrician and a nurse prepare the baby for the MRI according to our protocol. We double check all the steps: safety checks, metal checks, noise protection and monitoring equipment in the MRI conditional Lammers Neonatal incubator. The fluid infusions for the MRI conditional Braun system are also prepared. All the babies are monitored throughout the scan with similar monitoring equipment to that used in the NICU.

In ventilated babies we will continue their routine sedation (usually intravenous morphine). In non-ventilated inpatient babies, we will sedate for the MRI scan if necessary with Chloral Hydrate orally 50 mg/kg. This is already our current practice for most MR scans in babies with acute brain injury.

If the baby is an outpatient, we prepare him as well at least one hour before the scan. We will try to avoid sedation if he goes to sleep through a feed-and-wrap technique. If we need to give sedation (Chloral Hydrate), we will need to keep the baby monitored until he's awake and he managed to do a good feed.

In case of the baby being unstable in the scanner, there is a safety protocol in place. A resuscitation trolley and emergency equipment is in place adjacent to the 3T-MRI suite. At least one senior Registrar and a nurse or Advanced Nurse Neonatal Practitioner (ANNP) accompany the baby to and from the scanner and are present in the control room monitoring the baby throughout the scan.

Parents are welcome to accompany their baby in the Lammers Incubator over to the MRI ante-room to see where the scan is going to take place, see the facilities, monitoring, etc. They will then be asked to wait in the waiting room until the scan is finished.

If the baby wakes up, is unsettled or unstable, we will bring the baby out of the scanner and attend to the issue.

If the baby becomes unsettled before the end of the clinical scan, we will try to settle him down to be able to complete the sequences that are necessary for clinical information.

There are no specific risks for the newborn associated to the extra-sequences that this study involves as far as we know. The inconvenience is that the time of the scan

becomes slightly longer. If the baby wakes up during the extended scanner sequences, we will stop the scan and take the baby back to the neonatal unit. Parents will be kept informed at all times.

We will collect all the data acquired clinically as well as the extra neuromonitoring and neuroimaging sequences and analyse these.

Babies are routinely followed up and undergo assessment with Dr Angela Huertas-Ceballos at 3, 6, 12 and 24 months each with a formal Bayley III assessment. At the infancy visits we will also evaluate the following outcomes in the BabyLab – based in the Clinical Research Facility on the ground floor of the EGA Wing adjacent to outpatients:

Outcome	Test	Age (Corrected)		Examiner	Time	Location
Neuropsychology	Visual attention test	3m	+	Psychologist	20minζ	Baby Lab
(Memory, attention, inhibition, planning and/or processing speed)	ERP	6m	+	Psychologist	15 min	Baby Lab
	Delayed-response task	6m	+	Psychologist	10 min	Baby Lab
	A-not-B task	12m	+	Psychologist	5min	Baby Lab
	Means-End task	12m	+	Psychologist	5min	Baby Lab
	Deferred Imitation task	12m	+	Psychologist	10min	Baby Lab
Language/motor skills	Questionnaire	12m	+	Parent	20min	Baby Lab

Full details are included in the UCH PDP protocol (attached); please note this is a restricted set of assessments from the full BabyLab protocol.

The primary outcome is the Bayley composite scores (in Language, Motor and Cognition) at two years We will record all this data anonymously and analyse the relation between the early NIRS, MRI and MRS biomarkers and outcome. In further work we will evaluate our new measures made in infancy against the 2-year outcomes to determine if we can improve the predictive value of the neonatally acquired biomarkers.

The routine scanning protocol will comprise:

Sequence	Approx time to acquire
• High-resolution T1weighted 3D anatomical scan: MP-RAGE or other standard clinical acquisition for structural imaging	6 minutes
• T2w imaging anatomical scans: TSE or standard clinical acquisition for structural imaging	7.5 – 15 minutes (single or multiple orientations)
• Multi-direction Diffusion tensor-like imaging: standard clinical acquisition. Indices derived from DTI-like acquisition are thought to be sensitive to ischemia and to be correlated with outcome.	6-8 minutes
• Single voxel proton spectroscopy (PRESS): allows measurement of lactate in a small localised section of tissue.	6-8 minutes
• Additional positioning anatomical scans for MRS	1 minute

The total time taken for this is around 40 minutes

Additional sequences will include:

Sequence	Approx time to acquire
• Localised Phosphorus (^{31}P) MRS (ISIS): Measurements of energy metabolites and pH.	12 min
• Additional positioning anatomical scans for ^{31}P MRS	1 minute
• Quantitative measurement of perfusion (ASL): standard sequence to measure brain perfusion and/or angiography to assess blood delivery to the brain.	7-10 minutes
• Quantitative measurement of oxygen extraction fraction (e.g. TRUST): assessment of oxygen metabolism	8-10 minutes
• Long and short T_2 mobile proton exchange measurements (e.g. CEST): assessment of brain maturation (myelin), glucose metabolism and pH	10-15 minutes

The total time taken for this is around 45 mins

Feedback to parents: All MRI/MRS scans and EEG traces are reported by a clinical radiologist/physicists/neurophysiologist respectively. Feedback of relevant clinical information to parents occurs as part of the routine clinical care and is led by the attending neonatologist; this is recorded in the clinical case-record.

Outputs:

These data will be presented at national and international paediatric and radiological research meetings and written up for publication in peer-reviewed journals.

Study written and electronic records

- Each participant will be assigned a study identity code number, for use on all paper records, other study documents and the electronic database. The documents and database will also use the date of birth as a second identifier.
- All written records will be treated as confidential documents and held securely in accordance with regulations. The investigator will make a separate confidential record of the participant's name, date of birth, local hospital number or NHS number, and Participant Study Number, to permit identification of all participants enrolled in the study, for the purposes of later follow-up.
- All paper forms will be completed using black ballpoint pen. Errors shall be lined out but not obliterated by using correction fluid and the correction inserted, initialled and dated.
- The person completing each paper form shall sign and date each form.

Quality assurance & audit

Insurance and indemnity

- University College London holds insurance against claims from participants for harm caused by their participation in this clinical study. Participants may be able to claim compensation if they can prove that UCL has been negligent. However, if this clinical study is being carried out in a hospital, the hospital continues to have a duty of care to the participant of the clinical study. University College London does not accept liability for any breach in the hospital's duty of care, or any negligence on the part of hospital employees. This applies whether the hospital is an NHS Trust or otherwise.
- Insurance and indemnity for clinical study participants and study staff is covered within the NHS Indemnity Arrangements for clinical negligence claims in the NHS, issued under cover of HSG (96)48. There are no special compensation arrangements, but study participants may have recourse through the NHS complaints procedures.

Reporting Serious Unexpected Adverse Events

- All Serious Unexpected Adverse Events to a research subject in the study must be reported immediately to the sponsor using the following email address research-incidents@ucl.ac.uk.
- A Serious Adverse Event:
    - Results in death
    - Is life Threatening
    - Requires Hospitalisation or prolongation of hospitalisation

    - Results in persistent or significant disability or incapacity
    - Consists of a congenital anomaly or birth defect
    - Any other serious medical occurrence
- Serious Adverse Events will be documented from the point of enrolment until the patient is exited from study. Information recorded and reported shall include
    - A description of the event
    - The date of event onset
    - The relatedness of the event to the procedure
    - The expectedness of the event
    - The outcome of the event
    - The date the event was first noticed by, or reported to the investigator
- All ongoing Serious Adverse Events will be followed-up until the last study visit.

Reporting Incidents

- All incidents must be reported through the appropriate Trust incidents reporting system. Where no Trust is involved the incident should be reported by completing form at http://www.ucl.ac.uk/jro/postapproval
- Where the study is being conducted at UCLH then the incidents should be reported through Datix.
- An incident in a research study is:
    - Something that should not have happened OR
    - Something that should have happened but didn't ,
      which significantly effects any of the following:
        - the rights and well being of the research subject
        - the scientific value of the study
        - the compliance of the study with all relevant legal rules or ethics guidance including the Data Protection Act and the Human Tissue Act
        - The reputation of UCL

Conduct of the Study

- Study conduct will be subject to systems audit for inclusion of essential documents; permissions to conduct the study; CVs of study staff and training received; local document control procedures; consent procedures and recruitment logs; adherence to procedures defined in the protocol (e.g. inclusion / exclusion criteria, timeliness of visits); and accountability of study materials.
- Monitoring of study data shall include confirmation of informed consent; source data verification; data storage and data transfer procedures; local quality control checks and procedures, back-up and disaster recovery of any local databases and validation of data manipulation. The Study manager, or where required, a nominated designee of the Sponsor, shall carry out monitoring of study data as an ongoing activity.
- Data will be effectively double entered using SPSS Data Entry continuous comparison techniques to ensure accurate electronic data records
- Study data and evidence of monitoring and systems audits will be made available for inspection by the REC as required.

Data Management and analysis

- Access to all study documents is limited to the study personnel (see below) excepting that the CRF and all source documents will be made be available at all times for review by the Chief Investigator, Sponsor's designee and inspection by

relevant regulatory authorities.

- All study staff and investigators will endeavour to protect the rights of the study's participants to privacy and informed consent, and will adhere to the Data Protection Act, 1998. The Assessment procedures will only collect the minimum required information for the purposes of the trial. All records will be held securely, in a locked room, and a locked cabinet. Access to the information will be limited to the trial staff and investigators and any relevant regulatory authorities. Computer held data including the study database will be held securely and password protected. All data will be stored on a secure dedicated web server. Access will be restricted by user identifiers and passwords (encrypted using a one way encryption method).
    - Information about the study in the participant's medical records / hospital notes will be treated confidentially in the same way as all other confidential medical information.
    - A Neonatal Fellow and postdoctoral fellow (Physics and Bioengineering Dept), will carry out data analysis under supervision from the co-investigators. Where off-line analysis of data is undertaken these data are managed anonymously using a unique study identifier. Summary data are then returned to the main study database, which is again anonymised to maintain confidentiality.
    - Electronic data will be backed up every 24 hours to both local and remote media in encrypted format.
    - Data will be entered onto study forms and posted back to the study centre where they will be encoded for computer analysis using SPSS Data Entry and SPSS for Windows
    - Data will be analysed using appropriate categorical and continuous comparisons using SPSS and STATA statistical software packages. Regression analyses will be performed.
    - Electronic data will be archived at the completion of the study for a period of 25 years to allow for later follow up of this unique population. Paper records will be kept for 10 years after the last assessment is carried out on the population.

24.1.13_ v4.0

References:

1. Cady E, Costello AM, Dawson MJ, Delpy DT, Hope PL, Reynolds EO, Tofts PS, Wilkie DR. Non-invasive investigation of cerebral metabolism in newborn infants by phosphorus nuclear magnetic resonance spectroscopy.Lancet. 1983;1 (8333): 1059-1062
2. Azzopardi D, Wyatt JS, Cady EB, Delpy DT, Baudin J, Stewart AL, Hope PL, Hamilton PA, Reynolds EO. Prognosis of newborn infants with hypoxic-ischemic brain injury assessed by phosphorus magnetic resonance spectroscopy. Pediatr Res. 1989;25 (5): 445-451
3. Hope PL, Costello AM, Cady EB, Delpy DT, Tofts PS, Chu A, Hamilton PA, Reynolds EO, Wilkie Dr. Cerebral energy metabolism studied with phosphorus NMR spectroscopy in normal and birth-asphyxiated infants. Lancet. 1984; 2 (8399): 366-370
4. Therapeutic hypothermia with intracorporeal temperature monitoring for hypoxic perinatal brain injury: NICE guidelines: interventional procedures. 2010;

   http://www.nice.org.uk/nicemedia/live/11315/48809/48809.pdf
5. Tagin MA, Wollcott CG, Vincer MJ, Whyte RK, Stinson DA. Hypothermia for neonatal hypoxic ischemic encephalopathy: an updated systematic review and meta-analysis. Arch Pediatr Adolesc Med 2012;166 (6): 558-66
6. Robertson NJ, Cowan FM, Cox IJ, Edwards AD. Brain alkaline intracellular pH after neonatal encephalopathy. Ann Neurol 2002; 52(6): 732-742
7. Kendall GS, Robertson NJ, Iwata O, Peebles D, Raivich G. Pediatr Res. 2006; 59(2): 227-231.
8. Robertson NJ, Kato T, Bainbridge A, Chandrasekaran M, Iwata O, Kapetanakis A, Faulkner S, Cheong J, Iwata S, Hristova M, Cady E, Raivich G (2012). Methyl-isobutyl Amiloride Reduces Brain Lac/NAA, Cell Death and Microglial Activation in a Perinatal Asphyxia Model. J Neurochem 2012, *in press*.
9. Walker-Samuel S, Ramasawmy R, Torrealdea F, Rega M, Rajkumar V, Johnson SP, Richardson S, Gonçalves M, Parkes HG, Thomas DL, Pedley RB, Lythgoe MF, Golay X. In vivo imaging of glucose uptake and metabolism in tumors. Nat Med *In press*, 2012.
10. Zhou J, Payen JF, Wilson DA, Traystman RJ, van Zijl PC. Using amide proton signals of intracellular proteins and peptides to detect pH effects in MRI. Nat Med 2003; 9 (8): 1085-90
11. Papademetriou M, Tachtsidis I, Banaji M, Elliott M, Hoskote A, Elwell C. Regional cerebral oxygenation measured by multichannel near-infrared spectroscopy (optical topography) in an infant supported on venoarterial extracorporeal membrane oxygenation. J Thorac Cardiovasc Surg 2011;141(5):e31-3.

12. Tachtsidis I, Faulkner S, Bainbridge A, Cady EB, Golay X, Robertson N. Fusion of NIRS and MRS delivers novel multimodal investigation of neonatal HIE. XXVth International Symposium on CBF, Metabolism and Function 2011; Brain 2011(Barcelona, Spain).
13. Tisdall M.M., Tachtsidis I., Leung T.S., Elwell C.E., and Smith M. "Increase in cerebral aerobic metabolism by normobaric hyperoxia after traumatic brain injury" J. Neurosurg., 109:3, 424-432, (2008).
14. Tisdall M.M., Taylor C., Tachtsidis I., Leung T.S., Pritchard C., Elwell C.E., Smith M. “The effect on cerebral tissue oxygenation index of changes in the concentrations of inspired oxygen and end tidal carbon dioxide in healthy adult volunteers.” Anesthesia & Analgesia, 109(3):906-13 (2009).
15. Tachtsidis I., Tisdall M.M., Leung T.S., Pritchard C., Cooper C.E., Smith M., Elwell C.E. “The relationship between brain tissue haemodynamics, oxygenation and metabolism in the healthy human adult brain during hyperoxia and hypercapnea.” Advances in Experimental Medicine and Biology, 645, 315-320, (2009).
16. Tisdall M.M., Tachtsidis I., Leung T.S., Elwell C.E. and Smith M. “Near infrared spectroscopic quantification of changes in the concentration of oxidized cytochrome oxidase in the healthy human brain during hypoxemia.” Journal of Biomedical Optics, 12(2):024002, (2007).

University College London Hospitals NHS
NHS Foundation Trust

Project ID: 13/0013
REC Ref: 13/LO/0225

Patient Identification
Number for this trial: _____

Name of Researcher: Professor Nicola J Robertson

Neonatal Services
NNU Medical Secretaries
2nd Floor, North Wing
250 Euston Road
London NW1 2PG

Telephone: 0203 456 7890
Consultants' PA: 0203 447 8094

THE UCH BABY BRAIN STUDY

FORM FOR PARENTAL CONSENT

Please initial each box

1. I confirm that I have read and understand the information sheet dated 15 March 2013 (version. 4.1) for the above study. I have had the opportunity to consider the information, ask questions and have had these answered satisfactorily. ☐
2. I understand that the participation of my baby in this study (NIRS monitoring and extra sequences during MRI/MRS) is independent from other studies and I can withdraw from any of them separately at any time. ☐
3. I understand that the participation of my baby is voluntary and that I am free to withdraw at any time without giving any reason, without the medical care or legal rights of my baby being affected. ☐
4. I understand that relevant sections of my baby's medical notes and data collected during the study may be looked at by individuals from regulatory authorities or from the NHS Trust from the sponsor's representative from UCL, where it is relevant to my baby taking part in this research. I give permission for these individuals to have access to my baby's records. ☐
5. I agree that the NIRS, MRI/MRS and other MR sequences data, video recordings and EEG tracings can be used for further research and teaching purposes; the material will always be used anonymously and my child will not be identifiable in the data used. ☐
6. I understand that I will be invited back for 3 assessments over the first year after my child was born and a last assessment will be performed at 2 years of age. ☐
7. I agree that my baby may take part in the above study. ☐

Name of Child:		
Name of Parent:	Date	Signature
Name of Person taking consent:	Date	Signature

3 copies: one to be retained by parent, one placed in the clinical notes and one retained by the study office.

Version 4.1 15 March 2013

Appendix B

Publications